5.0 RESULTS OF ANALYSIS

The purpose of this section is to present the results for the analyses described in Section 4 of this PA.

Section 5.1 presents the Source Term Analysis and Release results process.

Section 5.2 presents peak groundwater concentrations for the radionuclides and chemicals discussed in Section 3.3.

Section 5.3 presents the Air Pathway and Radon release results.

Section 5.4 presents individual Biotic Pathway formulas used to calculate the doses to MOP.

Section 5.5 presents the results of the MOP Dose Analyses.

Section 5.6 presents the UA/SA.

Section 5.7 presents the Risk Analyses.

Section 5.8 presents the As Low As Reasonably Achievable (ALARA) Analyses.

5.1 Source Term Analysis and Release Results Process

The purpose of this section is to describe the process of evaluating modeled concentrations and dose and risk at exposure points for various pathways and exposure groups.

In the source term analyses, the release of radionuclides from the waste tanks was controlled, in most cases, by solubility, which will vary with the pH and/or with redox potential. All chemicals and some radionuclides are modeled as being released instantaneously from the CZ. In addition to solubility, the stabilized contaminant release rate for waste tanks was also impacted by the water flow through the waste tank, which varied by waste tank type and changed over time as the hydraulic properties of the waste tank materials changed. Results of the radionuclide and chemical environmental transport modeling to the HTF 100-meter boundary are summarized by aquifer in Section 5.2.1. These data are presented in either picocurie per liter for radionuclides or in microgram per liter for chemicals. In addition, the overall maximum concentrations for sensitivity run radionuclides by aquifer are provided.

Detailed modeling was performed on radionuclides determined to have the largest impact on dose and are discussed in Section 5.2.2 as "sensitivity run" radionuclides. Radionuclides are designated as sensitivity run radionuclides if 1) the radionuclides contributes greater than 0.1 mrem/yr to the MOP dose or 2) those radionuclides have a significant impact on progeny of the radionuclides that contributed greater than 0.1 mrem/yr to the MOP dose. Sensitivity run radionuclides were then modeled to determine concentration and dose to the MOP at the seeplines of UTR and Fourmile Branch.

The waste tank and ancillary equipment inventory of potentially airborne isotopes is used in conjunction with the methodology described in Section 4.5 to conservatively bound the air pathway dose. The air pathway dose at 100 meter and at the UTR and Fourmile Branch seeplines and the radon peak flux are calculated and presented in Section 5.3. The specific dose

calculation formulas for the individual elements of the biotic pathways for the MOP scenarios discussed in Section 4.2.3 are provided in Section 5.4. This includes the scenarios with the MOP at the 100-meter location as well as at the stream seeplines.

The peak total groundwater pathway doses are calculated using the pathway formulas discussed in Section 5.4 for the MOP at 100 meters and at the seeplines. The groundwater pathway doses are calculated utilizing the peak groundwater concentrations identified in Section 5.2 and presented in Section 5.5. The peak groundwater pathway dose is identified for the 10,000-year performance period.

The purpose of the UA/SA in Section 5.6 is to consider the effects of uncertainties in the conceptual models and sensitivities in the parameters used in the mathematical modeling. The uncertainty analysis was performed using the probabilistic model (i.e., the HTF GoldSim Model) discussed in Section 5.6.1. The probabilistic model provides the capability to vary multiple parameters simultaneously, so the concurrent effect of changes can be analyzed and the potential impacts of changes can be assessed. This capability allows for identification of parameters that are only of significance when varied at the same time as another parameter. This section also includes the deterministic sensitivity analyses and the barrier analyses performed using the HTF GoldSim Model, which provide additional information concerning which parameters are important to the HTF model.

The risk analysis discussed in Section 5.7 is based on ACP protocols for evaluating human health and ecological risk. The CMCOC were established by comparing modeled radionuclide activities and chemical concentrations at the 1-meter boundary to established regulatory limits. Modeled values for CMCOC at both the 100-meter boundary and the seeplines were used to determine risk to the MEI.

Section 5.8 presents the ALARA Analysis.

5.2 Environmental Transport of Radionuclides

The purpose of this section is to present the groundwater concentrations for all of the radionuclides and chemicals discussed in the source term screening section of the PA (Section 3.3). Maximum groundwater concentrations are presented for two exposure points, 1) 100 meters from the HTF and 2) the seeplines (UTR and Fourmile Branch). Results are presented for the three distinct aquifers modeled (UTR-UZ, UTR-LZ, and Gordon Aquifer).

The groundwater concentrations at 100 meters and at the seepline were calculated using the HTF PORFLOW Model for the Base Case discussed in Section 4.4.2.1. A summary of several key parameters used in the baseline HTF PORFLOW modeling case are provided in Table 5.2-1.

Table 5.2-1: Baseline Case

HTF Parameter	Baseline
Radiological inventory	Table 3.4-4
Non-Radiological inventory	Table 3.4-5
Solubilities (reduced and oxidized)	Table 4.2-5 and 4.2-6
Vadose K_d values	Table 4.2-29
Cementitious K_d values	Table 4.2-33
Cementitious material degradation times	Table 4.2-34
Type I basemat thickness (in)	30
Type II basemat Thickness (in)	42
Type III basemat thickness (in)	42
Type IIIA basemat thickness (in)	41
Type IV basemat thickness (in)	6.9025
Bypass fraction (% basemat with $K_d = 0$, represents fast flow path in GoldSim)	0%
Waste tank degradation case	Case A (Section 4.4.2.1)
Vadose zone thickness	Table 4.2-19
Type I tank liner failure (yr)[a]	11,397
Type II tank liner failure (yr) [b]	12,687
Type III/IIIA tank liner failure (yr)	12,751
Type IV tank liner failure (yr)	3,638
Ancillary equipment containment failure (yr)	510
Chemical transition of waste tank grout from reduced to oxidized (pore volumes)	371
Chemical transition of waste tank grout from Region II to Region III (pore volumes)	2,131

a Type I Tank 12 is modeled to have liner failure at the time of HTF closure
b Type II Tanks 14, 15, and 16 are modeled to have liner failure at the time of HTF closure

The uncertainties and sensitivities associated with the Base Case are discussed in detail in Section 5.6.

5.2.1 Groundwater Concentrations at 100 Meters

The 100-meter groundwater concentrations were calculated using the HTF PORFLOW Model, which divides the area around HTF into computational cells. The red line in Figure 5.2-1 is the demarcation line from which the 1-meter and 100-meter concentrations are calculated. The orange squares in Figure 5.2-1 identify aquifer source nodes that receive contaminant flux from vadose zone waste tank modeling. Source nodes are defined by locating source nodes associated with each waste tank varies from one to four. Two computational cells come closest to matching the physical waste tank area. Once source node concentrates the vadose zone flux, while three and four nodes dilute the source. Sixteen (55%) waste tanks utilize two source nodes, while five (17%), seven (24%), and one (3%) waste tanks have one, three, and four source nodes, respectively. A sensitivity case using a conservative tracer species and exactly two sources for each waste tank indicates a modest impact on 1-meter and 100-meter concentrations. At 100 meters, peak concentrations differed by less than 10% for 11 waste tanks, and 10 to 20% for the remaining two waste

tanks. At 1-meter nodes, peak concentrations differed by less than 10% for six waste tanks, 10 to 20% for five waste tanks, and 20 to 30% for two waste tanks. The average peak concentration for all waste tanks together was nearly identical for the two cases at both 1 meter and 100 meters. The smaller magenta squares indicate source nodes for certain ancillary (point) sources such as pump tanks and evaporators.

Figure 5.2-1: 100m Distance from HTF

Red Line = Demarcation line from which the 1-meter and 100-meter concentrations are calculated.
Red Diamonds = 1-meter distance from HTF
Green Diamonds = 100-meter distance from HTF

The green diamonds in Figure 5.2-1 show the 100-meter distance from HTF. Figure 5.2-2 illustrates the contaminant flow from the waste tanks using centerline stream traces. Since contaminant transport is not via a straight line, but by the applicable aquifers, the actual travel distance to reach 100 meters from the HTF boundary is greater than 100 meters for some sources. Table 5.2-2 shows the approximate distances a contaminant has to travel from each waste tank to reach a point 100 meters from the HTF boundary in the direction of the flow. The aquifer travel distances to the 100-meter boundary were scaled from the center of the waste tank location along the stream traces to the 100-meter boundary using information presented in Figure 5.2-2. The aquifer travel distances to the 100-meter boundary were measured from the center of the waste tank location along the 2-D stream trace to the center

of the hypothetical wells along the 100-meter boundary. A string was laid along the stream traces on Figure 5.2-2 scaled in feet and converted to meters.

Figure 5.2-2: Stream Traces from HTF

Table 5.2-2: Approximate Aquifer Travel Distance to HTF 100m Boundary

Waste Tank	100m Boundary (m)	Waste Tank	100m Boundary (m)
9	269	31	234
10	220	32	181
11	308	35	164
12	284	36	113
13	504	37	128
14	454	38	259
15	327	39	253
16	574	40	240
21	379	41	216
22	291	42	287
23	399	43	247
24	336	48	346
29	280	49	249
30	253	50	370
		51	234

The groundwater concentrations at 100 meters are assumed as the highest concentration in the range 100 meters or farther from the HTF. This assumption is supported by Figures 5.2-3 and 5.2-4, which present the plume that would result from a continuous (non-depleting) source of tracer (no decay, nor sorption). Figure 5.2-3 is a projection of plume centerline concentration onto a map view that displays the highest concentration at any location, irrespective of depth/aquifer. Similarly, Figure 5.2-4 is a projection of plume centerline onto the cross-sectional slice A-A shown in Figure 5.2-3. The plume was generated from a hypothetical constant source of a non-sorbing, non-decaying tracer placed in the waste tank source zones. The tracer plume illustrates groundwater flow directions and dispersion.

Peak concentration is observed to decrease monotonically with travel distance from the source zone, because of hydrodynamic dispersion. No physical mechanism exists to concentrate contamination beyond the source zone in the fully 3-D PORFLOW simulations. Hence, calculating the concentrations at 100 meters is adequate to capture the peak concentration that can occur at any location beyond 100 meters.

Figure 5.2-3: Contaminant Plume Leaving HTF (Aerial View)

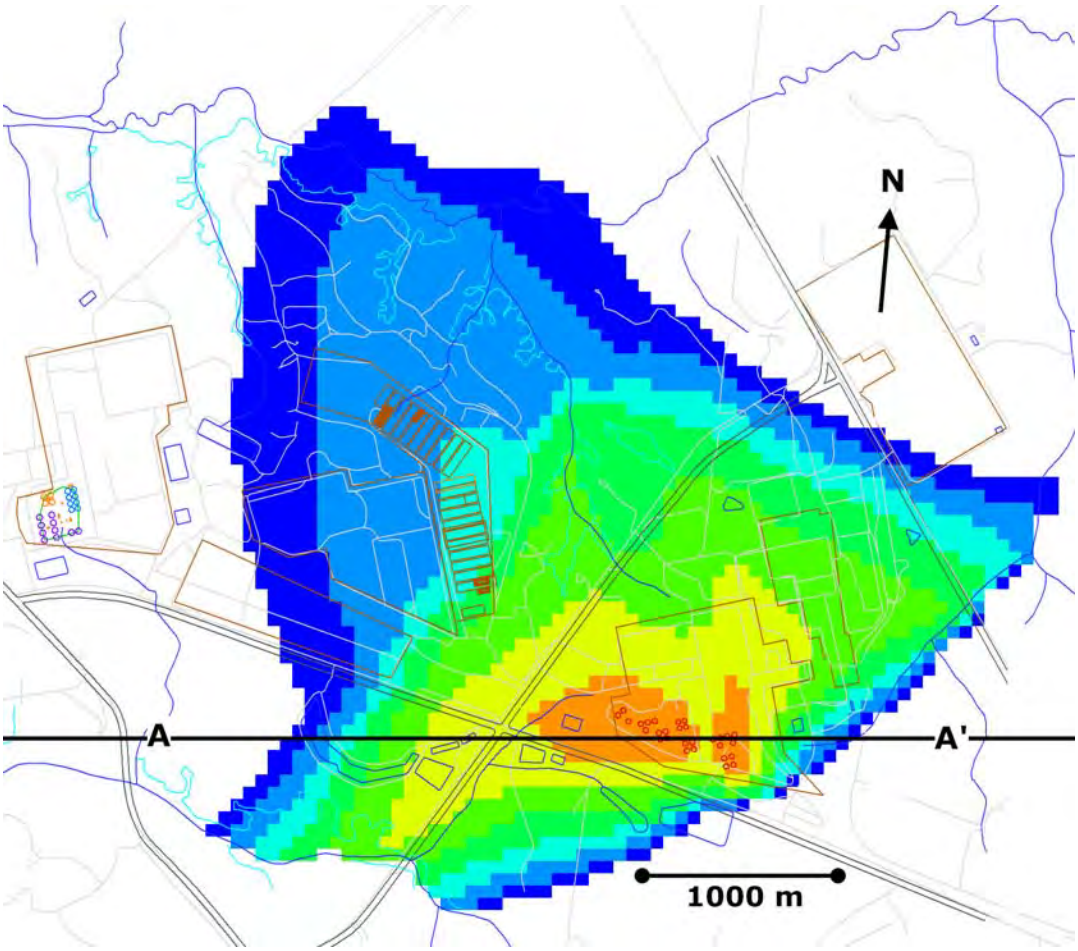

Figure 5.2-4: Contaminant Plume Leaving HTF (Cross Section View)

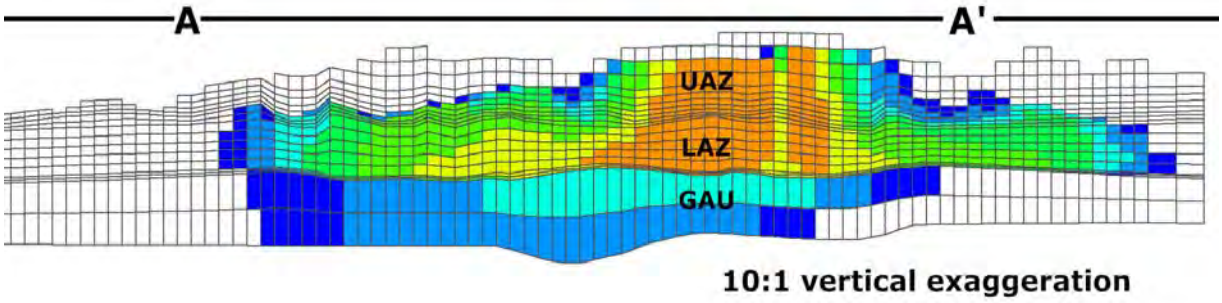

The PORFLOW 100-meter concentrations were calculated for six sectors (Sectors A through F) as shown on Figure 5.2-5. The peak concentration values for the 100-meter results are recorded for the depths of the three aquifer of concern (i.e., UTR-UZ, UTR-LZ, and Gordon Aquifer). The concentration for each aquifer represents peak concentration in any vertical computational mesh within the aquifer. The mesh vertical thicknesses (heights) in the computational model are less than 10 feet in the UTR-UZ, and less than 15 feet in the UTR-LZ. No well screen averaging was used in determining the concentrations for dose calculations because the typical well screen length of 20 feet is similar to the computational mesh height. Dividing the results into sectors was necessary to allow the large amount of concentration data to be stored from PORFLOW and used by the GoldSim dose calculator model, but also allowed variability in peak concentration for different areas of the HTF to be more easily evaluated. The six sectors were analyzed for each radionuclide and chemical to find the maximum groundwater concentrations at 100 meters from the HTF. The PORFLOW 1-meter concentrations were calculated for six sectors (Sectors A through F), as shown in Figure 5.2-5. Using the sectors to determine the highest groundwater concentrations causes the calculated peak doses to be higher than they actually are, since the peak concentrations are determined for each radionuclide independent of the location within the sector.

Figure 5.2-5: HTF PORFLOW 1m and 100m Model Evaluation Sectors

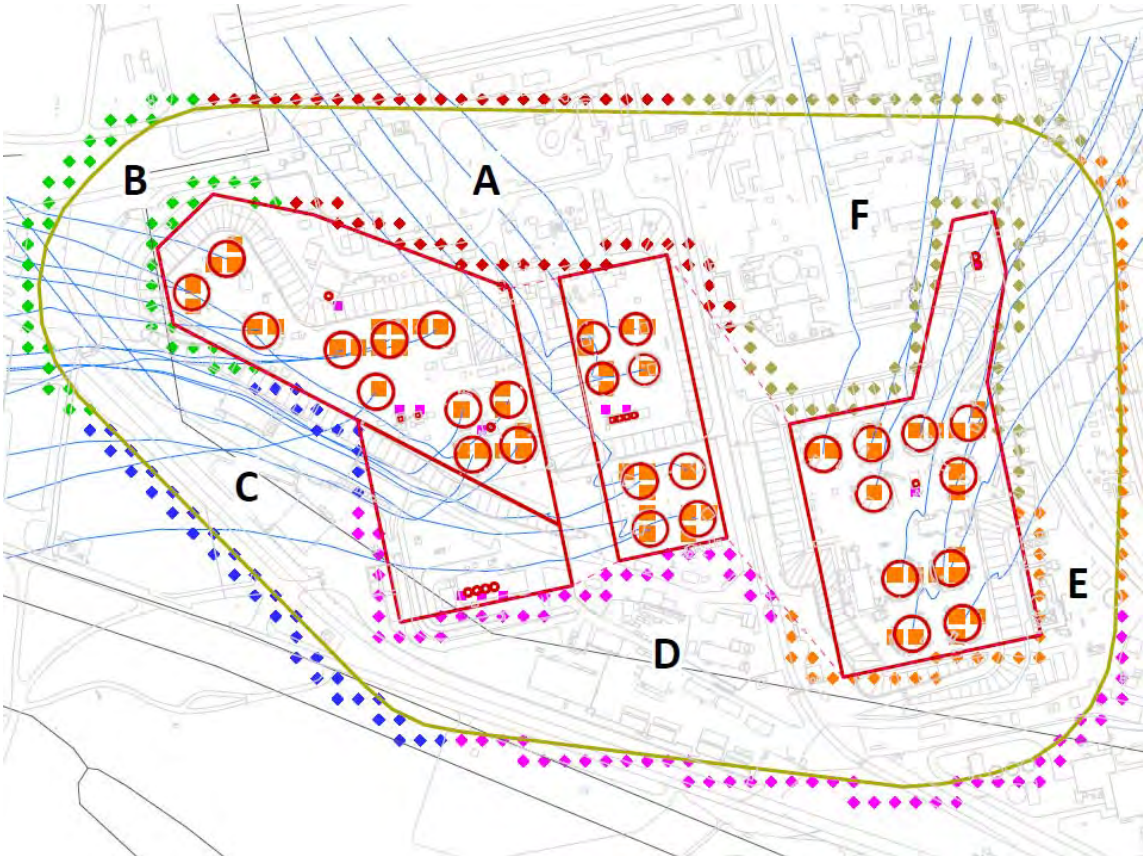

Note: The individual sectors at the 1-meter and 100-meter boundaries are indicated by unique diamond colors.

Tables 5.2-3 through 5.2-5 present the peak 100-meter radionuclide concentrations within the 10,000-year compliance period in each sector for the three aquifers. These radionuclide concentrations reflect the peak concentrations for each radionuclide in the sector. These values are conservatively high for the radionuclides present in multiple decay chains because the totals are simply the sum of the individual peaks within that sector for a given radionuclide, without regard to time or location. For example, if Pb-210 were present as a daughter product in six decay chains, those six concentrations would all be added (along with the initial Pb-210) together to arrive at a single Pb-210 concentration for that sector, even though the peaks for six daughters might have occurred at different times and at different locations within the sector. Tables 5.2-3 through 5.2-5 also list the MCL for each constituent with the derived values for beta and photo emitters from EPA 815-R-02-001. The MCLs provided in the reference are derived for 4 mrem/yr beta-gamma dose. The peak concentration from any time in 10,000 years for each beta-gamma emitter is compared to a specific MCL to determine their fraction. This was a conservative approach since peaks may occur at different times. To determine if the 4 mrem/yr beta-gamma limit is met, the sum of the fractions must be less than 1.0. The total alpha MCL includes Ra-226, but does not include radon or uranium. The radium MCL includes both Ra-226 and Ra-228. [SCDHEC R.61-58]

Table 5.2-3: Radiological 100m Concentrations for UTR-UZ

Rad	MCL (pCi/L) *	Sector A Concentration		Sector B Concentration		Sector C Concentration		Sector D Concentration		Sector E Concentration		Sector F Concentration	
		(pCi/L)	Yr Peak Occurs	(pCi/L)	Year Peak Occurs	(pCi/L)	Year Peak Occurs	(pCi/L)	Year Peak Occurs	(pCi/L)	Year Peak Occurs	(pCi/L)	Year Peak Occurs
Ac-227	N/A	7.4E-08	10,000	1.4E-06	10,000	7.5E-06	10,000	6.3E-08	1,808	6.7E-08	1,842	9.3E-08	1,486
Al-26	N/A	2.9E-11	10,000	2.0E-27	10,000	3.7E-13	10,000	1.9E-14	10,000	9.8E-16	10,000	1.1E-11	10,000
Am-241	Total α	7.2E-11	10,000	4.5E-26	10,000	2.8E-13	10,000	7.1E-15	10,000	1.2E-15	10,000	3.3E-11	10,000
Am-242m	Total α	2.2E-19	2,084	<1.0E-30	6,074	1.2E-23	2,506	1.2E-23	2,120	4.4E-30	4,516	5.7E-21	2,272
Am-243	Total α	6.7E-09	10,000	1.3E-25	10,000	2.7E-11	10,000	7.1E-13	10,000	1.1E-13	10,000	3.0E-09	10,000
C-14	2,000	8.6E-03	9,304	4.2E-01	6,772	2.8E+00	6,628	7.8E-03	9,454	3.8E-05	4,176	4.5E-03	9,996
Cf-249	Total α	2.3E-25	4,228	<1.0E-30	10,000	9.1E-29	5,358	1.7E-29	4,414	<1.0E-30	8,398	2.6E-26	5,094
Cf-251	Total α	1.2E-23	9,856	<1.0E-30	10,000	5.2E-26	10,000	4.8E-26	10,000	1.8E-28	10,000	5.4E-24	10,000
Cl-36	700	9.9E-03	586	2.4E-01	566	8.9E-01	566	1.5E-02	602	2.1E-01	530	3.2E+00	526
Cm-243	Total α	4.0E-30	850	<1.0E-30	1,812	<1.0E-30	414	<1.0E-30	332	<1.0E-30	1,538	<1.0E-30	892
Cm-244	Total α	<1.0E-30	234	<1.0E-30	1,310	<1.0E-30	260	<1.0E-30	208	<1.0E-30	716	<1.0E-30	260
Cm-245	Total α	6.5E-11	10,000	3.4E-26	10,000	2.4E-13	10,000	6.4E-15	10,000	1.0E-15	10,000	2.9E-11	10,000
Cm-247	Total α	1.3E-19	10,000	1.6E-28	10,000	5.6E-22	10,000	2.3E-22	10,000	2.1E-24	10,000	6.1E-20	10,000
Cm-248	Total α	1.4E-19	10,000	7.1E-29	10,000	5.5E-22	10,000	1.1E-22	10,000	2.2E-24	10,000	6.5E-20	10,000
Co-60	100	9.3E-29	66	<1.0E-30	200	2.4E-29	74	2.3E-29	60	<1.0E-30	168	2.4E-30	74
Cs-135	900	4.0E-03	6,202	1.9E-01	5,350	1.1E+00	5,220	5.4E-03	3,836	5.7E-03	3,924	7.5E-03	2,968
Cs-137	200	6.0E-08	750	1.9E-15	1,460	3.1E-09	808	2.9E-11	790	8.8E-11	964	5.4E-08	764
Eu-152	200	<1.0E-30	174	<1.0E-30	522	<1.0E-30	194	<1.0E-30	156	<1.0E-30	504	<1.0E-30	194
Eu-154	60	<1.0E-30	112	<1.0E-30	322	<1.0E-30	124	<1.0E-30	100	<1.0E-30	286	<1.0E-30	124
H-3	20,000	1.7E-03	92	7.9E-04	82	2.8E-02	64	2.0E-03	60	2.5E-08	76	7.8E-04	68
I-129	1	2.9E-04	696	5.2E-03	3,778	3.0E-02	3,766	4.5E-04	738	4.8E-04	744	6.4E-04	690
K-40	N/A	3.8E-04	1,862	8.0E-03	4,614	5.4E-02	4,496	6.3E-04	2,416	1.1E-03	962	1.7E-02	900
Nb-93m	1,000	2.6E+00	544	2.2E+01	9,990	1.4E+01	9,998	3.2E+00	9,980	3.7E+00	9,976	1.0E+01	9,858
Nb-94	N/A	2.9E-03	586	2.7E-02	580	2.2E-02	4,646	5.2E-03	602	5.5E-03	604	8.0E-03	580

Table 5.2-3: Radiological 100m Concentrations for UTR-UZ (continued)

Rad	MCL (pCi/L)*	Sector A Concentration		Sector B Concentration		Sector C Concentration		Sector D Concentration		Sector E Concentration		Sector F Concentration	
		(pCi/L)	Year Peak Occurs	(pCi/L)	Year Peak Occurs	(pCi/L)	Year Peak Occurs	(pCi/L)	Year Peak Occurs	(pCi/L)	Year Peak Occurs	(pCi/L)	Year Peak Occurs
Ni-59	300	4.9E-01	2,182	5.0E+00	2,158	2.4E+00	10,000	7.7E-01	2,900	8.2E-01	2,964	1.1E+00	2,314
Ni-63	50	2.0E-02	924	8.1E-04	1,656	3.9E-03	1,170	4.0E-05	1,016	1.2E-03	1,024	3.1E-02	962
Np-237	Total α	6.1E-02	1,352	6.3E-01	1,342	2.1E-01	1,500	1.0E-01	1,658	1.1E-01	1,688	1.5E-01	1,368
Pa-231	Total α	2.6E-05	10,000	4.7E-04	10,000	2.6E-03	10,000	2.1E-05	1,768	2.3E-05	1,808	3.2E-05	1,456
Pb-210	N/A	1.1E-05	10,000	6.7E-05	10,000	3.5E-04	10,000	5.7E-06	10,000	6.8E-06	10,000	2.8E-05	10,000
Pd-107	N/A	3.2E-04	2,184	5.2E-03	1,976	1.9E-02	1,924	5.2E-04	2,904	5.0E-03	1,114	7.8E-02	1,032
Pt-193	3,000	4.0E-10	804	5.0E-11	1,494	1.8E-06	806	2.9E-09	790	4.8E-07	960	1.8E-05	908
Pu-238	Total α	1.1E-12	1,468	<1.0E-30	3,826	1.1E-16	1,720	2.1E-17	1,480	3.3E-21	2,818	1.1E-13	1,684
Pu-239	Total α	4.1E-03	10,000	2.3E-10	10,000	4.0E-04	10,000	4.5E-06	10,000	8.1E-05	10,000	6.4E-03	10,000
Pu-240	Total α	1.1E-03	10,000	3.2E-11	10,000	1.1E-04	10,000	1.2E-06	10,000	2.2E-05	10,000	1.7E-03	10,000
Pu-241	300	2.6E-10	10,000	1.6E-25	10,000	1.0E-12	10,000	2.5E-14	10,000	4.2E-15	10,000	1.2E-10	10,000
Pu-242	Total α	8.3E-06	10,000	2.3E-13	10,000	8.2E-07	10,000	9.3E-09	10,000	1.7E-07	10,000	1.3E-05	10,000
Pu-244	Total α	3.8E-08	10,000	1.1E-15	10,000	3.9E-09	10,000	4.4E-11	10,000	7.8E-10	10,000	6.2E-08	10,000
Ra-226	Total α /Ra	9.1E-04	10,000	5.3E-03	10,000	2.8E-02	10,000	4.6E-04	10,000	5.5E-04	10,000	2.3E-03	10,000
Ra-228	Total Ra	9.0E-09	10,000	2.8E-15	10,000	4.0E-10	10,000	2.7E-12	10,000	4.8E-12	10,000	5.0E-09	10,000
Se-79	N/A	7.6E-08	10,000	5.6E-23	10,000	3.3E-09	10,000	3.9E-11	10,000	1.4E-11	10,000	3.7E-08	10,000
Sm-151	1,000	2.5E-17	1,536	<1.0E-30	4,286	5.6E-22	1,792	1.4E-21	1,534	1.6E-30	3,318	4.3E-19	1,652
Sn-126	N/A	3.3E-10	10,000	<1.0E-30	10,000	7.8E-13	10,000	1.0E-13	10,000	1.3E-16	10,000	5.7E-11	10,000
Sr-90	8	2.4E-05	708	3.2E-10	1,218	2.9E-06	706	2.4E-08	732	3.8E-07	820	2.7E-05	712
Tc-99	900	3.3E+01	796	3.1E+02	770	1.1E+02	812	5.1E+01	882	5.4E+01	890	6.9E+01	836
Th-229	Total α	1.7E-05	10,000	2.1E-06	10,000	2.1E-05	10,000	7.0E-07	10,000	3.4E-06	10,000	1.2E-04	10,000
Th-230	Total α	4.3E-06	10,000	6.6E-10	10,000	5.3E-06	10,000	5.4E-08	10,000	7.2E-07	10,000	3.0E-05	10,000
Th-232	Total α	2.0E-10	10,000	6.6E-17	10,000	7.5E-12	10,000	6.2E-14	10,000	1.1E-13	10,000	1.1E-10	10,000
U-232	Total U	1.8E-19	1,242	<1.0E-30	3,100	2.9E-22	1,436	4.7E-23	1,254	8.9E-27	2,312	2.3E-20	1,406

Table 5.2-3: Radiological 100m Concentrations for UTR-UZ (continued)

Rad	MCL (pCi/L) *	Sector A Concentration		Sector B Concentration		Sector C Concentration		Sector D Concentration		Sector E Concentration		Sector F Concentration	
		(pCi/L)	Year Peak Occurs	(pCi/L)	Year Peak Occurs	(pCi/L)	Year Peak Occurs	(pCi/L)	Year Peak Occurs	(pCi/L)	Year Peak Occurs	(pCi/L)	Year Peak Occurs
U-233	Total U	4.1E-04	10,000	1.8E-05	10,000	5.6E-04	10,000	1.1E-05	10,000	9.0E-05	10,000	2.2E-03	9,848
U-234	Total U	9.5E-04	10,000	6.5E-07	10,000	1.3E-03	10,000	1.5E-05	10,000	2.0E-04	10,000	4.9E-03	9,852
U-235	Total U	2.7E-06	10,000	1.8E-09	10,000	3.6E-06	10,000	4.3E-08	10,000	5.5E-07	10,000	1.4E-05	9,952
U-236	Total U	1.9E-05	10,000	1.2E-08	10,000	2.5E-05	10,000	3.0E-07	10,000	3.9E-06	10,000	1.0E-04	10,000
U-238	Total U	2.2E-05	10,000	1.5E-08	10,000	2.9E-05	10,000	3.4E-07	10,000	4.5E-06	10,000	1.1E-04	9,760
Zr-93	2,000	1.4E-07	10,000	1.8E-22	10,000	4.9E-09	10,000	3.9E-11	10,000	2.4E-11	10,000	7.3E-08	10,000
Total Alpha	**15**	**6.7E-02**	**N/A**	**6.3E-01**	**N/A**	**2.4E-01**	**N/A**	**1.0E-01**	**N/A**	**1.1E-01**	**N/A**	**1.6E-01**	**N/A**
Total Ra	**5**	**9.1E-04**	**N/A**	**5.3E-03**	**N/A**	**2.8E-02**	**N/A**	**4.6E-04**	**N/A**	**5.5E-04**	**N/A**	**2.3E-03**	**N/A**
Sum of beta-gamma MCL fractions		**4.1E-02**	**N/A**	**3.9E-01**	**N/A**	**1.8E-01**	**N/A**	**6.3E-02**	**N/A**	**6.8E-02**	**N/A**	**9.6E-02**	**N/A**

* MCL values for beta and photon emitters are calculated in EPA 815-R-02-001 based on 4 mrem/yr beta-gamma dose.
N/A = Not Applicable

Table 5.2-4: Radiological 100m Concentrations for UTR-LZ

Rad	MCL (pCi/L)*	Sector A Concentration		Sector B Concentration		Sector C Concentration		Sector D Concentration		Sector E Concentration		Sector F Concentration	
		(pCi/L)	Year Peak Occurs	(pCi/L)	Year Peak Occurs	(pCi/L)	Year Peak Occurs	(pCi/L)	Year Peak Occurs	(pCi/L)	Year Peak Occurs	(pCi/L)	Year Peak Occurs
Ac-227	N/A	2.6E-05	10,000	7.5E-05	10,000	7.5E-05	10,000	3.9E-07	10,000	2.0E-07	1,942	4.9E-07	10,000
Al-26	N/A	1.5E-17	10,000	<1.0E-30	10,000	1.1E-11	10,000	4.2E-13	10,000	8.9E-20	10,000	1.0E-17	10,000
Am-241	Total α	5.2E-17	10,000	<1.0E-30	10,000	1.0E-11	10,000	2.6E-13	10,000	7.2E-19	10,000	5.7E-17	10,000
Am-242m	Total α	<1.0E-30	3,820	<1.0E-30	7,392	1.0E-24	3,648	3.7E-25	3,290	<1.0E-30	6,618	<1.0E-30	3,988
Am-243	Total α	4.6E-15	10,000	1.4E-30	10,000	9.9E-10	10,000	2.6E-11	10,000	6.3E-17	10,000	5.0E-15	10,000
C-14	2,000	1.3E+01	7,814	5.5E+01	6,694	5.7E+01	6,598	6.6E+00	10,000	9.5E-05	10,000	2.1E+00	10,000
Cf-249	Total α	<1.0E-30	8,242	<1.0E-30	10,000	6.7E-28	7,430	4.4E-29	6,488	<1.0E-30	10,000	<1.0E-30	10,000
Cf-251	Total α	8.4E-30	10,000	<1.0E-30	10,000	1.6E-24	10,000	4.2E-26	10,000	<1.0E-30	10,000	8.2E-30	10,000
Cl-36	700	2.6E+00	592	3.6E+00	3,714	1.5E+01	524	9.5E-02	526	1.9E+00	530	4.4E+00	528
Cm-243	Total α	<1.0E-30	1,222	<1.0E-30	1,466	<1.0E-30	722	<1.0E-30	642	<1.0E-30	1,896	<1.0E-30	1,266
Cm-244	Total α	<1.0E-30	466	<1.0E-30	920	<1.0E-30	458	<1.0E-30	406	<1.0E-30	950	<1.0E-30	494
Cm-245	Total α	4.4E-17	10,000	<1.0E-30	10,000	9.0E-12	10,000	2.3E-13	10,000	5.7E-19	10,000	4.5E-17	10,000
Cm-247	Total α	9.2E-26	10,000	<1.0E-30	10,000	1.9E-20	10,000	5.0E-22	10,000	1.2E-27	10,000	9.6E-26	10,000
Cm-248	Total α	9.9E-26	10,000	<1.0E-30	10,000	2.0E-20	10,000	5.2E-22	10,000	1.3E-27	10,000	1.0E-25	10,000
Co-60	100	<1.0E-30	132	<1.0E-30	246	2.2E-30	116	<1.0E-30	102	<1.0E-30	250	<1.0E-30	138
Cs-135	900	1.8E+00	6,102	9.8E+00	5,308	1.0E+01	5,222	8.5E-02	4,674	1.5E-02	3,642	7.4E-02	6,078
Cs-137	200	5.1E-10	926	3.4E-14	1,212	3.9E-07	810	2.0E-09	796	7.0E-10	992	3.9E-09	970
Eu-152	200	<1.0E-30	348	<1.0E-30	692	<1.0E-30	344	<1.0E-30	304	<1.0E-30	674	<1.0E-30	368
Eu-154	60	<1.0E-30	222	<1.0E-30	442	<1.0E-30	220	<1.0E-30	196	<1.0E-30	396	<1.0E-30	236
H-3	20,000	1.9E+00	76	2.1E+00	86	6.5E+00	72	8.6E-01	72	1.6E-05	112	2.2E-01	90
I-129	1	1.1E-01	3,824	3.1E-01	3,770	3.1E-01	3,764	1.7E-02	1,408	1.4E-03	748	2.2E-02	1,510
K-40	N/A	2.4E-01	5,068	7.3E-01	4,542	7.6E-01	4,432	2.5E-02	4,136	1.0E-02	956	2.4E-02	4,788
Nb-93m	1,000	1.4E+01	10,000	7.6E+01	10,000	9.0E+01	10,000	1.0E+00	9,962	1.3E+01	9,916	1.7E+01	9,894
Nb-94	N/A	8.9E-02	10,000	2.1E-01	4,650	2.1E-01	4,646	7.0E-03	10,000	1.6E-02	594	1.7E-02	592

Table 5.2-4: Radiological 100m Concentrations for UTR-LZ (continued)

Rad	MCL (pCi/L)*	Sector A Concentration		Sector B Concentration		Sector C Concentration		Sector D Concentration		Sector E Concentration		Sector F Concentration	
		(pCi/L)	Year Peak Occurs	(pCi/L)	Year Peak Occurs	(pCi/L)	Year Peak Occurs	(pCi/L)	Year Peak Occurs	(pCi/L)	Year Peak Occurs	(pCi/L)	Year Peak Occurs
Ni-59	300	1.6E+01	10,000	6.9E+01	10,000	9.6E+01	10,000	1.2E+01	9,998	2.2E+00	2,742	7.4E+00	10,000
Ni-63	50	8.8E-03	1,098	6.9E-04	1,514	1.9E-01	860	2.1E-03	990	1.1E-02	1,028	3.4E-02	984
Np-237	Total α	3.0E-01	1,796	6.1E-01	1,390	4.6E-01	1,538	2.4E-02	2,342	2.9E-01	1,580	3.2E-01	1,536
Pa-231	Total α	8.9E-03	10,000	2.6E-02	10,000	2.6E-02	10,000	1.3E-04	10,000	6.8E-05	1,916	1.7E-04	10,000
Pb-210	N/A	4.4E-04	10,000	3.6E-03	10,000	6.8E-03	10,000	6.6E-04	10,000	2.4E-05	10,000	5.3E-05	10,000
Pd-107	N/A	4.7E-02	6,858	1.4E-01	6,078	2.7E-01	966	5.9E-03	10,000	4.5E-02	1,106	1.1E-01	1,066
Pt-193	3,000	1.6E-10	1,234	4.3E-09	1,188	2.3E-04	802	8.7E-07	812	4.4E-06	948	1.7E-05	926
Pu-238	Total α	4.6E-21	2,472	<1.0E-30	4,392	6.2E-16	2,242	4.5E-17	2,002	2.3E-24	3,926	1.3E-21	2,588
Pu-239	Total α	2.7E-05	10,000	3.5E-12	10,000	2.1E-02	10,000	1.2E-04	10,000	5.1E-04	10,000	3.4E-03	10,000
Pu-240	Total α	7.4E-06	10,000	9.6E-13	10,000	5.6E-03	10,000	3.1E-05	10,000	1.4E-04	10,000	9.1E-04	10,000
Pu-241	300	1.9E-16	10,000	<1.0E-30	10,000	3.7E-11	10,000	9.5E-13	10,000	2.6E-18	10,000	2.0E-16	10,000
Pu-242	Total α	5.6E-08	10,000	7.2E-15	10,000	4.3E-05	10,000	2.4E-07	10,000	1.0E-06	10,000	7.0E-06	10,000
Pu-244	Total α	2.6E-10	10,000	3.4E-17	10,000	2.0E-07	10,000	1.1E-09	10,000	4.9E-09	10,000	3.3E-08	10,000
Ra-226	Total α /Ra	3.6E-02	10,000	2.9E-01	10,000	5.4E-01	10,000	5.3E-02	10,000	1.9E-03	10,000	4.3E-03	10,000
Ra-228	Total Ra	1.6E-12	10,000	3.3E-17	10,000	1.4E-08	10,000	1.9E-10	10,000	2.8E-11	10,000	1.2E-10	10,000
Se-79	N/A	3.2E-13	10,000	1.2E-27	10,000	1.1E-07	10,000	2.2E-09	10,000	2.8E-14	10,000	1.9E-12	10,000
Sm-151	1,000	2.3E-30	2,652	<1.0E-30	4,926	3.2E-24	2,600	2.7E-24	2,362	<1.0E-30	4,400	<1.0E-30	2,772
Sn-126	N/A	2.2E-18	10,000	<1.0E-30	10,000	3.2E-12	10,000	3.5E-13	10,000	8.6E-23	10,000	3.5E-19	10,000
Sr-90	8	2.3E-06	816	4.7E-09	1,010	3.7E-04	704	1.6E-06	708	3.7E-06	816	1.6E-05	800
Tc-99	900	3.8E+02	782	5.3E+02	9,528	5.4E+02	9,502	6.6E+01	472	1.6E+02	886	1.7E+02	878
Th-229	Total α	3.6E-06	10,000	3.1E-06	10,000	4.0E-04	10,000	2.1E-06	10,000	3.1E-05	10,000	1.3E-04	10,000
Th-230	Total α	3.8E-07	10,000	7.9E-12	10,000	1.0E-04	10,000	4.8E-07	10,000	7.3E-06	10,000	3.1E-05	10,000
Th-232	Total α	4.1E-14	10,000	7.9E-19	10,000	2.6E-10	10,000	4.0E-12	10,000	7.6E-13	10,000	3.3E-12	10,000
U-232	Total U	6.0E-27	2,030	<1.0E-30	3,516	2.9E-21	1,828	1.7E-22	1,640	2.0E-29	3,144	1.4E-27	2,114

Table 5.2-4: Radiological 100m Concentrations for UTR-LZ (continued)

Rad	MCL (pCi/L)*	Sector A Concentration		Sector B Concentration		Sector C Concentration		Sector D Concentration		Sector E Concentration		Sector F Concentration	
		(pCi/L)	Year Peak Occurs	(pCi/L)	Year Peak Occurs	(pCi/L)	Year Peak Occurs	(pCi/L)	Year Peak Occurs	(pCi/L)	Year Peak Occurs	(pCi/L)	Year Peak Occurs
U-233	Total U	8.8E-05	10,000	3.5E-05	10,000	7.6E-03	10,000	5.0E-05	10,000	8.4E-04	10,000	2.8E-03	9,998
U-234	Total U	1.5E-04	10,000	7.1E-09	10,000	1.7E-02	10,000	1.2E-04	10,000	1.9E-03	10,000	6.4E-03	10,000
U-235	Total U	4.3E-07	10,000	2.0E-11	10,000	4.9E-05	10,000	3.1E-07	10,000	5.3E-06	10,000	1.8E-05	10,000
U-236	Total U	3.0E-06	10,000	1.3E-10	10,000	3.5E-04	10,000	2.2E-06	10,000	3.7E-05	10,000	1.3E-04	10,000
U-238	Total U	3.6E-06	10,000	1.6E-10	10,000	3.9E-04	10,000	2.5E-06	10,000	4.3E-05	10,000	1.4E-04	9,994
Zr-93	2,000	7.7E-13	10,000	1.3E-26	10,000	1.7E-07	10,000	2.7E-09	10,000	1.4E-13	10,000	7.8E-12	10,000
Total Alpha	**15**	**3.4E-01**	**N/A**	**9.3E-01**	**N/A**	**1.1E+00**	**N/A**	**7.8E-02**	**N/A**	**3.0E-01**	**N/A**	**3.3E-01**	**N/A**
Total Ra	**5**	**3.6E-02**	**N/A**	**2.9E-01**	**N/A**	**5.4E-01**	**N/A**	**5.3E-02**	**N/A**	**1.9E-03**	**N/A**	**4.3E-03**	**N/A**
Sum of beta-gamma MCL fractions		**6.1E-01**	**N/A**	**1.3E+00**	**N/A**	**1.4E+00**	**N/A**	**1.4E-01**	**N/A**	**2.1E-01**	**N/A**	**2.6E-01**	**N/A**

* MCL values for beta and photon emitters are calculated in EPA 815-R-02-001 based on a 4 mrem/yr beta-gamma dose.

N/A = Not Applicable

Table 5.2-5: Radiological 100m Concentrations for the Gordon Aquifer

Rad	MCL (pCi/L)*	Sector A Concentration		Sector B Concentration		Sector C Concentration		Sector D Concentration		Sector E Concentration		Sector F Concentration	
		(pCi/L)	Year Peak Occurs	(pCi/L)	Year Peak Occurs	(pCi/L)	Year Peak Occurs	(pCi/L)	Year Peak Occurs	(pCi/L)	Year Peak Occurs	(pCi/L)	Year Peak Occurs
Ac-227	N/A	6.2E-08	10,000	1.3E-07	10,000	3.8E-08	10,000	3.0E-10	10,000	3.1E-10	10,000	1.3E-09	10,000
Al-26	N/A	<1.0E-30	10,000	<1.0E-30	10,000	1.7E-24	10,000	1.4E-26	10,000	<1.0E-30	10,000	<1.0E-30	10,000
Am-241	Total α	<1.0E-30	10,000	<1.0E-30	10,000	1.0E-25	10,000	5.9E-28	10,000	<1.0E-30	10,000	<1.0E-30	10,000
Am-242m	Total α	<1.0E-30	5,082	<1.0E-30	8,146	<1.0E-30	5,144	<1.0E-30	4,644	<1.0E-30	7,962	<1.0E-30	5,264
Am-243	Total α	<1.0E-30	10,000	<1.0E-30	10,000	9.6E-24	10,000	5.9E-26	10,000	<1.0E-30	10,000	<1.0E-30	10,000
C-14	2,000	1.9E-04	10,000	5.3E-04	10,000	2.2E-04	10,000	3.3E-06	10,000	6.2E-10	10,000	5.7E-07	10,000
Cf-249	Total α	<1.0E-30	10,000	<1.0E-30	10,000	<1.0E-30	10,000	<1.0E-30	9,984	<1.0E-30	10,000	<1.0E-30	10,000
Cf-251	Total α	<1.0E-30	10,000	<1.0E-30	10,000	<1.0E-30	10,000	<1.0E-30	10,000	<1.0E-30	10,000	<1.0E-30	10,000
Cl-36	700	1.1E-02	636	1.1E-02	634	3.7E-03	588	6.5E-05	698	5.9E-05	656	2.6E-04	714
Cm-243	Total α	<1.0E-30	1,508	<1.0E-30	1,746	<1.0E-30	1,018	<1.0E-30	932	<1.0E-30	2,188	<1.0E-30	1,550
Cm-244	Total α	<1.0E-30	646	<1.0E-30	1,100	<1.0E-30	640	<1.0E-30	586	<1.0E-30	1,136	<1.0E-30	672
Cm-245	Total α	<1.0E-30	10,000	<1.0E-30	10,000	8.7E-26	10,000	5.3E-28	10,000	<1.0E-30	10,000	<1.0E-30	10,000
Cm-247	Total α	<1.0E-30	10,000	<1.0E-30	10,000	<1.0E-30	10,000	<1.0E-30	10,000	<1.0E-30	10,000	<1.0E-30	10,000
Cm-248	Total α	<1.0E-30	10,000	<1.0E-30	10,000	<1.0E-30	10,000	<1.0E-30	10,000	<1.0E-30	10,000	<1.0E-30	10,000
Co-60	100	<1.0E-30	178	<1.0E-30	284	<1.0E-30	172	<1.0E-30	154	<1.0E-30	302	<1.0E-30	186
Cs-135	900	1.1E-03	9,994	2.0E-03	9,998	6.0E-04	9,994	7.8E-06	10,000	4.6E-06	9,996	1.9E-05	10,000
Cs-137	200	6.4E-19	1,148	2.7E-17	1,106	1.0E-15	966	2.1E-18	984	2.2E-19	1,176	4.6E-19	1,172
Eu-152	200	<1.0E-30	484	<1.0E-30	824	<1.0E-30	480	<1.0E-30	440	<1.0E-30	812	<1.0E-30	504
Eu-154	60	<1.0E-30	308	<1.0E-30	528	<1.0E-30	308	<1.0E-30	282	<1.0E-30	482	<1.0E-30	320
H-3	20,000	1.7E-03	106	2.5E-03	102	2.0E-03	98	6.3E-05	96	2.3E-09	134	2.8E-05	118
I-129	1	1.4E-03	1,904	1.4E-03	1,892	5.8E-04	1,828	1.6E-05	1,822	9.0E-07	946	4.8E-05	2,040
K-40	N/A	4.4E-04	8,110	4.9E-04	7,540	1.7E-04	6,932	3.5E-06	7,028	6.3E-07	5,710	8.6E-06	9,538
Nb-93m	1,000	1.8E-02	9,998	4.3E-02	10,000	2.2E-02	10,000	1.5E-04	9,954	2.1E-03	9,898	4.1E-03	9,988
Nb-94	N/A	9.5E-04	10,000	1.1E-03	4,784	3.1E-04	10,000	7.9E-06	10,000	1.5E-05	666	3.4E-05	680

Table 5.2-5: Radiological 100m Concentrations for the Gordon Aquifer (continued)

Rad	MCL (pCi/L)*	Sector A Concentration		Sector B Concentration		Sector C Concentration		Sector D Concentration		Sector E Concentration		Sector F Concentration	
		(pCi/L)	Year Peak Occurs	(pCi/L)	Year Peak Occurs	(pCi/L)	Year Peak Occurs	(pCi/L)	Year Peak Occurs	(pCi/L)	Year Peak Occurs	(pCi/L)	Year Peak Occurs
Ni-59	300	2.0E-02	10,000	3.4E-02	10,000	1.9E-02	10,000	5.2E-04	10,000	7.0E-04	6,934	1.5E-03	7,758
Ni-63	50	8.1E-09	1,586	4.0E-08	1,402	7.7E-08	1,230	9.1E-10	1,382	6.4E-10	1,334	1.6E-09	1,354
Np-237	Total α	5.3E-04	3,060	5.8E-04	2,862	2.3E-04	2,526	9.9E-06	3,694	1.3E-04	3,124	3.0E-04	3,478
Pa-231	Total α	2.2E-05	10,000	4.4E-05	10,000	1.3E-05	10,000	1.0E-07	10,000	1.0E-07	10,000	4.5E-07	10,000
Pb-210	N/A	1.6E-08	10,000	4.3E-08	10,000	3.7E-08	10,000	8.4E-10	10,000	1.7E-11	10,000	4.5E-11	10,000
Pd-107	N/A	7.5E-05	10,000	1.3E-04	9,998	3.9E-05	10,000	2.5E-07	10,000	6.6E-07	6,710	1.5E-06	6,770
Pt-193	3,000	6.3E-14	1,124	2.6E-12	1,126	1.3E-11	1,002	2.3E-14	1,008	4.4E-14	1,174	9.6E-14	1,180
Pu-238	Total α	<1.0E-30	3,196	<1.0E-30	4,612	<1.0E-30	3,120	<1.0E-30	2,928	<1.0E-30	4,722	<1.0E-30	3,328
Pu-239	Total α	3.7E-18	10,000	8.8E-16	10,000	1.2E-12	10,000	2.5E-15	10,000	2.3E-16	10,000	6.1E-16	10,000
Pu-240	Total α	1.0E-18	10,000	2.4E-16	10,000	3.2E-13	10,000	6.6E-16	10,000	6.1E-17	10,000	1.7E-16	10,000
Pu-241	300	<1.0E-30	10,000	<1.0E-30	10,000	3.7E-25	10,000	2.0E-27	10,000	<1.0E-30	10,000	<1.0E-30	10,000
Pu-242	Total α	7.7E-21	10,000	1.8E-18	10,000	2.4E-15	10,000	5.1E-18	10,000	4.7E-19	10,000	1.3E-18	10,000
Pu-244	Total α	3.6E-23	10,000	8.5E-21	10,000	1.1E-17	10,000	2.4E-20	10,000	2.2E-21	10,000	5.9E-21	10,000
Ra-226	Total α /Ra	1.3E-06	10,000	3.5E-06	10,000	3.0E-06	10,000	6.7E-08	10,000	1.4E-09	10,000	3.6E-09	10,000
Ra-228	Total Ra	6.3E-21	10,000	5.1E-19	10,000	3.6E-17	10,000	5.5E-20	10,000	5.8E-20	10,000	1.8E-19	10,000
Se-79	N/A	1.5E-26	10,000	2.3E-29	10,000	1.5E-19	10,000	7.8E-22	10,000	1.2E-28	10,000	3.6E-27	10,000
Sm-151	1,000	<1.0E-30	3,496	<1.0E-30	5,592	<1.0E-30	3,552	<1.0E-30	3,244	<1.0E-30	5,264	<1.0E-30	3,614
Sn-126	N/A	<1.0E-30	10,000	<1.0E-30	10,000	2.2E-27	10,000	4.2E-29	10,000	<1.0E-30	10,000	<1.0E-30	10,000
Sr-90	8	9.4E-14	978	2.3E-12	916	1.7E-11	830	5.4E-14	888	2.8E-14	956	6.1E-14	958
Tc-99	900	2.7E+00	10,000	3.1E+00	10,000	8.3E-01	9,996	1.9E-02	828	9.6E-02	1,210	2.1E-01	1,280
Th-229	Total α	2.2E-08	10,000	2.3E-08	10,000	1.1E-08	10,000	4.2E-10	10,000	5.1E-09	10,000	1.2E-08	10,000
Th-230	Total α	1.5E-15	10,000	1.3E-13	10,000	1.0E-11	10,000	1.7E-14	10,000	1.7E-14	10,000	5.0E-14	10,000
Th-232	Total α	1.6E-22	10,000	1.3E-20	10,000	1.0E-18	10,000	1.8E-21	10,000	1.7E-21	10,000	5.1E-21	10,000
U-232	Total U	<1.0E-30	2,580	<1.0E-30	3,630	<1.0E-30	2,502	<1.0E-30	2,414	<1.0E-30	3,768	<1.0E-30	2,686

Table 5.2-5: Radiological 100m Concentrations for the Gordon Aquifer (continued)

Rad	MCL (pCi/L)*	Sector A Concentration		Sector B Concentration		Sector C Concentration		Sector D Concentration		Sector E Concentration		Sector F Concentration	
		(pCi/L)	Year Peak Occurs	(pCi/L)	Year Peak Occurs	(pCi/L)	Year Peak Occurs	(pCi/L)	Year Peak Occurs	(pCi/L)	Year Peak Occurs	(pCi/L)	Year Peak Occurs
U-233	Total U	3.0E-07	10,000	3.3E-07	10,000	1.4E-07	10,000	6.0E-09	10,000	6.8E-08	10,000	1.7E-07	10,000
U-234	Total U	1.3E-12	10,000	9.1E-11	10,000	5.0E-09	10,000	9.5E-12	10,000	1.4E-11	10,000	3.5E-11	10,000
U-235	Total U	3.5E-15	10,000	2.5E-13	10,000	1.4E-11	10,000	2.6E-14	10,000	3.7E-14	10,000	9.7E-14	10,000
U-236	Total U	2.4E-14	10,000	1.7E-12	10,000	9.5E-11	10,000	1.8E-13	10,000	2.6E-13	10,000	6.7E-13	10,000
U-238	Total U	2.9E-14	10,000	2.1E-12	10,000	1.1E-10	10,000	2.2E-13	10,000	3.1E-13	10,000	8.1E-13	10,000
Zr-93	2,000	1.1E-26	10,000	7.7E-29	10,000	1.1E-19	10,000	4.9E-22	10,000	2.7E-28	10,000	5.5E-27	10,000
Total Alpha	**15**	**5.5E-04**	**N/A**	**6.2E-04**	**N/A**	**2.5E-04**	**N/A**	**1.0E-05**	**N/A**	**1.3E-04**	**N/A**	**3.0E-04**	**N/A**
Total Ra	**5**	**1.3E-06**	**N/A**	**3.5E-06**	**N/A**	**3.0E-06**	**N/A**	**6.7E-08**	**N/A**	**1.4E-09**	**N/A**	**3.6E-09**	**N/A**
Sum of beta-gamma MCL fractions		**4.5E-03**	**N/A**	**5.0E-03**	**N/A**	**1.6E-03**	**N/A**	**3.9E-05**	**N/A**	**1.1E-04**	**N/A**	**3.0E-04**	**N/A**

* MCL values for beta and photon emitters are calculated in EPA 815-R-02-001 based on a 4 mrem/yr beta-gamma dose.

N/A = Not Applicable

If the sum of the beta-gamma ratios is greater than 1.0, the total beta-gamma for the sector is calculated to be greater than the MCL. The highest predicted ratio was in Table 5.2-4 for Sector C of the UTR-LZ with a summed ratio of 1.4. However, when the sum of the ratios of the beta-gamma emitters are evaluated more realistically on a per-year basis, the maximum value is in year 9,522 with a total ratio of 0.97, which is below the total beta-gamma MCL. A breakdown of the ratio of major constituents to their respective MCLs for year 9,522 for Sector C of the UTR-LZ at the 100-meter boundary is presented in Table 5.2-9.

In addition, as indicated in Table 5.2-3 through 5.2-5, on an individual constituent basis none of the radionuclides in any sector or aquifer at the 100-meter boundary exceeded their respective MCL.

Tables 5.2-6 through 5.2-8 show the peak 100-meter chemical concentrations within the 10,000-year performance period in each sector for the three aquifers. Nitrate and nitrite are modeled as nitrogen, therefore, the MCL for nitrate and nitrite (10,000 µg/L) is compared to the total nitrogen concentration.

Table 5.2-6: Chemical 100m Concentrations for UTR-UZ

Constituent	MCL (μg/L)	Sector A Concentration		Sector B Concentration		Sector C Concentration		Sector D Concentration		Sector E Concentration		Sector F Concentration	
		(μg/L)	Year Peak Occurs	(μg/L)	Year Peak Occurs	(μg/L)	Year Peak Occurs	(μg/L)	Year Peak Occurs	(μg/L)	Year Peak Occurs	(μg/L)	Year Peak Occurs
Ag	100	6.5E-05	10,000	6.9E-04	9,998	4.4E-04	10,000	6.1E-05	10,000	7.5E-05	10,000	1.9E-04	9,830
As	10	9.4E-07	10,000	2.3E-06	10,000	3.0E-06	10,000	8.6E-08	10,000	1.4E-07	10,000	1.3E-06	5,438
Ba	2,000	7.4E-04	3,888	7.5E-03	3,846	1.7E-02	6,592	1.1E-03	5,546	1.2E-03	5,704	1.5E-03	4,122
Cd	5	8.2E-04	3,262	8.6E-03	3,204	1.5E-02	7,604	1.4E-03	4,400	1.4E-03	4,318	2.6E-03	3,134
Cr	100	3.3E-03	1,508	3.4E-02	1,492	1.2E-01	4,534	5.3E-03	1,888	5.6E-03	1,926	8.2E-03	1,510
Cu	1,300	1.1E-04	8,098	1.2E-03	7,906	6.8E-04	10,000	1.8E-04	9,998	2.0E-04	9,868	4.2E-04	7,482
F	4,000	2.2E-02	586	2.9E-01	3,714	1.6E+00	3,710	4.0E-02	602	4.3E-02	604	6.2E-02	580
Fe	300	2.6E-03	10,000	1.4E-06	10,000	2.8E-03	10,000	3.3E-05	10,000	5.4E-04	10,000	1.4E-02	9,908
Hg	2	5.0E-08	10,000	7.0E-22	10,000	5.0E-09	10,000	1.9E-11	10,000	2.5E-11	10,000	2.9E-08	10,000
Mn	50	1.6E-02	2,032	3.1E-01	6,368	2.0E+00	6,020	1.5E-02	6,656	1.6E-02	6,906	1.9E-02	5,392
N	10,000	6.3E-03	2,182	6.4E-02	2,162	2.1E-02	2,466	9.6E-03	2,902	1.0E-02	2,954	1.4E-02	2,314
Ni	N/A	1.1E+00	586	9.7E+00	580	3.5E+01	3,710	1.9E+00	602	2.0E+00	604	2.9E+00	580
Pb	15	4.4E-12	10,000	<1.0E-30	10,000	1.0E-14	10,000	1.3E-15	10,000	1.6E-18	10,000	7.5E-13	10,000
Sb	6	1.1E-13	10,000	<1.0E-30	10,000	3.9E-16	10,000	7.6E-17	10,000	1.3E-20	10,000	1.2E-14	10,000
Se	5	9.7E-11	10,000	5.0E-26	10,000	4.4E-12	10,000	5.0E-14	10,000	1.8E-14	10,000	4.7E-11	10,000
U	30	6.5E-05	10,000	4.7E-08	10,000	8.8E-05	10,000	1.0E-06	10,000	1.3E-05	10,000	3.4E-04	9,806
Zn	5,000	8.5E-04	9,058	2.1E-02	7,968	1.2E-01	7,600	7.1E-04	4,412	7.4E-04	4,334	1.4E-03	3,134

Table 5.2-7: Chemical 100m Concentrations for UTR-LZ

Constituent	MCL (μg/L)	Sector A Concentration		Sector B Concentration		Sector C Concentration		Sector D Concentration		Sector E Concentration		Sector F Concentration	
		(μg/L)	Year Peak Occurs	(μg/L)	Year Peak Occurs	(μg/L)	Year Peak Occurs	(μg/L)	Year Peak Occurs	(μg/L)	Year Peak Occurs	(μg/L)	Year Peak Occurs
Ag	100	1.9E-04	9,998	5.9E-04	10,000	6.7E-03	10,000	4.8E-05	10,000	2.1E-04	10,000	3.2E-04	10,000
As	10	1.8E-06	10,000	2.5E-07	10,000	2.9E-05	10,000	3.2E-06	10,000	7.1E-07	6,496	1.7E-06	5,914
Ba	2,000	9.8E-02	8,322	3.4E-01	6,816	3.6E-01	6,376	1.7E-02	6,744	3.2E-03	6,216	1.3E-02	9,132
Cd	5	5.0E-02	9,298	1.5E-01	7,716	1.5E-01	7,568	5.0E-03	10,000	3.8E-03	3,900	4.6E-03	3,428
Cr	100	1.7E+00	8,924	1.2E+00	4,550	1.2E+00	4,506	6.8E-02	7,708	1.6E-02	1,774	7.2E-02	8,390
Cu	1,300	4.1E-04	10,000	1.4E-03	10,000	6.3E-03	10,000	5.5E-05	10,000	5.5E-04	9,842	7.2E-04	7950
F	4,000	5.5E+00	3,738	1.6E+01	3,712	1.6E+01	3,710	1.9E-01	560	1.2E-01	594	2.5E-01	630
Fe	300	3.6E-04	10,000	1.6E-08	10,000	4.7E-02	10,000	2.9E-04	10,000	5.1E-03	10,000	1.8E-02	9,998
Hg	2	1.0E-12	10,000	1.4E-25	10,000	1.7E-07	10,000	1.8E-09	10,000	6.2E-13	10,000	2.7E-11	10,000
Mn	50	1.4E+01	9,998	3.9E+01	6,392	4.1E+01	5,986	2.1E+00	5,282	4.8E-02	8,484	1.0E+00	8,226
N	10,000	3.1E-02	3,264	8.6E-02	10,000	1.4E-01	10,000	1.8E-02	10,000	2.7E-02	2,746	2.9E-02	2,658
Ni	N/A	5.9E+02	2,270	3.5E+02	3,714	3.5E+02	3,710	3.3E+01	564	5.8E+00	594	4.1E+01	620
Pb	15	3.0E-20	10,000	<1.0E-30	10,000	4.2E-14	10,000	4.5E-15	10,000	1.1E-24	10,000	4.6E-21	10,000
Sb	6	2.0E-22	10,000	<1.0E-30	10,000	5.1E-16	10,000	9.1E-17	10,000	1.8E-27	10,000	2.2E-23	10,000
Se	5	4.1E-16	10,000	1.5E-30	10,000	1.5E-10	10,000	2.8E-12	10,000	3.6E-17	10,000	2.5E-15	10,000
U	30	1.1E-05	10,000	4.9E-10	10,000	1.2E-03	9,998	7.5E-06	10,000	1.3E-04	10,000	4.3E-04	10,000
Zn	5,000	3.8E-01	9,212	1.2E+00	7,736	1.2E+00	7,576	1.4E-02	10,000	2.1E-03	3,942	2.4E-03	3,434

N/A = Not Applicable

Table 5.2-8: Chemical 100m Concentrations for Gordon Aquifer

Constituent	MCL (μg/L)	Sector A Concentration		Sector B Concentration		Sector C Concentration		Sector D Concentration		Sector E Concentration		Sector F Concentration	
		(μg/L)	Year Peak Occurs	(μg/L)	Year Peak Occurs	(μg/L)	Year Peak Occurs	(μg/L)	Year Peak Occurs	(μg/L)	Year Peak Occurs	(μg/L)	Year Peak Occurs
Ag	100	4.4E-09	10,000	2.3E-08	10,000	2.8E-08	10,000	3.1E-10	10,000	2.2E-10	10,000	5.5E-10	10,000
As	10	1.5E-12	10,000	2.7E-11	10,000	6.9E-11	10,000	5.1E-13	10,000	9.5E-13	10,000	2.4E-12	10,000
Ba	2,000	3.1E-05	10,000	6.4E-05	10,000	2.7E-05	10,000	4.6E-07	10,000	4.3E-07	10,000	7.8E-07	10,000
Cd	5	4.2E-05	10,000	1.0E-04	10,000	3.4E-05	10,000	2.0E-07	10,000	1.8E-06	9,608	4.0E-06	10,000
Cr	100	4.3E-03	9,998	4.2E-03	9,990	1.4E-03	9,364	2.9E-05	9,420	7.1E-06	3,528	8.0E-05	10,000
Cu	1,300	7.0E-08	10,000	2.5E-07	10,000	2.6E-07	10,000	2.7E-09	10,000	5.5E-09	10,000	1.3E-08	10,000
F	4,000	2.0E-02	748	3.6E-02	3,792	8.7E-03	3,782	2.0E-04	704	1.1E-04	666	7.3E-04	722
Fe	300	1.7E-12	10,000	1.2E-10	10,000	7.2E-09	10,000	1.4E-11	10,000	1.9E-11	10,000	4.7E-11	10,000
Hg	2	1.1E-25	10,000	3.8E-27	10,000	9.1E-19	10,000	3.7E-21	10,000	1.0E-26	10,000	1.9E-25	10,000
Mn	50	1.8E-03	10,000	2.9E-03	10,000	1.3E-03	10,000	2.3E-05	10,000	1.5E-06	10,000	1.2E-05	10,000
N	10,000	5.4E-05	10,000	6.6E-05	10,000	3.7E-05	10,000	1.3E-06	10,000	9.1E-06	7,010	2.0E-05	7,886
Ni	N/A	3.3E+00	734	3.3E+00	732	1.3E+00	694	3.3E-02	696	5.3E-03	666	1.1E-01	744
Pb	15	<1.0E-30	10,000	<1.0E-30	10,000	2.8E-29	10,000	<1.0E-30	10,000	<1.0E-30	10,000	<1.0E-30	10,000
Sb	6	<1.0E-30	10,000	<1.0E-30	10,000	<1.0E-30	10,000	<1.0E-30	10,000	<1.0E-30	10,000	<1.0E-30	10,000
Se	5	1.9E-29	10,000	<1.0E-30	10,000	2.0E-22	10,000	1.0E-24	10,000	<1.0E-30	10,000	4.7E-30	10,000
U	30	8.8E-14	10,000	6.2E-12	10,000	3.4E-10	10,000	6.5E-13	10,000	9.2E-13	10,000	2.4E-12	10,000
Zn	5,000	2.5E-04	10,000	7.6E-04	10,000	2.4E-04	10,000	3.4E-07	10,000	9.7E-07	9,602	2.1E-06	9,998

N/A = Not Applicable

Table 5.2-9: Beta-Gamma Emitters for Sector C - Year 9,522

C-14	=	2.3%
I-129	=	0.8%
Nb-93m	=	8.6%
Ni-59	=	25.2%
Tc-99	=	60.1%
Total	=	96.9%

The 100-meter radionuclide and chemical concentration curves (for 20,000 years) associated with the six sectors and three aquifers for the Base Case, as described in Section 4.4.2.1, are captured in Appendix B as follows:

- Appendix B.1 - 100-meter Radiological and Chemical Concentrations at the UTR-UZ (Sectors A through F)
- Appendix B.2 - 100-meter Radiological and Chemical Concentrations at the UTR-LZ (Sectors A through F)
- Appendix B.3 - 100-meter Radiological and Chemical Concentrations at the Gordon Aquifer (Sectors A through F)

To support further evaluation of sensitivity run radionuclides (e.g., individual waste tank contributions peak beyond the 10,000-year compliance period), additional 100-meter groundwater concentrations were calculated using the HTF PORFLOW Model. Appendix D contains 100,000-year curves for the 100-meter radionuclide concentrations for all of HTF (waste tank and ancillary inventories). Appendix E contains 20,000-year data curves for the 100-meter radionuclide concentrations for selected HTF sources, which included individual waste tanks and waste tank and ancillary equipment source groupings. The individual waste tank source runs were for Tanks 12, 13, 16, 22, 32, 36, 39, and 40. The waste tank and ancillary equipment source group model runs were for Type I (Tanks 9, 10, and 11), Type II (Tanks 14 and 15), Type IV (Tanks 21, 23, and 24), and Type III/IIIA (Tanks 29, 30, 31, 35, and 37). The transfer lines source for the "West Hill" was represented by the piping for Type III/IIIA tanks. The transfer lines source for the Type I and Type II tanks was represented by the piping for the Type II tanks. The remaining waste tanks and ancillary equipment were evaluated as a single group. These Base Case concentration results are for sensitivity run radionuclides only and are presented from the three aquifers of concern (UTR-UZ, UTR-LZ, and Gordon Aquifer) for Sectors A through F.

5.2.2 Sensitivity Run Radionuclide Determination

The purpose of this section is to present the methodology used to determine which radionuclides were most significant and to document which radionuclides would be considered a sensitivity run radionuclide. While all radionuclides identified in the HTF waste tank inventory (Section 3.3.2) were included in 100-meter groundwater modeling efforts, narrowing the catalog of radionuclides down to a sensitivity run radionuclide list allowed the analysis to concentrate on the few radionuclides that posed more risk and concentrated modeling efforts on the areas of greatest concern.

The sensitivity run radionuclides were determined based on the peak 100-meter groundwater concentrations by radionuclide provided in Tables 5.2-3 through 5.2-5 (it should be noted

that the peak concentration for each individual radionuclide is not necessarily in the same year). These concentrations were then run through the GoldSim dose calculator to determine dose rates by sector. Any radionuclide in a given sector with greater than 0.1 mrem/yr dose (assuming Base Case pathways and assumptions) anytime within 20,000 years at the 100-meter boundary was considered a sensitivity run radionuclide. The 0.1 mrem/yr screening threshold was considered sufficiently low, such that the seepline contribution of the radionuclides that were screened out would not appreciably affect the peak dose results, even accounting for cumulative pathway effects. In order to fully evaluate the contribution of the sensitivity run radionuclides, some radionuclides with a contribution of less than 0.1 mrem/yr at the 100-meter boundary were included because they had a significant (i.e., > 0.1 mrem/yr) impact on progeny; Am-241 (for Np-237), Am-243 (for Pu-239), Pu-238 (for Ra-226), Th-230 (for Ra-226), and U-234 (for Ra-226). Although Pu-239 dose did not exceed 0.1 mrem/yr dose in 20,000 years, it was included with the sensitivity run radionuclides for conservatism. The resulting sensitivity run radionuclides are Am-241, Am-243, I-129, Np-237, Pu-238, Pu-239, Ra-226, Tc-99, Th-230, and U-234. The screening conclusions are provided in Table 5.2-10.

Table 5.2-10: Determination of Sensitivity Run Radionuclides for the 100m Boundary

Radionuclide[a]	20,000 Peak Dose (mrem/yr)						Basis
	Sector A	Sector B	Sector C	Sector D	Sector E	Sector F	
Ac-227	0.00	0.00	0.00	0.00	0.00	0.00	
Al-26	0.00	0.00	0.00	0.00	0.00	0.00	
Am-241	0.00	0.00	0.00	0.00	0.00	0.00	**Np-237 parent**
Am-242m	0.00	0.00	0.00	0.00	0.00	0.00	
Am-243	0.00	0.00	0.00	0.00	0.00	0.00	**Pu-239 parent**
C-14	0.02	0.05	0.06	0.01	0.01	0.01	
Cf-249	0.00	0.00	0.00	0.00	0.00	0.00	
Cf-251	0.00	0.00	0.00	0.00	0.00	0.00	
Cl-36	0.01	0.01	0.02	0.00	0.00	0.01	
Cm-243	0.00	0.00	0.00	0.00	0.00	0.00	
Cm-244	0.00	0.00	0.00	0.00	0.00	0.00	
Cm-245	0.00	0.00	0.00	0.00	0.00	0.00	
Cm-247	0.00	0.00	0.00	0.00	0.00	0.00	
Cm-248	0.00	0.00	0.00	0.00	0.00	0.00	
Co-60	0.00	0.00	0.00	0.00	0.00	0.00	
Cs-135	0.04	0.05	0.04	0.03	0.03	0.04	
Cs-137	0.00	0.00	0.00	0.00	0.00	0.00	
Eu-152	0.00	0.00	0.00	0.00	0.00	0.00	
Eu-154	0.00	0.00	0.00	0.00	0.00	0.00	
H-3	0.00	0.00	0.00	0.00	0.00	0.00	
I-129	0.08	0.05	0.05	0.00	0.01	0.00	
K-40	0.05	0.06	0.06	0.05	0.05	0.05	
Nb-93m	0.06	0.04	0.04	0.02	0.03	0.03	
Nb-94	0.00	0.00	0.00	0.00	0.00	0.00	
Ni-59	0.07	0.03	0.01	0.00	0.00	0.00	
Ni-63	0.00	0.00	0.00	0.00	0.00	0.00	

Table 5.2-10: Determination of Sensitivity Run Radionuclides for the 100m Boundary (Continued)

Radionuclide[a]	20,000 Peak Dose (mrem/yr)						Basis
	Sector A	Sector B	Sector C	Sector D	Sector E	Sector F	
Np-237	0.05	**0.10**	0.08	0.02	0.05	0.05	**Dose > 0.1**
Pa-231	0.01	0.03	0.03	0.00	0.00	0.00	
Pb-210	0.02	0.05	0.07	0.01	0.01	0.01	
Pd-107	0.00	0.00	0.00	0.00	0.00	0.00	
Pt-193	0.00	0.00	0.00	0.00	0.00	0.00	
Pu-238	0.00	0.00	0.00	0.00	0.00	0.00	**Ra-226 parent**
Pu-239	0.01	0.00	0.08	0.00	0.01	0.03	**Dose approaching 0.1 at 20,000 yrs**
Pu-240	0.00	0.00	0.01	0.00	0.00	0.00	
Pu-241	0.00	0.00	0.00	0.00	0.00	0.00	
Pu-242	0.00	0.00	0.00	0.00	0.00	0.00	
Pu-244	0.00	0.00	0.00	0.00	0.00	0.00	
Ra-226	**0.20**	**0.54**	**0.79**	0.08	0.09	0.09	**Dose > 0.1**
Ra-228	0.00	0.00	0.00	0.00	0.00	0.00	
Se-79	0.00	0.00	0.00	0.00	0.00	0.00	
Sm-151	0.00	0.00	0.00	0.00	0.00	0.00	
Sr-90	0.00	0.00	0.00	0.00	0.00	0.00	
Tc-99	**0.44**	**0.62**	**0.62**	0.08	**0.20**	**0.20**	**Dose > 0.1**
Th-229	0.00	0.00	0.01	0.00	0.00	0.00	
Th-230	0.00	0.00	0.00	0.00	0.00	0.00	**Ra-226 parent**
Th-232	0.00	0.00	0.00	0.00	0.00	0.00	
U-232	0.00	0.00	0.00	0.00	0.00	0.00	
U-233	0.00	0.00	0.01	0.00	0.00	0.00	
U-234	0.00	0.00	0.02	0.00	0.00	0.00	**Ra-226 parent**
U-235	0.00	0.00	0.00	0.00	0.00	0.00	
U-236	0.00	0.00	0.00	0.00	0.00	0.00	
U-238	0.00	0.00	0.00	0.00	0.00	0.00	
Y-90	0.00	0.00	0.00	0.00	0.00	0.00	
Zr-93	0.00	0.00	0.00	0.00	0.00	0.00	

a Sensitivity run radionuclides are shaded gray.

Only the sensitivity run radionuclides were included in the initial seepline PORFLOW modeling run to determine seepline concentrations. The modeling was performed to 20,000 years and it included all aquifer and discharge locations for the Base Case (Case A). The maximum concentration per sensitivity run radionuclide at the seepline in 20,000 years was weighted to the corresponding maximum 100-meter concentration in 20,000 years for the same radionuclide. The resulting ratios were averaged to get an overall median ratio for the sensitivity run radionuclides (see Appendix F.1). Any sensitivity run radionuclide with a concentration at either the 100-meter boundary or the seepline of less than 1.0E-10 pCi/L was not utilized in determining the overall average ratio. The overall average ratio for the sensitivity run radionuclides was 3.47%; however, the ratio for the radionuclide that had the highest dose at the seepline, Np-237, has a ratio of 10% (see Appendix F.1). Therefore, a ratio of 10% was chosen for conservatism. The 10% ratio was then multiplied by the 100-meter concentration for the remaining radionuclides not modeled to get an estimated seepline concentration. The ratios are presented in Table 4.4-12. The concentrations at the seepline for the sensitivity run radionuclides and the weighted concentrations for the remaining radionuclides were then run through the GoldSim dose calculator to determine individual radionuclide dose at the seepline.

5.2.3 Groundwater Concentrations at the Seeplines

The seepline groundwater concentrations for sensitivity run radionuclides were calculated using the HTF PORFLOW Model, which grids the GSA surrounding the HTF. Figure 5.2-6 shows the HTF seeplines in relation to the HTF. The PORFLOW seepline concentrations are provided for two sectors (UTR and Fourmile Branch) and five aquifers (three outcropping to UTR and two outcropping to Fourmile Branch) as shown on Figure 5.2-6. The peak concentration values for the seepline results were recorded for the depths of the three aquifers of concern (i.e., UTR-UZ, UTR-LZ, and Gordon Aquifer). The diamond shapes on Figure 5.2-6 correspond to the PORFLOW calculated location where the applicable aquifer is outcropping. For example, the green diamonds represent the location where the Gordon Aquifer outcrops to UTR. For Fourmile Branch, there are only two sets of diamonds, since the Gordon Aquifer does not outcrop to Fourmile Branch.

Figure 5.2-6: HTF PORFLOW Seepline Evaluation Sectors

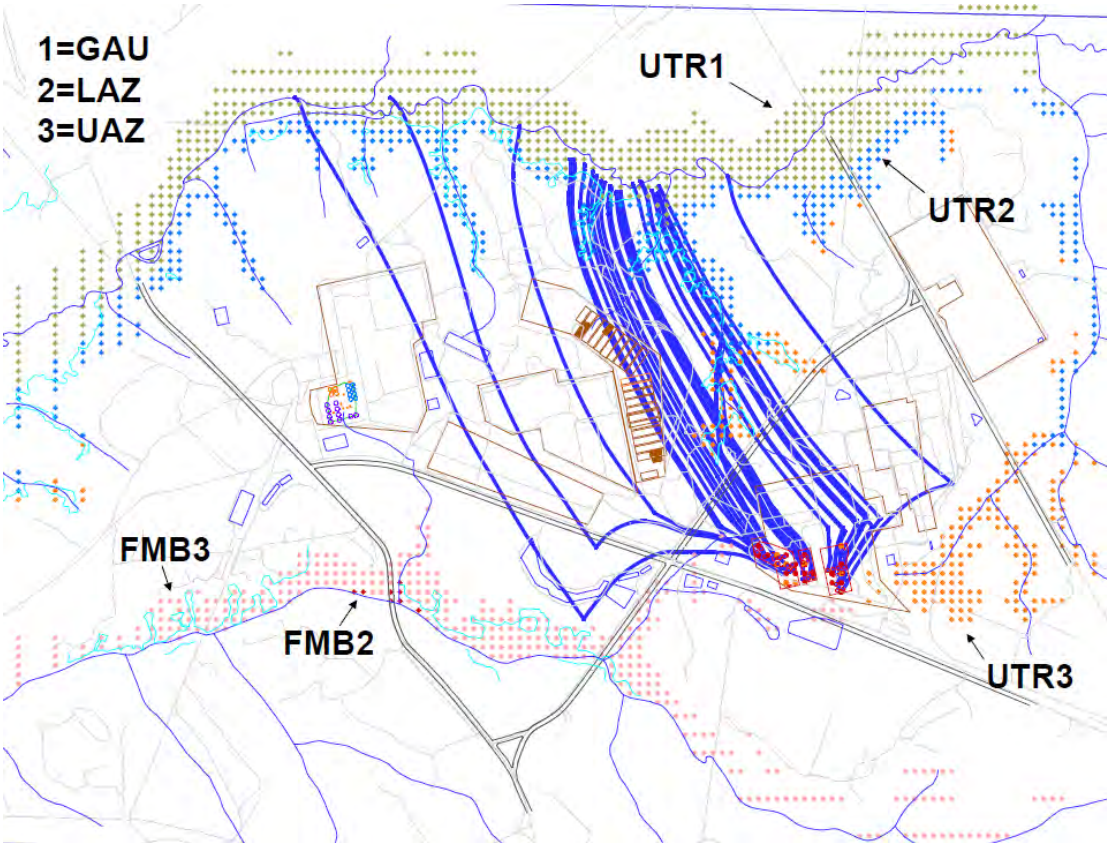

UTR1 = Gordon Aquifer Unit (GAU) outcropping to UTR
UTR2 = UTR-LZ (LAZ) outcropping to UTR
UTR3 = UTR-UZ (UAZ) outcropping to UTR
FMB2 = LAZ outcropping to Fourmile Branch
FMB3 = UAZ outcropping to Fourmile Branch

The five aquifers were analyzed for each sensitivity run radionuclide to find the maximum groundwater concentrations at each seepline. PORFLOW modeling point sources included individual waste tanks and waste tank and/or ancillary equipment groupings. The individual waste tank sources included Tanks 12, 13, 16, 22, 32, 36, 39, and 40. The waste tank source group modeling point that were run included Type I (Tanks 9, 10, and 11), Type II (Tanks 14 and 15), Type IV (Tanks 21, 23, and 24), and Type III/IIIA (Tanks 29, 30, 31, 35, and 37). The transfer lines source for the "West Hill" was represented by the piping for Type III/IIIA tanks. The transfer lines source for Type I and II tanks was represented by the piping for the Type II tanks. All remaining waste tanks and ancillary equipment were evaluated as a single group. The PORFLOW seepline concentrations were then modeled with the GoldSim dose calculator in order to derive doses for applicable dose pathways (e.g., swimming, boating, and fishing).

Tables 5.2-11 and 5.2-12 show the overall peak seepline radionuclide concentrations in the 10,000-year compliance period and to 20,000 years for the sensitivity run radionuclides by aquifer for the Base Case for UTR and Fourmile Branch, respectively. These values are

conservatively high for the radionuclides present in multiple decay chains because the totals are simply the sum of the individual peaks from all sources for a given radionuclide for the Base Case.

Table 5.2-11: Seepline Sensitivity Run Radionuclide Concentrations for UTR

Radionuclide	Peak Seepline Concentration 10,000 Years (pCi/L)	Location of Largest Contributor (Aquifer)	Year of Largest Contribution 10,000 Years	Peak Seepline Concentration 20,000 Years (pCi/L)	Location of Largest Contributor (Aquifer)	Year of Largest Contribution 20,000 Years
Am-241	1.1E-21	UTR-UZ	6,308	1.1E-21	UTR-UZ	6,308
Am-243	4.0E-18	UTR-UZ	10,000	3.6E-15	UTR-UZ	20,000
Np-237	1.5E-02	UTR-LZ	1,962	1.5E-02	UTR-LZ	1,962
Pu-238	9.3E-23	UTR-UZ	1,714	9.3E-23	UTR-UZ	1,714
Pu-239	5.5E-10	UTR-UZ	10,000	1.5E-05	UTR-UZ	20,000
Ra-226	5.5E-05	UTR-UZ	10,000	8.8E-03	UTR-UZ	17,156
Tc-99	1.2E+01	UTR-LZ	894	1.2E+01	UTR-LZ	894
Th-230	3.2E-11	UTR-UZ	10,000	1.6E-06	UTR-UZ	20,000
U-234	2.9E-08	UTR-UZ	10,000	2.6E-04	UTR-UZ	20,000

Table 5.2-12: Seepline Sensitivity Run Radionuclide Concentrations for Fourmile Branch

Radionuclide	Peak Seepline Concentration 10,000 Years (pCi/L)	Location of Largest Contributor (Aquifer)	Year of Largest Contribution 10,000 Years	Peak Seepline Concentration 20,000 Years (pCi/L)	Location of Largest Contributor (Aquifer)	Year of Largest Contribution 20,000 Years
Am-241	5.2E-18	UTR-UZ	5,756	5.2E-18	UTR-UZ	5,756
Am-243	1.4E-14	UTR-UZ	10,000	1.5E-10	UTR-UZ	20,000
Np-237	6.3E-02	UTR-UZ	1,234	6.3E-02	UTR-UZ	1,234
Pu-238	5.4E-19	UTR-UZ	1,600	5.4E-19	UTR-UZ	1,600
Pu-239	3.6E-08	UTR-UZ	10,000	6.0E-04	UTR-UZ	20,000
Ra-226	5.4E-03	UTR-UZ	10,000	8.8E-02	UTR-UZ	16,872
Tc-99	3.0E+01	UTR-UZ	738	3.0E+01	UTR-UZ	738
Th-230	2.0E-09	UTR-UZ	10,000	3.8E-05	UTR-UZ	20,000
U-234	1.6E-06	UTR-UZ	10,000	5.1E-03	UTR-UZ	20,000

Appendix C contains data curves showing the far-field (i.e., seepline) radionuclide concentrations (sensitivity run radionuclides for 20,000 years) for all of HTF (waste tank and ancillary inventories) for the Base Case.

5.3 Air Pathway and Radon Analyses

Section 4.5 describes the methods used to conservatively bound the dose from airborne radionuclides. The results in that section provided a dose to the MEI per curie of inventory for Type I and Type II tank configurations for the 10,000-year compliance period. These waste tank types were selected because they will have the least grout and concrete thickness above the stabilized CZ, the minimum assumed closure cap thickness over the waste tanks, and therefore, should produce the maximum flux of gaseous radionuclides at the ground surface.

Assuming that the HTF inventory is evenly distributed over the Type I or Type II tanks, the dose to the MEI can be calculated to conservatively bound the dose from airborne radionuclides. For the air pathway, the flux of eight radionuclides was modeled using PORFLOW. The DRFs that represent the dose to the receptor exposed to 1 curie of the specified radionuclide potentially released to the atmosphere were calculated at 100 meters, the Fourmile Branch seepline, and the UTR seepline. The estimated total waste tank and ancillary equipment inventory of selected potentially airborne isotopes at closure is summarized in Table 5.3-1.

Table 5.3-1: Projected Total HTF Inventory of Gaseous Radionuclides

Radionuclide	C-14	Cl-36	I-129	Se-79	Sn-126	H-3	Tc-99
Total HTF Inventory (Ci)	3.20E+01	1.58E-02	1.94E-03	3.84E+01	4.05E+01	3.20E+01	4.59E+01

Calculated exposure levels for Type I and Type II tanks for the 10,000-year MEI at 100 meters are presented in Tables 5.3-2 and 5.3-3, respectively. Calculated exposure levels for Type I and Type II tanks for the 10,000-year MEI at the Fourmile Branch (1,170 meter) seepline are presented in Tables 5.3-4 and 5.3-5, respectively. Calculated exposure levels for Type I and Type II tanks for the 10,000-year MEI at the UTR (2,360 meter) seepline are presented in Tables 5.3-6 and 5.3-7, respectively. The contribution of Sb-125 to the air pathways dose is insignificant based on the waste tank inventory and Sb-125 short half-life and is not included in the tables. As indicated in Figures 4.5-3 and 4.5-4, the maximum calculated fluxes occur within the first 1,000 years following facility closure.

Table 5.3-2: 100m Boundary DRFs and 10,000 Year Type I Tank Dose

Radionuclide	Peak Flux[a] (Ci/yr/Ci)	SRS 100m DRF[a] (mrem/Ci)	Dose to MEI at 100m Boundary[a] (mrem/yr/Ci)	HTF Inventory[b] (Ci)	MEI Dose at 100m Boundary (mrem/yr)
C-14	1.60E-05	8.1E-03	1.3E-07	3.20E+01	4.16E-06
Cl-36	9.53E-19	1.7E-02	1.6E-20	1.58E-02	2.53E-22
I-129	4.11E-22	1.2E+01	4.9E-21	1.94E-03	9.50E-24
Sb-125	1.31E-50	2.3E-01	3.0E-51	N/A	N/A
Se-79	5.51E-12	2.3E-02	1.3E-13	3.84E+01	4.99E-12
Sn-126	3.88E-61	1.1E+01	4.3E-60	4.05E+01	1.74E-58
H-3	2.93E-12	1.7E-04	5.0E-16	3.20E+01	1.60E-14
Tc-99	2.82E-47	6.4E-02	1.8E-48	4.59E+01	8.26E-47
Total Dose					4.16E-06

a SRNL-STI-2010-00135 (Table 10)
b Table 5.3-1

Table 5.3-3: 100m Boundary DRFs and 10,000 Year Type II Tank Dose

Radionuclide	Peak Flux[a] (Ci/yr/Ci)	SRS 100m DRF[a] (mrem/Ci)	Dose to MEI at 100m Boundary[a] (mrem/yr/Ci)	HTF Inventory[b] (Ci)	Dose to MEI at 100m Boundary (mrem/yr)
C-14	1.45E-05	8.1E-03	1.20E-07	3.20E+01	3.84E-06
Cl-36	8.64E-19	1.7E-02	1.50E-20	1.58E-02	2.37E-22
I-129	3.73E-22	1.2E+01	4.50E-21	1.94E-03	8.72E-24
Sb-125	1.19E-50	2.3E-01	2.70E-51	N/A	N/A
Se-79	5.00E-12	2.3E-02	1.10E-13	3.84E+01	4.22E-12
Sn-126	3.52E-61	1.1E+01	3.90E-60	4.05E+01	1.58E-58
H-3	2.66E-12	1.7E-04	4.50E-16	3.20E+01	1.44E-14
Tc-99	2.55E-47	6.4E-02	1.60E-48	4.59E+01	7.34E-47
Total Dose					3.84E-06

a SRNL-STI-2010-00135 (Table 18)
b Table 5.3-1

Table 5.3-4: Fourmile Branch Seepline DRFs and 10,000 Year HTF Type I Tank Dose

Radionuclide	Peak Flux[a] (Ci/yr/Ci)	Fourmile Branch 1,170m DRF[a] (mrem/Ci)	Dose to MEI at 1,170m[a] (mrem/yr/Ci)	HTF Inventory[b] (Ci)	Dose to MEI at 1,170m Seepline (mrem/yr)
C-14	1.60E-05	3.9E-03	6.2E-08	3.20E+01	1.98E-06
Cl-36	9.53E-19	9.5E-03	9.1E-21	1.58E-02	1.44E-22
I-129	4.11E-22	3.6E+00	1.5E-21	1.94E-03	2.91E-24
Sb-125	1.31E-50	1.5E-01	2.0E-51	N/A	N/A
Se-79	5.51E-12	1.4E-02	7.7E-14	3.84E+01	2.95E-12
Sn-126	3.88E-61	6.6E+00	2.6E-60	4.05E+01	1.05E-58
H-3	2.93E-12	8.0E-05	2.3E-16	3.20E+01	7.37E-15
Tc-99	2.82E-47	4.0E-02	1.1E-48	4.59E+01	5.05E-47
Total Dose					1.98E-06

a SRNL-STI-2010-00135 (Table 11)
b Table 5.3-1

Table 5.3-5: Fourmile Branch Seepline DRFs and 10,000 Year HTF Type II Tank Dose

Radionuclide	Peak Flux[a] (Ci/yr/Ci)	FMB 1,170m DRF[a] (mrem/Ci)	Dose to MEI at 1,170m [a] (mrem/yr/Ci)	HTF Inventory[b] (Ci)	Dose to MEI at 1,170m Seepline (mrem/yr)
C-14	1.45E-05	3.9E-03	5.7E-08	3.20E+01	1.82E-06
Cl-36	8.64E-19	9.5E-03	8.2E-21	1.58E-02	1.30E-22
I-129	3.73E-22	3.6E+00	1.3E-21	1.94E-03	2.52E-24
Sb-125	1.19E-50	1.5E-01	1.8E-51	N/A	N/A
Se-79	5.00E-12	1.4E-02	7.0E-14	3.84E+01	2.69E-12
Sn-126	3.52E-61	6.6E+00	2.3E-60	4.05E+01	9.31E-59
H-3	2.66E-12	8.0E-05	2.1E-16	3.20E+01	6.73E-15
Tc-99	2.55E-47	4.0E-02	1.0E-48	4.59E+01	4.59E-47
Total Dose					1.82E-06

a SRNL-STI-2010-00135 (Table 19)
b Table 5.3-1

Table 5.3-6: UTR Seepline DRFs and 10,000 Year Type I Tank Dose

Radionuclide	Peak Flux[a] (Ci/yr/Ci)	UTR 2,360m DRF[a] (mrem/Ci)	Dose to MEI at 2,360m[a] (mrem/yr/Ci)	HTF Inventory[b] (Ci)	Dose to MEI at 2,360m Seepline (mrem/yr)
C-14	1.60E-05	1.2E-03	1.9E-08	3.20E+01	6.08E-07
Cl-36	9.53E-19	3.2E-03	3.0E-21	1.58E-02	4.75E-23
I-129	4.11E-22	9.3E-01	3.8E-22	1.94E-03	7.37E-25
Sb-125	1.31E-50	5.2E-02	6.8E-52	N/A	N/A
Se-79	5.51E-12	4.8E-03	2.6E-14	3.84E+01	9.97E-13
Sn-126	3.88E-61	2.4E+00	9.3E-61	4.05E+01	3.77E-59
H-3	2.93E-12	2.5E-05	7.3E-17	3.20E+01	2.34E-15
Tc-99	2.82E-47	1.4E-02	3.9E-49	4.59E+01	1.79E-47
Total Dose					6.08E-07

a SRNL-STI-2010-00135 (Table 16)
b Table 5.3-1

Table 5.3-7: UTR Seepline DRFs and 10,000 Year Type II Tank Dose

Radionuclide	Peak Flux[a] (Ci/yr/Ci)	UTR 2,360m DRF[a] (mrem/Ci)	Dose to MEI at 2,360m[a] (mrem/yr/Ci)	HTF Inventory[b] (Ci)	Dose to MEI at 2,360m Seepline (mrem/yr)
C-14	1.45E-05	1.20E-03	1.70E-08	3.20E+01	5.44E-07
Cl-36	8.64E-19	3.20E-03	2.80E-21	1.58E-02	4.43E-23
I-129	3.73E-22	9.30E-01	3.50E-22	1.94E-03	6.79E-25
Sb-125	1.19E-50	5.20E-02	6.20E-52	N/A	N/A
Se-79	5.00E-12	4.80E-03	2.40E-14	3.84E+01	9.21E-13
Sn-126	3.52E-61	2.40E+00	8.40E-61	4.05E+01	3.40E-59
H-3	2.66E-12	2.50E-05	6.70E-17	3.20E+01	2.15E-15
Tc-99	2.55E-47	1.40E-02	3.60E-49	4.59E+01	1.65E-47
Total Dose					5.44E-07

a SRNL-STI-2010-00135 (Table 24)
b Table 5.3-1

For the radon air pathway, the Rn-222 flux resulted from five radionuclides, Pu-238, Ra-226, Th-230, U-234, and U-238 (Table 5.3-8). As shown in Figure 4.5-6, with the exception of Ra-226, the peak flux of Rn-222 occurs at the end of the 10,000-year compliance period. This is due to the long half-life for each of the parent radionuclides. For Ra-226, the peak flux of Rn-222 occurs within the first year of the simulation and declines gradually. Therefore, the peak dose of radon for the modeling period is assumed to be at 10,000 years. Section 4.5.3 describes other factors contributing to the conservative nature of the results.

Table 5.3-8: Projected Type I or II Tank Inventory of Isotopes Producing Rn-222

Radionuclide	Pu-238	U-238	U-234	Th-230	Ra-226
Type I or II Inventory[a] (Ci)	1.40E+03	1.60E-03	5.60E-03	1.00E-03	1.00E-03

a Table 3.4-4 Inventory from Type I or Type II tank with highest inventory

The peak instantaneous radon flux is found by multiplying the unit flux by the Type I or II tanks radon inventory then divided by the Type I or II tanks surface area. The inventory of isotopes contributing to the radon flux based on Type I or II tanks case is summarized in Tables 5.3-9 and 5.3-10, respectively. The peak instantaneous radon flux for Type I or II tanks, using the Type I and II tank inventory, is 1.81E-15 pCi/m^2/sec and 1.30E-17 pCi/m^2/sec, respectively.

The permissible radon flux for DOE facilities is addressed in DOE M 435.1-1 IV.P.(c) and states the radon flux requirement is that the release of radon shall be less than an average flux of 20 pCi/m^2/sec at the surface of the facility. The peak instantaneous radon flux for Type I and Type II tanks is below the regulatory limits. These results are highly conservative because of the assumption for the maximum Types I and II tank inventories is concentrated in a 1-foot layer in the waste tank. Section 4.5.3 describes other factors contributing to the conservative nature of the results.

Table 5.3-9: Peak Instantaneous Rn-222 Flux at Land Surface from Type I Tanks

Parent Source	Type I Inventory[a] (Ci)	Type I Inventory[b] (Ci/m^2)	Rn-222 Flux at Land Surface[c] (pCi/m^2/sec)/(Ci/m^2)	Peak Instantaneous Flux at Land Surface (pCi/m^2/sec)
Pu-238	1.40E+03	3.41E+00	5.01E-16	1.71E-15
U-238	1.60E-03	3.90E-06	1.72E-14	6.71E-20
U-234	5.60E-03	1.36E-05	1.42E-12	1.94E-17
Th-230	1.00E-03	2.44E-06	1.19E-11	2.90E-17
Ra-226	1.00E-03	2.44E-06	2.08E-11	5.07E-17
Total				1.81E-15

a Table 3.4-4 Inventory from Type I tank with highest inventory
b Total surface area of HTF is 410.43 m^2 (75-foot diameter waste tank)
c SRNL-STI-2010-00135 (Table 25)

Table 5.3-10: Peak Instantaneous Rn-222 Flux at Land Surface from Type II Tanks

Parent Source	Type II Inventory[a] (Ci)	Type II Inventory[b] (Ci/m^2)	Rn-222 Flux at Land Surface[c] (pCi/m^2/sec)/(Ci/m^2)	Peak Instantaneous Flux at Land Surface (pCi/m^2/sec)
Pu-238	1.40E+03	2.66E+00	4.59E-18	1.22E-17
U-238	1.60E-03	3.04E-06	1.58E-16	4.80E-22
U-234	5.60E-03	1.06E-05	1.30E-14	1.38E-19
Th-230	1.00E-03	1.90E-06	1.75E-13	3.32E-19
Ra-226	1.00E-03	1.90E-06	1.91E-13	3.62E-19
Total				1.30E-17

a Table 3.4-4 Inventory from Type II tank with highest inventory
b Total surface area of HTF is 527.18 m^2 (85-foot diameter waste tank)
c SRNL-STI-2010-00135 (Table 26)

The estimated annual dose from the inhalation of Rn-222 would be highest to an inadvertent intruder inhabiting the residence built directly above the waste tank. The dose to the MOP from the inhalation of Rn-222 would be significantly less than the estimated dose to the intruder because the residence of the MOP is at least 100 meters away from any waste tank. This intruder analysis assumes the peak Rn-222 concentration to be in equilibrium within the controlled volume of the basement of the residence built directly above the waste tank with the highest peak radon flux.

The estimated annual dose to an intruder from the inhalation of Rn-222 is dependent on the following:

- Concentration of Rn-222 in a controlled volume occupied by the intruder
- Intruder occupancy (fraction of year) in the controlled volume
- Breathing rate
- Rn-222 DCF

The controlled volume assumed in this analysis is a basement in a residential home that has a floor area of 200m^2 (2,150 ft^2) and 2.43-meter (8-foot) ceilings for a total volume of approximately 519m^3. The size of this controlled volume is based on the assumed values presented in NUREG-CR-4370, *Update of Part 61 Impacts Analysis Methodology*, Section 4.2.5.2. It is assumed that this controlled volume is situated above a Type I tank, which has the highest peak radon flux.

The buildup of Rn-222 in the basement is dependent on the production rate (P) and removal rate (R) of Rn-222. Based on Table 5.3-9, the peak instantaneous Rn-222 flux is 1.81E-15 pCi/m^2/sec. Taking no credit for intervening materials of construction (concrete, block, etc.) the production rate of Rn-222 entering the controlled volume is assumed to be at a constant rate equal to the peak flux times the basement floor area of 200m^2. Thus, P = 1.14E-05 pCi/yr. Assuming an air exchange rate of 1.0 *V*/hr taken from NUREG-CR-4370, Section 4.2.5.2, the removal rate is 8,760 *V*/yr. The greatest Rn-222 concentration is when the buildup is at equilibrium, which equals P/R, or 1.30E-09 picocurie. The peak Rn-222 concentration in the controlled volume is then estimated to be 2.51E-12 pCi/m3 (1.30E-09 pCi / 519m^3).

For this analysis, the intruder is assumed to occupy the controlled volume 100% of the time. The assumed nominal breathing rate is 5,548 m^3/yr. The DCF for Rn-222 inhalation is estimated based on 10 CFR 20. Assuming the occupational dose limit of 0.05 sieverts (5,000 millirem) specified in 10 CFR 20 and dividing by the annual limits on intake for Rn-222 of 100 microcuries (1.0E+08 pCi) in air from Table 1, Column 2 of Appendix B; the Rn-222 DCF is therefore estimated to be 5.0E-05 mrem/pCi.

The estimated dose to the intruder from the inhalation of Rn-222 is then calculated by the Rn-222 concentration in the controlled volume times the breathing rate times the DCF. Based on the inputs, the estimated annual dose from the inhalation of Rn-222 equals 2.51E-12 pCi/m^3 x 5,548 m^3/yr x 5.0E-05 mrem/pCi, or 6.96E-13 mrem/yr.

5.4 Biotic Pathways

The MOP exposure pathways are discussed in detail in Section 4.2.3.1. The HTF MOP scenario with 100-meter well water as a primary water source is graphically represented in Figure 4.2-30. The HTF MOP scenario with stream water as a primary water source is graphically represented in Figure 4.2-31. The individual elements of the MOP biotic pathways that were identified for analyses and inclusion in the two MOP scenarios are provided in this section. The GoldSim computer code was used to calculate doses utilizing the dose formulas provided below and utilizing the PORFLOW or GoldSim calculated 100-meter and seepline concentrations as inputs. Unless otherwise noted, formulas were based on those used in LADTAP or in the PA for the INL waste tank farm facility. [WSRC-STI-2006-00123, DOE-ID-10966] While these documents

were used as guides for the formulas, ultimately the basis for all the formulas can be traced to Regulatory Guide 1.109.

5.4.1 MOP at the 100-Meter Well Dose Pathways

The following MOP exposure pathways were used in calculating the dose to the MOP receptor with 100-meter well water as a primary water source. The stream is the secondary water source for the pathways involving swimming, fishing/boating, and fish ingestion. The stream concentrations used in the dose calculations for those secondary water source pathways are the peak aquifer concentrations (as discussed in Section 5.2.3), and conservatively assume no stream dilution. All transfer times are assumed negligible due to the half-lives of the radionuclides and the long-term analysis of the PA. Unit conversions are not explicitly stated in the equations, but are coded into GoldSim.

5.4.1.1 MOP at the 100-Meter Well Ingestion Dose Pathways

5.4.1.1.1 Ingestion of Water

Exposure route for water ingestion assumes the receptor uses a well as a drinking water source that is located 100 meters from the HTF waste tanks. The incidental ingestion of water from showering and during recreational activities is assumed negligible when compared to ingestion of drinking water. The dose from consumption of drinking water was calculated using the following formula.

$$D = C_{GW} \times U_W \times DCF$$

where:

D	=	dose from 1-year consumption of contaminated groundwater (rem/yr)
C_{GW}	=	radionuclide concentration in groundwater from the 100-meter well (pCi/L)
U_W	=	human consumption rate of water (L/yr), Table 4.6-9
DCF	=	ingestion DCF (rem/μCi), Table 4.7-1

5.4.1.1.2 Ingestion of Beef and Milk

Beef and dairy exposure route assumes cattle drink contaminated stock water and consume fodder irrigated with contaminated water. The stock water and irrigation water is from the 100-meter well. The fodder is contaminated from direct deposition of contaminated irrigation water on plants and from deposition of contaminated irrigation water in soil followed by root uptake by plants. The buildup of radionuclide concentration in the soil from successive years of irrigation is accounted for. The radionuclide concentration in fodder from deposition and root uptake is calculated using the following formulas.

$$C_f = C_{GW} \times I \times \left(LEAF + SOIL \times T_{StV}\right) \times F_I$$

$$LEAF = \frac{r \times \left(1 - e^{-\lambda_e t_V}\right)}{Y_V \times \lambda_e}$$

$$\lambda_e = \lambda_i + \lambda_w$$

$$SOIL = \frac{1 - e^{-\lambda_B t_b}}{\rho_S \times \lambda_B}$$

$$\lambda_L = \frac{P_R + I_R - E_R}{S_D \times \left(S_M + \rho_{SS} \times K_d\right)}$$

$$\lambda_B = \lambda_i + \lambda_L$$

where:

C_f	=	radionuclide concentration in fodder (pCi/kg)
C_{GW}	=	radionuclide concentration in groundwater from the 100-meter well (pCi/L)
I	=	irrigation rate (L/m^2-d), Table 4.6-8
$LEAF$	=	radionuclide deposition and retention on the vegetation leaves (m^{2}d/kg)
$SOIL$	=	radionuclide deposition and buildup rate in the soil (m^{2}d/kg)
T_{StV}	=	soil to vegetation ratio (unitless), Table 4.6-1
F_I	=	fraction of the time vegetation is irrigated (unitless), Table 4.6-8
r	=	fraction of material deposited on leaves that is retained (unitless), Table 4.6-8
λ_e	=	weathering and radiological decay constant (1/d)
t_V	=	time vegetation is exposed to irrigation (d), Table 4.6-7
Y_V	=	vegetation production yield (kg/m^2), Table 4.6-7
λ_i	=	radiological decay constant (1/d) [ln2/half-life of radionuclide *i*]
λ_w	=	weathering decay constant (1/d), Table 4.6-8
ρ_S	=	areal surface density of soil (kg/m^2), Table 4.6-8
t_b	=	buildup time of radionuclides in soil (d), Table 4.6-7
λ_B	=	soil buildup rate (1/d)
λ_L	=	soil retention rate (1/d)
P_R	=	precipitation rate (in/yr), Table 4.6-8
I_R	=	irrigation rate (in/yr), Table 4.6-8

E_R = evapotranspiration rate (in/yr), Table 4.6-8

S_D = depth of garden (cm), Table 4.6-8

S_M = soil moisture content (unitless), Table 4.6-8

ρ_{SS} = density of sandy soil (g/cm^3), Table 4.2-39

K_d = distribution coefficient (mL/g), Table 4.2-29

Following the cattle consumption of the contaminated water and fodder, the receptor consumes the contaminated beef and milk from the cattle. Beef and milk are treated separately. The dose is calculated using the following formulas.

Beef:

$$D = T_B \times \left(FF_B \times C_f \times Q_{FB} + C_{GW} \times Q_{WB}\right) \times DCF \times U_B \times F_B$$

Milk:

$$D = T_M \times \left(FF_M \times C_f \times Q_{FM} + C_{GW} \times Q_{WM}\right) \times DCF \times U_M \times F_M$$

where:

D = dose from 1-year consumption of contaminated beef or milk (rem/yr)

T_B = beef transfer coefficient (d/kg), Table 4.6-3

T_M = milk transfer coefficient (d/L), Table 4.6-2

FF_i = beef or milk cattle intake fraction from irrigated field/pasture (unitless), Table 4.6-9

C_f = radionuclide concentration in fodder, as defined above (pCi/kg)

Q_{Fi} = consumption rate of fodder by beef or milk cattle (kg/d), Table 4.6-9

C_{GW} = radionuclide concentration in groundwater from the 100-meter well (pCi/L)

Q_{Wi} = consumption rate of water by beef or milk cattle (L/d), Table 4.6-9

DCF = ingestion DCF (rem/μCi), Table 4.7-1

U_B = human consumption rate of beef (kg/yr), Table 4.6-9

U_M = human consumption rate of milk (L/yr), Table 4.6-9

F_B = fraction of meat produced locally (unitless), Table 4.6-7

F_M = fraction of milk produced locally (unitless), Table 4.6-7

5.4.1.1.3 Ingestion of Vegetables

The dose to humans from ingestion of contaminated leafy vegetables and produce is calculated assuming two contamination routes, 1) direct deposition of contaminated irrigation water on plants, and 2) deposition of contaminated irrigation water on soil followed by root uptake by plants. The buildup of radionuclide concentration in the soil from successive years of irrigation is accounted for. Leafy vegetables and produce are treated separately. The irrigation water is from the 100-meter well. The dose is calculated using the following formula.

$$D = C_{GW} \times I \times \left(LEAF + SOIL \times T_{StV}\right) \times DCF \times \left(U_{LV} \times k + U_{OV}\right) \times F_V \times F_I$$

where:

D	=	dose from 1-year consumption of contaminated vegetables (rem/yr)
C_{GW}	=	radionuclide concentration in groundwater from the 100-meter well (pCi/L)
I	=	irrigation rate (L/m^2-d), Table 4.6-8
$LEAF$	=	radionuclide deposition and retention rate on the vegetable's leaves, as defined in Section 5.4.1.1.2 (m^{2}d/kg)
$SOIL$	=	radionuclide deposition and buildup rate in the soil, as defined in Section 5.4.1.1.2 (m^{2}d/kg)
T_{StV}	=	soil to vegetation ratio (unitless), Table 4.6-1
DCF	=	ingestion DCF (rem/μCi), Table 4.7-1
U_{LV}	=	human consumption rate of leafy vegetables (kg/yr), Table 4.6-9
U_{OV}	=	human consumption rate of other vegetables (produce) (kg/yr), Table 4.6-9
k	=	fraction of material deposited on leaves that is retained after washing (unitless), Table 4.6-8
F_V	=	fraction of leafy vegetables and produce produced locally (unitless), Table 4.6-7
F_I	=	fraction of the time vegetables are irrigated (unitless), Table 4.6-8

5.4.1.1.4 Ingestion of Fish

Exposure route from fish ingestion assumes fish are caught from a stream contaminated from the aquifer, and the receptor in turn consumes the contaminated fish. The dose is calculated using the following formula.

$$D = C_{SW} \times U_F \times T_F \times DCF$$

where:

D	=	dose from 1-year consumption of contaminated fish (rem/yr)
C_{SW}	=	radionuclide concentration in water from the stream (undiluted aquifer) (pCi/L)
U_F	=	human consumption rate of finfish (kg/yr), Table 4.6-9
T_F	=	fish bioaccumulation factor (L/kg), Table 4.6-4
DCF	=	ingestion DCF (rem/μCi), Table 4.7-1

5.4.1.1.5 Ingestion of Soil

Exposure route from ingestion of soil assumes the soil is irrigated with groundwater from the 100-meter well and the receptor in turn consumes the contaminated soil. This formula was derived following the approach of the previous pathway calculations. A soil buildup factor was applied to account for the buildup of radionuclide concentration in the soil from successive years of irrigation. The radionuclide concentration in the soil and the dose is calculated using the following formulas.

$$D = C_D \times DCF \times U_D$$

$$C_D = C_{GW} \times I \times F_I \times SOIL$$

where:

D	=	dose from 1-year consumption of contaminated soil (rem/yr)
C_D	=	radionuclide concentration in soil irrigated with water from the 100-meter well (pCi/kg)
DCF	=	ingestion DCF (rem/μCi), Table 4.7-1
U_D	=	human consumption rate of dirt (kg/yr), Table 4.6-9
C_{GW}	=	radionuclide concentration in groundwater from the 100-meter well (pCi/L)
I	=	irrigation rate (L/m^2-d), Table 4.6-8
F_I	=	fraction of the time soil is irrigated (unitless), Table 4.6-8
$SOIL$	=	radionuclide deposition and buildup rate in the soil, as defined in Section 5.4.1.1.2 (m^{2}d/kg)

5.4.1.1.6 Ingestion of Poultry and Eggs

The poultry and egg exposure route assumes poultry drink contaminated stock water and consume fodder irrigated with contaminated water. The stock water and irrigation water is from the 100-meter well. The fodder is contaminated from direct deposition of contaminated irrigation water on plants and from deposition of contaminated irrigation water in soil followed by root uptake by plants. Following the poultry consumption of

the contaminated water and fodder, the receptor consumes the contaminated poultry and eggs. Poultry and eggs are treated separately. The concentration in fodder and the dose is calculated using the following formulas.

$$C_f = C_{GW} \times I \times \left(LEAF + SOIL \times T_{StV}\right) \times F_I$$

Poultry:

$$D = T_P \times \left(FF_P \times C_f \times Q_{FP} + C_{GW} \times Q_{WP}\right) \times DCF \times U_P \times F_P$$

Eggs:

$$D = T_E \times \left(FF_P \times C_f \times Q_{FP} + C_{GW} \times Q_{WP}\right) \times DCF \times U_E \times F_E$$

where:

D	=	dose from 1-year consumption of contaminated poultry or eggs (rem/yr)
C_f	=	radionuclide concentration in fodder (pCi/kg)
C_{GW}	=	radionuclide concentration in groundwater from the 100-meter well (pCi/L)
I	=	irrigation rate (L/m^2-d), Table 4.6-8
$LEAF$	=	radionuclide deposition and retention rate on the vegetation leaves, as defined in Section 5.4.1.1.2 (m^{2}d/kg)
$SOIL$	=	radionuclide deposition and buildup rate in the soil, as defined in Section 5.4.1.1.2 (m^{2}d/kg)
T_{StV}	=	soil to vegetation ratio (unitless), Table 4.6-1
F_I	=	fraction of the time vegetation is irrigated (unitless), Table 4.6-8
T_P	=	poultry transfer coefficient (d/kg), Table 4.6-5
T_E	=	egg transfer coefficient (d/kg), Table 4.6-6
FF_P	=	poultry or egg intake fraction from irrigated field/pasture (unitless), Table 4.6-9
Q_{FP}	=	consumption rate of fodder by poultry (kg/d), Table 4.6-9
Q_{WP}	=	consumption rate of water by poultry (L/d), Table 4.6-9
DCF	=	ingestion DCF (rem/μCi), Table 4.7-1
U_P	=	human consumption rate of poultry (kg/yr), Table 4.6-9
U_E	=	human consumption rate of eggs (kg/yr), Table 4.6-9
F_P	=	fraction of poultry produced locally (unitless), Table 4.6-7
F_E	=	fraction of eggs produced locally (unitless), Table 4.6-7

5.4.1.2 MOP at the 100-Meter Well Direct Exposure Dose Pathways

5.4.1.2.1 Direct Exposure from Irrigated Soil

Exposure route from direct contact to soil assumes the soil is irrigated with groundwater from the 100-meter well and the receptor in turn is exposed during time spent caring for a garden. The dose is calculated using the following formula.

$$D = C_D \times F_G \times DCF \times \rho_{SS}$$

where:

D	=	dose from 1-year direct exposure to contaminated soil (rem/yr)
C_D	=	radionuclide concentration in soil irrigated with water from the 100-meter well, as defined in Section 5.4.1.1.5 (pCi/kg)
F_G	=	fraction of time spent in garden (unitless), Table 4.6-9
DCF	=	external DCF, 15cm (rem/yr per μCi/m^3), Table 4.7-1
ρ_{SS}	=	density of sandy soil (g/cm3), Table 4.2-39

5.4.1.2.2 Direct Exposure from Swimming

Direct contact exposure route from swimming assumes the receptor receives dose from swimming in a stream contaminated from the aquifer. The dose is calculated using the following formula.

$$D = GF_S \times t_S \times C_{SW} \times DCF$$

where:

D	=	dose from 1-year direct exposure to contaminated stream water (rem/yr)
GF_S	=	swimming geometry factor (unitless), Table 4.6-9
t_S	=	time per year spent swimming (hr/yr), Table 4.6-9
C_{SW}	=	radionuclide concentration in water from the stream (undiluted aquifer) (pCi/L)
DCF	=	external DCF, water immersion (rem/yr per μCi/m^3), Table 4.7-1

5.4.1.2.3 Direct Exposure from Fishing/Boating

Direct contact exposure route for fishing/boating assumes the receptor receives dose from fishing or boating in a stream contaminated from the aquifer. The dose is calculated using the following formula.

$$D = GF_B \times t_B \times C_{SW} \times DCF$$

where:

D	=	dose from 1-year direct exposure to contaminated stream water (rem/yr)
GF_B	=	boating geometry factor (unitless), Table 4.6-9
t_B	=	time per year spent boating (hr/yr), Table 4.6-9
C_{SW}	=	radionuclide concentration in water from the stream (undiluted aquifer) (pCi/L)
DCF	=	external DCF, water immersion (rem/yr per μCi/m^3), Table 4.7-1

5.4.1.3 MOP at the 100-Meter Well Inhalation Dose Pathways

5.4.1.3.1 Inhalation during Irrigation

Exposure route from inhalation during irrigation assumes soil is irrigated with groundwater from the 100-meter well and the receptor in turn is exposed by breathing while the garden is irrigated but only during time spent caring for a garden. To account for the quantity of contaminants released into the air and available for inhalation, an Airborne Release Fraction (ARF) is included in the pathway formula. This ARF is conservatively assumed to be 1E-04 taken from DOE-HDBK-3010-94 and is used for all subsequent MOP water inhalation pathway calculations. This formula was derived following the approach of the previous pathway calculations. The dose is calculated using the following formula.

$$D = \frac{C_{GW} \times DCF \times U_A \times F_G \times C_{WA} \times ARF}{\rho_W}$$

where:

D	=	dose from 1-year inhalation of contaminated groundwater in the air from irrigation (rem/yr)
C_{GW}	=	radionuclide concentration in groundwater from the 100-meter well (pCi/L)
DCF	=	inhalation DCF (rem/μCi), Table 4.7-1
U_A	=	air intake (m^3/yr), Table 4.6-9
F_G	=	fraction of time spent in garden exposed to soil irrigated with contaminated groundwater (unitless), Table 4.6-9
C_{WA}	=	water contained in air at ambient conditions (g/m^3), Table 4.6-8
ARF	=	airborne release fraction (unitless), Table 4.6-8
ρ_W	=	water density (g/ml), Table 4.6-8

5.4.1.3.2 Inhalation during Showering

Exposure route from inhalation while showering assumes the receptor is exposed by breathing humid air within the shower. The source of water for the shower is the 100-meter well. This formula was derived following the approach of the previous pathway calculations. The dose is calculated using the following formula.

$$D = \frac{C_{GW} \times DCF \times U_A \times t_S \times C_{WS} \times ARF}{\rho_W}$$

where:

D	=	dose from 1-year inhalation of contaminated groundwater while showering (rem/yr)
C_{GW}	=	radionuclide concentration in groundwater from the 100-meter well (pCi/L)
DCF	=	inhalation DCF (rem/μCi), Table 4.7-1
U_A	=	air intake (m^3/yr), Table 4.6-9
t_S	=	fraction of time spent in shower (unitless), Table 4.6-9
C_{WS}	=	water contained in air at shower conditions (g/m^3), Table 4.6-8
ARF	=	airborne release fraction (unitless), Table 4.6-8
ρ_W	=	water density (g/mL), Table 4.6-8

5.4.1.3.3 Inhalation of Dust from Irrigated Soil

Exposure route from inhalation of irrigation soil assumes soil is irrigated with groundwater from the 100-meter well and the receptor is exposed by breathing dust during time spent caring for a garden. This formula was derived following the approach of the previous pathway calculations. The dose is calculated using the following formula.

$$D = U_A \times L_{SiA} \times C_D \times DCF \times F_G$$

where:

D	=	dose from 1-year inhalation of contaminated dust (rem/yr)
U_A	=	air intake (m^3/yr), Table 4.6-9
L_{SiA}	=	soil loading in air while working in a garden (kg/m^3), Table 4.6-8
C_D	=	radionuclide concentration in soil irrigated with water from the 100-meter well, as defined in Section 5.4.1.1.5 (pCi/kg)
DCF	=	inhalation DCF (rem/μCi), Table 4.7-1
F_G	=	fraction of time spent in garden exposed to soil irrigated with contaminated groundwater (unitless), Table 4.6-9

5.4.1.3.4 Inhalation While Swimming

Exposure route from inhalation while swimming assumes a stream contaminated from the aquifer and the receptor inhales saturated air. The dose is calculated using the following formula.

$$D = \frac{U_A \times GF_S \times t_S \times C_{SW} \times DCF \times C_{WA} \times ARF}{\rho_W}$$

where:

D	=	dose from 1-year inhalation of contaminated stream water while swimming (rem/yr)
U_A	=	air intake (m^3/yr), Table 4.6-9
GF_S	=	swimming geometry factor (unitless), Table 4.6-9
t_S	=	time per year spent swimming (hr/yr), Table 4.6-9
C_{SW}	=	radionuclide concentration in water from the stream (undiluted aquifer) (pCi/L)
DCF	=	inhalation DCF (rem/μCi), Table 4.7-1
C_{WA}	=	water contained in air at ambient conditions (g/m^3), Table 4.6-8
ARF	=	airborne release fraction (unitless), Table 4.6-8
ρ_W	=	water density (g/ml), Table 4.6-8

5.4.2 MOP at the Stream Dose Pathways

The MOP exposure pathways detailed below are used in calculating the dose to the HTF MOP receptor with stream water as a primary water source. The stream concentrations used in the dose calculations are the peak aquifer concentrations (as discussed in Section 5.2.3), and conservatively assume no stream dilution. All transfer times are assumed negligible due to the half-lives of the radionuclides and the long-term analysis of the PA. Unit conversions are not explicitly stated in the equations, but are coded into GoldSim.

5.4.2.1 MOP at the Stream Ingestion Dose Pathways

5.4.2.1.1 Ingestion of Water

Exposure route from ingestion of drinking water assumes the receptor uses water from a stream contaminated from the aquifer, as a drinking water source. The incidental ingestion of water from showering and during recreational activities is assumed negligible when compared to ingestion of drinking water. The dose from consumption of drinking water is calculated using the following formula.

$$D = C_{SW} \times U_W \times DCF$$

where:

D	=	dose from 1-year consumption of contaminated stream water (rem/yr)
C_{SW}	=	radionuclide concentration in water from the stream (undiluted aquifer) (pCi/L)
U_W	=	human consumption rate of water (L/yr), Table 4.6-9
DCF	=	ingestion DCF (rem/μCi), Table 4.7-1

5.4.2.1.2 Ingestion of Beef and Milk

Exposure route from ingestion of beef and dairy assumes cattle drink contaminated stream water and consume fodder irrigated with contaminated stream water. The fodder is contaminated from direct deposition of irrigation water on plants and from deposition of irrigation water on soil followed by root uptake by plants. The receptor in turn consumes the contaminated beef and milk from the cattle. Beef and milk are treated separately. The concentration in fodder and the dose is calculated using the following formulas.

$$C_f = C_{SW} \times I \times \left(LEAF + SOIL \times T_{StV}\right) \times F_I$$

Beef:

$$D = T_B \times \left(FF_B \times C_f \times Q_{FB} + C_{SW} \times Q_{WB}\right) \times DCF \times U_B \times F_B$$

Milk:

$$D = T_M \times \left(FF_M \times C_f \times Q_{FM} + C_{SW} \times Q_{WM}\right) \times DCF \times U_M \times F_M$$

where:

D	=	dose from 1-year consumption of contaminated beef or milk (rem/yr)
C_f	=	radionuclide concentration in fodder (pCi/kg)
C_{SW}	=	radionuclide concentration in water from the stream (undiluted aquifer) (pCi/L)
I	=	irrigation rate (L/m^2-d), Table 4.6-8
$LEAF$	=	radionuclide deposition and retention rate on the vegetation's leaves, as defined in Section 5.4.1.1.2 (m^{2}d/kg)
$SOIL$	=	radionuclide deposition and buildup rate in the soil, as defined in Section 5.4.1.1.2 (m^{2}d/kg)
T_{StV}	=	soil to vegetation ratio (unitless), Table 4.6-1
F_I	=	fraction of the time vegetation is irrigated (unitless), Table 4.6-8

T_B = beef transfer coefficient (d/kg), Table 4.6-3

T_M = milk transfer coefficient (d/L), Table 4.6-2

FF_i = beef or milk cattle intake fraction from irrigated field/pasture (unitless), Table 4.6-9

Q_{Fi} = consumption rate of fodder by beef or milk cattle (kg/d), Table 4.6-9

Q_{Wi} = consumption rate of water by beef or milk cattle (L/d), Table 4.6-9

DCF = ingestion DCF (rem/μCi), Table 4.7-1

U_B = human consumption rate of beef (kg/yr), Table 4.6-9

U_M = human consumption rate of milk (L/yr), Table 4.6-9

F_B = fraction of beef produced locally (unitless), Table 4.6-7

F_M = fraction of milk produced locally (unitless), Table 4.6-7

5.4.2.1.3 Ingestion of Vegetables

The dose to humans from ingestion of contaminated leafy vegetables and produce is calculated assuming two-contamination routes 1) direct deposition of contaminated irrigation water on plants and 2) deposition of contaminated irrigation water on soil followed by root uptake by plants. The irrigation water is from a stream contaminated from the aquifer. Leafy vegetables and produce are treated separately. The dose is calculated using the following formula.

$$D = C_{SW} \times I \times \left(LEAF + SOIL \times T_{StV}\right) \times DCF \times \left(U_{LV} \times k + U_{OV}\right) \times F_V \times F_I$$

where:

D = dose from 1-year consumption of contaminated vegetables (rem/yr)

C_{SW} = radionuclide concentration in water from the stream (undiluted aquifer) (pCi/L)

I = irrigation rate (L/m^2-d), Table 4.6-8

$LEAF$ = radionuclide deposition and retention rate on the vegetable's leaves, as defined in Section 5.4.1.1.2 (m^{2}d/kg)

$SOIL$ = radionuclide deposition and buildup rate in the soil, as defined in Section 5.4.1.1.2 (m^{2}d/kg)

T_{StV} = soil to vegetation ratio (unitless), Table 4.6-1

DCF = ingestion DCF (rem/μCi), Table 4.7-1

U_{LV} = human consumption rate of leafy vegetables (kg/yr), Table 4.6-9

U_{OV} = human consumption rate of other vegetables (produce) (kg/yr), Table 4.6-9

k = fraction of material deposited on leaves that is retained after washing (unitless), Table 4.6-8

F_V = fraction of leafy vegetables and produce produced locally (unitless), Table 4.6-7

F_I = fraction of the time vegetables are irrigated (unitless), Table 4.6-8

5.4.2.1.4 Ingestion of Fish

Exposure route from ingestion of fish assumes fish are caught from a stream contaminated from the aquifer, and the receptor in turn consumes the contaminated fish. The dose is calculated using the following formula.

$$D = C_{SW} \times U_F \times T_F \times DCF$$

where:

D = dose from 1-year consumption of contaminated fish (rem/yr)

C_{SW} = radionuclide concentration in water from the stream (undiluted aquifer) (pCi/L)

U_F = human consumption rate of finfish (kg/yr), Table 4.6-9

T_F = fish bioaccumulation factor (L/kg), Table 4.6-4

DCF = ingestion DCF (rem/μCi), Table 4.7-1

5.4.2.1.5 Ingestion of Soil

Exposure route from soil ingestion assumes soil is irrigated with water from a stream contaminated from the aquifer, and the receptor in turn consumes the contaminated soil. This formula was derived following the approach of the previous pathway calculations. The radionuclide concentration in the soil and the dose is calculated using the following formulas.

$$D = C_D \times DCF \times U_D$$

$$C_D = C_{SW} \times I \times F_I \times SOIL$$

where:

D = dose from 1-year consumption of contaminated soil (rem/yr)

C_D = radionuclide concentration in soil irrigated with stream water (undiluted aquifer) (pCi/kg)

DCF = ingestion DCF (rem/μCi), Table 4.7-1

U_D = human consumption rate of dirt (kg/yr), Table 4.6-9

C_{SW} = radionuclide concentration in water from the stream (undiluted aquifer) (pCi/L)

I = irrigation rate (L/m^2-d), Table 4.6-8

F_I = fraction of the time soil is irrigated (unitless), Table 4.6-8

SOIL = radionuclide deposition and buildup rate in the soil, as defined in Section 5.4.1.1.2 (m^2d/kg)

5.4.2.1.6 Ingestion of Poultry and Eggs

The poultry and egg exposure route assumes poultry drink contaminated stream water and consume fodder irrigated with contaminated stream water. The fodder is contaminated from direct deposition of irrigation water on plants and from deposition of irrigation water on soil followed by root uptake by plants. The receptor in turn consumes the contaminated poultry and eggs. Poultry and eggs are treated separately. The concentration in fodder and the dose is calculated using the following formulas.

$$C_f = C_{SW} \times I \times \left(LEAF + SOIL \times T_{StV}\right) \times F_I$$

Poultry:

$$D = T_P \times \left(FF_P \times C_f \times Q_{FP} + C_{SW} \times Q_{WP}\right) \times DCF \times U_P \times F_P$$

Eggs:

$$D = T_E \times \left(FF_P \times C_f \times Q_{FP} + C_{SW} \times Q_{WP}\right) \times DCF \times U_E \times F_E$$

where:

D = dose from 1-year consumption of contaminated poultry or eggs (rem/yr)

C_f = radionuclide concentration in fodder (pCi/kg)

C_{SW} = radionuclide concentration in water from the stream (undiluted aquifer) (pCi/L)

I = irrigation rate (L/m^2-d), Table 4.6-8

LEAF = radionuclide deposition and retention rate on the vegetation's leaves, as defined in Section 5.4.1.1.2 (m^2d/kg)

SOIL = radionuclide deposition and buildup rate in the soil, as defined in Section 5.4.1.1.2 (m^2d/kg)

T_{StV} = soil to vegetation ratio (unitless), Table 4.6-1

F_I = fraction of the time vegetation is irrigated (unitless), Table 4.6-8

T_P = poultry transfer coefficient (d/kg), Table 4.6-5

T_E = egg transfer coefficient (d/kg), Table 4.6-6

FF_P = poultry intake fraction from irrigated field/pasture (unitless), Table 4.6-9

Q_{FP} = consumption rate of fodder by poultry (kg/d), Table 4.6-9

Q_{WP} = consumption rate of water by poultry (L/d), Table 4.6-9

DCF = ingestion dose conversion factor (rem/μCi), Table 4.7-1

U_P = human consumption rate of poultry (kg/yr), Table 4.6-9

U_E = human consumption rate of eggs (kg/yr), Table 4.6-9

F_P = fraction of poultry produced locally (unitless), Table 4.6-7

F_E = fraction of eggs produced locally (unitless), Table 4.6-7

5.4.2.2 MOP at the Stream Direct Exposure Dose Pathways

5.4.2.2.1 Direct Exposure from Irrigated Soil

Exposure route from direct contact with irrigated soil assumes soil is irrigated with water from a stream contaminated from the aquifer and the receptor in turn is exposed during time spent caring for a garden. The dose is calculated using the following formula.

$$D = C_D \times F_G \times DCF \times \rho_{SS}$$

where:

D = dose from 1-year direct exposure to contaminated soil (rem/yr)

C_D = radionuclide concentration in soil irrigated with stream water, as defined in Section 5.4.2.1.5 (undiluted aquifer) (pCi/kg)

F_G = fraction of time spent in garden (unitless), Table 4.6-9

DCF = external DCF, 15 cm (rem/yr per μCi/m^3), Table 4.7-1

ρ_{SS} = density of sandy soil (g/cm^3), Table 4.2-39

5.4.2.2.2 Direct Exposure from Swimming

Exposure route from direct contact while swimming assumes the receptor receives dose from swimming in a stream contaminated from the aquifer. The dose is calculated using the following formula.

$$D = GF_S \times t_S \times C_{SW} \times DCF$$

where:

D = dose from 1-year direct exposure to contaminated stream water (rem/yr)

GF_S = swimming geometry factor (unitless), Table 4.6-9

t_S = time per year spent swimming (hr/yr), Table 4.6-9

C_{SW} = radionuclide concentration in water from the stream (undiluted aquifer) (pCi/L)

DCF = external DCF, water immersion (rem/yr per μCi/m^3), Table 4.7-1

5.4.2.2.3 Direct Exposure from Fishing/Boating

Exposure route from direct contact while fishing/boating assumes the receptor receives dose from fishing or boating in a stream contaminated from the aquifer. The dose is calculated using the following formula.

$$D = GF_B \times t_B \times C_{SW} \times DCF$$

where:

D	=	dose from 1-year direct exposure to contaminated stream water (rem/yr)
GF_B	=	boating geometry factor (unitless), Table 4.6-9
t_B	=	time per year spent boating (hr/yr), Table 4.6-9
C_{SW}	=	radionuclide concentration in water from the stream (undiluted aquifer) (pCi/L)
DCF	=	external DCF, water immersion (rem/yr per μCi/m^3), Table 4.7-1

5.4.2.3 MOP at the Stream Inhalation Dose Pathways

5.4.2.3.1 Inhalation during Irrigation

Exposure route from inhalation during irrigation assumes soil is irrigated with water from a stream contaminated from the aquifer, and the receptor in turn is exposed by breathing contaminated air only during the time spent caring for a garden while the garden is irrigated. This formula was derived following the approach of the previous pathway calculations.

$$D = \frac{C_{SW} \times DCF \times U_A \times F_G \times C_{WA} \times ARF}{\rho_W}$$

where:

D	=	dose from 1-year inhalation of contaminated stream water in the air from irrigation (rem/yr)
C_{SW}	=	radionuclide concentration in water from the stream (undiluted aquifer) (pCi/L)
DCF	=	inhalation DCF (rem/μCi), Table 4.7-1
U_A	=	air intake (m^3/yr), Table 4.6-9
F_G	=	fraction of time spent in garden exposed to soil irrigated with water from the stream (undiluted aquifer) (unitless), Table 4.6-9
C_{WA}	=	water contained in air at ambient conditions (g/m^3), Table 4.6-8
ARF	=	airborne release fraction (unitless), Table 4.6-8
ρ_W	=	water density (g/ml), Table 4.6-8

5.4.2.3.2 Inhalation While Showering

The exposure route for inhalation during showering assumes receptor exposed by breathing humid air within the shower. The source of water for the shower is a stream contaminated from the aquifer. This formula was derived following the approach of the previous pathway calculations. The dose is calculated using the following formula.

$$D = \frac{C_{SW} \times DCF \times U_A \times t_S \times C_{WS} \times ARF}{\rho_W}$$

where:

D	=	dose from 1-year inhalation of contaminated stream water while showering (rem/yr)
C_{SW}	=	radionuclide concentration in water from the stream (undiluted aquifer) (pCi/L)
DCF	=	inhalation DCF (rem/μCi), Table 4.7-1
U_A	=	air intake (m^3/yr), Table 4.6-9
t_S	=	fraction of time spent in shower (unitless), Table 4.6-9
C_{WS}	=	water contained in air at shower conditions (g/m^3), Table 4.6-8
ARF	=	airborne release fraction (unitless), Table 4.6-8
ρ_W	=	water density (g/ml), Table 4.6-8

5.4.2.3.3 Inhalation of Dust from Irrigated Soil

The exposure route for irrigated soil inhalation assumes soil is irrigated with water from a stream contaminated from the aquifer, and the receptor in turn is exposed by breathing contaminated dust during the time spent caring for a garden. This formula was derived following the approach of the previous pathway calculations. The dose is calculated using the following formula.

$$D = U_A \times L_{SiA} \times C_D \times DCF \times F_G$$

where:

D	=	dose from 1-year inhalation of contaminated dust (rem/yr)
U_A	=	air intake (m^3/yr), Table 4.6-9
L_{SiA}	=	soil loading in air while working in a garden (kg/m^3), Table 4.6-8
C_D	=	radionuclide concentration in soil irrigated with stream water, as defined in Section 5.4.2.1.5 (undiluted aquifer) (pCi/kg)
DCF	=	inhalation DCF (rem/μCi), Table 4.7-1
F_G	=	fraction of time spent in garden exposed to soil irrigated with water from the stream (undiluted aquifer) (unitless), Table 4.6-9

5.4.2.3.4 Inhalation While Swimming

The exposure route for inhalation during swimming assumes a stream contaminated from the aquifer and the receptor inhales saturated air. This formula was derived following the approach of the previous pathway calculations. The dose is calculated using the following formula.

$$D = \frac{U_A \times GF_S \times t_S \times C_{SW} \times DCF \times C_{WA} \times ARF}{\rho_W}$$

where:

D	=	dose from 1-year inhalation of contaminated stream water while swimming (rem/yr)
U_A	=	air intake (m^3/yr), Table 4.6-9
GF_S	=	swimming geometry factor (unitless), Table 4.6-9
t_S	=	time per year spent swimming (hr/yr), Table 4.6-9
C_{SW}	=	radionuclide concentration in water from the stream (undiluted aquifer) (pCi/L)
DCF	=	inhalation DCF (rem/μCi), Table 4.7-1
C_{WA}	=	water contained in air at ambient conditions (g/m^3), Table 4.6-8
ARF	=	airborne release fraction (unitless), Table 4.6-8
ρ_W	=	water density (g/ml), Table 4.6-8

5.5 Dose Analysis

The total peak doses are calculated utilizing the pathways identified in Section 5.4 for the MOP at the 100-meter boundary and the MOP at applicable streams (either UTR or Fourmile Branch) for the Base Case (Case A in Section 4.4.2). The peak doses are calculated using the peak groundwater concentrations identified in Section 5.2. A peak dose is identified for the 10,000-year compliance period. In addition, a peak dose associated with the sensitivity-run radionuclides is calculated through 100,000 years. The information after the compliance period is included to improve confidence in the overall PA model and not for comparison to performance objectives consistent with guidance in DOE Guide 435.1-1 Section IV.P.(2) and NUREG-1854 Section 4.1.1.1.

5.5.1 MOP at 100-Meter Groundwater Pathway Dose Results

The groundwater pathway peak doses for the six 100-meter sectors are calculated using the peak concentration for each radionuclide in the sector (a discussion of how peak concentrations are determined by sector is provided in Section 5.2). These groundwater pathway peak doses are the total dose associated with all the individual 100-meter well pathways identified in Section 5.4.

5.5.1.1 MOP 100-Meter Peak Annual Groundwater Pathway Dose

Table 5.5-1 presents a comparison of the 100-meter peak groundwater pathway doses for the different 100-meter sectors within both 10,000 and 20,000 years. In calculating the peak groundwater pathway dose, the highest radionuclide concentration within the vertical

computational meshes is used from each of the three distinct aquifers modeled (UTR-UZ, UTR-LZ, and the Gordon Aquifer).

Table 5.5-1: MOP at 100m Peak Groundwater Pathways Dose by Sector

Sector [a]	Peak Dose in 10,000 Years	Peak Dose in 20,000 Years
A	**0.5 mrem/yr (year 780)** Principal Radionuclide: Tc-99 (97%) Principal Pathways: Water Ingestion (68%) Vegetable Ingestion (23%)	**0.5 mrem/yr (year 780)** Principal Radionuclide: Tc-99 (97%) Principal Pathways: Water Ingestion (68%) Vegetable Ingestion (23%)
B	**0.8 mrem/yr (year 9,530)** Principal Radionuclides: Tc-99 (74%) Ra-226 (13%) Principal Pathways: Water Ingestion (71%) Vegetable Ingestion (21%)	**0.8 mrem/yr (year 9,530)** Principal Radionuclides: Tc-99 (74%) Ra-226 (13%) Principal Pathways: Water Ingestion (71%) Vegetable Ingestion (21%)
C	**1.0 mrem/yr (year 9,520)** Principal Radionuclides: Tc-99 (66%) Ra-226 (19%) Principal Pathways: Water Ingestion (73%) Vegetable Ingestion (20%)	**1.1 mrem/yr (year 20,000)** Principal Radionuclides: Ra-226 (74%) Pu-239 (8%) Principal Pathways: Water Ingestion (83%) Vegetable Ingestion (13%)
D	**0.08 mrem/yr (year 480)** Principal Radionuclide: Tc-99 (~100%) Principal Pathways: Water Ingestion (66%) Vegetable Ingestion (23%)	**0.1 mrem/yr (year 20,000)** Principal Radionuclides: Ra-226 (63%) Nb-93m (20%) Principal Pathways: Water Ingestion (63%) Fish Ingestion (26%)
E	**0.2 mrem/yr (year 890)** Principal Radionuclide: Tc-99 (95%) Principal Pathways: Water Ingestion (65%) Vegetable Ingestion (22%)	**0.2 mrem/yr (year 890)** Principal Radionuclide: Tc-99 (95%) Principal Pathways: Water Ingestion (65%) Vegetable Ingestion (22%)
F	**0.2 mrem/yr (year 880)** Principal Radionuclides: Tc-99 (90%) Np-237 (6%) Principal Pathways: Water Ingestion (66%) Vegetable Ingestion (22%)	**0.2 mrem/yr (year 880)** Principal Radionuclides: Tc-99 (90%) Np-237 (6%) Principal Pathways: Water Ingestion (66%) Vegetable Ingestion (22%)

a Sectors illustrated in Figure 5.2-5.

Figure 5.5-1 presents the peak doses to the 100-meter MOP receptor over time during the compliance period (10,000 years) for the 100-meter sectors. The peak 100-meter MOP groundwater pathway dose in the 10,000-year compliance period is 1.0 mrem/yr at year 9,520 in Sector C. Figure 5.5-2 presents the 100-meter MOP receptor doses within 20,000 years for the 100-meter sectors.

An overview of the modeling results indicate:

- Contaminant water concentrations and dose are directly influenced by flow direction (see Figures 5.2-2 and 5.2-5), timing of the loss of contaminant containment, and inventory location with respect to the 100-meter boundary.
- Early dose peaks (prior to year 2,500) are associated with the inventory from ancillary equipment (including transfer lines), from sand pads under Type II tanks, and tanks assumed to have failed steel liners at the time of closure (Tanks 12, 14, 15 and 16).
- Later dose peaks result from the loss of containment due to failure of the steel liner (Type IV tanks at year 3,638; Type I tanks at year 11,397; Type II tanks at year 12,687; and Type III and IIIA tanks at year 12,751). Loss of the steel liner initiates changes to the chemistry and radionuclide holding capability of the grout, which directly affects radionuclide release rates, as illustrated by the dose peaks.
- Peak doses to the MOP within 20,000 years at the 100-meter boundary are primarily from Tc-99 and Ra-226 (see Figures 5.5-3 through 5.5-6) from the groundwater pathways in Sectors A, B, and C.
- The all-pathways dose is the same as the groundwater pathways dose due to the negligible dose contribution from the air pathway, as presented in Section 5.3.

Figure 5.5-1: 100m Sector MOP Peak Groundwater Pathway Dose Results within 10,000 Years

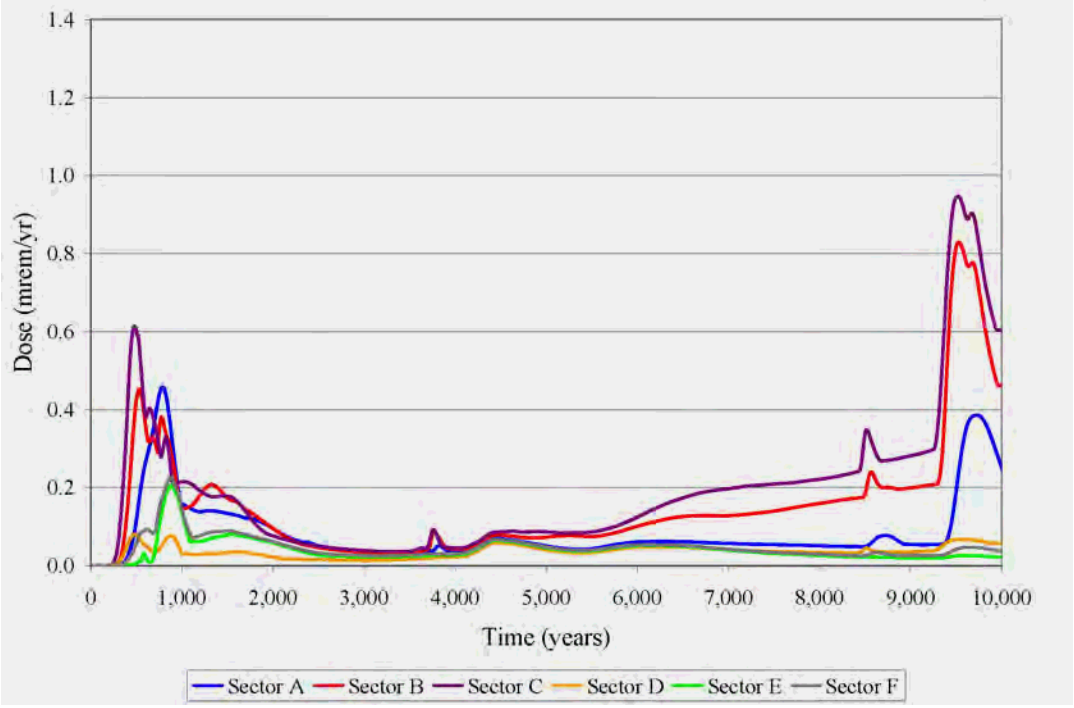

Figure 5.5-2: 100m Sector MOP Peak Groundwater Pathway Dose Results within 20,000 Years

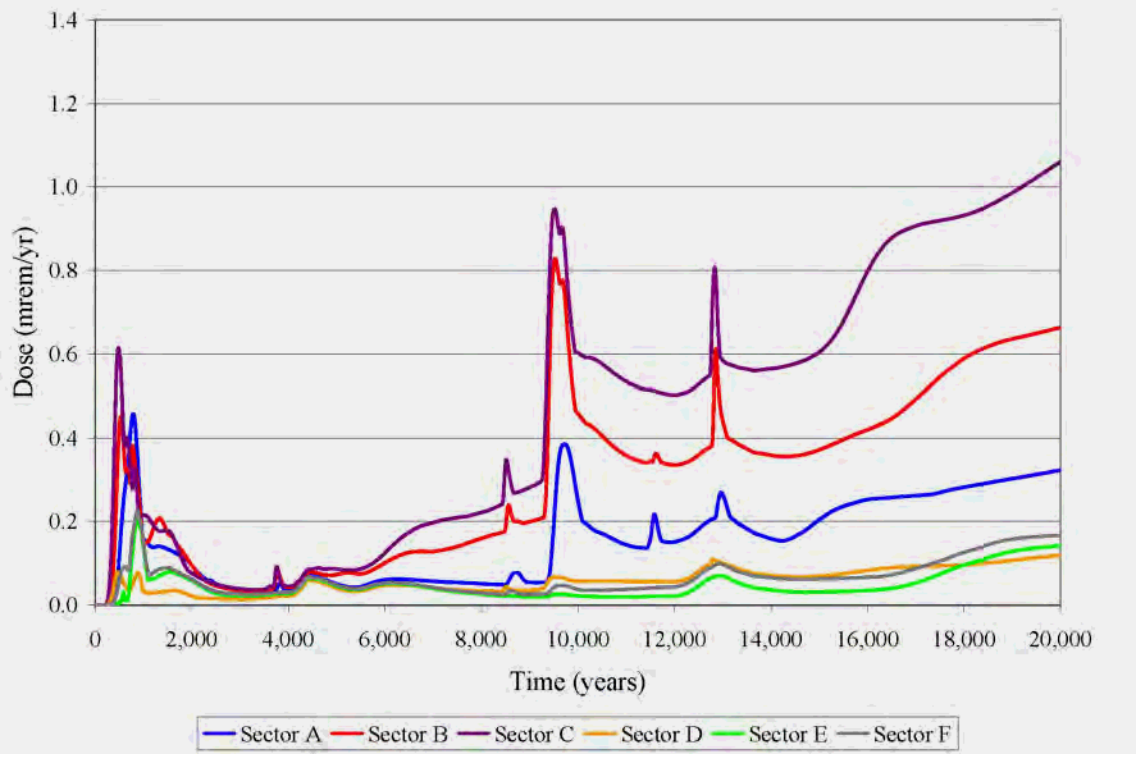

Provided below is a more detailed discussion of the peaks that appear in Figures 5.5-1 and 5.5-2. The discussion also relies upon information from Figures 5.5-3 through 5.5-6 relating to the individual radionuclide contributors to the groundwater pathway doses.

- The dose peaks prior to year 2,500 are influenced by ancillary equipment releases, in particular the transfer lines, which are distributed throughout the HTF and therefore affect all sectors. The timing of the ancillary equipment peaks is fairly consistent for all sectors, with the magnitude of the peak vary depending on what ancillary equipment other than the transfer lines are contributing to the peak (i.e., Sectors A, B, and C have more inventory sources, such as the PP and evaporators nearby). The ancillary equipment releases start when containment fails (at year 510). In contrast to the waste tanks (where solubility control was modeled as controlling waste release), the ancillary equipment releases were modeled as instantaneous, so the entire inventory in each ancillary equipment location is available for release at year 510.
- The peaks in the first 1,500 years after HTF closure are associated with Tc-99 and Np-237 from ancillary equipment (including transfer lines), from sand pads under Type II tanks, and from waste tanks that are assumed to have failed steel liners at the time of closure (Tanks 12, 14, 15, and 16). The Tc-99 travels quickly (distribution coefficient in soil of 0.6 mL/g) to the 100-meter boundary after the ancillary equipment containment fails (at year 510). The Tc-99 inventory in the sand pads under the Type II tanks is available for transport and contributes to a single peak soon thereafter. The Np-237 travels relatively quickly (distribution coefficient in soil of 3 mL/g), but does not travel as quickly as the Tc-99 due to soil retardation being greater for neptunium, so the peak associated with Np-237 is later and less acute. The basemat transitions from Oxidized Region II to Oxidized Region III at year 109 for the Type II tanks with a failed liner, and at year 1,350 for the Type I tanks with a failed liner.
- The small dose increase near year 3,700 is associated with I-129. This release is primarily associated with liner degradation of Type IV tanks. The contribution of I-129 to dose is quick because it travels rapidly (distribution coefficient in basemat of 15 mL/g, distribution coefficient in soil of 0.3 mL/g).
- The behavior between year 3,700 and 11,300 are tied to releases from the Type IV tanks and from waste tanks with initial liner failure. The Type IV tank liners are considered to fail at approximately year 3,700 while the Types I, II, and III/IIIA tanks do not fail until approximately years 11,400, 12,700, and 12,750, respectively (excepting those waste tanks, Tanks 12, 14, 15, and 16, that are modeled as being failed at the time of HTF facility closure). The releases from the CZs are potentially solubility limited, such that release fluxes from tank liners may vary by radionuclide dependant on its individual solubility controlled release rate from the CZ.
- The Sectors B and C doses between approximately year 6,000 and 20,000 years have a significant Ra-226 contribution. Although there is some initial Ra-226 inventory, this dose is primarily due to the decay of Ra-226 parent radionuclides (Pu-238, U-234, and Th-230) wherein Pu-238 comprises approximately 80% of the Ra-226 contribution; therefore, the radium travel time is tied to plutonium. Radium moves faster through concrete than plutonium (i.e., the radium distribution coefficient in

concrete of 100 mL/g is much lower than the plutonium distribution coefficient in concrete of 10,000 mL/g). Further, once the radium is released from the basemat, it moves even faster through the soil (distribution coefficient in soil of 25 mL/g), however it lags behind the Np-237 because radium is still being released primarily as a daughter product of Pu-238. The Ra-226 contribution starts ramping up almost as soon as the Type IV tank liners fail and steadily increases as more Ra-226 is produced from decay. The Ra-226 releases in Sector A increase at a slower rate than in Sectors B and C because the Type IV tanks have a thinner basemat for radium to travel through than the Type I and II tanks that primarily influence Sector A.

- There is a dose spike in Sectors B and C at approximately year 8,500 associated with Tc-99. These dose peaks are tied to concrete transition at year 8,392 in the Type II tanks that are modeled as having initially failed steel liners (Tanks 14, 15 and 16). At this time, the annulus concrete transitions from reducing to oxidized conditions. Sector A also experiences a slight dose increase however, the magnitude is smaller due to the greater distance between the Sector A 100-meter boundary and the Type II tanks.
- A second, larger dose spike from Tc-99 occurs in Sectors A, B, and C at around 9,500 years. This peak is tied to concrete transitions in the Type II tank (Tank 13) with the steel liner at year 9,126. Again, this is due to the annulus concrete transitioning from reducing to oxidized conditions.
- A third dose spike from Tc-99 occurs in Sectors A, B, and C starting at around 13,000 years. This peak is tied to the liner failures for Tank 13 (at approximately 12,700 years) and Type III/IIIA tanks (at approximately 12,750 years).
- As the waste tank annulus grout transitions to oxidizing grout, the relative Ra-226 doses from each respective waste tank type increases. When this transition occurs, the distribution coefficient for both radium and plutonium in the grout decreases (from 100 mL/g to 70 mL/g for radium and from 10,000 mL/g to 2,000 mL/g for plutonium). These changes result in faster transport of Ra-226 and its parent radionuclide (Pu-238). This is best depicted in Figure 5.5-6, which presents a series of "step" increases in the Ra-226 dose for Sector C, although Sectors A and B also experience significant contributions.
    - The first step (between about 6,000 and 9,000 years) corresponds to the annulus transition in Tank 12, which occurs at 6,549 years.
    - The next step (between 9,000 years and about 15,000 years) corresponds to the other Type I tanks and the Type II tanks, which experience transitions between 7,453 and 9,126, at which point the increase in Ra-226 becomes relatively steady.
    - The last step (starting around 15,000 years) is the steepest because it corresponds to the greatest number of waste tanks (Type III and IIIA tanks). The annulus grout in these waste tanks transitions from reducing to oxidizing between 14,577 and 14,762 years.
- Starting around year 14,000, Sectors B and C see large increases in Ra-226 doses. These are tied to Type III and IIIA tank liner failures (which occur at approximately 12,750 years) as Ra-226 travels though the waste tank basemats. The concrete basemats have a relatively low distribution coefficient for radium (basemat

distribution coefficient 70 to 100 mL/g) but are thick (41 to 43 inches for Type III/IIIA tanks). The differences in the release times are due to variation in the thicknesses of the basemats.

- Sectors E and F mirror the dose profiles from the other sectors in many ways but always with a smaller magnitude dose. Sectors E and F are both tied to Type IIIA tanks, which experience liner failure at approximately 12,750 years.
- Sector D is nearest to the Type II tanks. Tanks 14, 15, and 16 are modeled as having initially failed liners (at the time of HTF closure) whereas the liner for Tank 13 fails later at 12,700 years. However, the flow path's direction generally draws contaminants away from the Sector D 100-meter boundary. Therefore, results from Sector D are negligible, relative to the other sectors.

5.5.1.2 Individual Radionuclide Contributions to the MOP 100-Meter Peak Annual Groundwater Pathway Dose

For the individual radionuclide contributions analyses, Sectors A and C were selected for discussion. Sectors A, B, and C were the highest contributors to dose, as seen in Figures 5.5-1 and 5.5-2. Sector B had a dose profile that reflected conditions in both Sector A and Sector C, therefore discussion of Sector B would be superfluous.

Figures 5.5-3 and 5.5-4 present the relative contribution from individual radionuclides to the Sector A 100-meter groundwater pathway dose over time (10,000 and 20,000 years respectively). Figures 5.5-5 and 5.5-6 present the relative contribution from individual radionuclides to the Sector C 100-meter groundwater pathway dose over time (10,000 and 20,000 years respectively). Table 5.5-2 presents the relative contribution from the sensitivity-run radionuclides to the peak groundwater pathway doses for these two sectors. For Sector A, the peak groundwater pathway dose to the MOP at 100 meters during the 10,000-year compliance period is primarily associated with Tc-99 (97%). For Sector C, the peak groundwater pathway dose to the MOP at 100 meters during the 10,000-year compliance period is also primarily associated with Tc-99 (66%) and with Ra-226 (19%). The top individual radionuclide contributors (> 5% contribution) to the MOP peak groundwater pathway dose at 100 meters are Tc-99 and Ra-226.

Figure 5.5-3: Individual Radionuclide Contributors to the Sector A 100m Peak Groundwater Pathway Dose - 10,000 Years

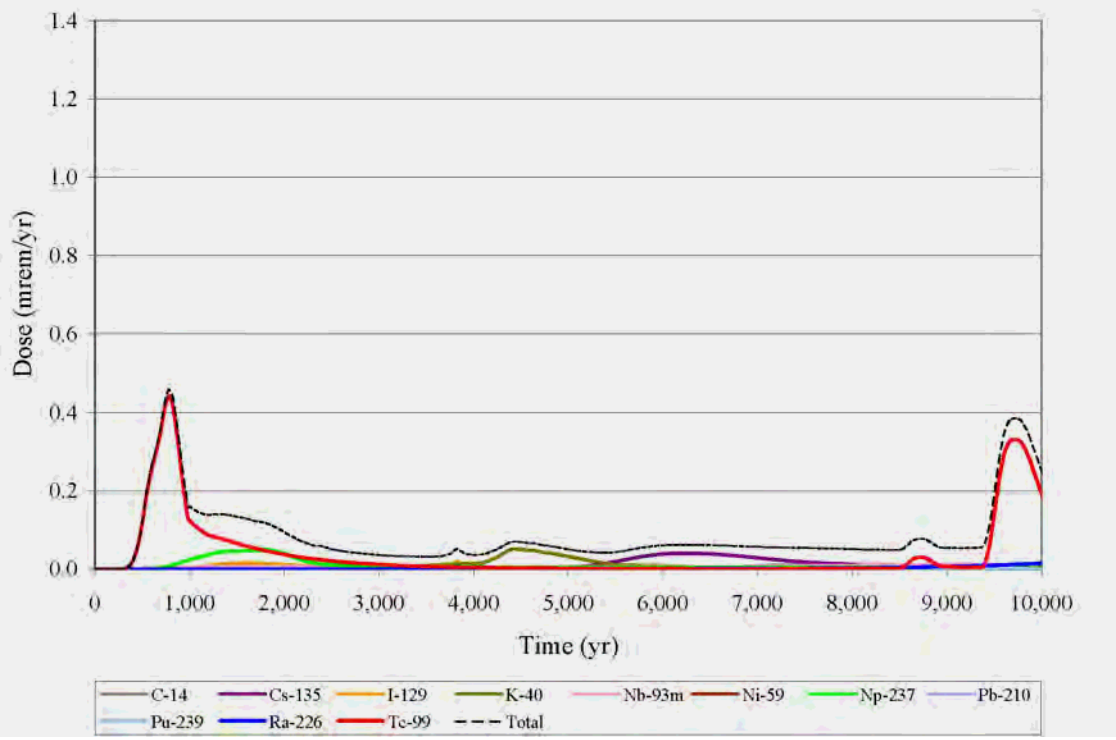

Figure 5.5-4: Individual Radionuclide Contributors to the Sector A 100m Peak Groundwater Pathway Dose - 20,000 Years

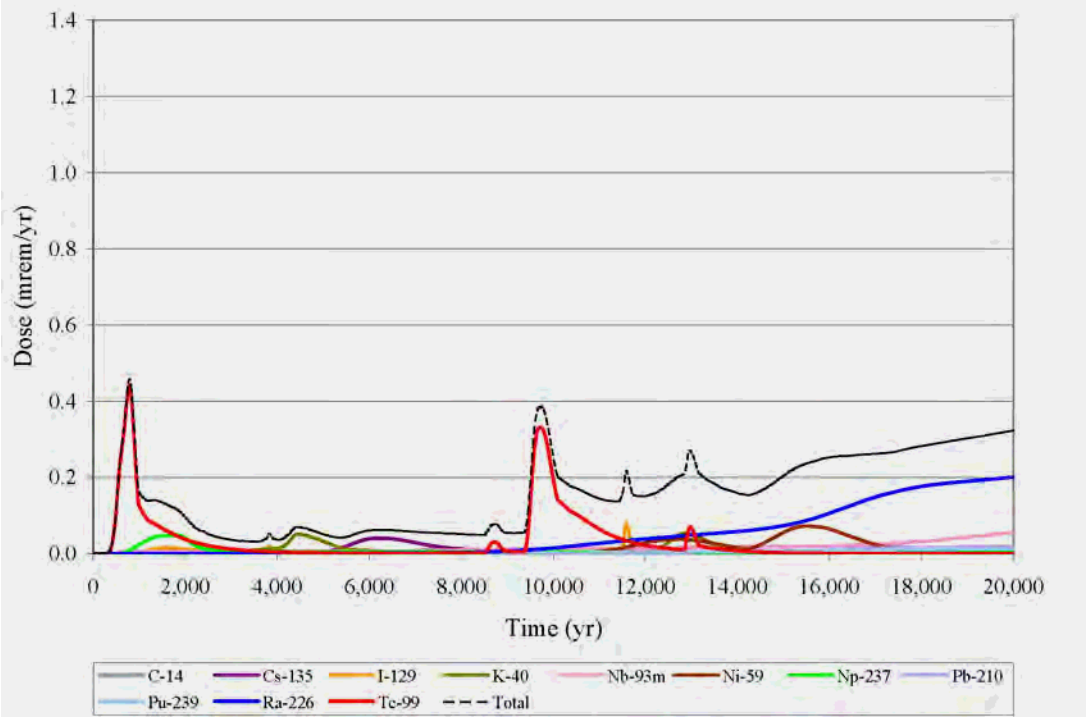

Figure 5.5-5: Individual Radionuclide Contributors to the Sector C 100m Peak Groundwater Pathway Dose - 10,000 Years

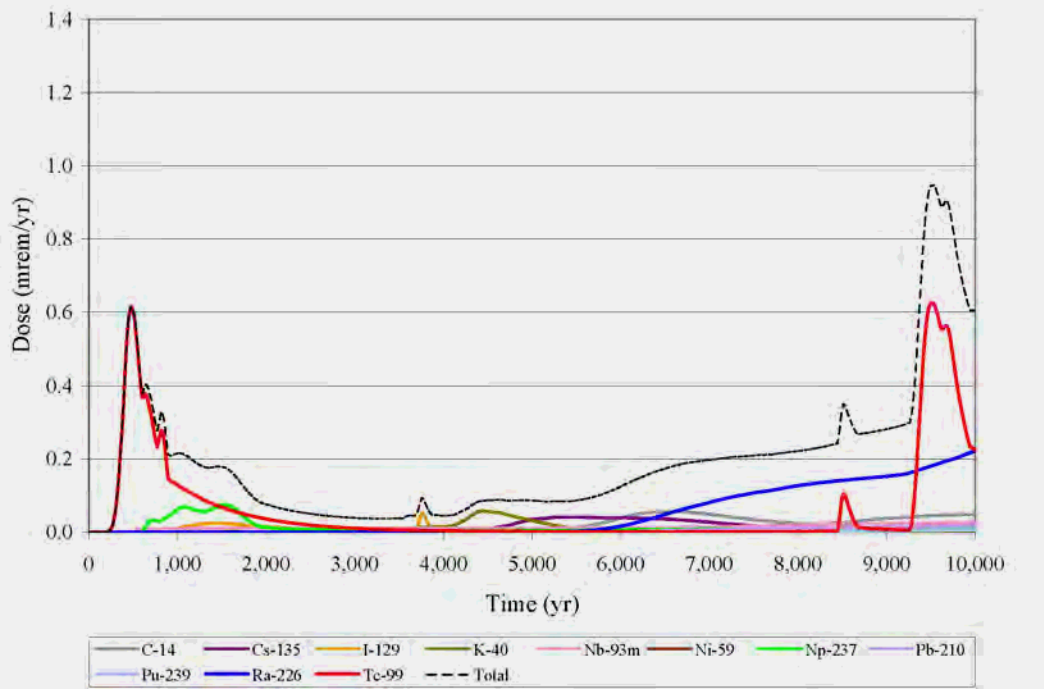

Figure 5.5-6: Individual Radionuclide Contributors to the Sector C 100m Peak Groundwater Pathway Dose - 20,000 Years

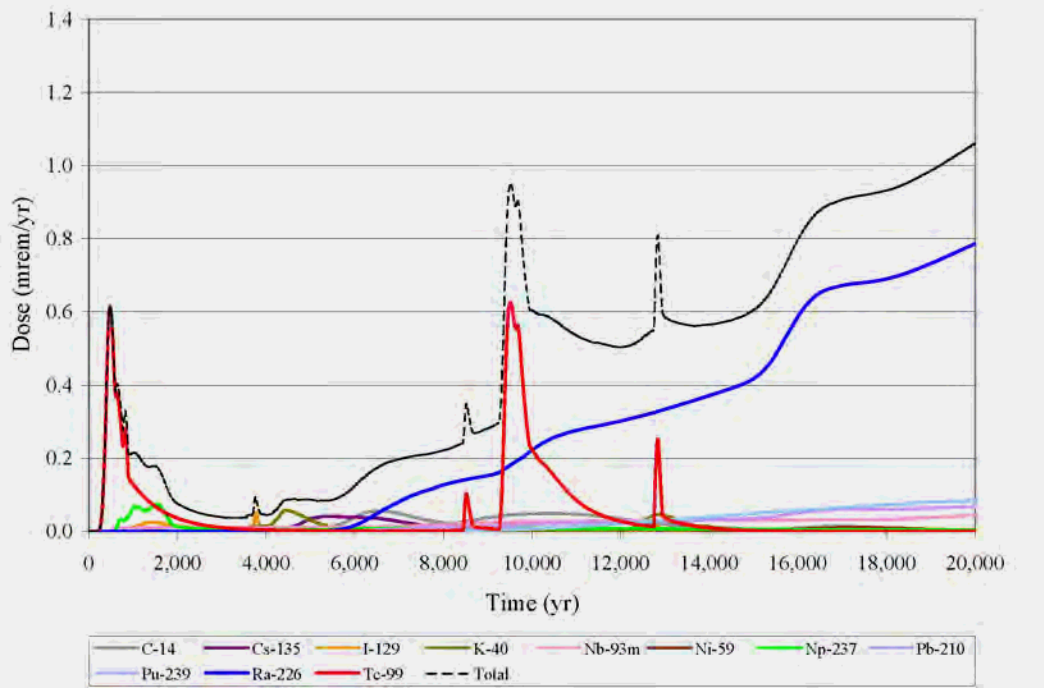

Table 5.5-2: MOP at 100m Peak Groundwater Pathway Dose Individual Radionuclide Contributions at Peak Years - Sectors A and C

Radionuclide	Contribution to Sector A Peak dose at year 780 (mrem/yr)	Percentage of Total Peak Dose	Contribution to Sector C Peak dose at year 9,520 (mrem/yr)	Percentage of Total Peak Dose
I-129	<0.01	<0.5%	<0.01	<0.5%
Np-237	<0.01	1.5%	<0.01	1%
Pu-239	<0.01	<0.5%	<0.01	0.6%
Ra-226	<0.01	<0.5%	0.18	19%
Tc-99	0.44	96.6%	0.62	66%
Others	<0.01	1.8%	0.13	13%
TOTAL	**0.46**	**100%**	**0.95**	**100%**

5.5.1.3 Individual Waste Tank Contributions to MOP 100-Meter Peak Annual Groundwater Pathway Dose

Table 5.5-3 presents the relative contributions from the waste sources, which will contribute to the Sectors A and C 100-meter MOP groundwater pathway doses at the year of the peak dose (780 years and 9,520 years, respectively). At year 780, the 100-meter peak groundwater pathway dose in Sector A is dominated by contributions from the transfer lines (which together contribute about 50% of the Sector A dose), followed by doses from the combined Type II tanks with early liner failure (Tanks 14, 15, and 16), which contribute about 46% of the dose.

Tank 13 is the primary contributor (68%) to the 100-meter peak groundwater pathway dose in Section C at year 9,520. Tank 13 has an intact liner during the 10,000-year compliance period, so this contribution is attributed to the inventory available in the sand pad under the waste tank. The other Type II tanks, along with the combined Type IV tanks (Tanks 21, 22, 23, and 24) make up most of the remaining contribution (16% and 15%, respectively) to the 100-meter peak groundwater pathway dose in Section C at year 9,520. The Type I tanks with intact liners and the Type III/IIIA tanks do not fail prior to 10,000 years and therefore do not contribute to dose within the 10,000-year compliance period. Appendix E contains the 100-meter radionuclide concentration curves (20,000 years) for Tanks 12, 13, 16, 22, 32, 36, 39, and 40, the transfer lines, and all other sources combined. Figures 5.5-7 and 5.5-8 present source contributions to the dose over 20,000 years for Sector A and Sector C, respectively. The figures display the sources presented in Table 5.5-3.

Figure 5.5-7: Individual Source Contributors to the Sector A 100m Peak Groundwater Pathway Dose - 20,000 Years

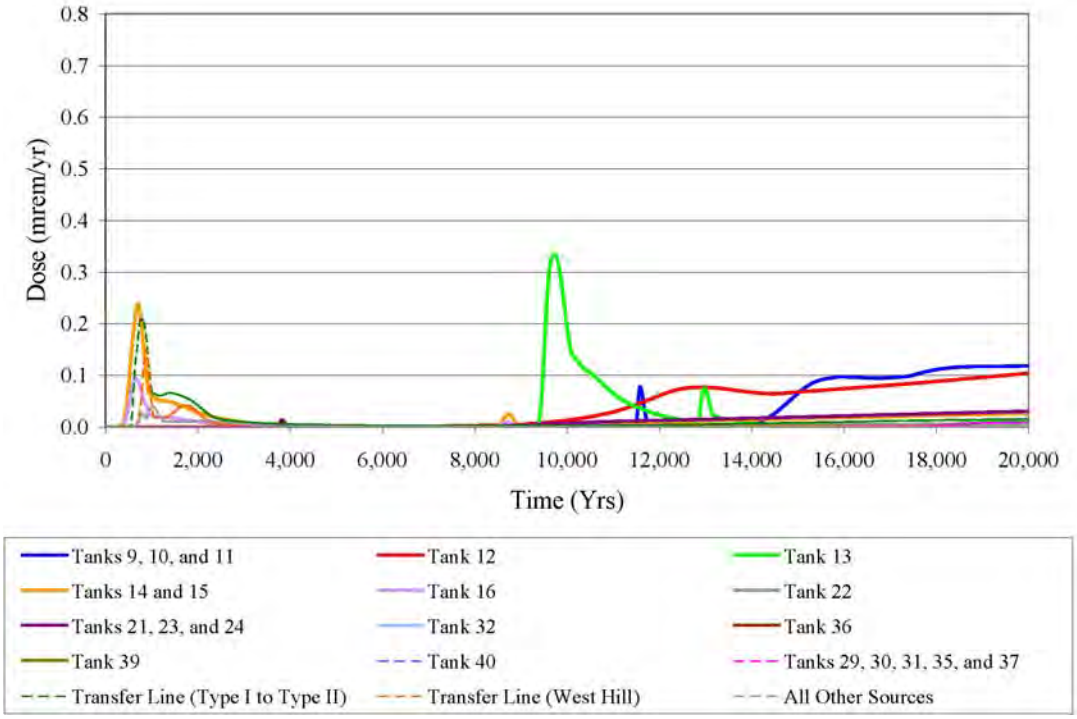

Figure 5.5-8: Individual Source Contributors to the Sector C 100m Peak Groundwater Pathway Dose - 20,000 Years

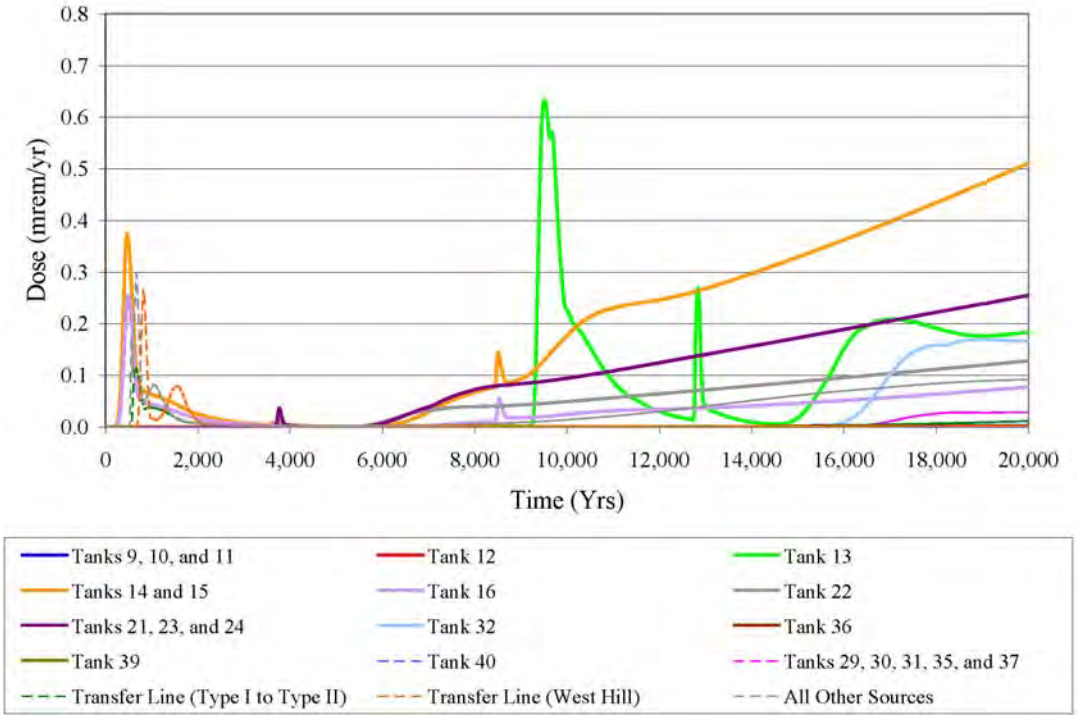

Table 5.5-3: MOP at 100m Peak Groundwater Pathway Dose Individual Source Contributions at Peak Years - Sectors A and C Peak

Waste Source [a]	Contribution to Sector A Peak Dose at year 780 (mrem/yr)	Percentage of Total Peak Dose	Contribution to Sector C Peak Dose at year 9,520 (mrem/yr)	Percentage of Total Peak Dose
Tank 12	<0.01	<0.5%	<0.01	<0.5%
Tank 13	<0.01	<0.5%	0.64	68%
Tanks 14 and 15	0.15	34%	0.13	14%
Tank 16	0.05	12%	0.02	2%
Tank 22	<0.01	<0.5%	0.05	5%
Tanks 21, 23, and 24	<0.01	<0.5%	0.09	10%
Transfer Line, Group 2 (Type I and Type II)	0.17	37%	<0.01	<0.5%
Transfer Line, Group 3 (West Hill)	0.06	13%	<0.01	<0.5%
All Other Sources	0.02	5%	0.01	1%
TOTAL	**0.46**	**100%**	**0.95**	**100%**

a The Type I tanks with intact liners (Tanks 9, 10, and 11), and the Type III/IIIA tanks (Tanks 29, 30, 31, 32, 35, 36, 37, 38, 39, 40, 41, 42, 43, 48, 49, 50, and 51) do not fail prior to the 10,000-year compliance period and are excluded from this table because their contributions to peak doses is 0%.

5.5.1.4 Individual Pathway Contributions to MOP 100-Meter Peak Annual Groundwater Pathway Dose

As stated previously, the total peak groundwater pathway dose results are the summation of the doses associated with all the individual 100-meter well pathways identified in Section 5.4. Table 5.5-4 presents the relative contributions from the individual groundwater pathways to the Sector A 100-meter MOP receptor dose at 780 years (the year of the peak dose). The primary contributors are water ingestion (68% of peak dose) and vegetable ingestion (23% of peak dose). Similarly, Table 5.5-5 presents the relative contributions from the individual groundwater pathways to the Sector C 100-meter MOP receptor dose at 9,520 years (the year of the peak dose). Like Sector A, the primary contributors for Sector C are water ingestion (73% of peak dose) and vegetable ingestion (20% of peak dose).

Table 5.5-4: MOP at 100m Peak Groundwater Pathway Dose Individual Contributions at Peak Years - Sector A

Pathway	Associated Contribution at year 780 (mrem/yr)	Percentage of Total Peak Dose	Principal Radionuclide Pathway Dose
Water Ingestion	3.1E-01	68%	Tc-99 (98%)
Vegetable Ingestion	1.1E-01	23%	Tc-99 (99%)
Fish Ingestion	1.6E-02	3.4%	Tc-99 (58%) Nb-93m (22%) K-40 (20%)
Egg Ingestion	1.0E-02	2.3%	Tc-99 (~100%)
Other Pathways	1.6E-02	3.3%	N/A

Pathway	Associated Contribution at year 780 (mrem/yr)	Percentage of Total Peak Dose (%)
Total Inhalation	2.0E-06	<0.5%
Total Ingestion	4.6E-01	~100%
Total Exposure	3.4E-07	<0.5%
TOTAL	**0.46**	**100%**

Table 5.5-5: MOP at 100m Peak Groundwater Pathway Dose Individual Contributions at Peak Years - Sector C

Pathway	Associated Contribution at year 9,520 (mrem/yr)	Percentage of Total Peak Dose	Principal Radionuclide Pathway Dose
Water Ingestion	6.9E-01	73%	Tc-99 (63%) Ra-226 (23%)
Vegetable Ingestion	1.9E-01	20%	Tc-99 (79%) Ra-226 (13%)
Fish Ingestion	2.1E-02	2.3%	Nb-93m (48%) Tc-99 (29%) Cs-135 (10%)
Beef Ingestion	1.8E-02	1.9%	Tc-99 (77%) C-14 (18%)
Other Pathways	2.9E-02	2.8%	N/A

Pathway	Associated Contribution at year 9,520 (mrem/yr)	Percentage of Total Peak Dose (%)
Total Inhalation	8.1E-06	<0.5%
Total Ingestion	9.5E-01	~100%
Total Exposure	1.7E-04	<0.5%
TOTAL	**0.95**	**100%**

Table 5.5-6 presents a comparison of the 100-meter peak water ingestion doses for the different 100-meter sectors within both 10,000 and 20,000 years. The early water ingestion doses (before year 3,000) are primarily associated with ancillary equipment (containment assumed breached at year 510) and Type II tanks. Figure 5.5-9 presents the water ingestion doses to the 100-meter MOP receptor over time during the 10,000-year compliance period for the 100-meter sectors. The highest 100-meter MOP water ingestion dose in the 10,000-year compliance period is a 0.69 mrem/yr dose in Sector C at year 9,520. Figure 5.5-10 presents the 100-meter MOP receptor water ingestion doses within 20,000 years for the 100-meter sectors. Figures 5.5-11 and 5.5-12 show the vegetable ingestion doses to the 100-meter MOP receptor for the 100-meter sectors within 10,000 and 20,000 years respectively.

Table 5.5-6: MOP at 100m Peak Water Ingestion Doses by Sector

Sector	Peak Water Ingestion Dose in 10,000 years (mrem/yr)	Principal Radionuclide	Peak Water Ingestion Dose in 20,000 years (mrem/yr)	Principal Radionuclide
A	0.31 (year 780)	Tc-99 (98%)	0.31 (year 780)	Tc-99 (98%)
B	0.59 (year 9,530)	Tc-99 (72%) Ra-226 (16%)	0.59 (year 9,530)	Tc-99 (72%) Ra-226 (16%)
C	0.69 (year 9,520)	Tc-99 (63%) Ra-226 (23%)	0.88 (year 20,000)	Ra-226 (76%) Pu-239 (8%)
D	0.05 (year 480)	Tc-99 (~100%)	0.08 (year 20,000)	Ra-226 (82%)
E	0.13 (year 890)	Tc-99 (98%)	0.13 (year 890)	Tc-99 (98%)
F	0.15 (year 880)	Tc-99 (91%) Np-237 (7%)	0.15 (year 880)	Tc-99 (91%) Np-237 (7%)

Figure 5.5-9: MOP at 100m Peak Water Ingestion Dose within 10,000 Years for the 100m Sectors

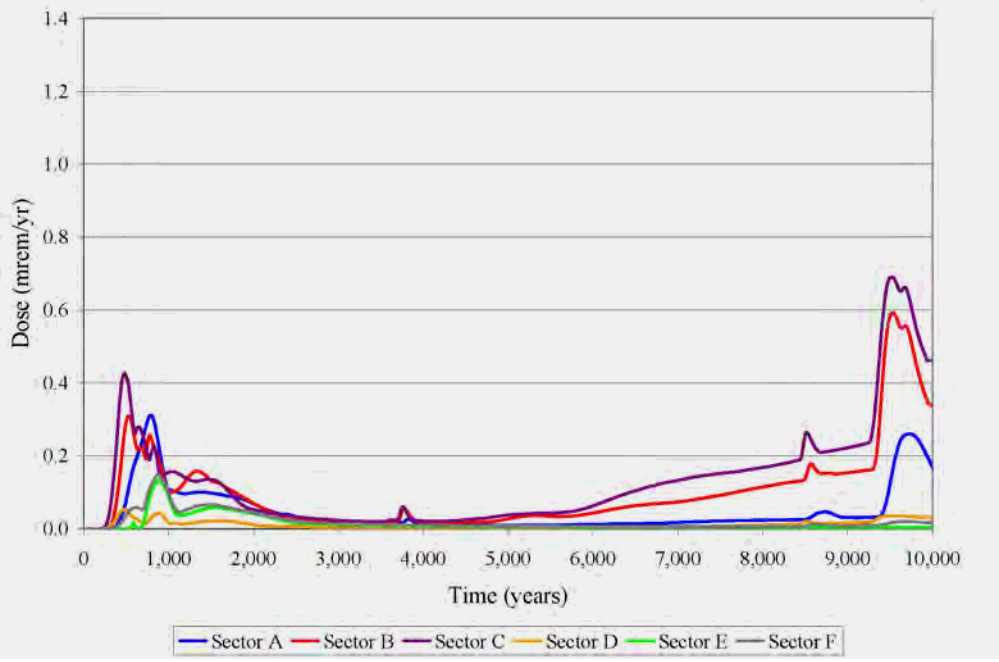

Figure 5.5-10: MOP at 100m Peak Water Ingestion Dose within 20,000 Years for the 100m Sectors

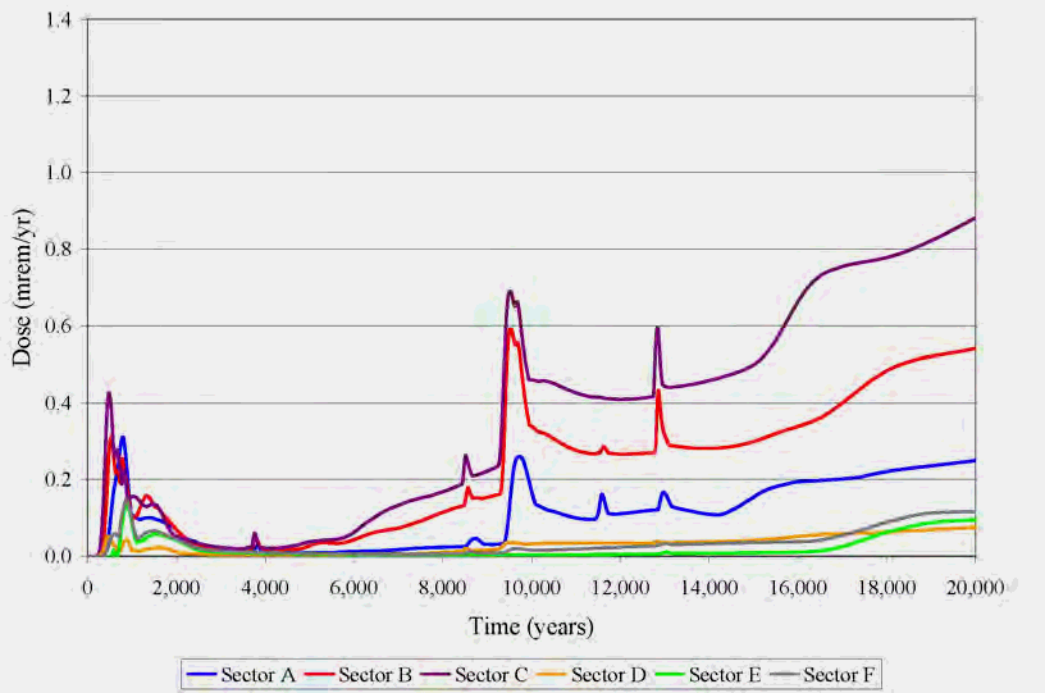

Figure 5.5-11: MOP at 100m Peak Vegetable Ingestion Dose within 10,000 Years for the 100m Sectors

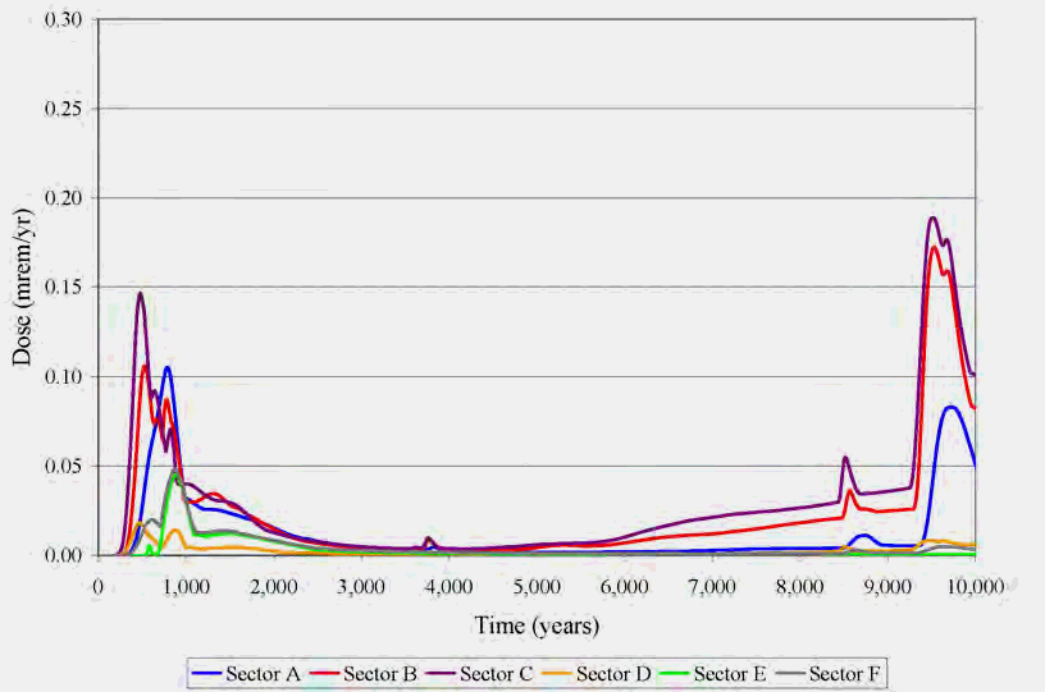

Figure 5.5-12: MOP at 100m Peak Vegetable Ingestion Dose within 20,000 Years for the 100m Sectors

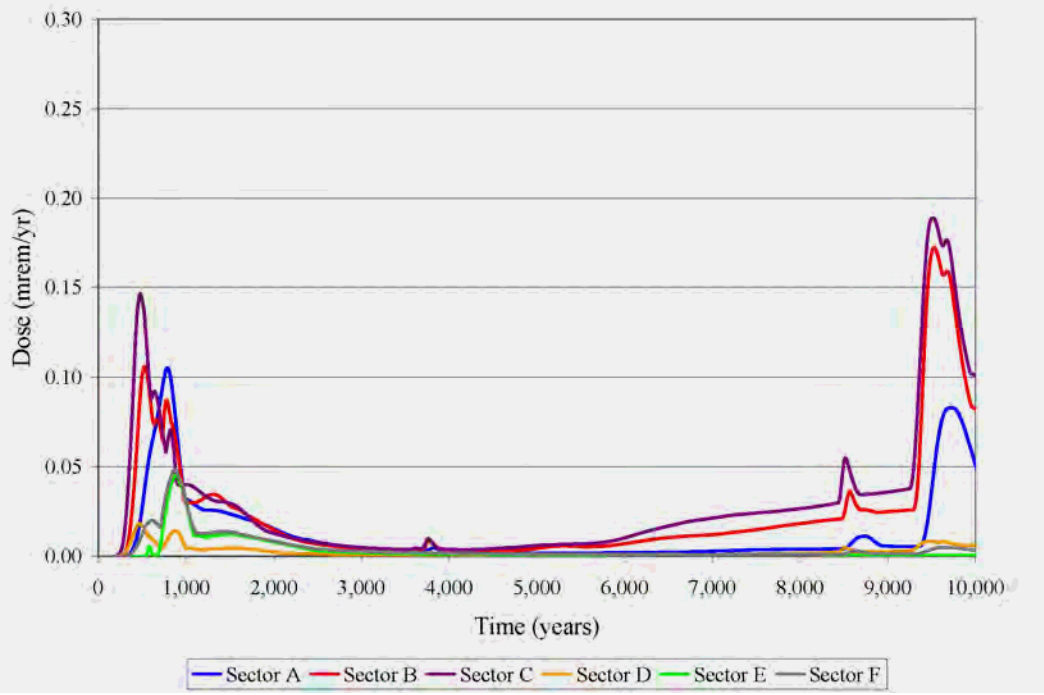

5.5.1.5 MOP 100-Meter Peak Annual Groundwater Pathway Dose Results for 100,000 Years

The peak groundwater pathway doses associated with the sensitivity run radionuclides are calculated for 100,000 years so that the dose behavior past the compliance period can be evaluated (Appendix D contains 100,000 year curves for the 100-meter radionuclide concentrations for all of HTF). These peak groundwater pathway doses are the total dose associated with every MOP 100-meter pathway identified in Section 5.4. Figure 5.5-13 shows the peak 100-meter groundwater pathway doses over time for 100,000 years for the six 100-meter sectors.

Figure 5.5-13: MOP at 100m Peak Groundwater Pathway Dose Results within 100,000 Years for the 100m Sectors

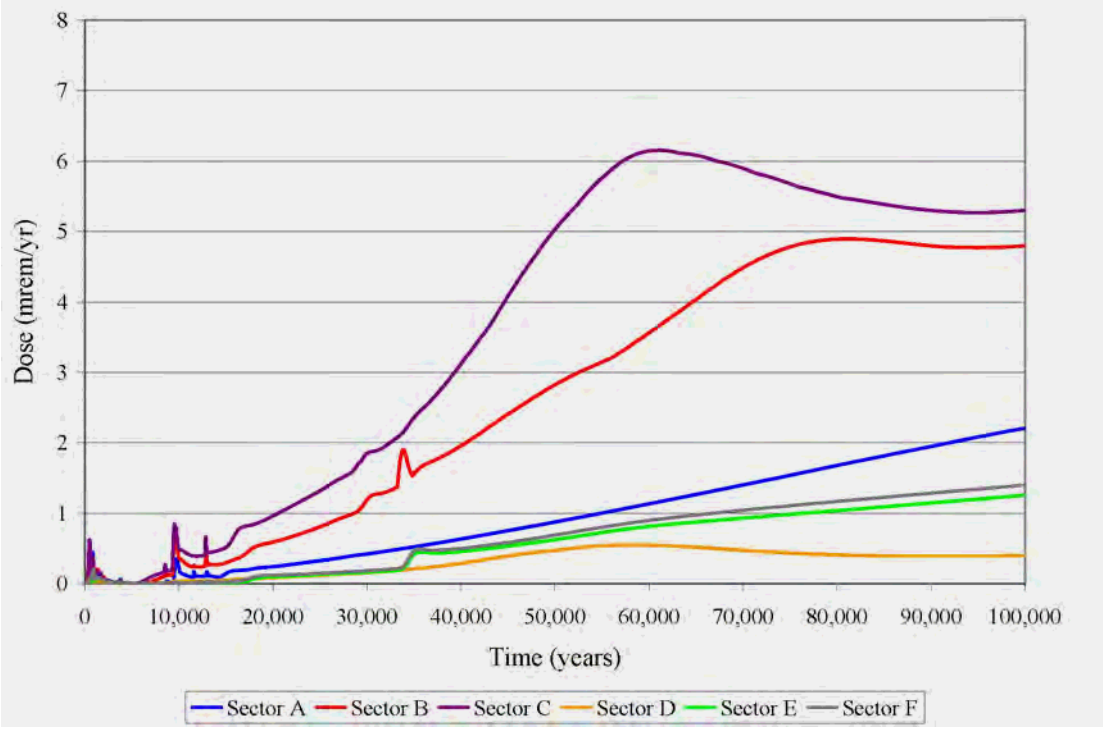

The approximate peak dose from Sector A is 6.2 mrem/yr at year 61,190 and is associated with Ra-226 (49% of the dose) and Pu-239 (44% of the dose). The long-term Ra-226 doses are driven by releases of slow-moving parent radionuclides with long half-lives. The dose peak is primarily associated with radionuclides with very long transport times (e.g., Pu-239) released from Type II and Type IV tanks.

The magnitude of this peak is conservative (higher than expected) due to the simplifying model assumption that all of the waste tanks of a given waste tank type fail simultaneously, which is considered unlikely to occur.

5.5.2 MOP at Stream Groundwater Pathway Dose Results

The peak groundwater pathway doses for two stream seeplines (Fourmile Branch and UTR) are calculated using the highest concentration for each radionuclide in the seepline sector (a discussion of how peak concentrations are determined by sector is provided in Section 5.2). In calculating the peak groundwater pathway dose, the highest radionuclide concentration is used from each of the distinct aquifers modeled (the UTR-UZ, UTR-LZ, and the Gordon Aquifer) for the two seepline sectors. The concentration for each aquifer represents peak concentration in any vertical computational mesh within the aquifer. The mesh vertical thicknesses (heights) in the computational model are less than 10 feet in the UTR-UZ, and less than 15 feet in the UTR-LZ. No well screen averaging was used in determining the concentrations for dose calculations because the typical well screen length of 20 feet is approximate to the computational mesh height. As discussed in Section 4.2.3.1.2, the stream dose analysis assumes direct ingestion of water from the stream location with no stream

dilution assumed. These peak groundwater pathway doses are the total dose associated with all the individual MOP stream pathways identified in Section 5.4.

5.5.2.1 MOP at Stream Peak Annual Dose

Table 5.5-7 presents a comparison of the MOP stream peak groundwater pathway doses for the two sectors. The peak groundwater pathway dose in the 10,000-year compliance period is associated with the Fourmile Branch. Figure 5.5-14 presents the peak groundwater pathway doses over time during the compliance period (10,000 years) for the two streams of concern (UTR and Fourmile Branch). The MOP at the stream peak groundwater pathway dose in the 10,000-year compliance period is a 0.047 mrem/yr groundwater pathway dose at year 740. Figure 5.5-15 presents the peak groundwater pathway stream doses within 20,000 years.

Table 5.5-7: MOP at Stream Peak Groundwater Pathways Dose

Stream[a]	Peak Dose in 10,000 Years[b]	Principal Radionuclides	Principal Pathways
Fourmile Branch	**0.047 mrem/yr (year 740)**	Tc-99 (~100%)	Water Ingestion (51%) Fish Ingestion (27%) Vegetable Ingestion (17%)
UTR	**0.018 mrem/yr (year 900)**	Tc-99 (~100%)	Water Ingestion (51%) Fish Ingestion (27%) Vegetable Ingestion (17%)

a Stream seeplines illustrated in Figure 5.2-6.
b For both streams, the 20,000 year peak dose occurs within 10,000 years of closure.

Figure 5.5-14: MOP at Stream Peak Groundwater Pathway Dose within 10,000 Years

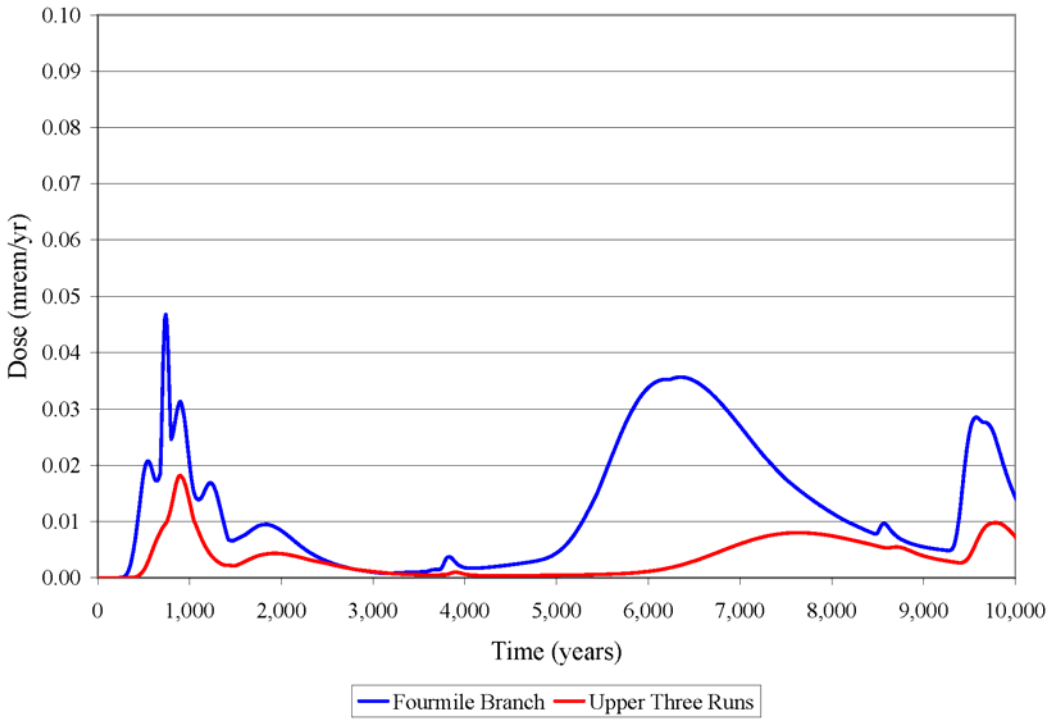

Figure 5.5-15: MOP at Stream Peak Groundwater Pathway Dose within 20,000 Years

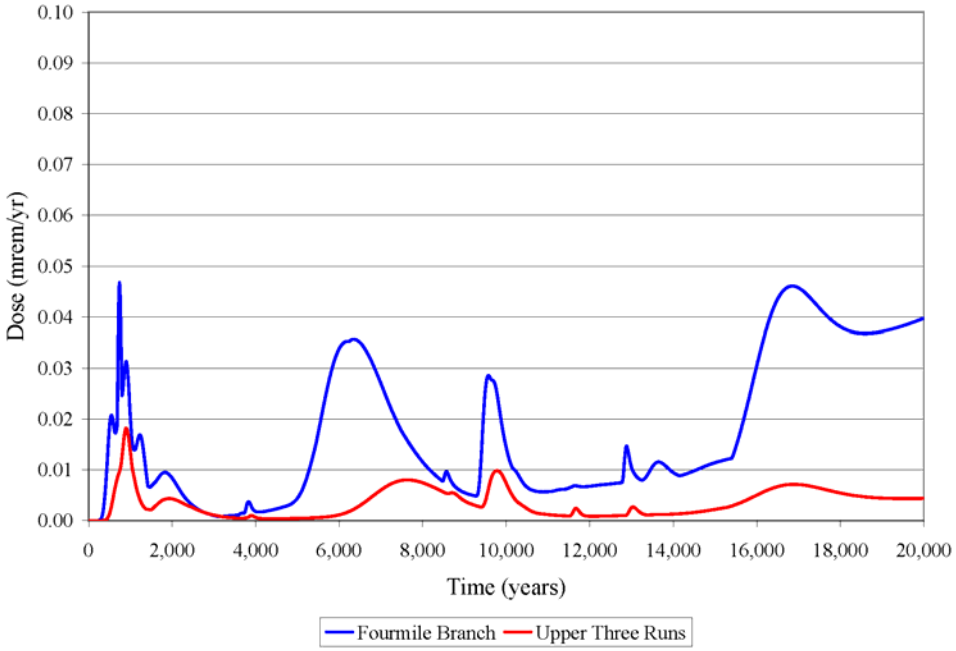

Figures 5.5-16 and 5.5-17 show the relative contribution from individual radionuclides to the groundwater pathway MOP dose at the stream within 20,000 years (Fourmile Branch and UTR, respectively).

Figure 5.5-16: Individual Radionuclide Contributors to the Fourmile Branch Groundwater Pathway Dose - 20,000 Years

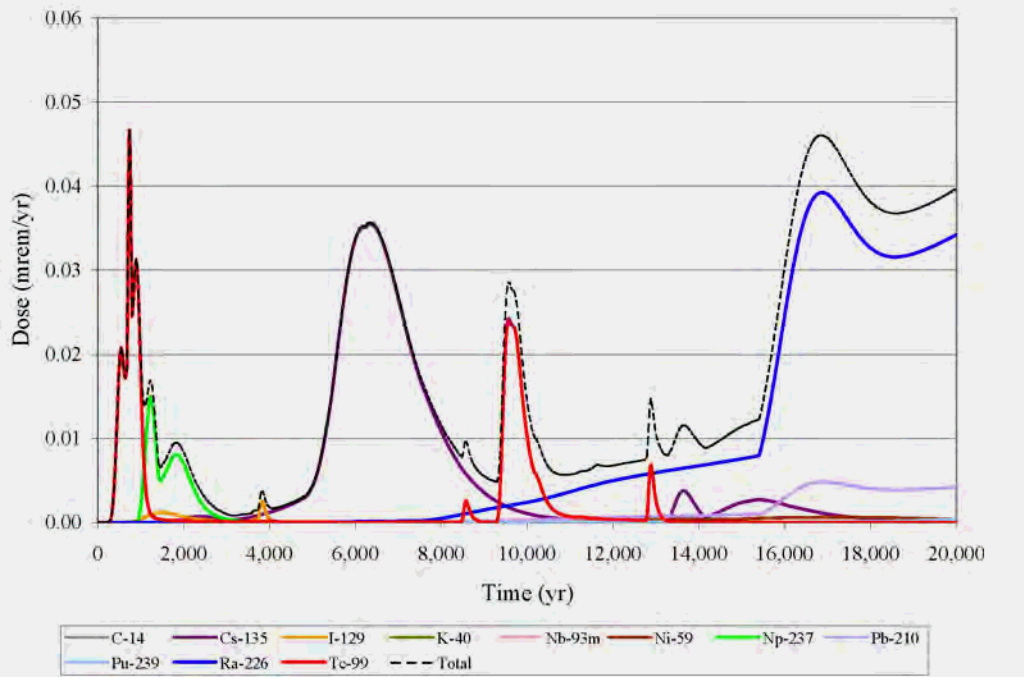

Figure 5.5-17: Individual Radionuclide Contributors to the UTR Groundwater Pathway Dose - 20,000 Years

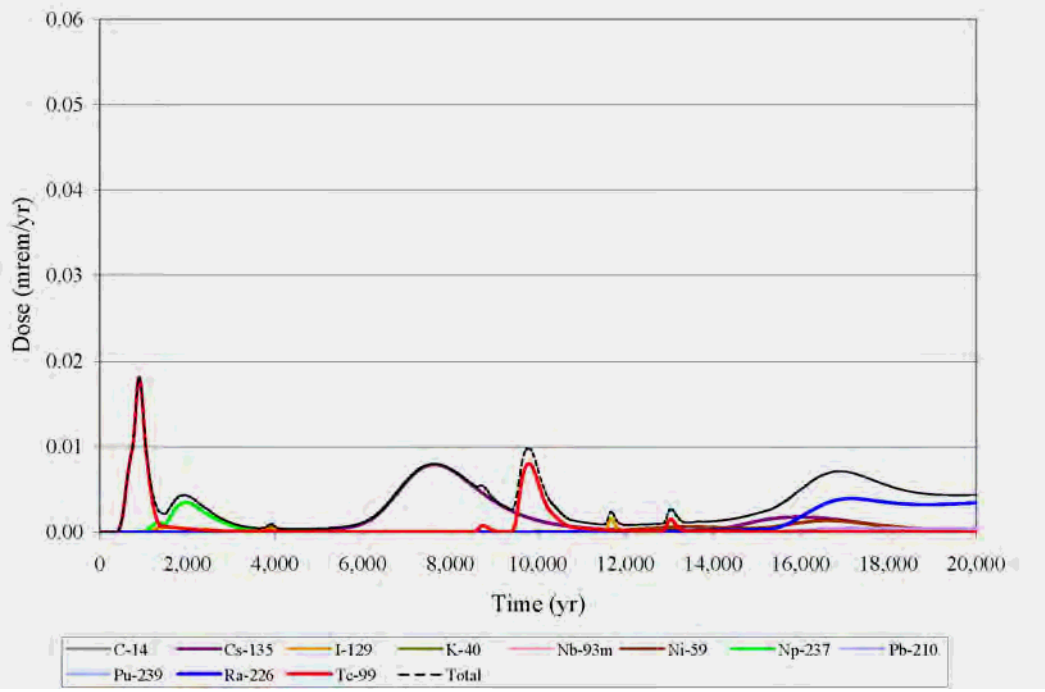

5.5.2.2 MOP at Stream Individual Pathway Contributors

Table 5.5-8 presents the relative contributions from the individual groundwater pathways to the Fourmile Branch MOP receptor dose at 740 years (the year of the peak Fourmile Branch dose). The primary contributors are water ingestion (51%), followed by fish ingestion (27%), and vegetable ingestion (17%). Table 5.5-9 presents the relative contributions from the individual groundwater pathways to the UTR MOP receptor dose at 900 years (the year of the peak UTR dose). The primary contributor to the UTR peak is water ingestion (51%), followed by fish ingestion (27%), and vegetable ingestion (17%).

Table 5.5-8: MOP at Stream Peak Groundwater Pathway Dose Individual Contributions for Fourmile Branch

Pathway	Associated Contribution at year 740 (mrem/yr)	Percentage of Total Peak Dose	Principal Radionuclide Pathway Dose
Water Ingestion	0.024	51%	Tc-99 (~100%)
Fish Ingestion	0.013	27%	Tc-99 (~100%)
Vegetable Ingestion	0.008	17%	Tc-99 (~100%)
All Others	0.002	5%	N/A
TOTAL	**0.047**	**100**%	

Table 5.5-9: MOP at Stream Peak Groundwater Pathway Dose Individual Contributions for UTR

Pathway	Associated Contribution at year 900 (mrem/yr)	Percentage of Total Peak Dose	Principal Radionuclide Pathway Dose
Water Ingestion	0.0093	51%	Tc-99 (~100%)
Fish Ingestion	0.0050	27%	Tc-99 (~100%)
Vegetable Ingestion	0.0032	17%	Tc-99 (~100%)
All Others	<0.001	5%	N/A
TOTAL	**0.021**	**100** %	

5.5.3 MOP All-Pathway Dose Results

The purpose of this section is to present the total all-pathway peak doses for both the MOP at 100 meters and the MOP at the stream. The total all-pathway doses include both the groundwater and air pathway contributors. As calculated in Section 5.3, the air pathway dose is negligible; therefore, the all-pathway dose is the same as the groundwater pathway dose. Figure 5.5-18 presents the all-pathway dose to the MOP at the 100-meter sectors.

Figure 5.5-18: MOP Peak 100m Sector All-Pathway Dose within 10,000 Years

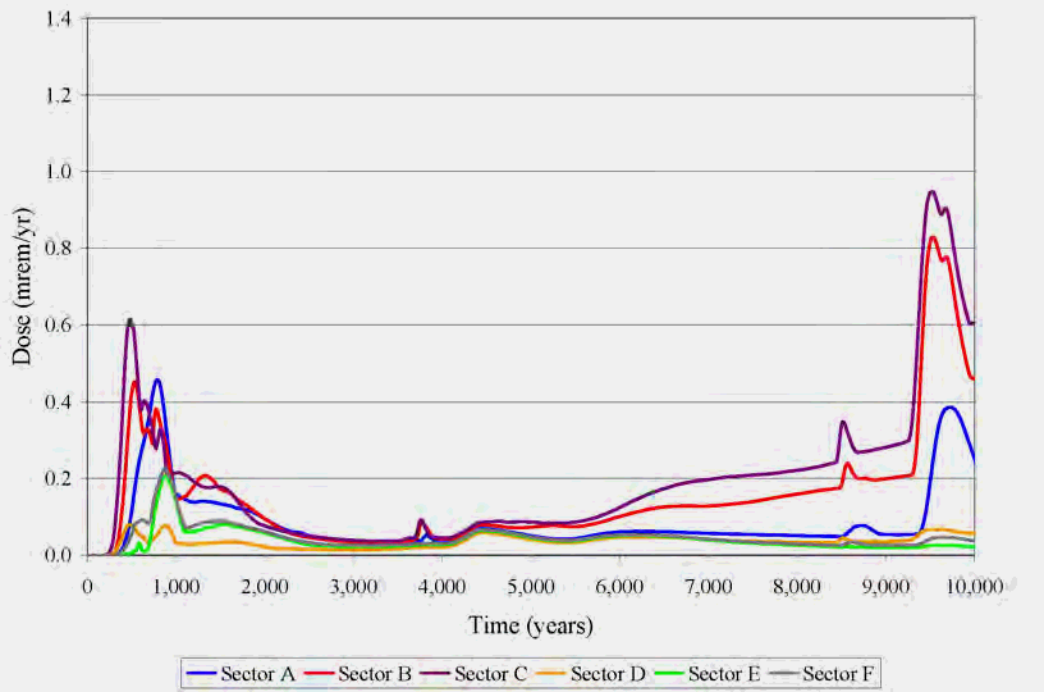

5.6 Uncertainty and Sensitivity Analyses

The purpose of the UA/SA is to consider the effects of uncertainties in the conceptual models used and examine model sensitivity to the parameters used in the mathematical models. This evaluation was conducted for analyses related to the MOP as well as those related to inadvertent intruders. These evaluations focused on key uncertainties and key sensitivities identified during modeling.

The UA/SA were primarily performed using a probabilistic model (i.e., the HTF GoldSim Model), as discussed in Sections 5.6.1 through 5.6.5. Section 5.6.1 summarizes the purpose, the key assumptions, and the approach used to develop the HTF GoldSim Fate and Transport Model (e.g., referred to as the HTF GoldSim Model, stochastic model, or probabilistic model). The abstracted probabilistic model is benchmarked against the deterministic HTF PORFLOW Model in Section 5.6.2. Section 5.6.3 identifies and defines the stochastic parameters applied in the probabilistic model. The analysis to evaluate how the uncertainty in model input parameters is propagated through the model to the selected model results, or endpoints, is detailed in Section 5.6.4. Section 5.6.5 documents the sensitivity analyses, which identifies the stochastic model input parameters most influential in determining the results (e.g., concentrations and potential dose). The barrier analyses documented in Section 5.6.6 compares the fluxes beneath the containment structures for several deterministic PORFLOW simulations, each representing a different barrier failure mode. The objective of this section is to evaluate the barrier's importance to releases to the saturated zone. Section 5.6.7 compares the deterministic PORFLOW Base Case dose time histories to the alternative Cases B through E, and to the no closure cap case.

The probabilistic model allows for varying multiple parameters simultaneously, so concurrent effects of changes in the model can be analyzed, and the potential impact of changes can be assessed. This assessment allows for identification of parameters that are only of significance when varied simultaneously with another parameter. The deterministic model single parameter analysis provides a method to evaluate parametric effects in isolation, so the importance of the uncertainty around a parameter of concern can be more effectively evaluated. Using both probabilistic and deterministic models for sensitivity analyses versus a single approach provides additional information concerning which parameters are of most importance to the HTF model.

5.6.1 Uncertainty and Sensitivity Analyses using Probabilistic Modeling

Uncertainty is inherent in simplified numeric models that attempt to replicate engineered or natural systems. Different types of uncertainty exist in modeling complex systems: uncertainty in possible future outcomes, uncertainty in the consequences of future outcomes, and uncertainty in the parameters used as input to these models. The objective of the probabilistic model is to provide the vehicle to quantify parameter uncertainty explicitly as a probability in order to bound the range of possible receptor dose outcomes, and to enable identification of those parameters strongly influencing dose.

5.6.1.1 HTF GoldSim Stochastic Fate and Transport Model

A probabilistic model was constructed to replicate fate and transport of HTF contaminant releases modeled using PORFLOW, in order to characterize parameter uncertainty and sensitivity (see Section 5.6.2 on benchmarking). The probabilistic model is necessarily

simpler than the PORFLOW groundwater model in its environmental transport calculations, but includes additional calculations that cannot be performed in PORFLOW. The probabilistic model is described in more detail in Section 4.4.4.2 and in the report *H-Area Tank Farm Stochastic Fate and Transport Model*. [SRR-CWDA-2010-00093]

The probabilistic model, developed using the GoldSim systems analysis software, accepts uncertainty and variability in the input parameters, the values of which can be defined using probability distributions. If a given model input (e.g., the porosity of sandy soil) is given a distribution, or range of values, then this distribution is sampled in the collection of Monte Carlo runs that constitutes a probabilistic analysis. The collective uncertainty of all stochastic (probabilistic) inputs is reflected in the range and distribution of modeled results, such as water concentrations or dose to hypothetical future human receptors. If an input parameter is given no range of input values, that is, if it is defined deterministically, then it contributes nothing to the overall uncertainty in the results. Few parameters have zero uncertainty. An example of a parameter without a defined range is the half-life of radionuclides.

Results for the HTF GoldSim Model uncertainty analyses are discussed in Section 5.6.4. Adopting a probabilistic approach also allows analysts to determine which model input parameters are the most significant to the results. This is done through sensitivity analyses, which identifies covariance between model inputs and results. Section 5.6.5 discusses the model sensitivity analyses.

5.6.1.2 HTF GoldSim Model Assumptions

A number of assumptions are necessary when simplifying complex engineered and natural systems for modeling purposes. The key model assumptions for the probabilistic model are summarized below:

Inventory Assumptions:

- The transfer line inventory used to calculate the "Drill-Cuttings" concentration for the acute and chronic intruder dose calculations is a projected inventory. [SRR-CWDA-2010-00023]

Transport Assumptions:

- At the intersection of PORFLOW stream traces and the 100-meter boundary surrounding the HTF, a line of hypothetical evaluation wells are located (See Figure 4.4-56 in Section 4.4.4.2). These evaluation wells are grouped based on their location in Sectors A through E. These "100-meter wells" are a point at which contaminant concentrations are evaluated for use in dose calculations compared with relevant performance measures. The assumption was made that contaminant transport distance is equal to the distance between the contaminant sources and these 100-meter wells along the stream trace.
- The MOP and intruder dose calculations require as input the contaminant concentration in the stream (Table 4.4-11, Section 4.4.4.2) to calculate the dose to the receptor from certain activities (e.g., fishing, swimming, and boating). The probabilistic model does not explicitly calculate stream concentrations. The

probabilistic model estimates the concentration of contaminants in the stream by applying a species dependent ratio to the GoldSim calculated concentration at the 100-meter well. This ratio is the ratio between the PORFLOW stream (e.g., seepline) concentrations for each radionuclide to the PORFLOW 100-meter well concentrations. Applying these ratios to estimate the stream concentrations is reasonably conservative because the water in the stream pathways would be subject to stream dilution, however, this is not accounted for when the raw seepline concentration from PORFLOW is used. Therefore, the ratio, which is based on the raw seepline concentration from PORFLOW, does not account for stream dilution. The calculation of this ratio is documented in Appendix F.1.

Dose Calculator Assumptions:

- The chronic intruder (Section 6.3) resides next to a Type I tank (Tank 11) and uses water from a well, drilled 1 meter from this waste tank. This waste tank was selected because it has high Tc-99 and Ra-226 releases to the saturated zone, and was considered a conservative representation of other waste tanks.
- The "Drill-Cuttings" concentration used in the acute and chronic intruder dose calculations assume the intruder drills into a 3-inch transfer line.

5.6.2 GoldSim Benchmarking

The HTF PORFLOW Model is a 3-D flow and transport model designed to simulate rigorously the transport and fate of radionuclides and non-radioactive species released from waste tanks and associated ancillary equipment located in the HTF. The HTF GoldSim Model is an abstraction of the HTF PORFLOW Model designed to perform UA/SA that would be prohibitive using a computationally intensive model like the HTF PORFLOW Model. The HTF PORFLOW Model is a deterministic model, in that it assumes single values for parameters used in the flow and transport calculations. One of the drawbacks to this type of model is that the selected parameter value may be conservative in most situations but under a unique set of conditions, the "conservatism" may actually force a non-pessimistic result. The HTF GoldSim Model offers the ability to test the sensitivity of the system to a range of parameter values. Therefore, the HTF GoldSim Model is necessarily a simplification of the HTF PORFLOW Model.

In abstract, spatially averaged flow rates from the HTF PORFLOW Model were used as input to the HTF GoldSim Model and controlled the transport of radionuclides and non-radioactive species through a simplified assemblage of the containment features (e.g., liner, basemat). While 3-D flow can take place within the containment structures, the HTF GoldSim Model is limited to 1-D flow through these features. In the saturated zone, the complex 3-D PORFLOW flow fields are represented by 1-D flow along PORFLOW generated stream traces. The 1-D GoldSim flow paths emanate from the upgradient edge of the containment feature's footprint and are broken down into two sections linked in series, one under the footprint where unsaturated zone releases are applied and one representing the remainder of the saturated zone outside the footprint. In the saturated zone, the timing of concentration breakthrough curve peaks generated by PORFLOW (for a conservative tracer) and the stream trace lengths were used to determine the flow velocities along the stream traces. For a more detailed description of the abstracted model, refer to Section 4.4.4.2.

The section presented below describes the process used to evaluate how well the GoldSim abstraction replicates the HTF PORFLOW Model. This process is referred to as "benchmarking" and is done to ensure the validity of the GoldSim abstraction. This is necessary to provide justification for the assumption that when the HTF GoldSim Model is simulated stochastically (e.g., multi-realizations are performed to test ranges of variable values), the results approximate the results of the HTF PORFLOW Model. Although key results of this evaluation are presented here, the detailed results can be found in the report, *H-Area Tank Farm Stochastic Fate and Transport Model* (SRR-CWDA-2010-00093).

5.6.2.1 Benchmarking Process Description

In the benchmarking effort, PORFLOW/GoldSim comparisons were performed in three phases. The first phase focuses on how well the abstraction model approximates the radionuclide releases from the waste tanks and ancillary equipment. The radionuclide releases to the saturated zone are used for this comparison, and are referred to below as "vadose zone mass release." The second phase focused on how well the abstraction model approximated the radionuclide transport behavior in the saturated zone. The radionuclide concentrations at a set of observation wells are examined for this task; these are referred to as the 100-meter observation well concentrations. The third phase compared PORFLOW dose results with GoldSim dose results, evaluating how well the timing and magnitude of the time histories matched. This third step verified that the physical and radiological processes controlling radionuclide transport were translated to the dose results, which is the metric used to evaluate whether HTF meets the dose performance objectives.

The benchmarking evaluation was conducted for Case A (e.g., Case A or Base Case) results, as well as for the alternative results (Case B through Case E). Table 4.4-1 (in Section 4.4.2) presents a summary of the various waste tank cases modeled.

The HTF modeling effort included five different modeling cases, 47 different source release locations, 6 different waste tank types (counting "no liner" waste tanks separately), 80-modeled radionuclides, and 28 hypothetical observation wells. A comparison of results for every radionuclide, at all locations for every scenario would be quite extensive. A selection process was devised to narrow the number of comparisons required, but would still ensure adequate model representation.

5.6.2.1.1 Representative Contaminant Sources

Of the 29 waste tanks in the HTF, nine representative waste tanks were selected for evaluation dependent on waste tank type, differences in environment or other considerations. The Table 5.6-1 summarizes the selected waste tanks and the rationale for their selection. A single ancillary equipment location was selected for each ancillary equipment unit type. Table 5.6-2 lists the representative ancillary equipment locations.

Table 5.6-1: Summary of Selected Waste Tanks

Representative Waste Tank	Waste Tank Type	Initial Liner Failed	Additional Reason for Inclusion?
Tank 9	Type I	N	N/A
Tank 12	Type I	Y	N/A
Tank 13	Type II	N	N/A
Tank 15	Type II	Y	N/A
Tank 16	Type II	Y	Initial inventory in the secondary sand pad
Tank 24	Type IV	N	N/A
Tank 31	Type III	N	N/A
Tank 36	Type IIIA	N	Located on west side of HTF
Tank 40	Type IIIA	N	Located on east side of HTF

N/A = Not Applicable

Table 5.6-2: Summary of Selected Ancillary Equipment

Representative	Type
HPT-7	Pump Tank
242-25H	Evaporator
Transfer Line Zone 3 or HTF-T-Line3	Transfer Line

5.6.2.1.2 Representative Radionuclides

Of the 80 radionuclides modeled in GoldSim, five were selected for the benchmarking comparison (Ra-226, Tc-99, I-129, Cs-135, and Np-237). Evaluation of individual radionuclides, as opposed to total dose, is important because each radionuclide behaves differently in the engineered and natural system. Because the HTF GoldSim Model is trying to replicate the transport system, evaluating individual radionuclides provides validation that the different modeling components are responding appropriately. Based on results from PORFLOW, the main contributors to total dose within 20,000 years include Ra-226 and Tc-99 (See Section 5.5, Table 5.5-2). These radionuclides were included in the benchmarking evaluation for this reason, but also because they (or their parent radionuclide) are affected by solubility controls in GoldSim.

The HTF GoldSim Model handles the influence of solubility limits in a more refined manner than PORFLOW. In the GoldSim simulations, all isotopes of uranium, for example, are considered simultaneously in the analysis. This means that GoldSim sums the concentration for each isotope of uranium together and evaluates if the solubility limit is reached at each time step. If the summed uranium concentration is higher than the solubility limit, uranium will precipitate out, thus limiting the amount of uranium released to the saturated zone. In the PORFLOW simulations, the isotopes are not summed together, but are considered separately for the duration of the simulation. PORFLOW therefore, is more likely to overestimate the mass released from the CZ. [SRS-REG-2007-00002, Section 5.6.2.1.2]

Because their transport is not subject to solubility control, Cs-135 and I-129 were chosen as benchmarking species. In the unsaturated zone, Cs-135 is more strongly sorbed than I-129, therefore they were both included for comparison. Because it is strongly sorbed to cementitious material and only slightly sorbed to soils in the unsaturated zone, Np-237 was selected.

5.6.2.1.3 Representative Observation Wells

Of the 28 observation wells, five were selected based on their proximity to the centerline of the PORFLOW generated stream traces, and their relative importance to peak dose. The observation wells used for the comparison are A3, B1, C2, E5, and F3 and are shown in Figure 4.4-56 (in Section 4.4.4.2).

5.6.2.2 Benchmarking Results

The Base Case represents what is considered the most likely scenario for the time-based degradation of the waste tank structure, including the degradation of the cementitious materials and the steel liner. For brevity, this section presents the Base Case mass release results for Tanks 9 (submerged Type I, no initial liner damage), 12 (submerged Type I, initial liner failed), 13 (submerged Type II, no initial liner damage), 24 (Type IV, no initial liner damage) and the saturated zone concentrations at Observation Well A3 only. In addition, to show the applicability of the HTF GoldSim Model for the other cases, total dose time history comparisons are presented for Cases A, D, and E. To review all benchmarking results, refer to SRR-CWDA-2010-00093. Note that the mass releases from waste tanks as presented here represent the source terms applied to the saturated zone. Their determination includes the influence of transport in the unsaturated zone for non-submerged waste tanks.

5.6.2.2.1 Tank 9 Mass Release from a Type I Tank with Intact Liner

Tank 9 is a submerged Type I tank with an initially intact liner that failed at year 11,397. Figures 5.6-1 through 5.6-5 display PORFLOW/GoldSim comparison plots of the mass released (mole per year) from Tank 9 for the following radionuclides, Ra-226, Tc-99, I-129, Np-237, and Cs-135. The curves indicate that the HTF GoldSim Model reproduces the HTF PORFLOW Model releases extremely well.

Figure 5.6-1: Mass Release from Type I Tank 9 - Ra-226 (Case A)

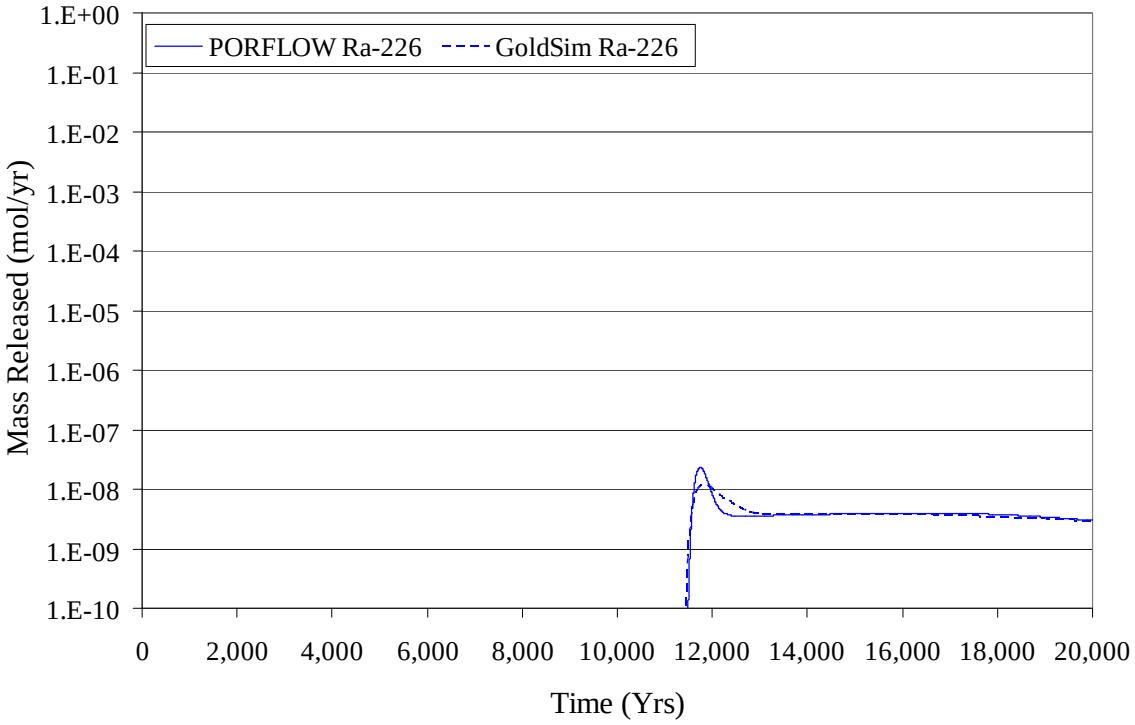

Figure 5.6-2: Mass Release from Type I Tank 9 - Tc-99 (Case A)

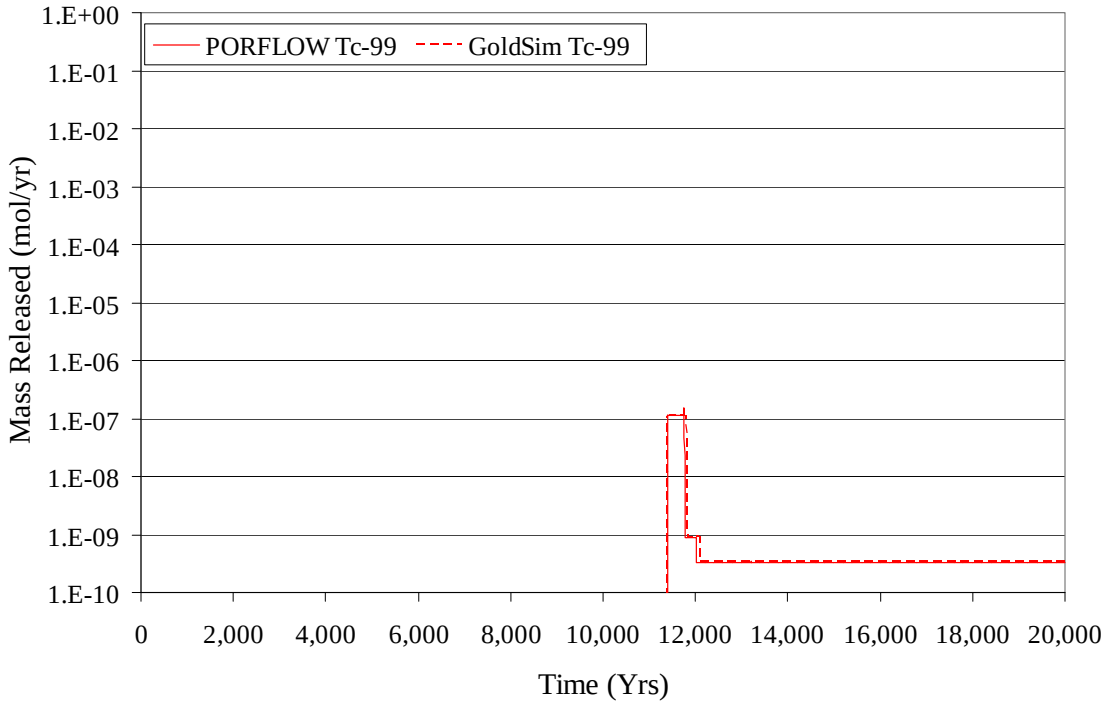

Figure 5.6-3: Mass Release from Type I Tank 9 - I-129 (Case A)

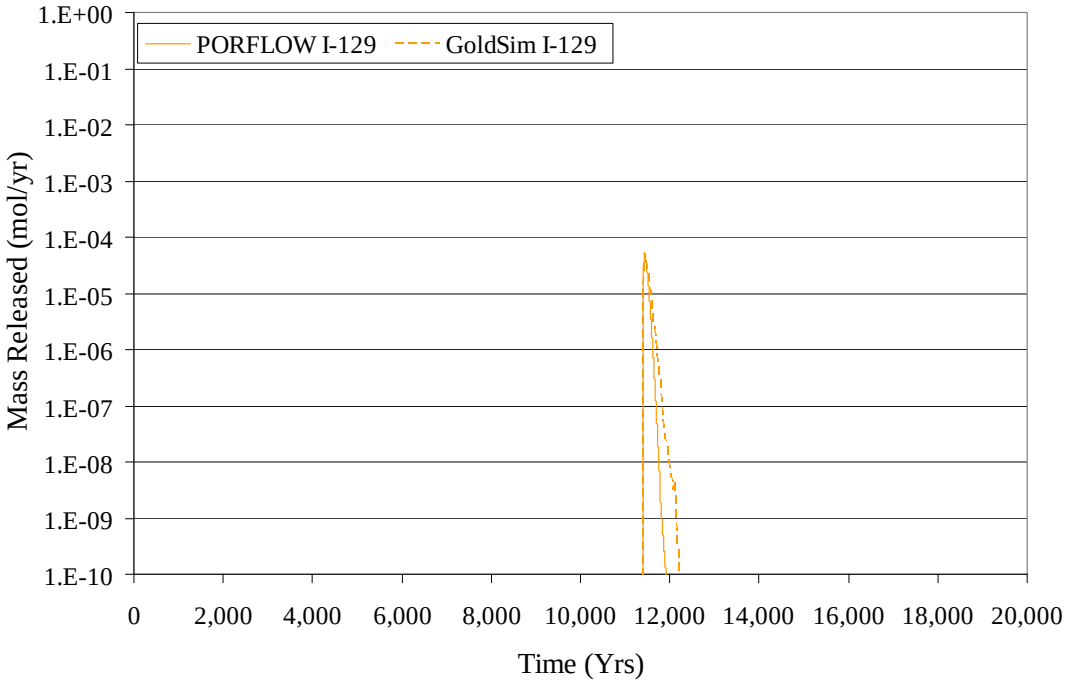

Figure 5.6-4: Mass Release from Type I Tank 9 - Np-237 (Case A)

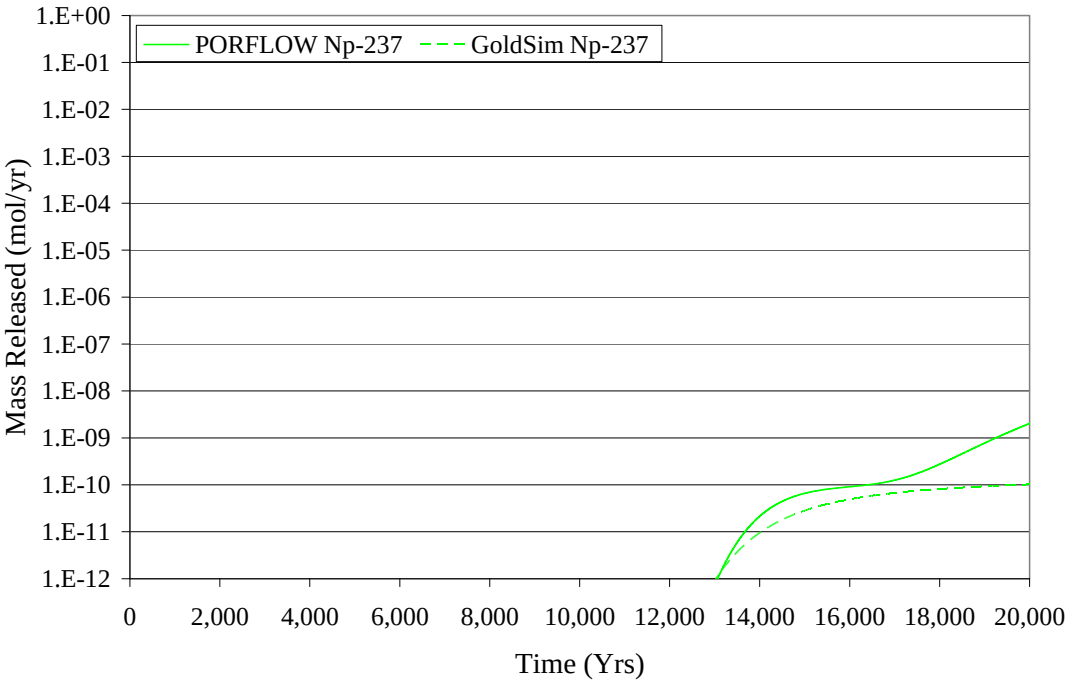

Figure 5.6-5: Mass Release from Type I Tank 9 - Cs-135 (Case A)

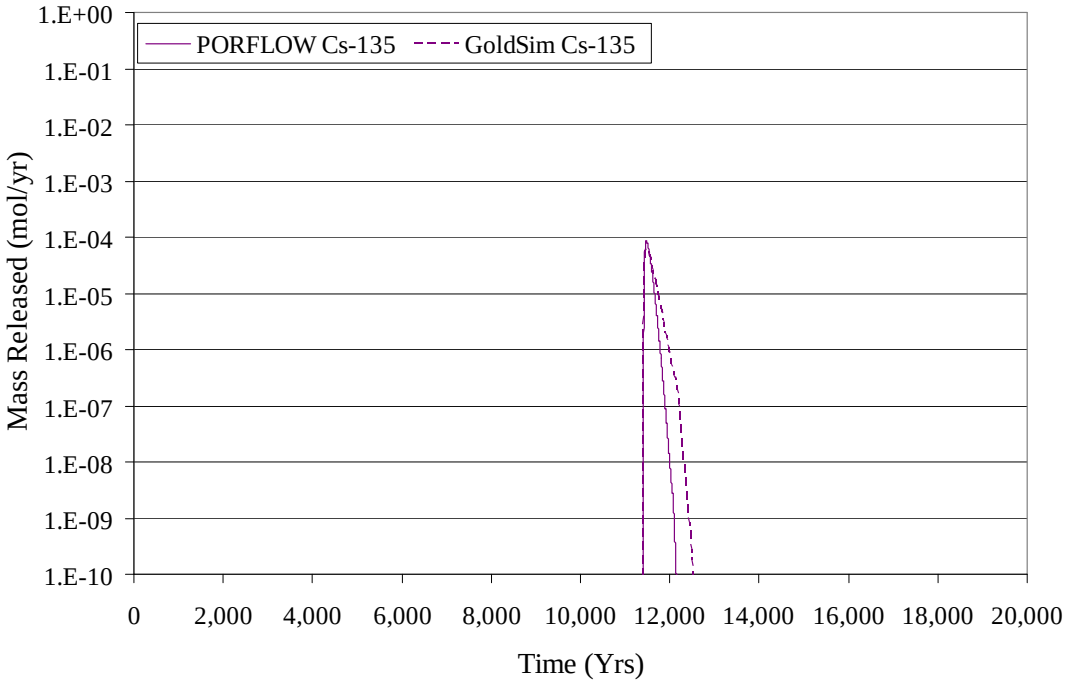

The close match between the curves representing Tank 9 Ra-226 releases (Figure 5.6-1) is significant because it indicates GoldSim also adequately represents the transport of the parents of Ra-226. The initial inventory of Ra-226 is relatively small. The majority of Ra-226 is generated through in-growth from the Pu-238→U-234→Th-230→Ra-226 chain making the initial inventory of Pu-238 important to the dose results and not the initial inventory of Ra-226.

In addition to being a major dose contributor, Tc-99 is strongly controlled by solubility limits. As Figure 5.6-2 illustrates, the GoldSim Tc-99 release overlies the PORFLOW release, indicating that the solubility control associated with the CZ is being accurately approximated in the HTF GoldSim Model.

Both the timing and the magnitude of the PORFLOW I-129 peak release displayed in Figure 5.6-3 are similar to the GoldSim results. The match is especially good at the higher concentrations. Note that the GoldSim results show a greater degree of numerical dispersion. Even though dispersion is not explicitly simulated in the GoldSim waste tank models, numerical dispersion associated with the use of mixing cells is implicit to the HTF GoldSim Model. [SRR-CWDA-2010-00093, Section 3.4]

Neptunium releases from Tank 9 are plotted in Figure 5.6-4 and are very low (< 1.0E-10 mol/yr for the GoldSim results) with the PORFLOW results showing an earlier breakthrough after 16,000 years.

Because its transport is not subject to solubility control and it is more strongly sorbed than I-129 in the unsaturated zone, Cs-135 was chosen as a benchmarking species. Figure 5.6-5 shows that there is a good match between the PORFLOW results and the GoldSim results for Cs-135 releases from Tank 9. The match is especially good at the higher concentrations.

5.6.2.2.2 Tank 12 Mass Release from a Type I Tank with Initial Liner Damage

Tank 12 is a submerged Type I tank with initial liner damage that is simulated as complete liner failure at the start of the simulation. Figures 5.6-6 through 5.6-10 display PORFLOW/GoldSim comparison plots of the mass released (mol/yr) from Tank 12 for the following radionuclides, Ra-226, Tc-99, I-129, Np-237, and Cs-135.

Figure 5.6-6: Mass Release from Type I Tank 12 - Ra-226 (Case A)

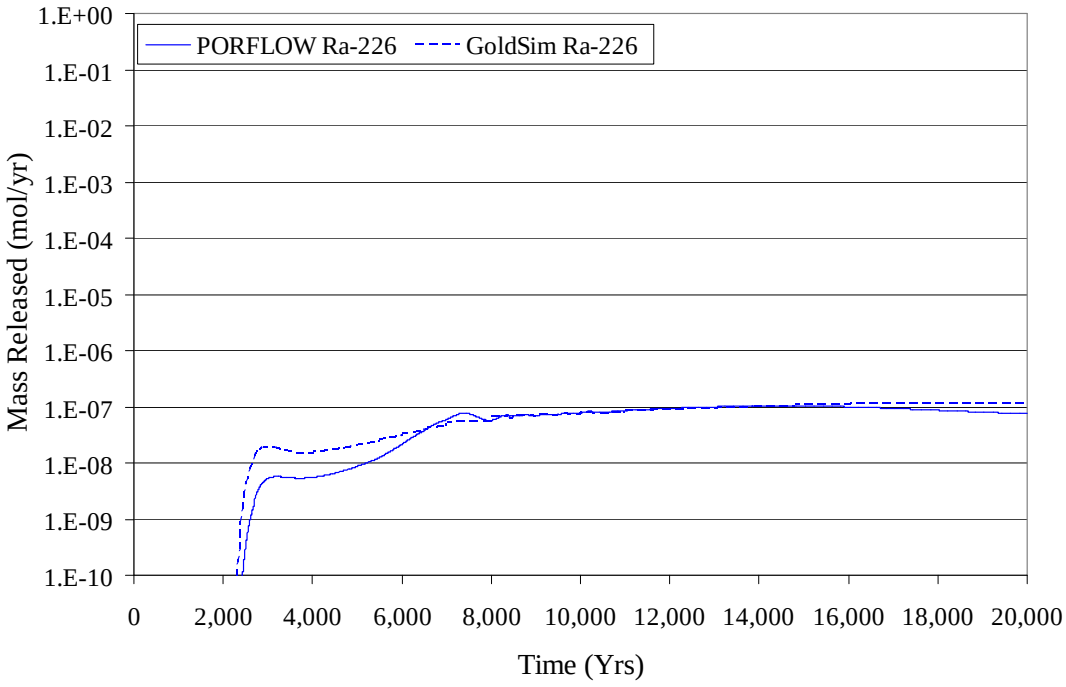

Figure 5.6-7: Mass Release from Type I Tank 12 - Tc-99 (Case A)

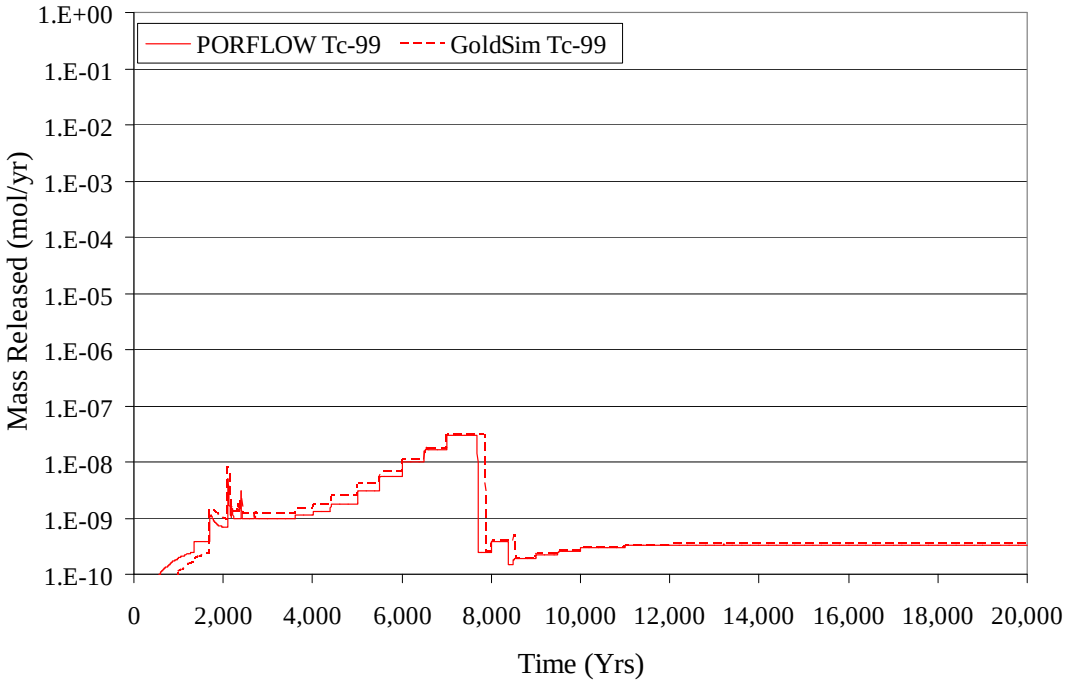

Figure 5.6-8: Mass Release from Type I Tank 12 - I-129 (Case A)

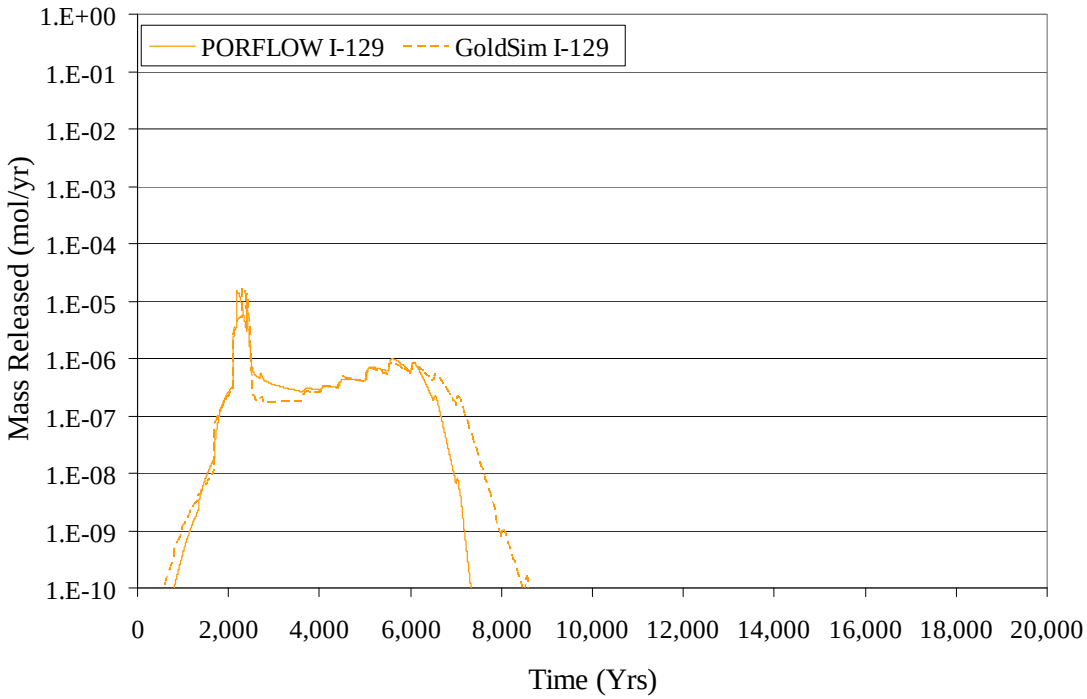

Figure 5.6-9: Mass Release from Type I Tank 12 - Np-237 (Case A)

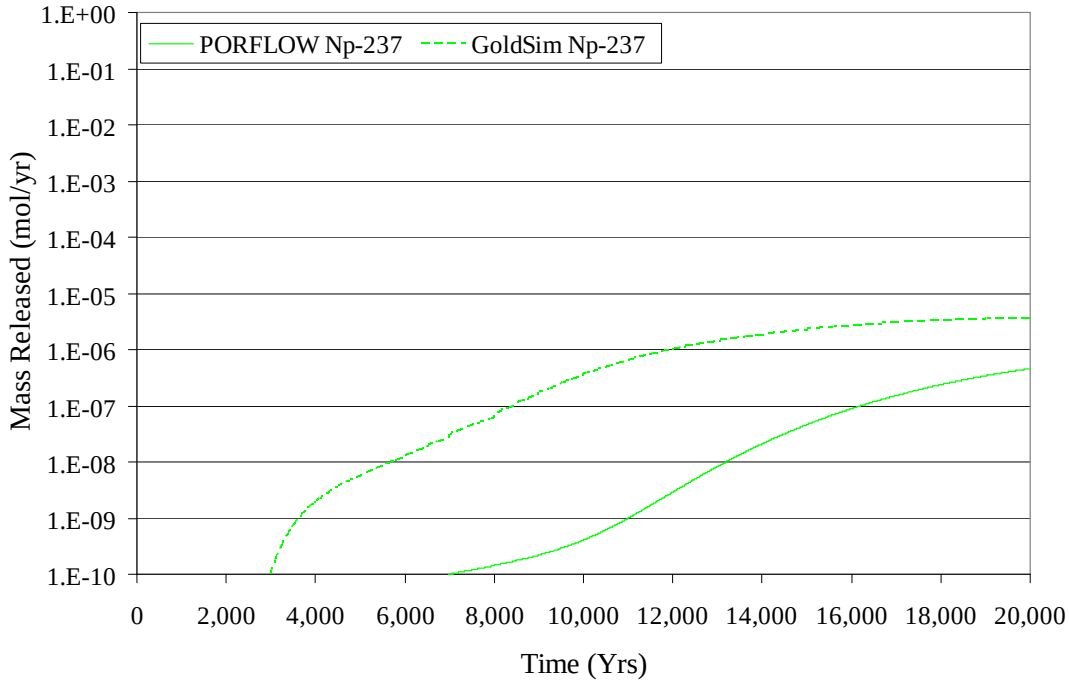

Figure 5.6-10: Mass Release from Type I Tank 12 - Cs-135 (Case A)

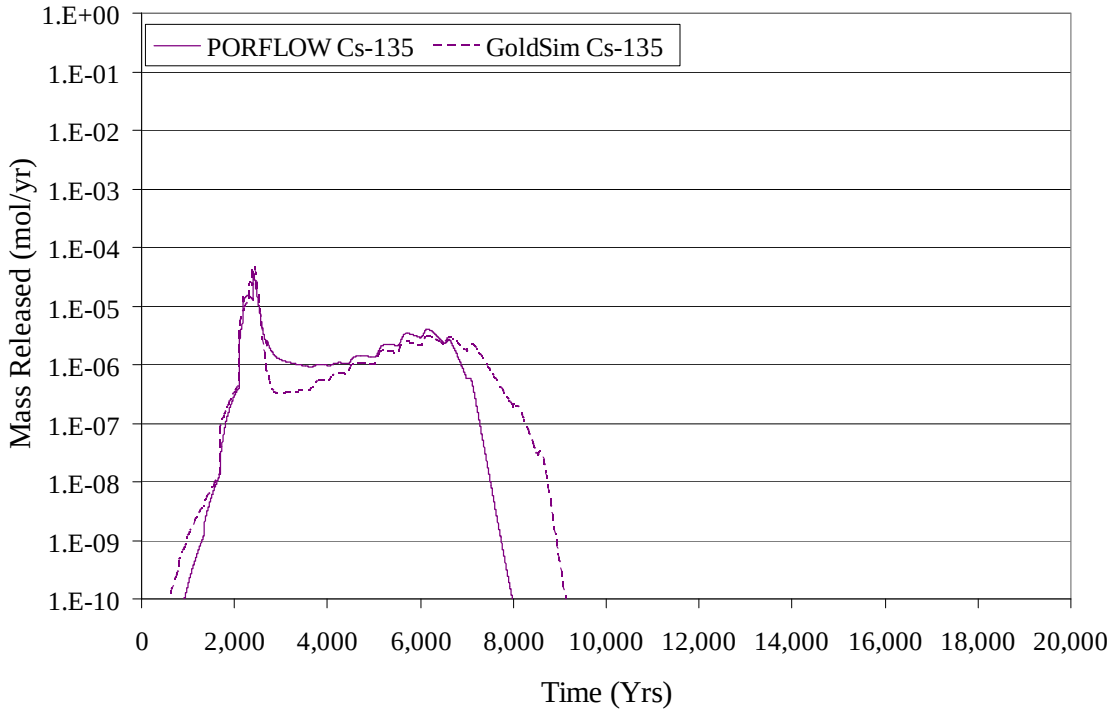

Figure 5.6-6 plots Tank 12 Ra-226 releases from PORFLOW and GoldSim. In the early years of the simulation and the later years, the HTF GoldSim Model overestimates the Ra-226 release, but the general trend of the release matches well between the two models.

As Figure 5.6-7 illustrates, the GoldSim Tc-99 release overlies the PORFLOW release, indicating that the solubility control associated with the CZ is being accurately approximated in the HTF GoldSim Model for the Type I tank. The more subtle changes in plateau levels reflect the changes in PORFLOW flow rates in conjunction with constant solubility limits. The dramatic decrease in the release rate of Tc-99 at year 7,690, for the PORFLOW simulation (7,840 years for the GoldSim simulation), reflects the transition of the waste tank grout and CZ from submerged Condition C (Reducing Region II), where Tc-99 has a high solubility limit, to submerged Condition D (Oxidizing Region II), where Tc-99 has a lower solubility limit. Dropping the solubility limit forces Tc-99 to precipitate, thus reducing the dissolved concentrations in the CZ and the associated releases.

Both the timing and the magnitude of the PORFLOW I-129 peak release displayed in Figure 5.6-8 are similar to the GoldSim results. The match is especially good at the peak concentrations, which occur between 2,000 and 2,500 years and correspond to the chemical transition of the concrete basemat from Oxidized Region II to Oxidized Region III. Iodine has a greater affinity to sorb to cementitious materials under the Region II conditions (I-129 K_d = 14 mL/g) than under Oxidized Region III conditions (I-129 K_d = 4 mL/g), therefore the transition results in peak I-129 release rates. The similarities in the curves indicate that GoldSim replicates the sorption processes in the cementitious materials for this radionuclide. Divergence in PORFLOW/GoldSim comparison curves after 7,000 years is likely associated with mass diffusing into the waste tank grout from the CZ, which results in an associated delayed release of the mass in the HTF GoldSim Model.

Figure 5.6-9 displays the PORFLOW and GoldSim Np-237 releases from Tank 12. The GoldSim Np-237, Tank 12 releases are greater for the entire simulation period by approximately three orders of magnitude. However, the general trends of the curves are similar. The differences between the GoldSim and PORFLOW Np-237 releases most likely reflect the greater influence of numerical dispersion in the HTF GoldSim Model in conjunction with the extremely large distribution coefficients of neptunium in the cementitious materials.

Figure 5.6-10 shows that there is a good match between the PORFLOW results and the GoldSim results for Cs-135 releases from Tank 12. Similar to the release of I-129 (Figure 5.6-8), the match reflects the trends well and is especially good at the higher concentrations.

5.6.2.2.3 Tank 13 Mass Release from a Type II Tank with an Intact Liner

Tank 13 is a submerged Type II tank with an intact liner. Type II tanks have a more complex engineered system, due in large part from the inclusion of the sand pads (primary and secondary) located beneath the primary and secondary liners (e.g., Figure 4.4-50 in Section 4.4.4.2), therefore flow and transport is consequently more complex for

these waste tanks. For Type II tanks, it is assumed some contaminant exists in the primary sand pad and annulus at the time of closure. It is also assumed for Tank 16 that some contaminant exists in the secondary sand pad. The mass in the primary sand pad, which is sandwiched between the primary and secondary liners, is capable of migrating out of the engineered barrier prior to liner failure, a process that is observed in the PORFLOW simulations. For Tank 13, a Type II tank with an intact liner, the initial exit route is from the sand pad to the annulus and upward through the annulus. The mass must first migrate above the 5-foot secondary liner vertical extension, before it can leave the system by migrating through the wall, into the concrete basemat, and finally into the saturated zone.

Although the HTF GoldSim Model meticulously simulates both flow and diffusion along the pathways described above, it assumes that the main mode of transport is diffusion out of the primary sand pad and upward through the annulus, until the liner fails. At the time of liner failure, downward vertical flow through the annulus is assumed as the critical process for transporting any mass that enters the annulus from the primary sand pad. This assumption is consistent with the inhibition of flow caused by the secondary liner.

Figures 5.6-11 through 5.6-15 display PORFLOW/GoldSim comparison plots of the mass released (mole per year) from Tank 13 for radionuclides Ra-226, Tc-99, I-129, Np-237, and Cs-135. Comparisons of the curves indicate that the HTF GoldSim Model adequately approximates the magnitude and the timing of the HTF PORFLOW Model releases for Type II tanks, with only small discrepancies.

Figure 5.6-11: Mass Release from Type II Tank 13 - Ra-226 (Case A)

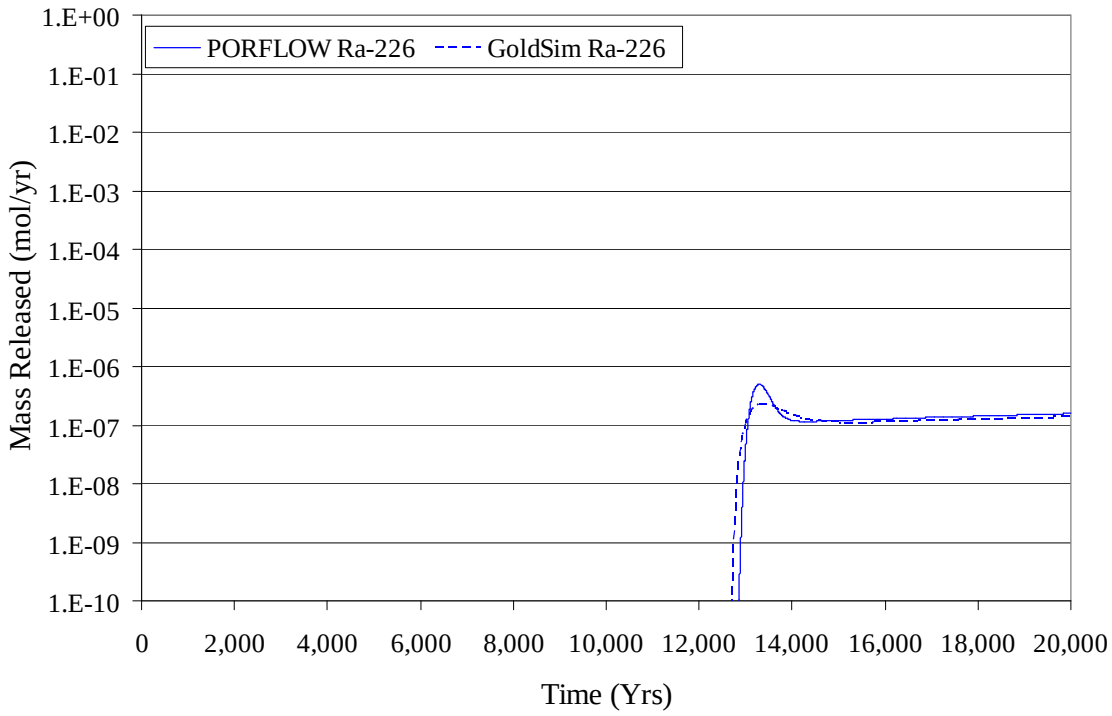

Figure 5.6-12: Mass Release from Type II Tank 13 - Tc-99 (Case A)

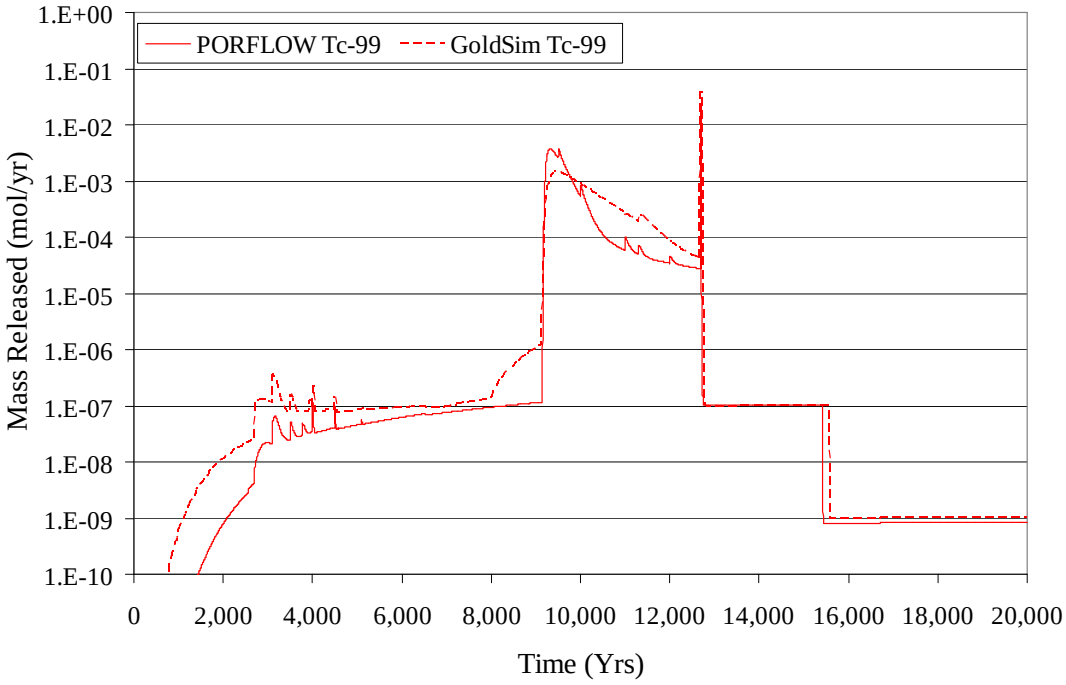

Figure 5.6-13: Mass Release from Type II Tank 13 - I-129 (Case A)

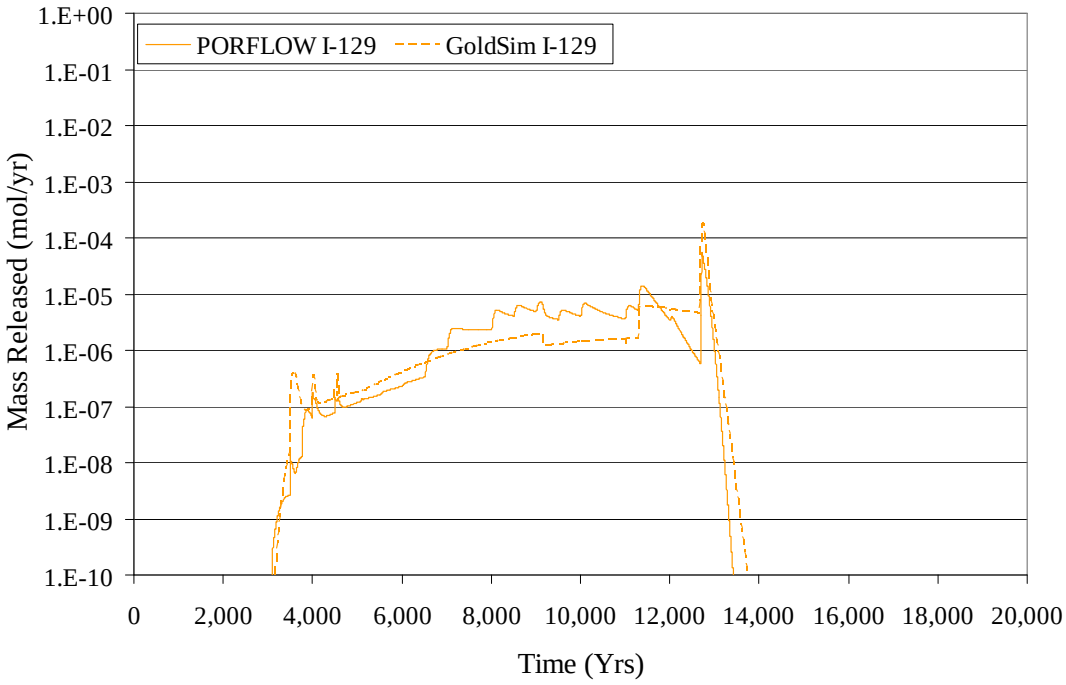

Figure 5.6-14: Mass Release from Type II Tank 13 - Np-237 (Case A)

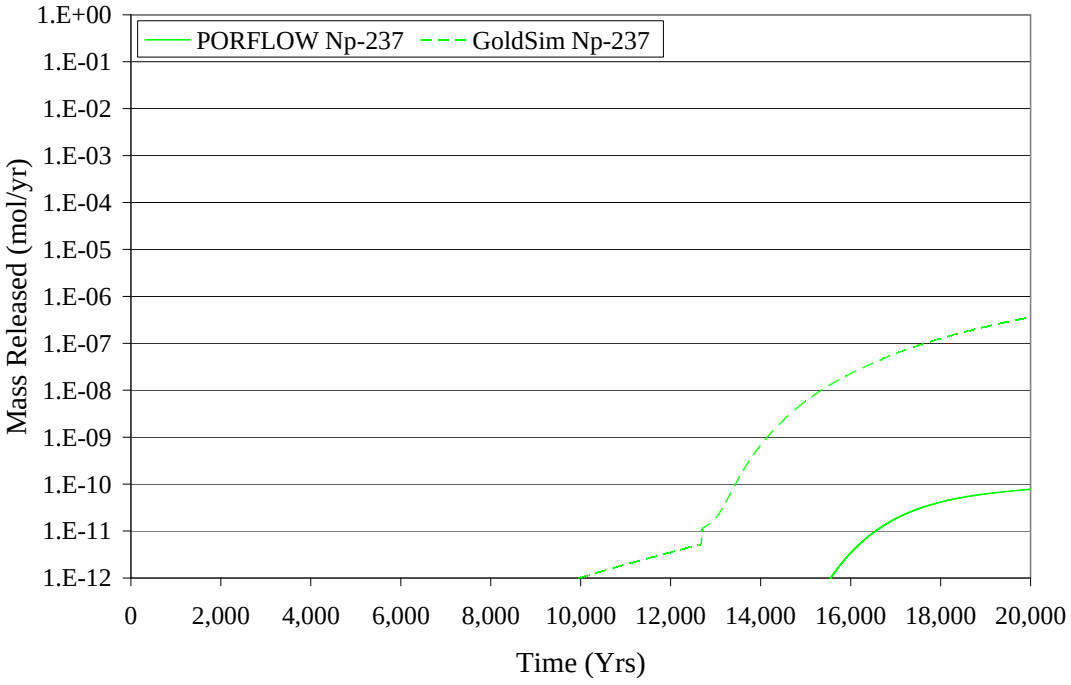

Figure 5.6-15: Mass Release from Type II Tank 13 - Cs-135 (Case A)

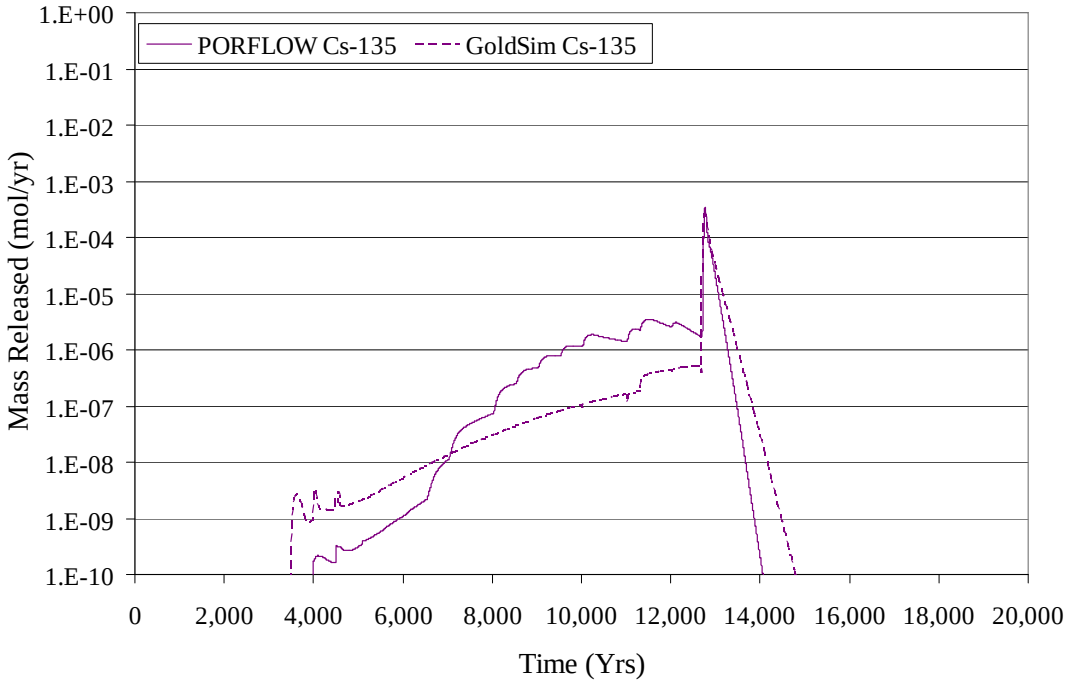

Figure 5.6-11 illustrates that GoldSim is able to replicate Ra-226 mass release from a Type II tank with an intact liner.

A noticeable increase in Tc-99 mass release is observed in Figure 5.6-12 just after 9,000 years. This pulse corresponds to the chemical transitions of the waste tank annulus concrete from Reducing Region II to Oxidizing Region II at 9,126 years. Prior to the chemical transition, the Tc-99 mass release from the HTF GoldSim Model reflects the general trends, but tends to overestimate the release. After the transition from a reducing to an oxidizing state, the two models show very similar behavior.

Figure 5.6-13 presents a good match between the PORFLOW results and the GoldSim results for I-129 releases from Tank 13. The match is especially good at the high peak concentration associated with the liner failure.

Figure 5.6-14 indicates that releases of Np-237 are very low for PORFLOW (< 1.0E-10 mol/L), but GoldSim releases of Np-237 from Tank 13 are higher than PORFLOW but only after the end of the compliance period. As discussed earlier, for the extremely high distribution coefficient species, such as neptunium, the release is generally more delayed in the HTF PORFLOW Model than in the HTF GoldSim Model.

Figure 5.6-15 shows that for Cs-135, the match between the PORFLOW results and the GoldSim results is not as good as for I-129 because of the higher distribution coefficient value for Cs-135, but the general release trends are still similar and the match is especially good at the high peak concentration associated with the liner failure.

5.6.2.2.4 Tank 24 Mass Release from a Type IV Tank with an Intact Liner

Tank 24 is a non-submerged Type IV tank with an intact liner that fails at 3,638 years. Figures 5.6-16 through 5.6-20 display PORFLOW/GoldSim comparison plots of the mass released (mole per year) from Tank 24 for the following radionuclides, Ra-226, Tc-99, I-129, Np-237, and Cs-135. The curves indicate that the HTF GoldSim Model reproduces the HTF PORFLOW Model releases extremely well.

Figure 5.6-16: Mass Release from Type IV Tank 24 - Ra-226 (Case A)

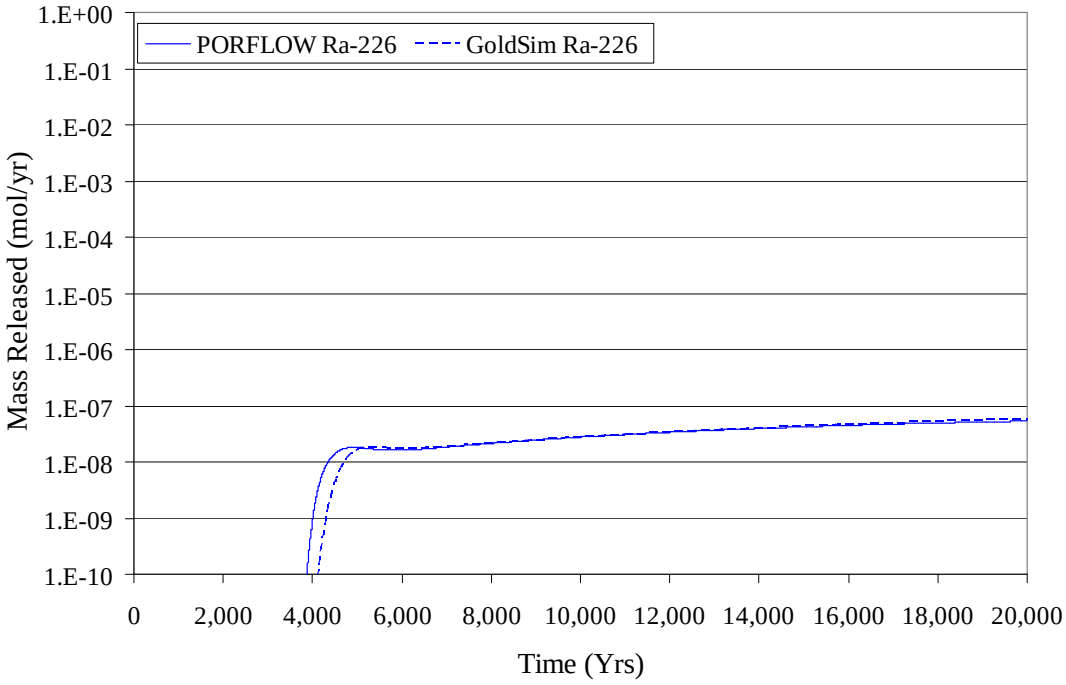

Figure 5.6-17: Mass Release from Type IV Tank 24 - Tc-99 (Case A)

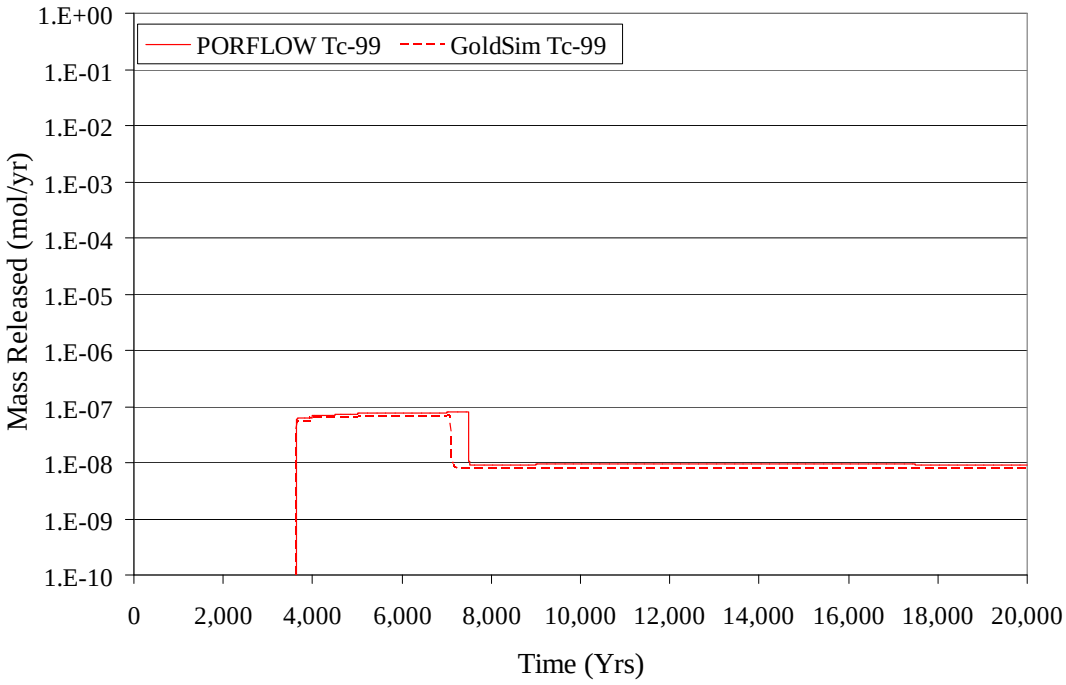

Figure 5.6-18: Mass Release from Type IV Tank 24 - I-129 (Case A)

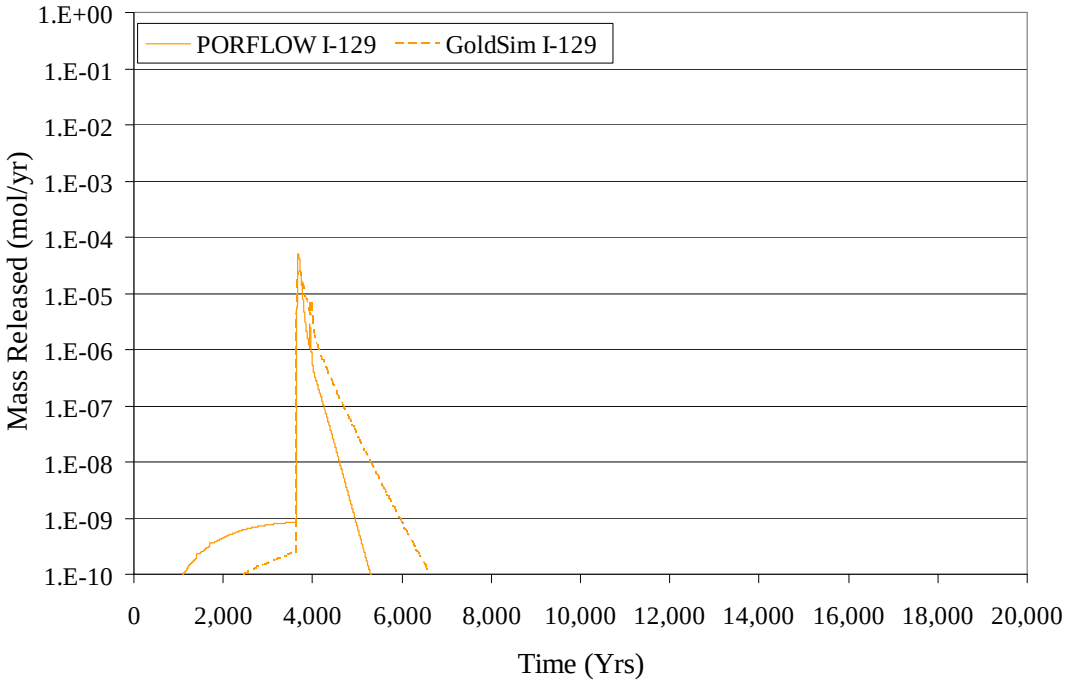

Figure 5.6-19: Mass Release from Type IV Tank 24 - Np-237 (Case A)

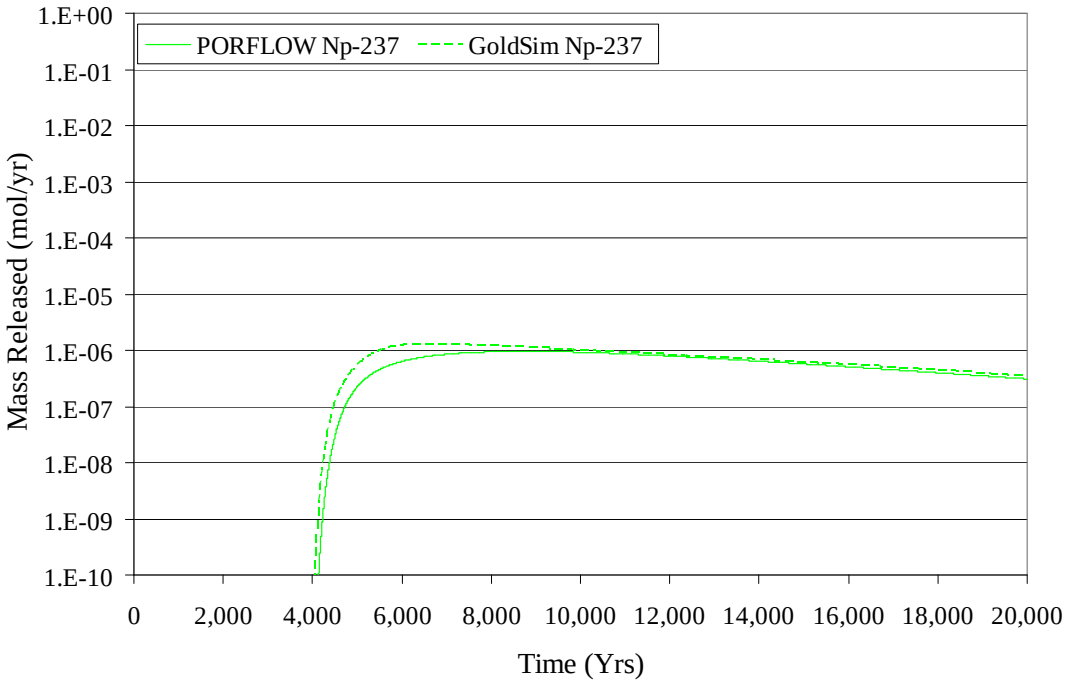

Figure 5.6-20: Mass Release from Type IV Tank 24 - Cs-135 (Case A)

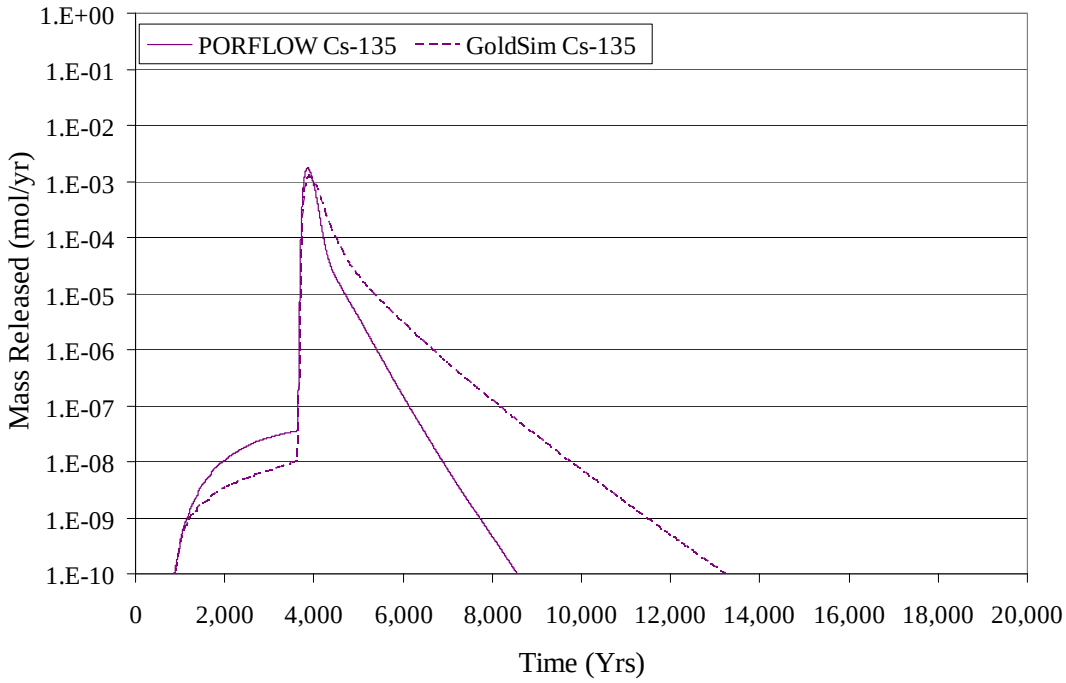

The close match between the curves representing Tank 24 Ra-226 releases (Figure 5.6-16) is once again significant because it indicates GoldSim also adequately represents the transport of the parents of Ra-226.

As Figure 5.6-17 illustrates, the GoldSim Tc-99 release closely overlies the PORFLOW release, indicating that the solubility control associated with the CZ is being accurately approximated in the HTF GoldSim Model. The CZ transition from Reducing Region II to Oxidizing Region II occurs at 7,491 years in the HTF PORFLOW Model, but a few hundred years earlier in the HTF GoldSim Model. The HTF GoldSim Model approximates the chemical transition times within the waste tank grout and the CZ independently, which explains why there is not a perfect match in the timing of the down-step.

Both the timing and the magnitude of the PORFLOW I-129 peak release displayed in Figure 5.6-18 are similar to the GoldSim results. A prolonged release effect is probably associated with a slightly greater amount of mass diffusing into the waste tank grout from the CZ. This results in a more dispersed release from the waste tank.

Figure 5.6-19 indicates that Np-237 releases match very well between the PORFLOW and GoldSim models for this non-submerged Type IV tank. The better Np-237 release match in the Type IV tanks compared to the Type I and II tanks is likely due to the lower degree of numerical dispersion in the basemat of the Type IV tanks. The Type IV tanks thinner basemat is approximated with the same number of cells as used for other waste tank types. This would decrease the degree of numerical dispersion in the basemat [SRR-CWDA-2010-00093, Section 3.4] Note that although the releases from the PORFLOW

and GoldSim models for Type IV tank Np-237 are dominated by the Cm-245 inventory, the Tank 24 results also compare favorably in simulations based on separate releases of the Np-237, Am-241, and Cm-245 inventory components.

Figure 5.6-20 shows that there is a good match between the PORFLOW results and the GoldSim results for Cs-135 releases from Tank 24. As with I-129 (Figure 5.6-18), the Cs-135 release is slightly more dispersed in the GoldSim results.

5.6.2.2.5 Observation Well A3 Saturated Zone Transport Behavior

The second phase of the benchmarking process focuses on how well the abstraction model approximates the radionuclide transport behavior in the saturated zone. The radionuclide concentrations in picocuries per liter at a set of observation wells were examined for this task. The observation wells used for the comparison are A3, B1, C2, E5, and F3. Only the results for observation Well A3 are presented here, however extensive results are provided in SRR-CWDA-2010-00093. This description is meant as an example of the benchmarking process.

The locations of the observation wells and the PORFLOW generated stream traces are shown in Figure 4.4-56 (Section 4.4.4.2). Based on the PORFLOW generated stream traces, Tank 9 releases are transported predominantly to Sector A wells, whereas the Tank 13 stream trace leads to Sector B. Note that the Tank 14 stream trace goes near Tank 13 and then veers north to Sector A (Figure 4.4-56, in Section 4.4.4.2). This is indicative of the complexity of the flow field.

Well A3

An examination of PORFLOW and GoldSim model generated Ra-226 concentrations presented in Figure 5.6-21 indicate that the GoldSim can provide a computationally efficient approximation of the 100-meter boundary concentrations. There is consistency in the trends observed in the two Ra-226 breakthrough curves, although GoldSim slightly overestimates the concentrations at early times.

Figure 5.6-21: Ra-226 Saturated Zone Concentration at Well A3 (Case A)

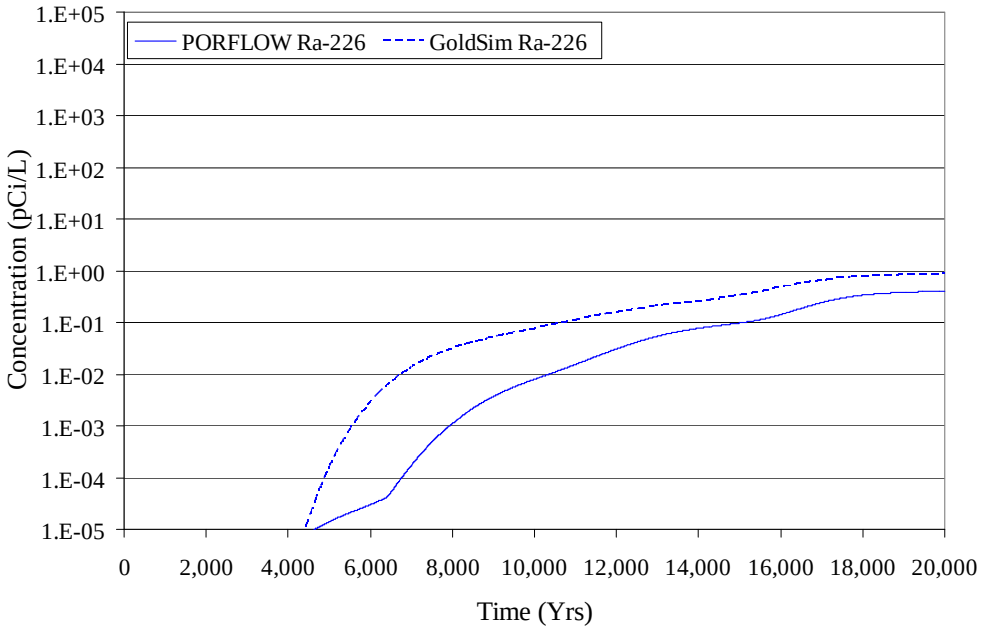

Figure 5.6-22 compares the Tc-99 breakthrough curves at Well A3. The GoldSim model reproduces the large first order trends displayed in the PORFLOW concentration data, however the magnitude of the concentration is lower in the GoldSim model after the initial peak (approximately 1,100 years) and after 9,000 years.

Figure 5.6-22: Tc-99 Saturated Zone Concentration at Well A3 (Case A)

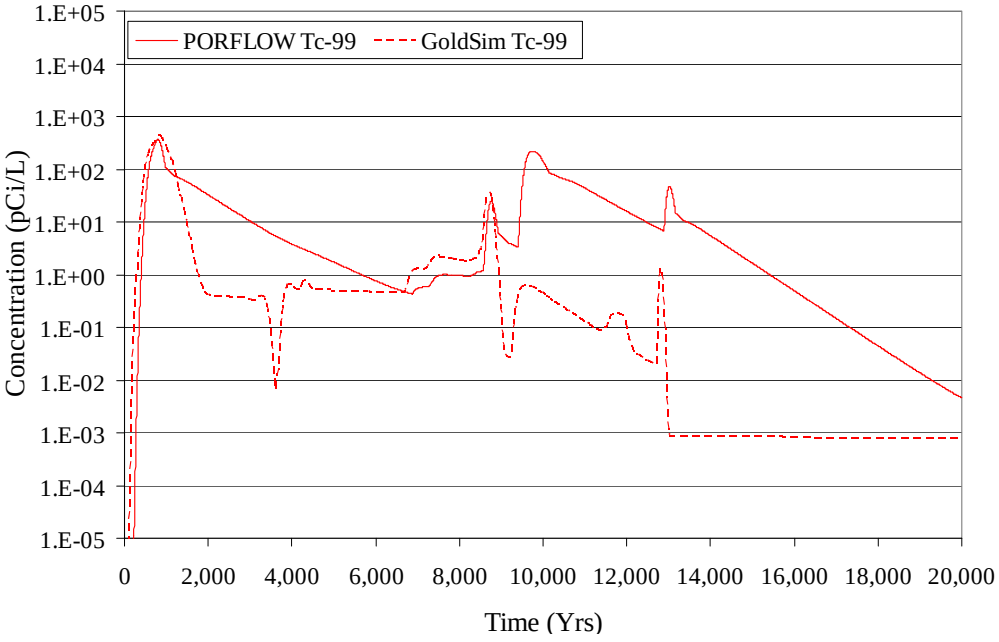

The differences are anticipated as the mass migration in PORFLOW is fully 3-D and the spreading effects due to the heterogeneous nature of the flow fields and the vertical spreading may promote differences. For example, as can be seen in Figure 5.6-23, mass released by Tank 13 will reach Wells A3 and B5 by two different flow paths in a PORFLOW simulation. There is a west to east trending flow path that is consistent with the stream trace from Tank 13 presented in Figure 4.4-56 (Section 4.4.4.2), but also a migration trend from southwest to northeast as mass migrates west of the source. The release from Tank 13 reaches Well A3 by dispersion only in the GoldSim model, which is not as effective at bringing mass to Well A3 as the advective transport in the PORFLOW simulations. Another example of this phenomenon is visible in Figure 5.6-24, which depicts the plume from Tank 16. The figure clearly illustrates the divergent trend in the HTF flow regime. Figure 5.6-25 provides an example of a good match between the GoldSim simulated Tc-99 breakthrough curve and the PORFLOW simulated Tc-99 breakthrough curve at Well B1. Concentrations at Well B1 are primarily from Tank 13 releases.

Figure 5.6-23: Conservative Constituent Release Plume from Tank 13

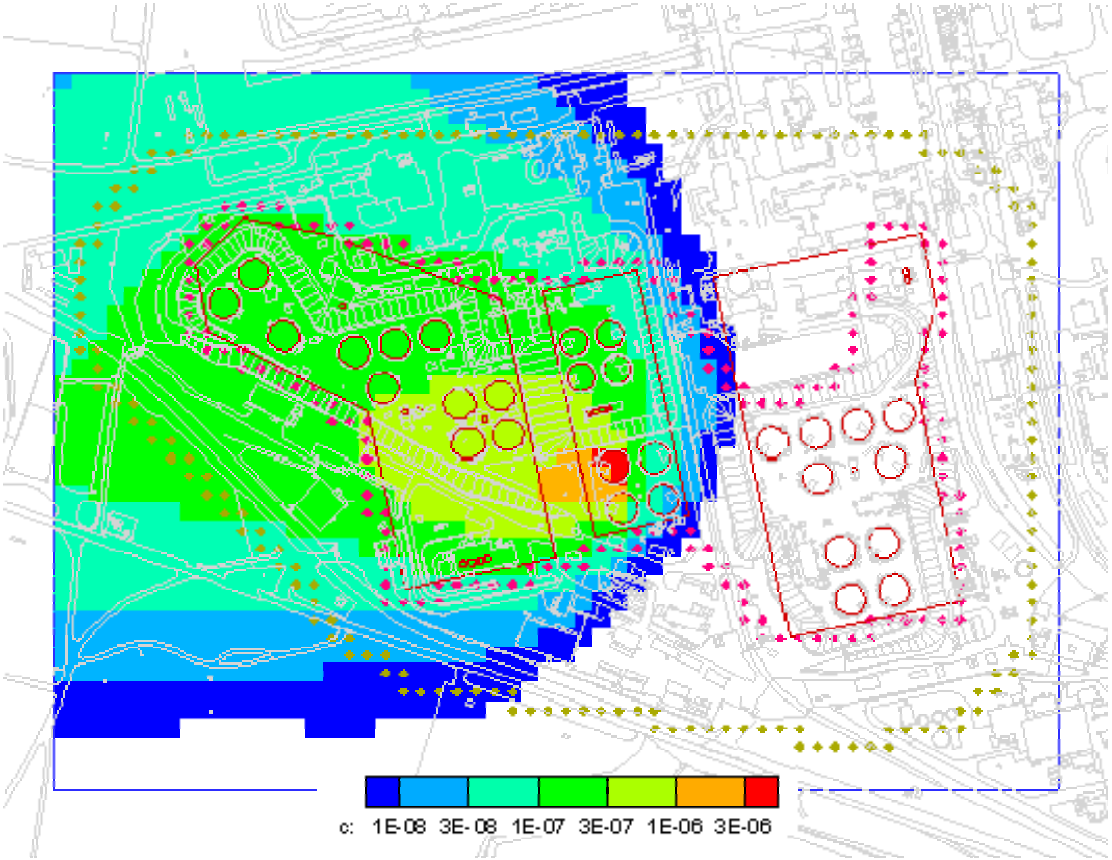

Note: Scale bar indicates concentration in mol/L produced by hypothetical constant source of 1 mol/yr. Location of waste tank is indicated in red.

Figure 5.6-24: Conservative Constituent Release Plume from Tank 16

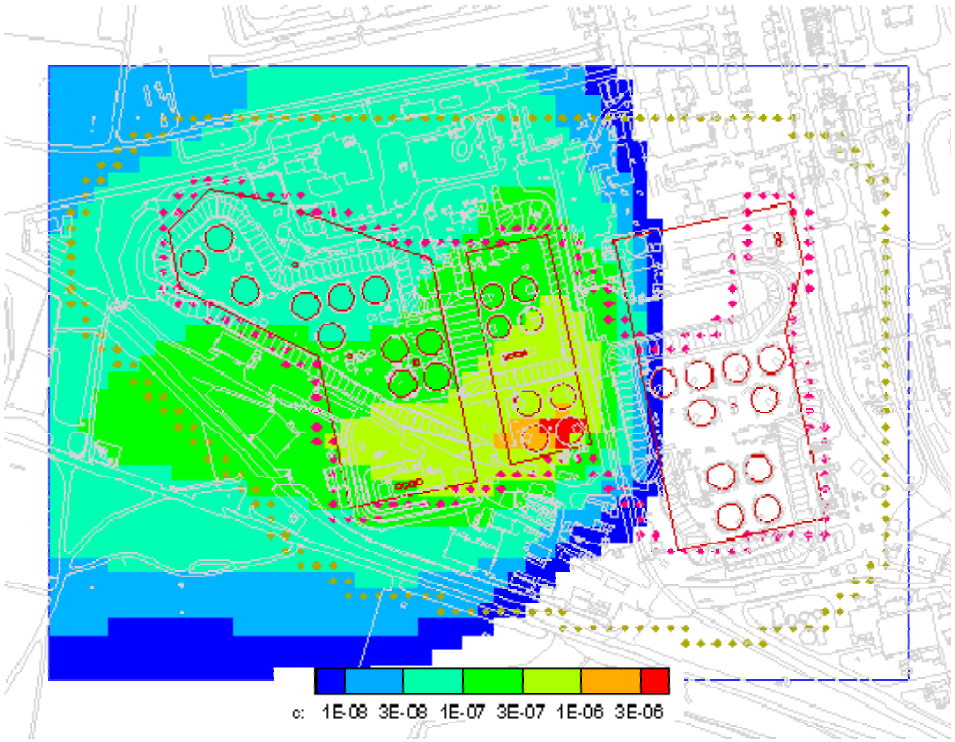

Note: Scale bar indicates concentration in mol/L produced by hypothetical constant source of 1 mol/yr. Location of waste tank is indicated in red.

Figure 5.6-25: Tc-99 Saturated Zone Concentration at Well B1 (Case A)

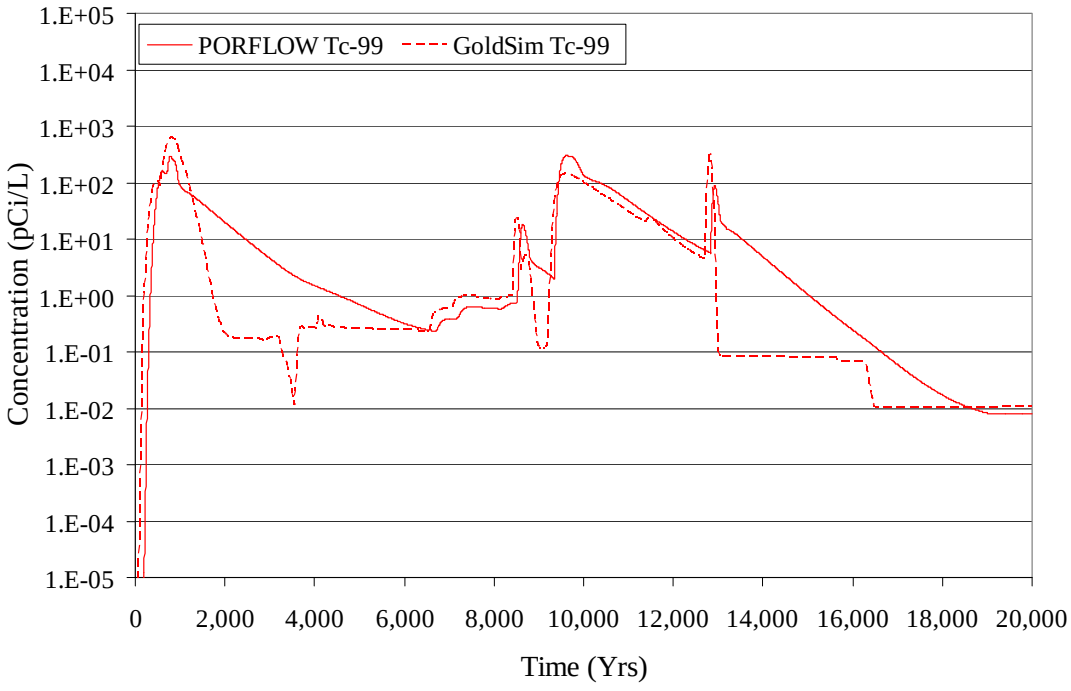

The differences between the GoldSim simulated breakthrough curves and PORFLOW results can be attributed to the difference in spatial scale between the two models. The PORFLOW results are based on maximum sampling point concentrations in each sector as taken from a relatively fine grid of sampling points within each sector. The GoldSim results are based upon the maximum values from a relatively few points located where streamlines from different waste tanks converge, decreasing the computation time while biasing the results towards locations where the peak values will occur. The use of the fine grid sampling will also have a tendency to produce more dispersed results.

Figure 5.6-26 shows a reasonable correlation between the I-129 100-meter concentration levels generated by PORFLOW and concentration levels produced by GoldSim. As was the case with the Tc-99 concentration comparison, the GoldSim model does not fully capture the release of the I-129 peak from Tank 13, but the does capture peaks from Tank 9 (see Figure 5.6-3) as well as from Tanks 10 and 11 (not shown).

Figure 5.6-26: I-129 Saturated Zone Concentration at Well A3 (Case A)

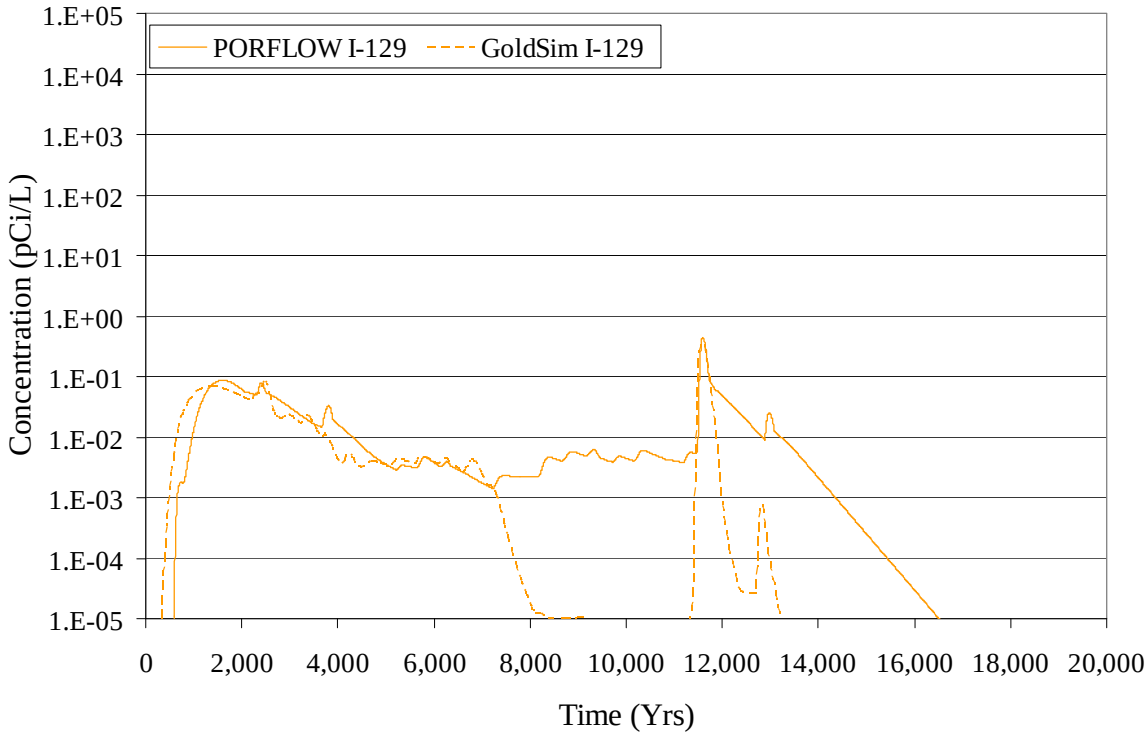

Figure 5.6-27 shows a reasonable correlation between the Np-237 100-meter concentration levels generated by PORFLOW and concentration levels produced by GoldSim.

Figure 5.6-27: Np-237 Saturated Zone Concentration at Well A3 (Case A)

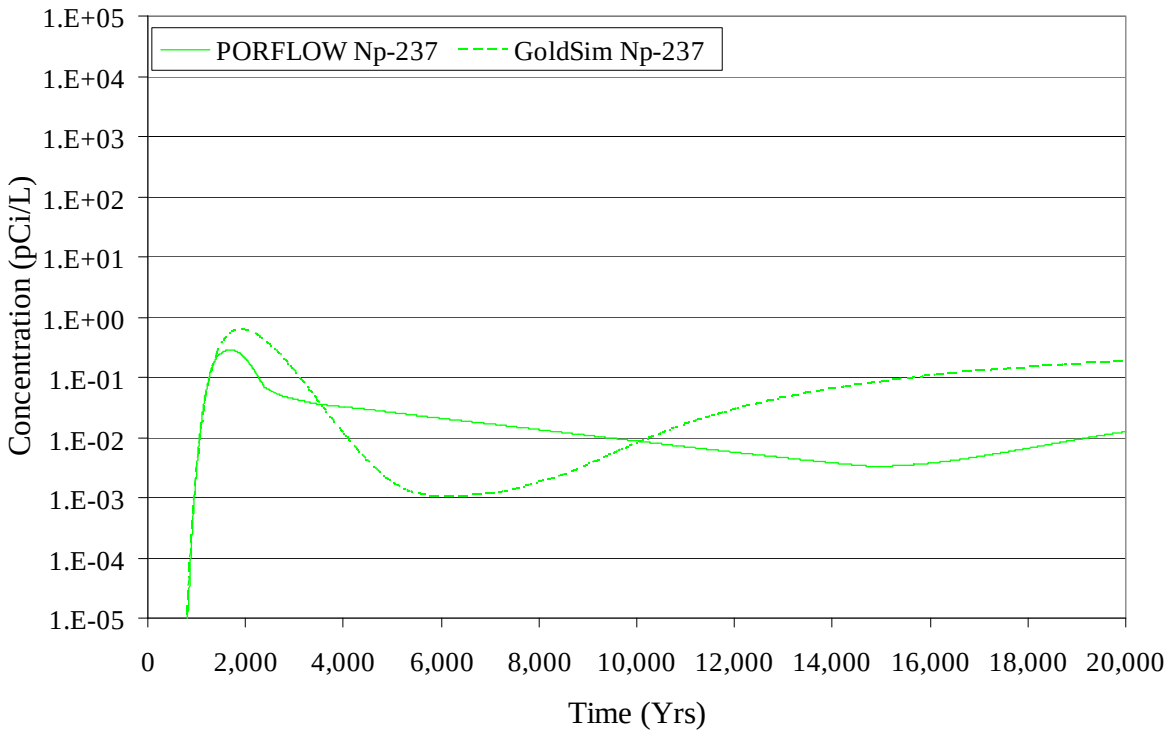

Figure 5.6-27 displays a reasonable correlation between the Np-237 100-meter concentration levels generated by PORFLOW and concentration levels produced by GoldSim.

Figure 5.6-28 also illustrates that the Cs-135 100-meter concentration trend generated by PORFLOW match well the 100-meter concentrations given by GoldSim for most of the 20,000-year simulation. Note that the GoldSim result shows a mass decrease at the end of the breakthrough curve. This may be caused by the lack of spreading due to advection or by mass being sorbed in clay layers being slowly released.

Figure 5.6-28: Cs-135 Saturated Zone Concentration at Well A3 (Case A)

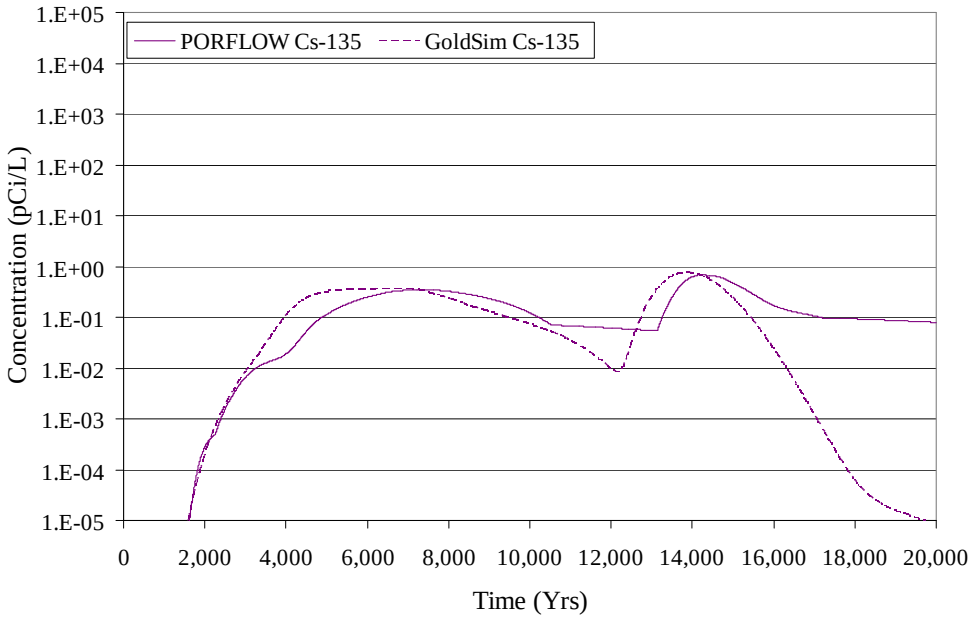

5.6.2.2.6 Total Dose Comparison for Cases A, D, and E

The third phase of the benchmarking process, which is an additional check on the appropriateness of GoldSim as a surrogate for the fully 3-D HTF GoldSim Model, is a comparison between total doses generated using PORFLOW and the HTF GoldSim Model. For this comparison, the Base Case is evaluated along with Cases D and E. Case D and E are selected because they have the largest releases, and therefore the greatest potential impact on dose.

For the Base Case, the comparison between the PORFLOW and GoldSim results presented in Figure 5.6-29 show that the GoldSim approximates the general trends quite well. The GoldSim results are slightly higher at the end of the simulation, but this is a conservative and acceptable approximation. For Case D, the comparison between the PORFLOW and GoldSim results in Figure 5.6-30 show that GoldSim still produces a good approximation of the HTF GoldSim Model. After 3,700 years, the HTF GoldSim Model results are slightly higher until the end of the simulation, but this is a conservative and acceptable approximation. The HTF PORFLOW Model does a good job of capturing the trends except for the early peak at approximately 1,400 years that is underestimated by approximately 1 mrem/yr. For Case E, the comparison between the PORFLOW and GoldSim results in Figure 5.6-31 show that the HTF GoldSim Model still produces a good approximation of the HTF PORFLOW Model. After 5,300 years, the HTF GoldSim Model results are slightly higher until the end of the simulation, but this is a conservative and acceptable approximation. The HTF GoldSim Model does a good job of capturing the trends except for very early time. The differences are likely due to transverse spreading due to flow in the HTF GoldSim Model and the changing of the peak dose observation position over time.

Figure 5.6-29: PORFLOW and GoldSim Dose Results Comparison for Case A

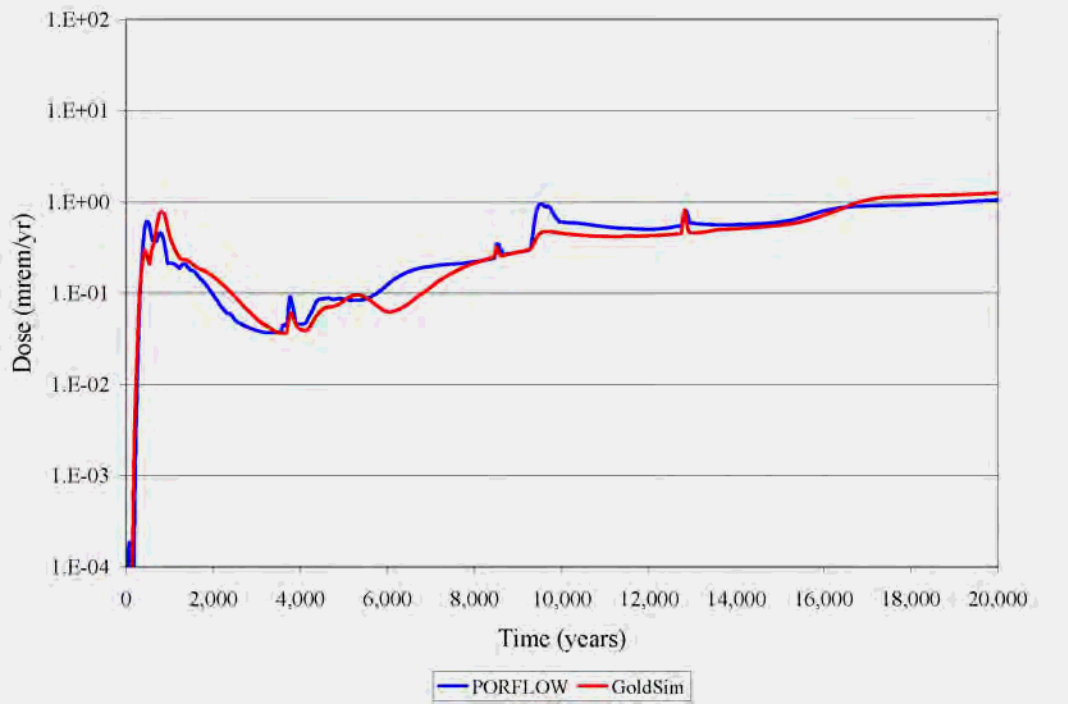

Figure 5.6-30: PORFLOW and GoldSim Dose Results Comparison for Case D

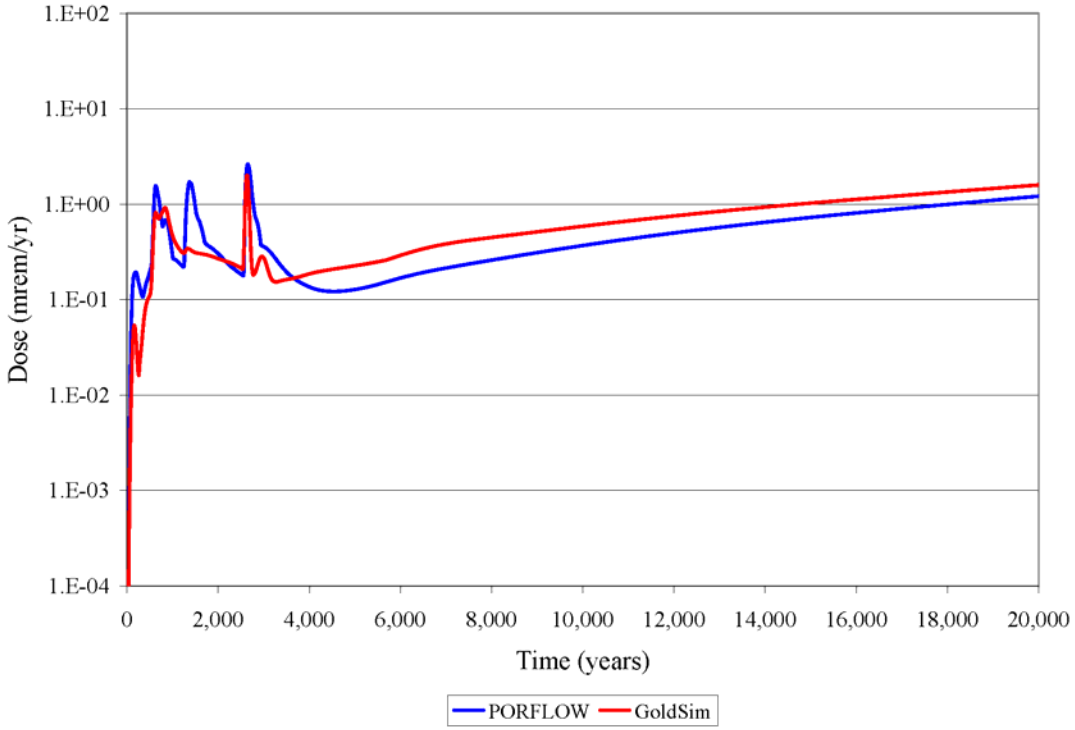

Figure 5.6-31: PORFLOW and GoldSim Dose Results Comparison for Case E

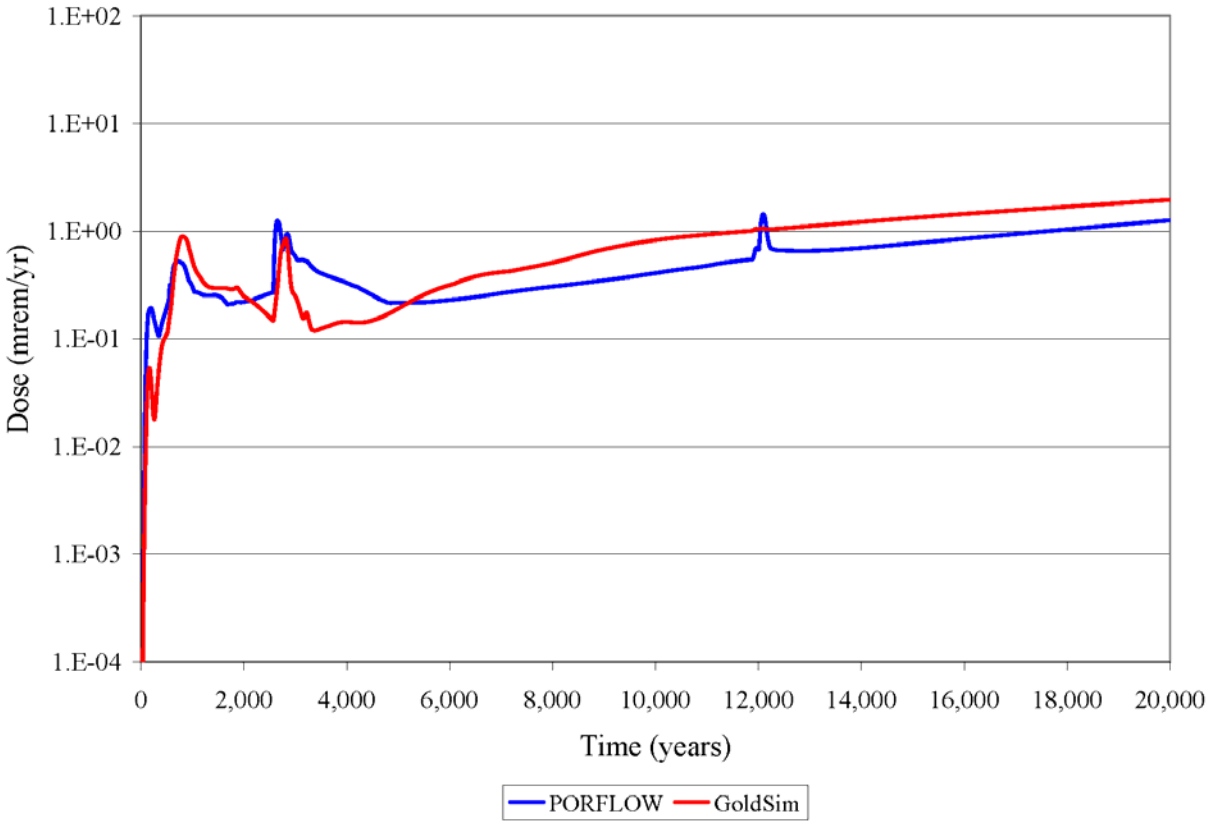

5.6.2.2.7 Influence of Using a Finer Discretization of the Basemat

The outcome of the preceding analysis for waste tank releases demonstrate an excellent match between the GoldSim and PORFLOW results for Tc-99, I-129, Cs-135, and Ra-226, but a much weaker match for Np-237. The cause of this weaker match for Np-237 is traced to a combination of factors including the discretizaton of the waste tank's basemat, the basemat thickness, and the highly adsorptive properties of Np-237 and its progenitors.

Figures 5.6-32 through 5.6-35 present representative results of Np-237 released from the basemats for representative Type I, Type II (initially failed and normal liner degradation), and Type III/IIIA tanks. GoldSim Np-237 releases had a tendency to be larger than the PORFLOW releases and initiate earlier in time. In comparison, modeled Np-237 releases from a Type IV tank, shown in Figure 5.6-36, present a very good comparison between GoldSim and PORFLOW. An important contributor to this effect is the thickness of the basemat and the discretization approach applied to the basemat in GoldSim. The modeled basemat thickness for the Type IV tanks is 6.9 inches and the basemat thickness for the other waste tank types ranges between 30 and 43 inches.

Figure 5.6-32: Mass Release from Type I Tank 12 (Case A)

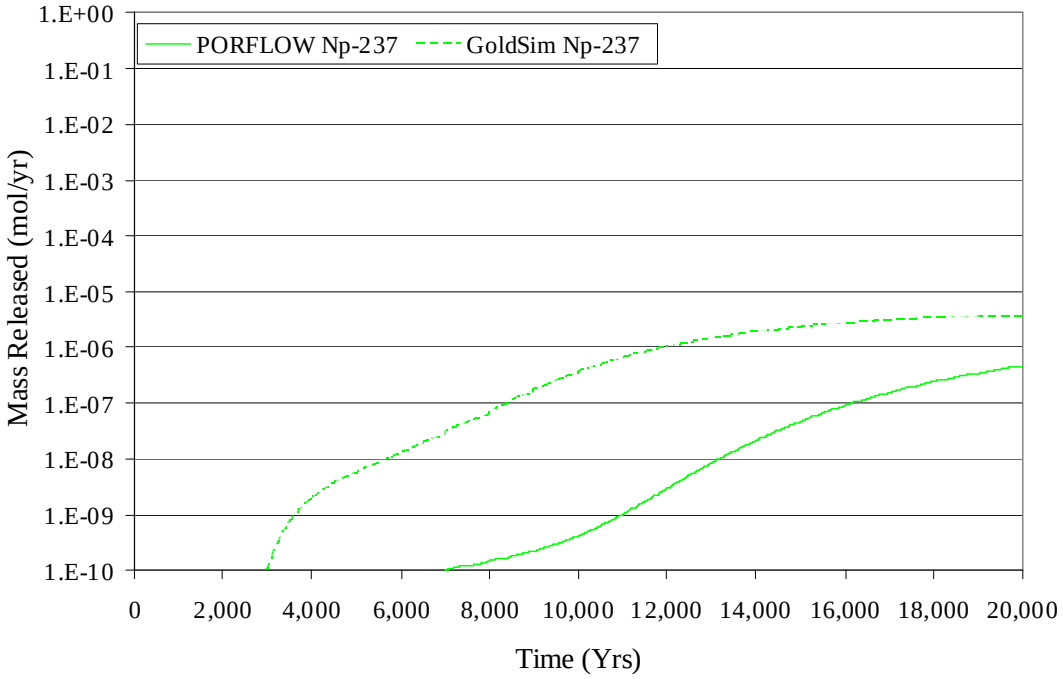

Figure 5.6-33: Mass Release from Type II Tank 13 (Case A)

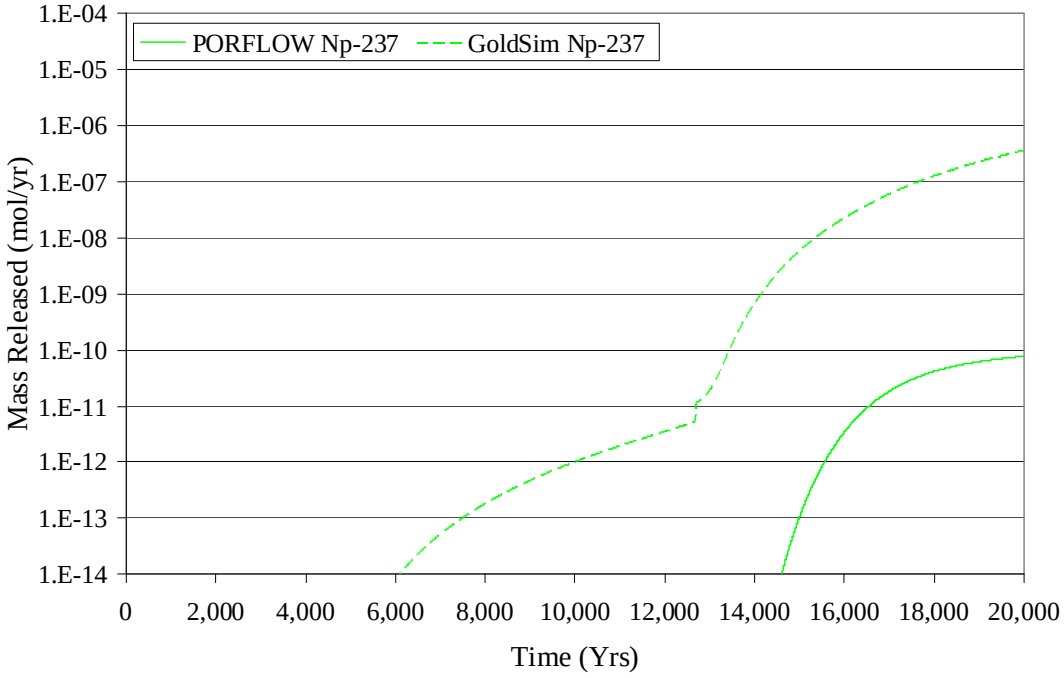

Figure 5.6-34: Mass Release from Type II Tank 15 (Case A)

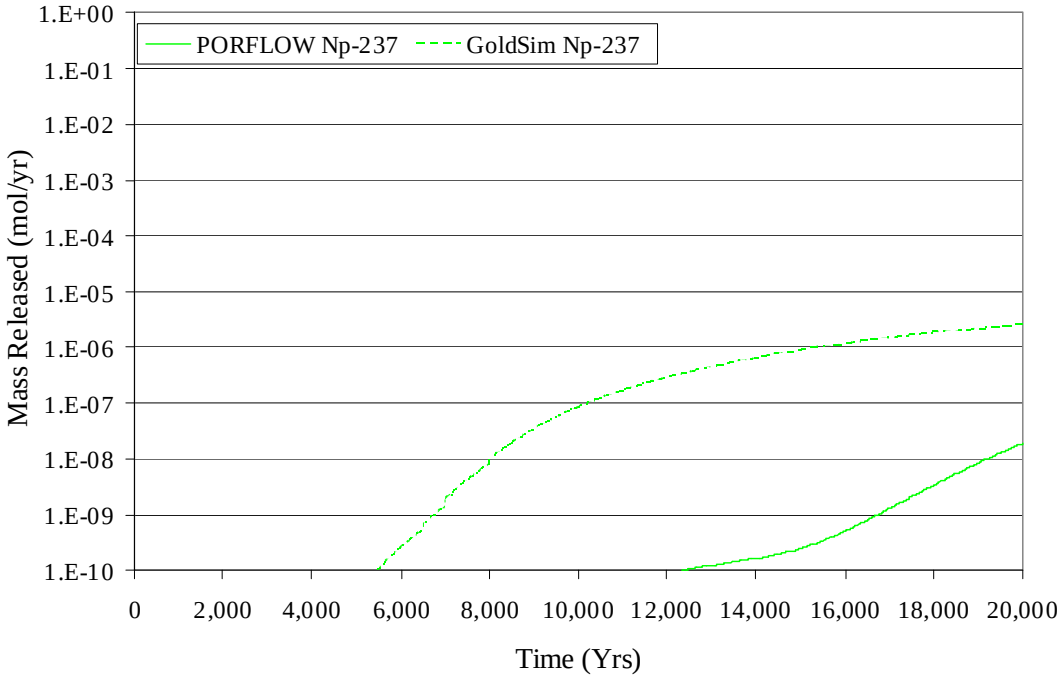

Figure 5.6-35: Mass Release from Type IIIA Tank 40 (Case A)

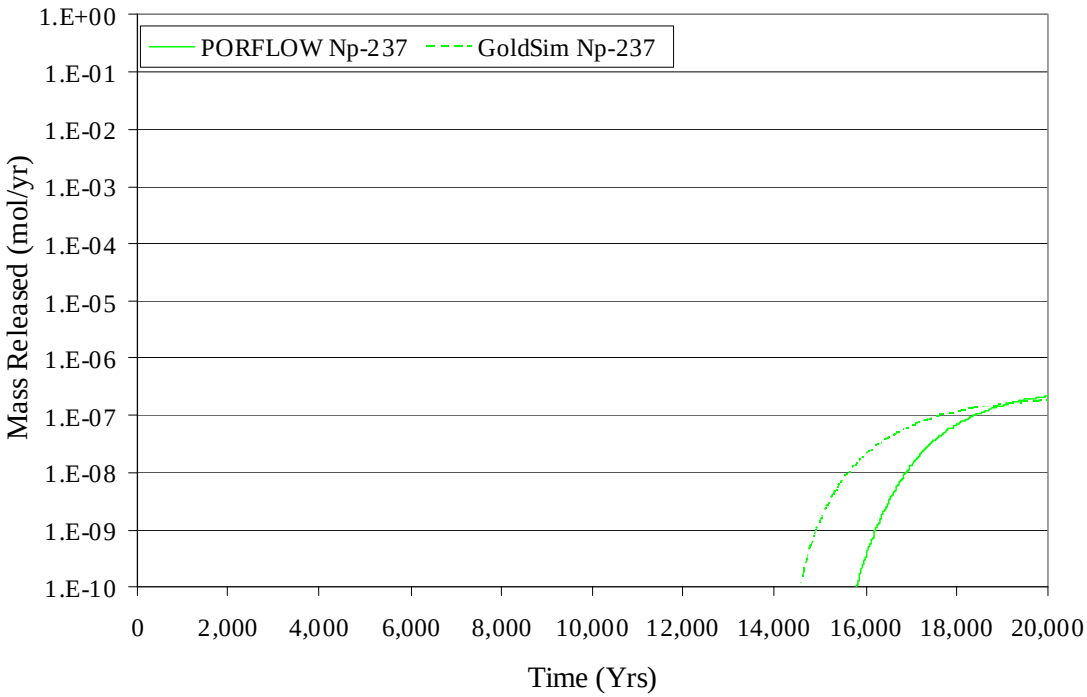

Figure 5.6-36: Mass Release from Type IV Tank 24 (Case A)

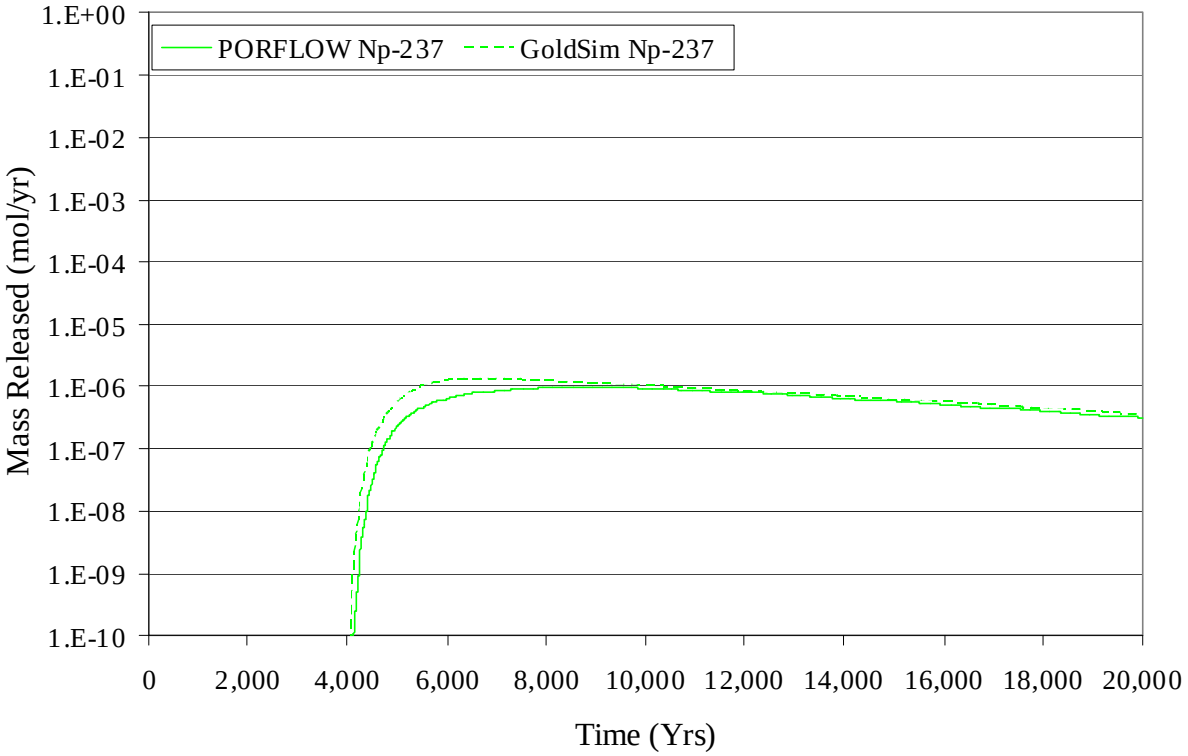

Table 4.2-33 indicates Np-237 and its principal decay chain Cm-245, Pu-241, and Am-241 are strongly sorbed and have the tendency to move slowly. A slower transport rate allows the radionuclide levels to be more strongly influenced by dispersive processes than radionuclides that are more mobile. More importantly, a difference in the degree of dispersion simulated by the two models could greatly influence the releases and lead to noticeable differences. Less retarded species are also influenced by the dispersion, but over much shorter release periods, the influence would be less perceptible.

The PORFLOW simulation sets all dispersivity terms to zero, effectively leaving only numerical dispersion. The level of numerical dispersion is a function of the models discretization of the basemat. Similarly, the waste tank release segment of the HTF GoldSim Model does not consider mechanical dispersion, but does subject releases through the basemat to numerical dispersion. In the HTF GoldSim Model, a set of cells is linked in series to represent a 1-D transport system. Longitudinal dispersivity is not explicitly defined in a series of GoldSim mixing cells, but implicitly the series is subject to numerical dispersion. The amount of numerical dispersion can be quantified as a function of the total length of the linked cell pathway and the number of cells defining the pathway. In a series of mixing cells, the numerical dispersivity (α_{num}) can be approximated as $\alpha_{num} \approx L/(2N)$ where L is the length of the string of cells and N is the number of cells. [GTG-2010b] Because the HTF GoldSim Model uses only five mixing cells to represent the basemat, and uses a more refined gridding that expands downward,

it is subject to much less numerical dispersion. To quantify the effects of the differences in numerical dispersion between the two models, the basemat portion of the HTF GoldSim Model was rebuilt with a construct of 30 mixing cells, which reduces the effective dispersivity by a factor of six.

By comparing Figures 5.6-37 through 5.6-40 with Figures 5.6-32 through 5.6-35 respectively, the influence of numerical dispersion on the GoldSim results can readily be seen. The GoldSim releases begin later, and over the analysis period, are effectively reduced. The releases are now similar to the HTF GoldSim Model releases. A comparison of Figure 5.6-41 with Figure 5.6-36 shows that for Type IV tanks, the increase from 5 to 30 mixing cells has little influence on the releases from the much thinner basemats. Since the discretization can have a large effect on any highly sorbed species, it is important to make sure from a risk-based perspective that the inclusion of a greater degree of dispersion in the basemat has little influence on total dose. Figure 5.6-42 presents the Base Case and new discretization deterministic GoldSim results and shows that increasing the number of mixing cells in the basemat has a negligible effect on the total dose results.

Figure 5.6-37: Revised Mass Release of Np-237 for Type I Tank 12

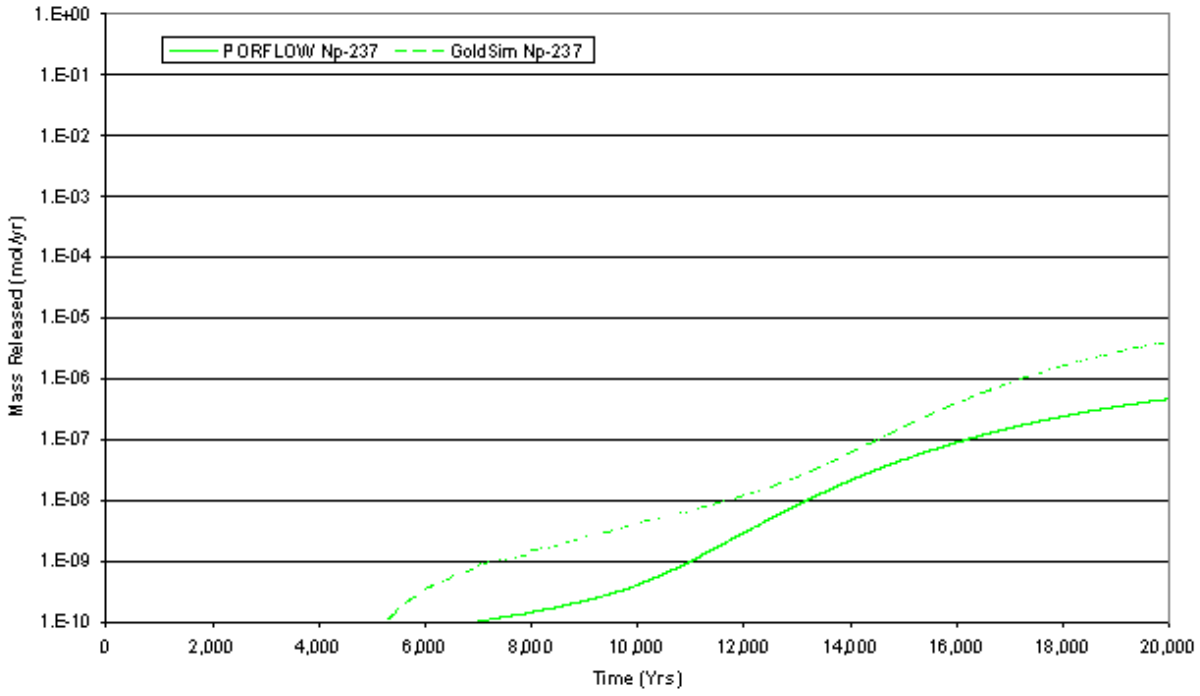

Figure 5.6-38: Revised Mass Release of Np-237 for Type II Tank 13

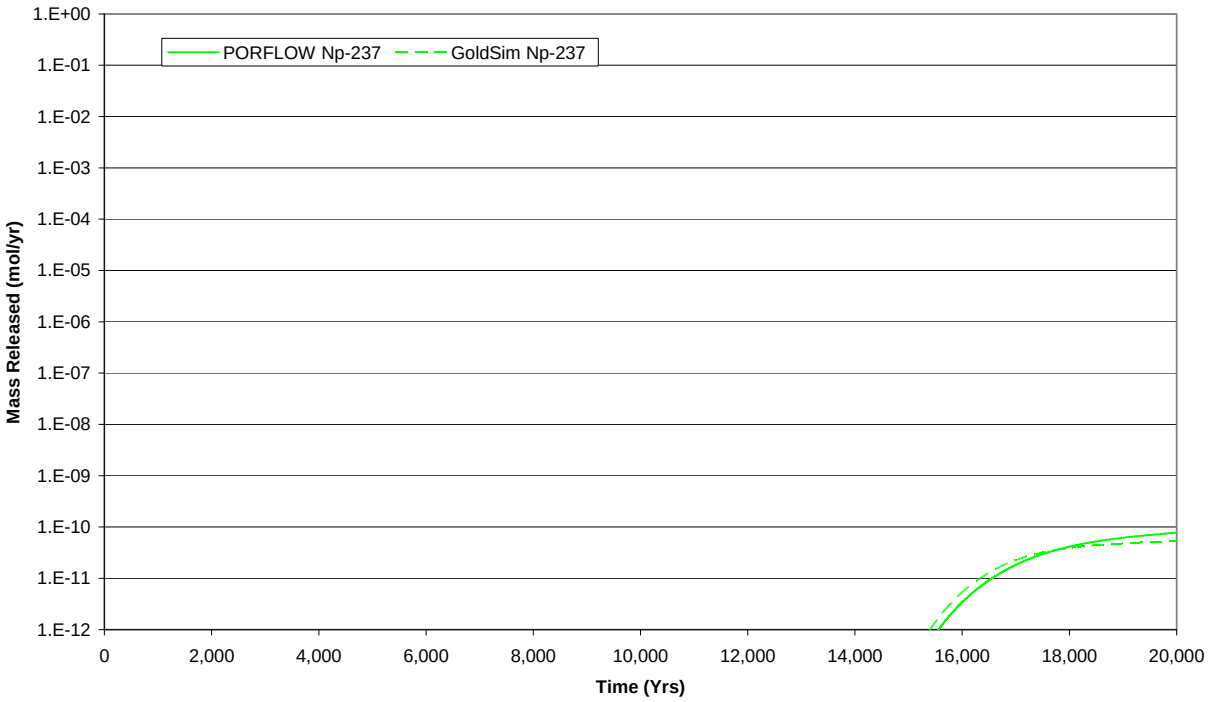

Figure 5.6-39: Revised Mass Release of Np-237 for Type II Tank 15

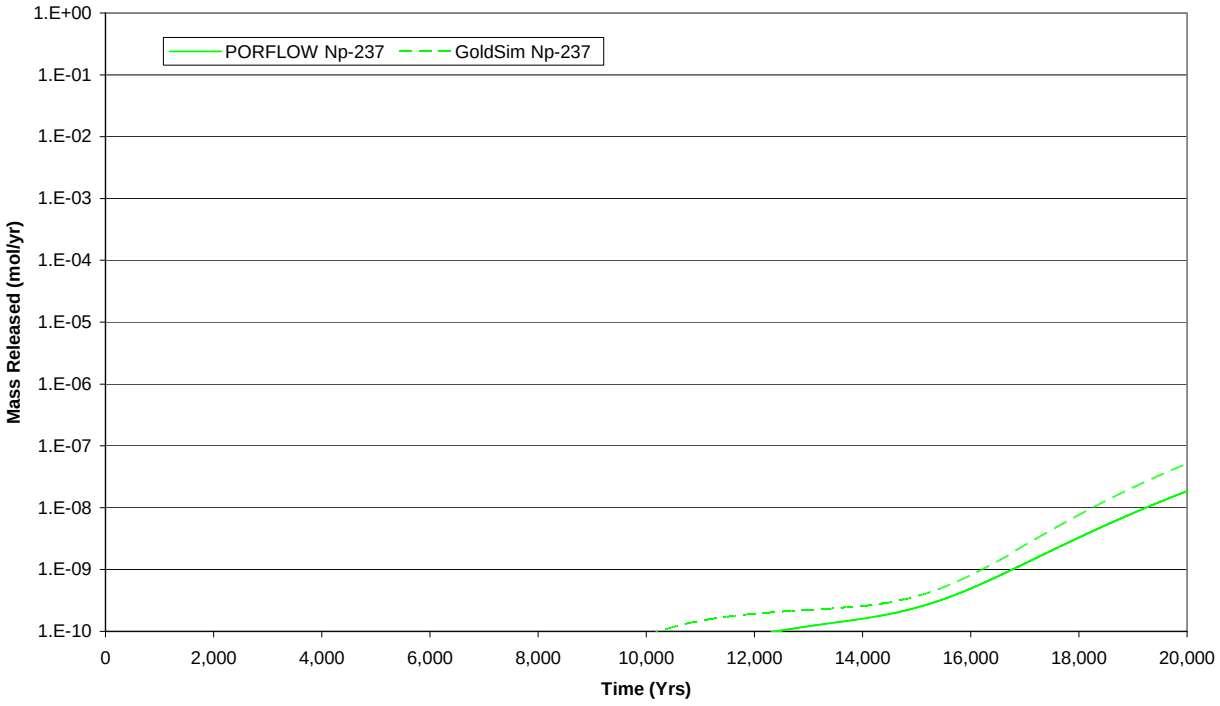

Figure 5.6-40: Revised Mass Release of Np-237 for Type IIIA Tank 40

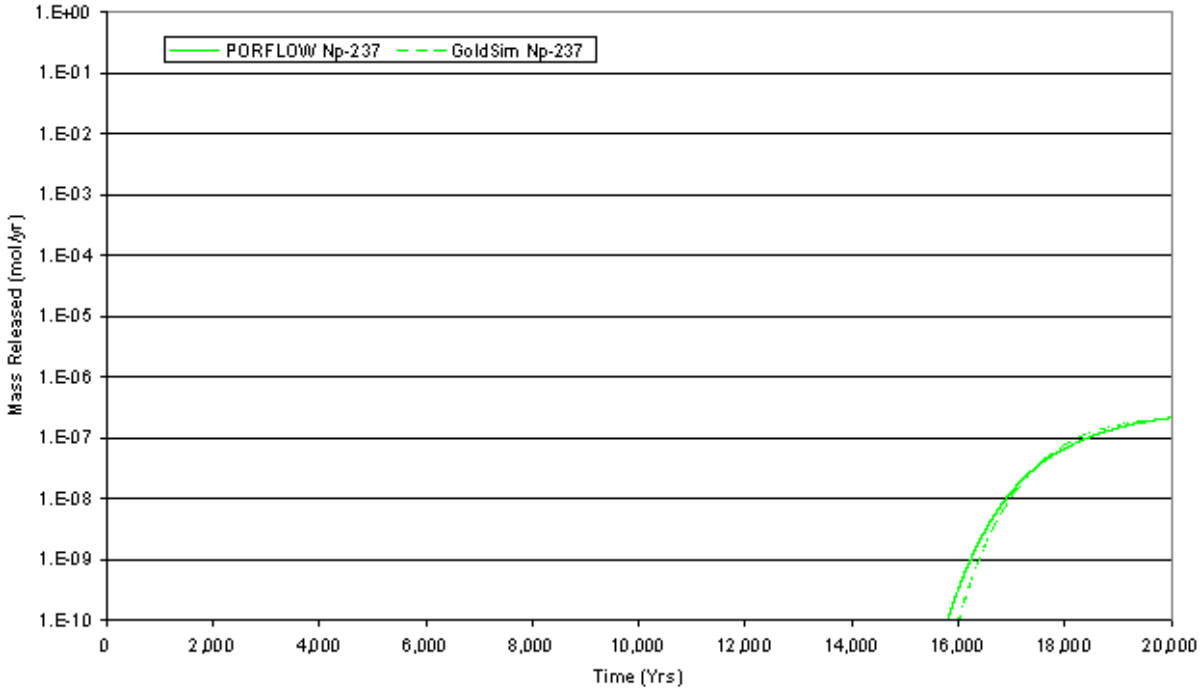

Figure 5.6-41: Revised Mass Release of Np-237 for Type IV Tank 24

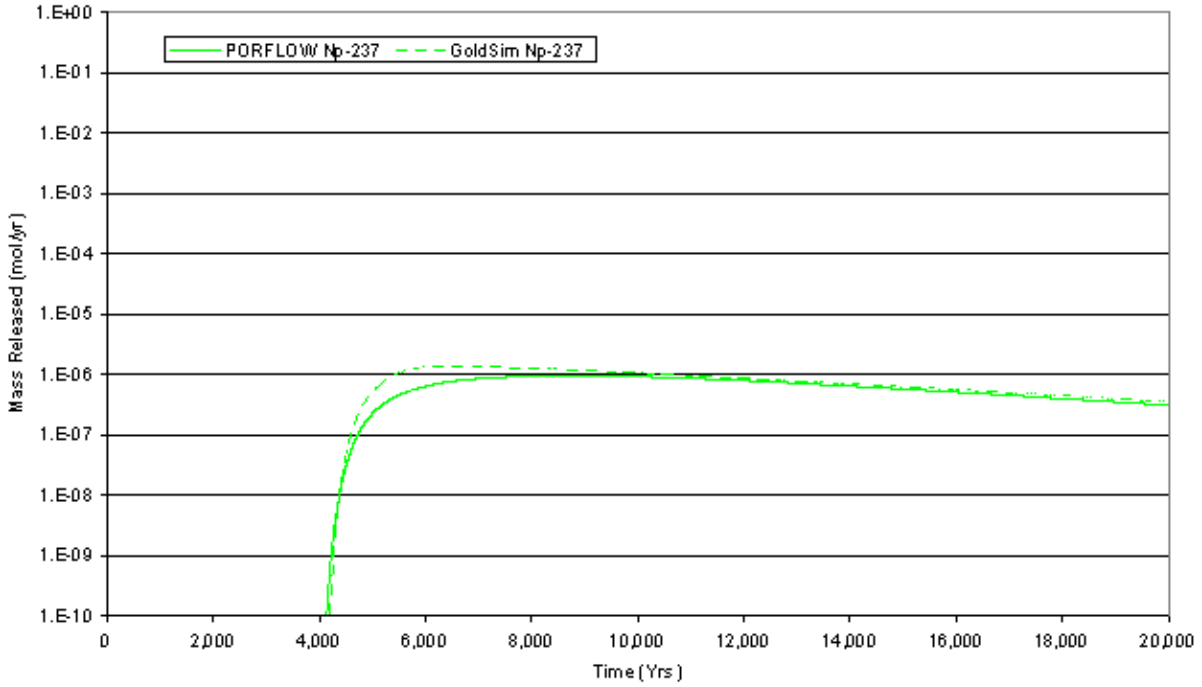

Figure 5.6-42: Comparison of GoldSim Base Case and Refined Basemat Total Dose Results

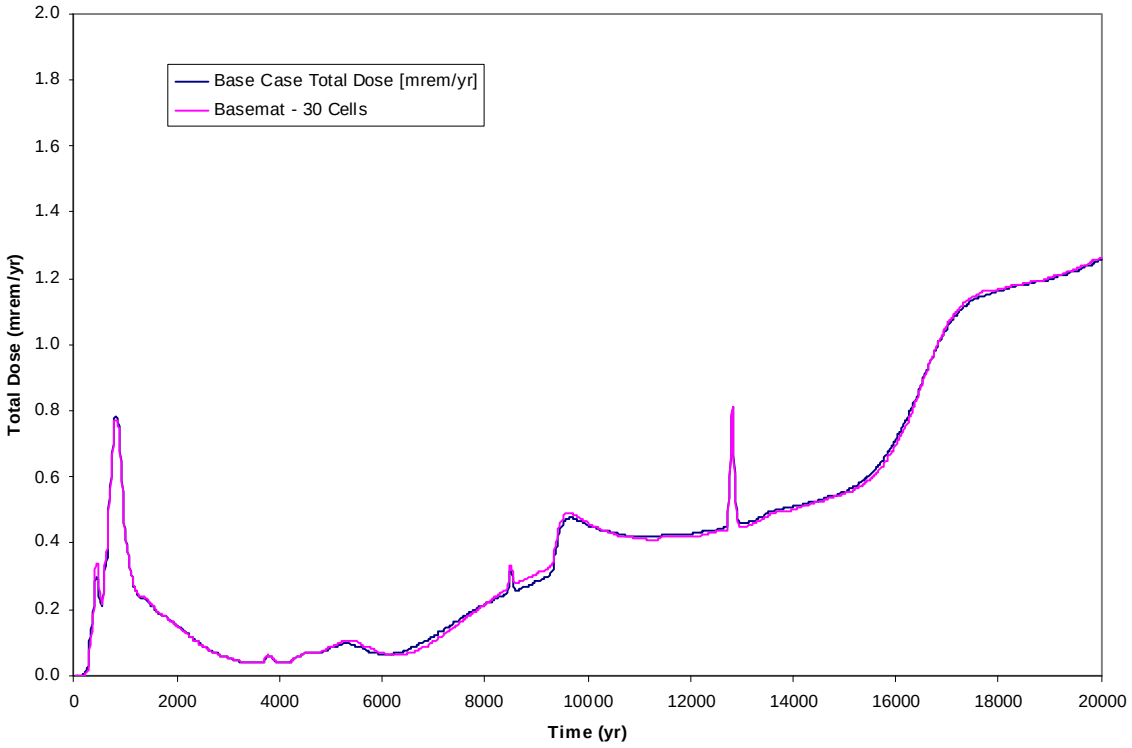

5.6.2.2.8 Benchmarking Summary

The radionuclides used for benchmarking were selected based on their contribution to total dose and because of their unique transport characteristics as either fast-moving (e.g., I-129 is not subject to solubility or sorption controls), slow-moving (e.g., Tc-99 is greatly influenced by solubility limits in the CZ), or produced by in-growth of slow-moving radionuclides (e.g., Ra-226 occurs mostly as in-growth from Pu-238, U-234, and Th-230, all controlled by solubility and sorption processes). By verifying the transport behavior of representative radionuclides, this verifies, by extension, other radionuclides included in the inventory that have similar transport characteristics.

It was confirmed that by increasing the number of mixing cells used to represent sections of the basemat a much closer comparison between the HTF GoldSim Model results and the GoldSim results can be obtained for highly adsorbing radionuclides, such as Np-237. It was also shown that from a risk-based perspective the increase in the number of mixing cells has little influence on total dose.

The results of the three phase benchmarking analysis provide validation that radionuclide release and transport, as simulated in the GoldSim model, mirror the deterministic PORFLOW release and transport behavior. Comparison of the final dose results further verify the agreement between the PORFLOW 3-D transport model and the simplified 1-D GoldSim model, providing confidence that the HTF GoldSim Model UA/SA results presented in Section 5.6.4 and Section 5.6.5 successfully propagate model uncertainty,

and identify the most dose sensitive parameters. For additional benchmarking results, refer to SRR-CWDA-2010-00093.

5.6.3 Parameters Evaluated in the HTF Probabilistic Model

A separate HTF Fate and Transport Model (e.g., also referred to as the HTF GoldSim Model, the stochastic model, or probabilistic model) was developed using the software program, GoldSim, to evaluate parameter sensitivity and the influence of parameter uncertainty on the migration of radionuclides and non-radioactive contaminants from the closed HTF to the accessible environment (see Section 4.4.4.2). The parameters selected for evaluation in the stochastic analyses were based on modeling experience, and the availability of generic and site-specific data to provide a basis for parameter ranges. For a complete description of the HTF GoldSim Model and the input stochastic data used in the model, refer to the report *H-Area Tank Farm Stochastic Fate and Transport Model* (SRR-CWDA-2010-00093).

This section summarizes the probabilistic distributions used in the HTF GoldSim Model. The stochastic parameters are organized by HTF GoldSim Model type. The HTF GoldSim Model contains both a transport sub-model as well as a dose calculator sub-model. The transport sub-model is an abstraction of the HTF PORFLOW flow and transport model, while the dose calculator sub-model takes the calculated contaminated concentrations at points of assessment, and applies exposure pathways and parameters (e.g., bioaccumulation factors, ingestion rates, DCFs, etc.) to determine the dose to the receptor (see Section 4.4.4.2). Uncertainty distributions have been applied to parameters within the transport sub-model as well as in the dose calculator sub-model and the basis and distribution type are discussed in the specific sections. Sections 5.6.3.1 through Section 5.6.3.11 describe the specific parameter distributions used in the transport sub-model. Section 5.6.3.12 presents the stochastic parameters applied in the dose calculator sub-model.

5.6.3.1 Radiological Inventory

The waste tank and ancillary equipment inventories in the HTF GoldSim Model control the total amount of contaminants available for release. Section 3.4 describes the basis for estimates of residual radiological inventory in the HTF waste tanks and ancillary equipment. The baseline, or deterministic, inventory used for each radionuclide is listed in Table 3.4-4. SRR-CWDA-2010-00023 details the process for selecting the baseline inventory. This report also includes a section on the selection of inventory distributions for probabilistic modeling.

The process used to estimate the waste tank residual material at operational closure created estimates that were both bounding and reasonable. Estimates were developed for all chemicals and radionuclides expected to occur in HTF, but those components expected to affect dose are closely scrutinized, and the values selected are intended to provide conservatism over what is expected to remain at operational closure.

The initial inventories are considered conservative estimates. For instance, in estimating residuals from reprocessed reactor spent fuel, maximum burn-up is assumed, consequently certain radionuclide byproducts are also maximized. An unknown amount of residual material characterized as fission products bearing PUREX Low Heat Waste actually originated as cladding waste or other low radionuclide bearing wastes that contain relatively small amounts of fission products. [LWO-PIT-2007-00025] Additional conservatism is

added to the estimate of residuals assumed to remain in the waste tanks after cleaning. It is probable that less residuals, thus a lower inventory of contaminants, will actually remain. These process-related uncertainties have not been quantified; instead, this uncertainty is accounted for by applying a lower and upper bound to the initial inventory estimates, using a log uniform distribution.

In the HTF GoldSim Model, a minimum and maximum multiplier (selected to be reasonably conservative based on scatter plots of sampled data from FTF Tanks 5, 18, and 19 presented in SRR-CWDA-2010-00023) is applied (between 0.01 and 10 are applied to both radionuclide and non-radiological chemical elements) to the initial inventory for each isotope and chemical constituent. The multipliers are presented in Table 5.6-3 and 5.6-4 and are based on the confidence in the initial estimate. The inventory multipliers were chosen based on the inventory estimate for each constituent and are listed in Tables 5.6-3 and 5.6-4. Below is description of basis for each multiplier. For radionuclides estimated by the nominal activity adjustment (1 curie or the detection limit), a maximum multiplier of one was used. Since the actual inventory is expected not to exceed the estimate, a multiplier was selected to reflect that idea. The minimum multiplier was set at two orders of magnitude below the estimate. There is uncertainty in the value for this multiplier because many of the radionuclides are based on the reaching the detection limits. The maximum of 10 were chosen based on SRR-CWDA-2010-00023 and used for those constituents that were not adjusted to the nominal activities (1 curie or the detection limit). In Figure 10.0-1 of SRR-CWDA-2010-00023, three waste tanks sample results are compared to predicted values. In general, the predicted values were within one order of magnitude of the sample results. Given that there are estimates that varied greater than one order of magnitude from actual, the maximum multipliers could have been increased to reflect each constituents range. Although due to the limited data set (i.e., sample results from only three waste tanks), the fact that zeolite was not accounted for in the original WCS sludge solids estimate (i.e., impacting Cs-137 estimates) and the fact that Tanks 18 and 19 do not reflect chemical cleaning impacts, a more generalized value was selected. The minimum of 0.01 was generally selected based on Figure 10.0-1 of SRR-CWDA-2010-00023. While the lower end of the range of data extended to less than 0.01, generally only one of the waste tanks' values were less than 0.01. Therefore, a minimum of 0.01 was conservatively selected. For those waste tanks that were not adjusted by the residual volume uncertainty step, a minimum of 0.1 was selected.

Table 5.6-3: Radiological Inventory Multipliers

	[a]Waste Tanks - Log Uniform Distribution - Minimums																												
Rad	**9**	**10**	**11**	**12**	**13**	**14**	**15**	**16**	**21**	**22**	**23**	**24**	**29**	**30**	**31**	**32**	**35**	**36**	**37**	**38**	**39**	**40**	**41**	**42**	**43**	**48**	**49**	**50**	**51**
Ac-227	0.01	0.01	0.01	0.01	0.01	0.01	0.01	0.01	0.01	0.01	0.01	0.01	0.01	0.01	0.01	0.01	0.01	0.01	0.01	0.01	0.01	0.01	0.01	0.01	0.01	0.01	0.01	0.01	0.01
Ag-108m	0.01	0.01	0.01	0.01	0.01	0.01	0.01	0.01	0.01	0.01	0.01	0.01	0.01	0.01	0.01	0.01	0.01	0.01	0.01	0.01	0.01	0.01	0.01	0.01	0.01	0.01	0.01	0.01	0.01
Al-26	0.01	0.01	0.01	0.01	0.01	0.01	0.01	0.01	0.01	0.01	0.01	0.01	0.01	0.01	0.01	0.01	0.01	0.01	0.01	0.01	0.01	0.01	0.01	0.01	0.01	0.01	0.01	0.01	0.01
Am-241	0.01	0.01	0.01	0.01	0.01	0.01	0.01	0.01	0.01	0.01	0.01	0.01	0.1	0.1	0.1	0.1	0.1	0.1	0.1	0.1	0.1	0.1	0.1	0.1	0.1	0.1	0.1	0.1	0.1
Am-242m	0.01	0.01	0.01	0.01	0.01	0.01	0.01	0.01	0.01	0.01	0.01	0.01	0.01	0.01	0.01	0.01	0.01	0.01	0.01	0.01	0.01	0.01	0.01	0.01	0.01	0.01	0.01	0.01	0.01
Am-243	0.01	0.01	0.01	0.01	0.01	0.01	0.01	0.01	0.01	0.01	0.01	0.01	0.01	0.01	0.01	0.01	0.01	0.01	0.01	0.01	0.01	0.01	0.01	0.01	0.01	0.01	0.01	0.01	0.01
Bi-210m	0.01	0.01	0.01	0.01	0.01	0.01	0.01	0.01	0.01	0.01	0.01	0.01	0.01	0.01	0.01	0.01	0.01	0.01	0.01	0.01	0.01	0.01	0.01	0.01	0.01	0.01	0.01	0.01	0.01
C-14	0.01	0.01	0.01	0.01	0.01	0.01	0.01	0.01	0.01	0.01	0.01	0.01	0.01	0.01	0.01	0.01	0.01	0.01	0.01	0.01	0.01	0.01	0.01	0.01	0.01	0.01	0.01	0.01	0.01
Ca-41	0.01	0.01	0.01	0.01	0.01	0.01	0.01	0.01	0.01	0.01	0.01	0.01	0.01	0.01	0.01	0.01	0.01	0.01	0.01	0.01	0.01	0.01	0.01	0.01	0.01	0.01	0.01	0.01	0.01
Cf-249	0.01	0.01	0.01	0.01	0.01	0.01	0.01	0.01	0.01	0.01	0.01	0.01	0.01	0.01	0.01	0.01	0.01	0.01	0.01	0.01	0.01	0.01	0.01	0.01	0.01	0.01	0.01	0.01	0.01
Cf-251	0.01	0.01	0.01	0.01	0.01	0.01	0.01	0.01	0.01	0.01	0.01	0.01	0.01	0.01	0.01	0.01	0.01	0.01	0.01	0.01	0.01	0.01	0.01	0.01	0.01	0.01	0.01	0.01	0.01
Cl-36	0.01	0.01	0.01	0.01	0.01	0.01	0.01	0.01	0.01	0.01	0.01	0.01	0.01	0.01	0.01	0.01	0.01	0.01	0.01	0.01	0.01	0.01	0.01	0.01	0.01	0.01	0.01	0.01	0.01
Cm-243	0.01	0.01	0.01	0.01	0.01	0.01	0.01	0.01	0.01	0.01	0.01	0.01	0.01	0.01	0.01	0.01	0.01	0.01	0.01	0.01	0.01	0.01	0.01	0.01	0.01	0.01	0.01	0.01	0.01
Cm-244	0.01	0.01	0.01	0.01	0.01	0.01	0.01	0.01	0.01	0.01	0.01	0.01	0.1	0.1	0.1	0.01	0.1	0.1	0.1	0.1	0.1	0.1	0.1	0.1	0.1	0.1	0.1	0.1	0.1
Cm-245	0.01	0.01	0.01	0.01	0.01	0.01	0.01	0.01	0.01	0.01	0.01	0.01	0.01	0.01	0.01	0.01	0.01	0.01	0.01	0.01	0.01	0.01	0.01	0.01	0.01	0.01	0.01	0.01	0.01
Cm-246	0.01	0.01	0.01	0.01	0.01	0.01	0.01	0.01	0.01	0.01	0.01	0.01	0.01	0.01	0.01	0.01	0.01	0.01	0.01	0.01	0.01	0.01	0.01	0.01	0.01	0.01	0.01	0.01	0.01
Cm-247	0.01	0.01	0.01	0.01	0.01	0.01	0.01	0.01	0.01	0.01	0.01	0.01	0.01	0.01	0.01	0.01	0.01	0.01	0.01	0.01	0.01	0.01	0.01	0.01	0.01	0.01	0.01	0.01	0.01
Cm-248	0.01	0.01	0.01	0.01	0.01	0.01	0.01	0.01	0.01	0.01	0.01	0.01	0.01	0.01	0.01	0.01	0.01	0.01	0.01	0.01	0.01	0.01	0.01	0.01	0.01	0.01	0.01	0.01	0.01
Co-60	0.01	0.01	0.01	0.01	0.01	0.01	0.01	0.01	0.01	0.01	0.01	0.01	0.01	0.01	0.01	0.01	0.01	0.01	0.01	0.01	0.01	0.01	0.01	0.01	0.01	0.01	0.01	0.01	0.01
Cs-135	0.01	0.01	0.01	0.01	0.01	0.01	0.01	0.01	0.01	0.01	0.01	0.01	0.1	0.1	0.1	0.1	0.1	0.1	0.1	0.1	0.1	0.1	0.1	0.1	0.1	0.1	0.1	0.1	0.1
Cs-137	0.01	0.01	0.01	0.01	0.01	0.01	0.01	0.01	0.01	0.01	0.01	0.01	0.1	0.1	0.1	0.1	0.1	0.1	0.1	0.1	0.1	0.1	0.1	0.1	0.1	0.1	0.1	0.1	0.1
Eu-152	0.01	0.01	0.01	0.01	0.01	0.01	0.01	0.01	0.01	0.01	0.01	0.01	0.1	0.1	0.1	0.1	0.1	0.1	0.1	0.01	0.01	0.01	0.01	0.01	0.01	0.01	0.01	0.01	0.01
Eu-154	0.01	0.01	0.01	0.01	0.01	0.01	0.01	0.01	0.01	0.01	0.01	0.01	0.1	0.1	0.1	0.1	0.1	0.1	0.1	0.1	0.1	0.1	0.1	0.1	0.1	0.1	0.1	0.1	0.1
Eu-155	0.01	0.01	0.01	0.01	0.01	0.01	0.01	0.01	0.01	0.01	0.01	0.01	0.01	0.01	0.01	0.01	0.01	0.01	0.01	0.01	0.01	0.01	0.01	0.01	0.01	0.01	0.01	0.01	0.01
Gd-152	0.01	0.01	0.01	0.01	0.01	0.01	0.01	0.01	0.01	0.01	0.01	0.01	0.01	0.01	0.01	0.01	0.01	0.01	0.01	0.01	0.01	0.01	0.01	0.01	0.01	0.01	0.01	0.01	0.01
H-3	0.01	0.01	0.01	0.01	0.01	0.01	0.01	0.01	0.01	0.01	0.01	0.01	0.01	0.01	0.01	0.01	0.01	0.01	0.01	0.01	0.01	0.01	0.01	0.01	0.01	0.01	0.01	0.01	0.01
I-129	0.01	0.01	0.01	0.01	0.01	0.01	0.01	0.01	0.01	0.01	0.01	0.01	0.01	0.01	0.01	0.01	0.01	0.01	0.01	0.01	0.01	0.01	0.01	0.01	0.01	0.01	0.01	0.01	0.01
K-40	0.01	0.01	0.01	0.01	0.01	0.01	0.01	0.01	0.01	0.01	0.01	0.01	0.01	0.01	0.01	0.01	0.01	0.01	0.01	0.01	0.01	0.01	0.01	0.01	0.01	0.01	0.01	0.01	0.01
Lu-174	0.01	0.01	0.01	0.01	0.01	0.01	0.01	0.01	0.01	0.01	0.01	0.01	0.01	0.01	0.01	0.01	0.01	0.01	0.01	0.01	0.01	0.01	0.01	0.01	0.01	0.01	0.01	0.01	0.01

Table 5.6-3: Radiological Inventory Multipliers (Continued)

	[a]Waste Tanks - Log Uniform Distribution - Minimums																											
Rad	**9**	**10**	**11**	**12**	**13**	**14**	**15**	**16**	**21**	**22**	**23**	**24**	**29**	**30**	**31**	**32**	**35**	**36**	**37**	**38**	**39**	**40**	**41**	**42**	**43**	**48**	**49**	**50**	**51**
Mo-93	0.01	0.01	0.01	0.01	0.01	0.01	0.01	0.01	0.01	0.01	0.01	0.01	0.01	0.01	0.01	0.01	0.01	0.01	0.01	0.01	0.01	0.01	0.01	0.01	0.01	0.01	0.01	0.01	0.01
Nb-93m	0.01	0.01	0.01	0.01	0.01	0.01	0.01	0.01	0.01	0.01	0.01	0.01	0.01	0.01	0.01	0.01	0.01	0.01	0.01	0.01	0.01	0.01	0.01	0.01	0.01	0.01	0.01	0.01	0.01
Nb-94	0.01	0.01	0.01	0.01	0.01	0.01	0.01	0.01	0.01	0.01	0.01	0.01	0.01	0.01	0.01	0.01	0.01	0.01	0.01	0.01	0.01	0.01	0.01	0.01	0.01	0.01	0.01	0.01	0.01
Ni-59	0.01	0.01	0.01	0.01	0.01	0.01	0.01	0.01	0.01	0.01	0.01	0.01	0.01	0.01	0.01	0.01	0.01	0.01	0.01	0.01	0.01	0.01	0.01	0.01	0.01	0.01	0.01	0.01	0.01
Ni-63	0.01	0.01	0.01	0.01	0.01	0.01	0.01	0.01	0.01	0.01	0.01	0.01	0.1	0.1	0.1	0.1	0.1	0.1	0.1	0.1	0.1	0.1	0.1	0.1	0.1	0.1	0.1	0.1	0.1
Np-237	0.01	0.01	0.01	0.01	0.01	0.01	0.01	0.01	0.01	0.01	0.01	0.01	0.1	0.1	0.1	0.1	0.1	0.1	0.1	0.1	0.1	0.1	0.1	0.1	0.1	0.1	0.1	0.1	0.1
Pa-231	0.01	0.01	0.01	0.01	0.01	0.01	0.01	0.01	0.01	0.01	0.01	0.01	0.01	0.01	0.01	0.01	0.01	0.01	0.01	0.01	0.01	0.01	0.01	0.01	0.01	0.01	0.01	0.01	0.01
Pb-210	0.01	0.01	0.01	0.01	0.01	0.01	0.01	0.01	0.01	0.01	0.01	0.01	0.01	0.01	0.01	0.01	0.01	0.01	0.01	0.01	0.01	0.01	0.01	0.01	0.01	0.01	0.01	0.01	0.01
Pd-107	0.01	0.01	0.01	0.01	0.01	0.01	0.01	0.01	0.01	0.01	0.01	0.01	0.01	0.01	0.01	0.01	0.01	0.01	0.01	0.01	0.01	0.01	0.01	0.01	0.01	0.01	0.01	0.01	0.01
Pt-193	0.01	0.01	0.01	0.01	0.01	0.01	0.01	0.01	0.01	0.01	0.01	0.01	0.01	0.01	0.01	0.01	0.01	0.01	0.01	0.01	0.01	0.01	0.01	0.01	0.01	0.01	0.01	0.01	0.01
Pu-238	0.01	0.01	0.01	0.01	0.01	0.01	0.01	0.01	0.01	0.01	0.01	0.01	0.1	0.1	0.1	0.1	0.1	0.1	0.1	0.1	0.1	0.1	0.1	0.1	0.1	0.1	0.1	0.1	0.1
Pu-239	0.01	0.01	0.01	0.01	0.01	0.01	0.01	0.01	0.01	0.01	0.01	0.01	0.1	0.1	0.1	0.1	0.1	0.1	0.1	0.1	0.1	0.1	0.1	0.1	0.1	0.1	0.1	0.1	0.1
Pu-240	0.01	0.01	0.01	0.01	0.01	0.01	0.01	0.01	0.01	0.01	0.01	0.01	0.1	0.1	0.1	0.1	0.1	0.1	0.1	0.1	0.1	0.1	0.1	0.1	0.1	0.1	0.1	0.1	0.1
Pu-241	0.01	0.01	0.01	0.01	0.01	0.01	0.01	0.01	0.01	0.01	0.01	0.01	0.1	0.1	0.1	0.1	0.1	0.1	0.1	0.1	0.1	0.1	0.1	0.1	0.1	0.1	0.1	0.1	0.1
Pu-242	0.01	0.01	0.01	0.01	0.01	0.01	0.01	0.01	0.01	0.01	0.01	0.01	0.01	0.01	0.01	0.01	0.01	0.01	0.01	0.01	0.01	0.01	0.01	0.01	0.01	0.01	0.01	0.01	0.01
Pu-244	0.01	0.01	0.01	0.01	0.01	0.01	0.01	0.01	0.01	0.01	0.01	0.01	0.01	0.01	0.01	0.01	0.01	0.01	0.01	0.01	0.01	0.01	0.01	0.01	0.01	0.01	0.01	0.01	0.01
Ra-226	0.01	0.01	0.01	0.01	0.01	0.01	0.01	0.01	0.01	0.01	0.01	0.01	0.01	0.01	0.01	0.01	0.01	0.01	0.01	0.01	0.01	0.01	0.01	0.01	0.01	0.01	0.01	0.01	0.01
Ra-228	0.01	0.01	0.01	0.01	0.01	0.01	0.01	0.01	0.01	0.01	0.01	0.01	0.01	0.01	0.01	0.01	0.01	0.01	0.01	0.01	0.01	0.01	0.01	0.01	0.01	0.01	0.01	0.01	0.01
Se-79	0.01	0.01	0.01	0.01	0.01	0.01	0.01	0.01	0.01	0.01	0.01	0.01	0.01	0.01	0.01	0.01	0.01	0.01	0.01	0.01	0.01	0.01	0.01	0.01	0.01	0.01	0.01	0.01	0.01
Sm-147	0.01	0.01	0.01	0.01	0.01	0.01	0.01	0.01	0.01	0.01	0.01	0.01	0.01	0.01	0.01	0.01	0.01	0.01	0.01	0.01	0.01	0.01	0.01	0.01	0.01	0.01	0.01	0.01	0.01
Sm-151	0.01	0.01	0.01	0.01	0.01	0.01	0.01	0.01	0.01	0.01	0.01	0.01	0.1	0.1	0.1	0.1	0.1	0.1	0.1	0.1	0.1	0.1	0.1	0.1	0.1	0.1	0.1	0.1	0.1
Sn-126	0.01	0.01	0.01	0.01	0.01	0.01	0.01	0.01	0.01	0.01	0.01	0.01	0.01	0.01	0.01	0.01	0.01	0.01	0.01	0.01	0.01	0.01	0.01	0.01	0.01	0.01	0.01	0.01	0.01
Sr-90	0.01	0.01	0.01	0.01	0.01	0.01	0.01	0.01	0.01	0.01	0.01	0.01	0.1	0.1	0.1	0.1	0.1	0.1	0.1	0.1	0.1	0.1	0.1	0.1	0.1	0.1	0.1	0.1	0.1
Tc-99	0.01	0.01	0.01	0.01	0.01	0.01	0.01	0.01	0.01	0.01	0.01	0.01	0.1	0.1	0.1	0.1	0.1	0.1	0.1	0.1	0.1	0.1	0.1	0.1	0.1	0.1	0.1	0.1	0.1
Th-229	0.01	0.01	0.01	0.01	0.01	0.01	0.01	0.01	0.01	0.01	0.01	0.01	0.01	0.01	0.01	0.01	0.01	0.01	0.01	0.01	0.01	0.01	0.01	0.01	0.01	0.01	0.01	0.01	0.01
Th-230	0.01	0.01	0.01	0.01	0.01	0.01	0.01	0.01	0.01	0.01	0.01	0.01	0.01	0.01	0.01	0.01	0.01	0.01	0.01	0.01	0.01	0.01	0.01	0.01	0.01	0.01	0.01	0.01	0.01
Th-232	0.01	0.01	0.01	0.01	0.01	0.01	0.01	0.01	0.01	0.01	0.01	0.01	0.1	0.1	0.1	0.01	0.1	0.1	0.1	0.1	0.1	0.1	0.1	0.1	0.1	0.1	0.1	0.1	0.1
U-232	0.01	0.01	0.01	0.01	0.01	0.01	0.01	0.01	0.01	0.01	0.01	0.01	0.01	0.01	0.01	0.01	0.01	0.01	0.01	0.01	0.01	0.01	0.01	0.01	0.01	0.01	0.01	0.01	0.01
U-233	0.01	0.01	0.01	0.01	0.01	0.01	0.01	0.01	0.01	0.01	0.01	0.01	0.1	0.1	0.1	0.01	0.1	0.1	0.1	0.1	0.1	0.1	0.1	0.1	0.1	0.1	0.1	0.1	0.1
U-234	0.01	0.01	0.01	0.01	0.01	0.01	0.01	0.01	0.01	0.01	0.01	0.01	0.1	0.1	0.1	0.1	0.1	0.1	0.1	0.1	0.1	0.1	0.1	0.1	0.1	0.1	0.1	0.1	0.1

Table 5.6-3: Radiological Inventory Multipliers (Continued)

	[a]Waste Tanks - Log Uniform Distribution - Minimums																												
Rad	**9**	**10**	**11**	**12**	**13**	**14**	**15**	**16**	**21**	**22**	**23**	**24**	**29**	**30**	**31**	**32**	**35**	**36**	**37**	**38**	**39**	**40**	**41**	**42**	**43**	**48**	**49**	**50**	**51**
U-235	0.01	0.01	0.01	0.01	0.01	0.01	0.01	0.01	0.01	0.01	0.01	0.01	0.1	0.1	0.1	0.1	0.1	0.1	0.1	0.1	0.1	0.1	0.1	0.1	0.1	0.1	0.1	0.1	0.1
U-236	0.01	0.01	0.01	0.01	0.01	0.01	0.01	0.01	0.01	0.01	0.01	0.01	0.01	0.01	0.01	0.01	0.01	0.01	0.01	0.01	0.01	0.01	0.01	0.01	0.01	0.01	0.01	0.01	0.01
U-238	0.01	0.01	0.01	0.01	0.01	0.01	0.01	0.01	0.01	0.01	0.01	0.01	0.1	0.1	0.1	0.01	0.1	0.1	0.1	0.1	0.1	0.1	0.1	0.1	0.1	0.1	0.1	0.1	0.1
Zr-93	0.01	0.01	0.01	0.01	0.01	0.01	0.01	0.01	0.01	0.01	0.01	0.01	0.1	0.1	0.1	0.1	0.1	0.1	0.1	0.1	0.1	0.1	0.1	0.1	0.1	0.1	0.1	0.1	0.1

	[b]Waste Tank - Log Uniform Distribution - Maximums																												
Rad	**9**	**10**	**11**	**12**	**13**	**14**	**15**	**16**	**21**	**22**	**23**	**24**	**29**	**30**	**31**	**32**	**35**	**36**	**37**	**38**	**39**	**40**	**41**	**42**	**43**	**48**	**49**	**50**	**51**
Ac-227	1	1	1	1	1	1	1	1	1	1	1	1	1	1	1	1	1	1	1	1	1	1	1	1	1	1	1	1	1
Ag-108m	1	1	1	1	1	1	1	1	1	1	1	1	1	1	1	1	1	1	1	1	1	1	1	1	1	1	1	1	1
Al-26	1	1	1	1	1	1	1	1	1	1	1	1	1	1	1	1	1	1	1	1	1	1	1	1	1	1	1	1	1
Am-241	10	10	10	10	10	10	10	10	10	10	10	10	10	10	10	10	10	10	10	10	10	10	10	10	10	10	10	10	10
Am-242m	1	1	1	1	1	1	1	1	1	1	1	1	1	1	1	1	1	1	1	1	1	1	1	1	1	1	1	1	1
Am-243	1	1	1	1	1	1	1	1	1	1	1	1	1	1	1	1	1	1	1	1	1	1	1	1	1	1	1	1	1
Bi-210m	1	1	1	1	1	1	1	1	1	1	1	1	1	1	1	1	1	1	1	1	1	1	1	1	1	1	1	1	1
C-14	1	1	1	1	1	1	1	1	1	1	1	1	1	1	1	1	1	1	1	1	1	1	1	1	1	1	1	1	1
Ca-41	1	1	1	1	1	1	1	1	1	1	1	1	1	1	1	1	1	1	1	1	1	1	1	1	1	1	1	1	1
Cf-249	1	1	1	1	1	1	1	1	1	1	1	1	1	1	1	1	1	1	1	1	1	1	1	1	1	1	1	1	1
Cf-251	1	1	1	1	1	1	1	1	1	1	1	1	1	1	1	1	1	1	1	1	1	1	1	1	1	1	1	1	1
Cl-36	1	1	1	1	1	1	1	1	1	1	1	1	1	1	1	1	1	1	1	1	1	1	1	1	1	1	1	1	1
Cm-243	1	1	1	1	1	1	1	1	1	1	1	1	1	1	1	1	1	1	1	1	1	1	1	1	1	1	1	1	1
Cm-244	10	10	10	10	10	10	10	10	10	10	10	10	10	10	10	1	10	10	10	10	10	10	10	10	10	10	10	10	10
Cm-245	1	1	1	1	1	1	1	1	1	1	1	1	1	1	1	1	1	1	1	1	1	1	1	1	1	1	1	1	1
Cm-246	1	1	1	1	1	1	1	1	1	1	1	1	1	1	1	1	1	1	1	1	1	1	1	1	1	1	1	1	1
Cm-247	1	1	1	1	1	1	1	1	1	1	1	1	1	1	1	1	1	1	1	1	1	1	1	1	1	1	1	1	1
Cm-248	1	1	1	1	1	1	1	1	1	1	1	1	1	1	1	1	1	1	1	1	1	1	1	1	1	1	1	1	1
Co-60	1	1	1	1	1	1	1	1	1	1	1	1	1	1	1	1	1	1	1	1	1	1	1	1	1	1	1	1	1
Cs-135	10	10	10	10	10	10	10	10	10	10	10	10	10	10	10	10	10	10	10	10	10	10	10	10	10	10	10	10	10
Cs-137	10	10	10	10	10	10	10	10	10	10	10	10	10	10	10	10	10	10	10	10	10	10	10	10	10	10	10	10	10
Eu-152	10	10	10	10	10	10	10	1	1	1	1	1	10	10	10	10	10	10	10	1	1	1	1	1	1	1	1	1	1

Table 5.6-3: Radiological Inventory Multipliers (Continued)

	[b]Waste Tank - Log Uniform Distribution - Maximums																												
Rad	**9**	**10**	**11**	**12**	**13**	**14**	**15**	**16**	**21**	**22**	**23**	**24**	**29**	**30**	**31**	**32**	**35**	**36**	**37**	**38**	**39**	**40**	**41**	**42**	**43**	**48**	**49**	**50**	**51**
Eu-154	10	10	10	10	10	10	10	10	10	10	10	10	10	10	10	10	10	10	10	10	10	10	10	10	10	10	10	10	10
Eu-155	1	1	1	1	1	1	1	1	1	1	1	1	1	1	1	1	1	1	1	1	1	1	1	1	1	1	1	1	1
Gd-152	1	1	1	1	1	1	1	1	1	1	1	1	1	1	1	1	1	1	1	1	1	1	1	1	1	1	1	1	1
H-3	1	1	1	1	1	1	1	1	1	1	1	1	1	1	1	1	1	1	1	1	1	1	1	1	1	1	1	1	1
I-129	1	1	1	1	1	1	1	1	1	1	1	1	1	1	1	1	1	1	1	1	1	1	1	1	1	1	1	1	1
K-40	1	1	1	1	1	1	1	1	1	1	1	1	1	1	1	1	1	1	1	1	1	1	1	1	1	1	1	1	1
Lu-174	1	1	1	1	1	1	1	1	1	1	1	1	1	1	1	1	1	1	1	1	1	1	1	1	1	1	1	1	1
Mo-93	1	1	1	1	1	1	1	1	1	1	1	1	1	1	1	1	1	1	1	1	1	1	1	1	1	1	1	1	1
Nb-93m	1	1	1	1	1	1	1	1	1	1	1	1	1	1	1	1	1	1	1	1	1	1	1	1	1	1	1	1	1
Nb-94	10	10	1	1	1	1	1	1	1	1	1	1	1	1	1	1	1	1	1	1	1	1	1	1	1	1	1	1	1
Ni-59	10	10	10	10	10	10	10	1	1	1	1	1	1	1	1	1	1	1	1	1	1	1	1	1	1	1	1	1	1
Ni-63	10	10	10	10	10	10	10	10	10	10	10	10	10	10	10	10	10	10	10	10	10	10	10	10	10	10	10	10	10
Np-237	10	10	10	10	10	10	10	10	10	10	10	10	10	10	10	10	10	10	10	10	10	10	10	10	10	10	10	10	10
Pa-231	1	1	1	1	1	1	1	1	1	1	1	1	1	1	1	1	1	1	1	1	1	1	1	1	1	1	1	1	1
Pb-210	1	1	1	1	1	1	1	1	1	1	1	1	1	1	1	1	1	1	1	1	1	1	1	1	1	1	1	1	1
Pd-107	1	1	1	1	1	1	1	1	1	1	1	1	1	1	1	1	1	1	1	1	1	1	1	1	1	1	1	1	1
Pt-193	1	1	1	1	1	1	1	1	1	1	1	1	1	1	1	1	1	1	1	1	1	1	1	1	1	1	1	1	1
Pu-238	10	10	10	10	10	10	10	10	10	10	10	10	10	10	10	10	10	10	10	10	10	10	10	10	10	10	10	10	10
Pu-239	10	10	10	10	10	10	10	10	10	10	10	10	10	10	10	10	10	10	10	10	10	10	10	10	10	10	10	10	10
Pu-240	10	10	10	10	10	10	10	10	10	10	10	10	10	10	10	10	10	10	10	10	10	10	10	10	10	10	10	10	10
Pu-241	1	1	10	10	10	10	10	10	10	10	10	10	10	10	10	10	10	10	10	10	10	10	10	10	10	10	10	10	10
Pu-242	1	1	1	1	1	1	1	1	1	1	1	1	1	1	1	1	1	1	1	1	1	1	1	1	1	1	1	1	1
Pu-244	1	1	1	1	1	1	1	1	1	1	1	1	1	1	1	1	1	1	1	1	1	1	1	1	1	1	1	1	1
Ra-226	1	1	1	1	1	1	1	1	1	1	1	1	1	1	1	1	1	1	1	1	1	1	1	1	1	1	1	1	1
Ra-228	1	1	1	1	1	1	1	1	1	1	1	1	1	1	1	1	1	1	1	1	1	1	1	1	1	1	1	1	1
Se-79	10	10	10	10	10	10	10	1	1	1	1	1	1	1	1	1	1	1	1	1	1	1	1	1	1	1	1	1	1
Sm-147	1	1	1	1	1	1	1	1	1	1	1	1	1	1	1	1	1	1	1	1	1	1	1	1	1	1	1	1	1
Sm-151	10	10	10	10	10	10	10	10	10	10	10	10	10	10	10	10	10	10	10	10	10	10	10	10	10	10	10	10	10
Sn-126	10	10	10	10	10	10	10	1	1	1	1	1	1	1	1	1	1	1	1	1	1	1	1	1	1	1	1	1	1
Sr-90	10	10	10	10	10	10	10	10	10	10	10	10	10	10	10	10	10	10	10	10	10	10	10	10	10	10	10	10	10

Table 5.6-3: Radiological Inventory Multipliers (Continued)

	[b]Tank - Log Uniform Distribution - Maximums																												
Rad	**9**	**10**	**11**	**12**	**13**	**14**	**15**	**16**	**21**	**22**	**23**	**24**	**29**	**30**	**31**	**32**	**35**	**36**	**37**	**38**	**39**	**40**	**41**	**42**	**43**	**48**	**49**	**50**	**51**
Tc-99	10	10	10	10	10	10	10	10	10	10	10	10	10	10	10	10	10	10	10	10	10	10	10	10	10	10	10	10	10
Th-229	1	1	10	10	10	10	10	1	1	1	1	1	1	1	1	1	1	1	1	1	1	1	1	1	1	1	1	1	1
Th-230	1	1	1	1	1	1	1	1	1	1	1	1	1	1	1	1	1	1	1	1	1	1	1	1	1	1	1	1	1
Th-232	1	1	10	10	10	10	10	10	1	1	1	1	10	10	10	1	10	10	10	10	10	10	10	10	10	10	10	10	10
U-232	1	1	1	1	1	1	1	1	1	1	1	1	1	1	1	1	1	1	1	1	1	1	1	1	1	1	1	1	1
U-233	10	10	10	10	10	10	10	10	10	10	10	10	10	10	10	1	10	10	10	10	10	10	10	10	10	10	10	10	10
U-234	10	10	10	10	10	10	10	10	10	10	10	10	10	10	10	10	10	10	10	10	10	10	10	10	10	10	10	10	10
U-235	1	1	10	10	10	10	10	1	1	1	1	1	10	10	10	10	10	10	10	10	10	10	10	10	10	10	10	10	10
U-236	1	1	1	1	1	1	1	1	1	1	1	1	1	1	1	1	1	1	1	1	1	1	1	1	1	1	1	1	1
U-238	10	10	10	10	10	10	10	1	1	1	1	10	10	10	10	1	10	10	10	10	10	10	10	10	10	10	10	10	10
Zr-93	10	10	10	10	10	10	10	10	10	10	10	10	10	10	10	10	10	10	10	10	10	10	10	10	10	10	10	10	10

a Shaded cells indicate radionuclides and waste tanks which apply 0.1 (as opposed to 0.01) as the minimum multiplier

b Shaded cells indicate radionuclides and waste tanks which apply 10 (as opposed to 1) as the maximum multiplier.

Table 5.6-4: Non-Radiological Inventory Multipliers for All Waste Tank Types

	Probability	Multiplier
All Non-Radiological Chemicals	0.25	0.01
	0.25	0.1
	0.25	1
	0.25	10

Several radionuclides listed in Table 5.6-3 have maximum multipliers equal to one, indicating that the initial inventory will not go above the deterministic baseline inventory. This was done for radionuclides where the inventory projections indicate they would remain below the detection limit (1.0E-4 curie), or where the adjusted inventory was 1.0 curie (Section 3.4.2.3) when the baseline inventory was set equal to the detection limit or 1.0 curie, it was a conservative adjustment of these inventory estimates. Therefore, an upper multiplier of 1.0 would be appropriate. The HTF GoldSim Model then adjusts the value to lower, more realistic values. As Table 5.6-3 and 5.6-4 indicate, the lower limit is either one order or two orders of magnitude less than the baseline inventory. For those components of the initial inventory expected to have a large impact on dose, and that had projected inventories greater than the detection limit, a multiplier of 10 is used for the upper bound. An example is Pu-238, which has a lower and upper multiplier equal to 0.01 and 10. Pu-238 decays to Ra-226, which is the radionuclide that drives peak dose in 20,000 years (Section 5.5). The initial inventory of Ra-226 is insignificant; rather it is the radioactive decay from its many parent radionuclides that control the concentration of Ra-226 and ultimately the dose from Ra-226. Because Pu-238 decay to Ra-226 is the largest contributor to the concentration of Ra-226, it was considered conservative to provide an upper bound an order of magnitude higher than the already conservative baseline estimate.

An initial inventory is assumed to exist in the Type II sand pads and annulus. An initial inventory is also assumed to exist in the ancillary equipment including the transfer lines. Both the sand pad and annulus initial inventory estimates were considered extremely conservative for the reasons described in SRR-CWDA-2010-00023, therefore, zero uncertainty was applied.

5.6.3.2 Waste Tank Cases

This section specifically considers the uncertainty accounted for by simulating different waste tank cases. As presented in Section 4.4.2, five different waste tank cases (Cases A through E) were simulated deterministically using the PORFLOW flow and transport model. The differences in the five conceptual models include 1) the existence of fast flow paths, 2) the timing of cementitious material degradation, 3) the timing of liner failure, and 4) the influence of the reducing capacity of the grout on the CZ. The differences between the five cases are summarized in Table 4.4-1 (Section 4.4.2).

A probability is applied to each case according to its likelihood of occurrence. The discrete distribution applied to the five scenarios presented in Table 5.6-5 is meant only to enable evaluation of the sensitivity of the case on dose. The applied values are not based on quantified data, but are instead relative relationships based on engineering judgment.

Table 5.6-5: Case Probability for All Waste Tank Types

Case	Probability[a]
A	50%
B	10%
C	30%
D	2.5%
E	7.5%

a Discrete distribution chosen using engineering judgment.

The following assumptions were used to inform the probability values:

- Fast flow paths, in the form of cracks through the cement barriers of the waste tanks (as represented by Cases B, C, D and E), are not likely to occur immediately at the time of closure. However, to be conservative, Case A was applied a 50% probability of occurrence, and the remaining fast flow cases a collective probability of 50%.
- Case B and C can be loosely grouped into a subgroup of fast flow paths through the grout but not the basemat. The grout is considered more likely to have a fast flow path (e.g., shrinkage gap) compared to the basemat, therefore a much smaller probability is applied to Cases D and E. Case B and C are given a probability of occurrence equal to 40%, while D and E have the collective probability equal to 10%.
- The 40% applied collectively to B and C and the 10% applied collectively to D and E are further refined by the likelihood of having instantaneous degradation of the cementitious materials at year 501. It was considered more likely that cementitious degradation would be gradual; therefore, B and D were given lower probabilities of occurrence than their counterparts were.

The impact of fast flow paths, the timing of liner failure, and cementitious material degradation time are represented both implicitly in the HTF GoldSim Model using case dependent flow fields and explicitly using stochastic parameters. Both are described in the following sections.

The HTF GoldSim Model was used only to model contaminant transport and therefore, flow is not calculated independently. Instead, the flow fields calculated in PORFLOW for each model component (e.g., grout, CZ, basemat, primary and secondary liner, annulus) were used as input to the HTF GoldSim Model. The unique set of PORFLOW flow fields used in the HTF GoldSim Model for each of the five failure cases, and applied to each model domain, are presented in SRR-CWDA-2010-00093. The inclusion points for the flow data in the HTF GoldSim Model is schematically depicted in Figure 4.4-50 for Type II tanks and Figure 4.4-51, for Non-Type II tanks (see Section 4.4.4.2). Having different flow fields for the various cases is the method by which uncertainties in parameters affecting flow (e.g., liner failure time and cementitious materials degradation time) are incorporated into the UA/SA.

5.6.3.3 Solubility

The solubility values applied to the CZ in the HTF GoldSim Model control contaminant release, with different solubility values resulting in different release rates. Table 4.2-5 and Table 4.2-6 (from Section 4.2.1) present the deterministic solubility values by controlling phase for all elements of interest at each of the chemical states of interest. For plutonium, neptunium, technetium, and uranium, the solubility values listed correspond to iron co-precipitation as the controlling mechanism.

As discussed in Section 4.2.1, there is large uncertainty in the calculation of solubility values within the waste cell. Much of the uncertainty is because of unknowns related to the CZ and how the conditions in this domain will evolve with time. Some of the uncertainty is due to the limited amount of thermodynamic data available for many of the radionuclides of interest. Uncertainty associated with the solubility model was managed largely through applying conservative modeling assumptions, specifically in determining the controlling phase for the element of interest.

For those radionuclides which have historically been of most concern at SRS (plutonium, uranium, neptunium, and technetium), distributions were assigned for both Reducing and Oxidizing Region II conditions. Tables 5.6-6 and 5.6-7 present the discrete distributions applied to the controlling phases for plutonium, uranium, neptunium, and technetium. The probabilities are weighted to account for the likelihood of the different controlling phases. The possibility of iron co-precipitation as a controlling phase was included in the probability distributions. The probabilities chosen are based on observations in the literature and expected thermodynamic stability. [WSRC-STI-2007-00544, Rev 2]

Table 5.6-6: Probability Distributions for Various Phases Controlling Reduced Region II Solubility

	Controlling Phase [a]	Solubility (mol/L)	Probability
Plutonium	$Pu(OH)_4$	1.7E-09	0.4
	PuO_2	1.3E-17	0.1
	Iron co-precipitation	7.0E-14	0.5
Neptunium	$Np(OH)_4$	4.8E-09	0.4
	NpO_2	2.6E-20	0.1
	Iron co-precipitation	2.0E-14	0.5
Technetium	Tc_2S_7	1.2E-32	0.4
	$TcO_2.2H_2O$	3.3E-08	0.1
	Iron co-precipitation	6.0E-13	0.5
Uranium	UO_2(am)	3.5E-05	0.25
	Uraninite	3.9E-10	0.15
	$CaUO_4$	6.9E-06	0.1
	Iron co-precipitation	7.0E-12	0.5

a Iron co-precipitation assumed to be controlling 50% of the time.

Table 5.6-7: Probability Distributions for Various Phases Controlling Oxidized Region II Solubility

	Controlling Phase[a]	Solubility (mol/L)	Probability
Plutonium	Pu(OH)4	3.0E-07	0.35
	PuO2	2.3E-15	0.1
	PuO2(OH)2	1.9E-11	0.05
	Iron co-precipitation	9.0E-15	0.5
Neptunium	NpO2(OH)(am)	6.8E-07	0.35
	Np2O5	9.6E-10	0.1
	NpO2	1.2E-10	0.05
	Iron co-precipitation	2.0E-15	0.5
Technetium	No solubility control	instantaneous release	0.5
	Iron co-precipitation	7.0E-14	0.5
Uranium	Becquerelite	3.4E-07	0.25
	CaUO4	1.8E-14	0.15
	Schoepite	1.8E-05	0.1
	Iron co-precipitation	9.0E-13	0.5

a Iron co-precipitation assumed to be controlling 50% of the time.

Uncertainties in predicting the controlling phase accounts for a large portion of the uncertainty in calculating the appropriate solubility. Uncertainties in the thermodynamic quantities also play an important role (Section 4.2.1). [WSRC-STI-2007-00544] Uncertainty in the controlling phase is presented above, while uncertainty in thermodynamic quantities is addressed by implementing four bounding conditions discussed in detail in Section 4.2.2. Changing the chemical conditions in the grout and CZ are implemented in GoldSim by modifying the chemical transition times in the CZ. This is discussed in Section 5.6.3.8.

5.6.3.4 Distribution Coefficient Values

The cementitious material (both concrete and grout) comprising the engineered barrier and the soil underlying the HTF have a propensity to slow the transport of certain radionuclides through the environment, thus retarding their arrival to a potential receptor. The ability of the cementitious materials or the soils to sorb the different radionuclides is represented using distribution coefficients. The ability of the material to sorb the radionuclide is dependent on the chemical condition of the environment. Tables 4.2-29 and 4.2-33 (Section 4.2.2) show the deterministic distribution coefficient values for the soils, for soils impacted by reducing cement leachate, and for the cementitious materials. Distribution coefficient values are element dependant and they vary depending on the chemical state of the system (e.g., young/old age; reducing/oxidizing regions). The bases for deterministic values are presented in Section 4.2.2 and in the report, *Geochemical Data Package for Performance Assessment Calculations Related to the Savannah River Site.* [SRNL-STI-2009-00473]

Groupings for the distribution coefficient values used in the HTF GoldSim Model were based on the approach described in SRNL-STI-2009-00150. This report recommends applying a lognormal distribution with maximum and minimum values based on the material under consideration. The shape of the lognormal distribution is based on the geometric standard deviation (GSD) that differs by the material under consideration and the magnitude of the

deterministic value for the distribution coefficient. Table 5.6-8 provides the distributions used in the HTF GoldSim Model for each of the materials. In Table 5.6-8, in the "Lognormal GSD" column certain conditions are defined to calculate the GSD. Here, the geometric mean (GM) is equal to the deterministic (baseline) value. For example, for clayey soils (and cement leachate impacted clayey soils), radionuclides with a deterministic distribution coefficient value less than 4 mL/g will have a lognormal GSD equal to 1.001, but for radionuclides with deterministic distribution coefficient values greater than 4 mL/g, the lognormal GSD is calculated as the product of 0.25 and the deterministic value. While a GSD of 1.001 results in a small distribution around the GM, this is only for elements that already have a low deterministic value and thus have low retardation which for soil include technetium, iodine, and astatine. Of particular interest is the technetium, which has a deterministic value in sandy soil of 0.6 mL/g and a small distribution around this value. The dispersion of technetium distribution coefficient values was evaluated in SRNS-STI-2008-00286 and the mean was 3.4 mL/g with a 95th percentile range of 2.4 to 4.4 mL/g. The deterministic value was already a pessimistic value based on the site-specific data and therefore, it would be inappropriate to allow the distribution around the modeled value to range lower.

Table 5.6-8: Distribution Coefficient Variability in the HTF GoldSim Model

Material Zone	Min	Max	Lognormal GSD	
Clayey Soils[b] and Cement Leachate Impacted Clayey Soils	0.5xGM[a]	1.5xGM	GM < 4.0 mL/g	GM = 4.0 mL/g or greater
			1.001 mL/g	0.25 x GM
Sandy Soils[c] and Cement Leachate Impacted Sandy Soils	0.25xGM	1.75xGM	GM < 2.7 mL/g	GM = 2.7 mL/g or greater
			1.001 mL/g	0.375 x GM
Cementitious Materials	0.25xGM	1.75xGM	GM < 2.7 mL/g	GM = 2.7 mL/g or greater
			1.001 mL/g	0.375 x GM

a GM = geometric mean of the lognormal distribution defined as the baseline value presented in Table 4.2-29 for soils, and cement leachate impacted soils and Table 4.2-33 for cementitious materials.
b Backfill layer
c Vadose zone and saturated zone

5.6.3.5 Basemat Thickness

The concrete floor thickness, also known as the basemat thickness in the HTF GoldSim Model, retards contaminant transport with its effectiveness related to the basemat distribution coefficient values and the basemat thickness. Section 4.4.1 shows the design dimensions used in the baseline modeling for the various waste tank types, including concrete basemat thickness. Section 3.2.1 provides design details for the various waste tank types, including details regarding the concrete basemat designs. The basemat thickness specified on construction drawings is used as the most likely basemat thickness, with other design details used to determine a probable maximum and minimum thickness of basemat concrete. A triangular distribution using these maximum, minimum, and the most likely value as the peak was utilized for basemat thickness in the stochastic analyses. Table 5.6-9 summarizes the values used in the HTF GoldSim Model.

Table 5.6-9: Basemat Thickness Variability in the HTF GoldSim Model

		Triangular	
Tank Type	**Deterministic (in)**	**Min (in)**	**Max (in)**
Type I	30	29	37
Type II	42	41.5	48.5
Type III	42	41.5	48.5
Type IIIA	41	40.5	45.5
Type IV	6.9025	6.7775	7.0275

The design details used as the basis for the various thicknesses are described below for each waste tank type.

5.6.3.5.1 Type IV Tank Concrete Floor Thickness

As described in Section 3.2, a Type IV tank basemat was specified to be 4-inches thick with a tolerance of plus 0.5 inch and minus 0.25 inch. A 3-inch cement topping was then poured over the basemat and given a float and trowel finish having a maximum tolerance of plus or minus 0.125 inch from a true level. Drainage channels, 1.625-inches deep and approximately 3.5-inches wide (3.625 inches at the top and 3.125 inches at the bottom), for use in leak detection were formed in the 3-inch deep basemat cement topping. The drainage channels cover less than 6% of the total foundation area.

Thickness Calculations

Minimum at channel location - 5.25 inches (4 + 2.875 - 1.625)

Minimum without channel - 6.875 inches (4 + 2.875)

Median at channel location - 5.375 inches (3 + 4 - 1.625)

Median without channel - 7 inches (3 + 4)

Maximum at channel location - 5.5 inches (4 + 3.125 - 1.625)

Maximum without channel - 7.125 inches (4 + 3.125)

Modeling Values Used

	Inches:	**Basis:**
Most likely:	6.9025	Weighted median (0.06 (5.375) + 0.94 (7))
Minimum:	6.7775	Weighted minimum (0.06 (5.25) + 0.94 (6.875))
Maximum:	7.0275	Weighted maximum (0.06 (5.5) + 0.94 (7.125))
Mean:	6.9025	Based on triangular distribution

5.6.3.5.2 Type I Tank Concrete Floor Thickness

As presented in Section 3.2, the working slab for a Type I tank is 4-inches thick. The working slab assumed tolerance is ± 0.5 inch based on the construction specification requirement of no visual variance in concrete level. [Spec-3019] A 30-inch reinforced concrete base (i.e., the basemat) sits on top of the working slab. The basemat assumed tolerance is ± 1 inch based on the construction specification requirement of no visual variance in concrete level. [Spec-3019] A 3-inch layer of grout sits on top of the basemat, and the primary container sits above the grout.

Modeling Values Used

	Inches:	**Basis:**
Most likely:	30.0	30-inch basemat
Minimum:	29.0	30-inch basemat - 1-inch tolerance on basemat
Maximum:	37.0	4-inch working slab + 30-inch basemat + 3-inch grout layer
Mean:	32.0	Based on triangular distribution

5.6.3.5.3 Type II Tank Concrete Floor Thickness

The modeling values used for Type II tanks are the same as for Type III tanks described in Section 3.2.

Modeling Values Used

	Inches:	**Basis:**
Most likely:	42.0	42-inch basemat (ignore drop panel)
Minimum:	41.5	42-inch basemat - 0.5-inch tolerance on basemat
Maximum:	48.5	6-inch working slab + 42-inch basemat + 0.5-inch tolerance on basemat (ignore drop panel)
Mean:	44.0	Based on triangular distribution

5.6.3.5.4 Type III Tank Concrete Floor Thickness

As described in Section 3.2, Type III tanks have a 6-inch working slab. The Type III tank basemat, made of reinforced concrete, has a 3 foot 6-inch minimum thickness (5 feet 4 inches at drop panel at waste tank center). The concrete finish shall have a tolerance of 0.125-inch per10 feet. The basemats in Type III tanks do not have leak detection slots.

Modeling Values Used

	Inches:	**Basis:**
Most likely:	42.0	42-inch basemat (ignore drop panel)
Minimum:	41.5	42-inch basemat - 0.5-inch tolerance on basemat
Maximum:	48.5	6-inch working slab + 42-inch basemat + 0.5-inch tolerance on basemat (ignore drop panel)
Mean:	44.0	Based on triangular distribution

5.6.3.5.5 Type IIIA Tank Concrete Floor Thickness

As described in Section 3.2, Type IIIA tanks have a 4-inch working slab. The Type IIIA tank basemat has a 3-foot 7-inch minimum thickness (6 feet 4 inches at drop panel at waste tank center). The concrete finish shall have a tolerance of 0.125-inch per10 feet. A grid of 2-inch deep interconnected radial channels is grooved into the concrete basemat upon which the secondary liner rests.

Modeling Values Used

	Inches:	**Basis:**
Most likely:	41.0	43-inch basemat - 2-inch drainage channels (ignore drop panel)
Minimum:	40.5	43-inch basemat - 2 inch drainage channels - 0.5-inch tolerance on basemat
Maximum:	45.5	4-inch working slab + 43 inch basemat - 2-inch drainage channels + 0.5-inch tolerance on basemat (ignore drop panel)
Mean:	42.3	Based on triangular distribution

5.6.3.6 Basemat Fast Flow

Cases A through E are differentiated, in part, by the presence or absence of a fast flow path, as well as a number of other parameters (Table 4.4-1, Section 4.4.2). Using separate model cases run deterministically enables evaluation of the sensitivity of the system to a fast flow path. However, a stochastic parameter was developed in the HTF GoldSim Model specifically to address the uncertainty associated with the existence of a fast flow path through the basemat, regardless of case. In other words, although the Cases A, B, and C do not have a fast flow path through the basemat, when run stochastically, a "basemat bypass factor" is applied to allow a fraction of flow to bypass the basemat. This bypass factor is implemented by setting the distribution coefficient for all radionuclides in the basemat equal to zero, effectively eliminating any retardation affects the basemat concrete provides.

The bypass fraction distribution is represented by a triangular distribution with zero being set as the most likely value (meaning 0% of flow bypasses the basemat) and the upper bound set at 0.1% (meaning 10% of flow bypasses the basemat). The distribution is based on the assumption that cracking in the basemat is not predicted to occur during the performance period. Although, some uncertainty was applied to represent void spaces forming all the way through the basemat, it was judged much more likely that the cracking would have a tendency to be self-sealing and would not create full channels; therefore, only 10% of flow bypasses the basemat.

5.6.3.7 Waste Tank and Ancillary Equipment Containment Failure Times

The containment failure times in the HTF GoldSim Model control initial contaminant release from the associated location (waste tank or ancillary equipment). Table 4.2-36 presents the deterministic liner failure times used in the HTF PA, while Table 5.6-10 shows the probabilistic distributions applied during stochastic modeling. The waste tank steel life estimates assume general corrosion and pitting (leading to stress corrosion cracking) are the primary corrosion mechanisms acting on the waste tank liners, as they are exposed to the CZ, grouted, and soil conditions. [SRNL-STI-2010-00047] Results used in the HTF GoldSim Model for Type I and Type II tanks partially submerged in groundwater are based on analyses presented in *Life Estimation of High Level Waste Tank Steel For H-Tank Farm Closure Performance Assessment* (SRNL-STI-2010-00047). In order to represent submerged waste tank conditions, which can have increased galvanic corrosion due to increased oxygen concentrations in wet soil, a high oxygen diffusion rate was selected (1.0E-4 cm^2/sec). Case A assumes there are no fast flow paths through the containment barriers. Under these conditions, it is reasonably bounding to assume carbon dioxide diffusion rates will be faster in the fast flow Cases B through E. Therefore, results corresponding to lower (1.0E-6 cm^2/sec) carbon dioxide diffusion rates were used to represent Case A. The results corresponding to the maximum evaluated carbon dioxide diffusion rates (1.0E-4 cm^2/sec) were selected for the remaining fast flow modeling cases (Cases B through E).

Table 5.6-10: Probability Distribution of Liner Failure Times by Waste Tank Types and Case

Case A		Case B,C,D, & E		Case A		Case B,C,D, & E		Case A		Case B,C,D, & E	
Type I[a,k]		Type I[b,k]		Type II[c,k]		Type II[d,k]		Type IV[e]		Type IV[f]	
Probability level	Value (yrs)	Probability level	Value (yrs)	Probability level	Value (yrs)	Probability level	Value (yrs)	Probability level	Value (yrs)	Probability level	Value (yrs)
0	3452	0	85	0	7443	0	123	0	152	0	38
0.005	8497	0.005	175	0.005	11358	0.005	330	0.005	444	0.005	42
0.025	8946	0.025	238	0.025	11796	0.025	473	0.025	655	0.025	45
0.1	9518	0.1	364	0.1	12272	0.1	757	0.1	1071	0.1	49
0.25	10182	0.25	587	0.25	12425	0.25	1258	0.25	1805	0.25	56
0.5	11397	0.5	1142	0.5	12687	0.5	2506	0.5	3638	0.5	75
0.75	12626	0.75	2703	0.75	12960	0.75	6018	0.75	8819	0.75	126
0.9	12994	0.9	7310	0.9	13131	0.9	12408	0.9	9639	0.9	280
0.975	13185	0.975	12265	0.975	13220	0.975	13017	0.975	10012	0.975	1050
0.995	13237	0.995	13033	0.995	13244	0.995	13201	0.995	10102	0.995	5107
1	13250	1	13250	1	13250	1	13250	1	10125	1	10125

Case A		Case B,C,D, & E		Case A		Case B,C,D, & E	
Type III[g]		Type III[h]		Type IIIA West[i]		Type IIIA West[j]	
Probability level	Value (yrs)	Probability level	Value (yrs)	Probability level	Value (yrs)	Probability level	Value (yrs)
0	6789	0	117	0	6789	0	117
0.005	12255	0.005	281	0.005	12255	0.005	281
0.025	12275	0.025	400	0.025	12275	0.025	400
0.1	12351	0.1	634	0.1	12351	0.1	634
0.25	12500	0.25	1047	0.25	12500	0.25	1047
0.5	12751	0.5	2077	0.5	12751	0.5	2077
0.75	13000	0.75	4986	0.75	13000	0.75	4986
0.9	13150	0.9	12341	0.9	13150	0.9	12341
0.975	13225	0.975	13010	0.975	13225	0.975	13010
0.995	13245	0.995	13201	0.995	13245	0.995	13201
1	13250	1	13250	1	13250	1	13250

From SRNL-STI-2010-00047: D_i units (cm^2/sec):

a Figure 43 $D_i(CO_2)$ = 1.0E-6, and $D_i(O_2)$ = 1.0E-4

b Figure 44 $D_i(CO_2)$ = 1.0E-4, and $D_i(O_2)$ = 1.0E-4

c Figure 46 $D_i(CO_2)$ = 1.0E-6, and $D_i(O_2)$ = 1.0E-4

d Figure 47 $D_i(CO_2)$ = 1.0E-4, and $D_i(O_2)$ = 1.0E-4

From WSRC-STI-2007-00061: D_i units (cm^2/sec):

e Table 37 $D_i(CO_2)$ = 1.0E-6, and $D_i(O_2)$ = 1.0E-6

f Table 38 $D_i(CO_2)$ = 1.0E-4, and $D_i(O_2)$ = 1.0E-6

g Table 34 $D_i(CO_2)$ = 1.0E-6, and $D_i(O_2)$ = 1.0E-6

h Table 35 $D_i(CO_2)$ = 1.0E-4, and $D_i(O_2)$ = 1.0E-6

i Table 34 $D_i(CO_2)$ = 1.0E-6, and $D_i(O_2)$ = 1.0E-6

j Table 35 $D_i(CO_2)$ = 1.0E-4, and $D_i(O_2)$ = 1.0E-6

k NOTE: Tank 12 (Type I) and Tanks 14, 15, and 16 (Type II) have no liner, therefore are set to fail at time = 0.01 years

The liner failure distributions used for the remaining waste tank types, Type III, IIIA, and IV, were taken directly from the probabilistic analyses presented in WSRC-STI-2007-00061. Similar to the submerged and partially submerged Tank I and Tank II analysis presented in SRNL-STI-2010-00047, the waste tank steel life estimates assume general corrosion and pitting are the main corrosion mechanisms degrading the liners as they are exposed to the CZ, grout, and soil conditions. Appropriate probability distributions were selected to represent Cases A through E, again, based on the oxygen and carbon dioxide diffusion rates. Fast flow Cases B through E applied the probabilities associated with faster carbon dioxide diffusion rates (1.0E-4 cm^2/sec) to maximize transport conditions, and Case A applied the probabilities associated with the slower carbon dioxide diffusion rates (1.0E-6 cm^2/sec). Because Type III/IIIA and IV tanks are considered unsaturated, the slower oxygen (1.0E-6 cm^2/sec) diffusion rate is considered adequate.

Each piece of ancillary equipment (with the transfer lines being treated as a collective inventory) was assumed in the HTF GoldSim Model to fail independently, with the failure time occurring between the time of first pit penetration (116 years) and 100% pitting penetration (approximately 1,000 years). The most probable time of ancillary equipment failure in the probabilistic HTF analyses assumed 25% pitting penetration time (510 years). A triangular distribution using these maximum and minimum and the most likely value as the peak was utilized for ancillary equipment containment failure in the stochastic analysis. More details concerning ancillary equipment containment failure are described in Section 4.4.2.6 and WSRC-STI-2007-00460.

The diffusion rates utilized for all cases are considered bounding (i.e., faster than are typically reported).

5.6.3.8 Transition Times between Chemical States

One of the key factors controlling the dose to downstream receptors is the chemical degradation of the grout and the chemical evolution in the CZ. The chemical state, defined in the HTF GoldSim Model as Region II or Region III, oxidizing or reducing, controls the selection of the solubilities and distribution coefficients applied to the different radionuclides in the engineered system, thus controlling their release rates. Section 4.2.1 discusses the model used to calculate the number of pore volumes required to pass through the waste tank before the grout transitions to different waste tank chemistry. The results of this model are summarized in Section 4.2.1, but further details can be found in Appendix B of the report, *Conceptual Model of Waste Release from the Contaminated Zone Closed Radioactive Waste Tanks*. [WSRC-STI-2007-00544] Table 4.2-18 presents the deterministic pore volumes required to cause a step change to a different chemical state. This table was used as input to the HTF GoldSim Model and is reproduced as Table 5.6-11. The timing of the various chemical transitions can be determined based on the flow rates through the system (which vary by component and by model case), and the waste tank pore volume. The calculated chemical transition times by waste tank are presented in Table 4.2-34 (Section 4.2.2).

Table 5.6-11: Pore Volume Distribution for Chemical Condition Step Change

Waste Tank Position	Transition[a]	Number of Pore Volumes Required		
		Deterministic (Most Likely)	Triangular Distribution	
			Minimum	Maximum
Non Submerged	Reduced Region II to Oxidized Region II (Step 1)	371	260	482
	Oxidized Region II to Oxidized Region III (Step 2)	2,131	1,066	3,197
Submerged	Condition C[b] to Condition D[b] (Step 1)	1,414	990	1,838
	Condition D[b] to Oxidized Region III (Step 2)	2,383	1,192	3,575

Modified from Table 4.2-18, Section 4.2.1 and based on results from WSRC-STI-2007-00544

a Step 1 = +/- 30 % of most likely; Step 2 = +/- 50 % of most likely

b Where Condition C =water flowing into the CZ is small fraction of groundwater mixed with the Reducing Region II grout pore fluid, and Condition D = water flowing into CZ is small fraction of groundwater mixed with Oxidizing Region II grout pore fluid.

Uncertainty in the timing of the chemical transitions is captured by sampling the number of pore volumes required to cause a step change to a different chemical state, instead of using the set deterministic value presented in Table 5.6-11. A triangular distribution is applied to each chemical transition using the range with the minimum and maximum values indicated in Table 5.6-11. The Step 1 minimum and maximum pore flush volumes are set based on ± 30% of the deterministic value, and Step 2 is set equal to ± 50% of the deterministic value. The variation provided by these values was judged reasonable to provide a distribution that showed the effects of uncertainty. Varying the transition time via the number of pore volumes required enables non-mechanistic probabilistic modeling of the multiple factors that could cause early or late transition (e.g., uncertainty in the initial grout formulation, flow differences, chemistry changes). The transition times can have a significant impact on results, as documented in Sections 5.6.4 and 5.6.6.

5.6.3.9 HTF Lower Vadose Zone Thickness

The lower vadose zone is a natural barrier that slows the transport of certain contaminants. Uncertainty in the retardation amount of the HTF lower vadose zone offers was captured in the HTF GoldSim Model using appropriate soil distribution coefficient values (presented above in Section 5.6.3.4) and variable vadose zone thicknesses. Table 4.2-31 presents the lower vadose zone thicknesses below the waste tanks used in the deterministic (baseline) analysis. [SRNL-STI-2010-00148] Negative values indicate the top of the slab is below the water table. The depth of the vadose zone beneath each waste tank varies in the HTF GoldSim Model based on the thickness of the saturated zone, as the thickness of the saturated zone increases, the depth of the vadose zone decreases; and as the thickness of the saturated zone decreases the depth of the vadose zone increases. The vadose zone does not have a stochastic thickness distribution, but instead is a function of the sampling of the saturated

zone thickness. The variability of the thickness of the saturated zone is discussed in Section 5.6.3.10.2.

5.6.3.10 Saturated Zone Flow Modeling Parameters

For source term releases, the modeling domain for the saturated zone begins at the upgradient edge of the waste tank and extends to the 100-meter boundary. Data input specific to the saturated zone includes, 1) data that describes the flow fields controlling the transport of mass released from the waste tanks and ancillary equipment and 2) data describing the geometry of the saturated zone and the spatial relationships between the sources (waste tanks and ancillary equipment) and the 100-meter boundary.

The HTF GoldSim Model flow fields were extracted from the HTF PORFLWOW Model (see Figures 4.4.-50 and 4.4-51 for input points, presented in Section 4.4.4.2). The flow fields vary by component and through time, and therefore reflect degradation of the barrier. The uncertainty associated with the flow fields is represented using different model cases, as described in Section 5.6.3.2.

Three modeling parameters of particular importance in describing the saturated zone geometry and spatial relationships are the Saturated Zone Darcy Velocity, Saturated Zone Thickness, and the Saturated Zone Width. Uncertainty was applied to the saturated zone model by applying probabilistic distributions to these parameters.

5.6.3.10.1 Saturated Zone Darcy Velocity

Groundwater flow in the saturated zone is approximated as a unidirectional flow field of constant Darcy velocity. The flow velocity is derived from a PORFLOW simulation where streamtraces were generated based on a particle released at the center of each source (waste tank or ancillary equipment). A particle path length to the 100-meter boundary from the streamtrace simulation and the time it took for the peak value of the breakthrough curves to reach the boundary were translated into averaged transport velocities. Darcy velocities were in turn derived from the transport velocities and the saturated zone porosity used in the HTF GoldSim Model as follows:

$$DarcyVelocity = TransportVelocity \times Porosity.$$

The waste tank-specific mean Darcy velocities in the saturated zone are presented in Table 5.6-12. These values are used in the HTF GoldSim Model.

Table 5.6-12: Mean Darcy Velocity from Waste Tanks

Waste Tank	Mean Darcy Velocity (ft/yr)
Tank 9	4.01
Tank 10	3.62
Tank 11	4.1
Tank 12	3.93
Tank 13	12.15
Tank 14	4.26
Tank 15	10.62
Tank 16	14.39
Tank 21	10.52
Tank 22	9.24
Tank 23	8.65
Tank 24	8.87
Tank 29	6.25
Tank 30	6.1
Tank 31	6.5
Tank 32	5.88
Tank 35	8.12
Tank 36	9.1
Tank 37	8.73
Tank 38	6.28
Tank 39	7.1
Tank 40	8.37
Tank 41	8.66
Tank 42	6.26
Tank 43	6.82
Tank 48	5.61
Tank 49	10.68
Tank 50	4.74
Tank 51	4.26

[SRR-CWDA-2010-00093]

The ancillary equipment-specific mean Darcy velocities in the saturated zone are presented in Table 5.6-13, and were derived using the same methodology as was for the waste tank-specific mean Darcy velocities. These values were used in the HTF GoldSim Model.

Table 5.6-13: Mean Darcy Velocity from Ancillary Equipment

Ancillary Equipment	Mean Darcy Velocity (ft/yr)
HPT2	4.31
HPT3	4.2
HPT4	4.13
HPT5	11.21
HPT6	10.71
HPT7	10.38
HPT8	10.1
HPT9	10.59
HPT10	10.41
E242_H	10.73
E242_16H	6.97
E242_25H	7.15
HTF_T_Line1	22.55
HTF_T_Line2	4.94
HTF_T_Line3	15.66
HTF_T_Line4	10.7
CTSO	6.13
CTSN	7.76

[SRR-CWDA-2010-00093]

Uncertainty associated with variable velocities in the saturated zone is accounted for by applying a uniform distribution with minimum and maximum values set equal to half the mean Darcy velocities presented in Table 5.6-12 and Table 5.6-13 and 1.5 times for the maximum.

5.6.3.10.2 Saturated Zone Thickness

In the HTF GoldSim Model, water leaving the unsaturated zone enters the saturated zone (i.e., the aquifer) as recharge, and this infiltrating water is mixed into the volume of aquifer water. The concentration in the cell at a given time is determined by the flow rate and mixing volume (flow face area times flow velocity time) in the aquifer. The aquifer thickness is therefore important to the receptor dose calculation, because it defines the cell volume, which directly affects the concentration.

Based on the estimates for the UTR-LZ of the UTR Aquifer reported in Table 7 of *Hydrogeologic Data Summary in Support of the H-Area Tank Farm Performance Assessment*, the deterministic saturated zone thickness value applied to the HTF GoldSim Model was fixed at 60 feet. [SRNL-STI-2010-00148, Rev 0] Sixty feet is selected because it falls within the range indicated from existing well data, and it is in agreement with modeled PORFLOW values.

The uncertainty associated with the variability in saturated zone thickness, presented in Table 5.6-14, is accounted for by applying a triangular distribution, centered around the deterministic value of 60 feet. The minimum value is set equal to 55 feet, while the maximum is set equal to 80 feet. The minimum and maximum values are based on the measured range reported for the UTR-LZ of the UTR Aquifer in the HTF area. [SRNL-STI-2010-00148]

Table 5.6-14: Distribution for Saturated Zone Thickness

	Triangular Distribution		
	Deterministic	**Minimum**	**Maximum**
Thickness (ft)	60	55	80

[Table 7, SRNL-STI-2010-00148]

5.6.3.10.3 Saturated Zone Width

The cross-sectional area of the cell network (representing the saturated zone) perpendicular to flow is defined as the product of the saturated zone width and the saturated zone thickness. The saturated zone width for waste tanks is defined as the diameter of the waste tank (Table 5.6-15). Because the waste tank diameter is known, there uncertainty is not considered for the waste tanks.

Table 5.6-15: Saturated Zone Width for Waste Tanks

Tank Type	Saturated Zone Width (ft)
Type I	75
Type II	85
Type III/IIIA	85
Type IV	85

[SRR-CWDA-2010-00093 Table 4.4-5]

For the ancillary equipment sources, the square root of the source area is used as the saturated zone width (Table 5.6-16). Because the mass released from the ancillary equipment sources is considered to be immediately applied to the unsaturated zone (or saturated zone if applicable) at a specific time, uncertainty on its distribution is considered. The uncertainty in the saturated zone width below ancillary equipment sources is described by a uniform distribution between 0.8 and 1.2 times the deterministic value of the saturated zone width.

Table 5.6-16: Saturated Zone Width for Ancillary Equipment

Ancillary Equipment	Saturated Zone Width (ft)
HPT2	10.63
HPT3	10.63
HPT4	10.63
HPT5	10.63
HPT6	10.63
HPT7	10.63
HPT8	10.63
HPT9	10.63
HPT10	10.63
E242_H	7.09
E242_16H	7.09
E242_25H	12.41
Transfer Lines 1	609.30
Transfer Lines 2	432.32
Transfer Lines 3	621.92
Transfer Lines 4	371.80
CTSO	7.09
CTSN	7.09

[SRR-CWDA-2010-00093 Table 4.4-6]

5.6.3.11 Well Depth

As discussed in the exposure pathways section of this PA (Section 4.2.3), the well water (located at the 100-meter boundary or seepline) may be used as a primary potable water source for a future resident (e.g., drinking water, showering) and may be used by the resident as a primary water source for agriculture (e.g., irrigation, livestock water). The hypothetical impacts to the MOP can be highly dependent on which aquifer the water is drawn. The report, *Evaluation of Well Drilling Records in the Vicinity of SRS from CY2005 Through CY2009* (SRR-CWDA-2010-00054), examines available on-site well drilling data, and information from regional commercial well drillers to determine probabilities associated with a future resident drilling into a particular aquifer. The deterministic HTF GoldSim Model assumes the water wells are drilled into the UTR-LZ.

The report SRR-CWDA-2010-00054 concludes that water wells drilled in the SRS area have a high probability of being located in the UTR-LZ or the deeper Gordon Aquifer (Table 5.6-17).

Table 5.6-17: Probability of Drilling into the Aquifers

Aquifer (Depth)	% of Total in GSA	Dilution Multiplier
UTR-UZ	4%	1
UTR-LZ	52%	1
Gordon Aquifer	44%	0.01

[SRR-CWDA-2010-00054]

To simulate the probability that the well source might be drilled into a lower aquifer (UTR-LZ or the Gordon Aquifer), the well depth probabilities in Table 5.6-17 were used as a stochastic in the HTF GoldSim Model. During the HTF GoldSim Model multi-realization simulation, 44% of the realizations used well water drilled from the Gordon Aquifer. For those realizations that drill into the Gordon Aquifer, a dilution multiplier was applied to the GoldSim calculated concentration values (Table 5.6-17). The dilution multiplier was set to 0.01, based on comparison of PORFLOW peak concentrations between the UTR-LZ and the Gordon Aquifer (Appendix F.2).

5.6.3.12 Bioaccumulation Factors and Human Health Exposure Parameters

The bioaccumulation factors (Section 4.6.1) and human health exposure (Section 4.6.2) parameters were used to calculate dose to the MOP and intruder in the dose calculator module of the HTF GoldSim Model for the different exposure pathways. A stochastic distribution was not applied to the bioaccumulation factors (e.g., transfer factors) in the HTF GoldSim Model because varying these factors has been shown to result in a negligible impact on dose results as was demonstrated in the response to the NRC comment on the SDF PA. [SRR-CWDA-2010-00033, Rev 1]

Other human health exposure factors, described in the following sections, were given a probabilistic distribution in the HTF GoldSim Model in order to evaluate the model's sensitivity to their uncertainty. The stochastic distributions applied to the human health exposure factors are presented in Tables 5.6-18 through 5.6-21.

Table 5.6-18: Stochastic Crop Exposure Times and Productivity

Parameter	GoldSim Parameter Name	Value		Min	Max
Vegetable crop exposure times to irrigation (d)	*VeggieExposureTime*	70		60	90
Buildup time of radionuclides in soil (d)[a]	*SoilBuildupTime*	9,125		N/A	N/A
Agricultural productivity (kg/m^2)[a]	*VegetationProductionYield*	2.2		0.7	4
Fraction of Foodstuff Produced Locally		**All-Pathway**	**Intruder**	**Min**	**Max**
Leafy vegetables and produce	*LocalGrown and LocalGrown_Intr*	0.173	0.308	0.1	0.5
Meat	*FracLocalBeef_MOP and FracLocalBeef_Intr*	0.306	0.319	0.1	0.5
Milk	*FracLocalMilk_MOP and FracLocalMilk_Intr*	0.207	0.254	0.1	0.5
Poultry and Egg[b]	*FracLocalChic_MOP and FracLocalChic_Intr*	0.306	0.319	0.1	0.5

[WSRC-STI-2007-00004, Table 3-1 except as noted]
a SRNL-STI-2010-00447
b ML083190829, Table B-1
N/A = Not applicable

Table 5.6-19: Stochastic Physical Parameters

Parameter	GoldSim Parameter Name	Value	Min	Max
Water Density (g/mL)	*WaterDens* (kg/m3)	1	N/A	N/A
Areal surface density of soil (kg/m^2)	*SurfaceSoilDensity*	240	180	270
Density of Sandy Soil (kg/m^3)[a]	*DryBulkDensity_SandySoil*	1,650	N/A	N/A
Airborne release fraction[b]	*ARF*	1.00E-04	N/A	N/A
Soil loading in air	*AirMassLoadingSoil*	1.00E-07	1.00E-09	3.00E-07
Depth of garden (cm)	*TillDepth and SoilThickness*	15	15	61
Water contained in air at ambient conditions (g/m^3)[c]	*AirWaterContent*	10	N/A	N/A
Water contained in air at shower conditions (g/m^3)[c]	*ShowerAirWaterContent*	41	N/A	N/A
Soil moisture content [d]	*SoilMoistureContent*	0.2086	N/A	N/A
Precipitation rate (in/yr)[d]	*PR*	49.1	N/A	N/A
Evapotranspiration rate (in/yr)[d]	*ER*	32.6	N/A	N/A
Irrigation rate (in/yr)	*IR*	52[e]	N/A	N/A
Irrigation rate ($L/d/m^2$)	*IrrigationRate*	3.6[e]	2.08	5.5
Fraction of the time that vegetation or soil is irrigated	*FracYearIrrigate*	0.2	0.2	0.25
Weathering decay constant (1/d)	*WeatheringDecayConst*	0.0495	0.03	0.0495
Fraction of material deposited on leaves that is retained	*LeafRetention*	0.25	0.2	0.25
Fraction of material deposited on leaves that is retained after washing	*WashingFactor*	1	N/A	N/A
Area of garden for family of four (m^2)	*GardenSize*	100	100	500
Well diameter (ft)	*WellDiameter*	0.667	N/A	N/A
Transfer line circumference (ft)	*PipeAreaperLength*	0.803	N/A	N/A
Well depth (ft)	*WellDepth*	100	N/A	N/A

[WSRC-STI-2007-00004, Table 3-2 except as noted]

a WSRC-STI-2006-00198, Table 5-18

b DOE-HDBK-3010-94

c HNF-SD-WM-TI-707

d WSRC-STI-2007-00184

e Based on an assumption of 1 in/wk = 0.36 cm/d. For a $1m^2$ area, 0.36 cm/d x 10,000 cm^2/m^2 x 1L/1,000 cm^3=3.6 $L/d/m^2$.

N/A = Not applicable

Table 5.6-20: Stochastic Individual Exposure Times and Consumption Rates

Parameter	GoldSim Parameter Name	Recommendation		
		Value	Min	Max
Breathing rate (m^3/yr)	*AirIntake*	5,548	1,267	11,600
Consumption Rate				
Soil (kg/yr)	*SoilConsumptionRate*	0.0365	N/A	N/A
Leafy vegetable (kg/yr)	*Leafy*	21	18	43
Other vegetable (kg/yr)	*Veg*	163	90	276
Meat (kg/yr)	*BeefConsumptionRate*	43	26	81
Poultry (kg/yr)[d]	*ChicConsumptionRate*	25	Table 5.6-21	
Egg (kg/yr)[d]	*EggConsumptionRate*	19	Table 5.6-21	
Finfish (kg/yr)	*FishConsumptionRate*	9	2.2	19
Milk (L/yr)	*MilkConsumptionRate*	120	73.7	230
Water (L/yr)	*WaterConsumptionRate*	337	184	730
Fodder-Beef cattle (kg/d)	*ConsumptionFodderBeef*	36	27	50
Fodder-Milk cattle (kg/d)	*ConsumptionFodderMilk*	52	36	55
Fodder-Poultry (kg/d)[d]	*ConsumptionFodderChic and ConsumptionFodderEgg* (clone)	0.1	NA	NA
Fraction of milk-cow feed is from pasture (fodder)	*FodderFractionMilk*	0.56	0.5	1
Fraction of beef-cow feed is from pasture (fodder)	*FodderFractionBeef*	0.75	0.5	1
Fraction of Poultry-feed is from pasture (fodder)	*FodderFractionChic and FodderFractionEgg* (clone)	1	NA	NA
Water (beef cow) (L/d)	*CattleWaterConsumptionBeef*	28	28	50
Water (milk cow) (L/d)	*CattleWaterConsumptionMilk*	50	50	60
Water (Poultry) (L/d)[d]	*ChicWaterConsumption and EggWaterConsumption* (clone)	0.3	NA	NA
Exposure Time				
Swimming (hr/yr)[a]	*AnnualSwimming*	7	N/A	N/A
Boating (hr/yr)[a]	*AnnualBoating*	22	N/A	N/A
Showering (min/d)	*ExposureFractionShower*	10	10	30
Fraction of time spent working in garden	*ExposureFractionGarden*	0.01	0.01	0.08
Boating geometry factor[b]	*BoatingGF*	0.5	N/A	N/A
Swimming geometry factor[b]	*SwimmingGF*	1	N/A	N/A
Fraction of year acute intruder is exposed to drill cuttings[c]	*FractionExposedtoCuttings*	0.0023	0.0011	0.0046

[WSRC-STI-2007-00004, Table 4-1 except as noted]

a SRNL-STI-2010-00447

b Conservative assumption

c Assumes 20 hours to complete well drilling, for baseline, 10 hours for minimum, and 40 hours for maximum

N/A = Not applicable

Table 5.6-21: Stochastic Human Consumption Rates for Poultry and Eggs

Parameter	GoldSim Parameter Name	Cumulative Probability	Value (kg/yr)
Human Consumption Rate of Poultry Mean Value = 25 kg/yr	*ChicConsumptionRate*	0	3.85
		0.01	3.85
		0.05	4.18
		0.1	5.94
		0.25	9.57
		0.5	19.85
		0.75	38.22
		0.9	50.83
		0.95	58.52
		0.99	72.81
		1	72.81
Parameter	**GoldSim Parameter Name**	**Cumulative Probability**	**Value (kg/yr)**
Human Consumption Rate of Eggs Mean Value = 19 kg/yr	*EggConsumptionRate*	0	2.8
		0.01	2.8
		0.05	4.5
		0.1	5.3
		0.25	8.23
		0.5	12.36
		0.75	21.35
		0.9	35.9
		0.95	47.35
		0.99	120.71
		1	120.71

[ML083190829, Table A-1]

Where available, site-specific values and distribution information obtained from WSRC-STI-2007-00004 and SRNL-STI-2010-00447 was used in determining the values and stochastic range to be evaluated. Where no specific guidance was available, a triangular distribution using maximum and minimum values from WSRC-STI-2007-00004 was implemented. The value used in the deterministic analysis was applied to the most likely value as defined in WSRC-STI-2007-00004 and SRNL-STI-2010-00447. For cases where site-specific distribution data was not available, it was judged reasonable to use the maximum and minimum values suggested in WSRC-STI-2007-00004. Although they may not be site-specific and have not been weighted for the purpose of the stochastic analysis, they provide a wide range of possible outcomes and were therefore better able to identify parameters of potential concern.

The documents WSRC-STI-2007-00004 and SRNL-STI-2010-00447 do not present human health exposure factors related to the dose from eating poultry and eggs. Therefore, the values related to the chicken and the egg dose pathways presented in Tables 5.6-18, 5.6-20 and 5.6-21 are based on parameter sets presented in *Description of Methodology for*

Biosphere Dose Model BDOSE. [ML083190829] Lacking specific site information for the fraction of poultry and eggs produced locally, ML083190829 assumes the same fraction used for locally produced beef for the SRS site, and this fraction was applied for the HTF dose to the receptors. Note a different value was used for the all-pathways dose versus the intruder dose (Table 5.6-18). Similarly, the minimum and maximum values used for SRS-specific fraction of locally produced beef were used for the minimum and maximum fraction of locally produced egg and poultry. The values representing the fraction of locally produced beef was selected for use in the chicken and egg pathway because out of the different food products produced locally, beef had the highest, most conservative fraction. The other various chicken and egg parameter values identified in Tables 5.6-20 and 5.6-21 were extracted from Table A-1 of ML083190829 and based on national averages.

A discussion of the basis for the drinking water ingestion rate distribution is included in Tables 5.6-18 through 5.6-21. The bases for the distributions presented in the summary tables are discussed in detail in WSRC-STI-2007-00004.

5.6.3.12.1 Drinking Water Ingestion

Ingestion of water is a key usage factor for the all-pathway and inadvertent intruder analyses. The rate of contaminated water consumption can vary by exposure scenario based on assumed access to the water supply. For the inadvertent intruder where the contaminated water is expected to come from a well, an assumption can be made that water from the well is only used for cooking. Likewise, for the all-pathway analyses the assumption could be made that total water intake comes from the community water supply. However, in the absence of site and/or regional specific surveys, national estimates are appropriate.

The RESRAD 511 L/yr (1.4 L/d) average water ingestion rate updated for use in the all-pathway analyses is based on EPA surveys published in the early 1990s. [ANL-EAD-4] The 730 L/yr (2 L/d) water ingestion rates for the inadvertent intruder are taken from *Site-Specific Parameter Values for the Nuclear Regulatory Commission's Food Pathway Dose Model* (ISSN 0017-9078 - Volume 62), and are based on 10 CFR 50, Appendix I rates for the MEI. The average rate for ingestion of drinking water listed in those sources is 370 L/yr (1 L/d). These publications consider indirect ingestion of water but do not consider whether the water was bottled or if it came from a community or commercial source.

An EPA drinking water survey estimates per capita ingestion of water using data from the combined 1994, 1995, 1996, and 1998 *Continuing Survey of Food Intakes by Individuals*, (EPA-822-R-00-001) conducted by the USDA. This publication considers indirect ingestion of water from food with water added at the final phase of food preparation and reports water consumption from community water, bottled water, water from other sources, missing source, and total water. Summary data found in EPA-822-R-00-001 Executive Summary provided a 337 L/yr water ingestion rate.

According to the EPA, direct water is plain water ingested directly, as a beverage, and indirect water is water added to foods and beverages during final preparation at home, or by food service establishments, such as school cafeterias and restaurants. An example of

indirect water is water added to dry cake mix. Community water is tap water from the community water supply. Bottled water is purchased, plain water. Other water is water obtained from a well or rain cistern (household's), spring (household's or public), or other source. Preparation water is water used to prepare foods and includes the water used to prepare foods at home and by local food service establishments (indirect water), as well as water added by commercial food manufacturers. Missing water source indicates that a survey participant responded, "don't know" or "not ascertained" to the survey question regarding the source of water. Total water is the sum of direct and indirect water from all sources, which includes community water, bottled water, other water, and missing sources. [EPA-822-R-00-001]

The EPA drinking water survey reports the mean per capita total water ingestion is 1,233 mL/person/d (450 L/yr) when viewed across genders and all age categories with 75% from community water, 13% from bottled water, 10% from other sources (well, spring and cistern, etc.), and 2% from non identified sources. This yields a per person mean of 924 mL/d (337 L/yr) from community water and 12.3 mL/d (4.5 L/yr) from other sources (well water). [EPA-822-R-00-001]

A value of 337 L/yr is used as the nominal water ingestion rate for all MOP and inadvertent intruder pathway analysis. In the stochastic analyses of this parameter, the water ingestion rate range was assumed to be as high as 730 L/yr (2 L/d), which, as discussed above, is a maximum evaluation point provided by the NRC. [Regulatory Guide 1.109] The lower range of the water ingestion rate range was set at 184 L/yr the minimum recommended water ingestion rate is cut in half (e.g., water or other liquids from a clean source are used instead of drinking water from a contaminated source). A triangular distribution is used in the stochastic analysis, which causes the mean value for this parameter to rise well above the most likely value (417 L/yr verses 337 L/yr).

5.6.4 HTF Probabilistic UA/SA Model

A separate model was developed in performing the UA/SA of the HTF PA calculations using the GoldSim system analysis software (Section 4.4.4.2). The model is intended to address the levels of uncertainty and sensitivity surrounding the PA calculations. The probabilistic UA/SA results can be used to place the deterministic analyses results (which are used to demonstrate compliance with the performance objectives) into context (i.e., to risk inform the deterministic results).

This section describes the uncertainty analyses, which is concerned with how the uncertainty in model input parameters is propagated through the model to the selected model results, or endpoints. These model endpoints are potential radiological doses to hypothetical human receptors and aqueous concentrations of specific contaminants. In contrast, the sensitivity analyses, discussed in Section 5.6.5, is focused on determining which of the many input parameters (called explanatory variables, in statistical parlance) are most responsible for determining the endpoints.

The probabilistic results of the HTF GoldSim Model are used to characterize the uncertainty manifested in the model input distributions. Some of these distributions are parameter values, such as material properties or water flow rates. Others are more oriented toward

model uncertainty, such as the stochastic that selects the waste tank case to choose for a given realization. Together, the distributions, defined as stochastic elements in GoldSim, are intended to capture the overall uncertainty in the model. These probabilistic model uncertainty analyses are not intended to quantify conceptual model uncertainty. Identification of conceptual model areas of importance is primarily accomplished throughout the combined sensitivity analyses (both stochastic and single parameter sensitivities). The sensitivity analyses highlight the portions of the conceptual model that most influence the model results.

The HTF UA/SA is based on inputs and results for the HTF GoldSim Model using version HTF Transport Model v0.015.gsm. Six model runs were performed for use in the uncertainty analyses.

One case uses all five waste tank cases, where each realization simulates a waste tank case according to its probability of occurrence (see Section 5.6.3 for waste tank case probability distribution), and the other five model runs use each of the individual cases described in Section 4.4.2. The names of the GoldSim models are listed below, under the relevant waste tank case description:

All five waste tank cases:

- All Cases - HTF Transport Model v0.015 UA AllCases r1000.gsm

Base Case waste tank scenario:

- Case A - HTF Transport Model v0.015 UA CaseA r1000.gsm

Fast flow waste tank scenarios (Cases B through E):

- Case B - HTF Transport Model v0.015 UA CaseB r1000.gsm
- Case C - HTF Transport Model v0.015 UA CaseC r1000.gsm
- Case D - HTF Transport Model v0.015 UA CaseD r1000.gsm
- Case E - HTF Transport Model v0.015 UA CaseE r1000.gsm

The model simulations listed above use the Monte Carlo method, which samples uncertain parameters. The random seed value of one is used. One-thousand realizations are simulated in the cases listed above, where each realization represents a unique possible future outcome. The Monte-Carlo method uses multi-realizations, where each realization uses sampled values from each of the uncertain parameters. All of the realizations combined cover the complete probabilistic range for each parameter. The results of the independent system realizations are then assembled into probability distributions of possible outcomes. The following sections summarize these results.

5.6.4.1 Uncertainty Analysis Summary Results

The most direct way to communicate the uncertain nature of the model results is to show graphs of certain key model endpoints. Statistics for maximum values (e.g., mean of the peaks) are summarized in Table 5.6-22 for any time step within 10,000 years. Table 5.6-23 presents the same summary statistics beyond 10,000 years (within 20,000 years for Cases A through E, and within 100,000 years for the All Cases).

Table 5.6-22: Stats on the Max Dose within 10,000 Years - Any Time Step

Cases Evaluated	Mean (mrem/yr)	Median (50th Percentile) (mrem/yr)	95th Percentile (mrem/yr)
All Cases - Maximum MOP dose within 10,000 years[a]	5.4	1.8	22.6
Case A - Maximum MOP dose within 10,000 years[b]	3.7	1.1	18.5
Case B - Maximum MOP dose within 10,000 years[c]	7.4	3.0	27.0
Case C - Maximum MOP dose within 10,000 years[d]	7.0	2.5	26.7
Case D - Maximum MOP dose within 10,000 years[e]	8.2	3.5	31.0
Case E - Maximum MOP dose within 10,000 years[f]	7.6	3.1	29.6

a From GoldSim model file HTF Transport Model v0.015 UA AllCases r1000.gsm
b From GoldSim model file HTF Transport Model v0.015 UA CaseA r1000.gsm
c From GoldSim model file HTF Transport Model v0.015 UA CaseB r1000.gsm
d From GoldSim model file HTF Transport Model v0.015 UA CaseC r1000.gsm
e From GoldSim model file HTF Transport Model v0.015 UA CaseD r1000.gsm
f From GoldSim model file HTF Transport Model v0.015 UA CaseE r1000.gsm

Table 5.6-23: Stats on the Max Dose beyond 10,000 Years - Any Time Step

Cases Evaluated	Mean (mrem/yr)	Median (50th Percentile) (mrem/yr)	95th Percentile (mrem/yr)
All Cases - Maximum MOP dose within 100,000 years[a]	34.1	17.7	129
Case A - Maximum MOP dose within 20,000 years[b]	10.1	3.7	41.9
Case B - Maximum MOP dose within 20,000 years[c]	25.2	7.3	118
Case C - Maximum MOP dose within 20,000 years[d]	18.5	5.7	80.3
Case D - Maximum MOP dose within 20,000 years[e]	24.7	7.7	115
Case E - Maximum MOP dose within 20,000 years[f]	17.4	5.8	77.4

a From GoldSim model file HTF Transport Model v0.015 UA AllCases r1000.gsm
b From GoldSim model file HTF Transport Model v0.015 UA CaseA r1000.gsm
c From GoldSim model file HTF Transport Model v0.015 UA CaseB r1000.gsm
d From GoldSim model file HTF Transport Model v0.015 UA CaseC r1000.gsm
e From GoldSim model file HTF Transport Model v0.015 UA CaseD r1000.gsm
f From GoldSim model file HTF Transport Model v0.015 UA CaseE r1000.gsm

The values in the tables focus on maximum doses (and concentrations) regardless of sector since the relevant performance metric is the maximum dose to any MOP outside the 100-meter buffer zone surrounding the HTF. The values in Tables 5.6-22 and 5.6-23 show the statistics (mean, median, and 95th percentile) for peak values of specific endpoints. This is not the same thing as the statistical time histories shown in the subsequent graphs, which summarize the dose values at each time step.

Figure 5.6-43 presents time history graphs showing statistical summaries, by time step, of the dose to the MOP based on the sector of highest dose within the 10,000-year compliance period, for the All Cases run. Figure 5.6-44 presents similar time history graphs for the All Cases run out to 100,000 years to ensure that the peak dose to the MOP is captured. Figures 5.6-45 through Figure 5.6-49 present-time history graphs showing statistical summaries by time step of the dose to the MOP based on the sector of highest dose within the 10,000-year compliance period for Cases A through E.

Figure 5.6-43: Time History Max MOP Dose - All Cases (0 to 10,000 Years)

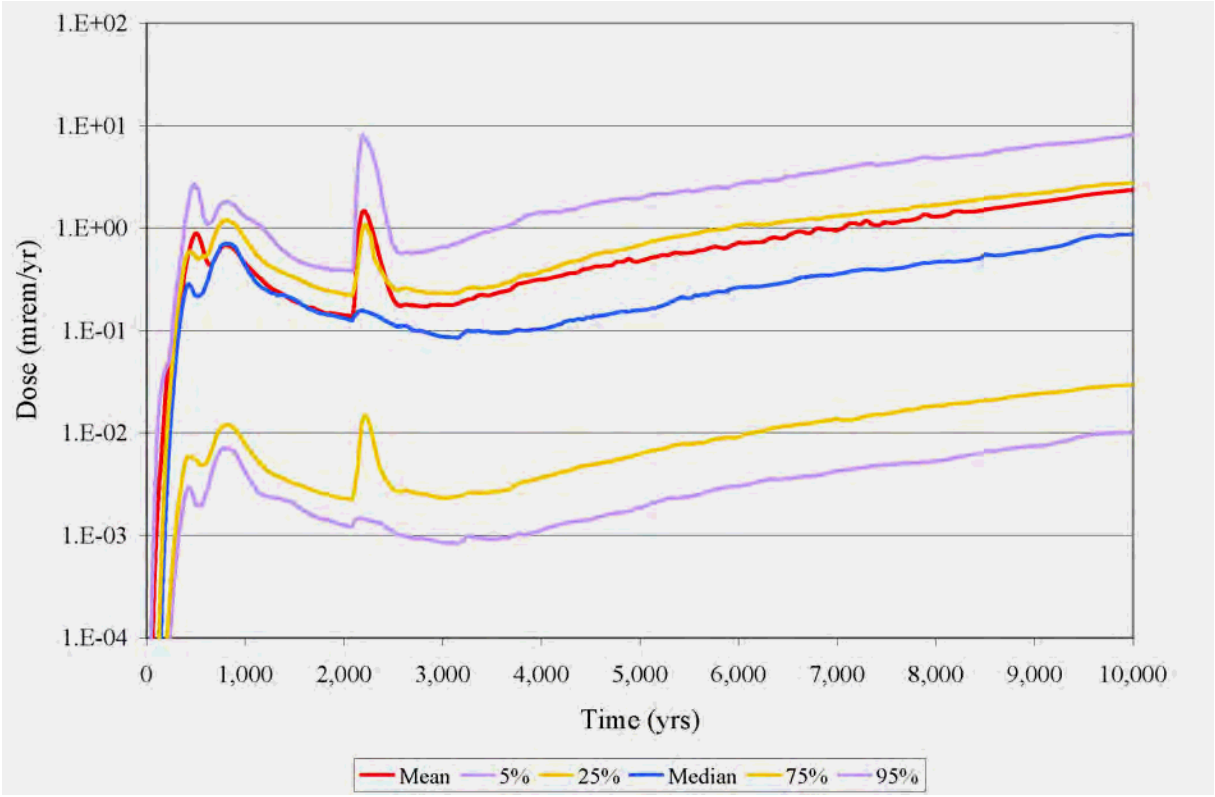

Figure 5.6-44: Time History Max MOP Dose - All Cases (0 to 100,000 Years)

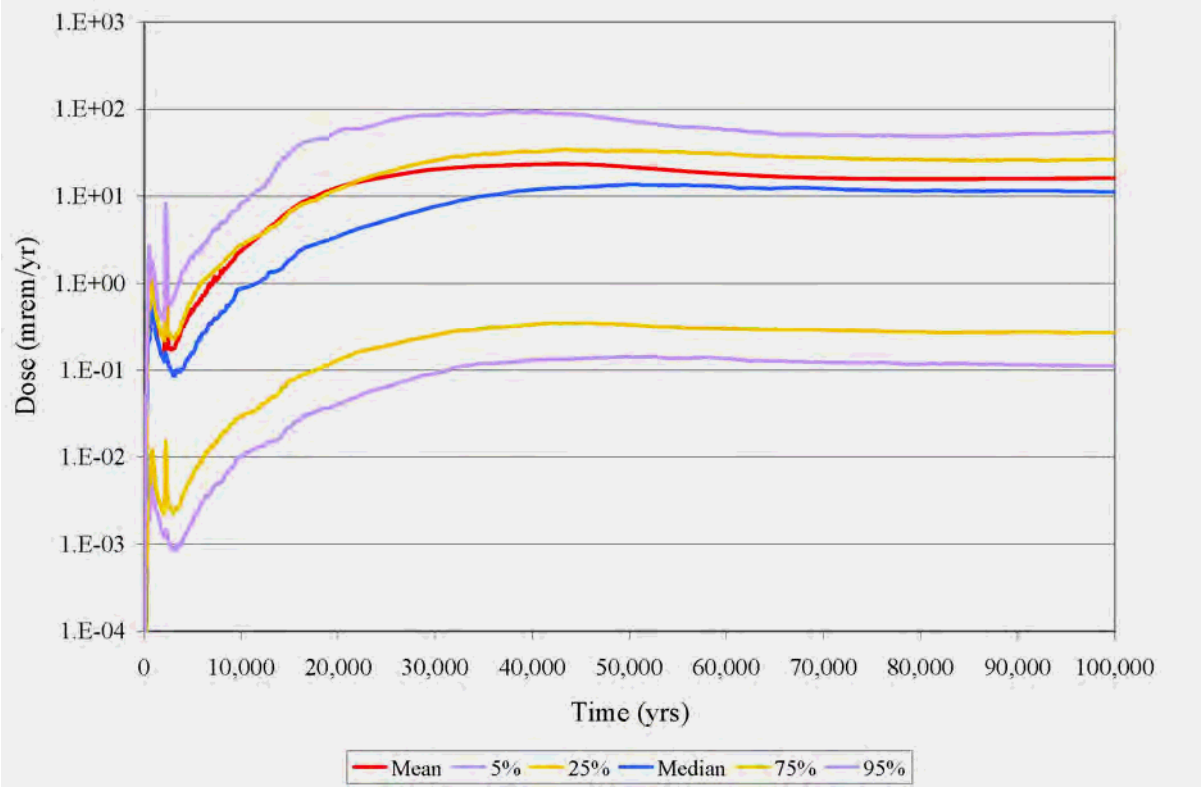

Figure 5.6-45: Time History Max MOP Dose - Case A (0 to 10,000 Years)

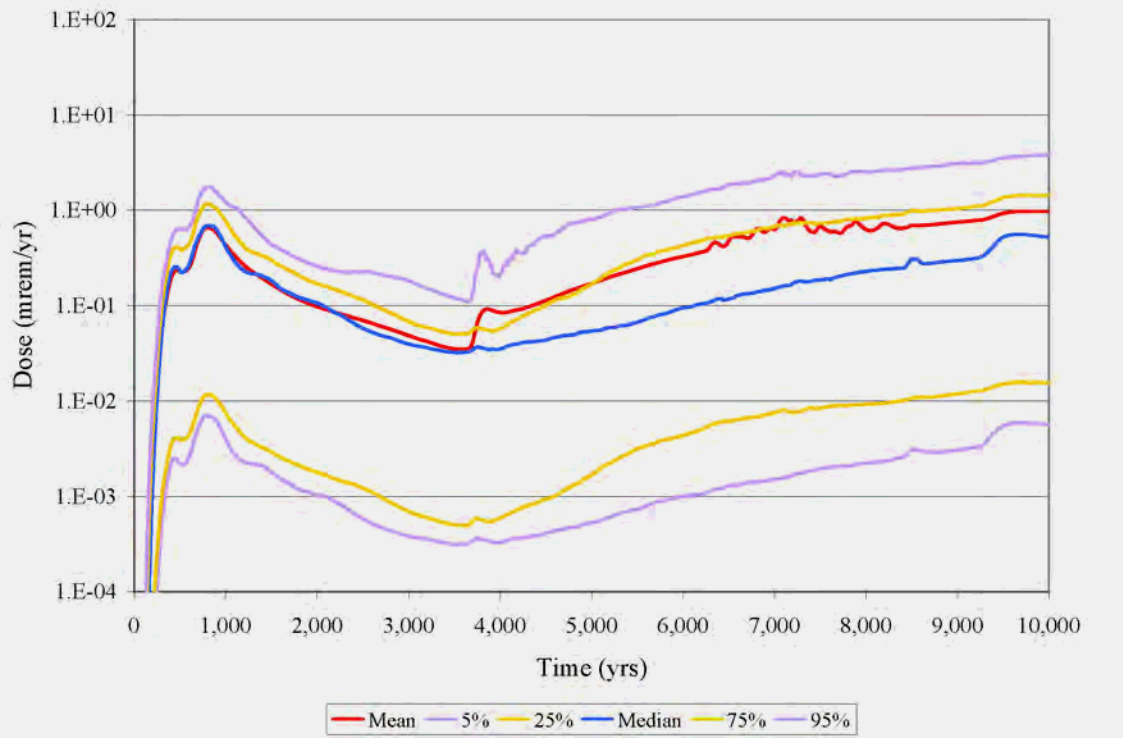

Figure 5.6-46: Time History Max MOP Dose - Case B (0 to 10,000 Years)

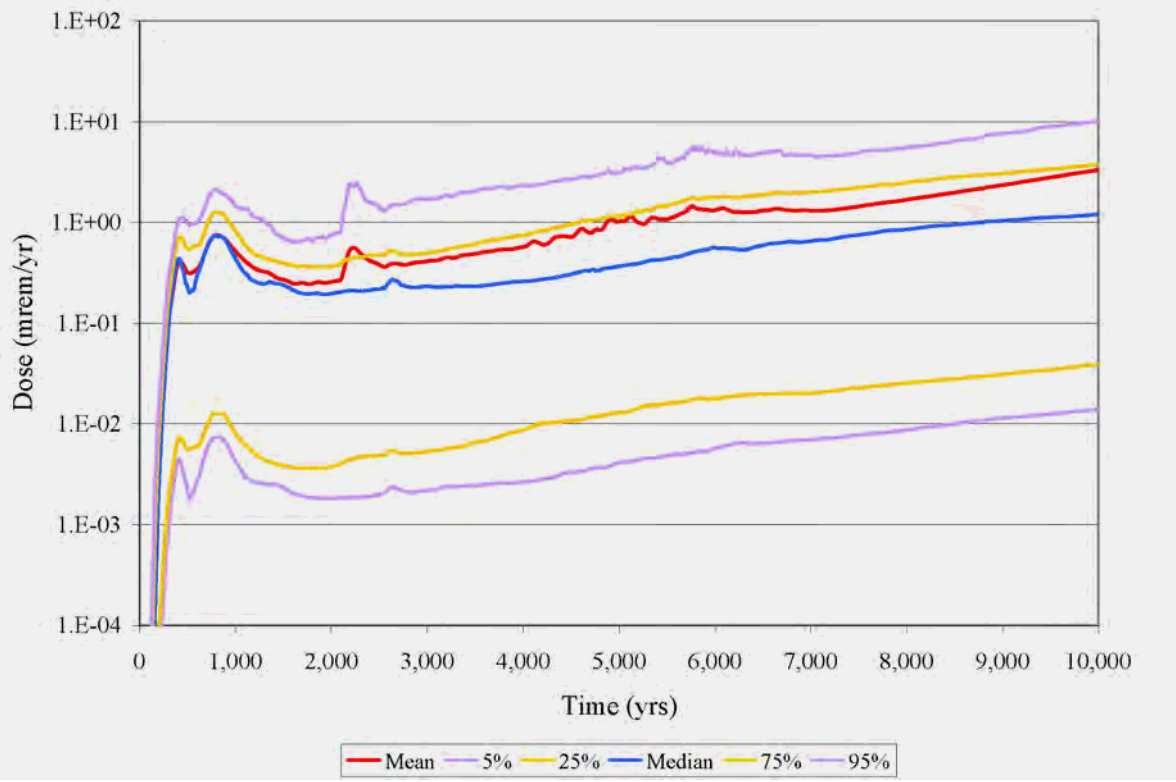

Figure 5.6-47: Time History Max MOP Dose - Case C (0 to 10,000 Years)

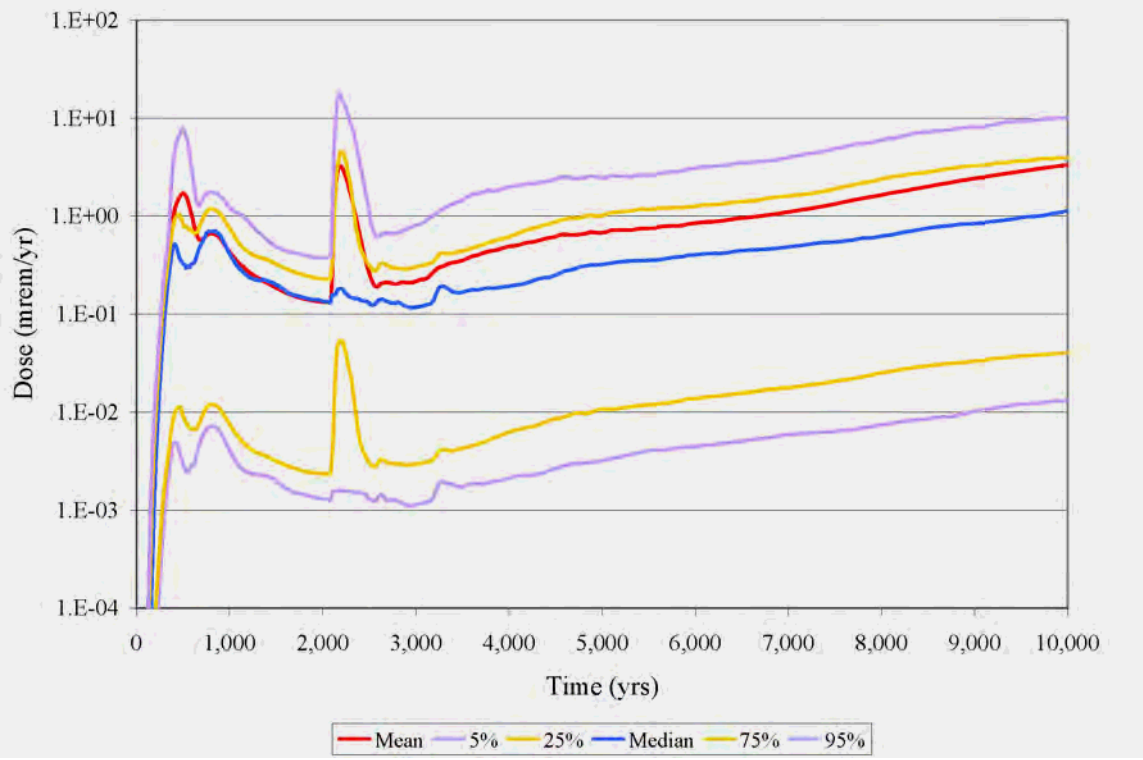

Figure 5.6-48: Time History Max MOP Dose - Case D (0 to 10,000 Years)

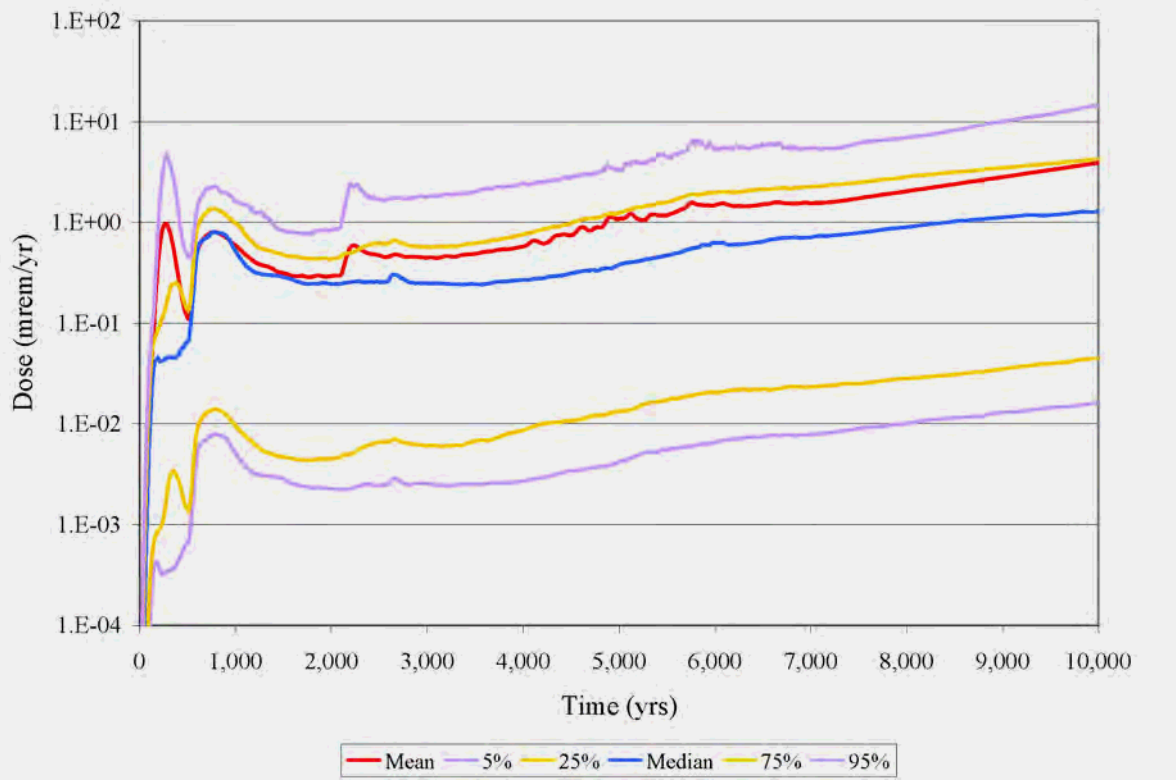

Figure 5.6-49: Time History Max MOP Dose - Case E (0 to 10,000 Years)

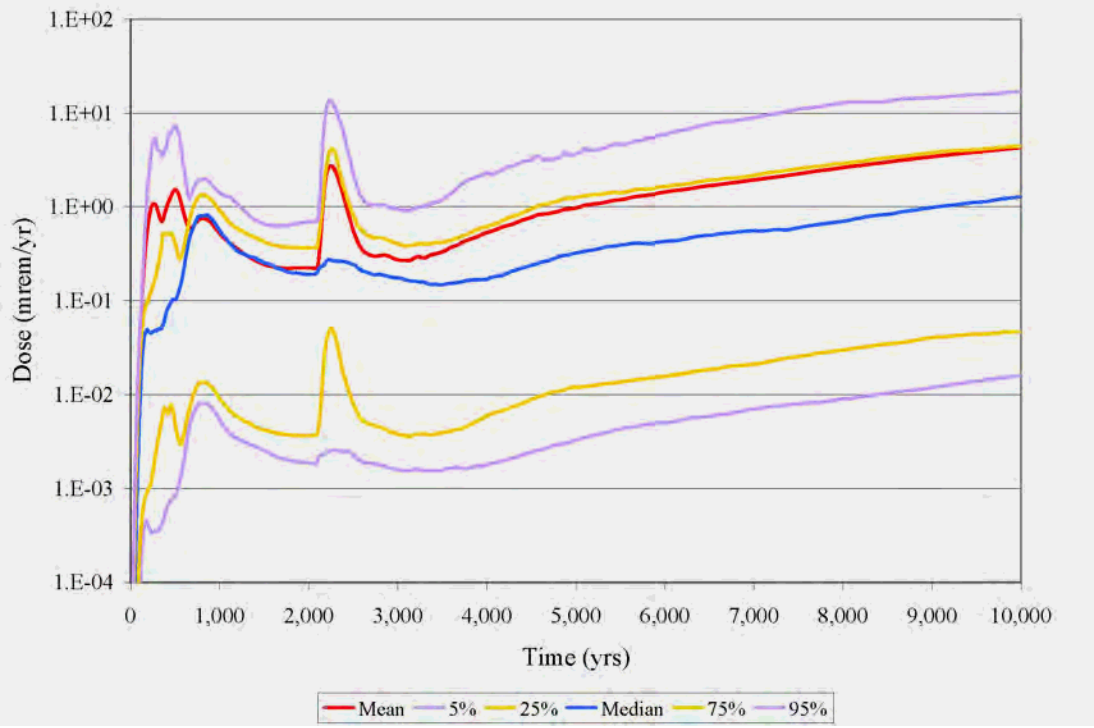

It is important to note that the tables and the time history figures do not present the same information. The tables show the statistics of the peak doses achieved in 10,000 years and 100,000 years. These are means (and medians and 95th percentiles) of the peak values in dose, no matter when that peak was achieved within the period (e.g., "mean of the peak"). In contrast, the figures account for the different times the peaks occur and by averaging all the realizations together can dampen the overall peak value. In other words, for each realization, every time step produces a maximum dose value achieved by accessing water in any of the sectors. Over the simulation period, every realization achieves a single maximum dose (or peak). All 1,000 realizations are averaged together to get a single mean time history. The single "mean" time history has its own peak. This is called the "peak of the mean."

The time history graphs show statistical summaries of the dose based on the sector of highest dose at each time step. As seen in Figure 5.6-43, the peak value of the mean dose within the 10,000-year compliance period occurs at 10,000 years with a value < 3 mrem/yr. The peak mean dose within 100,000 years shown in Figure 5.6-44 is < 26 mrem/yr, which occurs near 44,000 years. Also, note that the mean dose is higher than the median in Figures 5.6-43 and 5.6-44. This indicates that the mean time history curves are influenced by a few high outlier realizations.

The tables and graphs, while complementary, are not directly comparable since the tables list the maximum peak values achieved for each case evaluated, and the graphs display the statistics of time histories of doses (not just their peak values). For example, the approximate peak mean MOP dose within 100,000 years is 26 mrem/yr at 43,600 years, the mean of the peak doses achieved at any time in that 100,000 years is seen in Table 5.6-21 to be approximately 34 mrem/yr. The mean of the peaks is not the peak of the means.

It should be noted that 5th and 95th percentiles are significantly below and above the median value, respectively. The mean value is also driven higher, approaching the 75th percentile, by the input distributions. This indicates that the model has input distributions with long tails (e.g., lognormal distributions) or extreme values inherent in the distributions. It is somewhat expected that the mean value is higher than the median because many of the dominant distributions were established reasonably conservative, resulting in the distributions being skewed somewhat to the high end. This approach can inflate the variance in the uncertainty analyses causing a few realizations to dominate the uncertainty analyses results. The intent of Section 5.6.4.2 (Uncertainty Analyses Realizations of Interest) is to investigate which parameters are having the most impact on the uncertainty analyses.

Tables 5.6-22 and 5.6-23 show that the results from Cases B and D are very similar, as are the results from Cases C and E. A summary description of the waste tank cases is provided in Table 4.4-1. As shown in Table 4.4-1, Cases B and D have the same scenario settings, except that in Case D where there is a fast flow path through the basemat. The similarity of results between Cases B and D therefore indicate that the basemat provides little impedance to transport when severe hydraulic degradation of the cementitious materials is assumed. The basemat also provides little impedance to transport when there is a loss of reducing capacity as evidenced by the nearly identical statistics from Cases C and E, which also only differ in that Case E has the fast flow path through the basemat.

5.6.4.2 Uncertainty Analysis Insights

Based on the information presented in the uncertainty analyses section, the following general insights regarding the uncertainty analyses can be drawn.

- For Case A within 10,000 years, the mean of the MOP peak doses is 3.7 mrem/yr and the peak of the means dose is lower at 1.0 mrem/yr.
- For Case A within 10,000 years, at the location of highest dose, the 95th percentile of the peak MOP doses is 18.5 mrem/yr and the 95th percentile of the means of the MOP doses is lower at 3.8 mrem/yr.
- Based on the means of the peak doses reported in Table 5.6-22, the Case A uncertainty analysis dose results are lower than the dose results from the other uncertainty cases. The ratio of the mean of the peak dose for Case A to the mean of the peak dose from the All Cases run is 1.5. Cases B and D have similar dose results and the ratio of the mean of the peak dose for Case A to the mean of the peak dose for Case D is 2.2. Cases C and E have similar dose results and the ratio of the mean of the peak dose for Case A to the mean of the peak dose for Case E is 2.1.

For all of the uncertainty analyses runs, the mean value results are higher than the median results because many of the dominant distributions were established reasonably conservatively, resulting in the distributions being skewed somewhat to the high end. This conservative bias can lead to misleading analysis if only the mean values are considered.

5.6.4.3 Uncertainty Analysis Realizations of Interest

The purpose of this section is to investigate which individual parameters are having the most impact on the uncertainty analyses by analyzing those realizations whose results significantly affect the overall results. Recognizing that the realizations with the highest dose to the MOP may have a significant impact on the uncertainty analyses, the top five realizations for Cases A, D, and E were chosen for evaluation. Case A was selected because it is the Base Case, and Cases D and E were selected because they have the highest dose results. For each of these three cases, the evaluation was conducted by analyzing the top five realizations, which produce the highest peak dose to the MOP at 10,000 years. The highest dose consequences are those that have a combination of parameters with values significantly different from what is expected (e.g., the Base Case or deterministic values) such that when they occur concurrently they can produce significantly higher doses than anticipated. Parameters of possible interest are identified below, including those parameters that are different from the mean/median and have the greatest potential to influence the results.

5.6.4.3.1 Case A Realizations

The GoldSim model, HTF Transport Model v0.015 sensitivity analysis CaseA r5000 s1.gsm, was used to generate 5,000 realizations of Case A (e.g., enough to ensure sufficient coverage of uncertain parameter distributions). These 5,000 runs are the same runs used for the Case A sensitivity analysis presented in Section 5.6.5, and are used here to select single realizations that contribute to high dose results. Peak dose results for the 5,000 Case A realizations were investigated to identify the five realizations with the highest peak dose within the performance period. The results of this review are shown in

Table 5.6-24, with the Case A peak dose from the GoldSim gransport model run in deterministic mode (meaning all parameters use the baseline values) included in the table for comparison.

Table 5.6-24: Case A MOP Dose Results Using GoldSim Transport Model

Realization	Peak Dose (mrem/yr)	Time of Peak Dose (yr)	Major Pathway Contributors	Major Radionuclide Contributors
Deterministic Case [a]	0.78	810	Water Ingestion (68 %) Veg. Ingestion (23 %)	Tc-99 (96 %)
R 2710 [b]	118	6,650	Veg. Ingestion (66 %) Water Ingestion (30 %)	Tc-99 (100 %)
R 2456 [b]	90	7,610	Water Ingestion (53 %) Veg. Ingestion (40%)	Tc-99 (100 %)
R 3184 [b]	86	7,600	Veg. Ingestion (60 %) Water Ingestion (33 %)	Tc-99 (99 %)
R 3179 [b]	79	6,610	Veg. Ingestion (65 %) Water Ingestion (30 %)	Tc-99 (100 %)
R 4491 [b]	76	6,470	Veg. Ingestion (60 %) Water Ingestion (32 %)	Tc-99 (100 %)

a From HTF Transport Model v0.015 DeterministicCaseA.gsm (in Case A deterministic mode)
b From HTF Transport Model v0.015 sensitivity analysis CaseA r5000 s1.gsm

Inspection of Table 5.6-24 indicates that even though the peak dose from the individual realizations are significantly higher than the deterministic case and the identification of the major contributors to the dose with respect to the different biotic pathways and radionuclides are not different from the deterministic case. However, the major pathway contributor to dose differs by realization and the major radionuclide contributor to the dose is almost entirely from Tc-99 for the individual realizations, but for the deterministic case, the largest radionuclide contributor is Ra-226.

The individual realizations are analyzed below by identifying those stochastic elements that have a direct impact on the peak dose. Some initial interpretations of the deterministic model are required in order to do a detailed single realization analysis. Specifically, by identifying the individual waste tanks influencing the timing and magnitude of the deterministic peak dose, the number of key stochastic parameters can be narrowed for the single evaluation. Based on Table 5.6-24, the deterministic peak dose is driven by Tc-99. The steel liner failure times for the Case A deterministic simulation are as follows:

- Type I (intact liner) - 11,397 years
- Type II (intact liner) - 12,687 years
- Type IV (intact liner) -3,638 years
- Type IIIA (intact liner) - 12,751 years

Tanks 12, 14, 15, and 16 all have degraded liners at the beginning of the simulation. The timing of peak dose is between years 6,470 and 7,610 for the top realizations, therefore, the instantaneous releases from Tanks 12, 14, 15, and 16 due to the initially degraded

liners are not driving the Tc-99 peaks for these realizations, nor are the liner failures occurring after the end of the performance period. Instead, peak dose is likely driven by the Type IV tanks, which have early liner degradation. Because Tank 24 has an initial inventory an order of magnitude greater than Tanks 21, 22, and 23, it is likely that the deterministic peak is largely a function of the contribution from Tank 24.

Realization R 2710

As indicated in Table 5.6-24, the major radionuclide contributor to the peak MOP dose is Tc-99 (100%) with the major pathway contributors being vegetable ingestion (66%) and water ingestion (30%).

Stochastic elements influencing the release of Tc-99 with respect to the deterministic case are identified below. The deterministic value is presented within parentheses.

- Solubilities of technetium in Oxidized Region II = -1 [no solubility control] (7E-14 mol/L)
- Chemical transition from Reduced Region II to Oxidized Region II = 314 pore flushes (371 pore flushes)
- Inventory multiplier for Tc-99 in Tank 24 = 6.7 (1.0)
- Reducing Region II concrete distribution coefficient for technetium = 1,616 mL/g (5,000 mL/g)

Stochastic parameters affecting the estimate of the dose by pathway are identified below. The deterministic value is presented within parentheses.

- Water consumption rate = 526 L/yr (337 L/yr)
- Vegetable consumption rate = 249 kg/yr (163 kg/yr)
- Leafy vegetable consumption rate = 29 kg/yr (21 kg/yr)
- Fraction of year irrigating = 0.21 (0.2)
- Irrigation rate = 3.0 $L/m^2/d$ (3.6 $L/m^2/d$)
- Vegetation production yield = 0.147 kg/m^2 (2.2 kg/m^2)
- Fraction of vegetables grown locally = 0.47 (0.17)

Realization R 2456

As indicated in Table 5.6-24, the major radionuclide contributor to the peak MOP dose is Tc-99 (100%) with the major pathway contributors being water ingestion (53%) and vegetable ingestion (40%).

Stochastic elements affecting the release of Tc-99 with respect to the deterministic case are identified below. The deterministic value is presented within parentheses.

- Solubility of technetium in Oxidized Region II = -1 [no solubility control] (7E-14 mol/L)
- Chemical transition from Reduced Region II to Oxidized Region II = 414 pore flushes (371 pore flushes)
- Chemical transition from Oxidized Region II to Oxidized Region III = 1,854 pore flushes (2,131 pore flushes)

- Inventory multiplier for Tc-99 in Tank 24 = 9.5 (1.0)
- Reducing Region II concrete distribution coefficient for technetium = 1,252 mL/g (5,000 mL/g)

Stochastic parameters affecting the estimate of the dose by pathway are identified below. The deterministic value is presented within parentheses.

- Water consumption rate = 622 L/yr (337 L/yr)
- Vegetable consumption rate = 127 kg/yr (163 kg/yr)
- Leafy vegetable consumption rate = 22 kg/yr (21 kg/yr)
- Fraction of year irrigating = 0.22 (0.2)
- Irrigation rate = 4.3 $L/m^2/d$ (3.6 $L/m^2/d$)
- Vegetation production yield = 0.9 kg/m^2 (2.2 kg/m^2)
- Fraction of vegetables grown locally = 0.27 (0.17)

Realization R 3184

As indicated in Table 5.6-24, the major radionuclide contributors to the peak MOP dose is Tc-99 (99%) with the major pathway contributors being vegetable ingestion (60%) and water ingestion (33%).

Stochastic elements affecting the release of Tc-99 and Ra-226 with respect to the deterministic case are identified below. The deterministic value is presented within parentheses.

- Solubility of technetium in Oxidized Region II = -1 [no solubility control] (7E-14 mol/L)
- Chemical transition from Reduced Region II to Oxidized Region II = 408 pore flushes (371 pore flushes)
- Inventory multiplier for Tc-99 in Tank 24 = 8.3 (1.0)
- Reducing Region II concrete distribution coefficient for technetium = 3,294 mL/g (5,000 mL/g)

Stochastic elements of parameters affecting the estimate of the dose by pathway are identified below. The deterministic value is presented within parentheses.

- Water consumption rate = 343 L/yr (337 L/yr)
- Vegetable consumption rate = 251 kg/yr (163 kg/yr)
- Leafy vegetable consumption rate = 37 kg/yr (21 kg/yr)
- Fraction of year irrigating = 0.23 (0.2)
- Irrigation rate = 4.0 $L/m^2/d$ (3.6 $L/m^2/d$)
- Vegetation production yield = 2.9 kg/m^2 (2.2 kg/m^2)
- Fraction of vegetables grown locally = 0.29 (0.17)

Realization R 3179

As indicated in Table 5.6-24, the major radionuclide contributor to the peak MOP dose is Tc-99 (100%) with the major pathway contributors being vegetable ingestion (65%) and water ingestion (30%).

Stochastic elements affecting the release of Tc-99 with respect to the deterministic case are identified below. The deterministic value is presented within parentheses.

- Solubility of technetium in Oxidized Region II = -1 [no solubility control] (7E-14 mol/L)
- Chemical transition from Reduced Region II to Oxidized Region II = 309 pore flushes (371 pore flushes)
- Inventory multiplier for Tc-99 in Tank 24 = 8.8 (1.0)
- Reducing Region II concrete distribution coefficient for technetium = 7738 mL/g (5,000 mL/g)

Stochastic elements of parameters affecting the estimate of the dose by pathway are identified below. The deterministic value is presented within parentheses.

- Water consumption rate = 310 L/yr (337 L/yr)
- Vegetable consumption rate = 237 kg/yr (163 kg/yr)
- Leafy vegetable consumption rate = 29.3 kg/yr (21 kg/yr)
- Fraction of year irrigating = 0.22 (0.2)
- Irrigation rate = 2.5 $L/m^2/d$ (3.6 $L/m^2/d$)
- Vegetation production yield = 2.4 kg/m^2 (2.2 kg/m^2)
- Fraction of vegetables grown locally = 0.39 (0.17)

Realization R 4491

As indicated in Table 5.6-24, the major radionuclide contributor to the peak MOP dose is Tc-99 (100%) with the major pathway contributors being vegetable ingestion (60%) and water ingestion (32%).

Stochastic elements affecting the release of Tc-99 with respect to the deterministic case are identified below. The deterministic value is presented within parentheses.

- Solubility of technetium in Oxidized Region II = -1 [no solubility control] (7E-14 mol/L)
- Chemical transition from Reduced Region II to Oxidized Region II = 291 pore flushes (371 pore flushes)
- Inventory multiplier for Tc-99 in Tank 24 = 8.8 (1.0)
- Reducing Region II concrete distribution coefficient for technetium = 3675 mL/g (5,000 mL/g)

Stochastic elements of parameters affecting the estimate of the dose by pathway are identified below. The deterministic value is presented within parentheses.

- Water consumption rate = 578 L/yr (337 L/yr)
- Vegetable consumption rate = 163 kg/yr (163 kg/yr)
- Leafy vegetable consumption rate = 33 kg/yr (21 kg/yr)
- Fraction of year irrigating = 0.21 (0.2)
- Irrigation rate = 3.6 $L/m^2/d$ (3.8 $L/m^2/d$)
- Vegetation production yield = 2.6 kg/m^2 (2.2 kg/m^2)
- Fraction of vegetables grown locally = 0.30 (0.17)

5.6.4.3.2 Case D Realizations

The GoldSim model, HTF Transport Model v0.015 sensitivity analysis CaseD r2500 s1.gsm, was used to generate 2,500 realizations of Case D. These 2,500 runs are the same runs used for the Case D sensitivity analysis presented in Section 5.6.5, and are used here to select single realizations that contribute to high dose results. Peak dose results for the 2,500 Case D realizations were investigated to identify the five realizations with the highest peak dose within the performance period. The results of this review are shown in Table 5.6-25, with the Case D peak dose from the GoldSim transport model run in deterministic mode (meaning all parameters use the baseline values) included in the table for comparison.

Table 5.6-25: Case D MOP Dose Results Using the GoldSim Transport Model

Realization	Peak Dose (mrem/yr)	Time of Peak Dose (yr)	Major Pathway Contributors	Major Radionuclide Contributors
Deterministic Case [a]	2.11	2,630	Water Ingestion (68%) Veg Ingestion (22%)	Tc-99 (84%) Np-237 (4%)
R 2005 [b]	763	220	Water Ingestion (87%) Veg Ingestion (11%)	Sr-90 (100%)
R 1501 [b]	550	220	Water Ingestion (77%) Veg Ingestion (22%)	Sr-90 (100%)
R 2358 [b]	437	240	Water Ingestion (65%) Veg Ingestion (33%)	Sr-90 (100%)
R 1417 [b]	349	210	Water Ingestion (89%) Veg Ingestion (9%)	Sr-90 (100%)
R 2066 [b]	277	230	Water Ingestion (84%) Veg Ingestion (13%)	Sr-90 (100%)

a From HTF Transport Model v0.015 DeterministicCaseD.gsm (in Case D deterministic mode)
b From HTF Transport Model v0.015 sensitivity analysis CaseD r2500 s1.gsm

Inspection of Table 5.6-25 indicates that the peak dose from the individual realizations is significantly higher than the deterministic case and each peak occurs prior to 300 years for each realization. Each of the individual realizations is further analyzed below by identifying those stochastic elements that have a direct impact on the peak dose. Based on Table 5.6-25, the increase to the MOP dose with respect to the deterministic case is

expected to be from a significant increase in the release of Sr-90. Tanks 12, 14, 15, and 16 all have degraded liners at the beginning of the simulation. The realizations of interest are all realizations with a high Sr-90 inventory multiplier in one of these waste tanks that is failed initially. The timing of peak doses is earlier than year 300, since the short half-life of Sr-90 does not allow it to affect the dose at much later dates.

Realization R 2005

As indicated in Table 5.6-25, the major radionuclide contributor to the peak MOP dose is Sr-90 (100%), with the major pathway contributors being water ingestion (87%), and vegetable ingestion (11%).

Stochastic elements influencing the release and transport of Sr-90 with respect to the deterministic case are identified below. The deterministic value is presented within parentheses.

- Inventory multiplier for Sr-90 in Tank 12 = 0.04 (1.0)
- Inventory multiplier for Sr-90 in Tank 13 = 0.2 (1.0)
- Inventory multiplier for Sr-90 in Tank 14 = 7.9 (1.0)
- Inventory multiplier for Sr-90 in Tank 15 = 9.3 (1.0)
- Inventory multiplier for Sr-90 in Tank 16 = 1.9 (1.0)
- Sandy soils distribution coefficient for strontium = 1.3 mL/g (5 mL/g)
- Clayey soils distribution coefficient for strontium = 12.4 mL/g (17 mL/g)

Stochastic elements of parameters influencing the estimate of the dose by pathway are identified below. The deterministic value is presented within parentheses.

- Water consumption rate = 505 L/yr (337 L/yr)
- Vegetable consumption rate = 152 kg/yr (163 kg/yr)
- Leafy vegetable consumption rate = 21 kg/yr (21 kg/yr)

Realization R 1501

As indicated in Table 5.6-25, the major radionuclide contributor to the peak MOP dose is Sr-90 (100%), with the major pathway contributors being water ingestion (77%), and vegetable ingestion (22%).

Stochastic elements influencing the release and transport of Sr-90 with respect to the deterministic case are identified below. The deterministic value is presented within parentheses.

- Inventory multiplier for Sr-90 in Tank 12 = 4.9 (1.0)
- Inventory multiplier for Sr-90 in Tank 13 = 0.2 (1.0)
- Inventory multiplier for Sr-90 in Tank 14 = 3.2 (1.0)
- Inventory multiplier for Sr-90 in Tank 15 = 7.3 (1.0)
- Inventory multiplier for Sr-90 in Tank 16 = 4.4 (1.0)
- Sandy soils distribution coefficient for strontium = 1.5 mL/g (5 mL/g)
- Clayey soils distribution coefficient for strontium = 23.3 mL/g (17 mL/g)

Stochastic elements of parameters influencing the estimate of the dose by pathway are identified below. The deterministic value is presented within parentheses.

- Water consumption rate = 593 L/yr (337 L/yr)
- Vegetable consumption rate = 146 kg/yr (163 kg/yr)
- Leafy vegetable consumption rate = 36 kg/yr (21 kg/yr)

Realization R 2358

As indicated in Table 5.6-25, the major radionuclide contributor to the peak MOP dose is Sr-90 (100%), with the major pathway contributors being water ingestion (65%), and vegetable ingestion (33%).

Stochastic elements influencing the release and transport of Sr-90 with respect to the deterministic case are identified below. The deterministic value is presented within parentheses.

- Inventory multiplier for Sr-90 in Tank 12 = 0.3 (1.0)
- Inventory multiplier for Sr-90 in Tank 13 = 0.2 (1.0)
- Inventory multiplier for Sr-90 in Tank 14 = 0.2 (1.0)
- Inventory multiplier for Sr-90 in Tank 15 = 9.0 (1.0)
- Inventory multiplier for Sr-90 in Tank 16 = 1.8 (1.0)
- Sandy soils distribution coefficient for strontium = 1.7 mL/g (5 mL/g)
- Clayey soils distribution coefficient for strontium = 8.6 mL/g (17 mL/g)

Stochastic elements of parameters influencing the estimate of the dose by pathway are identified below. The deterministic value is presented within parentheses.

- Water consumption rate = 465 L/yr (337 L/yr)
- Vegetable consumption rate = 167 kg/yr (163 kg/yr)
- Leafy vegetable consumption rate = 20 kg/yr (21 kg/yr)

Realization R 1417

As indicated in Table 5.6-25, the major radionuclide contributor to the peak MOP dose is Sr-90 (100%), with the major pathway contributors being water ingestion (89%), and vegetable ingestion (9%).

Stochastic elements influencing the release and transport of Sr-90 with respect to the deterministic case are identified below. The deterministic value is presented within parentheses.

- Inventory multiplier for Sr-90 in Tank 12 = 0.1 (1.0)
- Inventory multiplier for Sr-90 in Tank 13 = 9.0 (1.0)
- Inventory multiplier for Sr-90 in Tank 14 = 0.9 (1.0)
- Inventory multiplier for Sr-90 in Tank 15 = 4.1 (1.0)
- Inventory multiplier for Sr-90 in Tank 16 = 1.2 (1.0)
- Sandy soils distribution coefficient for strontium = 1.3 mL/g (5 mL/g)
- Clayey soils distribution coefficient for strontium = 12.8 mL/g (17 mL/g)

Stochastic elements of parameters influencing the estimate of the dose by pathway are identified below. The deterministic value is presented within parentheses.

- Water consumption rate = 530 L/yr (337 L/yr)
- Vegetable consumption rate = 143 kg/yr (163 kg/yr)
- Leafy vegetable consumption rate = 26 kg/yr (21 kg/yr)

Realization R 2066

As indicated in Table 5.6-25, the major radionuclide contributor to the peak MOP dose is Sr-90 (100%), with the major pathway contributors being water ingestion (84%), and vegetable ingestion (13%).

Stochastic elements influencing the release and transport of Sr-90 with respect to the deterministic case are identified below. The deterministic value is presented within parentheses.

- Inventory multiplier for Sr-90 in Tank 12 = 5.8 (1.0)
- Inventory multiplier for Sr-90 in Tank 13 = 1.3 (1.0)
- Inventory multiplier for Sr-90 in Tank 14 = 2.3 (1.0)
- Inventory multiplier for Sr-90 in Tank 15 = 7.8 (1.0)
- Inventory multiplier for Sr-90 in Tank 16 = 4.6 (1.0)
- Sandy soils distribution coefficient for strontium = 1.7 mL/g (5 mL/g)
- Clayey soils distribution coefficient for strontium = 9.2 mL/g (17 mL/g)

Stochastic elements of parameters influencing the estimate of the dose by pathway are identified below. The deterministic value is presented within parentheses.

- Water consumption rate = 375 L/yr (337 L/yr)
- Vegetable consumption rate = 143 kg/yr (163 kg/yr)
- Leafy vegetable consumption rate = 41 kg/yr (21 kg/yr)

5.6.4.3.3 Case E Realizations

The GoldSim model, HTF Transport Model v0.015 sensitivity analyses CaseE r2500 s1.gsm, was used to generate 2,500 realizations of Case E. These 2,500 runs are the same runs used for the Case E sensitivity analysis presented in Section 5.6.5, and are used here to select single realizations that contribute to high dose results. Peak dose results for the 2,500 Case E realizations were investigated to identify the five realizations with the highest peak dose within the performance period. The results of this review are shown in Table 5.6-26, with the Case E peak dose from the GoldSim transport model run in deterministic mode (meaning all parameters use the baseline values) included in the table for comparison.

Inspection of Table 5.6-26 indicates that the peak dose from the individual realizations is significantly higher than the deterministic case and each peak occurs at less than 300 years for each realization. Each of the individual realizations is further analyzed below by identifying those stochastic elements that have a direct impact on the peak dose. Based on Table 5.6-25, the increase to the MOP dose with respect to the deterministic

case is expected to be from a significant increase in the release of Sr-90. Tanks 12, 14, 15, and 16 all have degraded liners at the beginning of the simulation. The realizations of interest are all realizations with a high Sr-90 inventory multiplier in one of these waste tanks that is failed initially. The timing of peak doses is earlier than year 300, since the short half-life of Sr-90 does not allow it to influence the dose at much later dates.

Table 5.6-26: Case E MOP Dose Results Using the GoldSim Transport Model

Realization	Peak Dose (mrem/yr)	Time of Peak Dose (yr)	Major Pathway Contributors	Major Radionuclide Contributors
Deterministic Case [a]	0.90	810	Water Ingestion (69%) Veg Ingestion (22%)	Tc-99 (92%) Np-237 (5%)
R 2005 [b]	839	210	Water Ingestion (87%) Veg Ingestion (11%)	Sr-90 (100%)
R 1501 [b]	573	220	Water Ingestion (77%) Veg Ingestion (22%)	Sr-90 (100%)
R 2358 [b]	451	240	Water Ingestion (65%) Veg Ingestion (33%)	Sr-90 (100%)
R 1417 [b]	358	210	Water Ingestion (89%) Veg Ingestion (9%)	Sr-90 (100%)
R 2066 [b]	293	230	Water Ingestion (84%) Veg Ingestion (9%)	Sr-90 (100%)

a From HTF Transport Model v0.015 DeterministicCaseE.gsm (in Case E deterministic mode)
b From HTF Transport Model v0.015 sensitivity analysis CaseE r2500 s1.gsm

Realization R 2005

As indicated in Table 5.6-26, the major radionuclide contributor to the peak MOP dose is Sr-90 (100%), with the major pathway contributors being water ingestion (87%), and vegetable ingestion (11%).

Stochastic elements influencing the release and transport of Sr-90 with respect to the deterministic case are identified below. The deterministic value is presented within parentheses.

- Inventory multiplier for Sr-90 in Tank 12 = 0.04 (1.0)
- Inventory multiplier for Sr-90 in Tank 13 = 0.2 (1.0)
- Inventory multiplier for Sr-90 in Tank 14 = 7.9 (1.0)
- Inventory multiplier for Sr-90 in Tank 15 = 9.3 (1.0)
- Inventory multiplier for Sr-90 in Tank 16 = 1.9 (1.0)
- Sandy soils distribution coefficient for strontium = 1.3 mL/g (5 mL/g)
- Clayey soils distribution coefficient for strontium = 12.4 mL/g (17 mL/g)

Stochastic elements of parameters influencing the estimate of the dose by pathway are identified below. The deterministic value is presented within parentheses.

- Water consumption rate = 505 L/yr (337 L/yr)
- Vegetable consumption rate = 152 kg/yr (163 kg/yr)
- Leafy vegetable consumption rate = 21 kg/yr (21 kg/yr)

Realization R 1501

As indicated in Table 5.6-26, the major radionuclide contributor to the peak MOP dose is Sr-90 (100%), with the major pathway contributors being water ingestion (77%), and vegetable ingestion (22%).

Stochastic elements influencing the release and transport of Sr-90 with respect to the deterministic case are identified below. The deterministic value is presented within parentheses.

- Inventory multiplier for Sr-90 in Tank 12 = 4.9 (1.0)
- Inventory multiplier for Sr-90 in Tank 13 = 0.2 (1.0)
- Inventory multiplier for Sr-90 in Tank 14 = 3.2 (1.0)
- Inventory multiplier for Sr-90 in Tank 15 = 7.3 (1.0)
- Inventory multiplier for Sr-90 in Tank 16 = 4.4 (1.0)
- Sandy soils distribution coefficient for strontium = 1.5 mL/g (5 mL/g)
- Clayey soils distribution coefficient for strontium = 23.3 mL/g (17 mL/g)

Stochastic elements of parameters influencing the estimate of the dose by pathway are identified below. The deterministic value is presented within parentheses.

- Water consumption rate = 593 L/yr (337 L/yr)
- Vegetable consumption rate = 146 kg/yr (163 kg/yr)
- Leafy vegetable consumption rate = 36 kg/yr (21 kg/yr)

Realization R 2358

As indicated in Table 5.6-26, the major radionuclide contributor to the peak MOP dose is Sr-90 (100%), with the major pathway contributors being water ingestion (65%), and vegetable ingestion (33%).

Stochastic elements influencing the release and transport of Sr-90 with respect to the deterministic case are identified below. The deterministic value is presented within parentheses.

- Inventory multiplier for Sr-90 in Tank 12 = 0.3 (1.0)
- Inventory multiplier for Sr-90 in Tank 13 = 0.2 (1.0)
- Inventory multiplier for Sr-90 in Tank 14 = 0.2 (1.0)
- Inventory multiplier for Sr-90 in Tank 15 = 9.0 (1.0)
- Inventory multiplier for Sr-90 in Tank 16 = 1.8 (1.0)
- Sandy soils distribution coefficient for strontium = 1.7 mL/g (5 mL/g)
- Clayey soils distribution coefficient for strontium = 8.6 mL/g (17 mL/g)

Stochastic elements of parameters influencing the estimate of the dose by pathway are identified below. The deterministic value is presented within parentheses.

- Water consumption rate = 465 L/yr (337 L/yr)
- Vegetable consumption rate = 167 kg/yr (163 kg/yr)
- Leafy vegetable consumption rate = 20 kg/yr (21 kg/yr)

Realization R 1417

As indicated in Table 5.6-26, the major radionuclide contributor to the peak MOP dose is Sr-90 (100%), with the major pathway contributors being water ingestion (89%), and vegetable ingestion (9%).

Stochastic elements influencing the release and transport of Sr-90 with respect to the deterministic case are identified below. The deterministic value is presented within parentheses.

- Inventory multiplier for Sr-90 in Tank 12 = 0.01 (1.0)
- Inventory multiplier for Sr-90 in Tank 13 = 9.0 (1.0)
- Inventory multiplier for Sr-90 in Tank 14 = 0.9 (1.0)
- Inventory multiplier for Sr-90 in Tank 15 = 4.1 (1.0)
- Inventory multiplier for Sr-90 in Tank 16 = 1.2 (1.0)
- Sandy soils distribution coefficient for strontium = 1.3 mL/g (5 mL/g)
- Clayey soils distribution coefficient for strontium = 12.8 mL/g (17 mL/g)

Stochastic elements of parameters influencing the estimate of the dose by pathway are identified below. The deterministic value is presented within parentheses.

- Water consumption rate = 530 L/yr (337 L/yr)
- Vegetable consumption rate = 143 kg/yr (163 kg/yr)
- Leafy vegetable consumption rate = 26 kg/yr (21 kg/yr)

Realization R 2066

As indicated in Table 5.6-26, the major radionuclide contributor to the peak MOP dose is Sr-90 (100%), with the major pathway contributors being water ingestion (84%), and vegetable ingestion (9%).

Stochastic elements influencing the release and transport of Sr-90 with respect to the deterministic case are identified below. The deterministic value is presented within parentheses.

- Inventory multiplier for Sr-90 in Tank 12 = 5.8 (1.0)
- Inventory multiplier for Sr-90 in Tank 13 = 1.3 (1.0)
- Inventory multiplier for Sr-90 in Tank 14 = 2.3 (1.0)
- Inventory multiplier for Sr-90 in Tank 15 = 7.8 (1.0)
- Inventory multiplier for Sr-90 in Tank 16 = 4.6 (1.0)
- Sandy soils distribution coefficient for strontium = 1.7 mL/g (5 mL/g)
- Clayey soils distribution coefficient for strontium = 9.2 mL/g (17 mL/g)

Stochastic elements of parameters influencing the estimate of the dose by pathway are identified below. The deterministic value is presented within parentheses.

- Water consumption rate = 375 L/yr (337 L/yr)
- Vegetable consumption rate = 143 kg/yr (163 kg/yr)
- Leafy vegetable consumption rate = 41 kg/yr (21 kg/yr)

5.6.4.3.4 Insights from the Realization Study

A review of the realizations with the highest peak doses indicates that the parameters most significant to Case A uncertainty analysis results are the parameters controlling the release of Tc-99. Realizations that do not apply Tc-99 solubility limits in the CZ result in greater Tc-99 releases, and therefore greater peak doses. The deterministic case allows dissolved Tc-99 concentrations up to 6.0E-13 mol/L (under Reduced Region II conditions), 7.0E-14 mol/L (under Oxidized Region II conditions), and 2.0E-15 mol/L (under Oxidized Region III conditions). When the solubility limit is lowered (as conditions become more oxidizing), more Tc-99 is forced to precipitate and is not released for transport. By removing solubility limits (as in Case A, all single realizations), Tc-99 dissolves in the pore fluid, becomes mobile and flushes through the system, thus maximizing Tc-99 releases.

When 1) the solubility limits on Tc-99 in the CZ are removed (for Oxidizing Region II), and 2) the inventory multiplier for Tc-99 in Tank 24 is between 6 and 10 forcing the already high initial inventory in Tank 24 to be maximized, Tc-99 becomes more important than all other radionuclides, and drives peak dose orders of magnitude higher. The high Tc-99 inventory multiplier in concert with no solubility limit allows Tc-99 to become more important than the other radionuclides, and drives the peak dose.

A review of the realizations with the highest peak doses indicates that the parameters most significant to Case D and Case E uncertainty analysis results are the parameters affecting Sr-90. The most significant parameters are both associated with Sr-90. The realizations of interest are all realizations with a high Sr-90 inventory multiplier in one of the tanks with degraded liners at the beginning of the simulation (Tanks 12, 14, 15, and 16). A high Sr-90 inventory can drive the peak dose early on, before the short half-life of Sr-90 makes it Sr-90 dose contribution insignificant. For the high inventory dose contribution to be maximized it had to occur in conjunction with a low distribution coefficient in sandy soil. The low distribution coefficient values for Sr-90 attributed to sandy soils (1.7 mL/g or less versus the deterministic value of 5 mL/g) allows for the rapid transport of Sr-90, such that the peak dose is achieved prior to the short Sr-90 half-life mitigating the Sr-90 dose contribution. The high inventory multiplier and low distribution coefficient values in sandy soil work together to allow Sr-90 to become more important than the other radionuclides, and drives the peak dose.

In summary, the parameters that influence the peak realizations can be significant and lead to higher dose only if they occur simultaneously. These scenarios are not likely because the parameters that lead to the high dose realizations do not have a common mode initiator that would have the tendency to have these independent parameters occur simultaneously. The high dose realizations do not have any "critical" parameters in

common. However, there are multiple parameters that have strong influence, and a smaller set of parameters with a very strong influence. Depending upon the alignment and number of parameters, they can combine to cause the peak dose to trend higher for a given realization. In addition, many of the parameters whose extreme, non-deterministic values lead to the high dose realizations have deterministic values supported by site-specific testing (e.g., soil distribution coefficient s).

5.6.5 Sensitivity Analysis using HTF Probabilistic Model

Given the uncertainties presented in Section 5.6.4, the next step was to identify those input parameters and other stochastic entities in the model that led to the uncertainties. Even in complex models, the results are often strongly dependent on only a handful of parameters. What is important for one result (e.g., the Tc-99 concentration in well water), may be insignificant for another, such as the maximum dose achieved within the 10,000-year period of performance. In fact, the maximum dose to the MOP will have different sensitivities at different times, since it is driven by the presence of different radionuclides. For example, a MOP dose may be dominated by Tc-99 at one time and by Pu-239 at another time, and these doses will be determined by different aspects of the model (different distribution coefficients, containment failure modes, etc.) Extracting the important model inputs for results of interest is the subject of the sensitivity analyses.

The results of the model output were analyzed using gradient boosting models (GBMs). The GBM modeling approach utilizes binary recursive partitioning algorithms that deconstruct a response into the relative influence from a given set of explanatory variables (stochastic model input parameters). [ISSN 0167-9473] This sensitivity analysis methodology identifies which stochastic model input parameters are most influential in determining the results, such as media concentrations or future potential doses.

The model was run using a Monte Carlo scheme, where each stochastic model input parameter is randomly sampled for each realization, and the realizations are then collectively analyzed as part of the sensitivity analyses. This sensitivity analysis is based on 5,000 realizations for Case A and 2,500 realizations each for Cases D and E. Cases B and C are similar to Cases D and E except for the basemat fast flow zone and therefore sensitive parameters for Cases B and C should be identified in the sensitivity analyses for Cases D and E.

5.6.5.1 Introduction to HTF Probabilistic Model Sensitivity Analysis

Complex modeling, such as the probabilistic modeling of the HTF, is needed to explore the dynamics of systems where multiple variables interact in a nonlinear manner. The probabilistic simulation approach used in the HTF GoldSim Model propagates uncertainty regarding the explanatory variables (e.g., inputs such as physical soil properties or inventory mass) through the model to the predicted response (model "endpoints", such as dose or concentration). Quantitative assessment of the importance of inputs is necessary when the level of uncertainty in the system response exceeds the acceptable threshold specified in the decision-making framework. One of the goals of sensitivity analyses is to identify which variables have distributions that exert the greatest influence on the response.

Sensitivity analyses deals with estimating influence measures for input variables. Influence measures can be estimated in either a qualitative or a quantitative context. A qualitative sensitivity analyses provides a relative ranking of the importance of input factors without incurring the computational cost of quantitatively estimating the percentage of the output variation accounted for by each input factor. For either approach, the estimates can be obtained either locally or globally within the parameter space. A local sensitivity analysis involves varying one explanatory variable while holding all other explanatory variables constant and assessing the impact on the model response. This is local in the sense that only a minimal portion of the full explanatory variable space is explored (i.e., the point at which the explanatory variables are held constant). Although local sensitivity analysis is useful in some applications, the region of possible realizations for the model of interest is left largely unexplored. Global sensitivity analysis attempts to explore the possible realizations of the model more completely. Global sensitivity methods such as the Fourier Amplitude Sensitivity Test require construction of model simulations in which a signal is embedded in each input parameter and then the strength of the signal in the model realizations is a measure of parameter sensitivity. This requires construction of a separate GoldSim model with distributions for input parameters constructed specifically for sensitivity analysis, rather than for uncertainty analysis.

The space of possible realizations for the model can be explored by using search curves or evaluation of multi-dimensional integrals using Monte Carlo methods. However, these approaches to global sensitivity analysis become more computationally intensive as the dimensionality of the model (i.e., the number of observations and explanatory variables) increases. In this case, the HTF GoldSim Transport Model includes nearly 3,000 stochastic parameters.

Because of the computational cost, sensitivity analyses of high-dimensional probabilistic models require efficient algorithms for practical application. Machine learning provides tools that allow for the partitioning of the variance in the model response to the input parameters by exploration of the realizations from a model run for uncertainty analysis. Two common machine-learning approaches that could be brought to bear for sensitivity analysis are bagging and boosting of regression trees. The advantages of machine learning approaches include the ability to fit non-monotonic and non-linear effects, the ability to fit parameter interaction effects, and the ability to visualize these effects and their interaction across the range of the response and input parameters. Bagging, boosting, and other machine learning approaches typically produce similar results for noisy data. [ISSN 0885-6125 Vol. 24, ISSN 0885-6125 Vol. 40] In the case of realizations from a probabilistic GoldSim model, each realization is a deterministic evaluation of the model and all the stochastic predictor variables are available. There is not any variation in the model response that is unexplainable (as is the case with observed data) and the choice of machine learning algorithm should have negligible impact on the results of the sensitivity analyses.

An implementation of Friedman's GBM approach is available in the *R* statistical software in the GBM package. [ISSN 0167-9473] To conduct the sensitivity analyses on the GoldSim model, 5,000 realizations of the model for Case A and 2,500 realizations each for Cases D and E were generated. A GBM analysis was conducted using the *R* GBM package on these realizations generating global sensitivity index (SI) and partial dependence visualization of

the impact of model input parameters on the model response. Details of this analysis are presented in Sections 5.6.5.2 and 5.6.5.3.

5.6.5.2 Model Fitting and Validation

This section presents detailed discussion of the statistical methods used in the sensitivity analyses. Global sensitivity is estimated here as the proportion of the variance of the response accounted for by each explanatory variable. This estimation is conducted by fitting GBM model predictions to realizations from the HTF GoldSim Model. Variance decomposition of the fitted GBM model is then used to estimate Sensitivity Indices (SIs). Under this decomposition approach, the goal is identify the most influential explanatory variables that are identified within a model. The necessary degree of model complexity is assessed using validation metrics based on comparison of model predictions with randomly selected subsets of the data. This approach uses the "deviance" of the model as a measure of goodness of fit. The concept of deviance is fundamental to classical statistical hypothesis tests (e.g., the common t-test can be derived using a deviance-based framework) and guides the model selection process applied here.

The GBM model fitting approach is based on finding the values of each explanatory variable that result in the greatest difference in means for the corresponding subsets of the response. For example, if there were only a single explanatory variable, the GBM would identify the value of the explanatory variable that corresponds to a split of the response into two parts such that no other split would result in corresponding groups of the response variable with a greater difference in means. When multiple explanatory variables are present, these multiple splits are referred to as "trees" and each tree results in an estimate (e.g., prediction) of the response. As multiple potential trees are evaluated, they are compared to the observed data using a loss function. The selection of the loss function is an influential aspect of the GBM process and depends on the distribution of the response variable. For data that are sufficiently skewed (e.g., non-normal), the absolute error loss function has a tendency to produce more reliable results.

There is a trade-off that exists when considering which loss function to use. The squared-error loss function tends to result in better fitting models but can do so at the expense of introducing spurious variables into the model selection process when the response distribution is sufficiently skewed. The absolute error loss function has a tendency to produce model predictions with more variability but is less likely to result in the selection of spurious variables into the model. For this application, the focus has been on using a deviance-based method to obtain models that identify the most important explanatory variables with respect to the observed variability in the response. To this end, the squared-error function was used in these applications.

Once a GBM model is constructed, each of the explanatory variables that exist in the model can be assigned an SI. The SI is obtained through variance decomposition and can be interpreted as the percentage of variability explained in the model by a given explanatory variable. The sum of the SIs across the entire set of explanatory variables in the model will approximately equal the coefficient determination of the linear regression of the GoldSim output versus the GBM predictions. The coefficient determination values for the HTF model

were typically high indicating the high degree of predictive power of the GBM in fitting the HTF GoldSim Model.

In order to assess the relationship between an individual explanatory variable and the response of interest, partial dependence plots are used (these are presented below for each endpoints of interest). The first panel of each plot depicts a density estimate of the simulated response from the HTF GoldSim Model. The percentiles of the response distribution in this panel are shaded to provide a context for the partial dependence plots presented in the remaining panels. The colors indicate the percentile range of the response as follows:

1. The 0 - 25th percentile region is shaded orange-brown.
2. The 25th - 50th percentile region is shaded dark yellow-green.
3. The 50th - 75th percentile region is shaded light green.
4. The 75th - 100th percentile region is shaded light blue.

The y-axis scale of the partial dependence plots is in units of the response distribution (the x-axis of the first panel). Given that each parameter has a different range and strength of influence on the response, the y-axes of the partial dependence panels depict only the range of the response over which a particular parameter is influential. If the original scale of the response were maintained on each partial dependence panel, then the influence of the least influential parameter would not be visible in many cases. To counteract this scale issue, the background of the partial dependence panels is shaded to depict the percentile of the response over which the parameter is influential. For example, if the background of the partial dependence plot under the partial dependence line is light blue, then that indicates the parameter's influence on the upper end of the response distribution (i.e., the 75th to 100th percentile of the response).

The partial dependence panels in each figure show the distributions of the explanatory variables (semi-transparent) and the partial dependence curve (blue line) shows changes in the response as a function of each explanatory variable. In the example provided (Figure 5.6-50), the variable has a triangular input distribution, and the dependence of the result on this parameter spans the entire range of the variable and explains 34.2% of the variation.

Figure 5.6-50: Example of a Result Probability Density and Partial Dependence Plot

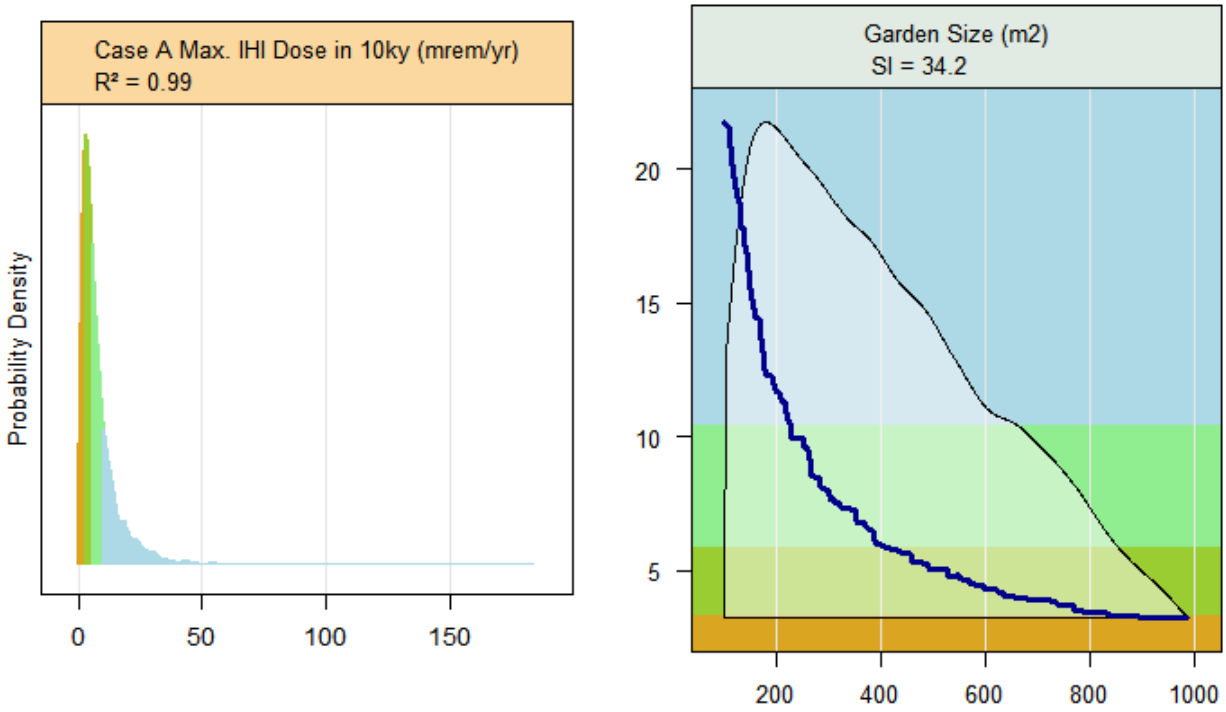

The partial dependence is determined through the integration across the joint density to obtain a marginal distribution. The integration is performed using a "weighted tree traversal" measure that is analogous to the more common integration procedures performed with Riemann or Lebesgue units of measure. The vertical axis of the partial dependence plot shows the change in the response variable as a function of the changes in the explanatory variable of interest. With standard linear regression techniques, it is assumed that the relationship between the response and the explanatory variable is a constant (e.g., the parameter estimates in the linear model). With the GBM approach, this relationship is not constrained by assumptions of linearity and the partial dependence plots show the data based estimate of the relationship between the response and the explanatory variable. This is especially useful for understanding the influence of changes in a single explanatory variable on the response, when integrating across all other explanatory variables.

5.6.5.3 Summary Statistics for Endpoints

Three GoldSim models were run for this sensitivity analyses, one model for the Base Case (failure Case A) and one model for each of the "fast flow" Cases D and E. All models were run for a 20,000-year period. The Case A model run is the file "HTF Transport Model v0.015 sensitivity analysis CaseA r5000 s1.gsm". The "s1" in the name refers to the value of the seed used for LHS of model input distributions. The "r5000" indicates the number of realization, in this case, 5,000 realizations. The exporting of results follows the simple procedure outlined in the model, in the *Sensitivity Analysis* container, wherein the tabulated raw data contents of the element *Endpoints_SA* are exported to files named exactly the same

as the model file but with the extension changed from ".gsm" to ".gsd" to indicate "GoldSim data". This process was repeated for Cases D and E. The model files are named "HTF Transport Model v0.015 sensitivity analysis CaseD r2500 s1.gsm" and "HTF Transport Model v0.015 sensitivity analysis CaseE r2500 s1.gsm," respectively. Each of these model files have a corresponding data file with the extension ".gsd."

Endpoints were selected for doses (actually TEDE) to a MOP and for an Inadvertent Human Intruder (IHI), as well as groundwater concentrations of selected radionuclides that contribute heavily to those doses. Doses are examined for maximum values within different periods (year 10,000 and year 20,000). A hypothetical "envelope" maximum dose from well water is considered, wherein the maximum total dose in any of several sectors, each containing a number of wells arranged along the 100-meter perimeter, is recorded at each time step.

For each endpoint, the most significant parameters identified by the sensitivity analysis are presented, along with the SI for each. Parameters with SI values below five are omitted from the presentation, since their contribution to the given endpoint is relatively low. Following the tables are a series of figures showing the partial dependence of each of the significant parameters for each endpoint. Summary statistics for the endpoints associated with the dose to the IHI are provided in Section 6.5.

In general, the GBM fits were quite good, with most of the coefficient determination values ranging from 0.92 to 1.0. The only exceptions to this observation were the coefficient determination values for the maximum MOP doses within 10,000 years for Cases D and E, which are 0.72 and 0.72, respectively. In the sample GBM fit plot given in Figure 5.6-51, the coefficient determination is 0.1. This tells us that the GBM statistical predictive model is able to mimic the GoldSim modeled results well, giving us confidence in the statistical analysis. The GBM fit values of coefficient determination are noted in Table 5.6-27 (for Case A), Table 5.6-28 (for Case D), and Table 5.6-29 (for Case E).

Figure 5.6-51: Example of a GBM Model Fit Plot

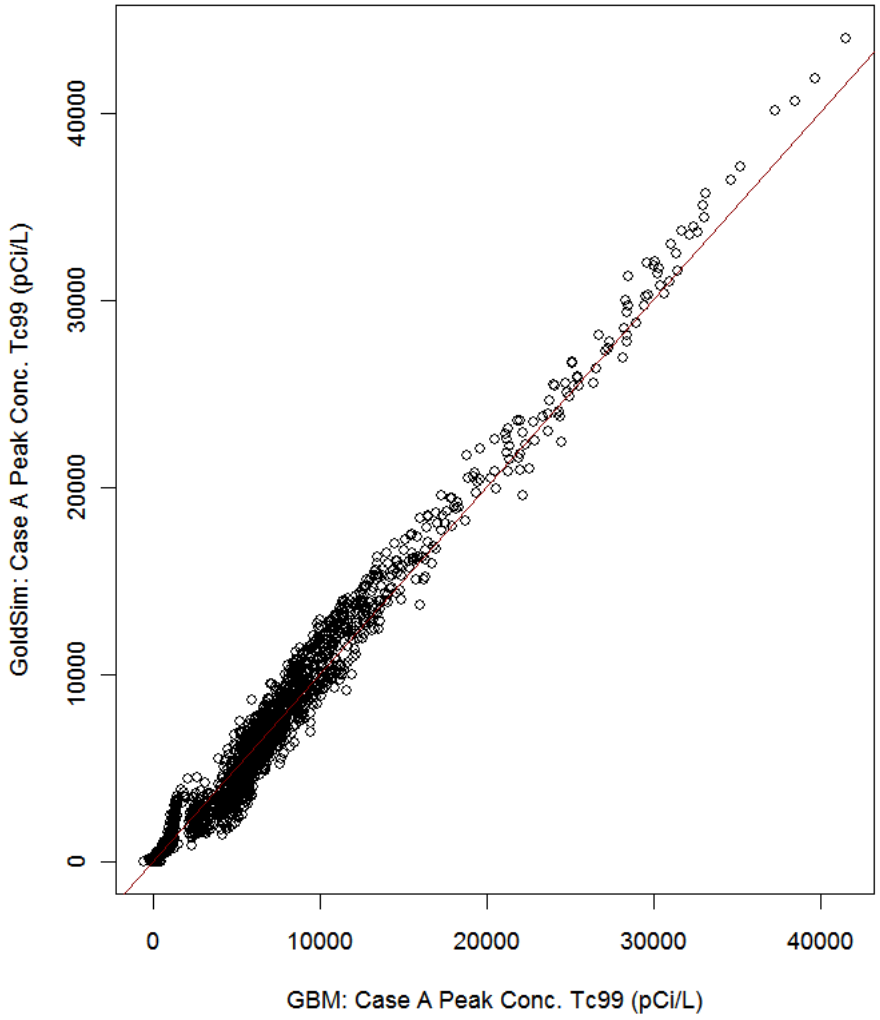

Table 5.6-27: Identification of the Most Sensitive Parameters for the Endpoints of Interest for Case A

Endpoint	SI Rank	Input Parameter	Sensitivity Index
Max MOP dose at any sector within 10,000 yr $R^2 = 1$	1	Technetium solubility in Oxidizing Region II cements	35
	2	Tank 24 inventory parameter for Tc-99	31.3
	3	Well completion stratum	14.9
Max MOP dose at any sector within 20,000 yr $R^2 = 0.92$	1	Well completion stratum	35.3
	2	Plutonium K_d in sandy soil	13.3
	3	Technetium solubility in Oxidizing Region II cements	7.67
Max conc. of I-129 at any sector within 20,000 yr $R^2 = 0.98$	1	Well completion stratum	74.9
	2	Tank Type II Case A liner failure time	7.81
Max conc. of Np-237 at any sector within 20,000 yr $R^2 = 0.99$	1	Well completion stratum	29
	2	Neptunium solubility in Oxidizing Region II cements	10.2
	3	Neptunium K_d in Oxidizing Region III cements	9.9
Max conc. of Pu-239 at any sector within 20,000 yr $R^2 = 0.97$	1	Well completion stratum	17.3
	2	Plutonium K_d in sandy soil	15.7
	3	Plutonium solubility in Oxidizing Region II cements	9.67
Max conc. of Ra-226 at any sector within 20,000 yr $R^2 = 0.99$	1	Well completion stratum	46.8
	2	Radium K_d in sandy soil	31.7
Max conc. of Tc-99 at any sector within 20,000 yr $R^2 = 1$	1	Technetium solubility in Oxidizing Region II cements	34.8
	2	Tank 24 inventory parameter for Tc-99	27.1
	3	Well completion stratum	21.9

Table 5.6-28: Identification of the Most Sensitive Parameters for the Endpoints of Interest for Case D

Endpoint	SI Rank	Input Parameter	Sensitivity Index
Max MOP dose at any sector within 10,000 yr $R^2 = 0.72$	1	Well completion stratum	9.71
	2	Strontium K_d in sandy soil	8.98
	3	Tank 15 inventory parameter for Sr-90	8.74
Max MOP dose at any sector within 20,000 yr $R^2 = 0.97$	1	Plutonium K_d in sandy soil	18.4
	2	Well completion stratum	17.1
	3	Plutonium solubility in Reducing Region II cements	9.42
Max conc. of I-129 at any sector within 20,000 yr $R^2 = 1$	1	Well completion stratum	89.2
Max conc. of Np-237 at any sector within 20,000 yr $R^2 = 1$	1	Well completion stratum	37.7
	2	Neptunium solubility in Reducing Region II cements	9.8
	3	Neptunium K_d in Oxidizing Region III cements	9.74
Max conc. of Pu-239 at any sector within 20,000 yr $R^2 = 0.99$	1	Well completion stratum	19.4
	2	Plutonium K_d in sandy soil	16.8
	3	Plutonium solubility in Reducing Region II cements	14
Max conc. of Ra-226 at any sector within 20,000 yr $R^2 = 0.99$	1	Well completion stratum	51.9
	2	Radium K_d in sandy soil	24.1
Max conc. of Tc-99 at any sector within 20,000 yr $R^2 = 1$	1	Tank 24 inventory parameter for Tc-99	31
	2	Well completion stratum	28.5
	3	Technetium solubility in Oxidizing Region II cements	26.1

Table 5.6-29: Identification of the Most Sensitive Parameters for the Endpoints of Interest for Case E

Endpoint	SI Rank	Input Parameter	Sensitivity Index
Max MOP dose at any sector within 10,000 yr $R^2 = 0.72$	1	Tank 15 inventory parameter for Sr-90	12.5
	2	Strontium K_d in sandy soil	9.42
	3	Well completion stratum	7.92
Max MOP dose at any sector within 20,000 yr $R^2 = 0.98$	1	Plutonium K_d in sandy soil	19.7
	2	Well completion stratum	12.6
	3	Plutonium solubility in Oxidizing Region II cements	11.3
Max conc. of I-129 at any sector within 20,000 yr $R^2 = 1$	1	Well completion stratum	67.3
	2	Tank Type II Cases B,C,D, & E liner failure time	18
	3	Darcy velocity of Tank 13	5.09
Max conc. of Np-237 at any sector within 20,000 yr $R^2 = 1$	1	Well completion stratum	37.7
	2	Neptunium solubility in Oxidizing Region II cements	30.6
Max conc. of Pu-239 at any sector within 20,000 yr $R^2 = 1$	1	Plutonium K_d in sandy soil	25.7
	2	Well completion stratum	22.8
	3	Plutonium K_d in Oxidizing Region III cements	15.6
Max conc. of Ra-226 at any sector within 20,000 yr $R^2 = 0.99$	1	Well completion stratum	51.2
	2	Radium K_d in sandy soil	26.6
Max conc. of Tc-99 at any sector within 20,000 yr $R^2 = 1$	1	Tank 24 inventory parameter for Tc-99	30.3
	2	Technetium solubility in Oxidizing Region II cements	29.5
	3	Well completion stratum	29

Cases A, D, and E were the cases run because, as the "Base Case" and the "Fast Flow" cases, these cases represent a cross section of the scenarios evaluated in the PA. The different waste tank cases are discussed in detail in Section 4.4.2. Since the HTF GoldSim Model is used only to model contaminant transport, flow profiles over time are calculated for each of these cases using the HTF PORFLOW Model. The HTF PORFLOW Model flow results are simplified into a 1-D steady state flow through the CZ to allow use in the HTF GoldSim Model.

The partial dependence plots shown in Figure 5.6-52 identify the most significant model input parameters in determining the maximum dose to a MOP within 10,000 years, assuming failure Case A. The GBM fit has an excellent coefficient determination of one. The dose is driven by radionuclide concentrations in water drawn from various wells, hence the MOP is exposed to the worst concentration in any sector at any given time step.

Figure 5.6-52: Partial Dependence Plot Max MOP Dose Any Sector within 10,000 Years, Case A

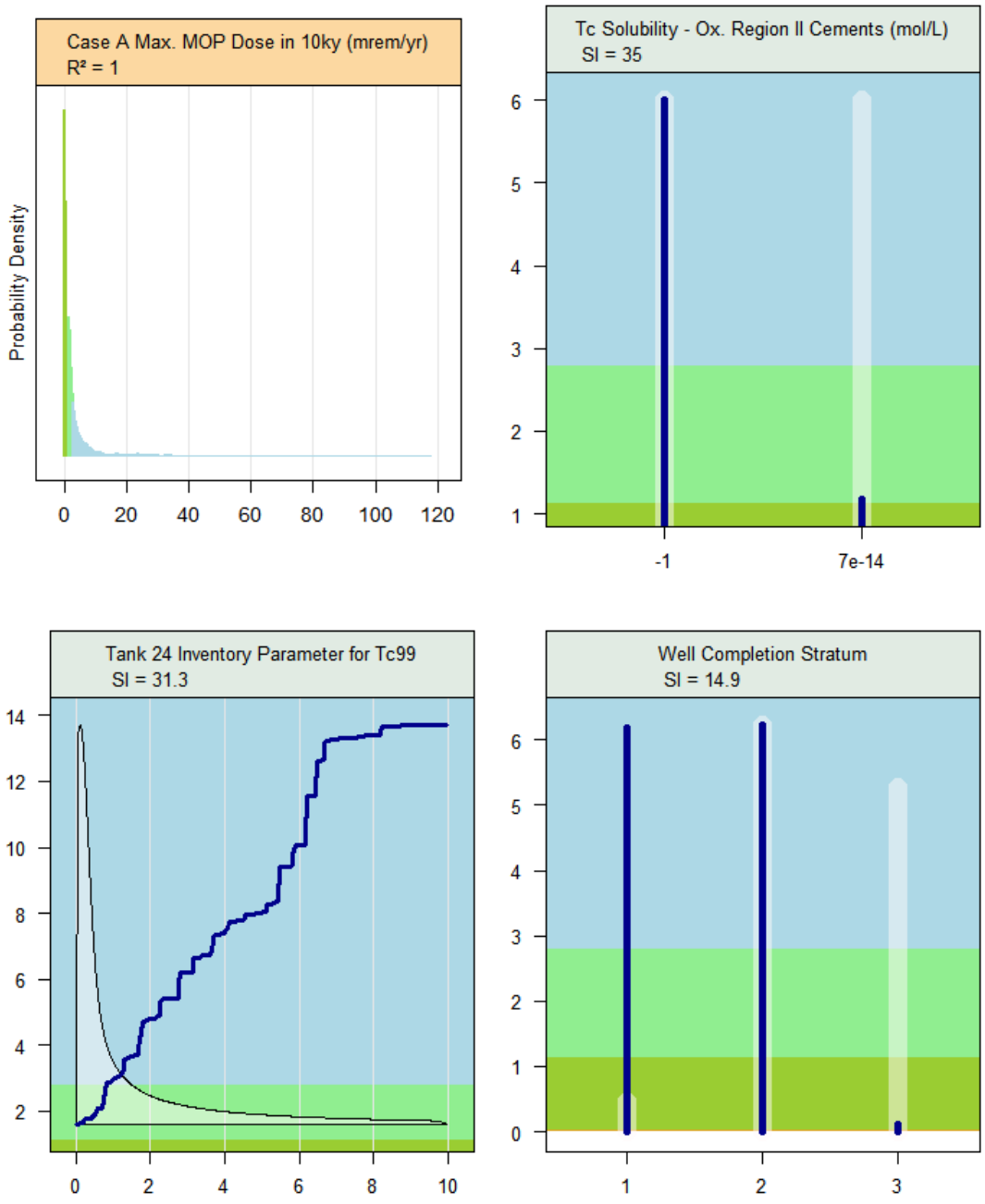

The most significant parameter is one that recurs in the sensitivity analysis, the solubility of a chemical element in the cementitious materials used to fill the waste tanks. In this case, the element is technetium, and its solubility in Oxidizing Region II cements is the parameter. Cementitious materials are modeled as six distinct types, each with its own chemical properties with respect to retardation and solubility of the chemical elements that make up the suite of radionuclides. The types are defined by a matrix of oxidizing versus reducing chemistry, and Region I, II, or III in age, or maturity. These regions are also known as stage I, II, and III, and are occasionally referred to in the model and the HTF PA as "young", "middle-aged", and "old" concretes or cements, respectively.

Note that solubilities in GoldSim are expressed in moles per liter, but a special definition of "-1" is made to indicate unlimited solubility. In the case of technetium in Oxidizing Region II cements, the parameter for solubility is limited to only two very different values: unlimited (-1), and 7.0E-14 mol/L.

The second most significant parameter in determining the value of the 10,000-year peak MOP dose endpoint is a log-normally distributed value that is used as a multiplier for the inventory of Tc-99 in Tank 24. Many similar inventory parameters show up as being quite significant throughout this analysis. Note that this parameter, which is used as a multiplier to the inventory, is positively correlated to dose, as we would expect. Higher inventories generally result in higher doses.

The third most significant parameter is the stochastic parameter for the water well completion stratum. This parameter has three discrete values, used to identify which aquifer a well is likely to be completed in (see the container *Saturated_Zone_Inputs\ WellCompletionDepth* in the HTF Transport Model). Values 1 and 2, which have likelihoods of 4% and 52%, respectively, correspond to shallow aquifers, which contain the bulk of the contamination. The value 3, sampled at 44%, identifies a deeper aquifer, which has only 0.01 of the concentration of the upper aquifers. Neither the likelihoods nor the concentration ratios have an uncertainty associated with them. The difference in concentrations in the upper and lower aquifers is naturally a strong discriminator for dose. It is not surprising that this parameter is influential in the dose, and is commonly seen as a sensitive parameter for many of these endpoints. More discussion of these parameters is also provided in Section 5.6.5.4.

Figure 5.6-53 shows SI plots for the same peak dose to a MOP from any well in any sector, and occurring any time within 20,000 years. Again, the model fit is good, with a coefficient determination of 0.92.

Figure 5.6-53: Partial Dependence Plot Max MOP Dose Any Sector within 20,000 Years, Case A

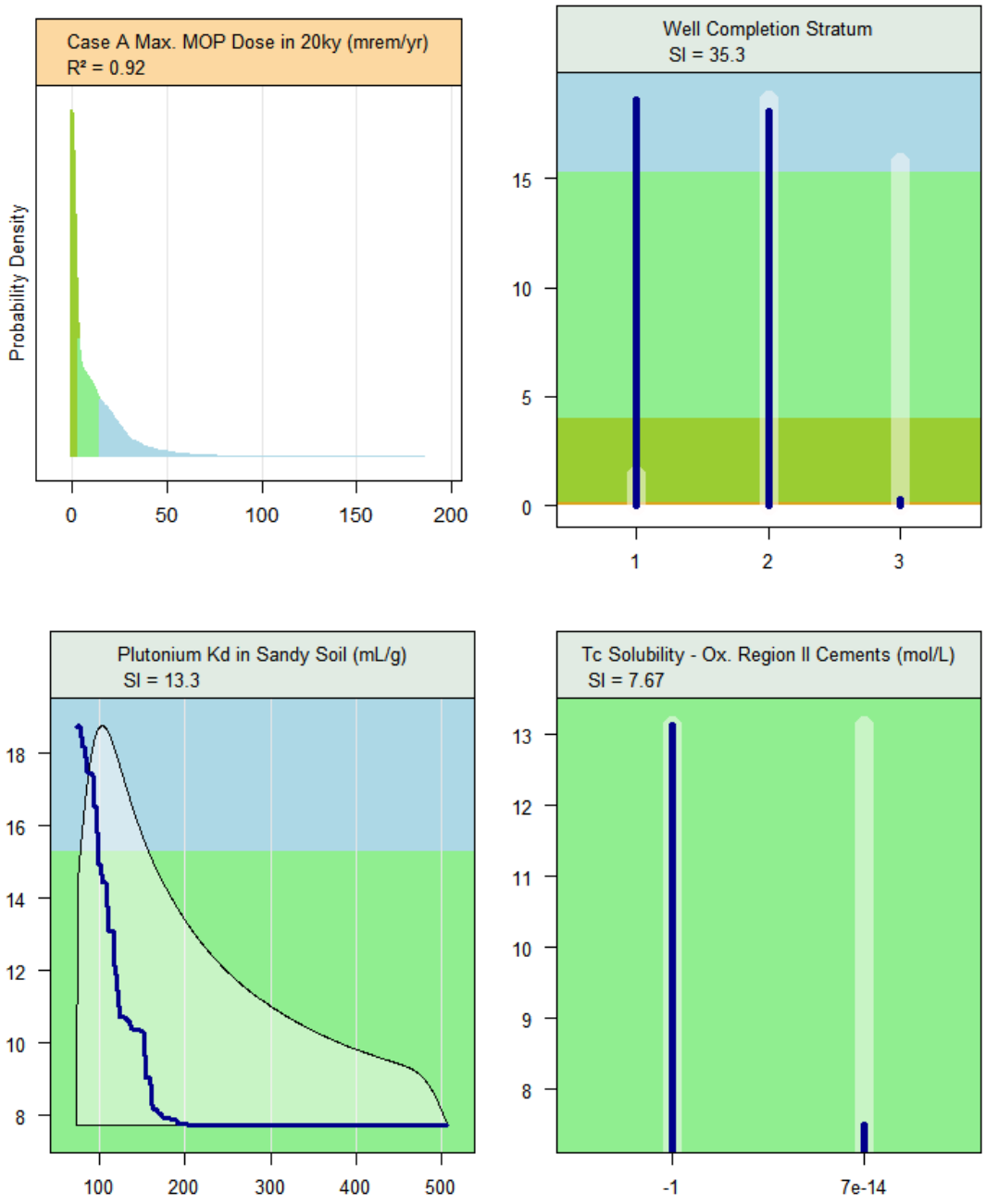

The most influential parameter is the well completion stratum, explaining over a third of the variation. Following that is the distribution coefficient of plutonium in sandy soil, with higher distribution coefficient values corresponding to lower doses. The third parameter is technetium solubility in Oxidizing Region II cements as seen in the previous figure.

The first of the aqueous concentration analyses is focused on the 20,000-year peak maximum concentration of I-129, shown in Figure 5.6-54. The coefficient determination of 0.98 shows that the GBM had a very good fit; hence these parameters are identified with high confidence. The first, with an SI of 74.9, is the well completion stratum, which has been previously described. Following this is the liner failure time for the Type II tanks.

Figure 5.6-54: Partial Dependence Plot Max Aqueous Concentration I-129 - 20,000 Years, Case A

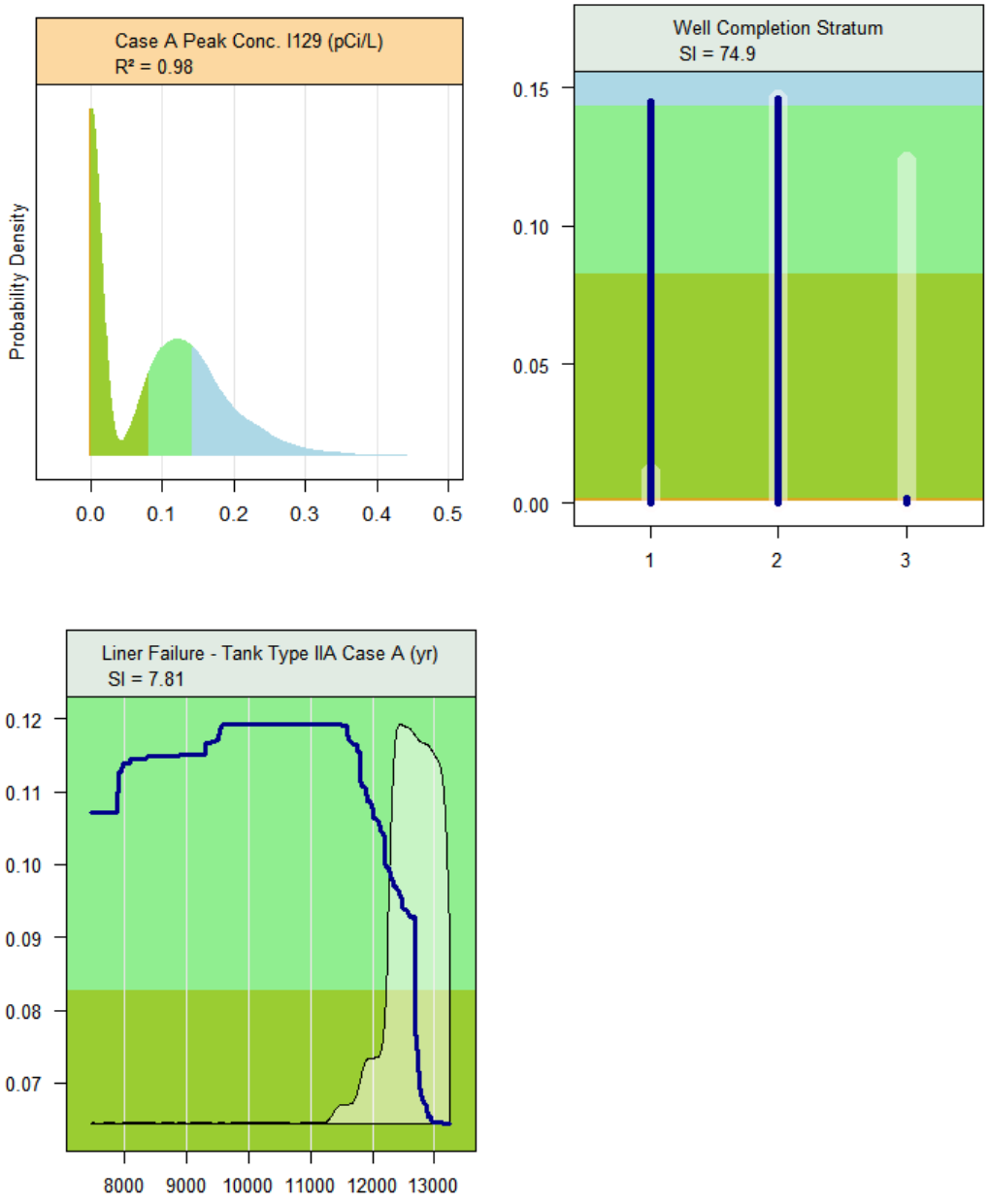

The 20,000-year peak concentration of Np-237 for Case A is shown in Figure 5.6-55. The coefficient determination of 0.99 is an excellent fit. Following the well completion stratum

are two parameters related to neptunium cementitious chemistry, neptunium's solubility in Oxidizing Region II (middle-aged) cements, and its distribution coefficient in Oxidizing Region III (old) cements. While the input distribution for neptunium distribution coefficient is a continuous function, the solubility is strongly discredited. This is because the input distribution is an attempt to represent the solubilities of neptunium in various chemical forms related to its oxidation state and the local water chemistry. Here, four discrete solubility values are represented. The implications of this distribution specification are discussed in the summary at the end of this section.

Figure 5.6-55: Partial Dependence Plot Max Aqueous Concentration Np-237 - 20,000 Years, Case A

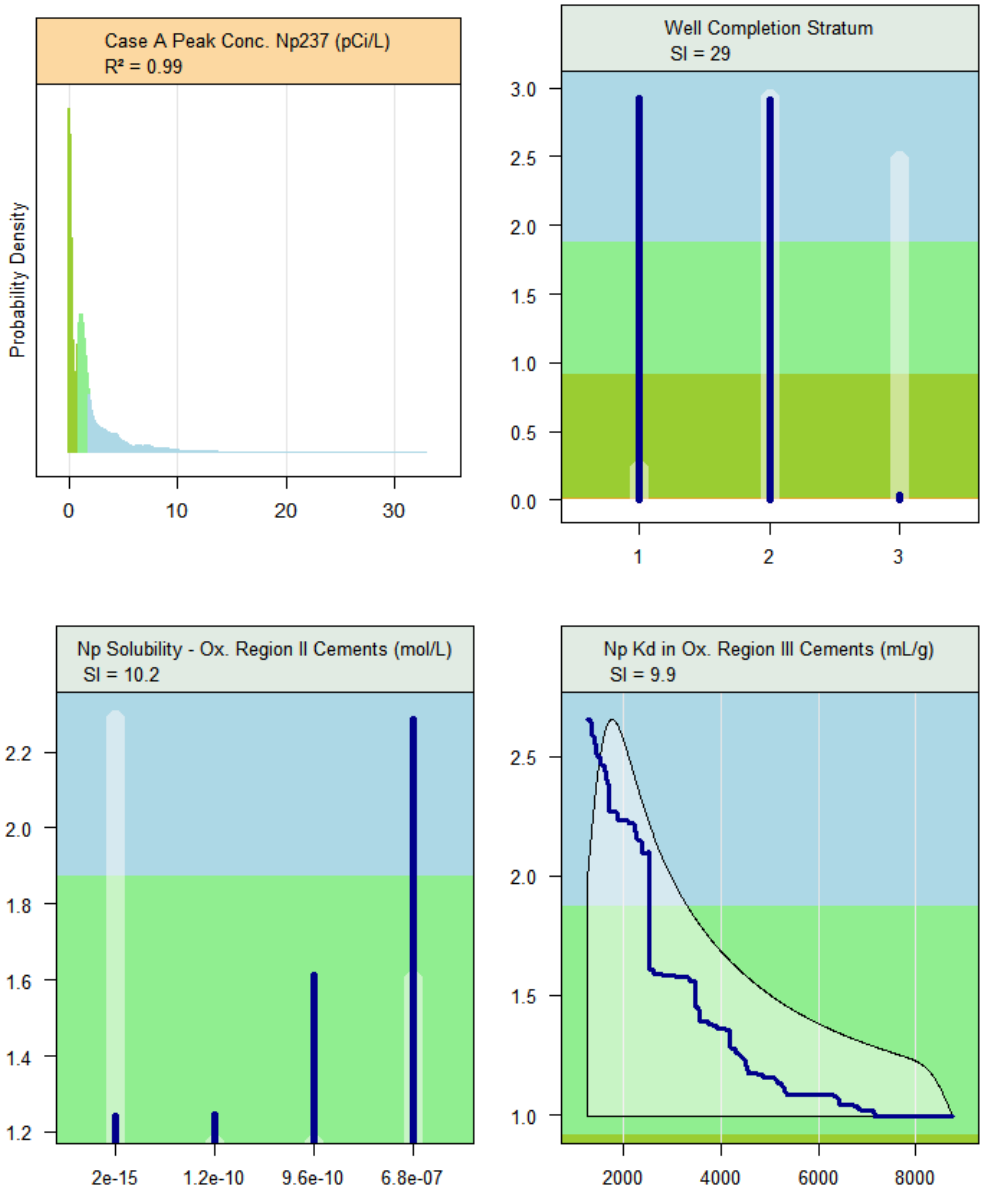

Figure 5.6-56 illustrates the most significant parameters in determining the maximum concentration of Pu-239 within 20,000 years. The water well completion stratum and the distribution coefficient of plutonium in the porous medium of sandy soil are two significant parameters, with a similar degree of influence. Following these is the plutonium solubility in Oxidizing Region II cements. Like the solubility of neptunium, this is given in four distinct values.

Figure 5.6-56: Partial Dependence Plot Max Aqueous Concentration Pu-239 - 20,000 Years, Case A

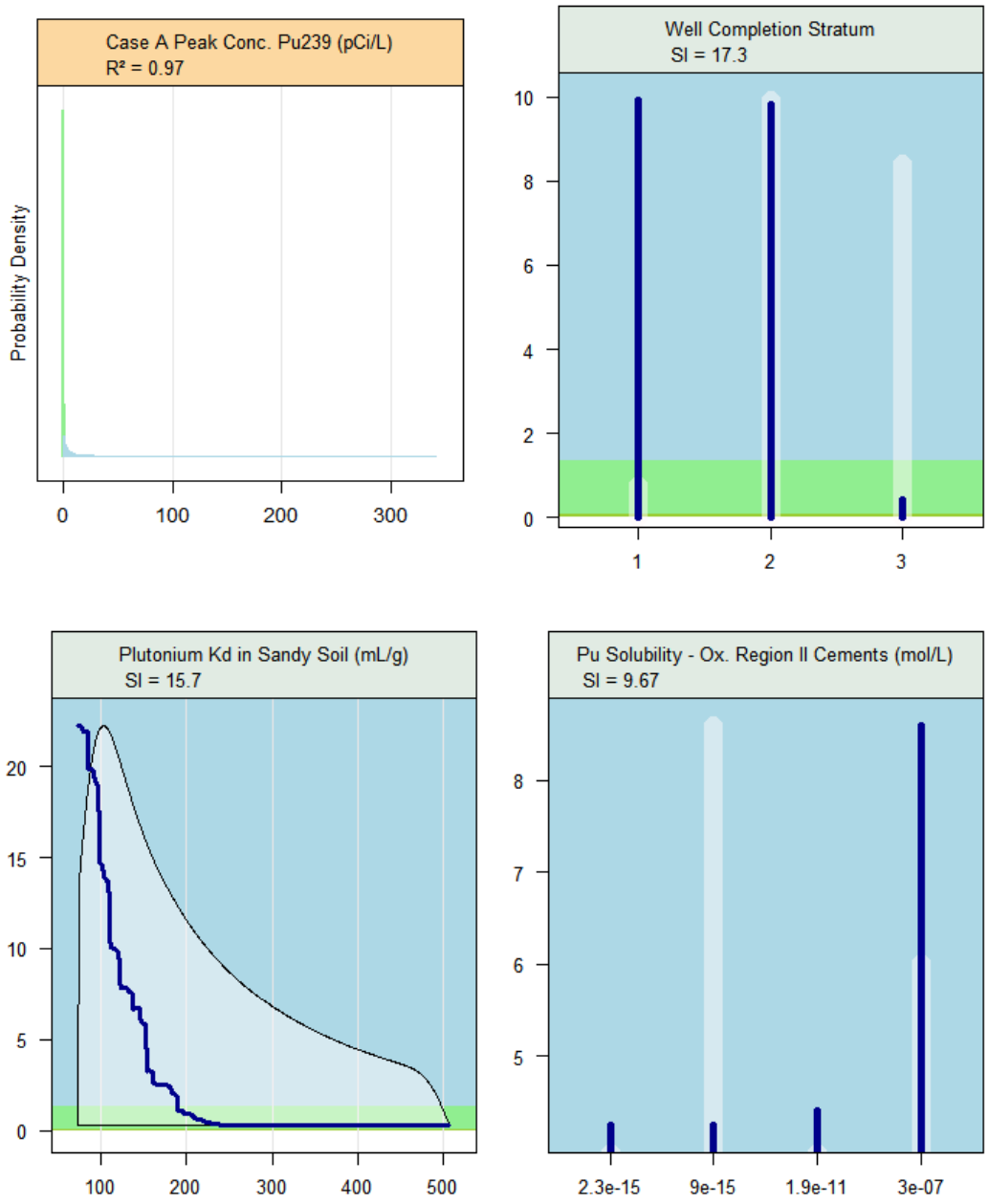

As shown in Figure 5.6-57, the 20,000-year peak aqueous concentration of Ra-226 has similar influences as shown above for the other radionuclide concentrations. The well depth parameter is again the most significant, followed by the distribution coefficient for radium in sandy soils.

Figure 5.6-57: Partial Dependence Plot Max Aqueous Concentration Ra-226 - 20,000 Years, Case A

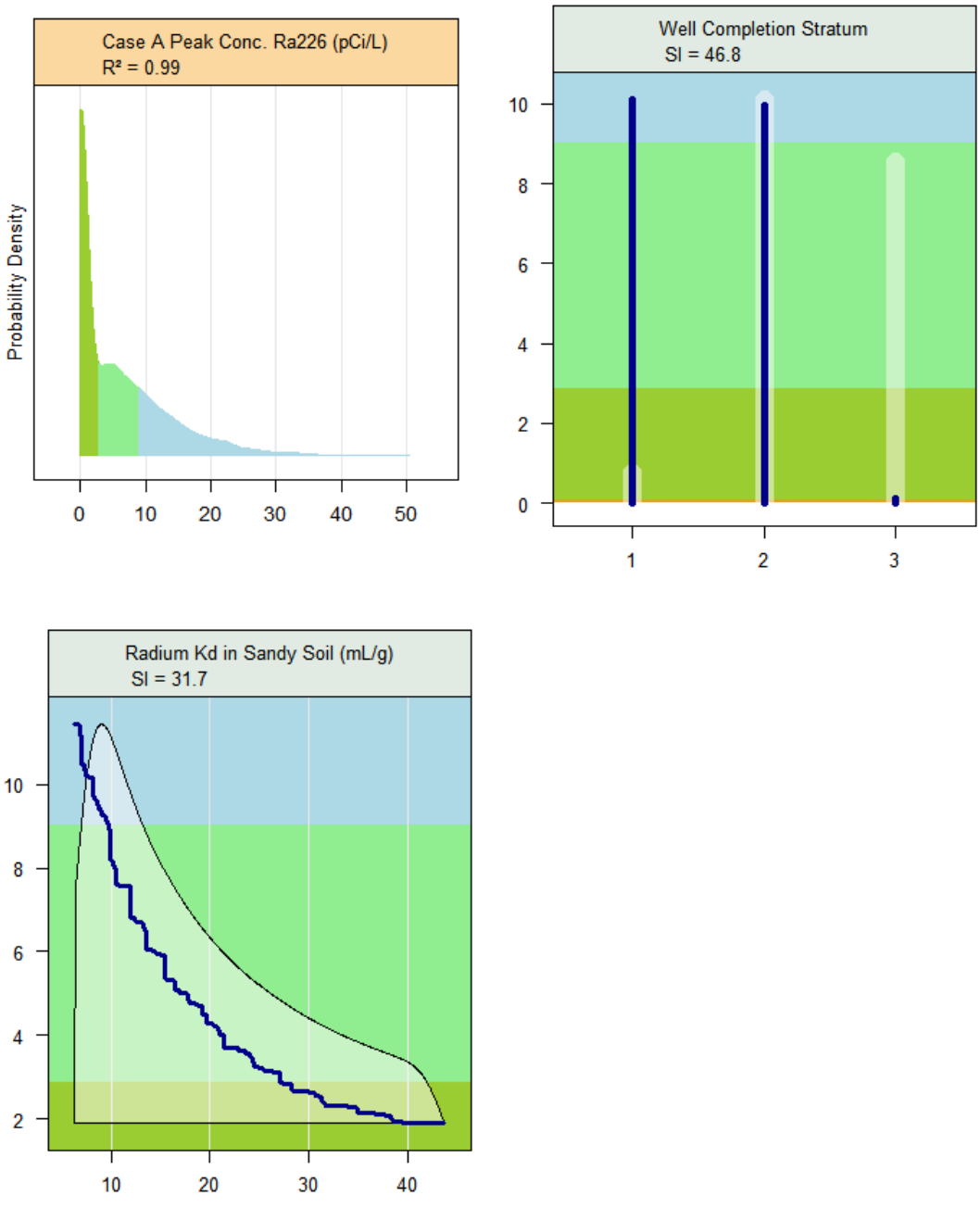

The 20,000-year peak maximum aqueous concentration of Tc-99 shows a dependence on familiar model input distributions, shown in Figure 5.6-58, and with a coefficient determination of 1.0, the fit is excellent. The most influential parameter is the technetium solubility in Oxidizing Region II cements. This is followed by the inventory parameter for Tc-99 in Tank 24. The third-ranked sensitive parameter is the well completion depth parameter.

Figure 5.6-58: Partial Dependence Plot Max Aqueous Concentration of Tc-99 - 20,000 Years, Case A

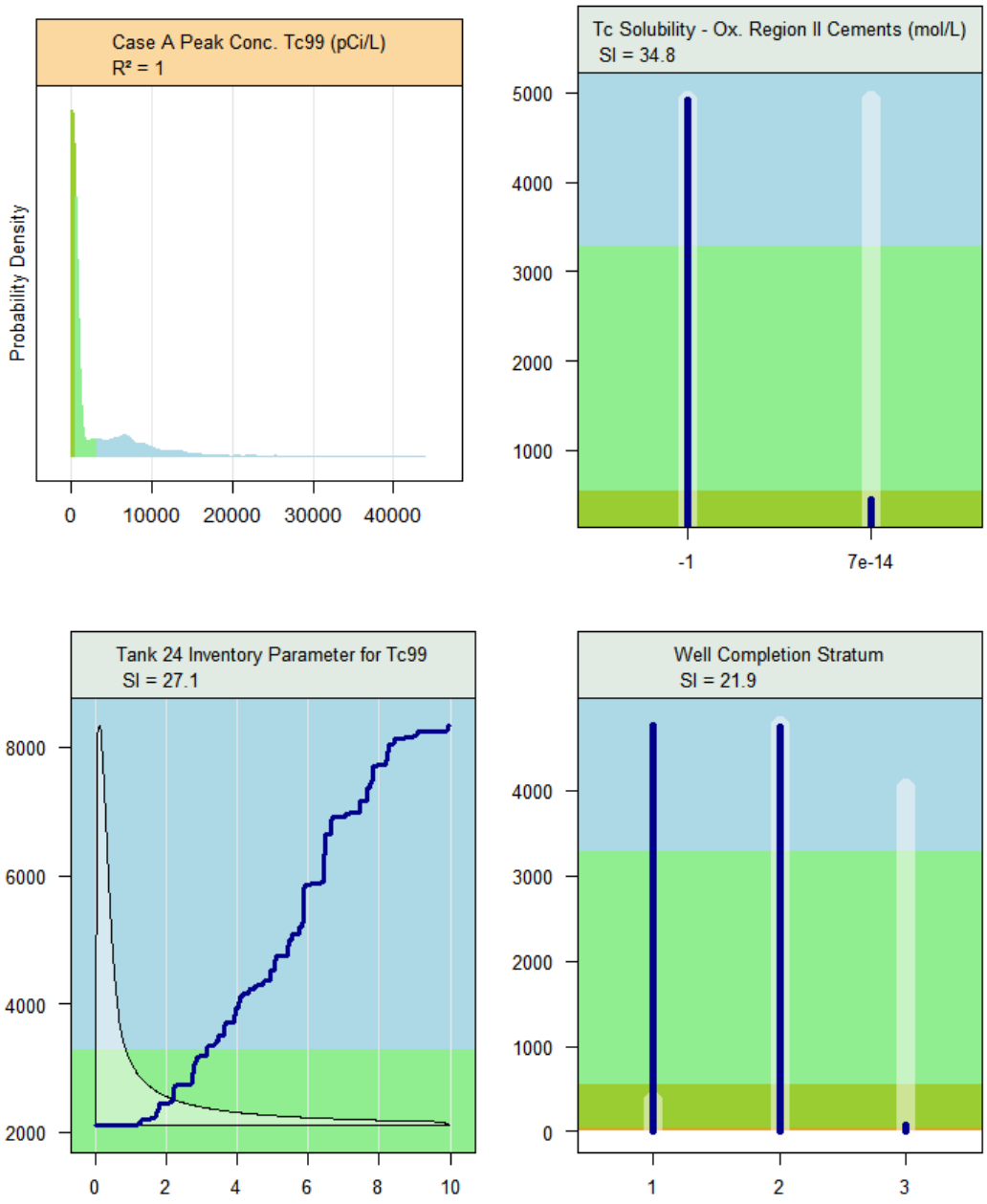

Figure 5.6-59 shows a GBM fit with a relatively low coefficient determination of 0.72, indicating less certainty in the sensitivity results for the maximum MOP Dose for Case D. Regardless, the well completion stratum parameter continues to be an important parameter in Case D. The other leading parameters relate directly to Sr-90, which is a significant dose contributor for early doses.

Figure 5.6-59: Partial Dependence Plot Max MOP Dose Any Sector - 10,000 Years, Case D

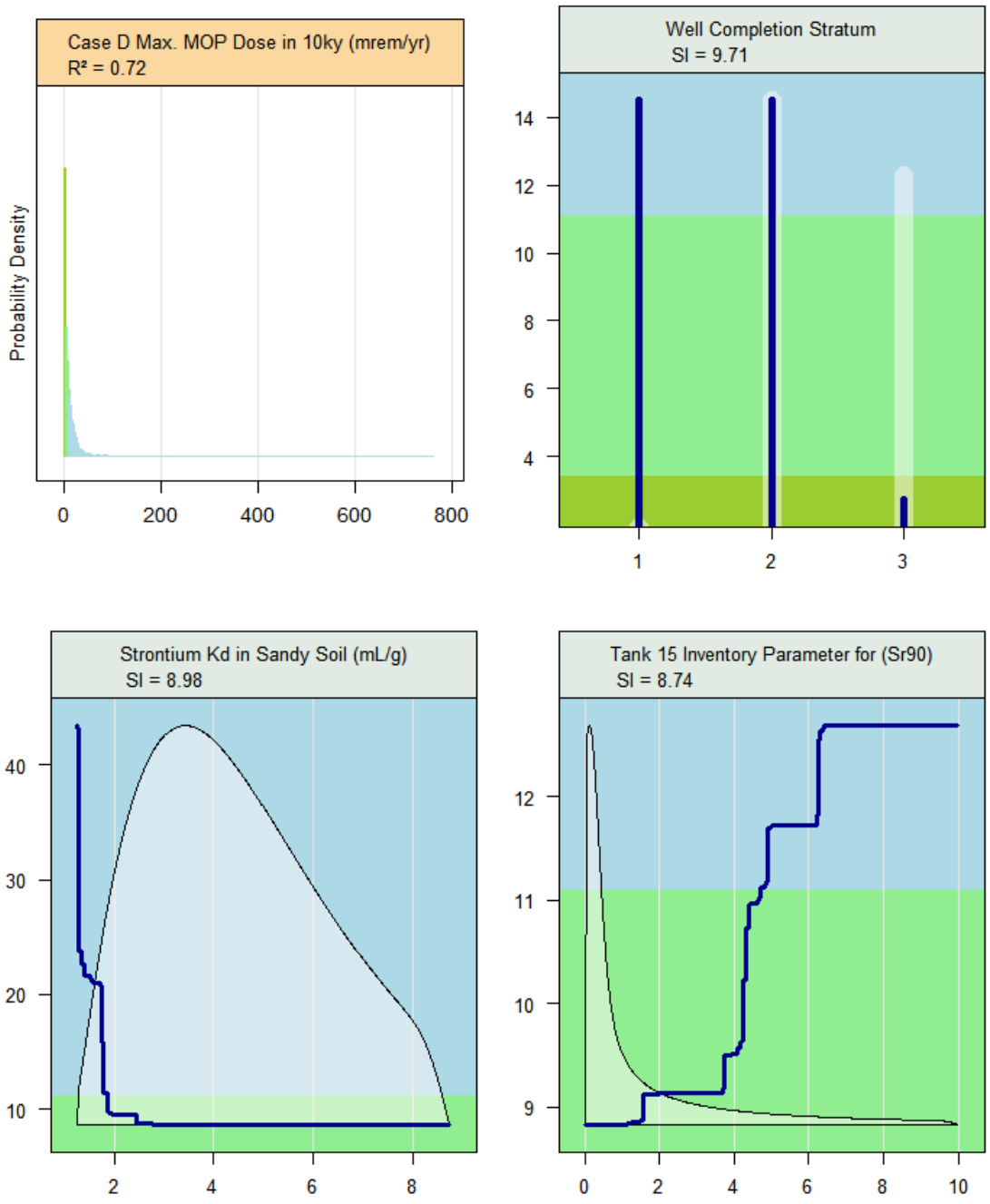

Figure 5.6-60 shows partial dependence plots for the same peak dose to a MOP from a well in any sector, but occurring any time within 20,000 years, rather than 10,000 years. The model fit is very good, with a coefficient determination of 0.97.

Figure 5.6-60: Partial Dependence Plot Max MOP Dose Any Sector - 20,000 Years, Case D

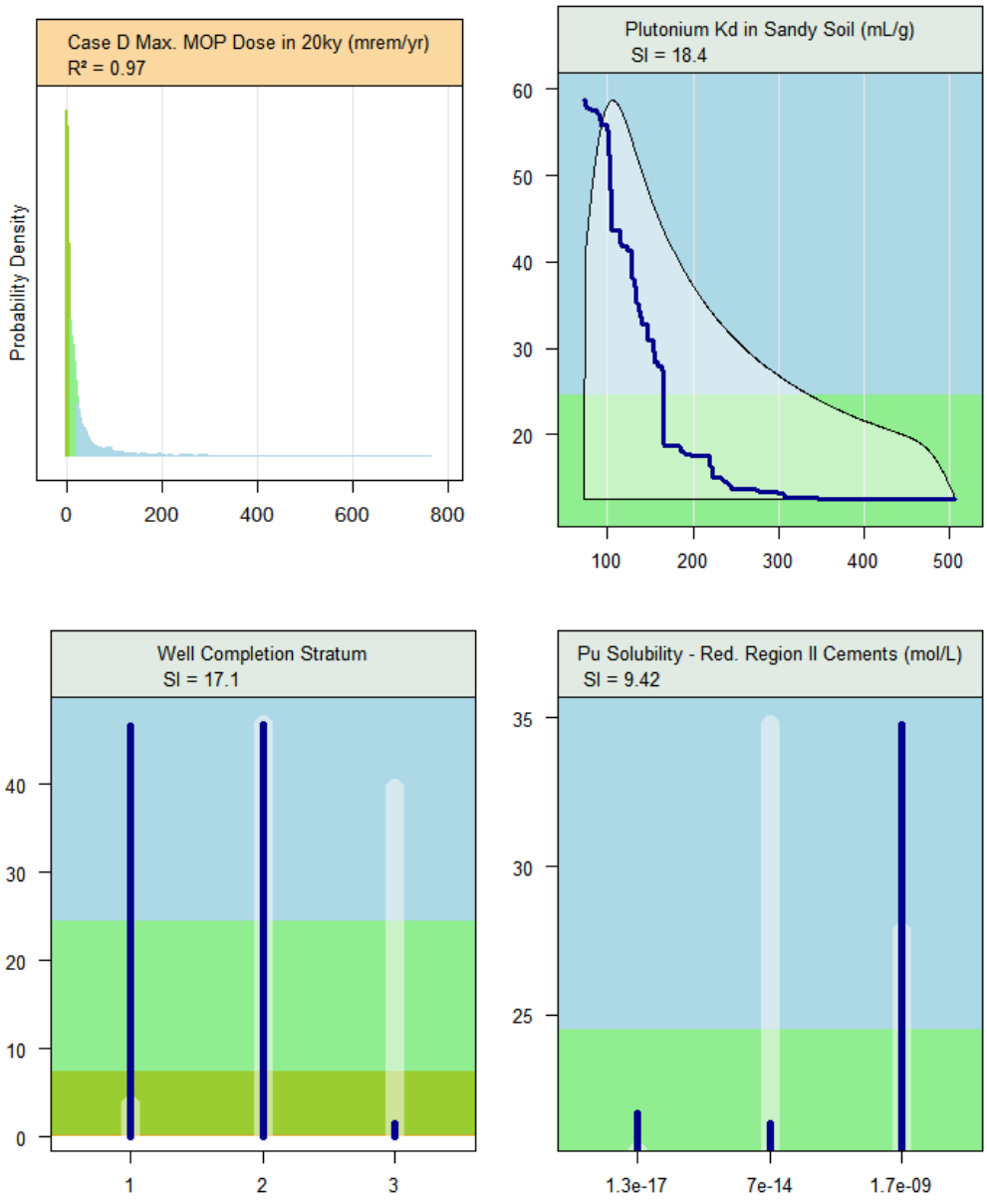

The dose is dominated by Pu-239 and Pu-240, and the plutonium distribution coefficient in sandy soil and its solubility in Reducing Region II cements rank first and third in influence, respectively. Second is the water well completion stratum parameter.

The 20,000-year peak concentration of I-129 at any sector for Case D is shown in Figure 5.6-61. The coefficient determination of 1.0 shows an excellent model fit. The well completion stratum parameter is the most influential input distribution, to the exclusion of others. The stratum parameter produces an SI of 89.2 with respect to variation in iodine concentrations.

Figure 5.6-61: Partial Dependence Plot Max Aqueous Concentration I-129 - 20,000 Years, Case D

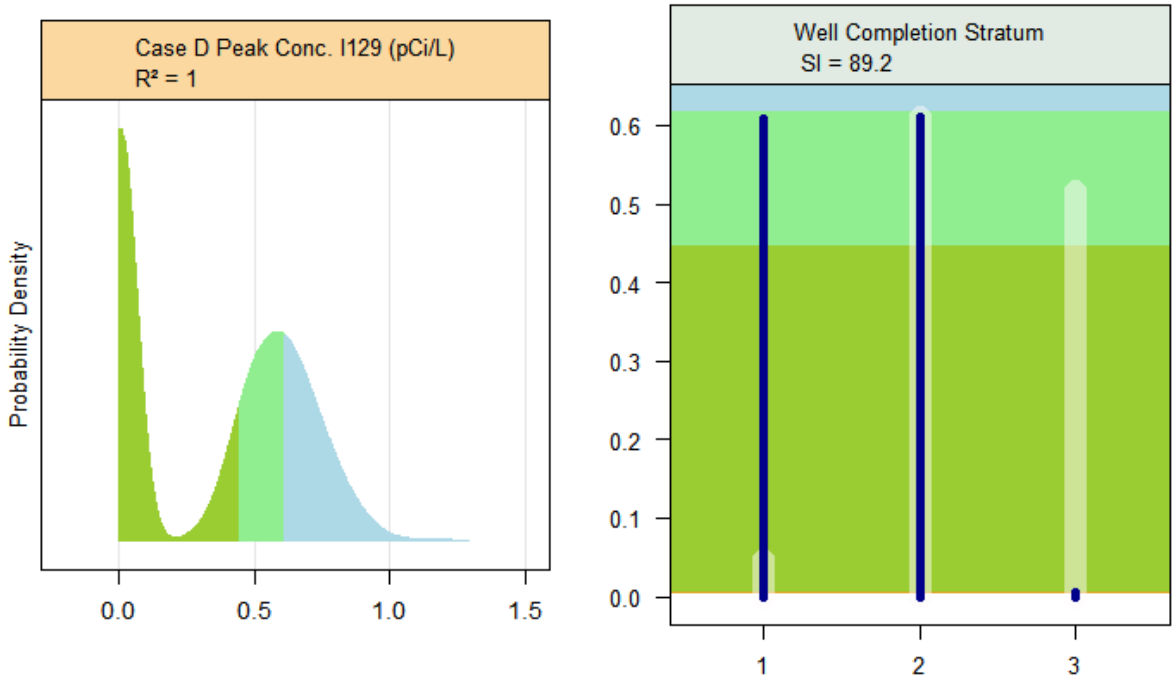

The Case D 20,000-year peak concentration of Np-237 is shown in Figure 5.6-62. The coefficient determination of 1.0 is an excellent fit. Following the well completion stratum is the solubility for neptunium in Reducing Region II cements and the distribution coefficient for neptunium in Oxidizing Region III cements.

Figure 5.6-62: Partial Dependence Plot Max Aqueous Concentration Np-237 - 20,000 Years, Case D

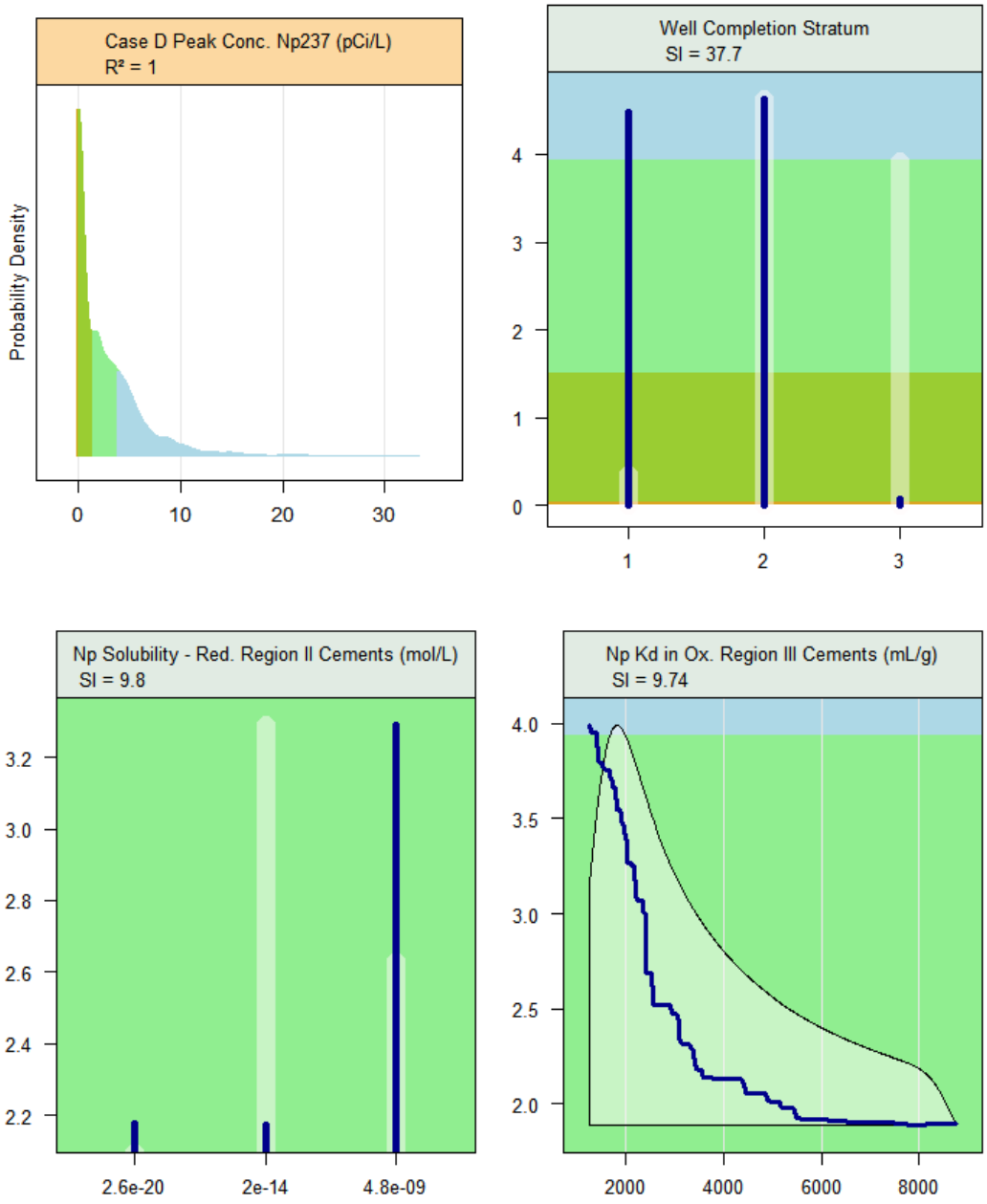

The 20,000-year peak concentration of Pu-239 is shown in Figure 5.6-63. The coefficient determination of 0.99 is a very good fit. Following the well completion stratum are two parameters related to plutonium chemistry, plutonium distribution coefficient in sandy soil and its solubility in Reducing Region II (middle-aged) cements.

Figure 5.6-63: Partial Dependence Plot Max Aqueous Concentration Pu-239 - 20,000 Years, Case D

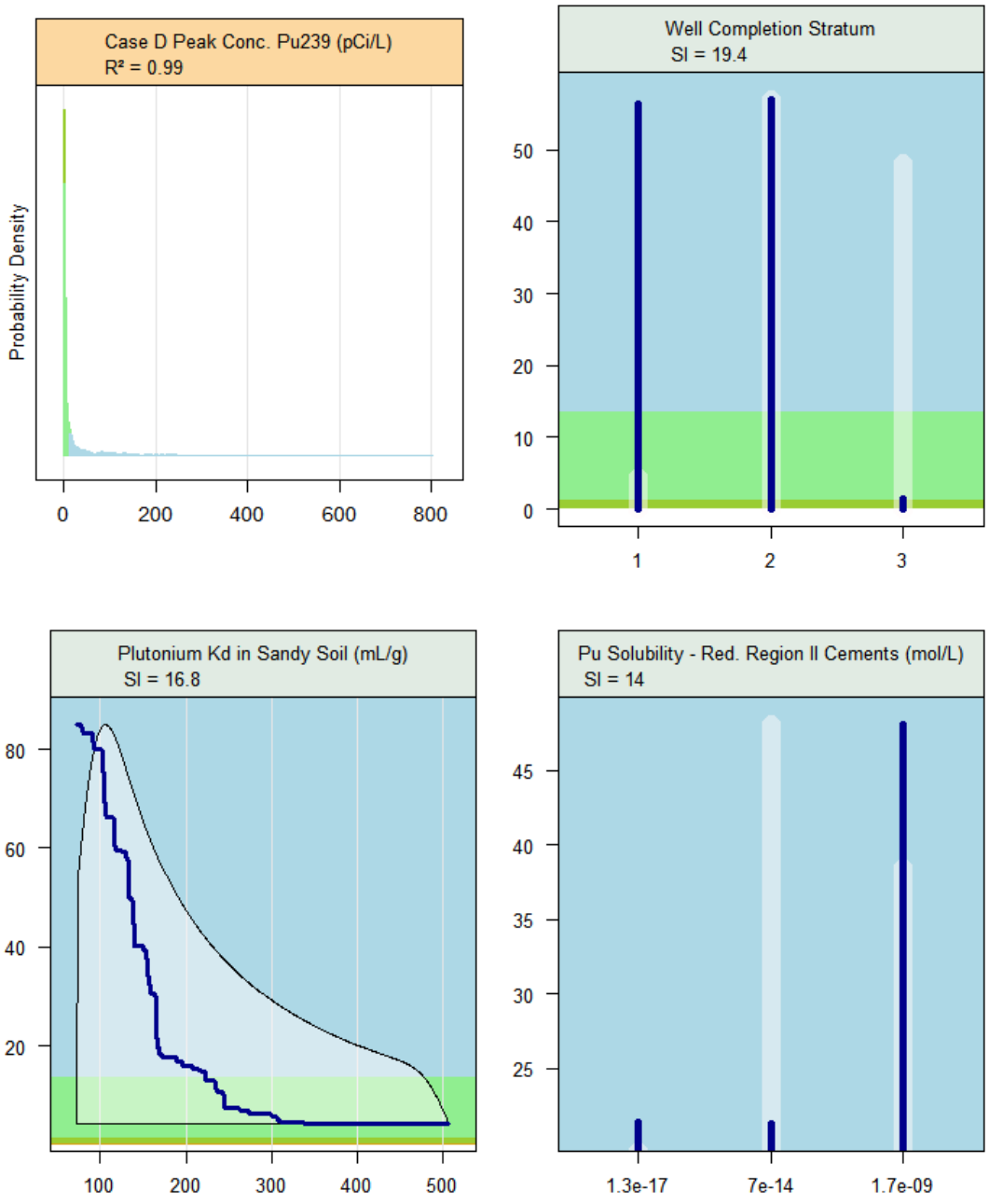

Similar to the 20,000-year peak aqueous concentration of I-129, the peak concentration of Ra-226 is dominated by the water well completion stratum parameter, as shown in Figure 5.6-64. A minor influence is identified for the distribution coefficient of radium in sandy soils.

Figure 5.6-64: Partial Dependence Plot Max Aqueous Concentration Ra-226 - 20,000 Years, Case D

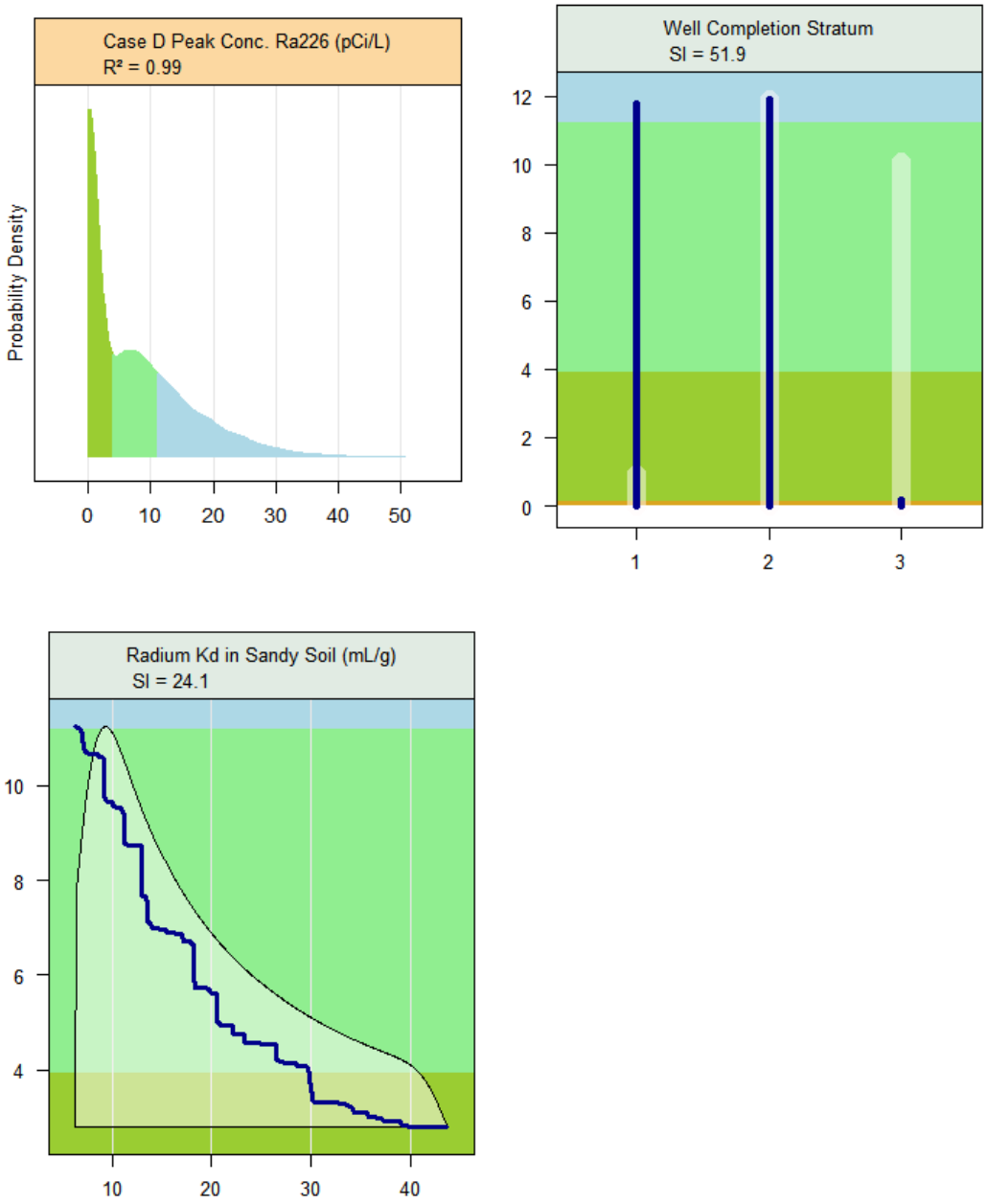

As shown in Figure 5.6-65, the influence on the 20,000-year peak maximum aqueous concentration of Tc-99 for Case D also includes a heavy influence from the well completion depth (the second-ranked parameter) and a coefficient determination of 1.0, the fit is very good. The top-ranked sensitive parameter is the Tank 24 inventory for Tc-99. Third is the solubility of technetium in Oxidizing Region II cements. Overall, these results are similar to those obtained for Tc-99 peak concentrations for Case A.

Figure 5.6-65: Partial Dependence Plot Max Aqueous Concentration Tc-99 - 20,000 Years, Case D

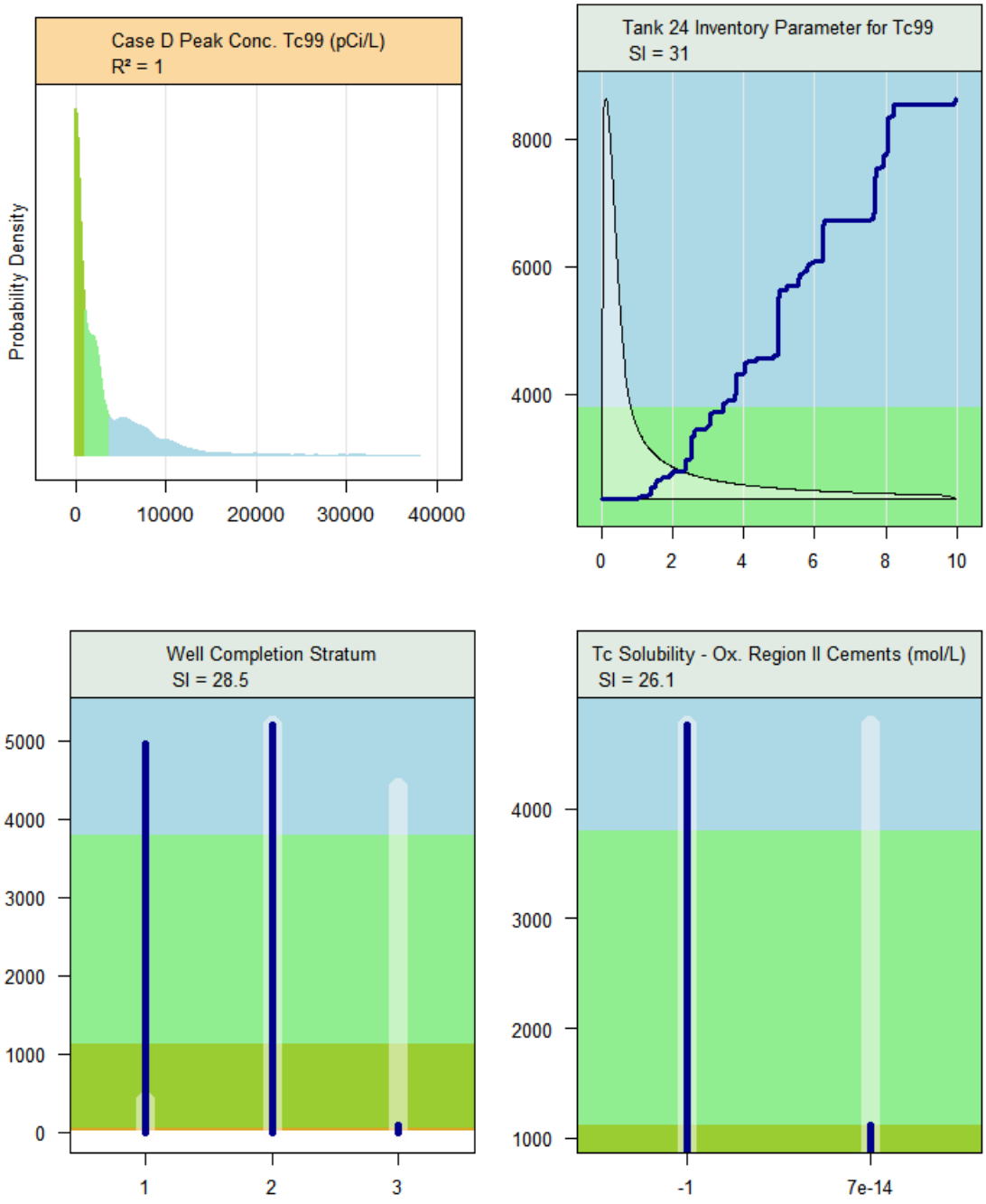

As with Case D, Figure 5.6-66 identifies the well completion stratum and two parameters related to Sr-90 as the top three most sensitive parameters. The GBM fit has a relatively low coefficient determination of 0.72.

Figure 5.6-66: Partial Dependence Plot Max MOP Dose Any Sector - 10,000 Years, Case E

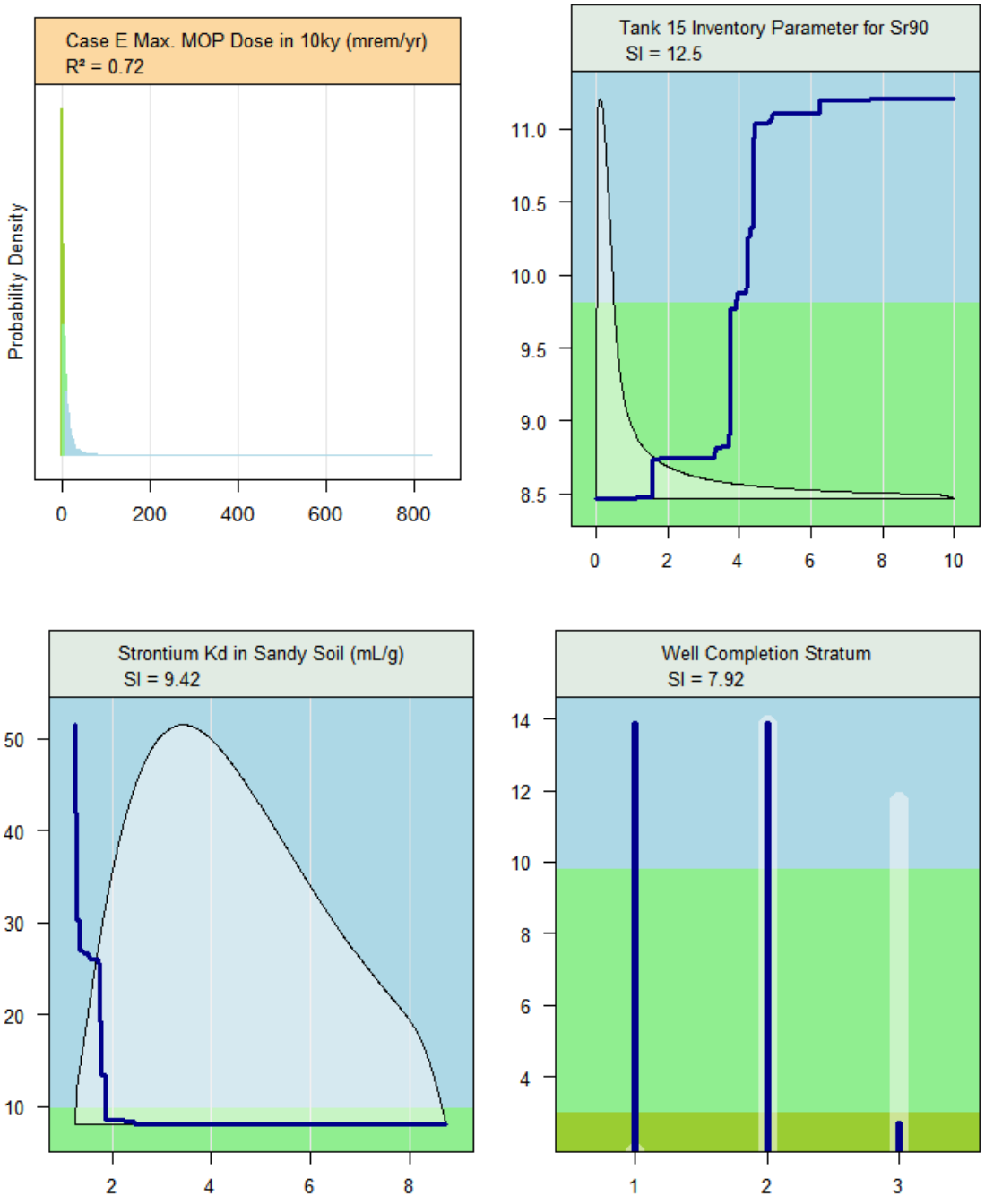

Figure 5.6-67 shows SI plots for the same maximum dose to a MOP from any sector, but occurring any time within 20,000 years, rather than 10,000 years. The model fit has a coefficient determination of 0.98.

Figure 5.6-67: Partial Dependence Plot Max MOP Dose Any Sector - 20,000 Years, Case E

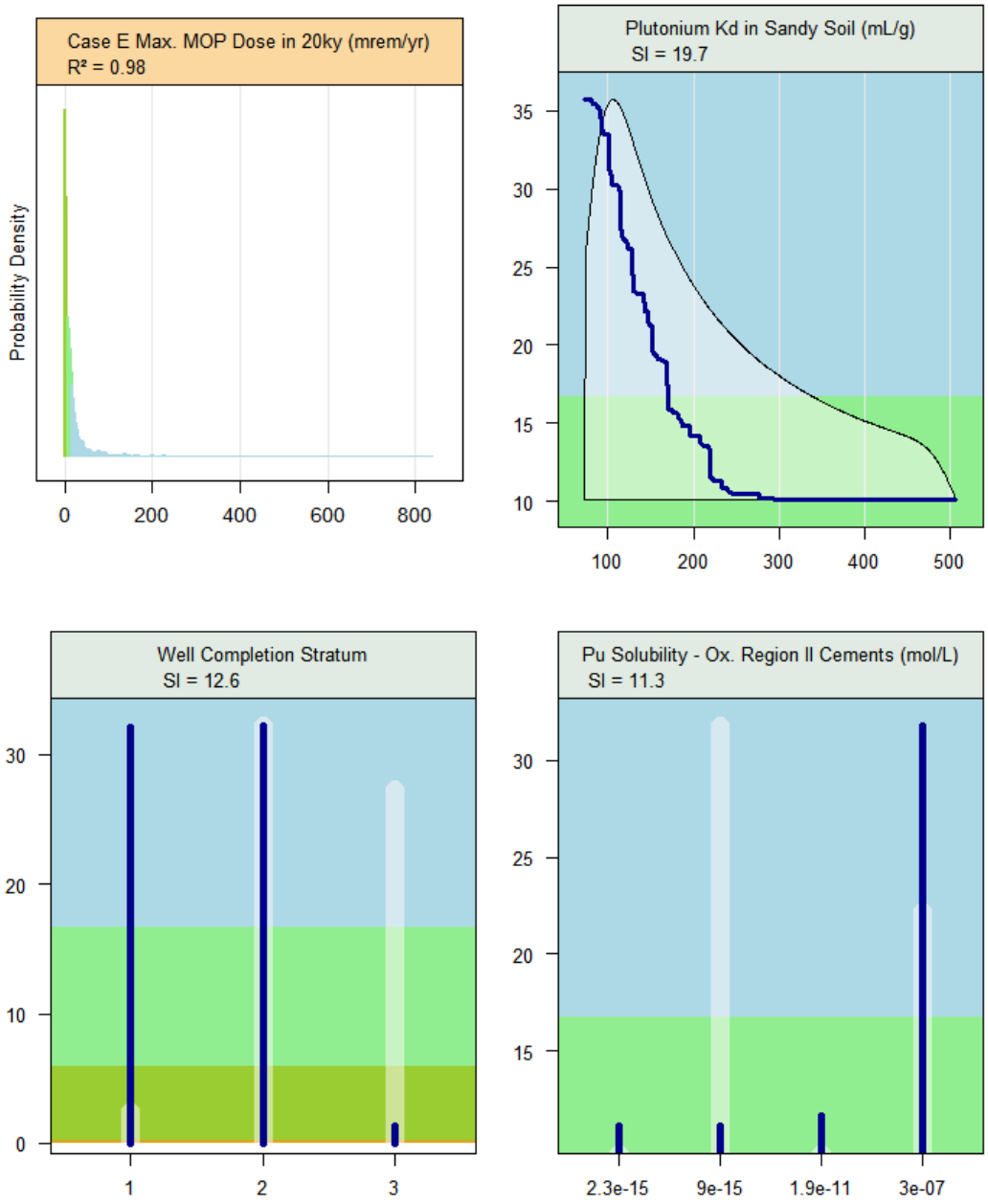

As with Case D, this dose is dominated by Pu-239 and Pu-240. The plutonium distribution coefficient in sandy soil and its solubility in Oxidizing Region II, cements rank first and third in influence, respectively. Second is the water well completion stratum parameter.

The 20,000-year peak concentration of I-129 at any sector for Case E is shown in Figure 5.6-68. The coefficient determination of 1.0 indicates an excellent fit of the GBM statistical model to the GoldSim results. The well completion stratum parameter has the most influence

on the I-129 concentration. Following that are the liner failure time for Type II tanks for Cases B, C, D, and E, and the Darcy velocity for Tank 13.

Figure 5.6-68: Partial Dependence Plot Max Aqueous Concentration I-129 - 20,000 Years, Case E

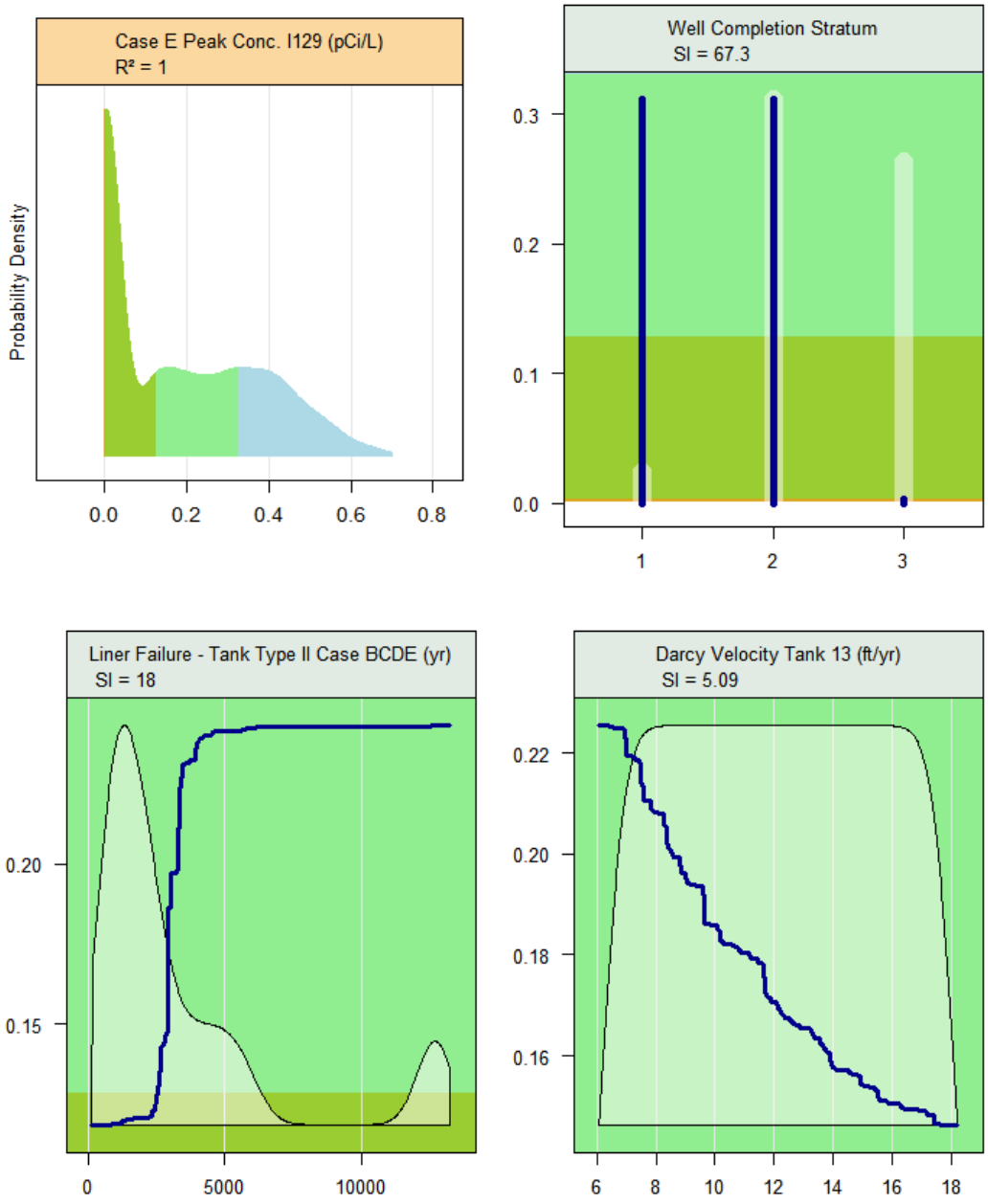

The Case E 20,000-year peak concentration of Np-237 is shown in Figure 5.6-69. The coefficient determination of 1.0 indicates an excellent fit of the GBM statistical model to the GoldSim results. Following the well completion stratum is the solubility of neptunium in Oxidizing Region II (middle-aged) cements.

Figure 5.6-69: Partial Dependence Plot Max Aqueous Concentration Np-237 - 20,000 Years, Case E

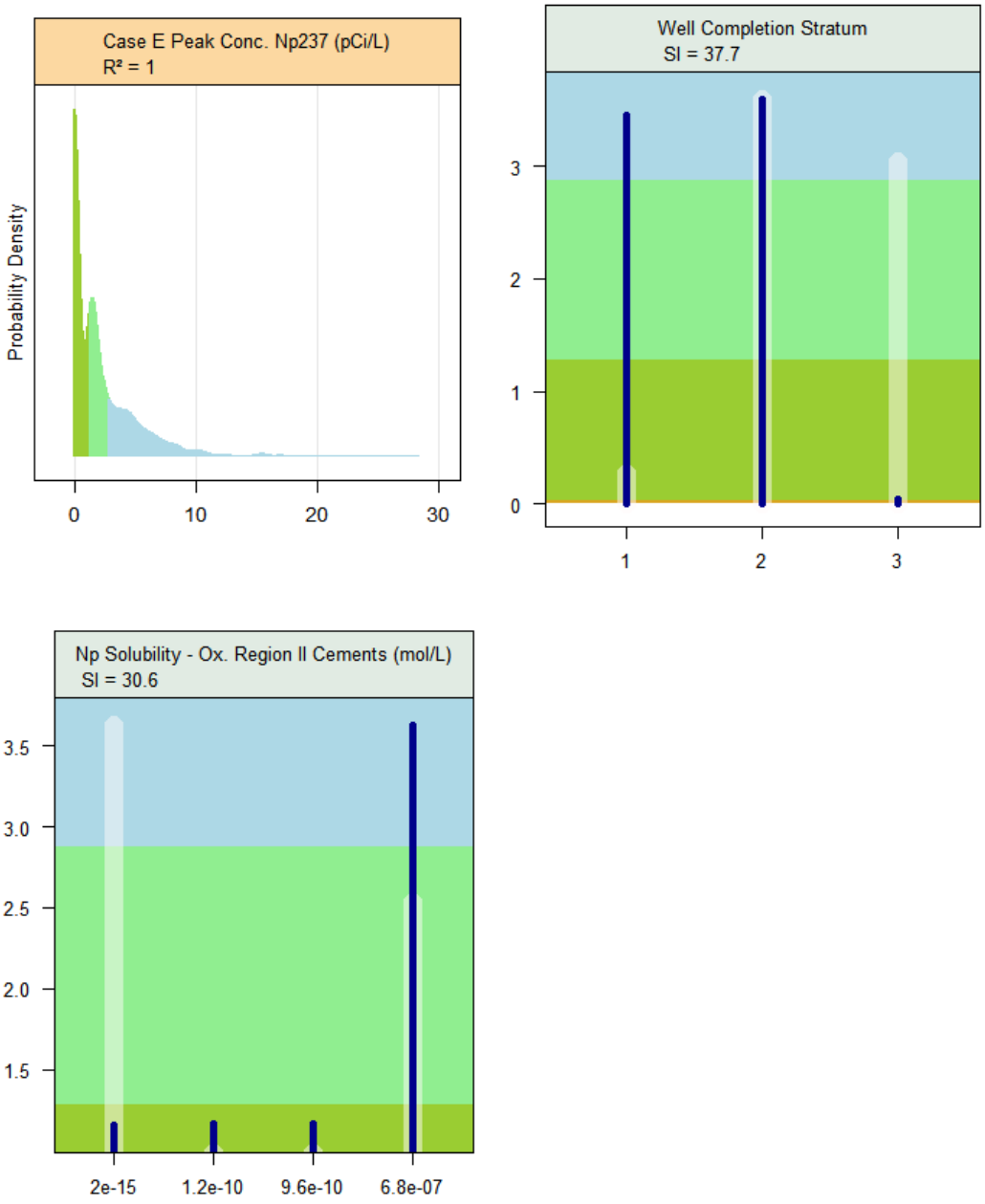

The Case E 20,000-year peak concentration of Pu-239 is shown in Figure 5.6-70. The coefficient determination of 1.0 is an excellent fit. The three most influential parameters are similar to those identified for this endpoint in Case D. Plutonium distribution coefficient in sandy soil is the most significant, followed closely by the well completion stratum. Third is the plutonium solubility in Oxidizing Region III (old-aged) cements.

Figure 5.6-70: Partial Dependence Plot Max Aqueous Concentration Pu-239 - 20,000 Years, Case E

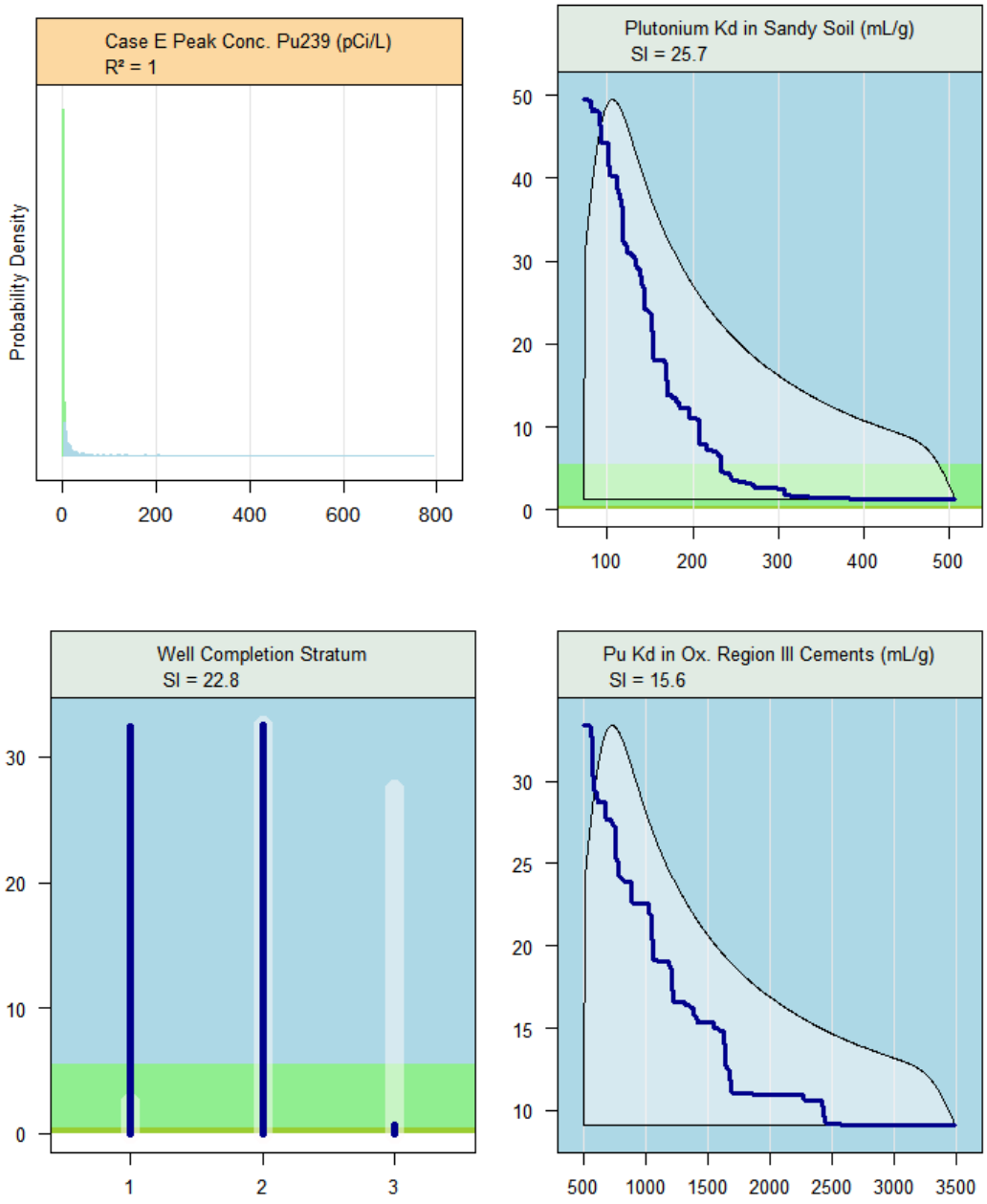

Like the 20,000-year peak aqueous concentration of I-129, the peak concentration of Ra-226 is due almost completely to the water well completion stratum parameter, as shown in Figure 5.6-71. A minor influence is identified for the distribution coefficient of radium in sandy soils. This is essentially identical to the influences seen for this endpoint assuming Case D. The coefficient determination of the GBM fit is 0.99.

Figure 5.6-71: Partial Dependence Plot Max Aqueous Concentration Ra-226 - 20,000 Years, Case E

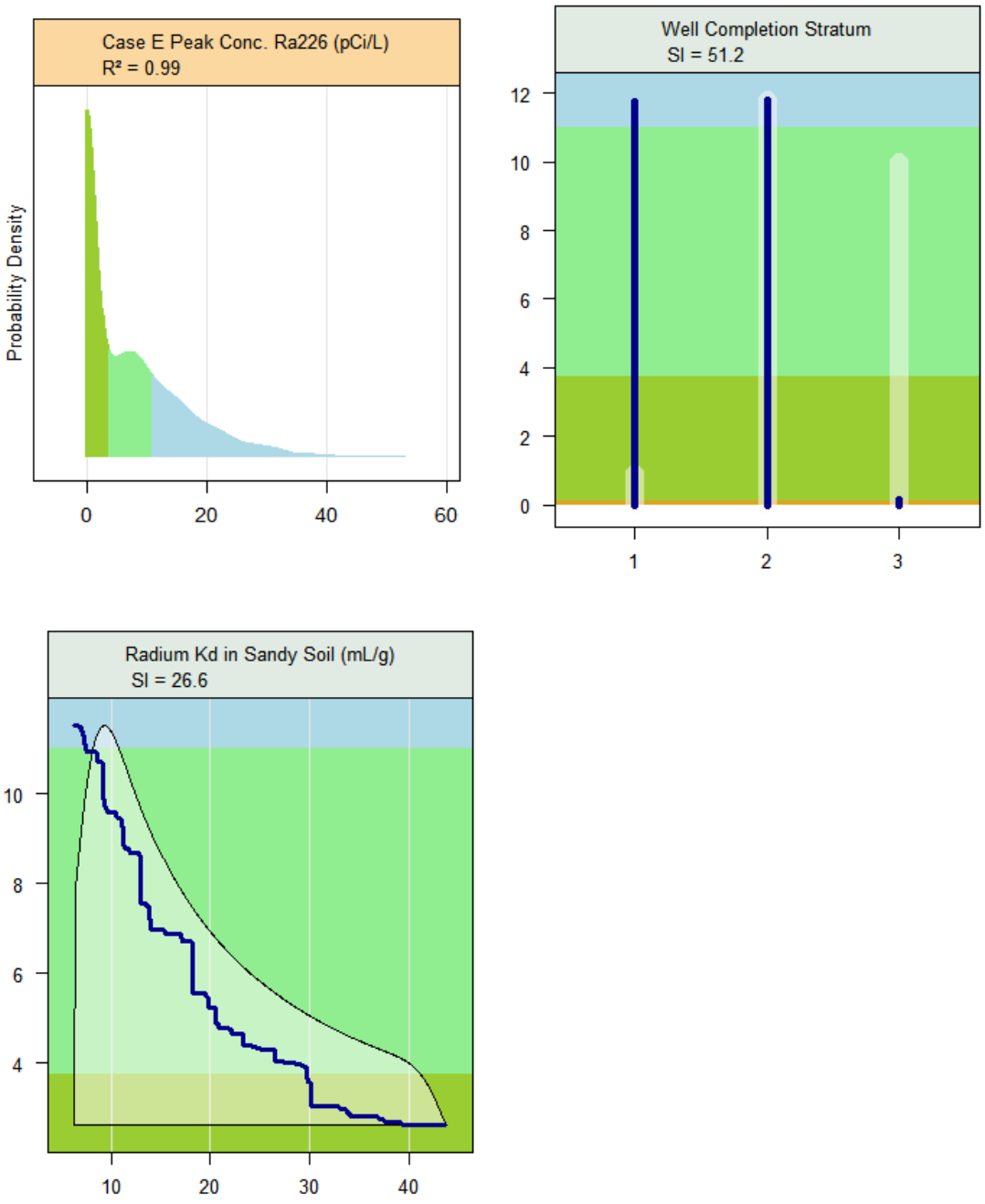

The 20,000-year peak maximum aqueous concentration of Tc-99 for Case E is also dominated by the inventory parameter for Tc-99 in Tank 24, as shown in Figure 5.6-72, and with a coefficient determination of 1.0, the fit is excellent. The second most influential parameter is solubility of technetium in Oxidizing Region II cements. The third-ranked

sensitive parameter is the completion depth of the well. Overall, these results are similar to those obtained for Tc-99 peak concentrations for both Cases A and D.

Figure 5.6-72: Partial Dependence Plot Max Aqueous Concentration Tc-99 - 20,000 Years, Case E

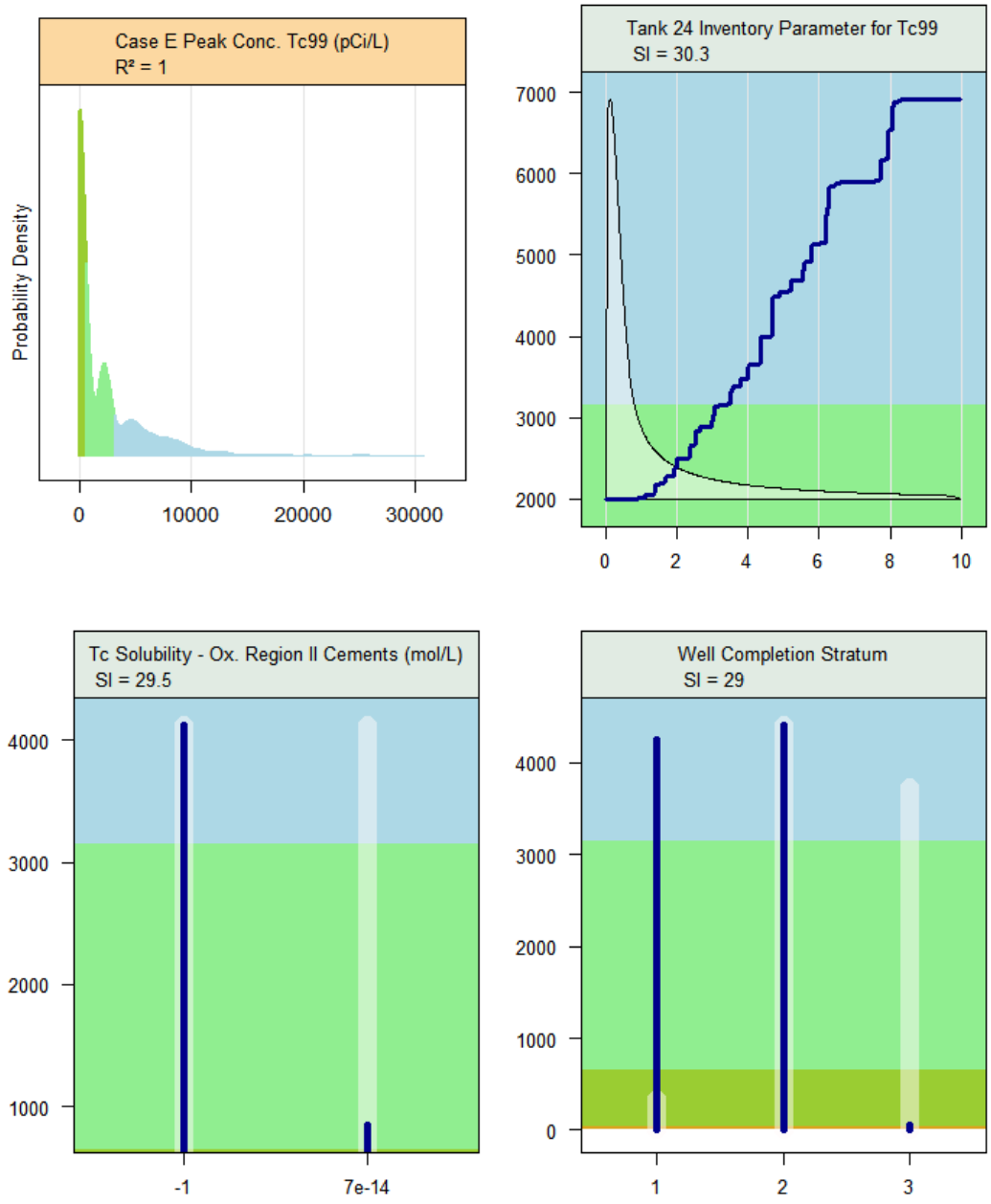

5.6.5.4 Summary of the Sensitivity Analysis

The sensitivity analysis of the HTF GoldSim Model was very successful in identifying significant parameters for the selected endpoints. In the present analysis, GBM fitting has very high coefficient determination values, and relationships between input variables and result endpoint variations are clear.

Several recurring themes appeared in the sensitivity analyses:

- The water well completion stratum parameter appeared in the top three sensitive parameters in almost every aqueous concentration and MOP dose endpoint.
- Specific distribution coefficient values are generally significant. About half of the endpoints were dependent on the distribution coefficient of plutonium and radium in sandy soil, or on the distribution coefficient of neptunium in Oxidizing Region III cements.
- Aqueous solubilities of the elements neptunium, plutonium, and technetium, in cementitious materials (specifically Oxidizing Region II cements) are quite significant in determining well water concentrations and doses.
- The timing of the failure of the waste form for Cases B, C, D, and E (grouped into the same stochastic within the HTF GoldSim Model) for Type I tank is influential to determining the peak concentration of I-129 for Case E.
- A common influential variable type is an inventory multiplier parameter. Specific common inventory parameters are for Pu-238 in Tank 11, Tc-99 in Tank 24, and I-129 in Tanks 9, 10, and 12.
- In the Case A MOP dose endpoint, the stochastic variable related to the ingestion of local well water is significant.

The water well completion stratum parameter is described in Section 5.6.3.11 and is based on well drilling records in counties bordering the SRS and concentration ratios developed from PORFLOW results.

The importance of distribution coefficient values in the performance assessment of the closure system has been recognized and is an area of continued testing and analysis. Section 5.6.3.4 provides the results of current testing and analysis to develop the stochastic used in the model.

The representation of element-specific solubilities in cementitious materials is based on analysis reported in Section 4.2.1 and the stochastic is developed in Section 5.6.3.3.

The timing of liner failure is dependent on the tank type and case, as described in Section 5.6.3.7.

The strong and persistent influence of the inventory parameter on radionuclide concentrations, for various radionuclides in various waste tanks was anticipated. The basis for the initial residual inventories in the various waste tanks is provided in Section 3.3 and the development of the inventory multiplier stochastic is described in Section 5.6.3.1. The concentration of Ra-226 is influenced by the inventory multiplier on Pu-238 in Tank 11 because Pu-238 is a parent to Ra-226 and its inventory multiplier ranges from 0.01 to 10 in the Type I tanks.

The peak MOP dose within 20,000 years for Case A is influenced by the water ingestion. Its stochastic is based on data provided in Section 5.6.3.12.

The sensitivity analyses performed two important functions 1) it provided important feedback about which input parameters (and over what ranges) are most significant to specific endpoints, and 2) it identified parts of the model for which improved modeling implementation could prove most beneficial.

5.6.6 Barrier Analysis using the PORFLOW Deterministic Model

The purpose of this section is to evaluate the total barrier capability offered by the engineered and natural system and provide a systematic analysis of each barrier to waste migration. The barrier analyses will assess the contribution of individual barriers (e.g., closure cap, grout, CZ, liner, and natural barrier) by comparing contaminant flux results under various barrier conditions. The barrier analyses will compare the difference in flux between intact and degraded barriers, while minimizing the contribution of the other barriers to the extent possible. Time histories of flux below the waste tanks (e.g., at the water table for unsaturated waste tanks and exiting the basemat for submerged waste tanks) from PORFLOW for the no closure cap barrier are provided in Appendix H.1 and for all other barrier cases, including the Base Case, they are provided in Appendix I.

5.6.6.1 Barrier Analysis Scope

The barrier analysis was carried out for the waste tanks listed in Table 5.6-30. Each waste tank type is represented in this list, as well as representative Type I and Type II tanks with initially failed liners (e.g., Tank 12 and Tank 15). Table 5.6-31 lists the radionuclides selected for barrier analysis, along with a description of their significance. The radionuclides chosen for analysis were the radionuclides with the most impact on dose and those possessing differing transport characteristics (e.g., distribution coefficient values, solubility limits). The analysis point for each barrier is the radionuclide flux below the waste tank (e.g., at the water table for unsaturated waste tanks and exiting the basemat for submerged waste tanks). The Base Case (Case A) initial inventory for each waste tank is used for all barrier analyses cases and alternative cases (e.g. the inventory estimates are the same).

A selection of the barrier analysis results is presented. Specifically, because Type II tanks (both initially degraded and initially intact) and Type IV tanks are predominant contributors to dose, time histories displaying radionuclide flux from these waste tank types will be the focus (except for the natural barrier analysis which presents Type IV and Type IIIA tanks because submerged waste tanks were not part of that analysis). The Type II tanks are unique in that they are modeled with an initial radionuclide inventory in their primary sand pad and annulus (Tank 16 also includes an initial inventory in the secondary sand pad).

Table 5.6-30: Summary of Waste Tanks Selected for Barrier Analysis

Representative Waste Tank	Waste Tank Type	Initially Failed Liner?
Tank 9	Type I (submerged)	N
Tank 12	Type I (submerged)	Y
Tank 13	Type II (submerged)	N
Tank 15	Type II (submerged)	Y
Tank 21	Type IV	N
Tank 36	Type III A	N

Table 5.6-31: Summary of Radionuclides Selected for Barrier Analysis

Radionuclide of Interest	Half-Life (yrs)	Significant Characteristics
Tc-99	2.11E+05	Significant dose contributor, long-lived, redox sensitive, K_d/solubility controlled
Ra-226	1.60E+03	Significant dose contributor, short-lived, not redox sensitive, K_d /solubility controlled, generated through ingrowth from the Pu-238→U-234→Th-230 chain
Pu-239	2.41E+04	Long-lived, redox sensitive, K_d/solubility controlled
I-129	1.57E+07	Significant dose contributor, long-lived, not redox sensitive, no solubility controls
Np-237	2.14E+06	Long-lived, K_d/solubility controlled, generated through ingrowth from Cm-245→ Pu-241 →Am-241 chain

The ten run configurations considered in the barrier analyses are detailed in Tables 5.6-32 and 5.6-33. In addition, waste tank releases generated using the alternative scenario settings for Cases B and C will also be evaluated (see Section 4.4.2 and Table 4.4-1 for a summary of the conceptual models for these two cases). Table 5.6-32 identifies the barrier analysis parameters for the five PORFLOW material zones that are varied (natural barrier, closure cap, grout, CZ, waste tank liner, and waste tank concrete including existing basemat, wall, and roof). Table 5.6-32 also describes the nominal (N), partially degraded (P), and fully degraded (F) condition for each material zone. Table 5.6-33 lists the physical condition of the material zone for each of the ten run configurations. The barrier analyses includes the PORFLOW Base Case, which uses the nominal barrier properties and a degraded run configuration (run 2) where every zone other than the CZ is modeled as fully degraded. There are also specific barrier cases associated with each material zone to evaluate the capabilities of each barrier configuration by holding other material zone conditions constant while varying the condition of the zone being assessed. Additional information regarding the material zones for the various barriers is provided in Sections 4.2.1 and 4.2.2.

Table 5.6-32: Barrier Analysis Variability

Material Zone	N (Nominal)	P (Partially Degraded)	F (Fully Degraded)
Closure Cap	Infiltration profile per Base Case (Table 4.2-23)	N/A	Infiltration constant at 16.45 in/yr [WSRC-STI-2007-00184]
Grout (K_d controlled)	Hydraulic properties (e.g., failure date) and chemical properties unchanged per Base Case	N/A	Hydraulic properties of failed grout at time 0 - chemical properties unchanged. High flow throughout grout causes grout to impart reducing capacity onto CZ.
CZ (Solubility controlled)	CZ initial solubility limits are those associated with Base Case	N/A	Solubility controls are removed for Tc-99 and Ra-226, and set to very high levels for remaining radionuclides.
Waste Tank Liner [a]	Later liner failure (based on grouted CO_2 diffusion coefficient of 1E-06)	Early liner failure (based on grouted CO_2 diffusion coefficient of 1E-04)	No Liner at time 0
Waste Tank Concrete [c] (K_d controlled)	Hydraulic properties (e.g., failure date) and chemical properties unchanged per Base Case.	N/A	Hydraulic properties of failed concrete - initial chemical properties unchanged. Chemical transitions are a function of the "failed" flow fields.
Natural Barrier [b] (K_d controlled)	Native soil K_d values are set equal to Base Case values	N/A	Native soil K_d values are as defined in Table 5.6-33.

a The liner barrier analysis does not apply to waste tanks with initially failed waste tank liners (e.g., Tanks 12 and 15 for this analysis).

b The natural barrier is equal to the unsaturated native soil zone below the basemat of the waste tanks, therefore, this analysis only applies to the unsaturated waste tanks, which include Type's IV and III/IIIA tanks.

c Includes basemat, wall, and roof cementitious materials.

N/A = Not applicable

Table 5.6-33: Barrier Analyses Configuration Case Summary by Material Zone

Configuration		PORFLOW Base Case	Fully Degraded	Waste Tank Liner[a]			CZ		Natural Barrier		Closure Cap
Barrier Case		N/A	2	3	4	5	6	7	8	9	N/A
Material Zone	Closure Cap	N	F	F	F	N	F	N	N	F	F
	Grout	N	F	F	F	N	F	N	N	F	N
	CZ	N	N	N	N	N	F	F	N	N	N
	Liner	N	F	N	P	P	F	N	N	F	N
	Concrete (basemat, wall, roof)	N	F	F	F	N	F	N	N	F	N
	Natural Barrier	N	F	F	F	N	F	N	F	N	N

a For Tank 12 and 15, liner is failed at time zero, therefore partial liner barrier analysis and liner barrier analysis are not applicable.

N = Nominal
P = Partially degraded
F = Fully degraded
N/A = Not applicable

Chemical transition times for the different barrier configuration cases are discussed and presented in Section 5.6.6.2. Time histories displaying flux below the waste tanks for each of the barrier configuration cases are included in Appendix I. The results of the barrier analyses are presented in Section 5.6.6.3. To aid the evaluation of the barriers, the flux results from Appendix I are re-plotted for the radionuclides and waste tanks of interest such that only the run configurations pertaining to the specific barrier are included. These barrier specific plots are included in Appendix N, however, only a selection of the plots are included in Section 5.6.6.3.

5.6.6.2 Barrier Analysis Transition Times

The release of contaminants from the CZ is controlled by solubility, which is affected by the chemistry of the pore fluid that travels through the CZ as described in Section 4.2.3. The pore fluid in the CZ enters into the CZ from the grout above the CZ. The contaminants that are released from the CZ travel through the waste tank basemat, which delays their travel based on the distribution coefficient value, which is also dependent on the chemistry of the pore fluid that travels through the basemat. Therefore, the various barrier cases will influence the times that the cementitious barriers (grout, CZ, annulus, and waste tank basemat, etc.) transition from one chemical state to another. The transition times also vary by waste tank type.

In addition to the chemical transition times, the liner failure time and the hydraulic degradation of the waste tank components are also important to transport and the timing of radionuclide releases from the waste tanks. A selection of the transition times for the waste tanks are included in Figures 5.6-73 through 5.6-89, and illustrate the chemical transition times, the hydraulic degradation transition times, and the liner failure times for all barrier

cases. Transitions for the annulus, waste tank grout, and CZ for Type II tanks, Type II tanks with initially degraded liner, and Type IV tanks are provided for reference for the discussion in Section 5.6.6.3. Note the chemical and hydraulic degradation of the other cementitious components (roof, wall, and basemat) can be important to radionuclide transport, however the transition times are not presented here because in general, their transitions are secondary to the transitions in the annulus (Type II tanks), waste tank grout, and CZ.

Figure 5.6-73: Waste Tank Grout Chemical Transitions - Type II Tank

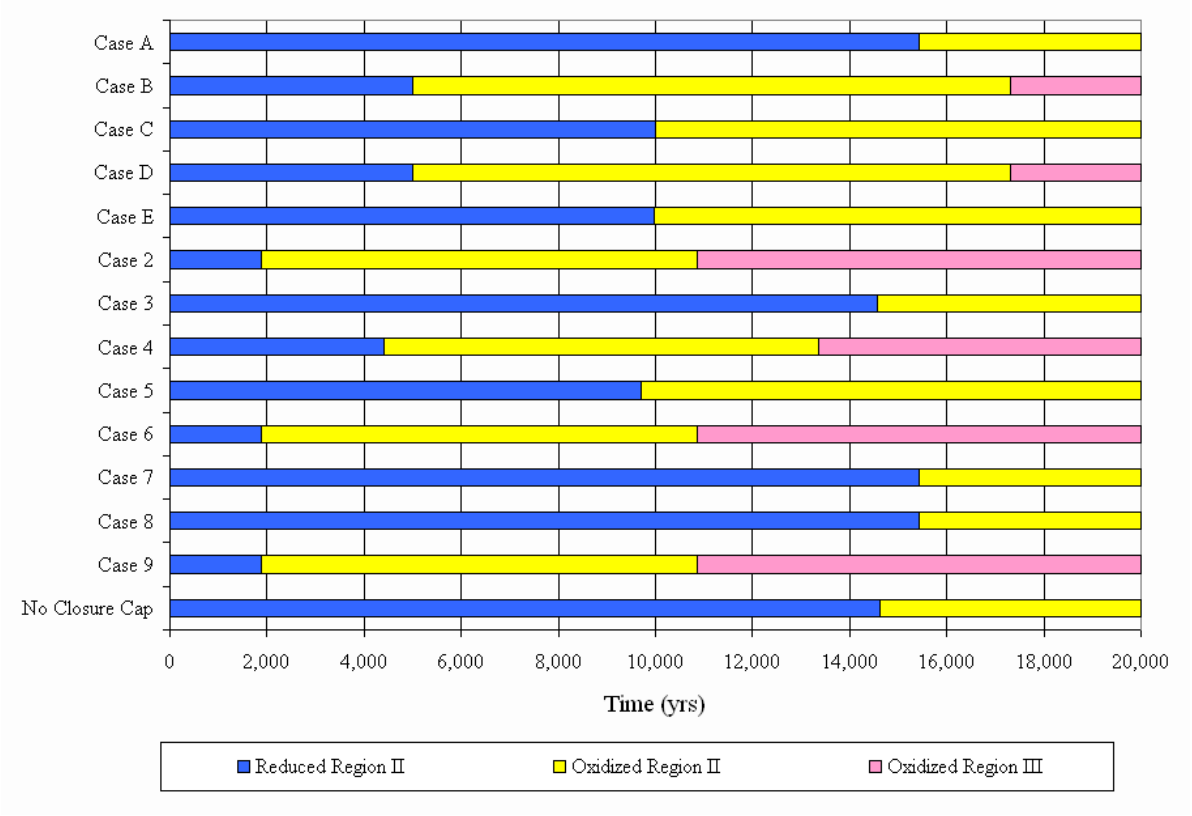

Figure 5.6-74: CZ Chemical Transitions - Type II Tank

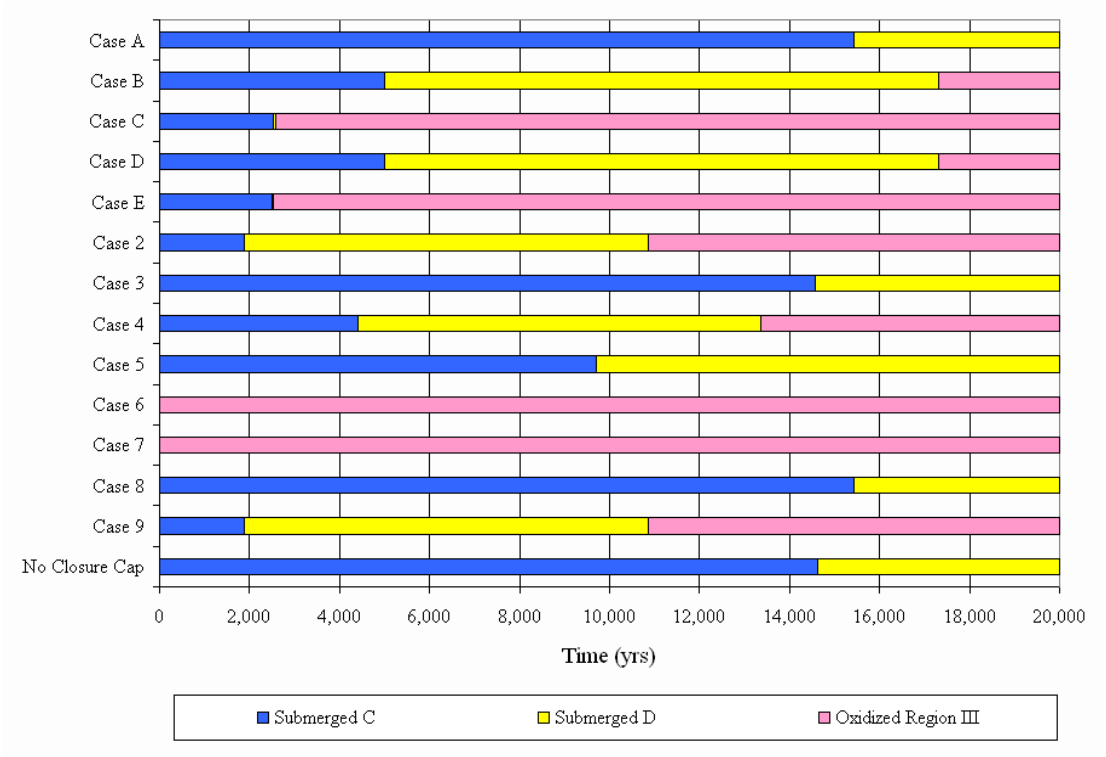

Figure 5.6-75: Annulus Chemical Transitions - Type II Tank

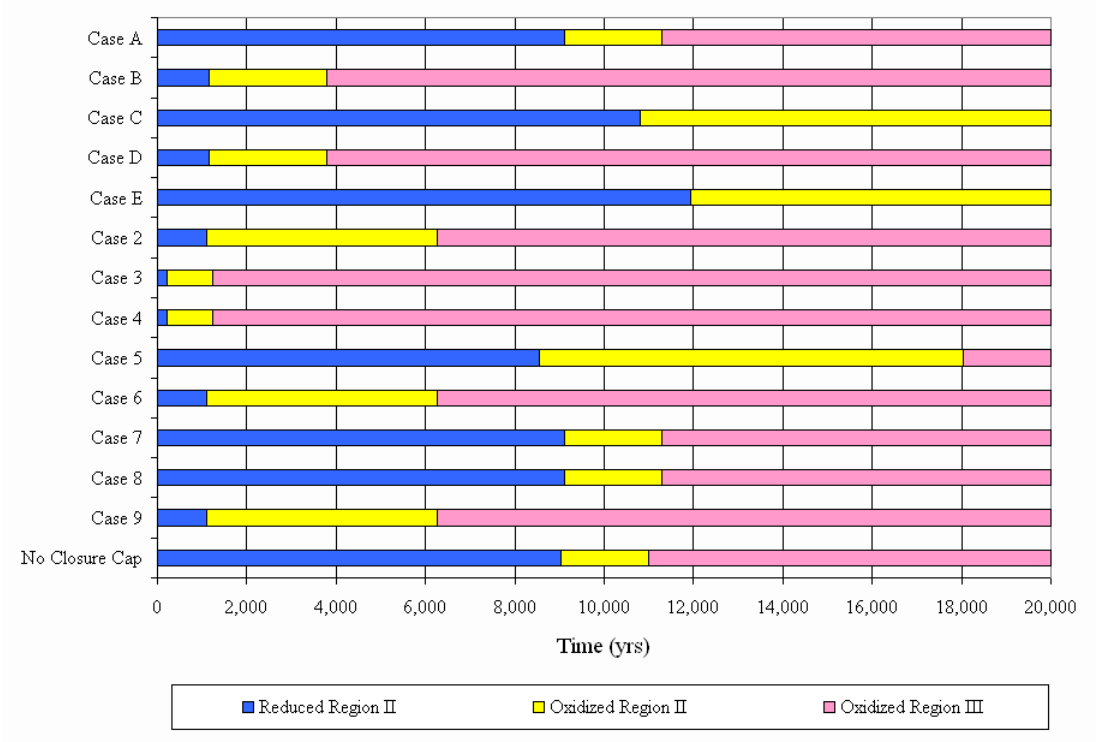

Figure 5.6-76: Waste Tank Grout and Annulus Hydraulic Degradation - Type II Tank

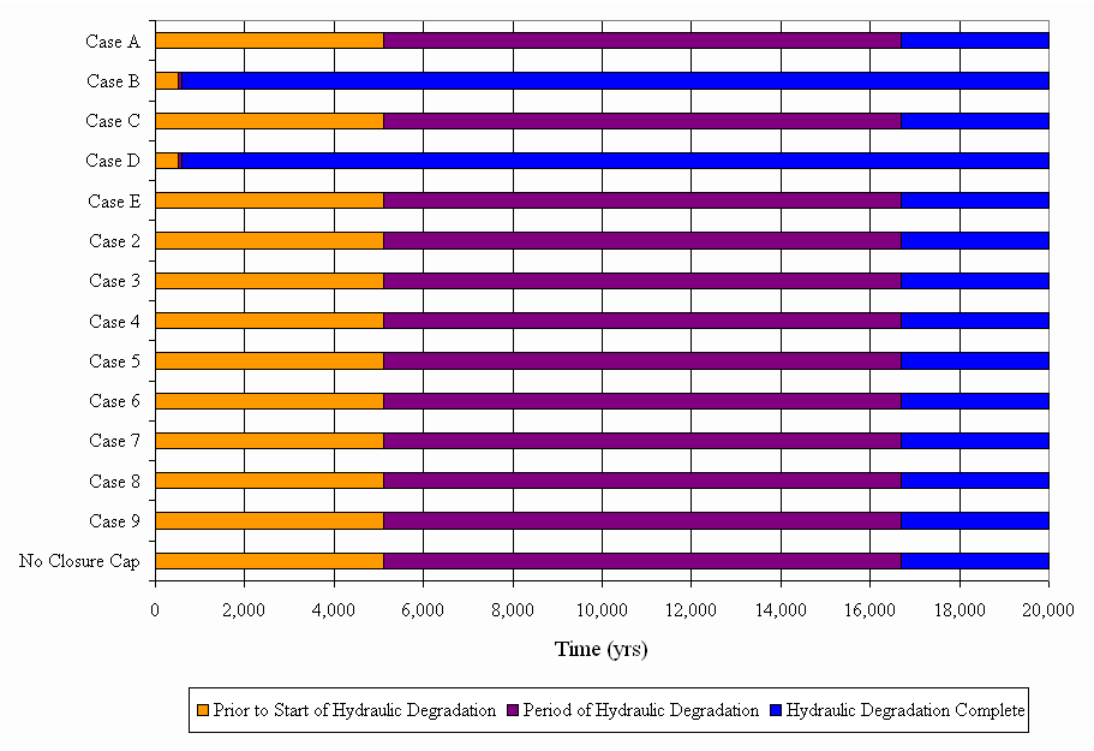

Figure 5.6-77: CZ Hydraulic Degradation - Type II Tank

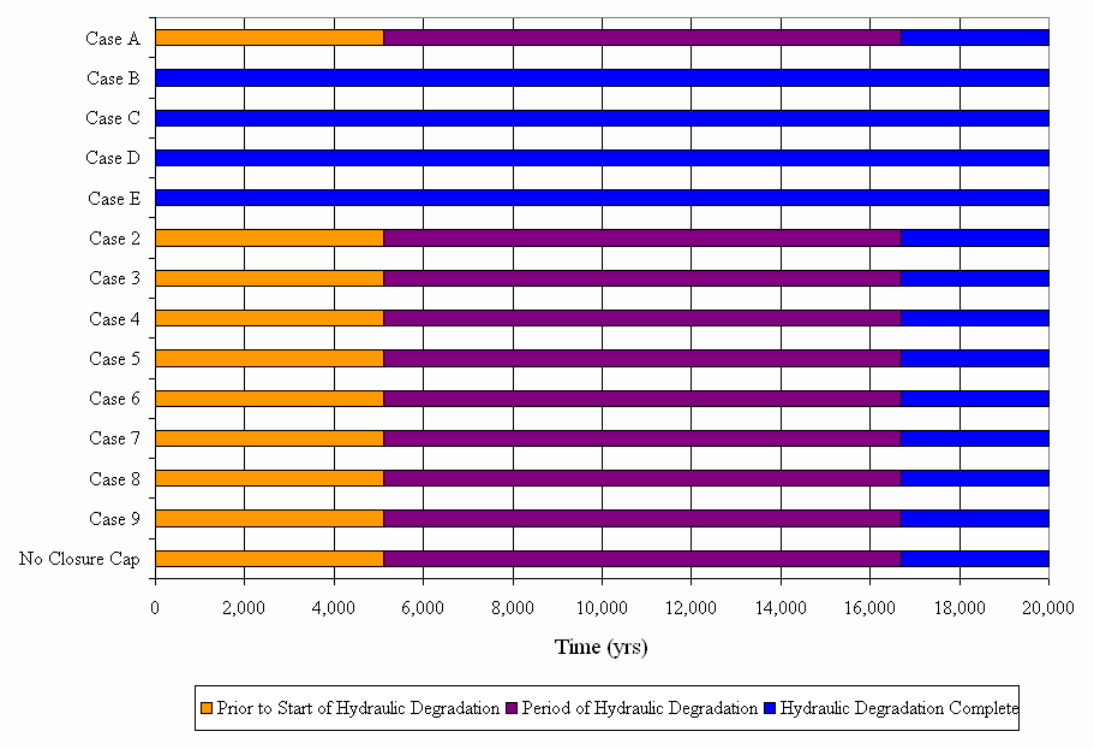

Figure 5.6-78: Waste Tank Liner Failure - Type II Tank

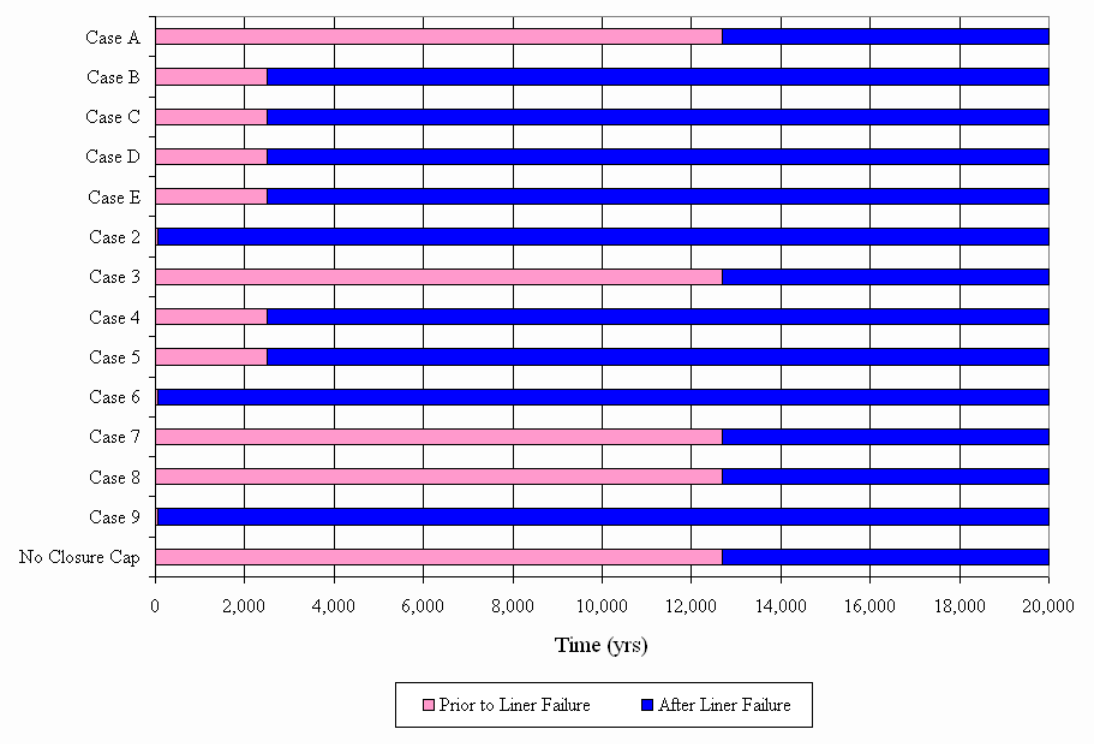

Figure 5.6-79: Waste Tank Grout (No Liner) Chemical Transitions - Type II Tank

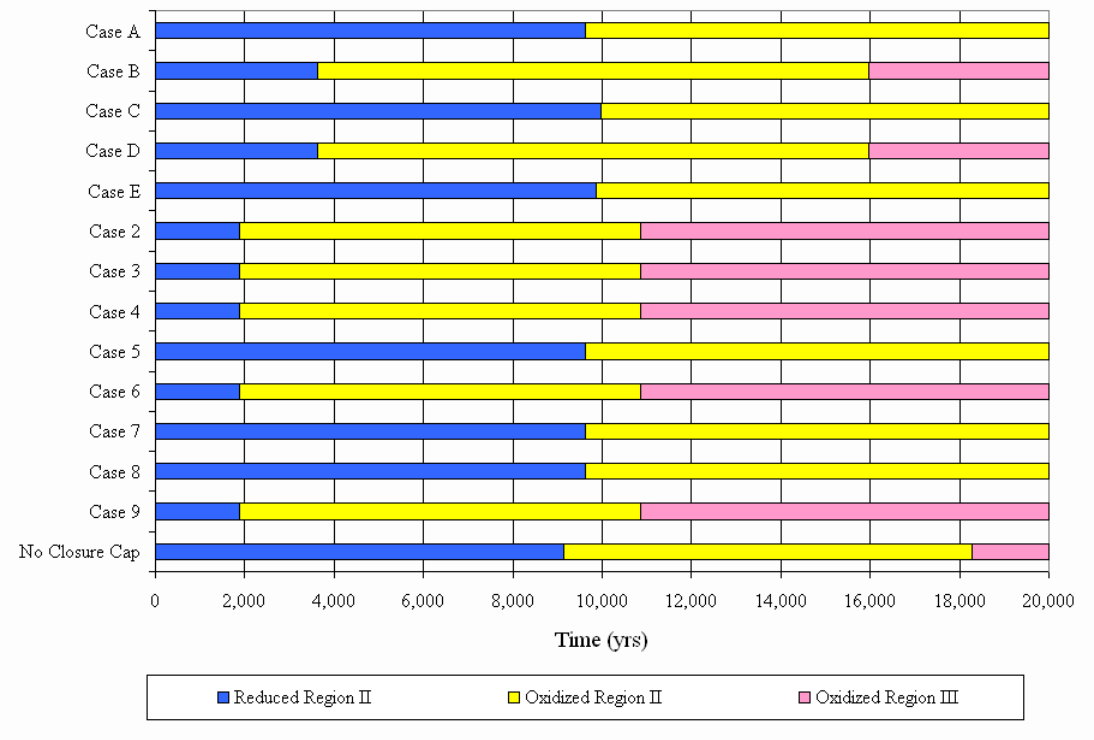

Figure 5.6-80: CZ (No Liner) Chemical Transitions - Type II Tank

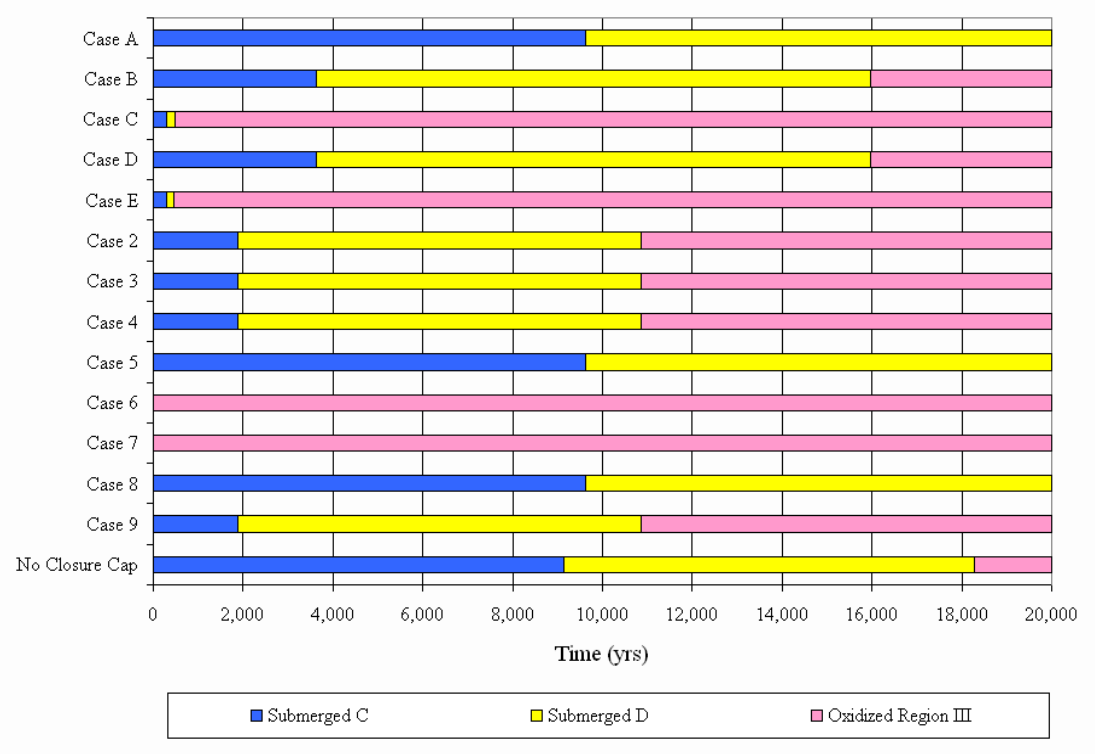

Figure 5.6-81: Annulus (No Liner) Chemical Transitions - Type II Tank

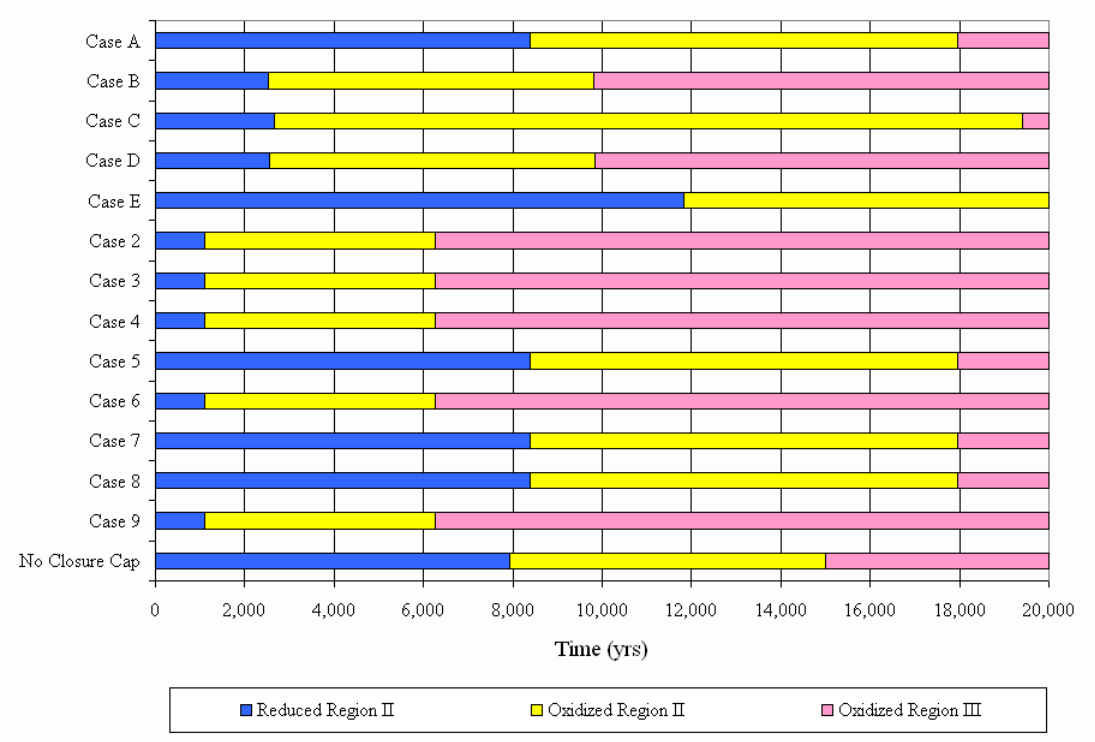

Figure 5.6-82: Waste Tank Grout (No Liner) Hydraulic Degradation - Type II Tank

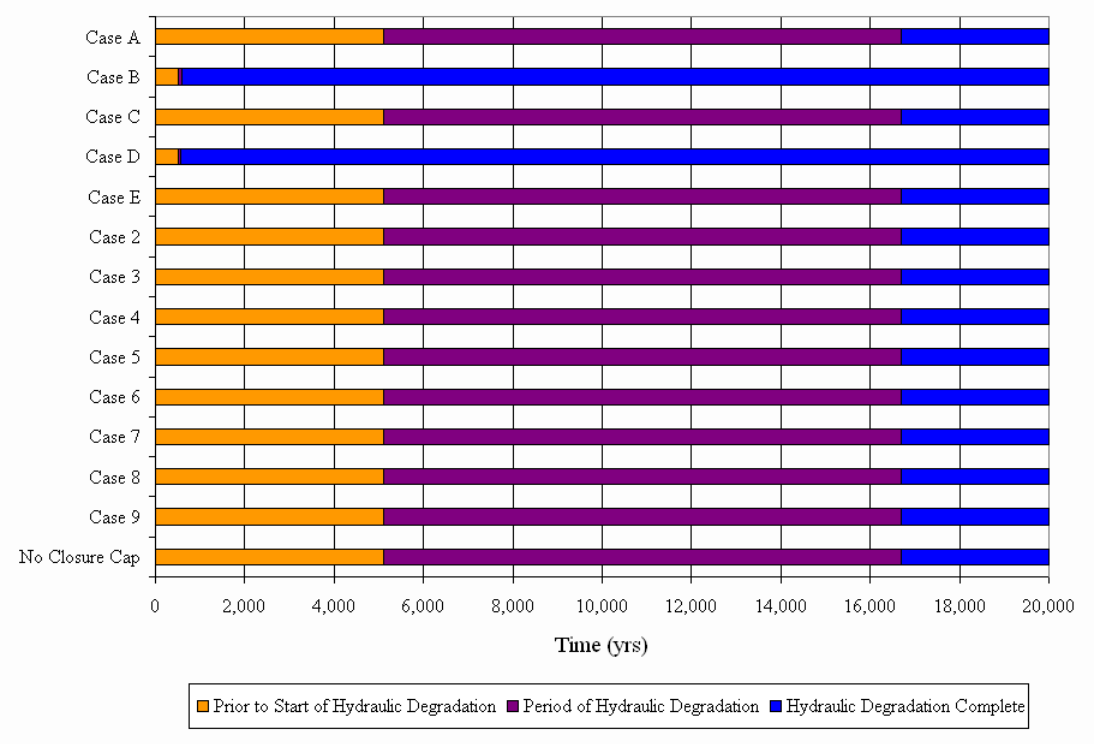

Figure 5.6-83: CZ (No Liner) Hydraulic Degradation - Type II Tank

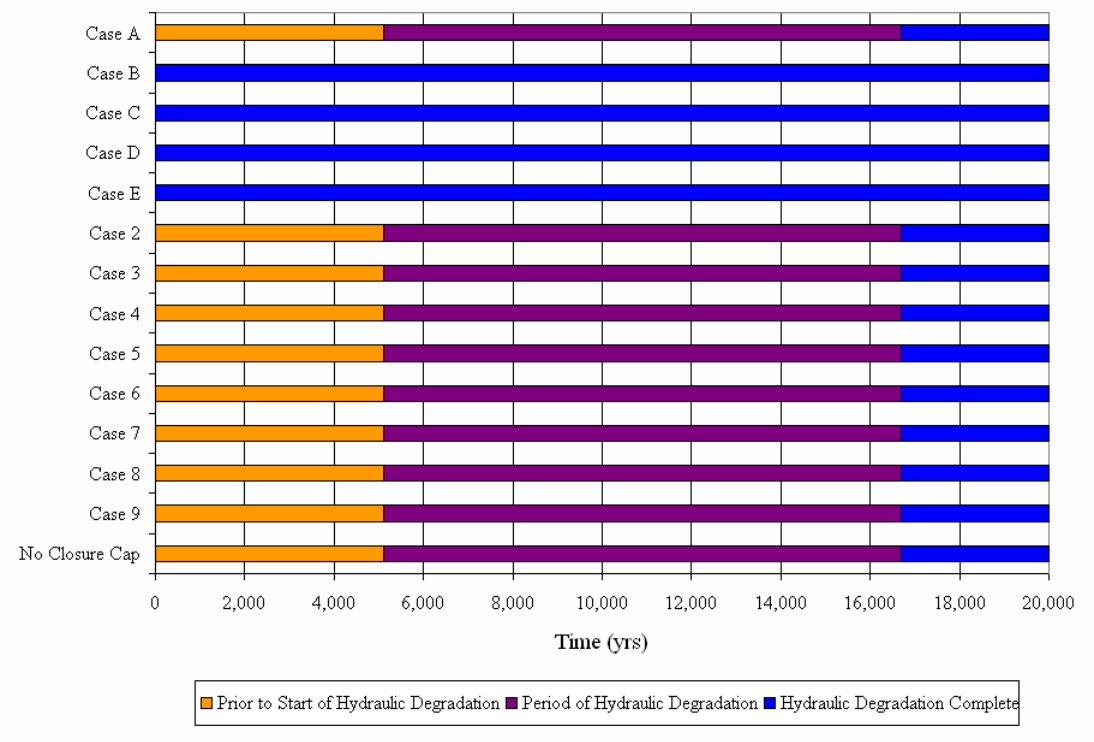

Figure 5.6-84: Annulus (No Liner) Hydraulic Degradation - Type II Tank

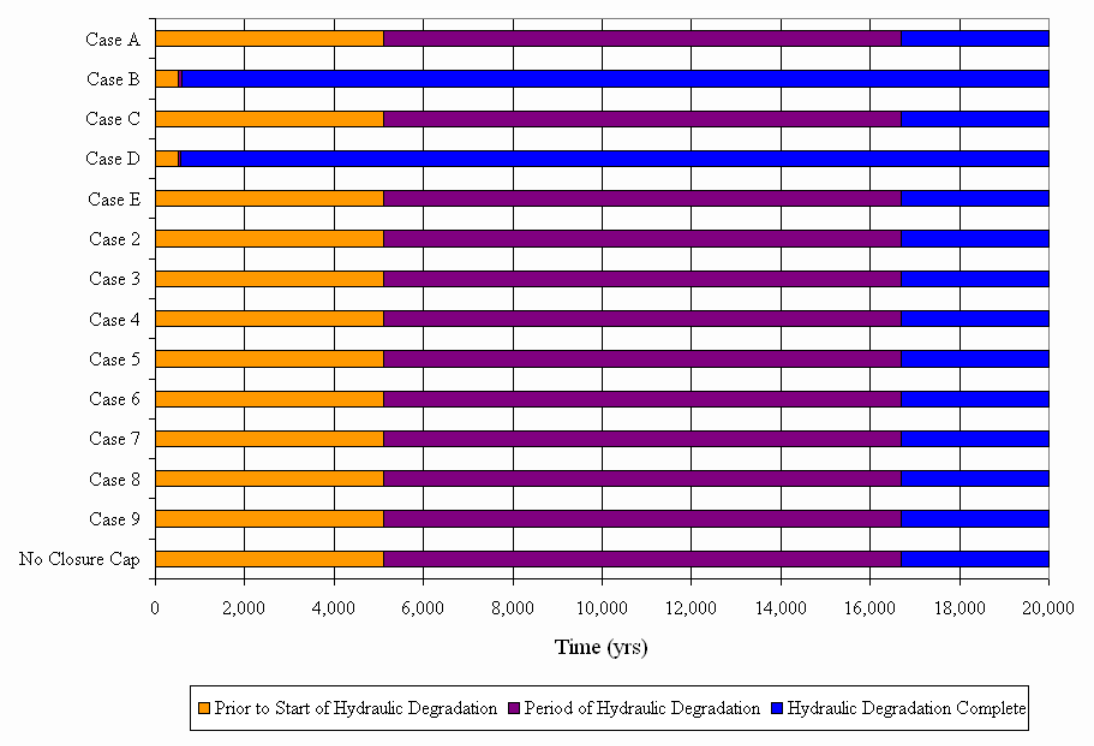

Figure 5.6-85: Waste Tank Grout Chemical Transitions - Type IV Tank

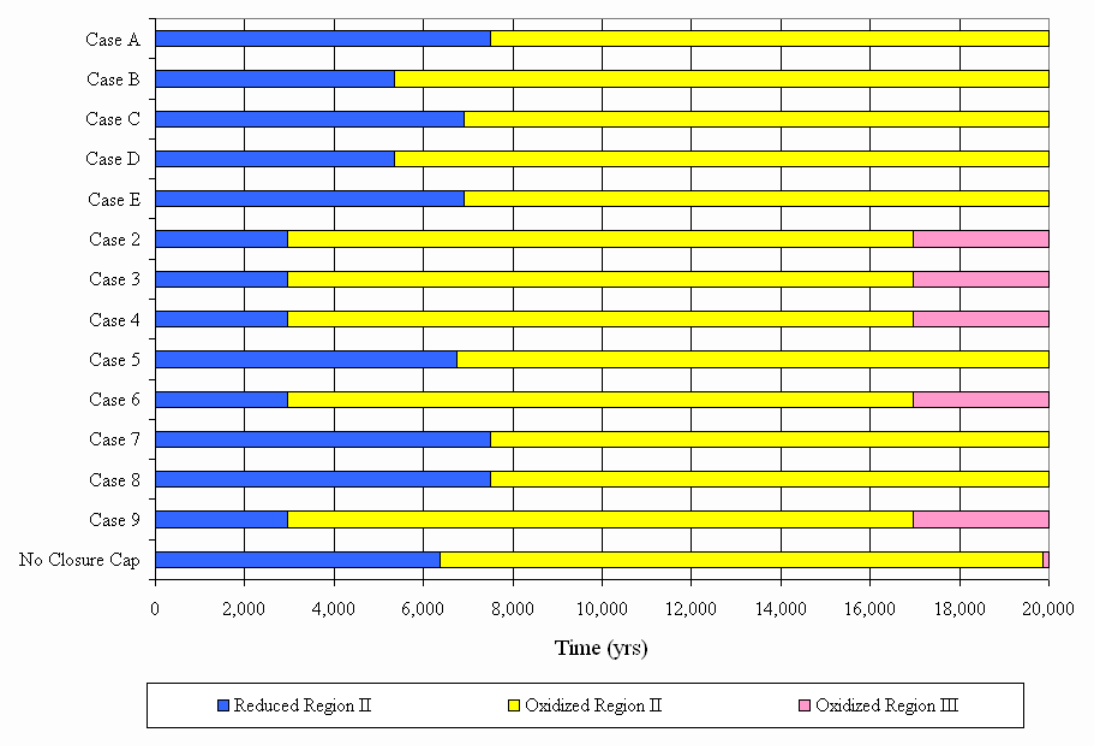

Figure 5.6-86: CZ Chemical Transitions - Type IV Tank

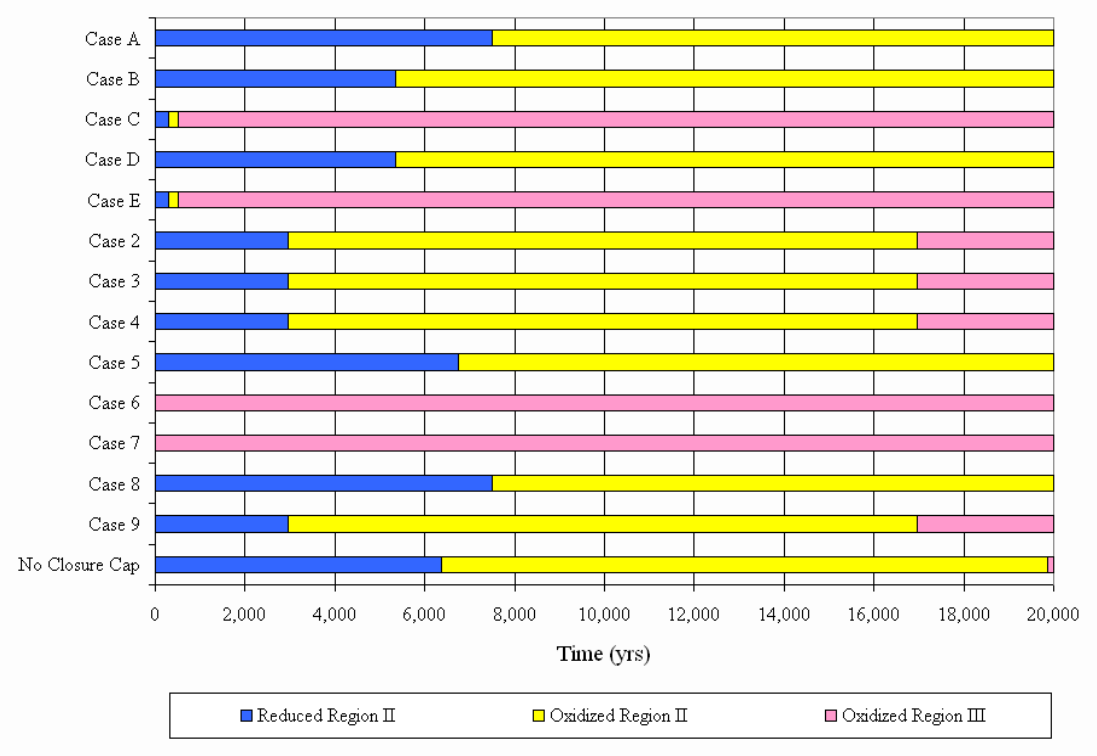

Figure 5.6-87: Waste Tank Grout Hydraulic Degradation - Type IV Tank

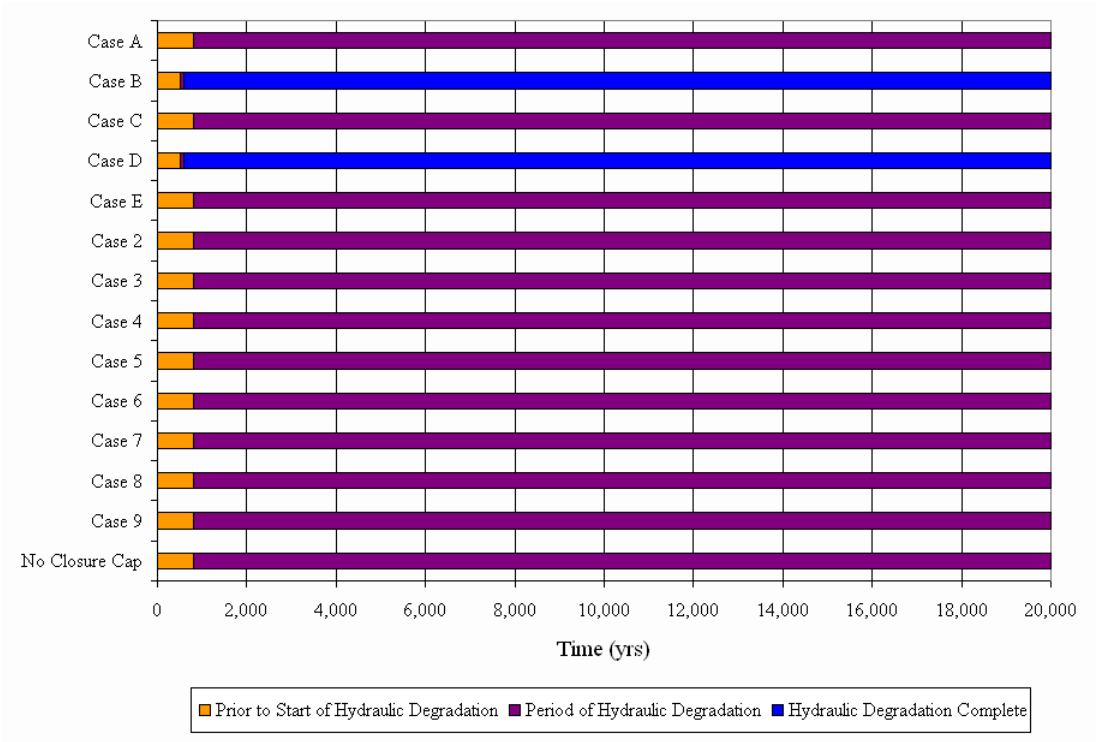

Figure 5.6-88: CZ Hydraulic Degradation - Type IV Tank

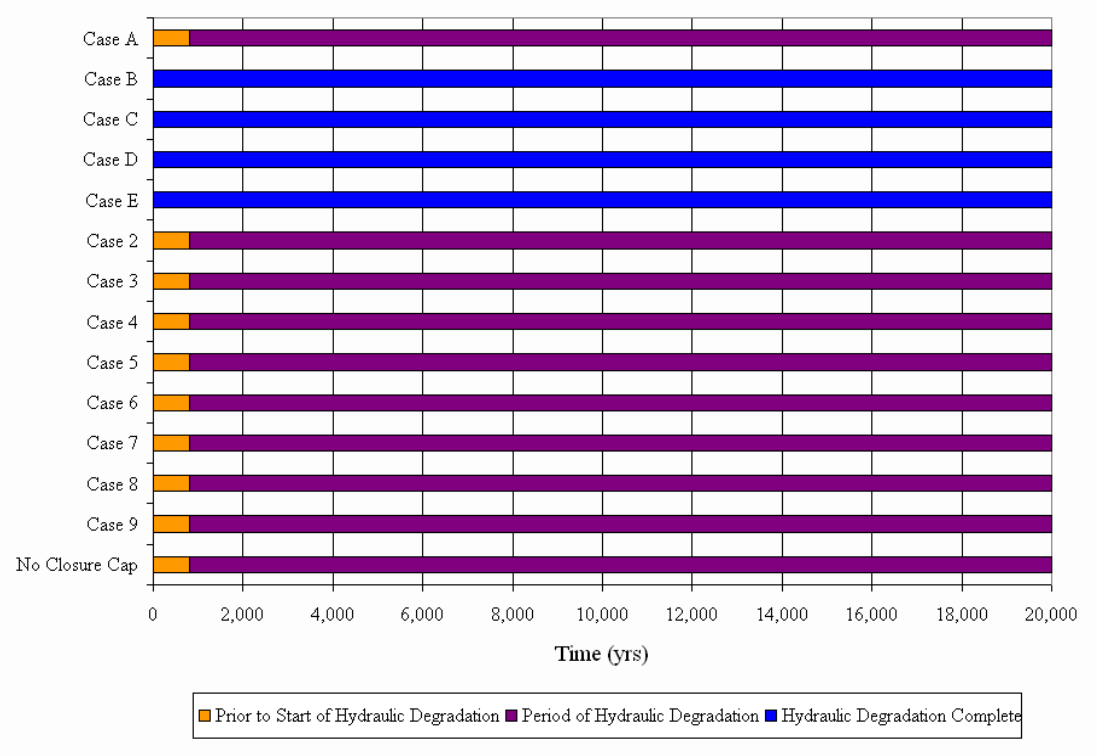

Figure 5.6-89: Waste Tank Liner Failure - Type IV Tank

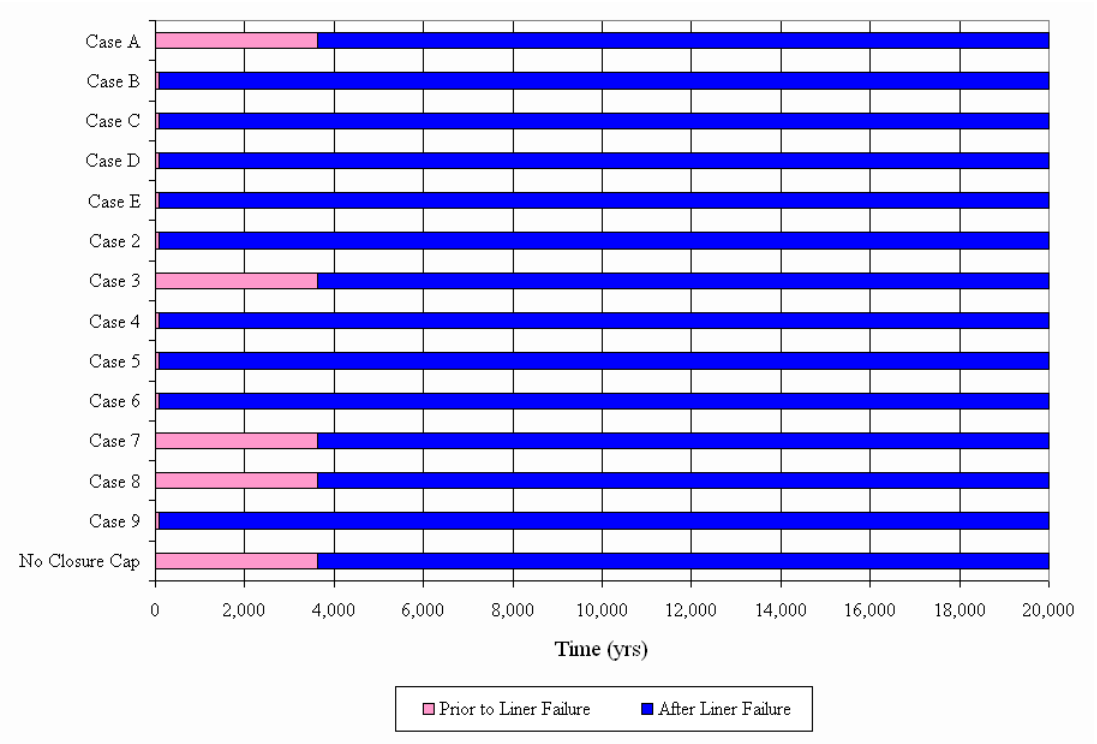

5.6.6.3 Summary of Results by Barrier

This section compares different barrier failure run configurations and they affect the timing and magnitude of peak flux, below the waste tanks, during the 20,000-year simulation period. The simulations were run for 20,000 years in order to evaluate processes that can take thousands of years. This section also considers each barrier's ability to prevent or retard radionuclide migration, by considering the behavior of the radionuclide through time under failed and nominal barrier conditions. Radionuclide flux below the waste tanks (e.g., at the water table for unsaturated waste tanks and exiting the basemat for submerged waste tanks) from PORFLOW for the no closure cap barrier are provided in Appendix H.1 and Appendix I provides all other barrier run configurations, including the Base Case. The following barriers are considered here, the closure cap, waste tank grout, CZ, waste tank liner, and the natural barrier. The faster-moving radionuclides, Tc-99, Ra-226, and I-129 are graphed on a single plot for each barrier separately from the slower-moving radionuclides, Np-237 and Pu-239. Note that flux values for the slower radionuclides, Np-237 and Pu-239, have the tendency to be very small values, therefore the y-axis for these figures vary accordingly from figure to figure. Every waste tank from Table 5.6-30 is plotted for each barrier and is provided in Appendix N. A number of the graphs from Appendix N, illustrating the impact on the release for selected radionuclides, are provided in the discussion that follows.

5.6.6.3.1 Closure Cap

Closure cap barrier capability is estimated by comparing the timing and magnitude of peak fluxes and the time history curves for the Base Case (PORFLOW Case A) and the no closure cap (No Cap) sensitivity case. The two cases were simulated using the deterministic GoldSim model. Using the HELP model, background infiltration was estimated to be 16.45 in/yr. [WSRC-STI-2007-00184 Figure 29 and Table 31] This is analogous to modeling a "soils only" closure cap with no barrier, drainage, or erosion control layers. The impact of removing the engineered closure cap barrier is determined by comparing the timing and magnitude of peak fluxes for the No Cap sensitivity case with the Base Case. This analysis evaluates fluxes out of the waste tanks to understand the barrier's impact on the transport behavior of specific radionuclides. However, Section 5.6.7 evaluates the importance of this barrier on the total projected dose to the MOP. Refer to Section 5.6.7 for further details on the closure cap impact on dose.

Figures 5.6-90 through 5.6-92 compare Base Case fluxes with the No Cap fluxes from Tank 13 (submerged Type II tank with initially intact liner), Tank 15 (submerged Type II tank with initially degraded liner), and Tank 21 (unsaturated Type IV tank), respectively. The figures illustrate the impact of the closure cap on the fast-moving radionuclides, Tc-99, Ra-226, and I-129. All three figures indicate that inclusion of the closure cap (Base Case) provides a small delay and reduction in radionuclide releases to the saturated zone. Removal of the closure cap in the No Cap sensitivity case allows for increased flow to the vadose zone leading to an increase in the mass released from the CZ. The increase in flow also results in slightly earlier chemical transition times in the different waste tank components. The releases from the annulus, sand pads (Type II tanks only), waste tank grout, and CZ are influenced the most by the earlier transition times. The waste tank grout transition time coincides with the CZ transition times.

Figure 5.6-90: Fast-Moving Radionuclide Fluxes Tank 13 (No Cap)

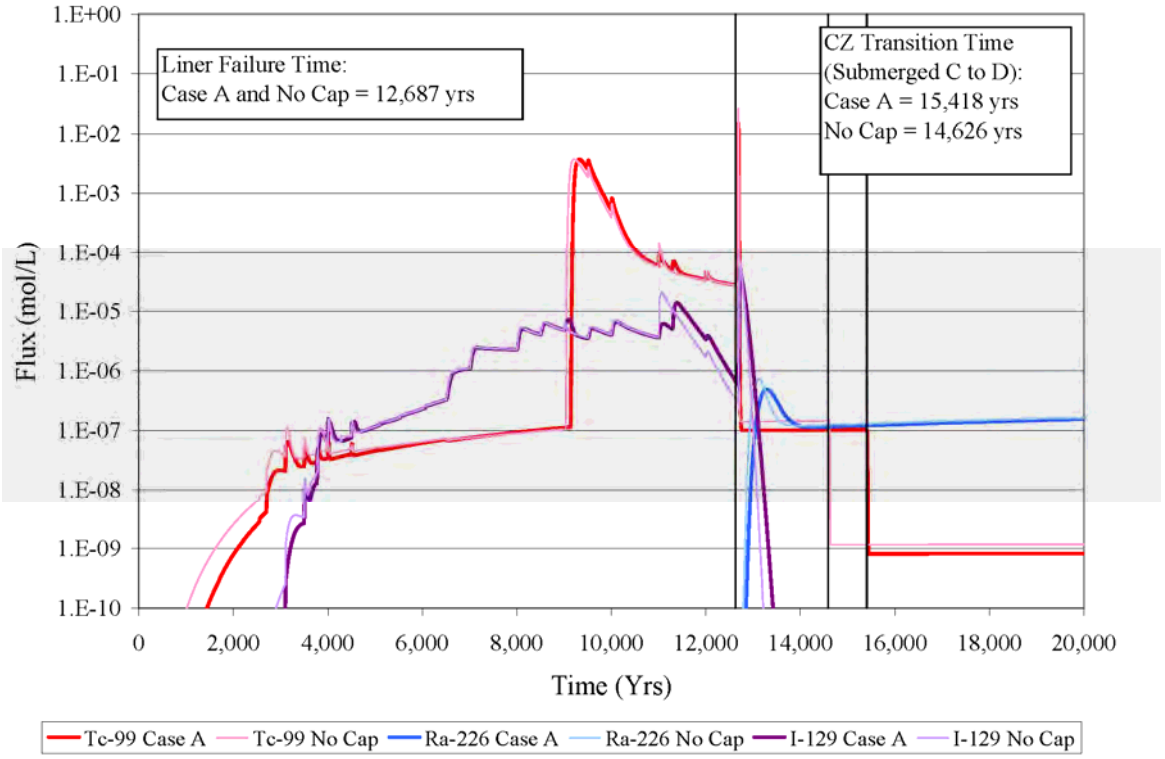

Figure 5.6-91: Fast-Moving Radionuclide Fluxes Tank 15 (No Cap)

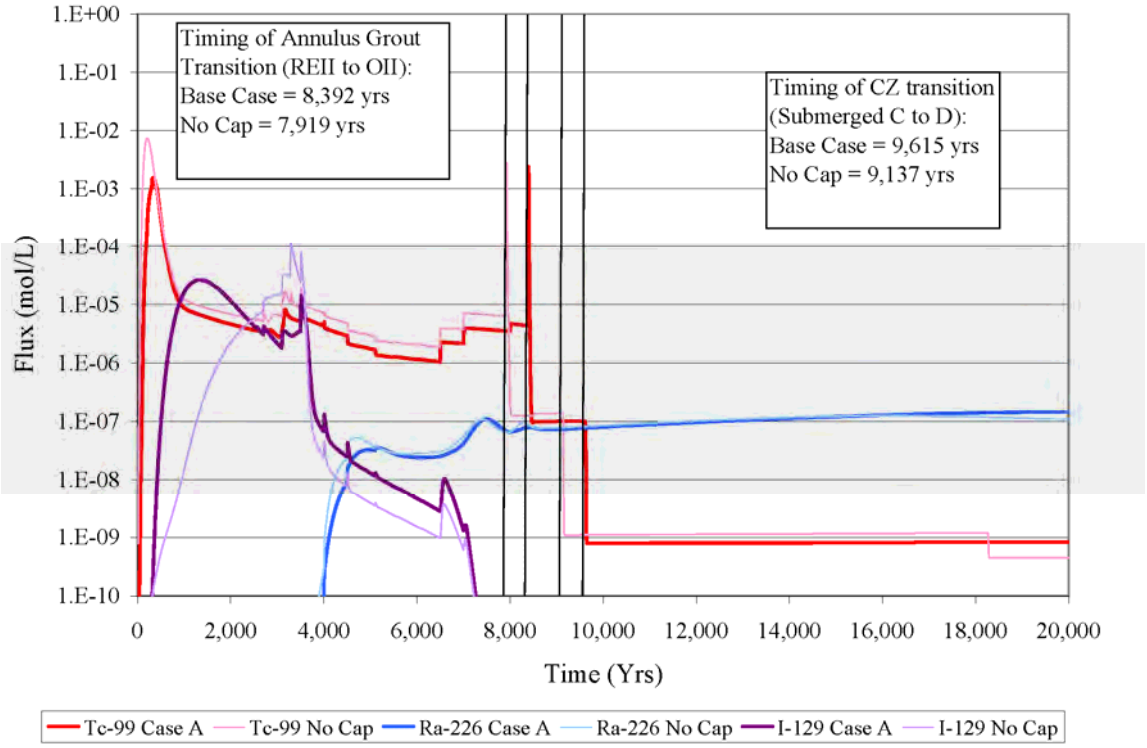

Figure 5.6-92: Fast-Moving Radionuclide Fluxes Tank 21 (No Cap)

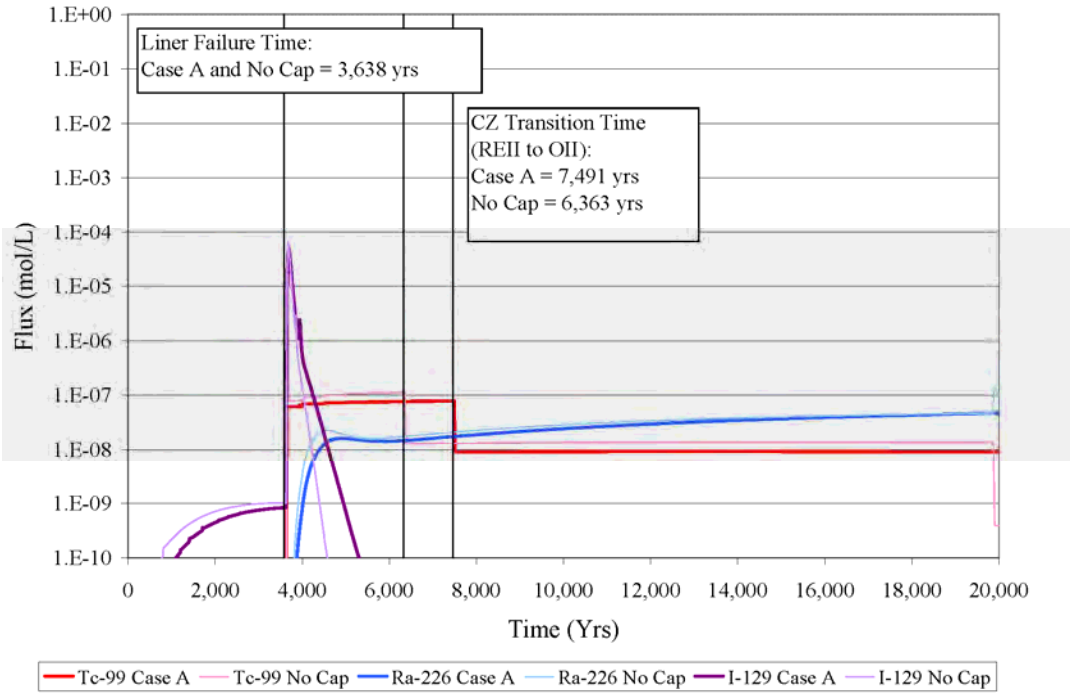

Comparison of the timing and magnitude of the peak fluxes for each radionuclide from the three waste tanks presented in Figures 5.6-90 through 5.6-92 indicate that for Tc-99, the closure cap has the most impact on releases from Tank 15, the submerged Type II tank with an initially degraded liner (Figure 5.6-91). The Tc-99 peak flux from this waste tank occurs approximately 200 years earlier than in the Base Case and is less than an order of magnitude greater. In contrast, the I-129 peak flux is delayed from Tank 15 in the No Cap sensitivity case compared to the Base Case, while Ra-226 behaves similarly in all waste tanks types (e.g., peak Ra-226 flux occurs earlier and is higher in magnitude in the No Cap sensitivity case).

The closure cap is moderately effective as a barrier for those mobile radionuclides not greatly influenced by sorption onto oxidized cementitious material (e.g., Tc-99, Ra-226, and I-129). The impact of the closure cap is greater for the slow-moving radionuclides, Pu-239 and Np-237, however because these radionuclides take time to move through the system, the impact is only relevant later (> 5,000 yrs). Plutonium and neptunium move slowly through the system due to high distribution coefficient values in cementitious materials. Figure 5.6-93 and Figure 5.6-94 compare fluxes from Tank 15 and Tank 21, respectively, for the Base Case to the No Cap sensitivity case. Tank 13 tank fluxes for Np-237 and Pu-239 are so low that they are not plotted here. The increased flow in the No Cap sensitivity case causes earlier and higher magnitude fluxes of Pu-239 and Np-237 out of the waste tanks. As the cements become more oxidizing with time, more of the highly sorbed Pu-239 and Np-237 are released in the No Cap sensitivity case. While the less sorptive radionuclides show only a moderate impact from the closure cap, Pu-239 and Np-237 show about an order of magnitude increase in flux or more without the closure cap.

Figure 5.6-93: Slow-Moving Radionuclide Fluxes Tank 15 (No Cap)

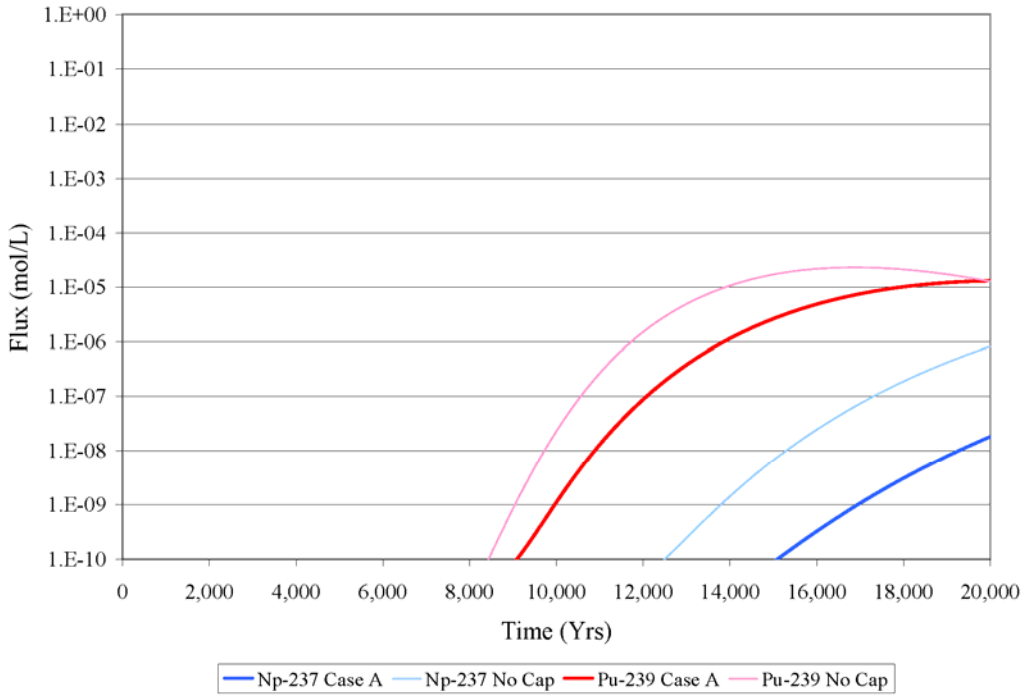

Figure 5.6-94: Slow-Moving Radionuclide Fluxes Tank 21 (No Cap)

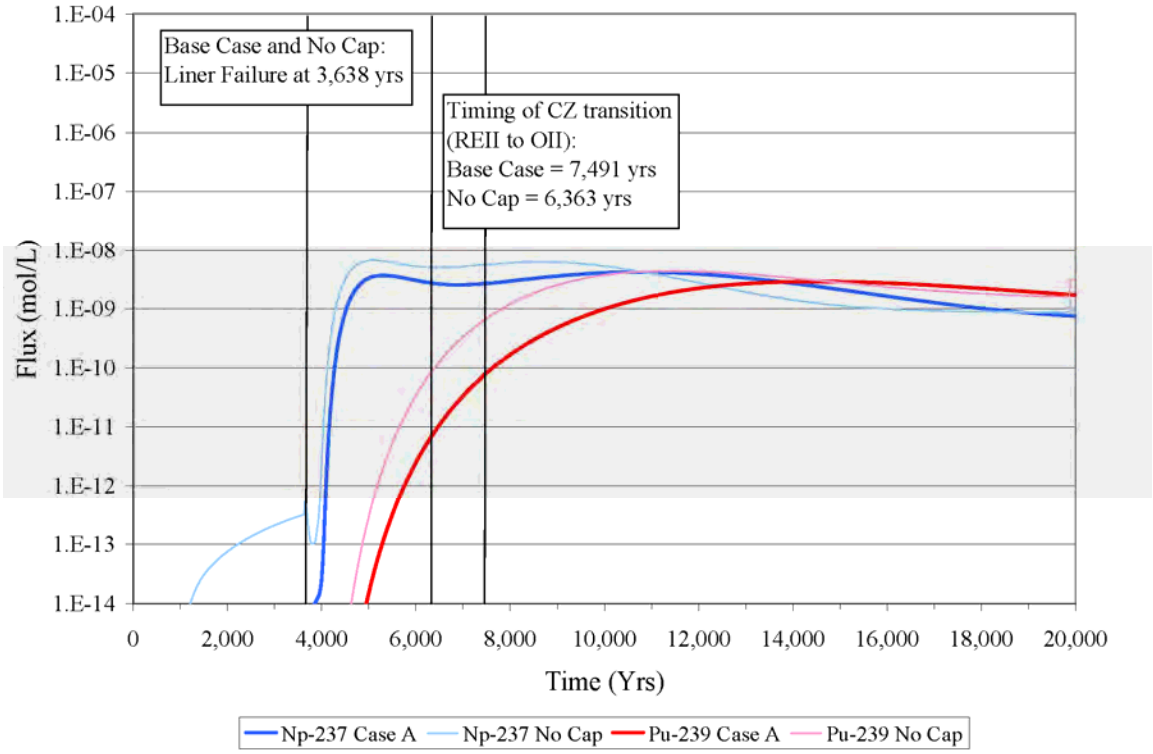

5.6.6.3.2 Waste Tank Grout

Using the alternative scenario settings for Cases B and C described in Section 4.4.2 and summarized in Table 4.4-1 the deterministic GoldSim model was simulated and the radionuclide fluxes from selected waste tanks are evaluated to assess the impact of the grout as a barrier to radionuclide migration. Both Case B and C were modeled with a fast flow path through the grout and early failure of the waste tank liners based on the times presented in Table 4.2-36. Case B differs from Case C in that the waste tank grout, annulus grout, and other cementitious barriers in the former case hydraulically failed at year 501, while Case C gradually fails these barriers (according to Table 4.2-34). Additionally, the full reducing capacity of the grout is imparted on the CZ in Case B, as would be the case with waste tank grout that is hydraulically degraded. In contrast, because the grout retains its integrity for a long time, Case C is modeled as having the reducing capacity of the CZ only. The dominant flow for Case C is through the fast flow channel on the edge of the grout, bypassing the influence of this reducing zone. Comparing these cases will provide insight to the effectiveness of the intact waste tank grout on radionuclide fluxes.

Figures 5.6-95 through 5.6-97 compare Case B fluxes with Case C fluxes from Tank 13 (submerged Type II tank with initially intact liner), Tank 15 (submerged Type II tank with initially degraded liner), and Tank 21 (unsaturated Type IV tank), respectively. The figures illustrate the impact of 1) the grout reducing capacity and 2) the grout integrity on the migration of the fast-moving radionuclides, Tc-99, Ra-226, and I-129. Relevant transition times for the two cases are compared by waste tank in Table 5.6-34, and are required to interpret the release behavior in Figures 5.6-95 through 5.6-97.

Figure 5.6-95: Fast-Moving Radionuclide Fluxes Tank 13 (Grout)

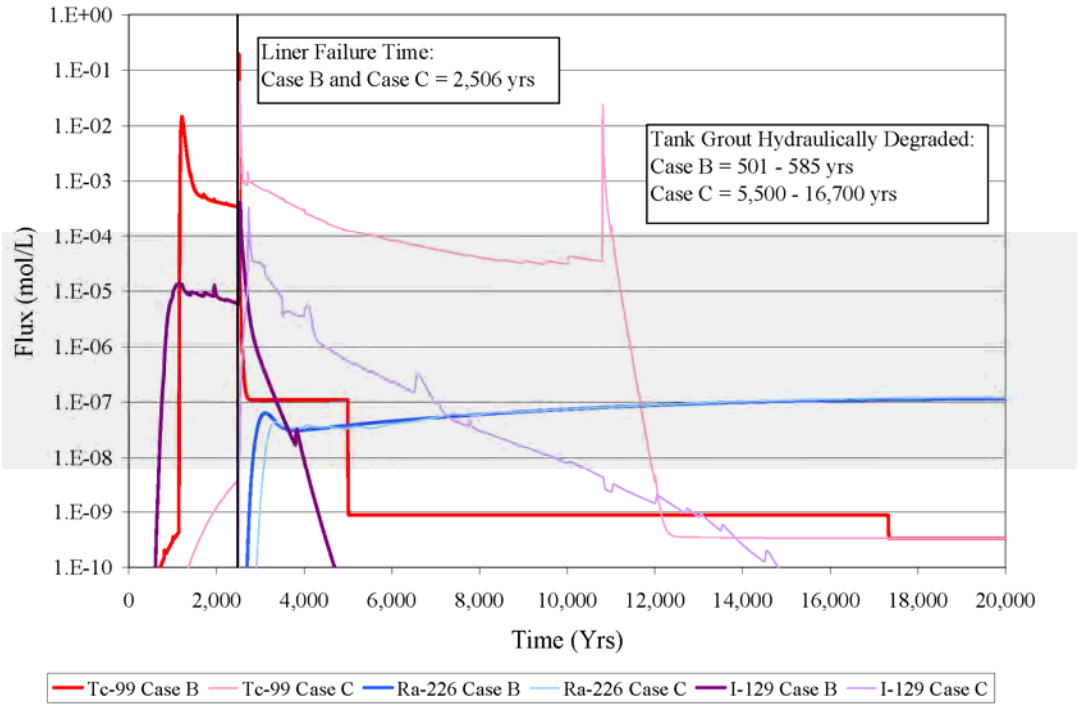

Figure 5.6-96: Fast-Moving Radionuclide Fluxes Tank 15 (Grout)

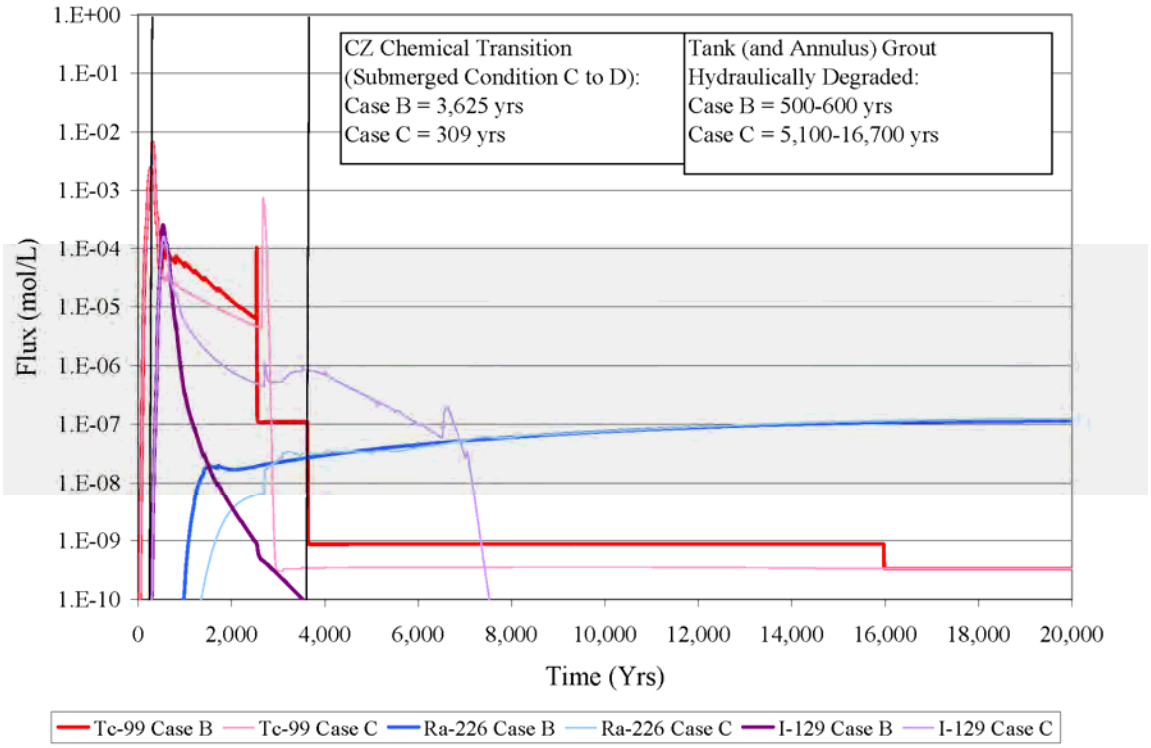

Figure 5.6-97: Fast-Moving Radionuclide Fluxes Tank 21 (Grout)

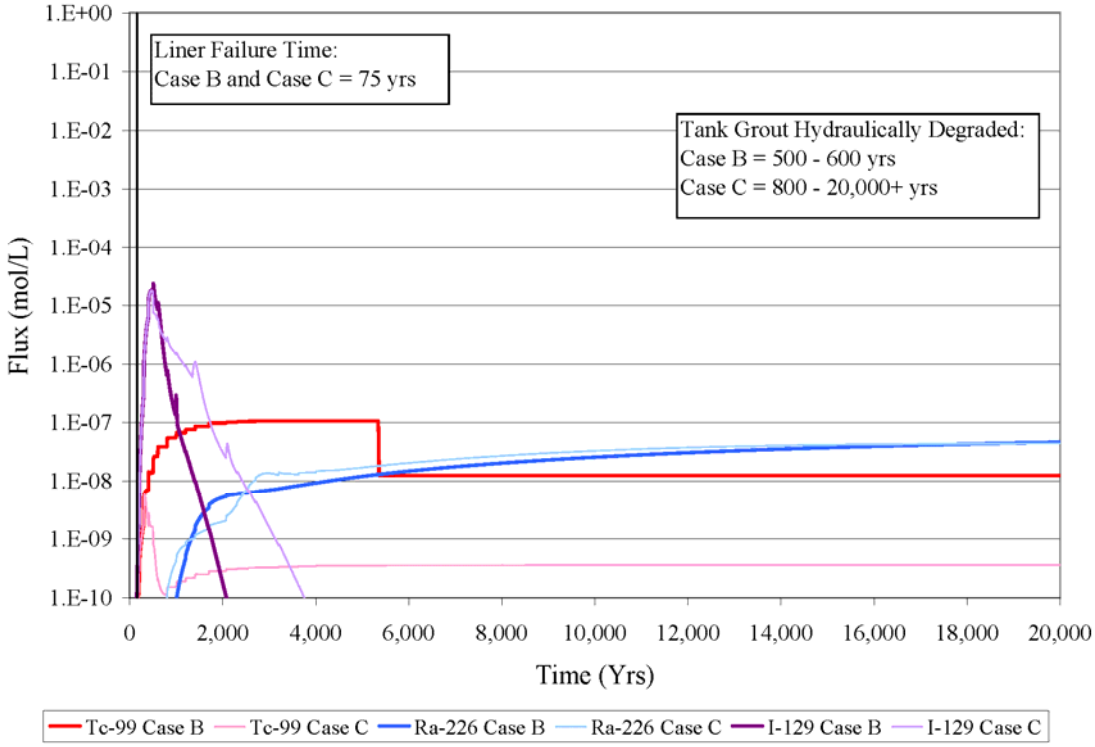

Table 5.6-34: Transition Times by Waste Tank - Case B and C

	Year of Occurrence	
Type of Transition	**Case B**	**Case C**
Type II Tank - Tank 13		
Liner fails hydraulically	2,506	2,506
Basemat (OII to OIII)	585	2,719
Concrete degrades hydraulically	500-585	2,550-5,100
Waste tank grout degrades hydraulically	500-585	5,100-16,700
Annulus grout (REII to OII)	1,143	10,805
Waste tank grout (REII to OII)	4,990	9,993
CZ (Submerged C to Submerged D)	4,990	2,518
CZ (Submerged D to OIII)	17,323	2,575
Type II Tank (No Liner) - Tank 15		
Liner fails hydraulically	N/A	N/A
Basemat (OII to OIII)	89	89
Concrete degrades hydraulically	500	2,550-5,100
Waste tank grout degrades hydraulically	500-600	5,100-16,700
Annulus grout (REII to OII)	2,530	2,657
Waste tank grout (REII to OII)	3,625	9,965
CZ (Submerged C to Submerged D)	3,625	309
CZ (Submerged D to OIII)	15,969	493
Type IV Tank - Tank 21		
Liner fails hydraulically	75	75
Basemat (OII to OIII)	988	1,350
Concrete degrades hydraulically	500-600	400-800
Waste tank grout degrades hydraulically	500-600	800-20,000+
Annulus grout (REII to OII)	NA	NA
Waste tank grout (REII to OII)	5,346	6,896
CZ (REII to OII)	5,346	302
CZ (OII to OIII)	20,000+	501

Note: Information extracted from Tables 4.4-4, 4.4-5 and 4.4-9
REII = Reducing Region II
OII = Oxidized Region II
OIII = Oxidized Region III
N/A = Not Applicable

Releases of the fast-moving radionuclides (e.g., Tc-99, Ra-226, and I-129) from Tank 13 are compared for Case B and C in Figure 5.6-95. A vertical line on the graph indicates the liner failure time for both cases at 2,506 years. Significant releases of Tc-99 and I-129 occur prior to the liner failure in Case B, but not Case C, because of the early hydraulic degradation (at 500 to 585 years) of the annulus grout in the former case. This allows rapid transport of inventory out of the annulus. In Case B, transport of Tc-99 out of the annulus is further enhanced due to a marked decrease in sorption of Tc-99 (because of the chemical transition at 1,143 years). When the liner fails, a pulse of radionuclides leave the waste tank (from inventory in the CZ) but fluxes are reduced at a much faster rate in Case B. Releases for Case B following liner failure are greatly suppressed by several orders of magnitude relative to Case C, especially for Tc-99 and I-129. In the absence of high flow rates in the waste tank grout in Case C, upward diffusion of Tc-99, I-129 and Ra-226 from the CZ becomes an important, dominant process, promoting storage of these radionuclides in the grout. This explains the much higher release rates in Case C after liner failure, as transport of the radionuclides finds another path of exit, from the grout through the annulus and wall.

Additionally, these graphs provide information regarding the impact of the early CZ transition time characteristic of Case C. While Case B releases of I-129 and Ra-226 mirror Case C releases (after liner failure) but at a slower rate, the Case B Tc-99 releases behave differently than Case C Tc-99 releases. This is due to the difference between Case B and Case C chemical transitions for the CZ (and for the annulus). Tc-99 releases are strongly controlled by solubility limits in the CZ, whereas I-129 has no solubility limits, and Ra-226 only weakly. Therefore, I-129 and Ra-226 reflect similar curves to Case C, while the Tc-99 curves reflect the changing solubility limits in the CZ and the timing of annulus transition, both vary by case.

Case B Tc-99 releases from the CZ are controlled by the submerged Condition C solubility limit until 4,990 years, at which time the CZ transitions to the lower technetium solubilities prevalent in submerged Condition D solubility limit. For the remainder of the Case B simulation, Tc-99 releases are held at the solubility limit in the CZ. The submerged Condition C solubility limit to Condition D solubility limit transition occurs immediately following the liner failure in Case C, but releases for Case C are mostly coming from the annulus and the waste tank grout until after 12,000 years therefore, the step is overshadowed by the change in flow fields accompanying the loss of liner integrity. For Case C, the Tc-99 in the grout is due to upward diffusion from the CZ before liner failure.

The late Tc-99 spike (at 10,830 years) in Case C is due to the annulus grout transitioning from Reducing Region II (where Tc-99 has a high distribution coefficient of 5,000 mL/g) to Oxidizing Region II (Tc-99 has a very low distribution coefficient of 0.8 mL/g), which flushes the remaining Tc-99 out of the annulus. Once the Tc-99 is gone from the annulus, the releases revert to the solubility controlled releases out of the CZ.

In Figure 5.6-96, Tank 15 that has a degraded liner at year zero, the annulus grout transitions at approximately the same time for both cases. The degraded grout in Case B results in slightly higher I-129 and Ra-226 peaks, but more dramatic is the faster

transport out of the system for I-129. Tc-99 in Tank 15 is controlled mostly by the inventory from the sand pads and annulus at early times, and later by the solubility of the CZ.

Figure 5.6-97 illustrates the fast-moving radionuclide release behavior from Tank 21 (Type IV tank). Figure 5.6-97 illustrates that the degraded grout in Case B promotes faster transport of I-129 (and Ra-226) out of the system, while Tc-99 curves are again predominantly controlled by the solubility limits in the CZ (and there is no sand pad or annulus inventory to be a second source of Tc-99).

Releases of slow-moving radionuclides, Np-237 and Pu-239, from Tank 15 are displayed in Figure 5.6-98. The figure indicates releases from Case B, the case with early grout degradation, are earlier and one to two orders of magnitude greater than releases in Case C. Slow-moving radionuclide releases from Tank 13 and Tank 21 show the same behavior.

Figure 5.6-98: Slow-Moving Radionuclide Fluxes Tank 15 (Grout)

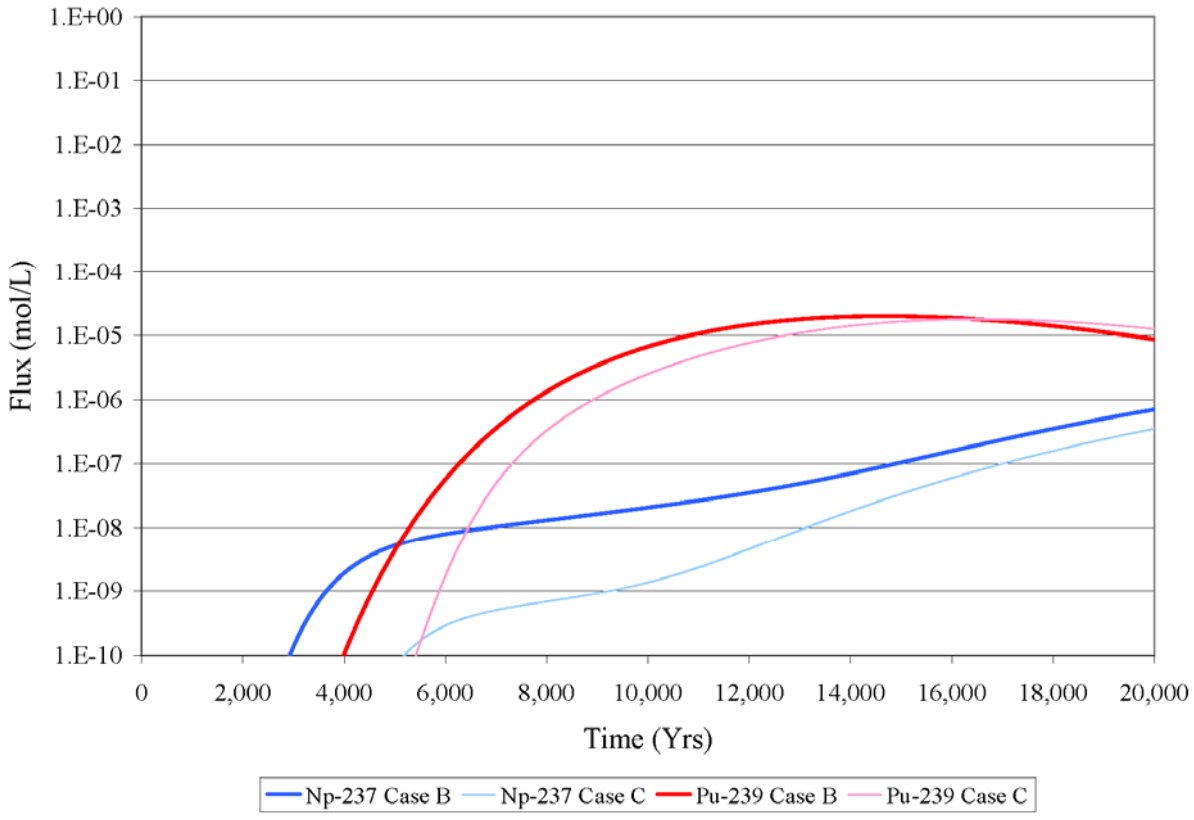

5.6.6.3.3 Contamination Zone (Barrier Cases 6 and 7)

The CZ barrier analyses removed the solubility limits applied to radionuclides in the CZ in the sensitivity conditions to evaluate the retarding affect this barrier has on Base Case releases. In the CZ Barrier Case 7, all of the barriers, except the CZ, are assumed to behave per the Base Case. All solubility controls are removed for Tc-99, Ra-226, and I-129, and set to very high concentrations for all other radionuclides in sensitivity condition, Barrier Case 7. These same solubility settings are used for sensitivity condition, Barrier Case 6 while the assumption for all other barriers is that they are fully degraded. The degraded configuration (Barrier Case 2) modeled the CZ under nominal conditions according to Tables 4.2-5 and 4.2-6, with all barriers except the CZ assumed to be fully degraded. The Base Case is compared to Barrier Case 7 to evaluate fast-moving radionuclide releases, while Barrier Case 2 (is compared to Barrier Case 6 releases to evaluate the CZ impact on slow-moving radionuclide releases.

The fast-moving radionuclide releases for Tank 13, Tank 15, and Tank 21 are provided in Figures 5.6-99, 5.6-100, and 5.6-101, respectively. The releases from Tank 15 are provided in Figure 5.6-102 as an example of the release behavior for the slow-moving radionuclides. It is expected that when the solubility limits in the sensitivity cases are removed, radionuclide releases will increase. When the radionuclide aqueous concentration in the CZ reaches the solubility concentration limit (or solubility limit); the radionuclide will precipitate to a solid form, and thus will not be available in aqueous form for transport out of the CZ. Low solubility limits in the CZ promote increased precipitation and decreased releases.

Figure 5.6-99: Fast-Moving Radionuclide Fluxes Tank 13 (CZ)

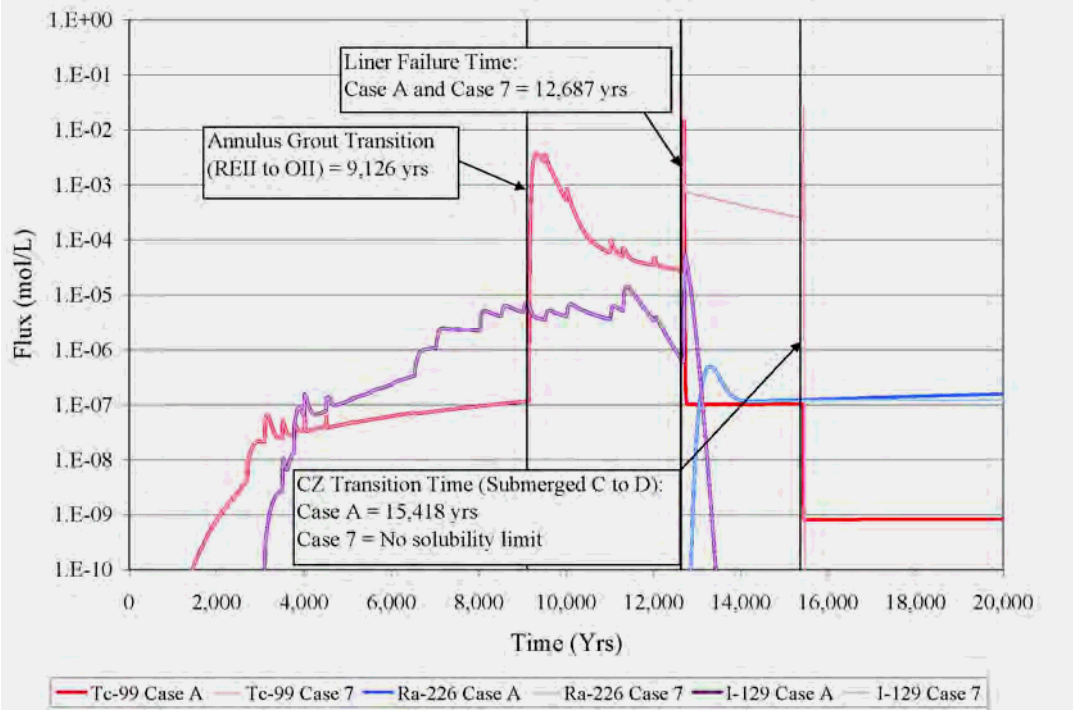

Figure 5.6-100: Fast-Moving Radionuclide Fluxes Tank 15 (CZ)

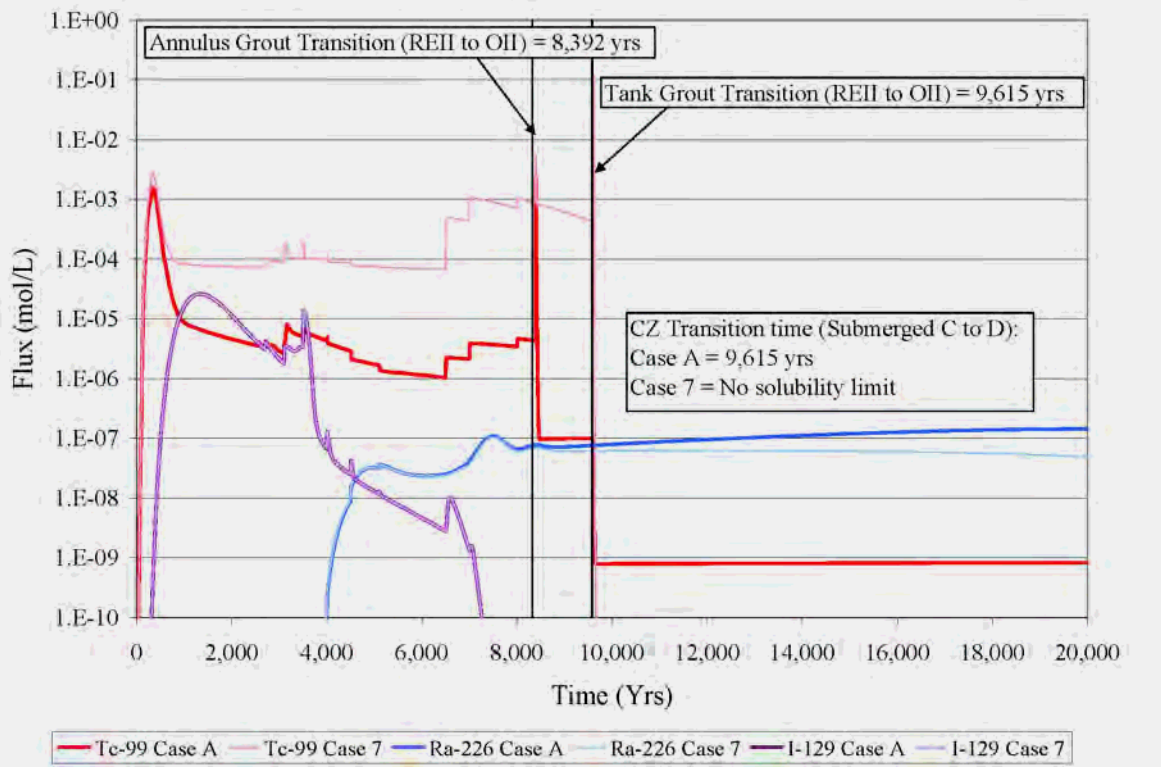

Figure 5.6-101: Fast-Moving Radionuclide Fluxes Tank 21 (CZ)

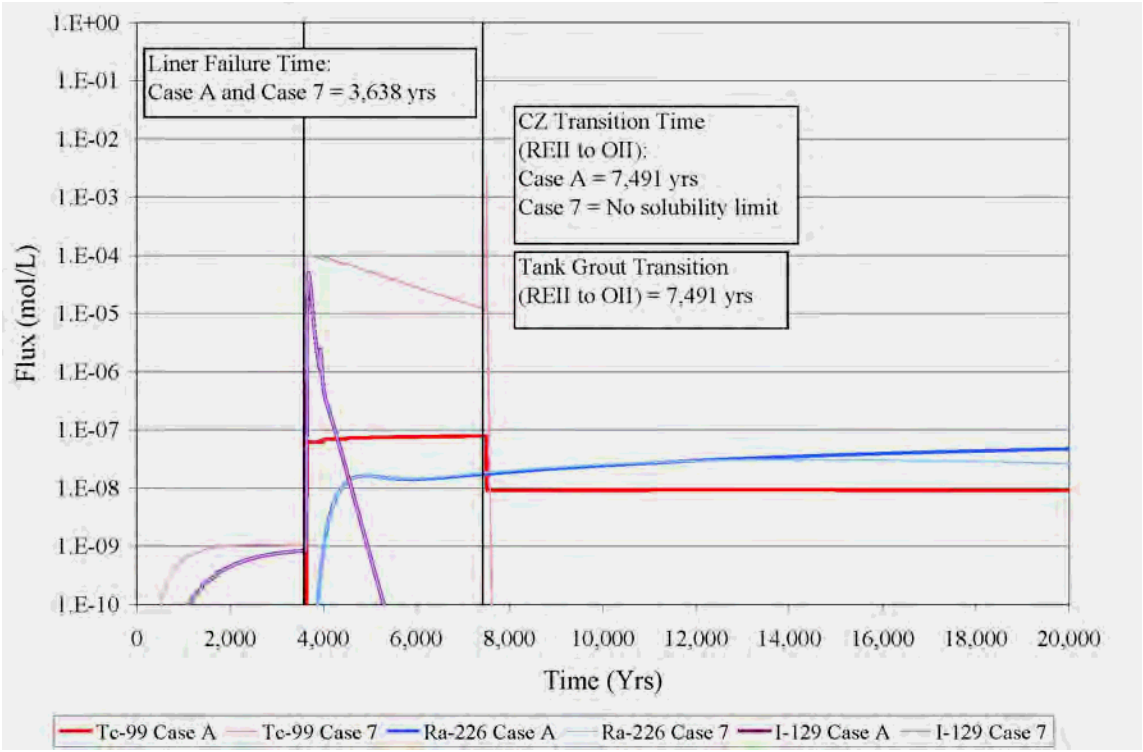

Figure 5.6-102: Slow-Moving Radionuclide Fluxes Tank 15 (CZ)

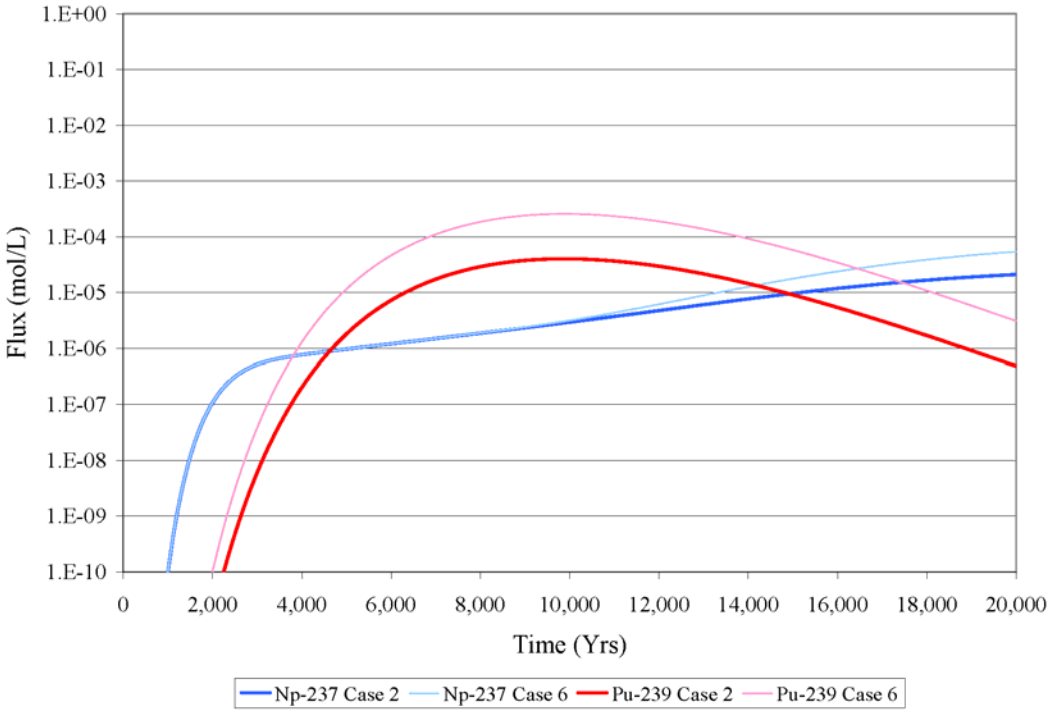

As expected, the radionuclides with solubility controls in the CZ are impacted in the sensitivity cases (e.g., releases increase), most notably Tc-99 and Pu-239 (and Np-237 later). As defined in Tables 4.2-5 and 4.2-6, I-129 is modeled with instantaneous releases (e.g., no solubility limit) therefore; there is no impact in the sensitivity case. Figures 5.6-99 through 5.6-101 also show no impact on Ra-226 releases. The reason Ra-226 is not impacted is that the radium concentration in the CZ never reaches the solubility limit, which is set to a relatively high concentration.

Although Ra-226 is relatively insensitive to the chemical condition of the CZ, the release of Ra-226 is strongly dependent on the availability of the release of the radionuclides whose decay produces Ra-226, most notably Pu-238. Plutonium is solubility controlled; therefore, it is possible that given a large enough initial inventory of Pu-238, Ra-226 could be affected. This also explains the late time increase in Np-237 releases relative to the Base Case (Figure 5.6-101). While Np-237 is relatively insensitive to the chemical condition of the CZ, Np-237's parent radionuclides (Cm-245→Pu-241→Am-241→Np-237) are frequently at their solubility limits.

In Figure 5.6-99, Tc-99 releases from the two cases are identical prior to liner failure (12,687 years) because releases originate in the sand pad and annulus, and are not subject to the solubility controls in the CZ. The sand pad and annulus Tc-99 inventory is depleted by the time the liner fails and CZ sourced Tc-99 releases become dominant. At this time, Barrier Case 7 releases are more than three orders of magnitude greater than the Base Case, indicating that Tc-99 concentrations are controlled by the solubility constraints in the CZ in Tank 13 at this late time.

Both Figure 5.6-100 and Figure 5.6-101 show that Tc-99 releases from Tank 15 (Type II tank with initially degraded liner) and Tank 21 are controlled at early times by the solubility limit. The Base Case releases are suppressed by more than three orders of magnitude. Pu-239 releases from Tank 15 indicate an order of magnitude increase when solubility controls are removed (Figure 5.6-102).

5.6.6.3.4 Liner (Barrier Cases 3, 4, and 5)

The liner barrier analysis compared three different barrier cases against the Base Case (Case A) and the degraded parameter (Barrier Case 2):

- Barrier Case 3: Nominal CZ and liner, with all other barriers degraded and the nominal liner failure time is based on a grouted carbon dioxide diffusion coefficient of 1E-06
- Barrier Case 4: Nominal CZ, liner fails early based on grouted carbon dioxide diffusion coefficient of 1E-04, all other barriers degraded
- Barrier Case 5: Nominal CZ, liner fails early based on grouted carbon dioxide diffusion coefficient of 1E-04, all other barriers intact

The degraded configuration (Barrier Case 2), which is compared to Barrier Case 4 in order to evaluate the impacts of liner failure on slow-moving radionuclides, was modeled with no liner present starting at year zero and the CZ set to nominal conditions (See Tables 4.2-5 and 4.2-6 for solubility tables). For the Base Case model, liner failure times vary with waste tank design, owing to differences in liner properties between the waste tanks. The failure times are provided in Table 4.2-36 (Section 4.2.2). The Base Case is compared to Barrier Case 5 to illustrate the impacts of liner failure on the fast-moving radionuclides. Barrier Case 3 results are not presented here because they are not significantly different from the Barrier Cases 4 and 5 comparison plots. Note, this analysis does not apply to waste tanks with initially failed liners (e.g., Tanks 12 and 15), as the nominal cases for these liners are the same as the failed conditions.

For non-Type II and IV tanks, releases from the waste tanks initiate following liner failure. However, the existence of inventory in the Type II sand pads and annulus allow for early releases from Type II tanks. Similarly, although a very small amount of flow is allowed through the liners for all waste tank types, the thinner basemat of the Type IV tanks, combined with no secondary liner result in a slightly larger amount of flow through the Type IV tanks. Because peak dose to the MOP is controlled primarily by the Type II and IV tanks (Section 5.5), the impact of varying the liner failure time in these waste tanks is presented here.

Figures 5.6-103 and 5.6-104 present the impacts of early liner failure on the transport of fast-moving radionuclides, Tc-99, I-129, and Ra-226 in Tank 13 (Type II tank, intact liner) and Tank 21 (Type IV tank). In Figure 5.6-98, in the Base Case, Tc-99 releases prior to liner failure (12,687 yrs) are primarily from the sand pad and annulus inventory. The first Tc-99 peak at 9,380 occurs due to the annulus chemical transition from Reducing Region II, where Tc-99 is held up in the annulus due to a high distribution coefficient (5,000 mL/g), to Oxidizing Region II, where Tc-99 is released because Tc-99 has a lower distribution coefficient (0.8 mL/g) in this chemical environment. The second

Tc-99 peak (12,710 years) occurs immediately after liner failure, which corresponds to the annulus transition from Oxidizing Region II to Oxidizing Region III, where Tc-99 has an even lower distribution coefficient (0.5 mL/g). This transition results in additional Tc-99 being flushed from the annulus (and any Tc-99 in the waste tank grout from upward diffusion from the CZ). For the remainder of the simulation Tc-99 releases are limited by the solubility controls applied to the CZ.

Figure 5.6-103: Fast-Moving Radionuclide Fluxes Tank 13 (Liner Failure)

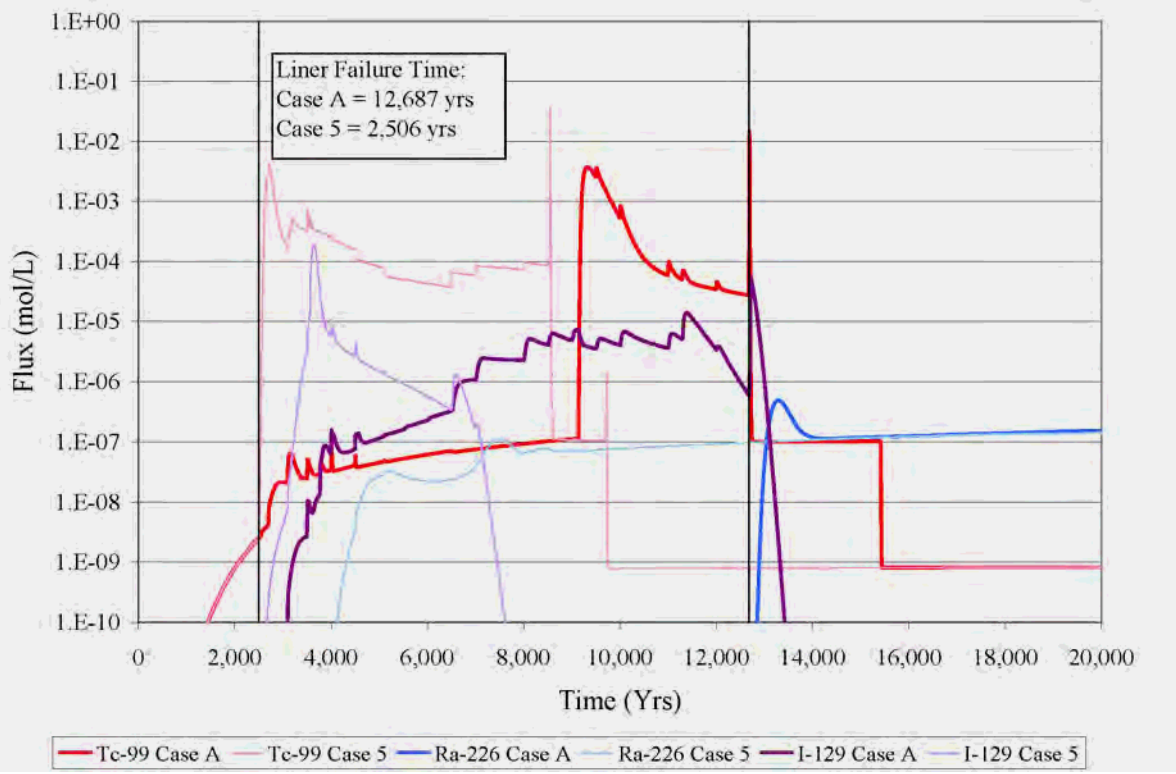

Figure 5.6-104: Fast-Moving Radionuclide Fluxes Tank 21 (Liner Failure)

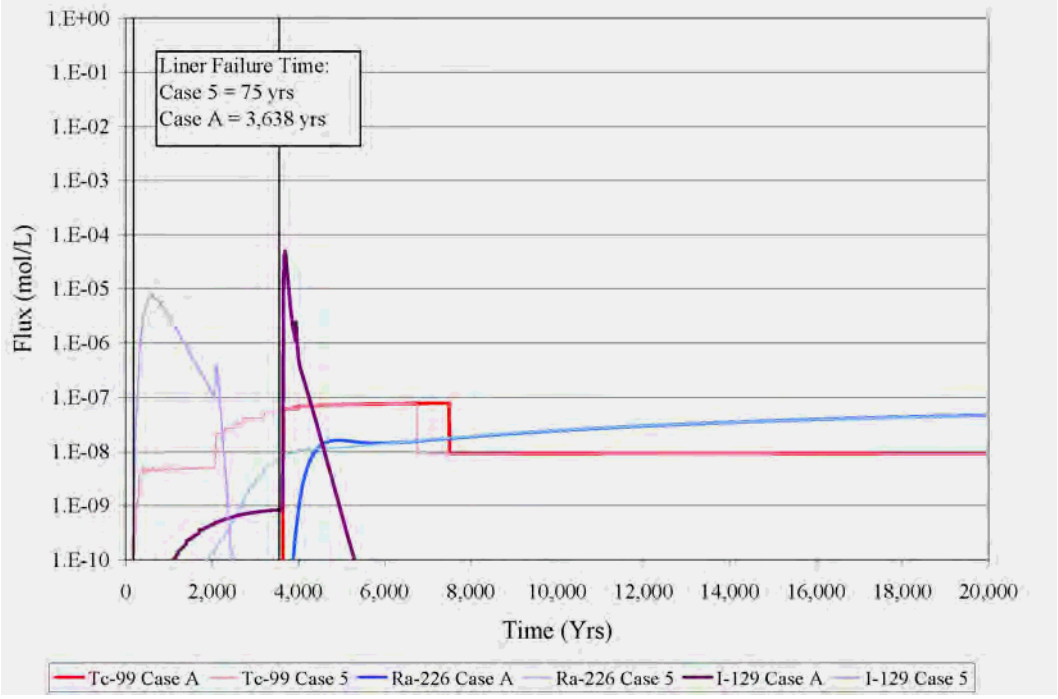

Failing the Tank 13 liner more than 10,000 years earlier causes the peak Tc-99 flux to occur more than 4,000 years earlier (Figure 5.6-103). The cause of the peak differs from the Base Case, in that the Barrier Case 5 peak is from the annulus transition from Reducing Region II to Oxidizing Region II (at 8,542 years), while the Base Case peak is from liner failure. The magnitude of the peak flux in Barrier Case 5 is slightly higher. Similarly, the I-129 peak flux is higher in magnitude (less than one order of magnitude) and occurs more than 9,000 years earlier in the sensitivity case. In contrast, the Ra-226 peak flux, while it does occur nearly 6,000 years earlier, the later Base Case peak is higher in magnitude due to the contribution of parent radionuclides.

Figure 5.6-104 displays the fast-moving radionuclide releases from Tank 21. Liner failure in the Base Case occurs at 3,683 years and 75 years in the sensitivity case. There is little difference in the Tc-99 releases because both release curves are solely controlled by the solubility limits in the CZ, and unlike Type II tanks, there is no other source of Tc-99 inventory in the Type IV tanks. In contrast, peak fluxes for both I-129 and Ra-226 occur earlier by more than 3,000 years in the former, and more than 1,000 years in the latter case. The earlier I-129 peak is nearly an order of magnitude lower in the sensitivity case, while the earlier Ra-226 peak is only slightly lower.

The affect of early liner degradation on the slow-moving radionuclides, Pu-239 and Np-237 in Tank 13 are illustrated in Figures 5.6-105. The liner is failed at the onset of the simulation period in the degraded parameter (Barrier Case 2), and the liner is failed at 2,506 years in the sensitivity case (Barrier Case 4). The magnitude of the peak Pu-239 flux is nearly the same in both runs, while the Np-237 peak flux is approximately one order magnitude less in Barrier Case 4, which had the later liner failure. Both peak fluxes

occur at the end of the simulation period. Differences in the fluxes at earlier times are more pronounced, with Np-237 flux for Barrier Case 4 several orders of magnitude less than the degraded configuration. This is because the liner failure delay results in a delay in the onset of both Pu-239 and Np-237 releases in Barrier Case 4.

Figure 5.6-105: Slow-Moving Radionuclide Fluxes Tank 13 (Liner Failure)

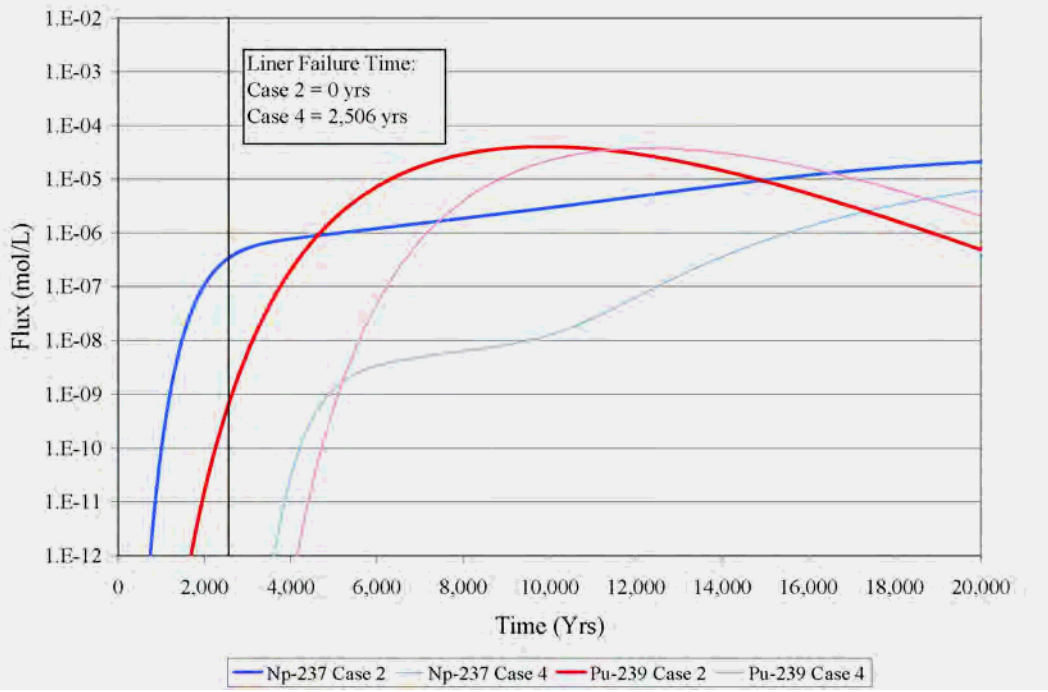

5.6.6.3.5 Natural Barrier (Barrier Cases 8 and 9)

Natural barrier capability is estimated by comparing the timing and magnitude of peak fluxes and the time history curves for failed natural barriers compared to those with nominal conditions. The natural barrier is considered the material zone and is called native soil in the HTF GoldSim Model and it exists immediately below the basemat. Submerged waste tanks (e.g., Tanks 9, 12, 13, and 15) are not included in this analysis because the native soil below the waste tank basemat is saturated. Therefore, only Tank 21, and Tank 36, the non-submerged, unsaturated waste tanks are presented in this section. The nominal condition for the native soil in the unsaturated waste tanks is to apply cement leachate impacted soil distribution coefficients initially. The "failed" natural barrier condition applies lower distribution coefficient values for each element. Using lower distribution coefficient values will maximize radionuclide migration through the natural barrier. The distribution coefficient values used for nominal natural barrier conditions and "failed" natural barrier conditions are presented in Table 5.6-35 for the radionuclides of interest, Tc-99, I-129, Ra-226, Pu-239, and Np-237. Note that the failed, cement leachate impacted sandy soil distribution coefficient for I-129 was simulated using the value 0.01 mL/g, instead of 0 mL/g. However, as the following section indicates, varying the I-129 soil distribution coefficient between 0.01 and 0 mL/g has little impact on the results.

Table 5.6-35: K_d Values Applied to Natural Barrier Sensitivity Cases

Radionuclides	Nominal Values [a]		Failed Values	
	Sandy Soil (mL/g)[d]	Cement Leachate Impacted Sandy Soil (mL/g)[c]	Minimum - Sandy Soil (mL/g)[d]	Minimum - Cement Leachate Impacted Sandy Soil (mL/g)[c]
I-129	0.3	0	0.07	0.01[b]
Np-237	3	5	0.75	1.12
Pu-239	290	580	72.5	145
Ra-226	25	75	1.25	3.75
Tc-99	0.6	0.1	0.15	0.01

a From Table 4.2-29

b The failed, cement leachate impacted sandy soil distribution coefficient for I-129 was simulated using the value 0.01 mL/g, instead of 0 mL/g. However, this low value had little impact on the results; therefore, the simulation was not rerun

c Applied to unsaturated waste tanks (Type III, IIIA, and IV Tanks) initially

d Values applied to unsaturated waste tanks (Type III, IIIA, and IV tanks) upon transition to non-cement leachate impacted soil

Barrier Cases 2 and 8 apply the failure conditions for the natural barrier. Case A compares to Barrier Case 8 as these cases use the nominal settings for the other barriers; whereas Barrier Case 2 compares to Barrier Case 9 as these cases use the degraded settings for the other barriers (closure cap, grout, concrete, and liner).

Figures 5.6-106 and 5.6-107 present the impact of failing the natural barrier on the fast-moving radionuclide releases in Tank 21 and 36, respectively. Figures 5.6-108 and 5.6-109 present the impact of failing the natural barrier on the slow-moving radionuclides in Tank 21 and 36, respectively.

Figure 5.6-106: Fast-Moving Radionuclide Fluxes Tank 21 (Natural Barrier)

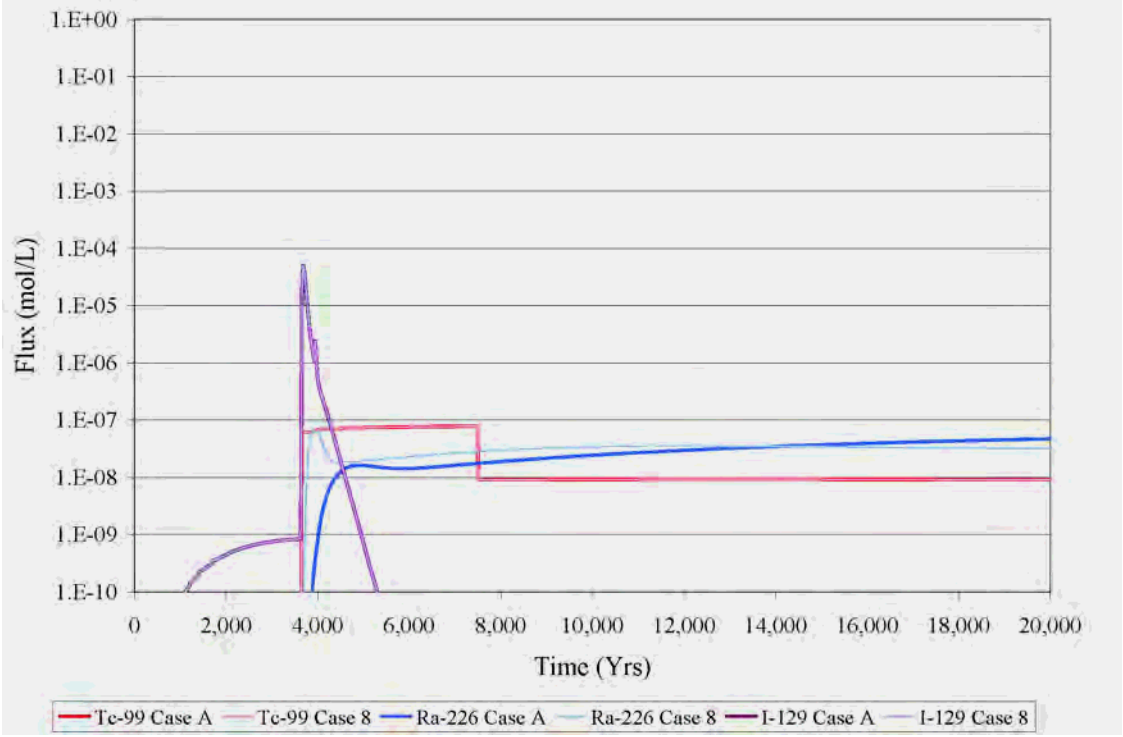

Figure 5.6-107: Fast-Moving Radionuclide Fluxes Tank 36 (Natural Barrier)

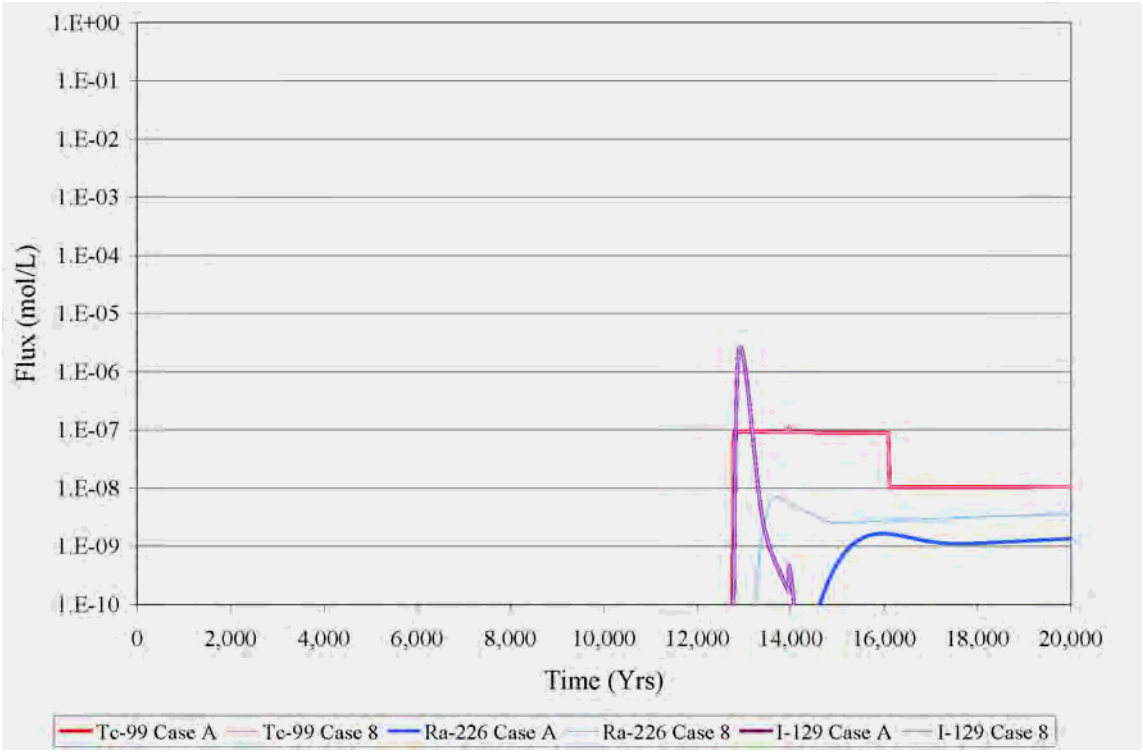

Figure 5.6-108: Slow-Moving Radionuclide Fluxes Tank 21 (Natural Barrier)

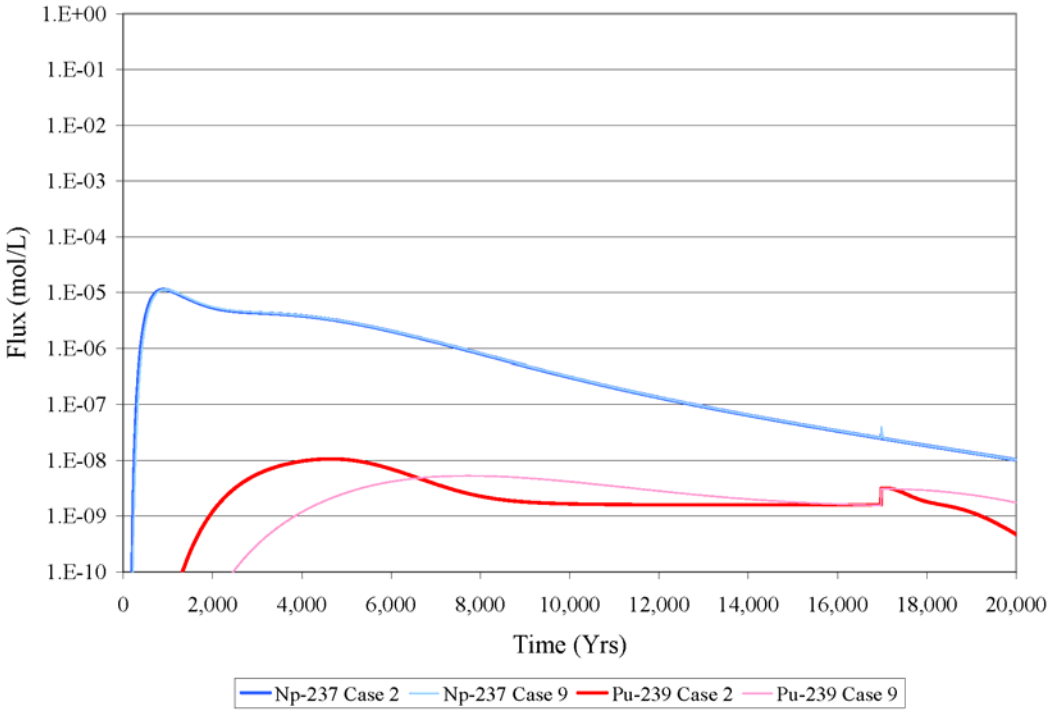

Figure 5.6-109: Slow-Moving Radionuclide Fluxes Tank 36 (Natural Barrier)

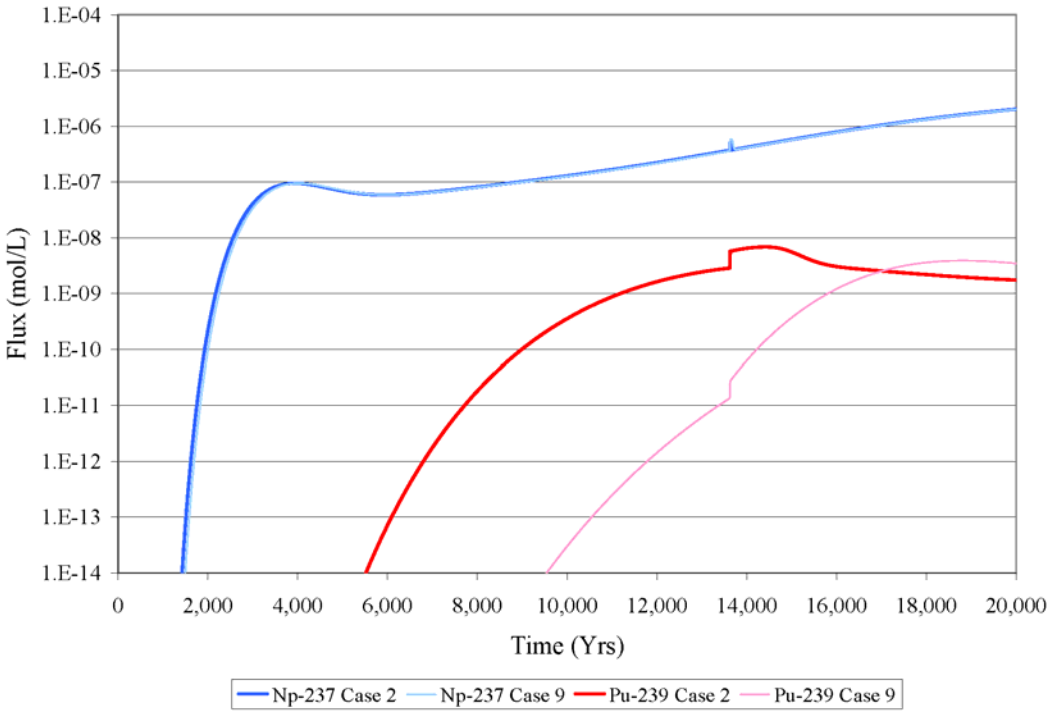

The natural barrier has no appreciable impact on those radionuclides that have little to no affinity to sorb to soil (e.g., Tc-99, I-129, and Np-237). For those radionuclides that do sorb, the natural barrier provides a moderate (e.g., Ra-226) to significant (e.g., Pu-239) impact, commensurate with their relative sorptive capacity and thickness of the native soil zone below the waste tank (more impact is apparent in Tank 36 due to a thicker vadose zone). Under nominal conditions, sorption in the vadose zone is increased for these radionuclides. Consequently, because less sorption is occurring in the failed case, radionuclides influenced by sorption onto soil have higher releases early on. However, with time, the failed cases become depleted, allowing the nominal case, which has more mass available, to overtake the failed case (e.g., Pu-239). Figures 5.6-106 and 5.6-107 indicate that the natural barrier delays Ra-226 releases between 500 and 1,000 years, whereas peak releases of Pu-239 are delayed by as much as 3,000 years (Figure 5.6-109). The natural barrier dampens peak Ra-226 flux by less than one order of magnitude, while the Pu-239 peak flux is not significantly different.

5.6.6.4 Barrier Analysis General Conclusions

The barriers with the most impact on releases from the source waste tanks are the liners, the CZ, and the waste tank grout. The closure cap and the natural barrier have less of an impact on radionuclide fluxes. The importance of the barrier on radionuclide transport is element specific for the CZ, the waste tank grout and the natural barrier, whereas the liner and closure cap are inclined to have a similar affect for all radionuclides. Although an independent barrier analysis of the annulus grout was not done, it is apparent from the interpretation of the time histories presented that the timing of annulus grout transition (Type II tanks) greatly influences the timing of Tc-99 peaks. The annulus transition triggers a large decrease in Tc-99 sorption onto the annulus grout (from a distribution coefficient of 5,000 mL/g to 0.8 mL/g). This transition combined with a significant inventory in the annulus (some initiated in the sand pads) produces significant releases prior to liner failure.

Liner failure has the largest impact on the timing of peak flux for the different radionuclides. The earlier a waste tank liner fails, the earlier the peak release for that radionuclide. Depending on the time of early failure, the peak flux can occur earlier by thousands of years. The change in the magnitude of the peaks varies by waste tank type and radionuclide. The liner is an effective barrier to radionuclide migration because it is designed to prevent flow and mass transport out of the waste tanks. Failure of the liner allows mass built up behind the liner to be rapidly flushed from the bottom of the waste tanks. Secondary effects of liner failure include increased physical degradation of the grout, which influences the timing of solubility changes in the CZ and distribution coefficient transitions in the cementitious materials and vadose zone. In this way, the timing of liner failure strongly controls peak flux.

The CZ, which mostly impacts peak Tc-99 and Pu-239 releases (and Np-237 in later years), acts to delay and dampen the Tc-99 peak fluxes by several orders of magnitude, however it has no impact on the transport of I-129 and Ra-226. The CZ also dampens the Pu-239 peak flux by approximately one order of magnitude; however, it does not affect the timing of the flux peak. The CZ effectively dampens the flux of Tc-99 and Pu-239 out of the waste tanks because 1) these radionuclides are strongly controlled by solubility, and 2) their aqueous

concentration in the CZ remains at or close to the solubility limit. If their aqueous concentrations were less, the CZ would be less effective at limiting the release of these radionuclides.

The integrity of the waste tank grout plays an important role in delaying the releases of I-129, Ra-226, Np-237, and Pu-239; although the peak magnitude is not significantly different. The integrity of the waste tank grout indirectly affects the Tc-99 releases, in that degraded waste tank grout has the ability to impart its reducing capacity onto the CZ, which causes the CZ chemical transitions to occur later. The impact of the grout on Type II tanks (both with and without a liner) is more difficult to discern because the radionuclide releases are overprinted by the inventory coming from the sand pads and annulus. More specifically, the large fluctuations in the hydraulic conductivity through the grout can greatly change the flow fields through the waste tank system, including redirecting flow through the annulus, which acts as a sink/source of inventory prior to liner failures.

The closure cap plays an important role in that it limits flow into and through the tanks, at least in the first few thousand years. The impact of the faster flow in the first few thousand years from removal of this barrier results in greater Np-237 and Pu-239 releases by as much as two orders of magnitude. The natural barrier dampens radionuclide releases especially for those radionuclides with higher soil distribution coefficients (e.g., plutonium and radium, as well as the parents of radium and neptunium); however, this barrier plays a lesser role in controlling peak releases.

5.6.7 Sensitivity Analysis using the HTF Deterministic Model

This section presents the sensitivity of the HTF closure system to alternative waste tank cases, and the sensitivity of the system to the nominal waste tank conditions with no closure cap (referred to as the No Cap Case). Although certain conditions used in the alternative cases are not supported by experimental data (e.g., complete degradation of cementitious material in one time step at 501 years) simulation of alternative scenarios with worse case settings provides insight into parameter importance to groundwater dose. Similarly, simulating the Base Case (Case A) with the closure cap material zone set equal to the estimated natural infiltration rate (e.g., 16.45 in/yr) provides insight into the importance of this feature on the 100-meter groundwater pathway dose.

Section 5.6.7.1 summarizes the alternative waste tank cases used in the analyses. Section 5.6.7.2 presents the impact of the various waste tank scenarios on dose at 100 meters for Cases B through E using the deterministic PORFLOW model. Section 5.6.7.3 summarizes the No Cap Case, while 5.6.7.4 presents the impact of assuming a no closure cap condition on dose at 100 meters, also using the deterministic PORFLOW model. The results are compared to the Base Case results presented in Section 5.5.

5.6.7.1 Alternative Scenario Analysis using the PORFLOW Deterministic Model

To simulate potential conditions in the HTF closure system over the modeling period, five waste tank cases (Cases A through E) are analyzed. Case A results are considered the Base Case and are presented in Section 5.5. The alternate cases allow evaluation of system behavior while varying key components of the conceptual model. Section 4.4.2 describes the different cases in detail.

Each case starts out with the system closed as planned, with waste tanks and ancillary equipment filled with grout and the closure cap in place. Expected degradation of the closure cap materials over time are simulated using the increasing infiltration rates shown in Table 3.2-14 (and are the same for all five cases). Each waste tank case is simulated using the waste release process described in Section 4.2.1 and the material properties described in Section 4.2.2.2.

The differences between the five waste tank cases are summarized in Table 4.4-1. Cases A through E vary according to whether 1) a fast flow channel through the grout and basemat exists, 2) the cementitious materials degrade at 501 years in a single time step, 3) the liner fails early, and 4) the grout volume is used to calculate the chemical transition time. These four factors define the physical and chemical transition times for each waste tank type. The transition times are provided in Table 4.4-9 for each waste tank and case and are discussed in Section 4.4.3. The property transitions in the waste tank system control the timing and magnitude of contaminant releases, and therefore the tables will aid the interpretation of the dose results. Additional process change timelines for the different tank types associated with Case A through E are provided in Section 4.4.3 (Tables 4.4-2 through Table 4.4-9).

5.6.7.2 Alternative Scenario MOP 100-Meter Groundwater Pathway Dose

The 100-meter radionuclide concentrations for Cases B through E (documented in Appendices J thru M) were used to calculate the total dose associated with the individual MOP peak 100-meter groundwater pathways identified in Section 5.4 (a discussion of how peak concentrations are determined by sector is provided in Section 5.2). Table 5.6-36 compares the peak 100-meter groundwater pathway doses within 10,000 years for Cases A through E for Sector C, the sector with the highest dose for all cases. The peak 100-meter groundwater pathway dose time histories for the six 100-meter sectors are shown for Cases B through E in Figures 5.6-110, 5.6-112, 5.6-114, and 5.6-116. The individual radionuclide contributions for the various cases are shown in Figures 5.6-111, 5.6-113, 5.6-115, and 5.6-117. The total dose is also plotted with the individual radionuclides to see their relative contribution. Because the majority (> 93%) of the peak dose comes from Tc-99 for the alternative cases, the focus of this discussion is on the dose contribution from Tc-99.

Table 5.6-36: Peak Groundwater Pathway Dose at 100m for Sector C (Cases A through E)

Case	Peak Dose (mrem/yr)	Year	Principle Radionuclide(s) and Percent Contribution to Peak
Case A	1	9,520	Tc-99 66%, Ra-226 19%
Case B	2.6	2,650	Tc-99 97%
Case C	2.4	2,680	Tc-99 ~100%
Case D	2.6	2,650	Tc-99 ~100%
Case E	1.3	2,650	Tc-99 93%

Figure 5.6-110: Case B MOP Groundwater Pathway Dose

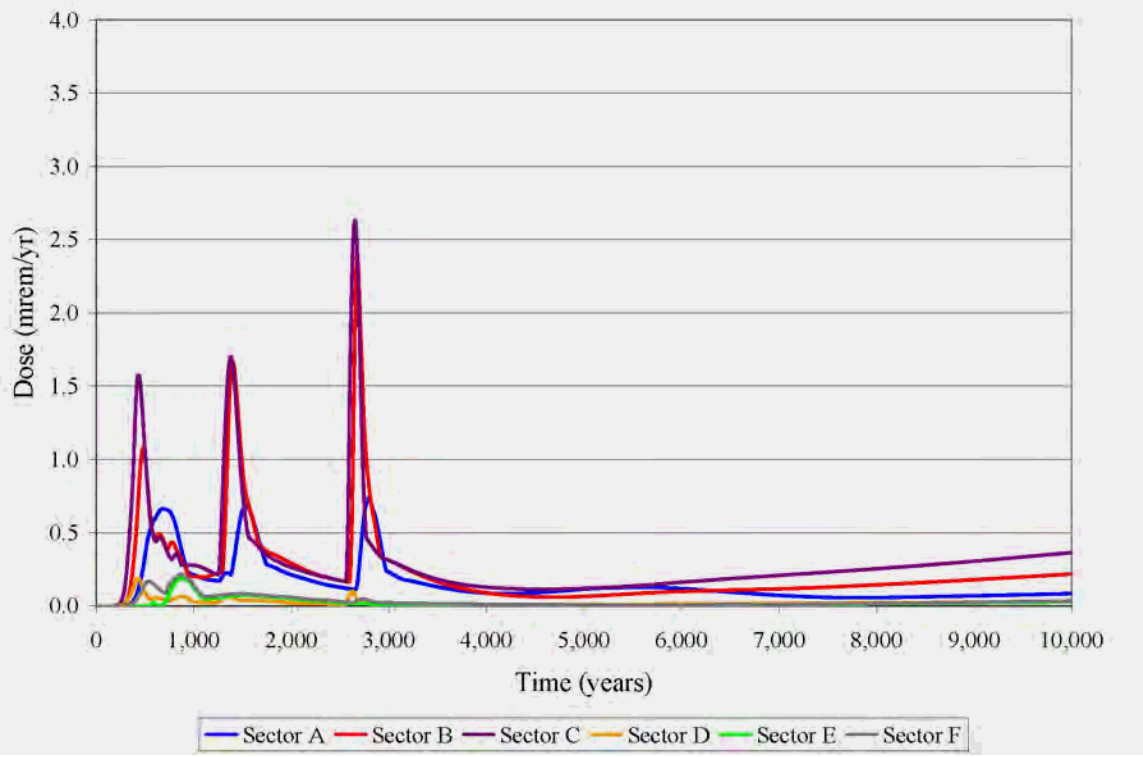

Figure 5.6-111: Case B Individual Radionuclide Contributors to the MOP Groundwater Pathway Dose

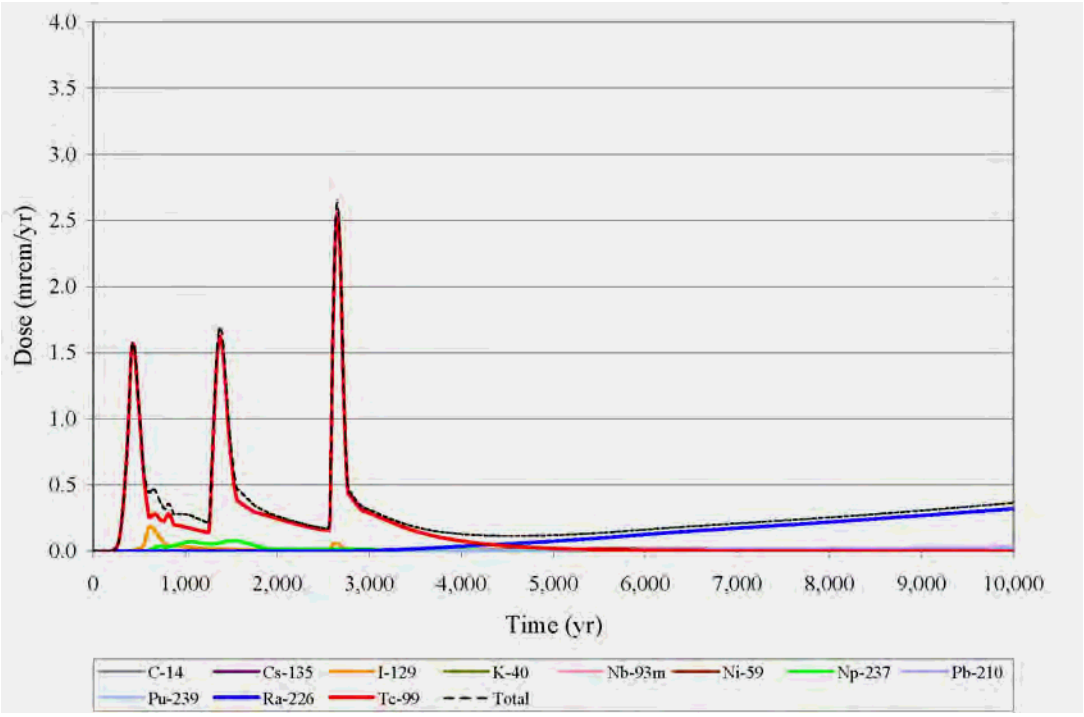

Figure 5.6-112: Case C MOP Groundwater Pathway Dose

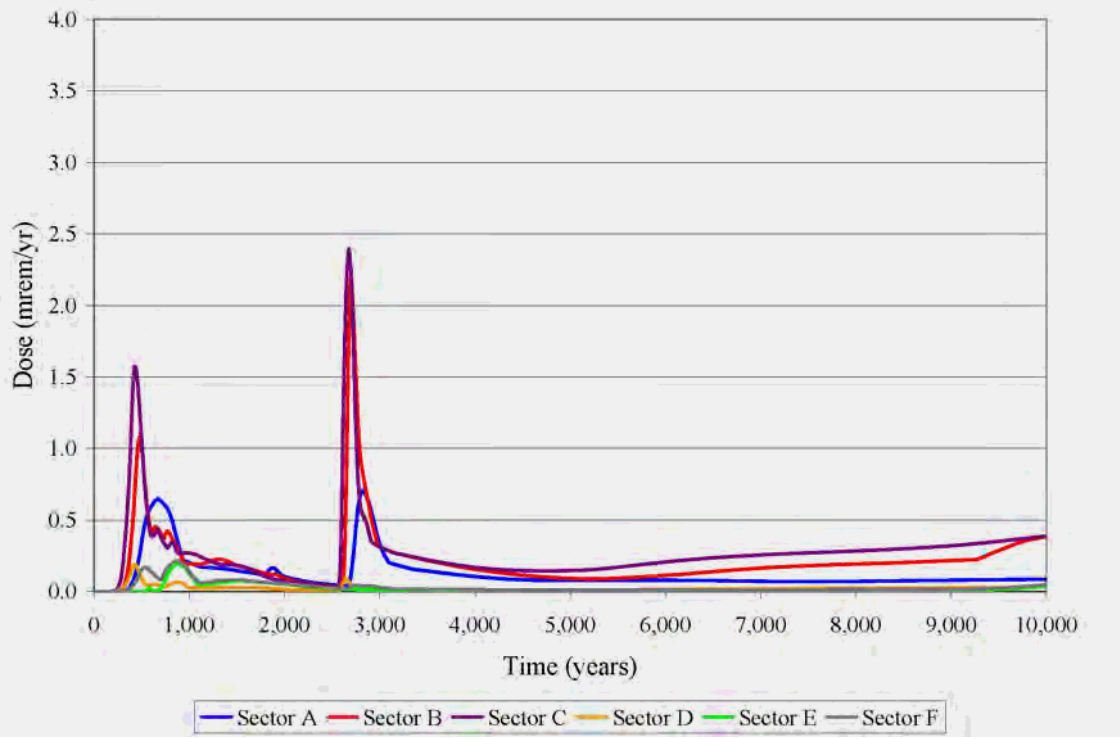

Figure 5.6-113: Case C Individual Radionuclide Contributors to the MOP Groundwater Pathway Dose

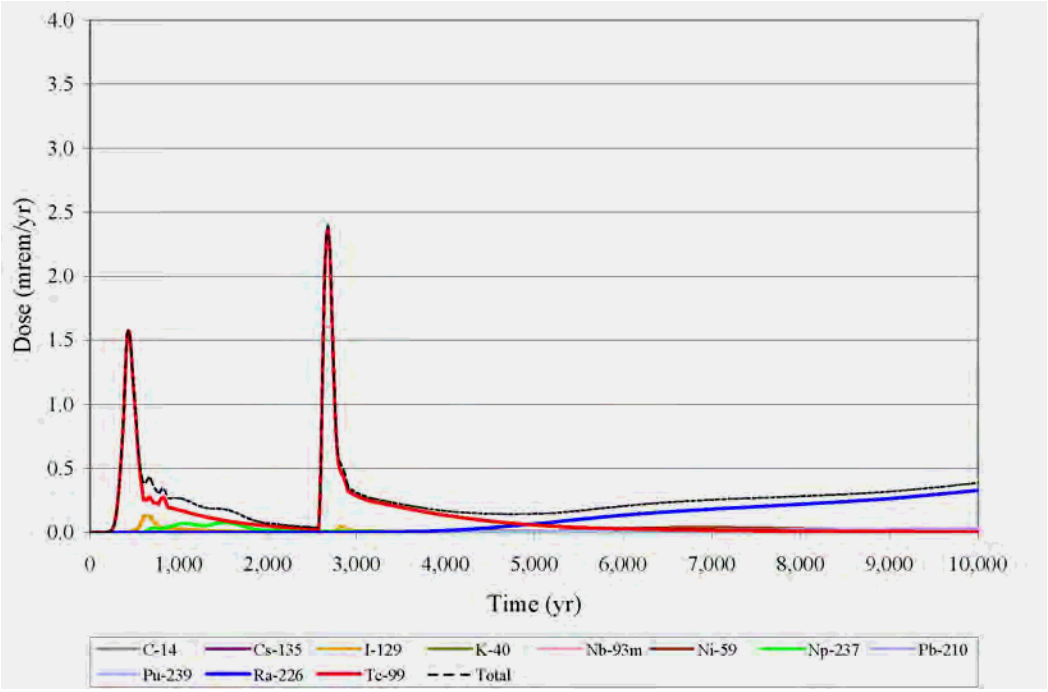

Figure 5.6-114: Case D MOP Groundwater Pathway Dose

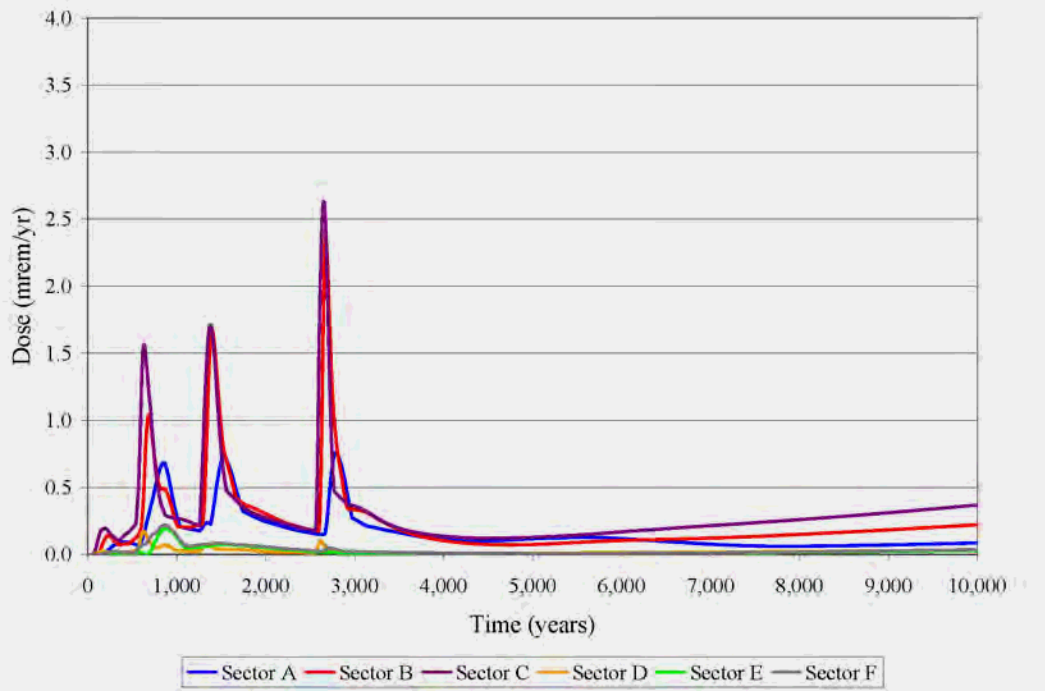

Figure 5.6-115: Case D Individual Radionuclide Contributors to the MOP Groundwater Pathway Dose

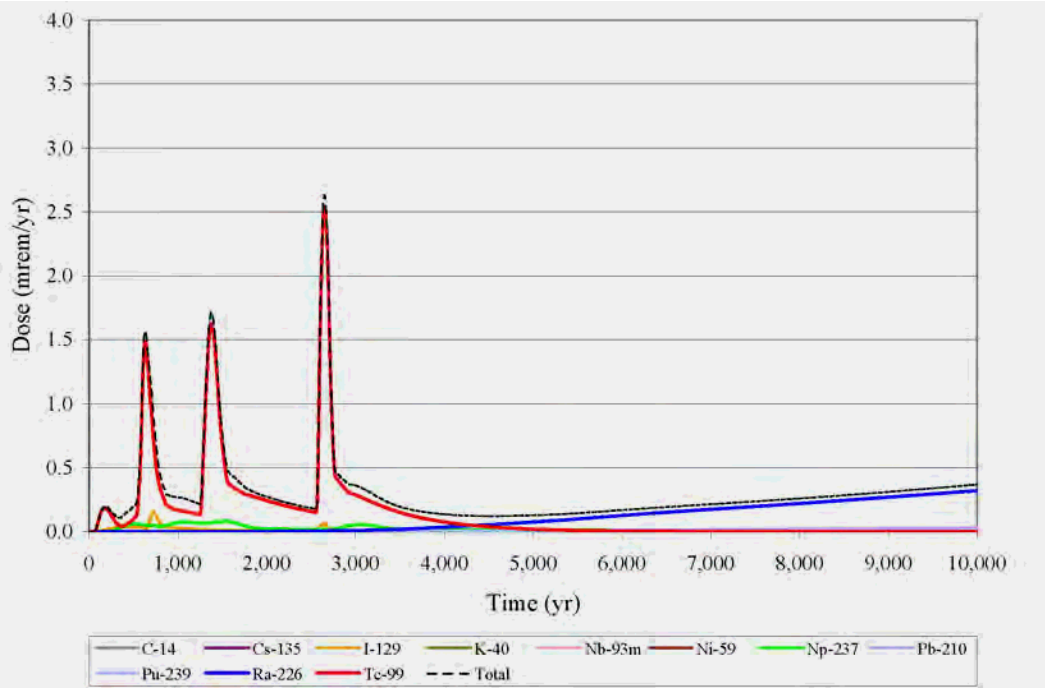

Figure 5.6-116: Case E MOP Groundwater Pathway Dose

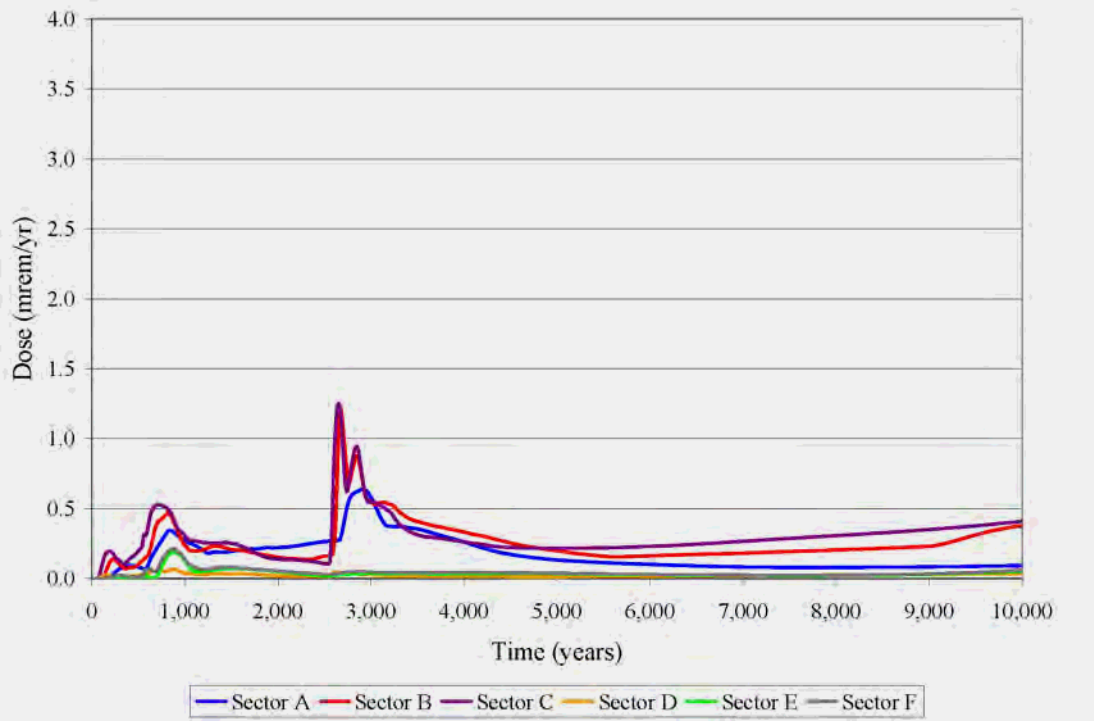

Figure 5.6-117: Case E Individual Radionuclide Contributors to the MOP Groundwater Pathway Dose

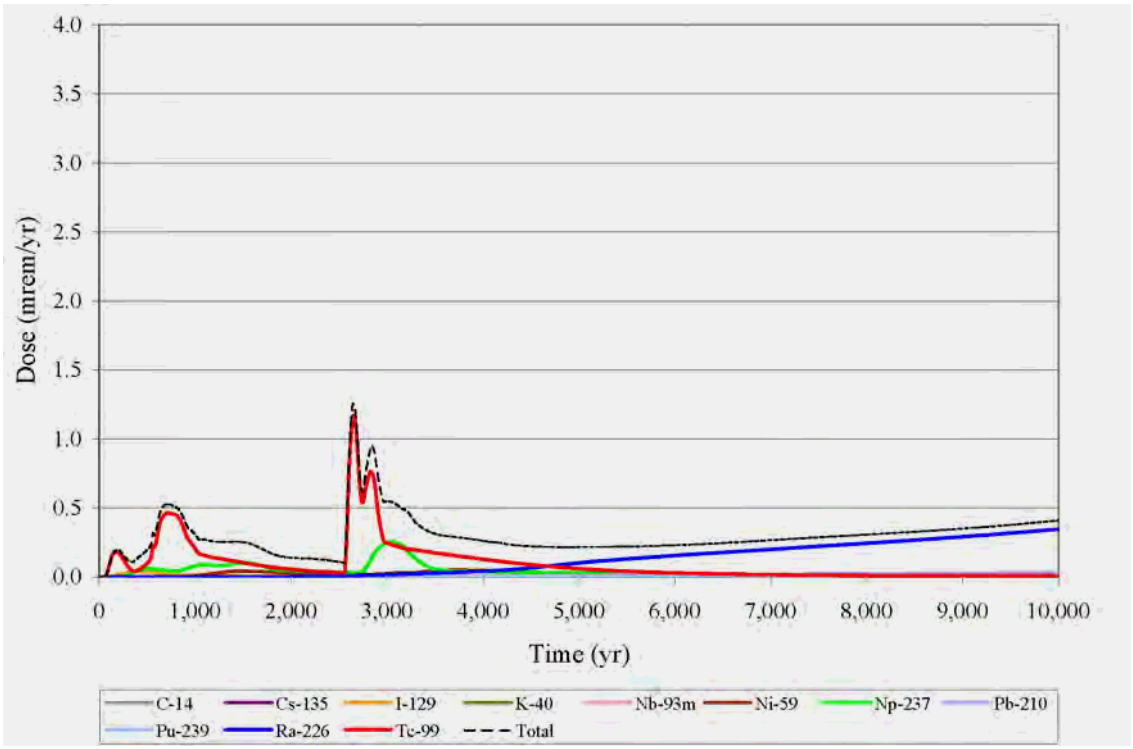

The alternative case 100-meter groundwater pathway dose results are similar to the Base Case results in that Sector C produces the highest dose over the compliance period. The alternative case results for this sector are displayed in Figure 5.6-118 against the Case A results from Section 5.5 (Figure 5.5-1). The alternative cases differ from the Base Case result in that the peak doses for Sector C in the alternative cases occur earlier than for Case A and are primarily from the contribution of Tc-99 as opposed to the late-time contribution of Ra-226 (Figure 5.5-3 compared with Figures 5.6-111, 5.6-113, 5.6-115, and 5.6-117, and Table 5.6-36). Table 5.6-36 indicates that the alternative cases result in peak groundwater pathway doses between 1.3 and 2.6 mrem/yr around 2,650 years as opposed to the later (e.g., 9,520 years) 1.0 mrem/yr Base Case peak.

Figure 5.6-118: All Case Comparison MOP Groundwater Pathway Doses

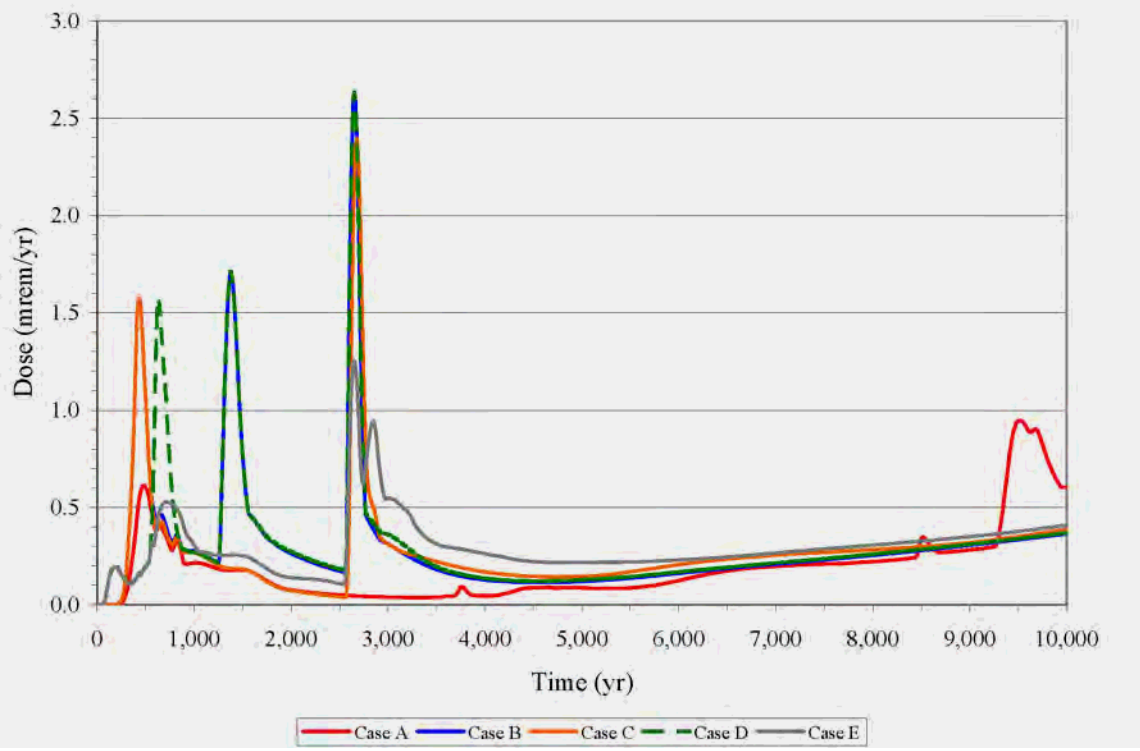

Stream traces indicate that Sector C concentrations are predominantly from Type II and IV tank releases. As presented in the benchmarking discussion (Section 5.6.2), the Type II tanks require modeling of components (sand pad and annulus) because in addition to an initial inventory in the CZ, these waste tanks are assumed to have an initial inventory in the primary sand pad and annulus. Tank 16 also has an initial inventory in the secondary sand pad.

Comparison of the peaks for the different cases displayed in Figure 5.6-118 indicates that all cases have an early peak. The early peak (between 440 and 750 years) for all cases is driven by early Tc-99 releases from Type II tanks with an initially degraded liner. The release is enhanced in Cases A through D by the transition of the basemat concrete from Oxidized Region II to Oxidized Region III. Additionally, the existence of a fast flow path through the grout for the alternative cases is sufficient to change the flow fields enough in the Type II tanks, that flow through the annulus and sand pads is lower for Case A. The flow through the

annulus and sand pads for Case E is also low relative to B, C, and D because of the existence of the fast flow through the basemat. Case D still has sufficient flow through the annulus, despite having the existence of the fast flow channel through the basemat because the cementitious materials are hydraulically degraded at year 501.

A second distinct peak, centered at 1,380 years occurs in Cases B and D, but is absent (or delayed) in Cases A, C, and E. Both the timing and magnitude of the peak is the same in B and D. This is expected, because both cases assume a fast flow path around the grout (e.g., from grout shrinkage), instantaneous degradation of the cementitious materials at 501 years, early liner failure per Table 4.2-36, and the full reducing capacity of the waste tank grout imparted onto the CZ. Case D differs from Case B in that it also models a fast flow path through the waste tank basemat, in addition to the fast flow path through the grout. Tables 4.4-2 through 4.4-9 confirm that these two cases have similar timing of different processes in the tanks. Table 4.4-4 indicates that the second peak is driven by Tc-99 releases from Type II tanks (with initially intact liners) following the transition of the annulus grout from Reducing Region II, where Tc-99 has a high cementitious material distribution coefficient of 5,000 mL/g, to Oxidized Region II where Tc-99 has the very low distribution coefficient of 0.8 mL/g. The absence of this peak in Cases A, C, and E is due to a long delay in the onset of this transition. Table 4.4-4 indicates that the annulus transitions after the end of the compliance period for Case C and E and at 9,126 years for the Base Case (which drives the Case A peak around 9,500 years).

The largest peak for the alternative cases centers around 2,650 years and is driven by the combination of Type II liner failure (Tank 13), and the annulus grout transition from Reducing Region II to Oxidized Region II in the Type II tanks with initially degraded liners (Tanks 14, 15, and 16). The contribution from Ra-226 overtakes the contribution from Tc-99 later (between 4,500 years and 5,000 years) mostly due to ingrowth from parent products. Radionuclide releases from Type IV tanks are important in the Base Case after their liner fails (e.g., 3,638 years). However, contributions from Type IV tanks in alternative Cases B through E (which have liner failures at 75 years) are overshadowed by the early contributions from Type II tanks.

Comparison of the alternative cases with the Base Case indicates that Type II tanks (with and without intact liners), which are important contributors to dose for the Base Case at later times become very important contributors to dose early on when a fast flow channel through the grout (and basemat for Case D and E) is modeled. The early chemical transition due to increased flow through the annulus and sand pads controls the timing and magnitude of the peak in most cases. Increased flow through the annulus resulted from the hydraulic degradation of the cementitious material at 501 years for Cases B and D, but also when normal degradation of the cementitious material was combined with the fast flow channel through the waste tank grout. The alternative cases indicate that the earlier transition times and changing flow through the annulus leads to an earlier peak dose by almost 7,000 years and an increase in the magnitude of the peak by as much as 1.6 mrem/yr.

5.6.7.3 PORFLOW Deterministic Model - No Closure Cap Analysis

The no closure cap analysis evaluates the sensitivity of the 100-meter groundwater pathway dose to the engineered closure cap. The deterministic Base Case (Case A) is simulated using

PORFLOW, but the closure cap material zone is set equal to background infiltration for the No Cap Case. Using the HELP model, background infiltration was estimated to be 16.45 in/yr. [WSRC-STI-2007-00184 Figure 29 and Table 31] This is analogous to modeling a soils only closure cap with no barrier, drainage, or erosion control layers. The impact of removing the engineered closure cap is determined by comparing the timing and magnitude of the dose peaks of the sensitivity case with the Base Case. For a comparison of radionuclide fluxes below the waste tanks for these two cases, see the no cap barrier analysis in Section 5.6.6.

5.6.7.4 No Closure Cap MOP 100-Meter Groundwater Pathway Dose

The 100-meter radionuclide concentrations for the No Cap Case (documented in Appendix H) are used to calculate the total dose associated with the individual MOP peak 100m groundwater pathways identified in Section 5.4 (a discussion of how peak concentrations are determined by sector is provided in Section 5.2). Table 5.6-37 compares the peak 100-meter groundwater pathway doses within 10,000 years for Cases A and the No Cap Case for Sector C, the sector with the highest dose. Figure 5.6-119 displays the No Cap Case peak 100-meter groundwater pathway dose time histories by sector. Figure 5.6-120 displays the individual radionuclide contributions to Sector C for the No Cap Case. The total dose is also plotted with the individual radionuclides to see their relative contribution.

Table 5.6-37: Peak Groundwater Pathway Dose at 100m - Sector C (Case A and No Cap Case)

Case	Peak (mrem/yr)	Year	Principle Radionuclide(s) and Percent Contribution to Peak
Case A	1	9,520	Tc-99 66%, Ra-226 19%
No Cap	3	350	Tc-99 ~100%

Figure 5.6-119: No Cap Case MOP Groundwater Pathway Dose

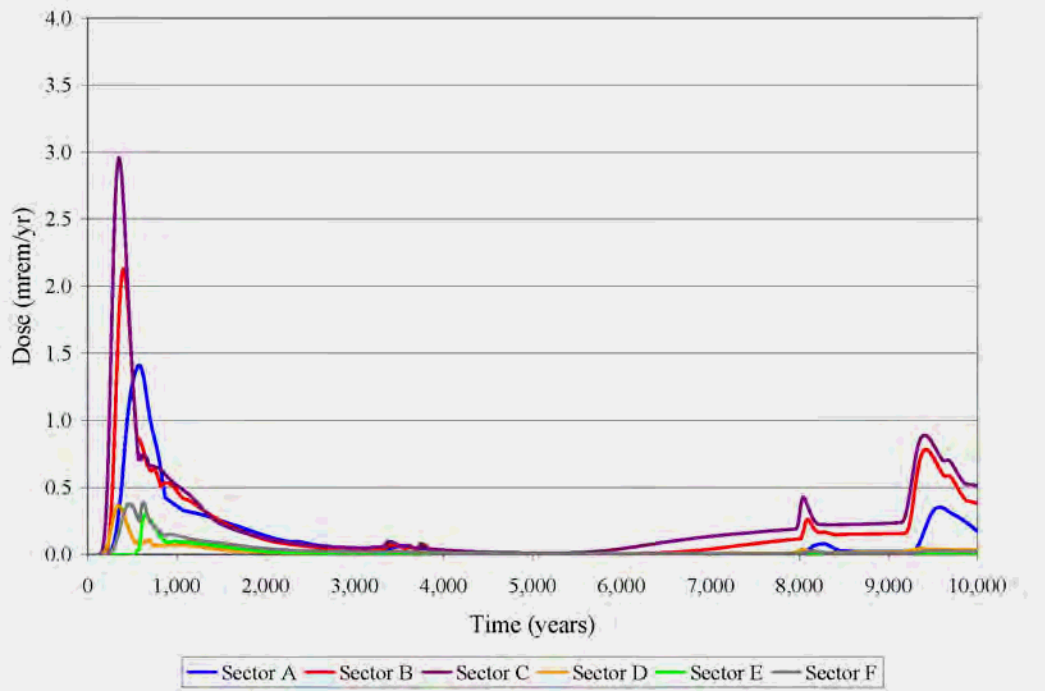

Figure 5.6-120: No Cap Case Individual Radionuclide Contributors to MOP Groundwater Pathway Dose

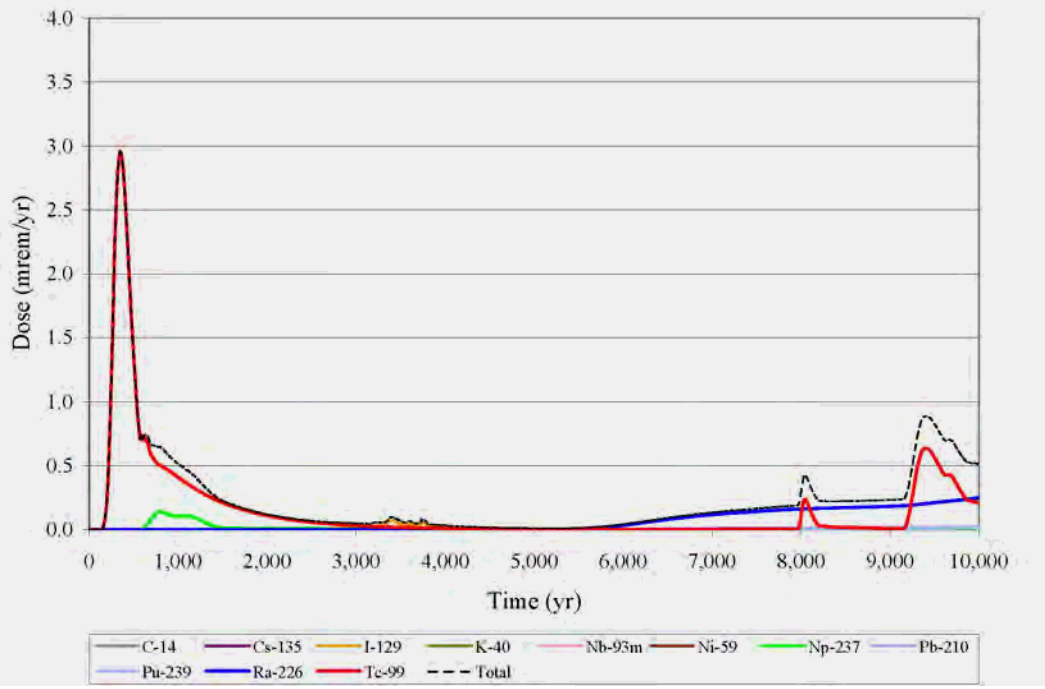

Comparison of the Base Case with the No Cap Case in Figure 5.6-121 indicates that removal of the closure cap increases the approximate early peak dose to 2.4 mrem/yr. The increased flow causes more mass to be released from the waste tanks with initially degraded liners (Tanks 14, 15, and 16), and from the waste tanks with inventory in the sand pads. In addition to higher magnitude peaks, the timing of the peaks in the No Cap Case are earlier relative to the Base Case resulting from earlier chemical transition times from the increase in flow through the system.

Figure 5.6-121: Sector C 100m Groundwater Pathway Doses, Base Case, and No Cap Comparison

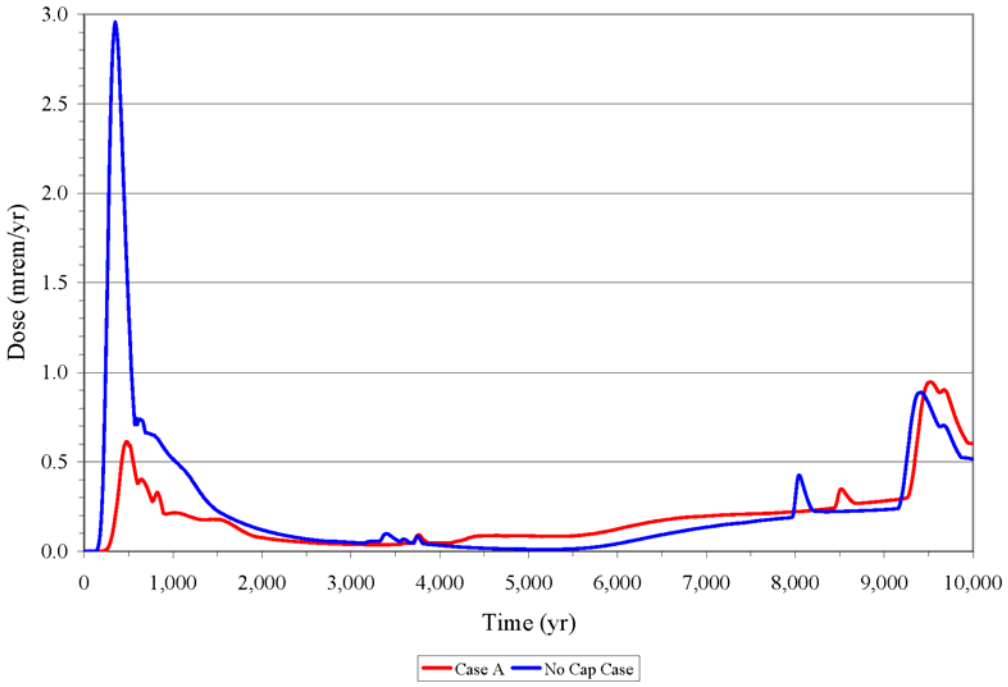

5.6.7.5 Synergistic Sensitivity Case 100-Meter Dose Results

In order to address uncertainty related to three Base Case key modeling parameters, a synergistic sensitivity case was developed using the PORFLOW deterministic model. The three parameters analyzed further are gas transport impacts on reducing grout, liner failure times, and solubility controlling phases. The synergistic case evaluates the combined results of pessimistic assumptions regarding these three key modeling parameters.

The starting point for the case development is Case C. As described in Section 4.4.2.3, Case C models a fast flow path that bypasses the reducing grout fill and thus the reducing grout is not assumed to affect the chemistry of the infiltrating water. This assumption causes the solubility phase to change from Reducing to Oxidized in tens to hundreds of years following closure (for waste tanks with initially failed liners) or failure of the waste tank liner as seen in Tables 4.4-2 through 4.4-9. This assumption addresses the uncertainty related to the duration of the Base Case reducing conditions by eliminating the influence of the reducing grout fill.

There were two additional modifications to the Case C model to address the other two parameters. In Case C, the waste tank liners are assumed to fail earlier than the Base Case with Type I liners failing at 1,142 years, Type II liners at 2,506 years, Type III/IIIA liners at 2.077 years and Type IV liners at 75 years (except for Tanks 12, 14, 15, and 16 which are assumed failed at time of closure). To address the synergistic impact of earlier liner failure, the failure time for Type I, II and III/IIIA tanks was modeled at 500 years while the liner failure time for Type IV tanks was modeled at 75 years.

The second modification to Case C was made to address alternative solubility controlling phases. The Base Case assumed iron co-precipitation as the controlling phase for plutonium, technetium, uranium, and neptunium. To address the synergistic impact of alternate solubility controlling phases for Reducing Region II and Oxidized Region II conditions the synergistic case assumes the maximum solubility phase from Table 7 of WSRC-STI-2007-00544 for non-submerged waste tanks (i.e., Type III/IIIA and IV tanks), and the phases from Table 5 of WSRC-STI-2007-00544 for submerged waste tanks (i.e., Type I and II tanks). For Oxidized Region III, all values are utilized from Table 4 of WSRC-STI-2007-00544. Table 5.6-38 presents the values modeled for this case.

Table 5.6-38: Synergistic Case Solubility Controlling Phases vs. Base Case

	Run	Reduced Region II Solubility (mol/L)		Oxidized Region II Solubility (mol/L)		Oxidized Region III Solubility (mol/L)
		Non-submerged	Submerged	Non-submerged	Submerged	All tanks
Pu	Base Case	7.0E-14 (Fe co-prec)	8.0E-14 (Fe co-prec)	9.0E-15 (Fe co-prec)	7.0E-16 (Fe co-prec)	2.0E-16 (Fe co-prec)
	Sensitivity Run	1.7E-09 ($Pu(OH)_4$)	1.7E-09 ($Pu(OH)_4$)	3.0E-7 ($Pu(OH)_4$)	4.5E-10 ($PuO_2(OH)_2$)	5.7E-5 ($Pu(OH)_4$)
Tc	Base Case	6.0E-13 (Fe co-prec)	7.0E-13 (Fe co-prec)	7.0E-14 (Fe co-prec)	5.0E-15 (Fe co-prec)	2.0E-15 (Fe co-prec)
	Sensitivity Run	3.3E-8 ($TcO_2.H_2O$)	1.1E-31 (Tc_2S_7)	No solubility control - Modeled as instantaneous release	No solubility control - Modeled as instantaneous release	No solubility control - Modeled as instantaneous release
U	Base Case	7.0E-12 (Fe co-prec)	8.0E-12 (Fe co-prec)	9.0E-13 (Fe co-prec)	6.0E-14 (Fe co-prec)	2.0E-14 (Fe co-prec)
	Sensitivity Run	3.5E-05 (UO_2)	3.5E-05 (UO_2)	1.8E-5 (Schoepite)	2.5E-7 (Becquerelite)	3.4E-5 (Becquerelite)
Np	Base Case	2.0E-14 (Fe co-prec)	2.0E-14 (Fe co-prec)	2.0E-15 (Fe co-prec)	2.0E-16 (Fe co-prec)	5.0E-17 (Fe co-prec)
	Sensitivity Run	5.1E-9 (NpO)	1.6E-9 ($Np(OH)_4$)	6.8E-7 ($NpO_2(OH)$)	2.5E-5 ($NpO_2(OH)$)	1.3E-4 ($Np(OH)_4$)

Figures 5.6-122 and 5.6-123 display the peak MOP dose time histories by sector for the synergistic case for 10,000 years and 20,000 years, respectively. Figure 5.6-124 displays the individual radionuclide contributions to Sector C (i.e., the peak sector) for up to 20,000 years. Figure 5.6-125 displays a comparison of the Base Case, Case C, and the synergistic case.

Figure 5.6-122: Synergistic Case MOP Dose by Sector - 10,000 Years

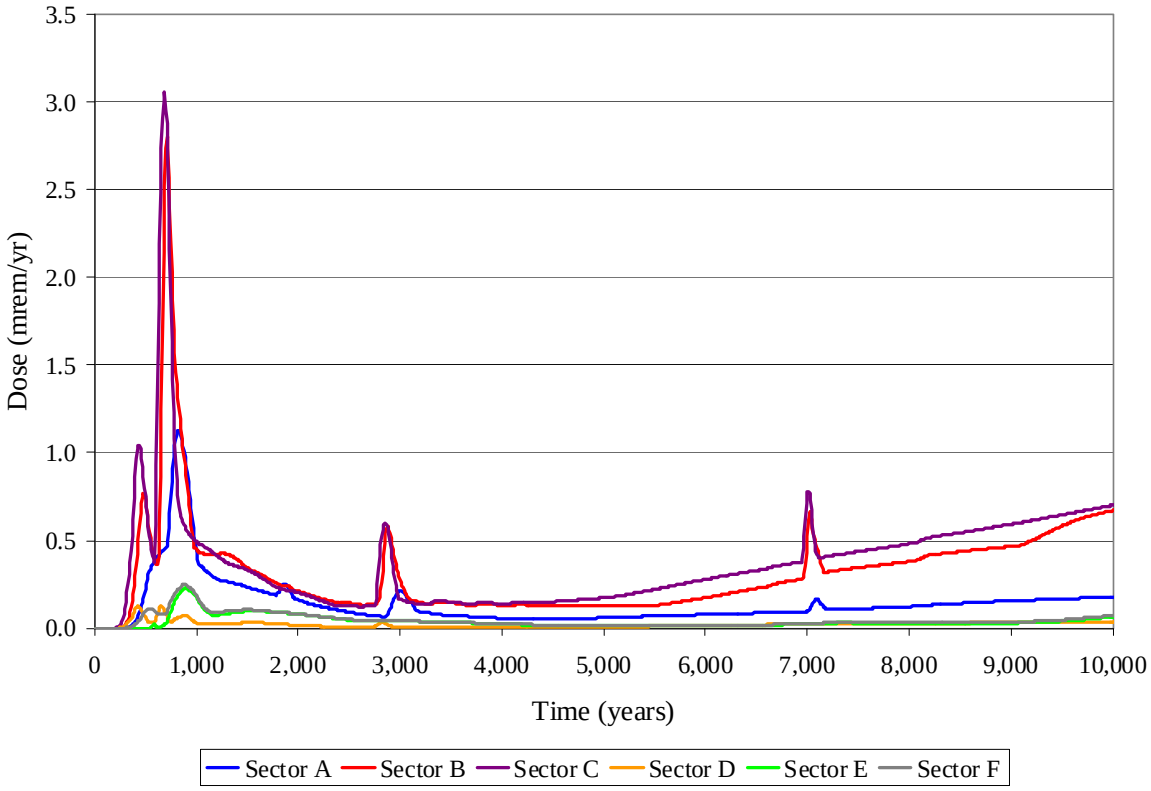

Figure 5.6-123: Synergistic Case MOP Dose by Sector - 20,000 Years

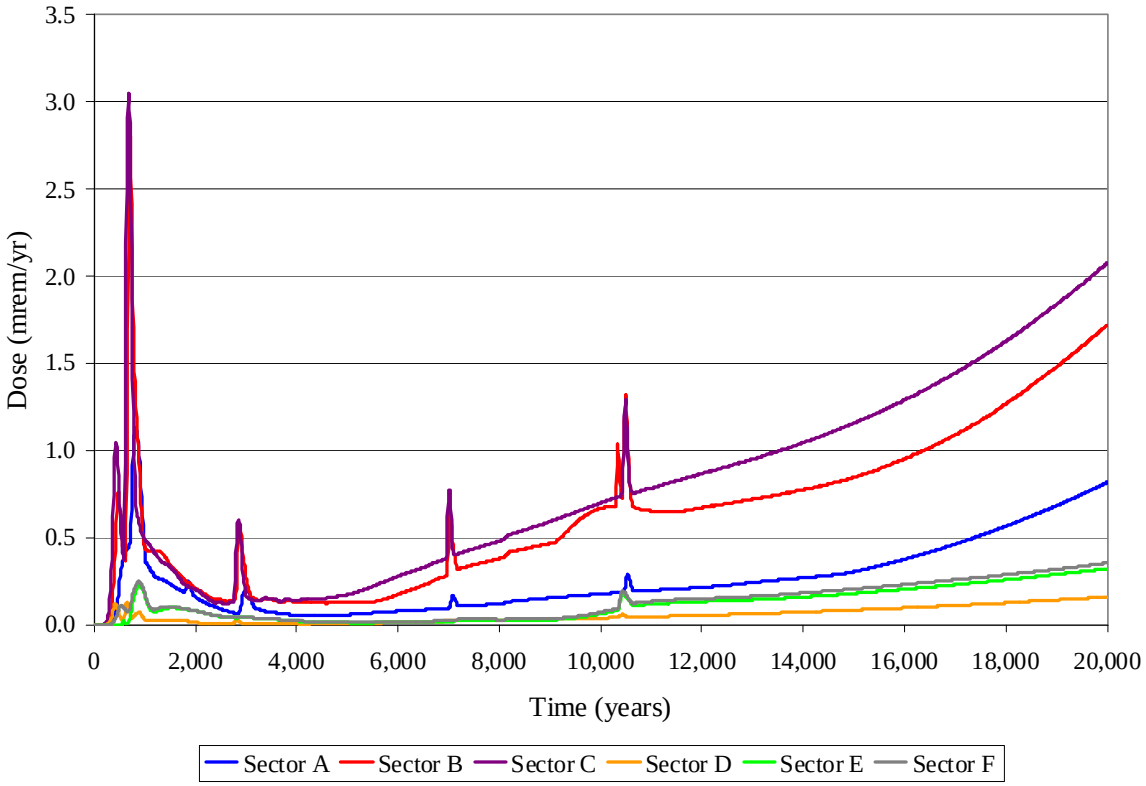

Figure 5.6-124: Synergistic Case Individual Radionuclide Contributors to MOP

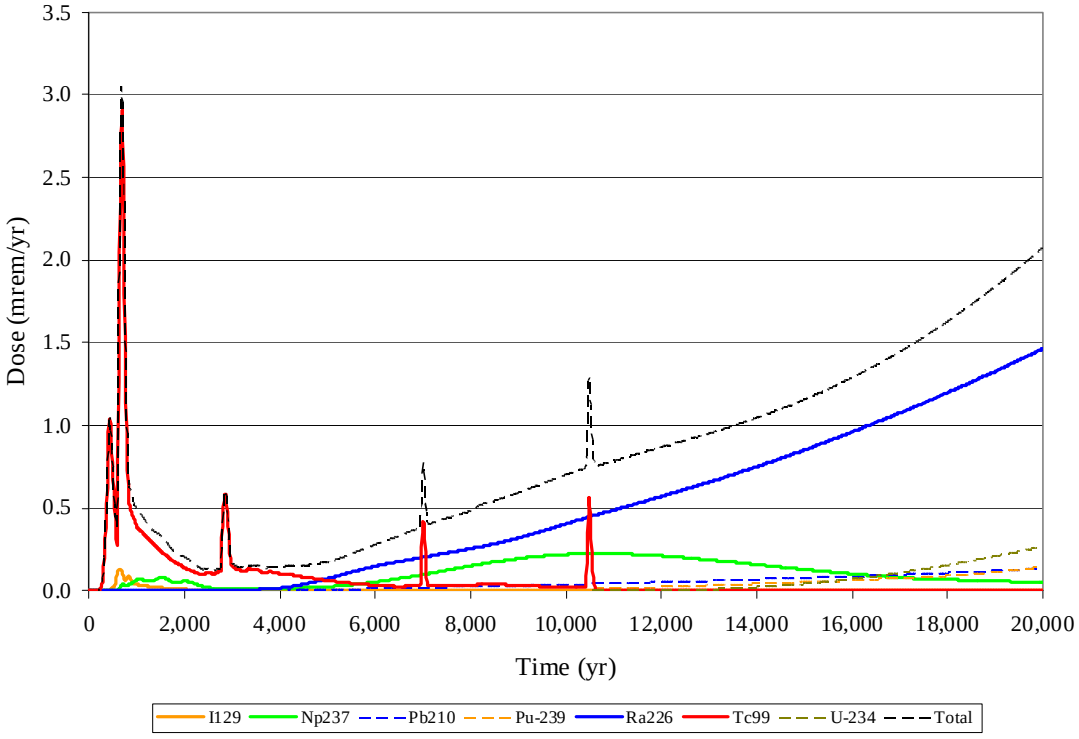

Figure 5.6-125: Sector C Base Case, Case C, and Synergistic Case Comparison

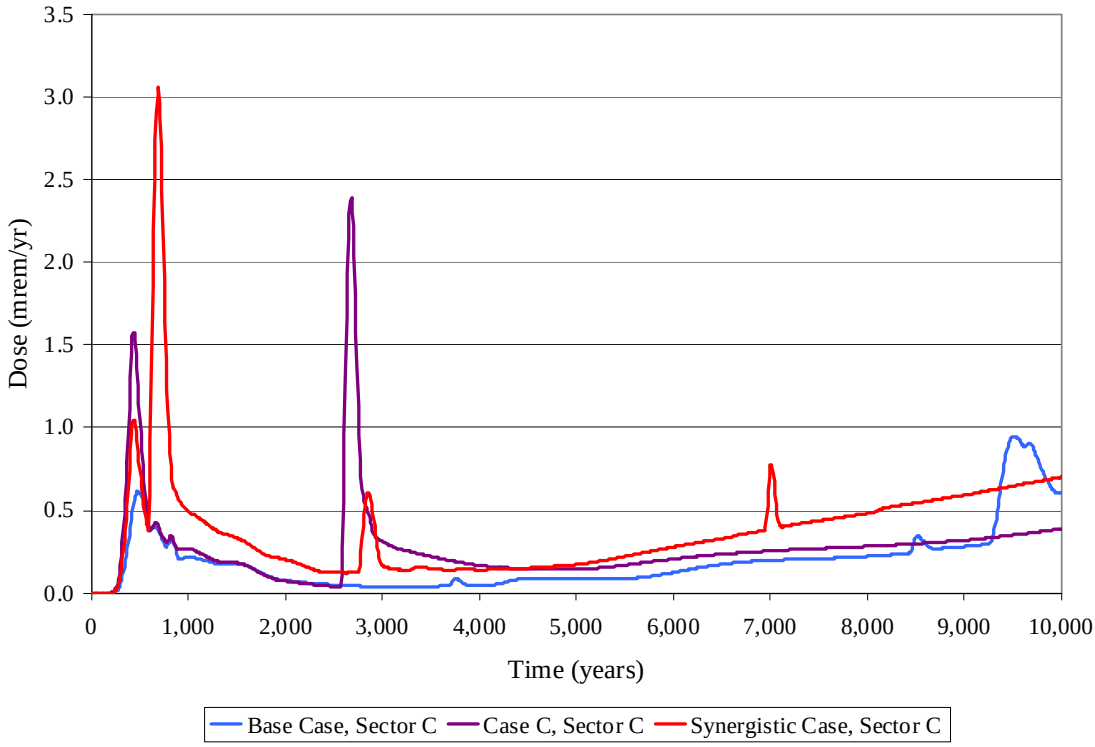

The results indicate that the impacts associated with the synergistic case parameter changes result in dose peaks that are higher in magnitude and earlier in time than the Base Case or Case C results. This is expected as the pessimistic parameter changes modeled would increase the magnitude of the releases due to the solubility phases, and lack of reducing grout impacts and move the peaks earlier in time due to the liner failure time and lack of reducing grout. Although the peaks are higher in magnitude and earlier in time than the Base Case or Case C, the magnitude only increases to approximately 3 mrem/yr and therefore provides reasonable assurance that the performance objectives would not be exceeded.

5.6.8 Sensitivity Analysis Using the HTF Probabilistic Model

This section presents the sensitivity of the closure system to alternative conditions using the GoldSim probabilistic model.

5.6.8.1 Influences of Flow Field Changes

This sensitivity analysis information is designed to evaluate the potential effects of changes in the water table divide on the analysis results. The GoldSim radionuclide transport model is an abstraction of the HTF GoldSim Model. The GoldSim saturated zone sub-model is constructed from spatial and velocity data associated with specific stream traces generated from the HTF GoldSim Model. For this reason, the HTF GoldSim Model is not amenable to changing the groundwater flow patterns without the development of a GoldSim model from which 1) groundwater flow velocities, 2) path lengths along the stream traces, and 3) the lengths of perpendiculars from the analysis wells to the stream traces can be abstracted. Modifying the PORFLOW generated flow field would yield less than satisfactory results

since arguably; there are no criteria to establish the appropriateness of the new flow field over the existing one. Still, from a risk-based perspective, it is necessary to be able to provide an estimate of an upper bound for the total dose to a MOP, assuming that the groundwater divide traversing the HTF could shift.

Since neither the HTF PORFLOW or GoldSim models are readily amenable to a standalone analysis pertaining to major changes in the flow field, such as would be seen if the location of the groundwater divide changes within the tank farm, it was decided to take a simple conservative approach using the HTF GoldSim Model by summing up the maximum dose concentrations from the individual sectors (Sectors A through F), as shown in Figure 5.6-126. Note that for the HTF GoldSim Model, because none of the stream traces presented in Figure 5.6-126 cross the 100-meter boundary in Sector D, Sector D was not analyzed for dose and therefore, there is no contribution from that sector in this analysis. Despite there being no contribution from Sector D, for simplicity the text will refer to the summation as the summation of results from Sectors A through F. Also, note that the total dose values presented in Section 5.5 (for specific time steps) represent the maximum of total dose values taken from Sectors A through F. The Base Case (Case A) will be used for this analysis.

Figure 5.6-126: PORFLOW Stream Traces with Hypothetical 100m Boundary and Associated GoldSim Well Locations

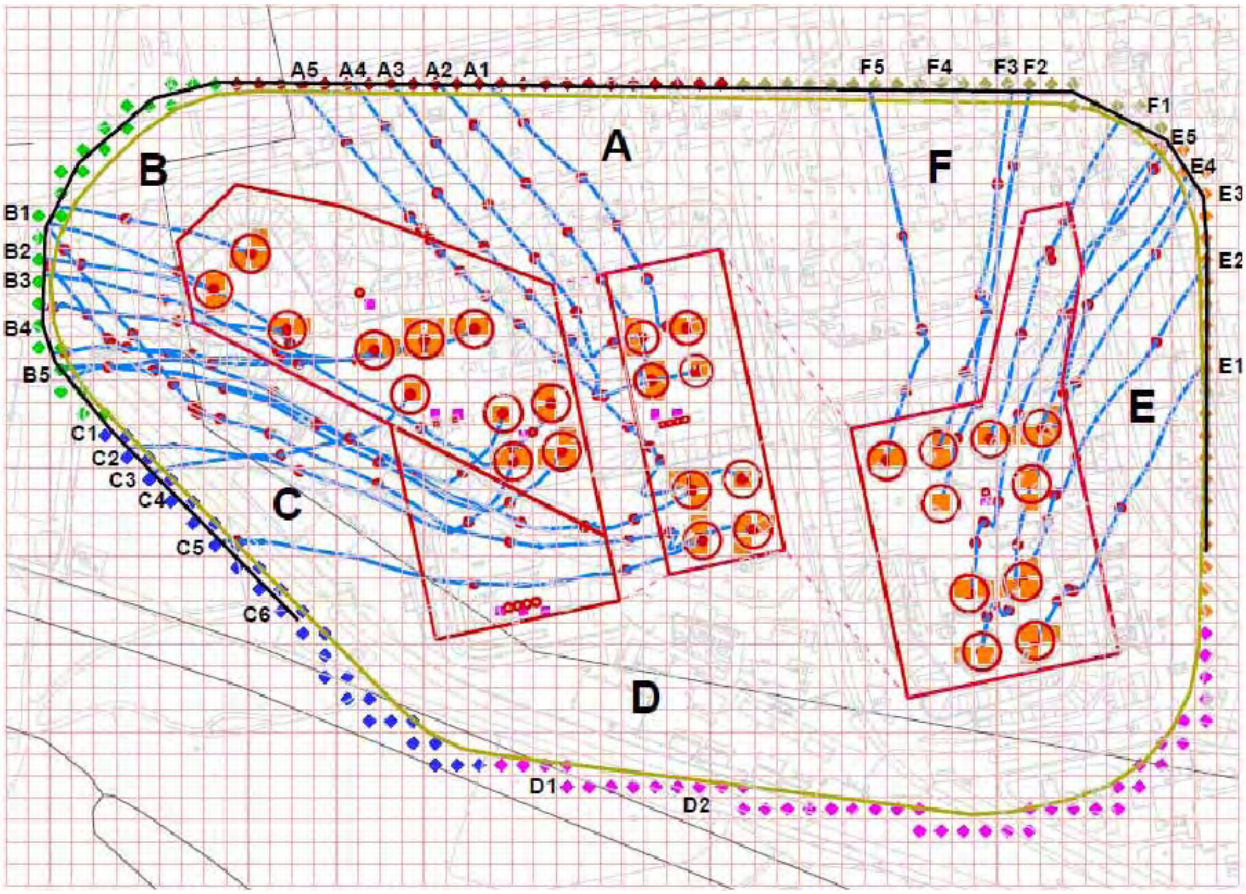

Insight to the sensitivity of the system to changes in the groundwater divide can be obtained by assuming all waste tank releases converge. It is recognized that conceptually, the superposition of localized peak dose values from all sectors is physically inconsistent. Although summing the peak concentrations is unrealistic, it does provide a conservative assumption, which is applicable in a bounding calculation. Additionally, an important insight pertaining to the sensitivity of the system to flow rates can be derived by systematically varying the flow rates. To evaluate the influence of potential changes in stream trace Darcy velocities, a set of three additional GoldSim simulations were performed where the Darcy velocity for each waste tank and ancillary equipment release were set to the maximum, minimum, and mean Darcy velocity values. This was done to prove that increasing (or decreasing) the Darcy velocity can have both attenuating and conservative effects. On the attenuating side, there is more water available for dilution. On the conservative side, the radionuclides will migrate faster increasing the influence of the more highly sorbing radionuclides over the time period of interest and offsetting the attenuating effect of radionuclide decay. The fact that stream trace lengths are not changed is a necessary simplification, but in general, since some of the pathway lengths could increase and some could decrease it is assumed that this would be an offsetting assumption.

As shown in Figure 5.6-127, summing the locally maximized dose values for all sectors will, as expected, have a limited effect on the dose increases. Since the Base Case result is based on the largest of those locally maximized dose values, the magnitude of the summation of doses is limited to five times the Base Case value, which means that all sectors have the same maximum total doses. As can be seen in Figure 5.6-127 and Table 5.6-39, superposition of the Base Case doses for each sector generates an early-time peak of approximately 2.4 mrem/yr, or approximately three times the Base Case equivalent of 0.8 mrem/yr. The early-time peak is formed by the release of Tc-99 from the primary sand layer in the Type II tanks. This early-time peak also represents the peak dose over the first 10,000 years. At 20,000 years, the peak dose based on the summed doses is 3.6 mrem/yr, or once again, approximately three times the Base Case dose at that time of 1.3 mrem/yr.

Figure 5.6-127: Comparison of Base Case Results with Sum of Max Dose - All Sectors, Base Case Model

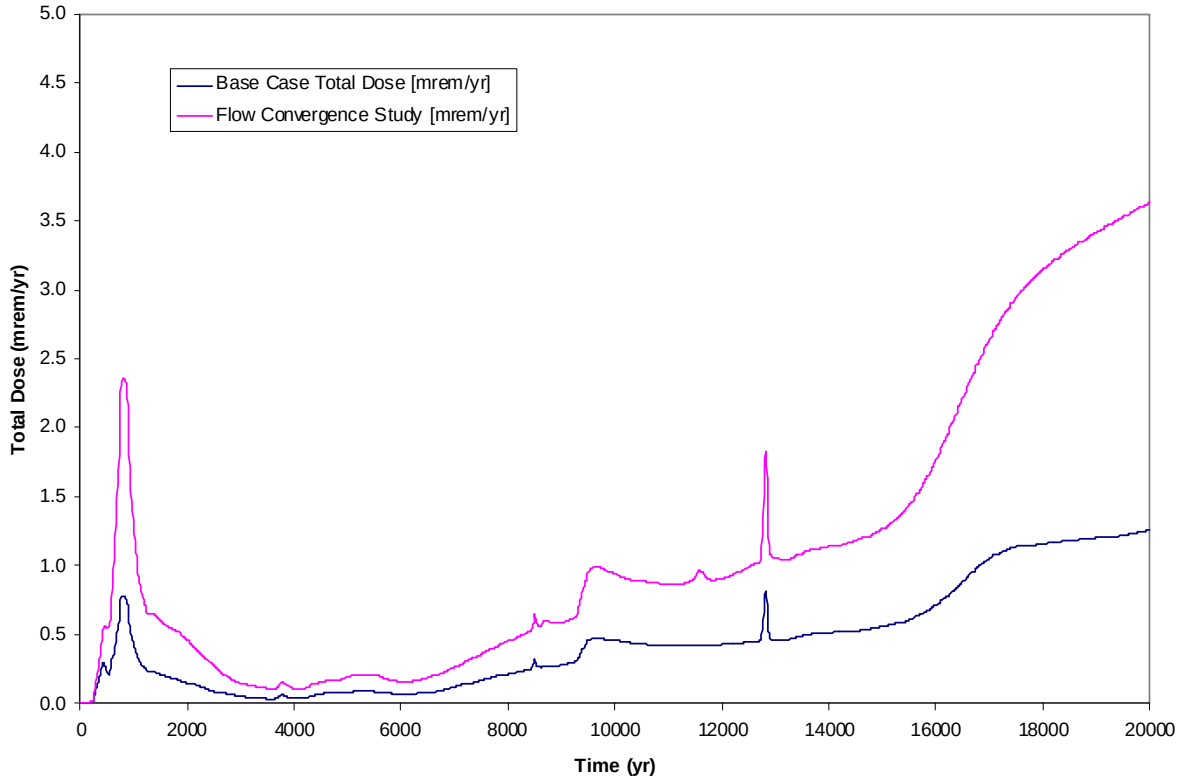

Table 5.6-39: Peak Dose Results for Various Time Periods

Run ID	Early Peak Dose (mrem/yr)	Time of Early Peak Dose (yr)	10,000-Year Peak Dose (mrem/yr)	Time of 10,000-Year Peak Dose (yr)	20,000-Year Peak Dose (mrem/yr)	Time of 20,000-Year Peak Dose (yr)
Base Case	0.8	810	0.8	810	1.3	20,000
Sum of All Sectors	2.4	810	2.4	810	3.6	20,000
Sum of All Sectors (Max)	1.7	790	1.7	790	4.4	20,000
Sum of All Sectors (Min)	5.3	1010	5.3	1010	1.8	20,000
Sum of All Sectors (Mean)	2.9	860	2.9	860	3.9	20,000

To evaluate the sensitivity of concentrations (and associated doses) at the 100-meter boundary to changes in flow-field velocities, three additional GoldSim simulations were performed. The first of the simulations assumed that the Darcy velocities for all sources (waste tanks and ancillary equipment) were the same value, the maximum value for all of the waste tank releases from

Table 5.6-40. Therefore, the saturated zone Darcy velocity for each source was set to 14.39 ft/yr. As can be seen by comparing Figure 5.6-128 to Figure 5.6-127, if the Darcy velocities for all waste tanks and ancillary equipment releases are increased to the waste tank specific maximum, the early-time peak radionuclide dose decreases, from approximately 2.4 mrem/yr to 1.7 mrem/yr. This change reflects the influence of increased flow on non-sorbing and slightly sorbing species, such as Tc-99. The increase in Darcy velocity (except for the Tank 16 release) will increase the volume water mixing with the solute as the plume spreads. This early peak, which arrives in 810 years, also represents the peak total dose over the first 10,000 years of the simulation. At later time (20,000 years), the faster movement of the more highly sorbed radionuclides such as Pu-239 promotes an increase of the peak dose from approximately 3.6 mrem/yr to 4.4 mrem/yr.

Table 5.6-40: Average Saturated Zone Darcy Velocities for Waste Tanks

Tank	Mean Darcy Velocity (ft/yr)
Tank 9	4.01
Tank 10	3.62[a]
Tank 11	4.1
Tank 12	3.93
Tank 13	12.15
Tank 14	4.26
Tank 15	10.62
Tank 16	14.39[b]
Tank 21	10.52
Tank 22	9.24
Tank 23	8.65
Tank 24	8.87
Tank 29	6.25
Tank 30	6.1
Tank 31	6.5
Tank 32	5.88
Tank 35	8.12
Tank 36	9.1
Tank 37	8.73
Tank 38	6.28
Tank 39	7.1
Tank 40	8.37
Tank 41	8.66
Tank 42	6.26
Tank 43	6.82
Tank 48	5.61
Tank 49	10.68
Tank 50	4.74
Tank 51	4.26
Mean Value	7.37

[SRR-CWDA-2010-00093]

a Minimum Darcy Velocity

b Maximum Darcy Velocity

Figure 5.6-128: Comparison of Base Case Results with Sum of Max Dose - All Sectors, Max Velocity Analysis

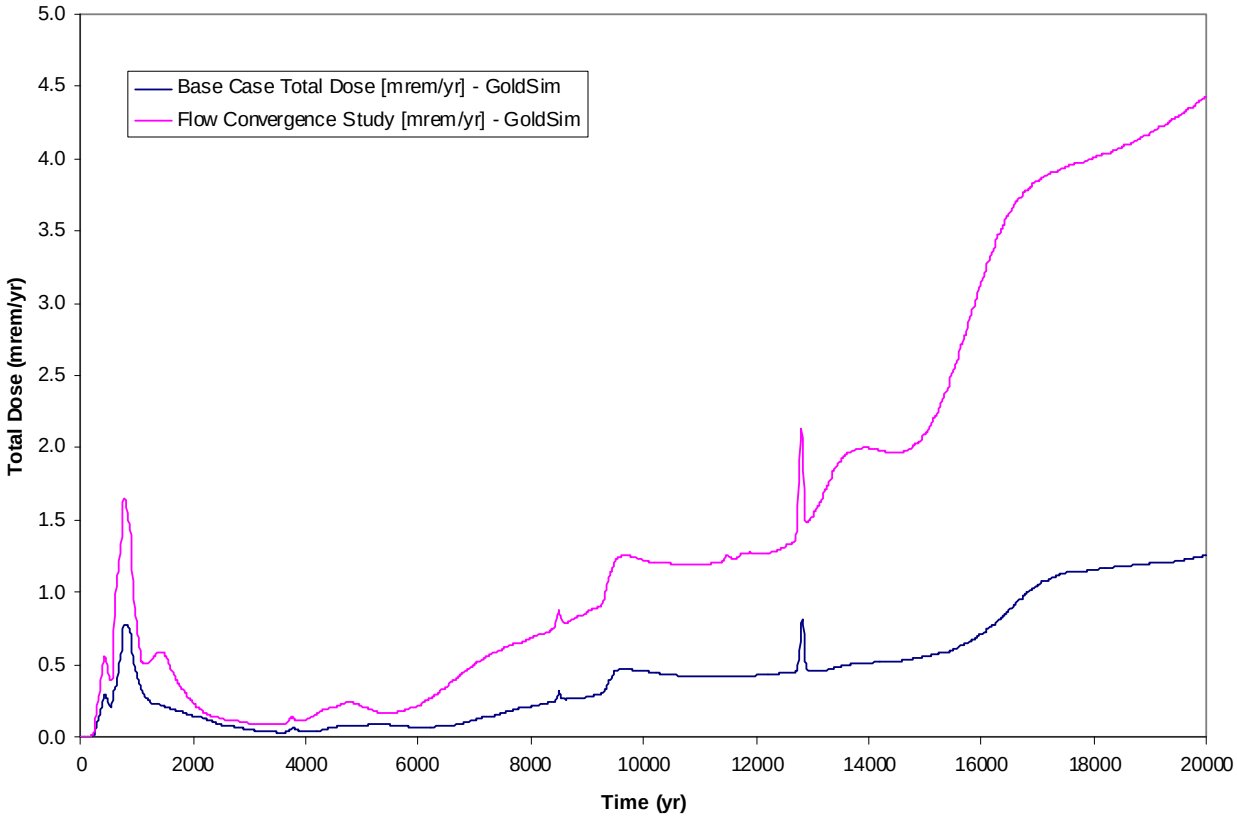

The second of the simulations assumed that the Darcy velocities for all sources (waste tanks and ancillary equipment) were the same value, the minimum value for all of the waste tank releases from Table 5.6-40. Therefore, the saturated zone Darcy velocity for each source was set to 3.62 ft/yr. As can be seen by comparing Figure 5.6-129 to Figure 5.6-127, if the Darcy velocities for all waste tanks and ancillary equipment releases are decreased to the waste tank specific minimum, the early-time peak radionuclide dose increases from approximately 2.4 mrem/yr to 5.3 mrem/yr. This change reflects the influence of decreased flow on non-sorbing and slightly sorbing species, in this case Tc-99. Less water is available for mixing and associated dilution of the mass. This early peak, which arrives at 1010 years, also represents the peak total dose over the first 10,000 years of the simulation. At later time (20,000 years), the slower movement of the more highly sorbed radionuclides such as Pu-239 causes a decrease of the peak dose from approximately 3.6 mrem/yr to 1.8 mrem/yr.

Figure 5.6-129: Comparison of Base Case Results with Sum of Max Dose - All Sectors, Min Velocity Analysis

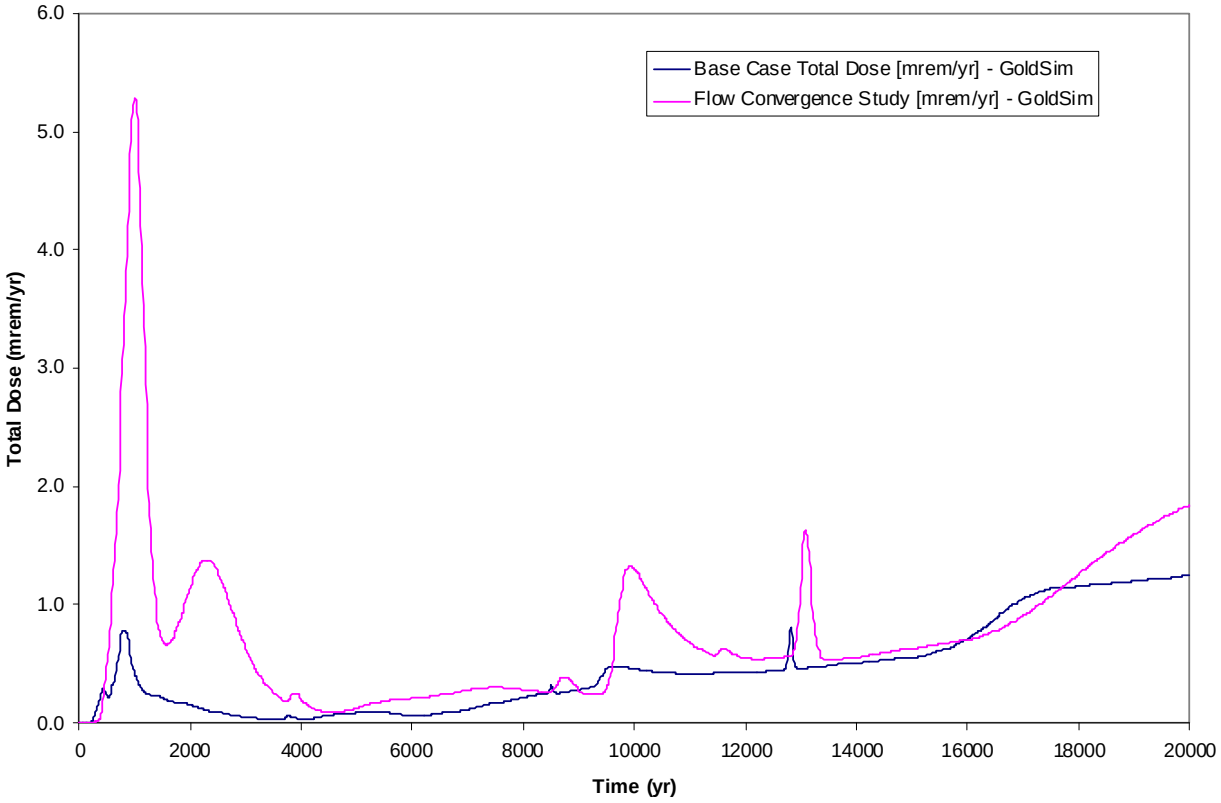

The third of the simulations assumed that the Darcy velocities for all sources (waste tanks and ancillary equipment) were the same value, the mean value for all of the waste tank releases from Table 5.6-40. Therefore, the saturated zone Darcy velocity for each source was set to 7.37 ft/yr. As can be seen by comparing Figure 5.6-130 to Figure 5.6-127, if the Darcy velocities for all waste tanks and ancillary equipment releases are set to the mean of the waste tank specific values, the early-time peak radionuclide dose increases from approximately 2.4 mrem/yr to 2.9 mrem/yr. This early peak, which arrives in 860 years, also represents the peak total dose over the first 10,000 years of the simulation. At later time (20,000 years), the movement of the more highly sorbed radionuclides such as Pu-239 promotes an increase of the peak dose from approximately 3.6 mrem/yr to 3.9 mrem/yr.

Figure 5.6-130: Comparison of Base Case Results with Sum of Max Doses - All Sectors, Mean Velocity Analysis

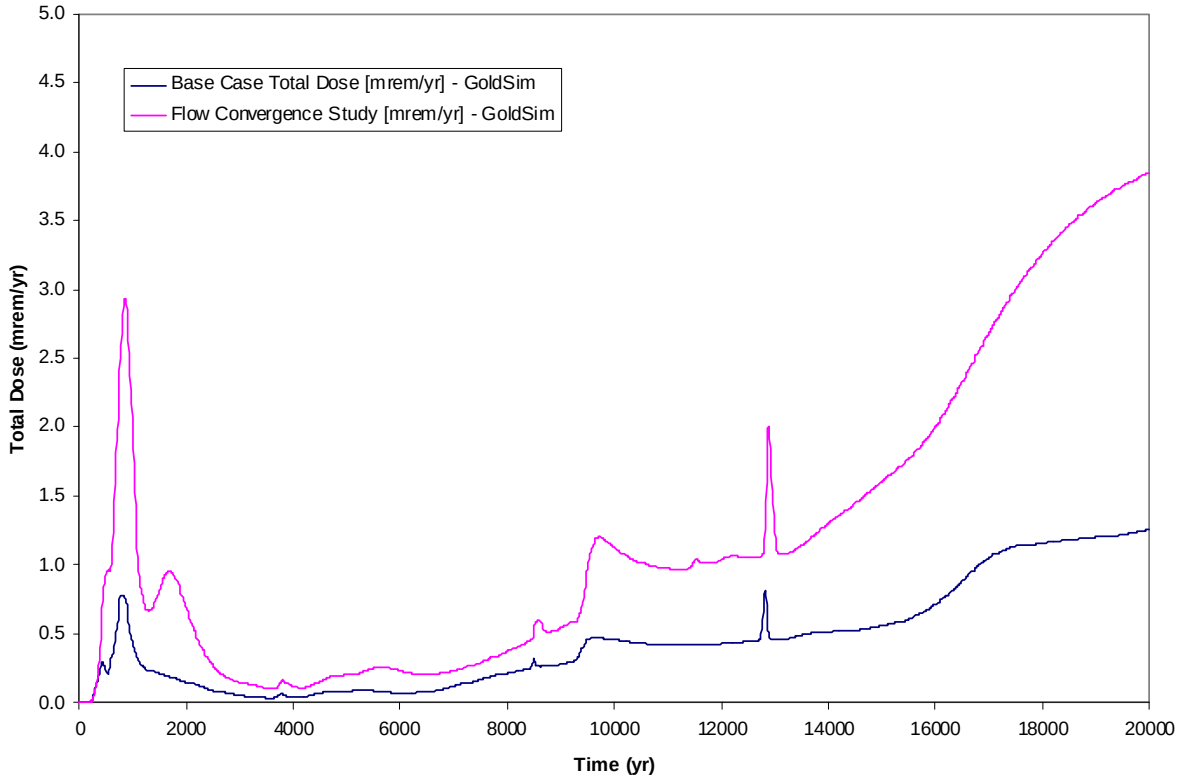

The analysis indicates that although a change in the water table divide could change the flow directions and velocities associated with releases from individual waste tanks (and ancillary equipment), it is unlikely that it would lead to a peak dose that would exceed the performance objective. Additionally, the analysis showed the sensitivity of the system to the saturated zone Darcy velocities, which are likely to change if the water table divide location changes. The analysis also reflected the sensitivity of the system to sorption, especially for highly sorbing radionuclides such as Pu-239.

5.7 RCRA/CERCLA Risk Analysis

The RCRA/CERCLA risk assessment for the HTF closure follows the ACP protocols for human health and ecological risk assessments. [ERD-AG-003_F.17, ERD-AG-003_P.1.4, ERD-AG-003_P.1.5, ERD-AG-003_P.5.2, and ERD-AG-003_P.10.1] Based on available characterization data and estimated volume of residual material expected to remain in each of the waste tanks and ancillary equipment, the chemical and radiological inventory used for PA modeling has been calculated for HTF as discussed in Section 3.3. As discussed in Section 4.8, the placement of a low-permeability closure cap with at least 10 feet of clean backfill soil will ensure that the surface soils (0 to 1 foot) and the subsurface soils (1 to 4 feet) will not be contaminated and that there is no pathway for human health or ecological risk. The potential receptors of contamination include:

- The industrial worker excavating deep soil containing PTSM
- The resident who will be exposed to groundwater (ingestion, inhalation, and dermal contact)

Modeling was conducted to determine the peak concentrations of the non-radiological and radiological contaminants in the groundwater over 10,000 years.

5.7.1 Principal Threat Source Material

The PTSMs are the materials that include or contain hazardous substances, pollutants, or contaminants that act as a reservoir for migration of contamination to groundwater, surface water, or air, or that act as a source for direct exposure. The EPA defines PTSM as the source materials considered highly toxic or mobile that generally cannot be reliably contained or would present a significant risk to human health or the environment should exposure occur. [OSWER 9380.3-06FS]

The HTF waste tanks and ancillary equipment will contain a heel of highly contaminated material that would present a significant risk should exposure occur, so they are, by definition, PTSM. The waste tanks and the heels remaining in the waste tanks will be stabilized and then covered as part of waste tank closure. This approach is consistent with ACP remediation of reactor seepage basins, which contain highly contaminated soils determined to be PTSM. No additional evaluation will be made to determine that the source material is PTSM.

5.7.2 Contaminant Migration Constituents of Concern

The CMCOC were identified through a system that is consistent with both ACP protocols and the PA. The CMCOC were identified by modeling the release of contaminants and their travel through the vadose zone. The basis of the CMCOC evaluation is the same model used for the PA to meet 10 CFR 61 requirements. The concentrations of contaminants that are modeled to reach the water table are compared to the MCL or RSLs/PRGs, in cases where the constituent does not have an MCL. Any constituents that are predicted to exceed these standards (i.e., fraction greater than 1.0) in the groundwater directly beneath HTF (1 meter from boundary) are identified as CMCOC as shown in Tables 5.7-1 and 5.7-2. The CMCOC identified using the described protocols are, Np-237, Pu-239, Pu-240, Se-79, Tc-99, U-233, U-234, and manganese.

Table 5.7-1: Groundwater Radionuclide Concentrations at 1m from HTF

Radionuclide	MCL** (pCi/L)	Residential Tap Water PRG* (pCi/L)	Peak Concentration (pCi/L) 1 to 10,000 Years	Fraction of MCL or PRG at 1m
Ac-227	N/A	2.37E-01	1.6E-04	6.9E-04
Al-26	N/A	2.75E+00	1.2E-01	4.3E-02
Am-241	N/A	4.58E-01	1.6E-01	3.5E-01
Am-242m	N/A	6.74E-01	7.7E-06	1.1E-05
Am-243	N/A	4.62E-01	6.9E-02	1.5E-01
C-14	2.0E+03	MCL used	1.5E+02	7.3E-02
Cf-249	N/A	3.75E-01	8.7E-14	2.3E-13
Cf-251	N/A	3.61E-01	1.3E-08	3.7E-08
Cl-36	7.0E+02	MCL used	3.2E+01	4.5E-02
Cm-243	N/A	5.03E-01	7.2E-12	1.4E-11
Cm-244	N/A	5.70E-01	1.3E-10	2.3E-10
Cm-245	N/A	4.58E-01	9.7E-05	2.1E-04
Cm-247	N/A	4.79E-01	3.0E-05	6.3E-05
Cm-248	N/A	5.00E-03	3.0E-05	6.0E-03
Co-60	1.0E+02	MCL used	3.5E-14	3.5E-16
Cs-135	9.0E+02	MCL used	3.3E+01	3.7E-02
Cs-137	2.0E+02	MCL used	1.1E-02	5.7E-05
Eu-152	6.0E+01	MCL used	1.6E-11	2.6E-13
Eu-154	2.0E+02	MCL used	5.8E-11	2.9E-13
H-3	2.0E+04	MCL used	3.5E+01	1.8E-03
I-129	1.0E+00	MCL used	6.8E-01	6.8E-01
K-40	N/A	1.93E+00	1.86E+00	9.6E-01
Nb-93m	1.0E+03	MCL used	2.9E+02	2.9E-01
Nb-94	N/A	6.13E+00	4.5E-01	7.3E-02
Ni-59	3.0E+02	MCL used	1.5E+02	4.9E-01
Ni-63	5.0E+01	MCL used	1.2E+01	2.3E-01
Np-237	N/A	7.71E-01	1.0E+00	1.3E+00
Pa-231	N/A	2.75E-01	5.6E-02	2.0E-01
Pb-210	N/A	5.41E-02	3.3E-02	6.0E-01
Pd-107	N/A	1.90E+02	5.0E-01	2.6E-03
Pt-193	3.0E+03	MCL used	1.1E-02	3.7E-06
Pu-238	N/A	3.64E-01	1.2E-01	3.3E-01
Pu-239	N/A	3.53E-01	2.0E+00	5.6E+00
Pu-240	N/A	3.53E-01	9.6E-01	2.7E+00
Pu-241	N/A	2.71E+01	3.7E-04	1.4E-05
Pu-242	N/A	3.72E-01	3.3E-03	8.8E-03
Pu-244	N/A	3.48E-01	1.5E-05	4.3E-05

Table 5.7-1: Groundwater Radionuclide Concentrations at 1m from HTF (Continued)

Radionuclide	MCL** (pCi/L)	Residential Tap Water PRG* (pCi/L)	Peak Concentration (pCi/L) 1 to 10,000 Years	Fraction of MCL or PRG at 1m
Ra-226+Ra-228	5.0E+00	MCL used	2.6E+00	5.2E-01
Se-79	N/A	6.53E+00	9.4E+00	1.4E+00
Sm-151	1.0E+03	MCL used	1.9E-02	1.9E-05
Sn-126	N/A	1.86E+00	2.3E-02	1.2E-02
Sr-90	8.0E+00	MCL used	2.9E-01	3.6E-02
Tc-99	9.0E+02	MCL used	9.5E+02	1.1E+00
Th-229	N/A	2.13E-01	1.1E-01	5.1E-01
Th-230	N/A	5.23E-01	2.0E-02	3.8E-02
Th-232	N/A	4.71E-01	5.9E-05	1.3E-04
U-232	N/A	1.63E-01	8.8E-09	5.4E-08
U-233	N/A	6.63E-01	1.6E+00	2.3E+00
U-234	N/A	6.74E-01	2.4E+00	3.5E+00
U-235	N/A	6.84E-01	5.7E-03	8.3E-03
U-236	N/A	7.11E-01	3.1E-02	4.4E-02
U-238	N/A	7.44E-01	2.4E-02	3.2E-02
Zr-93	2.0E+03	MCL used	4.0E-02	2.0E-05

Note CMCOC are shaded gray in the table

* Residential tap water PRGs are provided in tables at http://epa-prgs.ornl.gov/radionuclides/download/rad_master_prg_table_pci.pdf based on a target cancer risk of 1.0E-06

** MCL values for beta and photon emitters are calculated in EPA 815-R-02-001 based on a beta-gamma 4 mrem/yr dose

N/A = Not Available

Table 5.7-2: Groundwater Chemical Concentrations at 1m from HTF

Chemical	MCL** (µg/L)	Tap Water RSLs* (µg/L)	Peak Concentration (µg/L) 1 to10,000 Yrs	Fraction of MCL or PRG at 1m
Ag	1.0E+02	MCL used***	2.4E-01	2.4E-03
As	1.0E+01	MCL used	3.0E-03	3.0E-04
Ba	2.0E+03	MCL used	8.3E-01	4.1E-04
Cd	5.0E+00	MCL used	3.4E-01	6.8E-02
Cr	1.0E+02	MCL used	3.8E+00	3.8E-02
Cu	1.3E+03	MCL used	1.0E-01	7.9E-05
F	4.0E+03	MCL used	3.5E+01	8.7E-03
Fe	3.0E+02	MCL used***	1.6E+00	5.3E-03
Hg	2.0E+00	MCL used	5.7E-01	2.9E-01
Mn	5.0E+01	MCL used***	9.7E+01	1.9E+00
N	1.0E+04	MCL used	1.3E+03	1.3E-01
Ni	N/A	7.3E+02	2.2E-01	3.0E-04
Pb	1.5E+01	MCL used	2.8E-02	1.9E-03
Sb	6.0E+00	MCL used	3.1E-03	5.2E-04
Se	5.0E+01	MCL used	1.8E-04	3.6E-06
U	3.0E+01	MCL used	5.6E-03	1.9E-04
Zn	5.0E+03	MCL used***	2.7E+00	5.4E-04

Note CMCOC are shaded gray in the table
* RSLs are calculated at: http://www.epa.gov/reg3hwmd/risk/human/rb-concentration_table/Generic_Tables/index.htm, calculated based on a Non-cancer Hazard Index = 1
** EPA 816-F-09-0004
*** EPA 816-F-10-079
N/A = Not Available

Manganese - Manganese has a peak concentration of 97 µg/L at 1 meter compared to the secondary MCL of 50 µg/L. The peak concentration occurs approximately 5,214 years following HTF closure. As shown in Table 5.7-3, the peak concentration drops to 41 µg/L at 100 meters (which is below the secondary MCL).

Neptunium-237 - Np-237 does not have an MCL, so the peak concentration of 1.0 pCi/L at 1 meter is compared to the PRG of 7.7E-01 pCi/L. [http://epa-prgs.ornl.gov/radionuclides/download/rad_master_prg_table_pci.pdf] This peak concentration occurs 544 years following HTF closure. As shown in Table 5.7-3, the peak concentration drops to 6.3E-01 pCi/L at 100 meters (which is below the PRG).

Plutonium-239 - Pu-239 does not have an MCL, so the peak concentration of 2.0 pCi/L at 1 meter is compared to the PRG of 3.5E-01 pCi/L. [http://epa-prgs.ornl.gov/radionuclides/download/rad_master_prg_table_pci.pdf] This peak concentration occurs 2,540 years following HTF closure. As shown in Table 5.7-3, the peak concentration drops to 2.1E-02 pCi/L at 100 meters (which is below the PRG).

Plutonium-240 - Pu-240 does not have an MCL, so the peak concentration of 9.6E-01 pCi/L at 1 meter is compared to the PRG of 3.5E-01 pCi/L. [http://epa-prgs.ornl.gov/radionuclides/download/rad_master_prg_table_pci.pdf] This peak

concentration occurs 2,218 years following HTF closure. As shown in Table 5.7-3, the peak concentration drops to 5.6E-03 pCi/L at 100 meters (which is below the PRG).

Selenium-79 - Se-79 does not have an MCL so the peak concentration of 9.4 pCi/L at 1 meter is compared to the PRG of 6.5 pCi/L. [http://epa-prgs.ornl.gov/radionuclides/download/rad_master_prg_table_pci.pdf] This peak concentration occurs 10,000 years following HTF closure. As shown in Table 5.7-3, the peak concentration drops to 1.1E-07 pCi/L at 100 meters (which is below the PRG).

Technetium-99 - Tc-99 has a peak concentration of 950 pCi/L at 1 meter, compared to the MCL of 900 pCi/L. [EPA 815-R-02-001] This peak concentration occurs 9,510 years following HTF closure. As shown in Table 5.7-3, the peak concentration drops to 540 pCi/L at 100 meters (which is below the MCL).

Uranium-233 - U-233 does not have an MCL so the peak concentration of 1.6 pCi/L at 1 meter is compared to the PRG of 6.6E-01 pCi/L. [EPA 815-R-02-001] This peak concentration occurs at approximately 10,000 years following HTF closure. As shown in Table 5.7-3, the peak concentration drops to 7.6E-03 pCi/L at 100 meters (which is below the PRG).

Uranium-234 - U-234 does not have an MCL, so the peak concentration of 2.4 pCi/L at 1 meter is compared to the PRG of 6.7E-01 pCi/L. [EPA 815-R-02-001] This peak concentration occurs at approximately 7,196 years following HTF closure. As shown in Table 5.7-3, the peak concentration drops to 1.7E-02 pCi/L at 100 meters (which is below the PRG).

Table 5.7-3: Groundwater Concentrations of CMCOC at 100m

Contaminant	MCL (pCi/L[a] or µg/L[b])	Residential Tap Water PRG (pCi/L)	Peak Concentration at 100m (pCi/L[a] or µg/L[b]) 1 to 10,000 Yrs	Fraction of MCL or PRG at 100m
Mn	5.0E+01[b]	MCL used	4.1E+01[b]	8.2E-01
Np-237	N/A	7.7E-01	6.3E-01	8.2E-01
Pu-239	N/A	3.5E-01	2.1E-02	6.0E-02
Pu-240	N/A	3.5E-01	5.6E-03	1.6E-02
Se-79	N/A	6.5E+00	1.1E-07	1.7E-08
Tc-99	9.0E+02[a]	MCL used	5.4E+02	6.0E-01
U-233	N/A	6.6E-01	7.6E-03	1.2E-02
U-234	N/A	6.7E-01	1.7E-02	2.5E-02

a pCi/L
b µg/L

5.7.3 Evaluation of Results

The CMCOC are often addressed by the placement of a low permeability cap as is planned for the HTF closure (described in Section 3.2.4). Sections 2.4.2 and 2.4.3 describe the *SRS Long Range Comprehensive Plan* (PIT-MISC-0041) as founded on the following:

- The entire site will be owned and controlled by the federal government in perpetuity
- The property will be used only for industrial purposes
- Site boundaries will remain unchanged
- Residential use will not be allowed

Therefore, a scenario in which an inadvertent intruder establishes a residence on the HTF and obtains drinking water from the water table below is very unlikely. A more probable location for the MEI would be at either the UTR seepline located approximately 2 miles northwest of the HTF or the Fourmile Branch seepline, approximately 1 mile south of the HTF. As discussed previously, all isotopes, including total beta-gamma emitters, meet the MCLs or PRGs at the 100-meter boundary in 10,000 years and therefore would be below the MCLs or PRGs at either seepline in 10,000 years.

5.8 ALARA Analysis

The SRS has an ALARA program and processes established in company level policies and procedures that are well documented. [E7-1 - Procedure DE-DP-384, ESH-RPS-2005-00208] The goal of the ALARA process is the attainment of the lowest practical dose level after taking into account social, technical, economic, and public policy considerations. Depending on the situation, the ALARA analysis can range from simple qualitative statements evaluating different operation and disposal options for LLW to rigorous quantitative analyses that consider individual and collective doses to the MOP. The rigor of the ALARA analysis should be commensurate with the magnitude of the calculated dose and the decisions to be made regarding the disposal facility. Based on the results of the HTF PA, a qualitative assessment of ALARA alternative disposal analysis is justified. Additionally, an in-depth ALARA cost-benefit analysis is not appropriate at this time, because the cost of new technology and personnel exposures will not be available until following final waste tank cleaning and sampling operations. A more in-depth ALARA analysis will be completed as part of the DOE O 435.1 Tier 2 closure authorization documentation.

The ALARA process is applied to HTF in several ways, 1) making conservative assumptions when modeling tank farm waste inventory, releases, and dose to receptors, 2) by evaluating waste tank cleaning and stabilization alternatives, and 3) by implementing cleaning processes prior to waste tank closure that remove the highly radioactive radionuclides to the maximum extent practical. Each is described below.

The following excerpts are from the two governing regulations that define performance objects.

DOE M 435.1-1, Chapter IV, P.(2)(f) states:

> *Performance assessments shall include a demonstration that projected releases of radionuclides to the environment shall be maintained as low as reasonable achievable (ALARA).*

DOE G 435.1-1 provides additional guidance on meeting this requirement. The Guide states in part:

> *that the goal of the ALARA process is not the attainment of a particular dose level (or, in this case, level of release), but rather the attainment of the lowest practical dose level after taking into account social, technical, economic, and public policy considerations. The PA should include assessments that focus on alternatives for LLW disposal. ALARA is meant to provide a documented answer to the question: "Have I done all that I can reasonably do to reduce radiation doses or releases to the environment?*

Code of Federal Regulations, 10 CFR 61, Section 61.41, *Protection of the General Population from Releases of Radioactivity*, states:

> *Reasonable effort should be made to maintain releases of radioactivity in effluents to the general environment as low as is reasonable achievable.*

The DOE's approach to radiation protection is based on meeting the performance objectives identified in DOE M 435.1-1 and 10 CFR 61. These documents specify maximum doses for various pathways based upon the ALARA principle.

The HTF PA modeling effort provides evidence of the SRS efforts to reduce radioactive releases to the general environment to levels ALARA. Considerable conservatisms are applied during the modeling effort and are summarized in Section 7.2. One of the appreciable conservatisms is the evaluation point for dose. In the HTF PA modeling, radionuclide dose to receptors is evaluated at a 1-meter and 100-meter buffer zones surrounding HTF and at the seepline. However, based on SRS land use plans, no MOP will have unrestricted access to the HTF, because current SRS boundaries will remain unchanged, and the land will remain under the ownership of the federal government, consistent with the site's designation as a NRMP. By demonstrating protection to the 1-meter and the 100-meter boundary, the PA is also demonstrating public protection at the site boundary (approximately 5 miles away). In fact, the dose due to radionuclides at the site boundary would only be greatly diminished in comparison to the 1-meter and 100-meter boundary dose, because as radionuclides travel a greater distance through the air and subsurface, the more dispersion and dilution occurs. Therefore, the PA demonstrates protection of the public at the site boundary to a much greater degree than at the 1-meter or 100-meter boundary.

Social, technical, economic and public policy aspects were considered in the alternative disposal analysis included in the EIS for waste tank closure. [Section 3.2.3, DOE-EIS-0303] In May 2002, DOE issued the EIS on waste tank cleaning and stabilization alternatives. DOE studied five alternatives:

1. Empty, clean, and fill waste tank with grout
2. Empty, clean, and fill waste tank with sand
3. Empty, clean, and fill waste tank with saltstone
4. Clean and remove waste tanks
5. No action

The EIS concluded the "empty, clean, and fill with grout" was the preferred option with the best approach to minimize human health and safety risks associated with operational closure of waste tanks. [DOE-EIS-0303]

In addition, the NDAA Section 3116, and DOE M 435.1-1 require that highly radioactive radionuclides be removed to the maximum extent practical. [NDAA_3116] This basic ALARA principle is accomplished through the cleaning of the waste tanks prior to closure. Section 3.3.2 delineates the estimations of waste tank inventory after waste tank cleaning.

In summary, the analysis of alternative disposal techniques; the application of cleaning the waste tanks to the maximum extent practical; the stabilization of the remaining inventory with grout; and meeting the performance objectives of DOE M 435.1-1 and 10 CFR 61 are all evidence of the application of ALARA in limiting the release of radionuclides into the environment. Furthermore, an additional ALARA analysis will be performed following closure of HTF to support the CERCLA closure, including the final design considerations for the closure cap to evaluate further opportunities to reduce environmental releases. Therefore, the principle of ALARA is satisfied.